

Curtin Medical School

**An exploration into common mechanisms of oxidative damage in
models of demyelinating disease and neurotrauma**

**Lillian May Toomey
0000-0001-9435-6128**

**This thesis is presented for the Degree of
Doctor of Philosophy
of
Curtin University**

September 2022

Declaration

To the best of my knowledge and belief this thesis contains no material previously published by any other person except where due acknowledgment has been made.

This thesis contains no material that has been accepted for the award of any other degree or diploma in any university.

The research presented and reported in this thesis was conducted in compliance with the National Health and Medical Research Council Australian (NHMRC) code for the care and use of animals for scientific purposes 8th edition (2013). The proposed research study received animal ethics approval from the University of Western Australia Animal Ethics Committee, Approval Numbers #RA/3/100/1613 and #RA/3/100/1485, with reciprocal approval from the Curtin University Animal Ethics Committee, Approval Numbers #ARE2019-4 and #ARE2017-4.

All schematic figures are original illustrations created with BioRender.com.

Signature:



Date: 23rd September 2022

Abstract

Multiple sclerosis (MS) is a chronic inflammatory disease which is characterised by demyelinated lesions, or areas of the brain where the myelin sheath that facilitates correct neuronal signalling is lost. This disease has been traditionally considered to have a primarily autoimmune aetiology but is now being increasingly acknowledged to be multifaceted and complex with primary oligodendrocyte death and innate neuroinflammation occurring in the absence of peripheral immune cell infiltration. Current immunomodulatory treatments only slow MS disease progression rather than halt it completely, which suggests that therapeutics that are more effective in targeting this innate central nervous system (CNS) damage may also be required to improve the quality of life for those living with MS. Neurotrauma, such as traumatic brain injury (TBI), is the damage caused by an external force acting upon the CNS. There are currently no effective pharmacological therapies clinically available for treating those who have experienced neurotrauma. The literature surrounding damage specifically to white matter following neurotrauma is presented in the thesis as a published narrative review article. Neurotrauma shares similar mechanisms of damage to MS, therefore to facilitate rapid advancement of knowledge and potentially assist in the development of effective treatments for both of these disorders, it is important to deepen the understanding of these commonalities between MS and neurotrauma. One such damage mechanism shared between the two conditions is oxidative stress, which is the damage caused by overwhelming levels of reactive oxygen species (ROS). Oligodendrocyte precursor cells (OPCs) are particularly vulnerable to the deoxyribonucleic acid (DNA) damage that results from heightened oxidative stress. Therefore, the core goal of this thesis was to establish the framework and commence initial experiments for investigation into broader shared mechanisms of oxidative damage between MS and neurotrauma.

The first aim of the thesis was to demonstrate the generalisability of a combinatorial treatment for ameliorating pathology in models of MS & neurotrauma. To address this, the initial work presented in the thesis utilises a combinatorial ion channel inhibitor treatment for neurotrauma and MS and encompasses two published papers that I have contributed to during candidature. Both studies utilised a combination of lomerizine, YM872 and Brilliant Blue G (BBG) to limit excess calcium ion (Ca^{2+}) influx into cells. This therapeutic strategy resulted in significant improvements for myelin outcomes in both models, which suggests that similar Ca^{2+} -associated mechanisms underpin the myelin structure abnormalities in the two conditions. This research also assessed whether the ion channel inhibitor combination results in an anti-inflammatory effect in the periphery when systemically delivered following neurotrauma, however no effect of either injury or treatment on circulating chemokine and cytokine levels was observed at the acute three day timepoint post-injury. Nevertheless, the generalisability of this combinatorial ion channel inhibitor treatment in the two animal models further supports the theory that deepening the understanding of the common

mechanisms between neurotrauma and MS will potentially assist in the development of effective treatments for both of these disorders.

The second aim of the thesis was to establish the framework & commence initial experiments investigating shared mechanisms of oxidative damage to oligodendroglia in models of MS & neurotrauma. Initially, it was intended that this thesis would use the cuprizone model of demyelinating disease to answer a series of research questions regarding the effects of oxidative DNA damage on the oligodendrocyte cell cycle, as part of a larger collaborative study. To address these questions as the second aim of the thesis, a large-scale experiment utilising cuprizone was designed and performed. However, upon both behavioural and tissue analysis, it was evident that the administered cuprizone wasn't effective at inducing demyelinating pathology. Therefore, a subsequent study was performed to directly compare powdered and pelleted cuprizone feed formulations to determine the optimal delivery technique for effective cuprizone toxicity. In this comparison, a 0.2% cuprizone model was employed at an early 3 week timepoint, with the cuprizone fed to mice in either a powdered or pelleted form, with appropriate control groups for both feed formulations. Comprehensive analysis of the tissue revealed that the cuprizone pellets were a more effective method of inducing the desired demyelinating disease pathology than cuprizone powder. Interestingly, the formulation of the control feed was also shown to influence oligodendroglial dynamics, with a reduction in oligodendroglial density in mice fed powdered control feed compared to those fed pelleted control feed. These findings, presented as a published paper, highlight the necessity for researchers to utilise appropriate feed formulations for mice fed both cuprizone and control feed, and will inform future research to allow for more optimal study designs when assessing cuprizone-induced toxicity. Due to the time constraints of this degree and the large scale, collaborative nature of the project as a whole, it was no longer feasible for this aspect of my research to form a substantial part of the thesis, so my contribution to the wider study is described.

Oxidative stress has also been associated with dysfunction of the blood-brain barrier (BBB) in a variety of injuries and diseases. Perivascular OPCs have emerged as having a key role in modulating BBB integrity, however the potential influence of oxidative damage to OPCs to this oligovascular niche is currently unknown. Similar to OPCs, pericytes are also particularly susceptible to oxidative damage. The third aim of this thesis was to determine whether oxidative DNA damage to perivascular OPCs and pericytes at the BBB are associated with increased BBB permeability in models of both MS and neurotrauma. The partial optic nerve model of neurotrauma was employed to assess the relationship between oxidative stress, BBB dysfunction and cellular proliferation at 1 day post-injury. The level of observed BBB dysfunction increased with injury with a strong significant correlation to the degree of cellular DNA damage. Specifically, there was an increase in the level of DNA damage within both neural/glial antigen 2 (NG2)+ glia in optic nerve vulnerable to secondary

degeneration, a cellular population comprised primarily of OPCs and pericytes. Similarly, there was an increase in the level of DNA damage within platelet-derived growth factor receptor α (PDGFR α) glia, a population comprised primarily of OPCs. Altogether, this indicated a particular vulnerability of OPCs to oxidative DNA damage. The density of newly derived and proliferating cells with DNA damage also significantly increased with injury, with PDGFR α ⁺ OPCs identified as the major proliferating, DNA damaged cell type at 1 day post-injury. These results provide insights into oxidative damage mechanisms within the optic nerve at an acute timepoint following neurotrauma and further highlighted oxidative stress as a worthy target for future investigations. A parallel study investigated the extent of oxidative stress to perivascular OPCs and pericytes at the BBB in the cuprizone model of demyelinating disease, at early timepoints where the BBB has been previously shown to be dysfunctional. COVID-19 associated laboratory shutdowns led to delays in tissue analysis throughout the PhD program and therefore discussion of this work is confined to experimental design.

The thesis closes with a discussion of the outcomes presented within the context of the wider literature and directions for future research into the commonalities in damage mechanisms between MS and neurotrauma.

Acknowledgements

The creation of a thesis is never due exclusively to the efforts of just one individual and this thesis is no exception to that rule. Consequently, there are numerous people I would like to thank and acknowledge who have greatly contributed to this academic journey.

First and foremost, I would like to thank my primary supervisor Prof. Melinda (Lindy) Fitzgerald. Your advice and wealth of knowledge has helped me immensely to navigate my research and produce a final thesis that I am proud to submit. When we first met in your old office in Curnow to discuss upcoming Honours projects in mid-2016, who would've thought we'd be here just over six years later. It's not been a smooth road to get to this point but I am honestly so grateful for your support and patience throughout this journey. It has been amazing to have had such a strong female role model during my time in academia and I feel privileged to have had this opportunity to learn, grow and work under your guidance.

I would also like to thank my secondary supervisor A/Prof. Ryu Takechi for providing editorial assistance with the thesis, as well as the entire Fitzgerald laboratory, both past and present. Every one of you has helped me along this journey in your own special way and you have all become my lab family over these past few years. In particular, I would like to acknowledge Dr. Chidozie (Dozie) Anyaegbu, Melissa (Mel) Papini, Carole Bartlett, Dr. Sarah Hellewell, Dr. Brittney Lins, Terence (Terry) McGonigle, Andrew Warnock, Alexander (Alex) Wright, and Eleanor (Ellie) Denham. However, I would especially like to express my deepest gratitude to Dozie for essentially becoming an honorary supervisor towards the end of this degree. Your resolute belief that this PhD would and could be done infinitely helped spur me on and I'm so grateful for everything you have done to help make this completed thesis a reality.

I would like to acknowledge MS Research Australia and the Perron Institute for Neurological and Translational Science for providing personal scholarship funding throughout this degree in the form of the MS Research Australia Postgraduate Scholarship and the Byron Kakulas Prestige Top-Up Scholarship respectively. Thank you to the Australian Government for supporting me through an Australian Government Research Training Program Fee Offset Scholarship.

A huge thank you to Curtin University for providing me with this PhD opportunity. Additionally, I would like to express my gratitude to Sandy Goodin and the UWA Animal Care team who have assisted with each of my various projects and who have all been so accommodating and understanding.

I could not have completed this journey without Aleksandra (Ola) Gozt, who has been my main companion and postgraduate partner in crime throughout this entire doctoral degree. We have shared in each other's successes and failures, and supported each other through the anxiety and imposter syndrome that comes hand-in-hand with the graduate school journey. It has been so

comforting to know that I can always lean on you and know that you fully understand my experiences traversing the world of academia and scientific research. You are such an intelligent and kind person that I am so proud and lucky to call my best friend. Your unconditional support has been worth more than words can actually express.

Thank you to all of my friends outside of the Fitzgerald group who have remained encouraging and reassuring over the last four and a half years, especially Briarna Popis who has been a key emotional support throughout this degree. To the online scientific community that I have become a part of during my PhD, thank you for your encouraging and kind words that never failed to give me the motivation and strength I needed to push through. I would also like to shout out all of my extended family in England, but in particular Charlotte Davey. Additionally, thank you to the Driver family who have welcomed me into their lives and whose family dinners have provided a welcomed distraction from the thesis through the combined efforts of Sahara and Ari.

I would also like to express gratitude to my father, Steve Toomey. Though you are over in Brisbane and we have not been able to see each other as often as we may have liked in the past few years, I am always grateful for your support. To my little brother, Alex Gledstone, I hope this PhD thesis will inspire you to follow your passions and let your inner nerd shine brighter than a diamond in Minecraft.

A huge thank you goes to my stepdad, David Letts, who has been an enormous help to me throughout this degree. Your intelligence and enthusiasm for knowledge constantly inspire me and I always learn something new and interesting when I talk to you. I'm so grateful that I have you in my life and I know that you'll be there for me no matter what.

To my mum, Victoria Davey, I honestly do not think I would be where I am today without your unwavering belief in my ability to succeed. You have always instilled in me the value of education and now I've reached the pinnacle of academic qualifications. Our coffee dates, Wednesday walks at Yanchep and Lake Monger, summer swims and trips to the theatre are memories I'll always cherish. Thank you for supporting me in everything I do and I am beyond grateful to call you my mum.

Finally, I would like to thank my wonderful partner, Oliver Driver. Oliver, are my absolute favourite person in the whole world and I cannot imagine finishing this huge part of my life without you. I will never be able to thank you enough for everything you have done to help me get this PhD done. You accept me as I am without any limitations and you make me feel so loved and seen in a way that I've never experienced before. You always listen to me talk about my research and even though you spell oligodendrocyte as olagdengicyte or oligendicyte, I know that you would help me with this thesis at the drop of a hat if you could. Your endless understanding, love and patience

throughout this PhD journey has been astonishing; you are my rock. I love you so much and I cannot wait to see what life has in store for us as we move now towards the next chapter in our story together.

*You have experienced becoming,
learned a lot more about what's inside you,
and you have made your soul grow.*

– Kurt Vonnegut Jr.

Copyright Statement

I have obtained permission from the copyright owners to use any third-party copyright material reproduced in the thesis (e.g. questionnaires, artwork, unpublished letters), or to use any of my own published work (e.g. journal articles) in which the copyright is held by another party (e.g. publisher, co-author). Further information regarding the obtained permissions to use third party copyright material can be found in Appendix D.

Attribution of Research Outputs

Warnock, A.*, **Toomey L.M.***, Wright, A.J., Fisher, K., Won, Y., Anyaegbu, C., and Fitzgerald, M. 2020. Damage mechanisms to oligodendrocytes and white matter in central nervous system injury: The Australian context. *Journal of Neurotrauma* 37, 739-769. doi.org/10.1089/neu.2019.6890

* *Equal contribution*

Location in thesis: Chapter 1, Section 1.3

Author	Signature	Conception & Design	Interpretation & Discussion	Creation of Figures & Tables	Final Editorial Changes	Total % Contribution
Toomey, L.M.	X	3	25	10	4.5	42.5
Warnock, A.		7.5	25		10	42.5
Wright, A.J.			5			5
Fisher, K.						
Won, Y.						
Anyaegbu, C.					3	
Fitzgerald, M.			2			3

Toomey L.M., Papini, M., Lins, B., Wright, A.J., Warnock, A., McGonigle, T., Bartlett, C.A., Hellewell, S.C., Anyaegbu, C., and Fitzgerald, M. 2021. Cuprizone feed formulation influences the extent of demyelinating disease pathology. *Scientific Reports*, 11(1), 1-16. doi.org/10.1038/s41598-021-01963-3

Location in thesis: Chapter 4, Section 4.5

Author	Signature	Conception & Design	Acquisition of Data	Data Analysis	Creation of Figures & Tables	Interpretation & Discussion	Final Editorial Changes	Total % Contribution	
Toomey, L.M.	X	5	25	13	10	15	5	73	
Papini, M.			5					5	
Lins, B.			4					4	
Wright, A.J.			5					5	
Warnock, A.									
McGonigle, T.									
Bartlett, C.A.									
Hellewell, S.C.									
Anyaegbu, C.					4		2	1	7
Fitzgerald, M.			2				3	1	6

Toomey L.M., Bartlett C.A., Gavriel N., Majimbi M., Gopalasingam G., Rodger J., Fitzgerald M. 2019. Comparison of ion channel inhibitor combinations for limiting secondary degeneration following partial optic nerve transection. *Scientific Reports* 9: 1-10. doi.org/10.1038/s41598-019-51886-3

Location in thesis: Appendix A.

Author	Signature	Conception & Design	Acquisition of Data	Data Analysis	Creation of Figures & Tables	Interpretation & Discussion	Final Editorial Changes	Total % Contribution
Toomey, L.M.	X	4	24	10	10	15	5	68
Bartlett, C.A.			10					10
Gavriel, N.			3					3
McGonigle, T.			2	1				3
Majimbi, M.			2					2
Gopalasingam, G.								
Rodger, J.						3		3
Fitzgerald, M.			6				3	2

Gopalsingam G., Bartlett C.A., McGonigle T., Majimbi M., Warnock A., Ford A., Gough A., **Toomey L.M.**, Fitzgerald M. 2019. The effects of a combination of ion channel inhibitors on pathology in a model of demyelinating disease. *Multiple Sclerosis and Related Disorders* 34: 1-8. doi.org/10.1016/j.msard.2019.06.005

Location in thesis: Appendix B.

Author	Signature	Conception & Design	Acquisition of Data	Data Analysis	Creation of Figures & Tables	Interpretation & Discussion	Final Editorial Changes	Total % Contribution	
Gopalasingam, G.			8	7	2	3		20	
Bartlett, C.A.		5	7					12	
McGonigle, T.			7	5	3		2	17	
Majimbi, M.			3	5	2			10	
Warnock, A.					2		2	4	
Ford, A.			1	1				2	
Gough, A.			1					1	
Toomey, L.M.					2	13	2	17	
Fitzgerald, M.			8				5	4	17

Publications, Conference Presentations & Awards

Primary Publications Included in Thesis Body

Warnock A. *, **Toomey L.M.***, Wright A.J., Fisher K., Won Y., Anyaegbu C., Fitzgerald M. 2020. Damage mechanisms to oligodendrocytes and white matter in central nervous system injury: The Australian context. *Journal of Neurotrauma* 37(5): 739-769. doi.org/10.1089/neu.2019.6890
**equal contribution*

Toomey L.M., Papini, M., Lins, B., Wright, A.J., Warnock, A., McGonigle, T., Bartlett, C.A., Hellewell, S.C., Anyaegbu, C., and Fitzgerald, M. 2021. Cuprizone feed formulation influences the extent of demyelinating disease pathology. *Scientific Reports*, 11(1), 1-16. doi.org/10.1038/s41598-021-01963-3

Secondary Publications Included in Appendices

Toomey L.M., Bartlett C.A., Gavriel N., McGonigle, T., Majimbi M., Gopalasingam G., Rodger J., Fitzgerald M. 2019. Comparing modes of delivery of a combination of ion channel inhibitors for limiting secondary degeneration following partial optic nerve transection. *Scientific Reports* 9: 1-10. doi.org/10.1038/s41598-019-51886-3

Gopalasingam G., Bartlett C.A., McGonigle T., Majimbi M., Warnock A., Ford A., Gough A., **Toomey L.M.**, Fitzgerald M. 2019. The effects of a combination of ion channel inhibitors on pathology in a model of demyelinating disease. *Multiple Sclerosis and Related Disorders* 34: 1-8. doi.org/10.1016/j.msard.2019.06.005

Toomey L.M., Papini, M.G., Clarke, T.O., Wright, A.J., Denham, E., Warnock, A., McGonigle, T., Fitzgerald M., Anyaegbu, C. 2023. Secondary degeneration of oligodendrocyte precursor cells occurs as early as 24 hours after optic nerve injury in rats. *International Journal of Molecular Sciences* 24(4): 3463. doi.org/10.3390/ijms24043463

Additional Publications Not Included in Thesis

Naidu, P.S.R.*, Gavriel, N.*, Gray, C.G.G.*, Bartlett, C.A., **Toomey, L.M.**, Kretzmann, J.A., Patalwala, D., McGonigle, T., Denham, E., Hee, C., Ho, D., Taylor, N.L., Norret, M., Smith, N., Dunlop, S.A., Iyer, K.S., & Fitzgerald, M., 2019. Elucidating the inability of functionalized nanoparticles to cross the blood brain barrier and target specific cells *in vivo*. *ACS Applied Materials and Interfaces* 11(25): 22085-22095. doi.org/10.1021/acsami.9b01356

**equal contribution*

Toomey, L.M., Bartlett, C.A., Majimbi, M., Gopalasingam, G., Rodger, J., & Fitzgerald, M., 2019. Comparison of ion channel inhibitor combinations for limiting secondary degeneration following partial optic nerve transection. *Experimental Brain Research*, 237: 161-171. doi.org/10.1007/s00221-018-5414-0

Giacci M.K., Bartlett C.A., Smith N.M., Iyer K.S., **Toomey L.M.**, Jiang H., Guagliaro P., Kilburn M.R., Fitzgerald M. 2018. Oligodendroglia are particularly vulnerable to oxidative damage after neurotrauma *in vivo*. *Journal of Neuroscience* 38(29): 6491-6504. doi.org/10.1523/JNEUROSCI.1898-17.2018

Conference Presentations

International

Toomey, L.M.*, Anyaegbu, C.*, Clarke, T.O., Papini, M., Wright, A.J., Denham, E., Warnock, A., Lins, B., McGonigle, T., Bartlett, C.A., & Fitzgerald M., 2020. Investigating the Role of Oxidative DNA Damage to NG2+ Cells in BBB Dysfunction Following a Partial Optic Nerve Transection. *Cold Spring Harbour Laboratory Glia in Health and Disease*. Poster presentation.

**equal contribution*

National

Toomey, L.M.*, Warnock, A.*, Anyaegbu, C.*, Clarke, T.O., Denham, E., Bartlett, C.A., & Fitzgerald M., 2019. Investigating the Role of Oxidative DNA Damage to NG2+ Cells in BBB Dysfunction Following a Partial Optic Nerve Transection. *Australian Neurotrauma Workshop*. Poster presentation. **equal contribution*

Local

Toomey, L.M., Papini, M., Lins, B., Wright, A.J., Warnock, A., McGonigle, T., Bartlett, C.A., Anyaegbu, C., & Fitzgerald, M., 2021. Powdered vs Pelleted: The Ultimate Cuprizone Showdown. *Australian Medical Research Society Medical Research Week WA Symposium*. Oral presentation.

Toomey, L.M., Papini, M., Lins, B., Wright, A.J., Warnock, A., McGonigle, T., Bartlett, C.A., Anyaegbu, C., & Fitzgerald, M., 2020. Powdered vs Pelleted: The Ultimate Cuprizone Showdown. *Perron Institute Symposium*. Oral presentation.

Toomey, L.M., Papini, M., Wright, A.J., Lins, B., Warnock, A., McGonigle, T., Bartlett, C., Fitzgerald, M., 2020. The importance of cuprizone feed formulation on inducing demyelinating disease pathology. *Symposium of Western Australian Neuroscience*. Poster presentation.

Toomey, L.M.*, Anyaegbu, C.*, Clarke, T.O., Denham, E., Warnock, A., Bartlett, C.A., & Fitzgerald M., 2019. Investigating the Role of Oxidative DNA Damage to NG2+ Cells in BBB Dysfunction Following a Partial Optic Nerve Transection. *Symposium of Western Australian Neuroscience*. Oral presentation. **equal contribution*

Toomey, L.M., Warnock, A., Denham, E., McGonigle, T., & Fitzgerald, M., 2019. The role of oxidative DNA damage to oligodendroglia in demyelinating disease. *Perron Institute Student Seminar Series*. Oral presentation.

Toomey, L.M., Takechi, R., & Fitzgerald, M., 2019. The role of DNA damage to oligodendroglia in demyelination. *Perron Institute Symposium*. Invited oral presentation.

Awards and Scholarships

iPREP Biodesign, 2021: *iPREP Biodesign Placement Scholarship*

Perron Institute Symposium, 2020: *First Prize People's Choice Award (Scientific Talk)*

Multiple Sclerosis Research Australia, 2019: *MS Research Australia Postgraduate Scholarship*

Perron Institute for Neurological and Translational Science, 2018: *Byron Kakulas Prestige Top-Up Scholarship*

Australian Government Research Training Program, 2018: *Fee Offset Scholarship*

Table of Contents

Declaration	1
Abstract	2
Acknowledgements	5
Copyright Statement	8
Attribution of Research Outputs	9
Publications, Conference Presentations & Awards	13
Table of Contents	16
Abbreviations	21
List of Thesis Figures	24
Chapter 1. Literature Review	27
<i>1.1. Introduction</i>	27
<i>1.2. Multiple Sclerosis</i>	27
1.2.1. Prevalence, Diagnosis and Symptomology	27
1.2.2. Disease Subtypes	30
1.2.3. Genetic & Environmental Risk Factors	31
1.2.4. Demyelination as a Hallmark of MS	32
1.2.4.1. Oligodendroglia and Myelin	32
1.2.4.2. Demyelinated Plaques	37
1.2.4.3. Normal Appearing White Matter	39
1.2.4.4. Remyelination and Shadow Plaques	39
1.2.5. Human MS Pathophysiology	39
1.2.5.1. “Outside-In” Hypothesis	39
1.2.5.2. “Inside-Out” Hypothesis	41
1.2.6. Current Therapeutic Strategies for MS.....	41
1.2.7. The Cuprizone Model of Demyelinating Disease.....	42
1.2.7.1. Mechanism of Cuprizone Toxicity	42
1.2.7.2. Cuprizone Pathophysiology Within the Corpus Callosum	43
1.2.7.3. Pathophysiology in Other Brain Regions.....	46
1.2.7.4. Behavioural Changes in the Cuprizone Model	46
1.2.7.5. Limitations of the Cuprizone Model.....	47
<i>1.3. Neurotrauma</i>	48
1.3.1. Introducing “Damage mechanisms to oligodendrocytes and white matter in central nervous system injury: The Australian context”	48
1.3.2. Partial Optic Nerve Transection Model.....	80
<i>1.4. Common Mechanisms of Damage In MS and Neurotrauma</i>	81
1.4.1. Overview of Common Mechanisms	81

1.4.2. Oxidative Burst	81
1.4.3. Glutamate Excitotoxicity and Changes in Ca ²⁺ Dynamics	82
1.4.4. Mitochondrial Dysfunction.....	84
1.4.5. Oxidative Stress	84
1.4.6. Oxidative DNA Damage.....	85
1.4.6.1. Nucleobase Modifications and Base Excision Repair	86
1.4.6.2. Single- and Double-Strand DNA Breaks and Repair.....	89
1.4.6.3. Oligodendroglial Susceptibility to Oxidative DNA Damage	90
1.5. Concluding Remarks.....	90
Introduction to Series One.....	93
Chapter 2. Generalisability of a Combinatorial Ion Channel Inhibitor Treatment for Neurotrauma and Demyelinating Disease	94
2.1. Delivery of a Combinatorial Ion Channel Inhibitor Treatment	94
2.2. Comparing Local and Systemic Delivery of a Combinatorial Ion Channel Inhibitor Treatment for Limiting Peripheral Cytokines and Chemokines Following Neurotrauma.....	96
2.2.1. Data Obtained Prior to Candidature.....	96
2.2.2. Rationale for Luminex Analysis	96
2.2.3. Study Design and Procedures	97
2.2.3.1. Experimental Groups and Treatment Delivery Strategy.....	97
2.2.3.2. Priming Osmotic Mini-Pumps	99
2.2.3.3. Surgical Procedures.....	99
2.2.3.4. Collection of Blood Samples	100
2.2.3.5. Luminex Assay	101
2.2.4. Effect of the Combinatorial Treatment on Plasma Cytokine and Chemokine Concentrations	103
2.2.5. Study Conclusions	104
2.3. Utilising the Combinatorial Ion Channel Inhibitor Treatment in Demyelinating Disease.....	105
2.4. Concluding Remarks.....	106
Introduction to Series Two	107
Chapter 3. Commencing Initial Experiments into Common Mechanisms of Oxidative Damage to Oligodendroglia	108
3.1. Initial Cohort Rationale.....	108
3.2. Initial Cuprizone Cohort.....	109
3.2.1. Study Design and Animal Procedures	109
3.2.2. Animal Weights.....	111
3.2.3. Behavioural Assessments	113
3.2.3.1. Rotarod Test.....	113
3.2.3.2. Open Field Test.....	116
3.2.3.3. Optokinetic Nystagmus Test.....	118

3.2.4. Histological Tissue Analysis	119
3.2.4.1. Luxol Fast Blue	120
3.2.4.2. Myelin Black-Gold II.....	121
3.2.5. Issues Regarding Efficacy of Cuprizone Pellets.....	122
3.3. <i>Optimisation of Freezing Protocols</i>	123
3.3.1. Rationale	123
3.3.2. Confirming Freezing Issues	123
3.3.3. Optimising Freezing Duration	125
3.3.3.1. Impact of Freezing Duration on Tissue Quality.....	126
3.3.3.2. Impact of Freezing Duration on Tissue Antigenicity.....	127
3.4. <i>Concluding Remarks</i>	130
Chapter 4. Characterisation and Optimisation of the Cuprizone Model of Demyelinating Disease.....	131
4.1. <i>Study Rationale</i>	131
4.2. <i>Study Design and Animal Procedures</i>	132
4.3. <i>Optimisation of Immunohistochemistry</i>	133
4.4. <i>Study Outcomes</i>	135
4.5. <i>Introducing “Cuprizone feed formulation influences the extent of demyelinating disease pathology”</i>	136
4.6. <i>Concluding Remarks and Continuing Experimental Work</i>	153
4.6.1. Additional Contributions to Ongoing Experimental Work.....	153
Introduction to Series Three	154
Chapter 5. Review of the Blood-Brain Barrier in Health and Disease.....	155
5.1. <i>The Blood-Brain Barrier</i>	155
5.1.1. Structure of the Cerebrovasculature	155
5.1.2. Cells at the Blood-Brain Barrier	156
5.1.2.1. Endothelial Cells	156
5.1.2.2. Astrocytes and Neurons	157
5.1.2.3. Pericytes	157
5.1.2.4. OPCs	158
5.2. <i>Blood-Brain Barrier Dysfunction</i>	159
5.2.1. BBB Dysfunction in MS.....	160
5.2.2. BBB Dysfunction in Neurotrauma	162
5.3. <i>The Blood-Brain Barrier and Oxidative Stress</i>	164
5.4. <i>Concluding Remarks</i>	165
Chapter 6. Investigating Oxidative Stress in NG2+ Glia in Blood-Brain Barrier Dysfunction Following Neurotrauma.....	166
6.1. <i>Tissue Analysis Pipeline Development</i>	166

6.1.1. Rationale and Design of Immunohistochemical Analyses	166
6.1.2. Initial ImageJ Analysis Pipeline	169
6.2. <i>Study Design and Animal Procedures</i>	171
6.3. <i>Variability in Blood Vessel Location and Morphology in the Optic Nerve</i>	172
6.4. <i>Optimisation of Immunohistochemistry Protocols</i>	175
6.5. <i>Analysing Immunohistochemical Outcomes</i>	177
6.6. <i>Investigating the Relationship Between Oxidative Stress, BBB Dysfunction and Cellular Proliferation in Neurotrauma</i>	179
6.6.1. Effect of Injury on the Level of Oxidative DNA Damage	179
6.6.2. Effect of Injury on BBB Integrity	181
6.6.3. Effect of Injury on Cellular Proliferation	182
6.7. <i>Concluding Remarks</i>	184
Chapter 7. Investigating Oxidative Stress in NG2+ Glia in Blood-Brain Barrier Dysfunction in Demyelinating Disease	185
7.1. <i>Study Design and Animal Procedures</i>	185
7.2. <i>Animal Weights</i>	187
7.3. <i>Plans for Remaining Experimental Work</i>	190
7.3.1. Initial Optimisation of Immunohistochemical Tissue Analysis	190
7.3.2. GeoMx Spatial Proteomic Analysis.....	191
7.4. <i>Concluding Remarks</i>	194
Chapter 8. General Discussion and Final Remarks	195
8.1. <i>Translating Knowledge of Common Damage Mechanisms</i>	195
8.2. <i>Implications for Increased Efficacy of Cuprizone-Containing Pellets</i>	196
8.2.1. Potential Variations Between the Two Suppliers of Cuprizone-Containing Pellets	196
8.2.2. Implications of Increased Efficacy of a Pelleted Cuprizone Feed Formulation for the Cuprizone Literature and Future Studies	198
8.2.2.1. Importance of Control Feed Formulation	198
8.2.2.2. Importance of Cuprizone-Containing Feed Formulation.....	200
8.3. <i>Oxidative DNA Damage and the Blood-Brain Barrier in MS and Neurotrauma</i>	201
8.3.1. Relationship Between Oxidative Stress and Blood-Brain Barrier Dysfunction	201
8.3.2. Cell Specific Oxidative DNA Damage	202
8.3.3. Relationship Between Oxidative Stress and Cell Proliferation	204
8.4. <i>Pathological Differences Between MS and Neurotrauma</i>	207
8.5. <i>Potential Therapeutic Strategies</i>	210
8.5.1. Combinatorial Ion Channel Inhibitor Treatment	210
8.5.2. Anti-Oxidant Therapies	211

8.5.2.1. Metformin	212
8.5.3. Important Considerations for Developments of Therapeutics	212
8.6. <i>Broader Clinical Applicability and Translatability</i>	213
8.6.1. Cuprizone Model of Demyelinating Disease Compared to Human MS Pathology	214
8.6.2. Partial Optic Nerve Transection Compared to Human Neurotrauma.....	216
8.7. <i>Final Concluding Remarks</i>	217
References	219
Appendix A. Introducing “Comparing modes of delivery of a combination of ion channel inhibitors for limiting secondary degeneration following partial optic nerve transection”	276
Appendix B. Introducing “The effects of a combination of ion channel inhibitors on pathology in a model of demyelinating disease”	287
Appendix C. Introducing “Secondary degeneration of oligodendrocyte precursor cells occurs as early as 24 hours after optic nerve injury in rats”	296
Appendix D. Detailed Copyright Statements.....	312

Abbreviations

3-NT	3-Nitrotyrosine
53BP1	p53-binding protein 1
8OHDG	8-Hydroxy-2-deoxyguanosine
8-OxoG	8-Oxoguanine
AKT	Protein kinase B
AMPA	α -amino-3-hydroxy-5-methyl-4-isoxazolepropionic acid
APE1	Apurinic/apyrimidinic endonuclease-1
APP	Amyloid precursor protein
ASPA	Aspartoacylase
ATM	Ataxia-telangiectasia mutated serine/threonine kinase
ATP	Adenosine triphosphate
BBB	Blood-brain barrier
BBG	Brilliant Blue G
BSA	Bovine serum albumin
Ca ²⁺	Calcium ion
Caspr	Contactin-associated protein
CC1	Adenomatous polyposis coli
CNPase	2',3'-Cyclic nucleotide-3'-phosphodiesterase
CNS	Central nervous system
Cuprizone	N,N'-Bis(cyclohexylideneamino)oxamide
CXCL1	Chemokine (C-X-C motif) ligand 1
DNA	Deoxyribonucleic acid
DPX	Dibutylphthalate polystyrene xyelene
DSP	Digital spatial profiling
EAE	Experimental autoimmune encephalomyelitis
EdU	5'Ethynyl-2-deoxyuridine
ELISA	Enzyme-linked immunosorbent assay
ERK	Extracellular signal-regulated kinase
G-CSF	Granulocyte-colony stimulating factor
Gd	Gadolinium
GM-CSF	Granulocyte-macrophage colony-stimulating factor
Gro- α	Growth-regulated oncogene α
HNE	4-Hydroxynonenal
ICH	Ion channel inhibitor combinatorial treatment

IgG	Immunoglobulin G
IFN γ	Interferon gamma
IL	Interleukin
IP-10	Interferon gamma-induced protein 10
MAG	Myelin-associated glycoprotein
MAPK	Mitogen-activated protein kinase
MBP	Myelin basic protein
MCP	Monocyte chemoattractant protein
MEK	Mitogen-activated protein kinase
MHC	Major histocompatibility complex
MIP	Macrophage inflammatory protein
MnSOD	Manganese superoxide dismutase
MOG	Myelin oligodendrocyte glycoprotein
MRI	Magnetic resonance imaging
MS	Multiple sclerosis
mTOR	Mammalian target of rapamycin
Na ⁺	Sodium ion
NADPH	Nicotinamide adenine dinucleotide phosphate hydrogen
NF-L	Neurofilament light
NG2	Neural/glial antigen 2
NHMRC	National Health and Medical Research Council of Australia
NMDA	N-methyl-D-aspartate
NSE	Neuron-specific enolase
OCT	Optimal temperature compound
OGG1	8-Oxoguanine glycosylase
Olig2	Oligodendrocyte transcription factor 2
OPC	Oligodendrocyte precursor cell
PBS	Phosphate buffered solution
PDGFR α	Platelet-derived growth factor receptor α
PDGFR β	Platelet-derived growth factor receptor β
PI3K	Phosphatidylinositol 3-kinase
PLP	Proteolipid protein
Pol β	DNA polymerase β
PPMS	Primary progressive multiple sclerosis
RANTES	Regulated on activation normal T cell expressed and secreted

RECA	Rat endothelial cell antigen-1
RNA	Ribonucleic acid
RNS	Reactive nitrogen species
ROS	Reactive oxygen species
RPMS	Relapsing-progressive multiple sclerosis
RRMS	Relapse-remitting multiple sclerosis
S100b	S100 calcium-binding protein B
SAPE	Streptavidin-phycoerythrin
SOX10	SRY-related HMG-box 10
SPMS	Secondary progressive multiple sclerosis
TBI	Traumatic brain injury
TMEV	Theiler's murine encephalomyelitis virus
TNF α	Tumour necrosis factor α
UV	Ultraviolet
VGCC	Voltage-gated Ca ²⁺ channel
VGluT1	Vesicular glutamate transporter 1
XRCC1	X-ray cross-complementing protein-1
ZO-1	Zonula occludens 1

List of Thesis Figures

Chapter 1. Literature Review

Figure 1.1. Common symptoms of MS.....	29
Figure 1.2. Disease progression of the four different subtypes of MS.	30
Figure 1.3. The oligodendroglial lineage.	33
Figure 1.4. Structure of the myelin sheath.	34
Figure 1.5. Demyelination in MS.....	37
Figure 1.6. Four main types of early human MS lesions.	38
Figure 1.7. Peripheral immune cell-mediated damage to oligodendrocytes and myelin.	40
Figure 1.8. Comparison of behavioural and functional symptomology in MS and in the cuprizone model of demyelinating disease.	47
Figure 1.9. Schematic of a partial optic nerve transection.	81
Figure 1.10. Relevant forms of oxidative DNA damage.	86
Figure 1.11. Mechanism of base excision repair to remove 8OHdG and 8-oxoG from DNA for maintaining genomic integrity.....	88
Figure 1.12. Flow diagram of the forthcoming thesis structure.....	92

Chapter 2. Generalisability of a Combinatorial Ion Channel Inhibitor Treatment for Neurotrauma and Demyelinating Disease

Figure 2.1. Experimental groups for the additional combinatorial ion channel inhibitor treatment cohort.	98
Figure 2.2. Ion channel inhibitor treatment strategy.	99
Figure 2.3. Experimental design for the additional combinatorial ion channel inhibitor treatment cohort.	101
Figure 2.4. Luminex assay protocol for use on rat plasma samples.	102
Figure 2.5. Effect of injury and combinatorial ion channel inhibitor treatment on the plasma concentration of cytokine and chemokine analytes.	104
Figure 2.6. Effect of combinatorial ion channel inhibitor treatment on myelin outcomes. .	106

Chapter 3. Commencing Initial Experiments into Common Mechanisms of Oxidative Damage to Oligodendroglia

Figure 3.1. The effect of oxidative DNA damage to oligodendroglia in models of neurotrauma and Alzheimer's disease.....	109
Figure 3.2. Experimental design for the initial cuprizone cohort.	111
Figure 3.3. Effect of cuprizone on animal weights.	112
Figure 3.4. Schematic of behavioural tests performed.....	113

Figure 3.5. Effects of cuprizone administration on Rotarod test outcomes.....	114
Figure 3.6. Effects of cuprizone administration on Rotarod test outcomes with a revised protocol.	116
Figure 3.7. Effects of cuprizone administration on open field test outcomes.....	118
Figure 3.8. Histological assessments of myelin quality comparing 3 week control and cuprizone tissue using a Luxol Fast Blue stain.	120
Figure 3.9. Histological assessments of myelin quality comparing 3 week control and cuprizone tissue using a Myelin Black-Gold II Stain.	122
Figure 3.10. Freezing apparatus.	124
Figure 3.11. Comparison of different freezing times in a bath of isopentane.....	125
Figure 3.12. Comparison of different freezing times on tissue quality.....	127
Figure 3.13. Comparison of different freezing methods on antigenicity.....	129

Chapter 4. Characterisation and Optimisation of the Cuprizone Model of Demyelinating Disease

Figure 4.1. Expected demyelinating disease pathology within the corpus callosum following 3 weeks of cuprizone intoxication.	132
Figure 4.2. Experimental design for the direct comparison between powdered and pelleted cuprizone formulations.	133
Figure 4.3. The modified immunohistochemistry protocol for use on mouse brain tissue sections.....	134

Chapter 5. Review of the Blood-Brain Barrier in Health and Disease

Figure 5.1. Structure and cellular components of the cerebrovasculature.....	156
Figure 5.2. Summary of differences between disruptive and non-disruptive changes to the BBB.....	160

Chapter 6. Investigating Oxidative Stress in NG2+ Glia in Blood-Brain Barrier Dysfunction Following Neurotrauma

Figure 6.1. The detection of four fluorescent wavelengths by confocal laser scanning microscopy.....	167
Figure 6.2. Immunohistochemical panels designed to assess the role of oxidative damaged OPCs and pericytes at the BBB following neurotrauma.....	168
Figure 6.3. ImageJ analysis pipeline developed to investigate the role of oxidative damaged OPCs and pericytes in BBB dysfunction following neurotrauma.	170
Figure 6.4. Experimental design for cohort investigating BBB dysfunction following a partial optic nerve transection.	172

Figure 6.5. Representative images demonstrating the variability in blood vessel location and morphology across adjacent transverse sections of the optic nerve.....	173
Figure 6.6. Modified immunohistochemistry protocol for use on rat optic nerve tissue sections.....	176
Figure 6.7. Effects of injury for oxidative DNA damage within the ventral nerve.	180
Figure 6.8. Effects of injury for BBB dysfunction and oxidative DNA damage within the ventral nerve.....	181
Figure 6.9. Effects of injury for cellular proliferation and oxidative DNA damage within the ventral nerve.....	183

Chapter 7. Investigating Oxidative Stress in NG2+ Glia in Blood-Brain Barrier Dysfunction in Demyelinating Disease

Figure 7.1. Experimental groups for cohort investigating oxidative stress and BBB dysfunction in the cuprizone model of demyelinating disease.	186
Figure 7.2. Experimental design for cohort investigating BBB dysfunction during cuprizone intoxication.....	187
Figure 7.3. Effects of cuprizone intoxication and quantity of feed consumption on animal weights.	189
Figure 7.4. Optimisation of the CD31 primary antibody on mouse brain tissue.	191
Figure 7.5. GeoMx spatial proteomics experimental workflow.	192
Figure 7.6. GeoMx panel designed to assess the role of oxidative damage to perivascular OPCs and pericytes during early cuprizone intoxication.....	192

Chapter 8. General Discussion and Final Remarks

Figure 8.1 Workflow of the generalised feed pelleting process.	197
Figure 8.2 Schematic of the approximate relative ratios of proliferating and non-proliferating oligodendroglial cells in the ventral nerve following a partial optic nerve transection.	205

Chapter 1. Literature Review

1.1. Introduction

MS is a chronic inflammatory demyelinating disease that has traditionally been considered to have a primarily autoimmune aetiology (Sospedra & Martin 2005). However, it is becoming increasingly understood that MS may rather originate with primary early degeneration of oligodendrocytes and myelin, in what has been dubbed the “inside-out” hypothesis (Titus et al. 2020). Neurotrauma is the damage caused by an external force acting upon the CNS for which there are currently no effective treatments available (Kobeissy 2015). Oxidative stress, or the damage caused by overwhelming levels of ROS (Birben et al. 2012), is a key feature of both MS lesions (Gilgun-Sherki et al. 2004) and neurotrauma (Cornelius et al. 2013). In particular, oxidative stress can cause damage to DNA, including hydroxylation of DNA nucleic acid bases (Arnett et al. 2005), single-stranded DNA breaks, and double-stranded DNA breaks (Woodbine et al. 2011). OPCs, the cells that possess the capacity to differentiate into myelinating oligodendrocytes, are particularly vulnerable to this DNA damage (Giacci *et al.*, 2018b). The work presented throughout this thesis aims to establish the relevant framework and commence the initial experiments for investigation into shared mechanisms of oxidative damage between these two conditions.

The following review chapter will be divided into three key components. Firstly, the literature surrounding MS prevalence, diagnosis, and symptomology will be examined, before exploring demyelination as a hallmark of MS and the varying schools of thought surrounding human MS pathophysiology. The relevant cuprizone model of demyelinating disease will be discussed to provide context for the forthcoming work introduced later in this thesis. Next, the literature surrounding neurotrauma will be reviewed, primarily presented as a co-first author review article published in the *Journal of Neurotrauma*. Common mechanisms of damage between MS and neurotrauma will then be explored with a strong emphasis on the mechanisms underlying oxidative stress, in particular oxidative DNA damage and the inherent susceptibility of OPCs to oxidative stress. Finally, concluding remarks and thesis aims will be presented along with a brief outline of the subsequent thesis chapters.

1.2. Multiple Sclerosis

1.2.1. Prevalence, Diagnosis and Symptomology

MS is a chronic inflammatory demyelinating disease of the CNS (Kutzelnigg et al. 2005). MS is the leading cause of non-traumatic neurological disability in young adults, with more than 2.5 million people living with the disease worldwide (Trapp & Nave 2008). The disease initially presents when a patient is either in their 20s or 30s, with approximately twice as many females developing the

disease than men (Noseworthy et al. 2000). Initial presentation often includes a broad range of symptoms, including reduced dexterity, sensory disturbances, optic neuritis, diplopia, fatigue, tremor and ataxia (Hauser & Oksenberg 2006; Rolak 2003), depending on lesion location (Brownlee et al. 2017). Based on the 2017 revisions of the McDonald criteria, people must present with multiple lesions in distinct anatomical locations and must develop new lesions over time in order to be diagnosed with MS (Thompson et al. 2018). Magnetic resonance imaging (MRI) is the gold standard diagnostic test performed for an MS diagnosis, with nearly all people with MS showing MRI abnormalities (Brownlee et al. 2017; Offenbacher et al. 1993). MRI can also be useful to exclude other disorders that show similar clinical presentation to MS (Filippi et al. 2016). Examination of cerebrospinal fluid and testing of neurophysiological visual evoked potentials can be used as diagnostic tools, however they are less specific and are instead often used in combination with MRI (Brownlee et al. 2017; McDonald et al. 2001). Following diagnosis, people with MS are commenced on immunomodulatory or immunosuppressant therapies but these treatments only slow disease progression rather than halt it completely (Lassmann et al. 2007). Within 15 years of disease onset, 50% of people with MS will need assistance with walking (Weinshenker et al. 1989), and 75% of people with MS will experience bladder dysfunction (Betts et al. 1993). However, since MS can affect any area of the CNS, overall MS symptomology is unpredictable and heterogeneous, and can differ greatly between people and even within one person over time (Ghasemi et al. 2017). The more common symptoms of MS are presented in Figure 1.1.

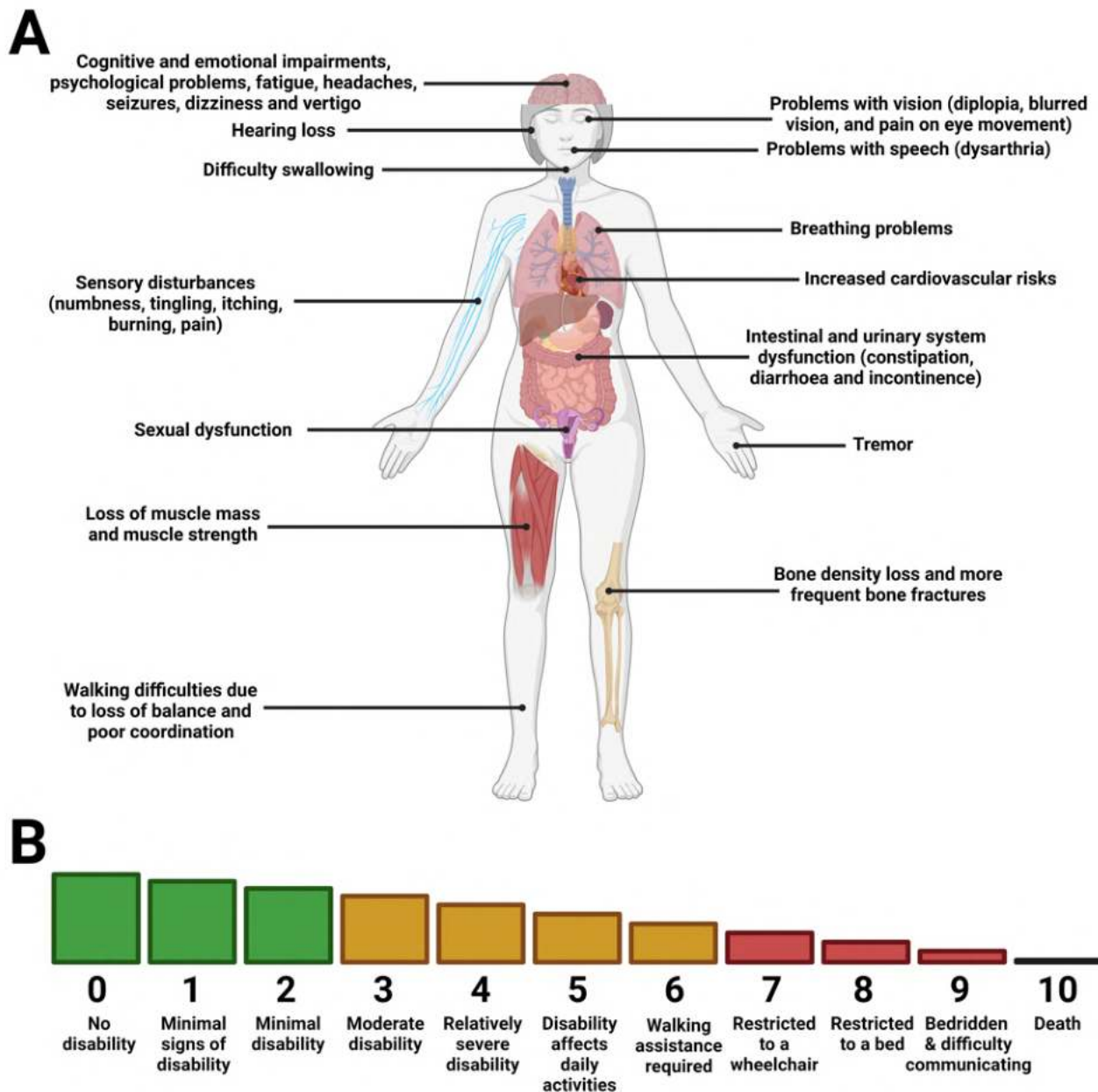


Figure 1.1. Common symptoms of MS. (A) MS can result in a wide array of symptoms that can contribute to the overall disease burden (Alusi et al. 2001; Cosman et al. 1998; Ghasemi et al. 2017; Wens et al. 2014). (B) The severity of MS symptoms can be measured using the Expanded Disability Status Scale, which quantifies the involvement and contribution of discrete neurological functional systems towards overall disability status, ultimately resulting in a score between 0 and 10 (Kurtzke 1983). Original illustration created using BioRender.com.

Quality of life is consistently reduced in people with MS compared with the general population (Amato et al. 2001; Benedict et al. 2005; McCabe & McKern 2002; Nortvedt et al. 1999). People with MS experience increased strain upon professional goals and ambitions, with less than 10% of people with severe MS able to maintain employment, and over 50% of people with MS having to either reduce the numbers of hours worked or change to less demanding careers, often resulting in substantial income loss (Kobelt et al. 2006). Additionally, mental health issues present more frequently in people with MS. People with MS have an approximately 50% lifetime incidence rate of

a major depressive disorder and a 36% lifetime incidence rate of anxiety, compared to 16.2% and 25% respectively for the general population (Chwastiak & Ehde 2007; Siegert 2005), and are significantly more likely to have a co-morbidity with bipolar spectrum disorder (Edwards & Constantinescu 2004). People with MS are 7-8 times more likely to attempt suicide (Hauser & Oksenberg 2006), with up to 15% of deaths of people with MS being the result of suicide (Chwastiak & Ehde 2007; Sadovnick et al. 1991).

1.2.2. Disease Subtypes

According to the United States of America National Multiple Sclerosis Society Advisory Committee (Lublin & Reingold 1996), there are four subtypes of MS depending on disease progression (Figure 1.2).

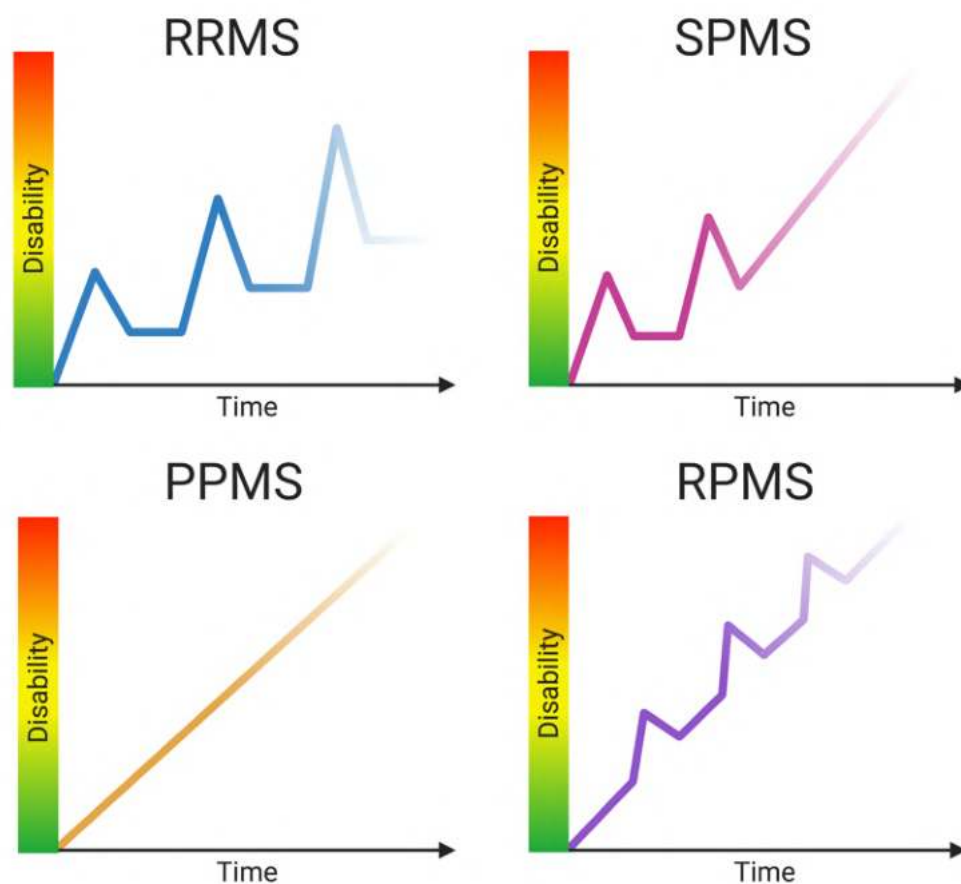


Figure 1.2. Disease progression of the four different subtypes of MS. Speed and nature of progression adapted from Lublin and Reingold, 1996. Abbreviations: RRMS, relapse-remitting multiple sclerosis; SPMS, secondary progressive multiple sclerosis; PPMS, primary progressive multiple sclerosis; RPMS, relapse-progressive multiple sclerosis. Original illustration created using BioRender.com.

The most common form of MS is relapse-remitting (RRMS), which affects 85% of people with MS (Goldenberg 2012; Lublin & Reingold 1996). This phenotype is characterised by periods of demyelination and symptomatic presentation, followed by remyelination and attenuation of symptoms (Prakash et al. 2008). The second subtype is secondary progressive (SPMS), in which

people no longer have periods of remission, rather the disease continues to progress to further disability (Lublin & Reingold 1996; Tremlett et al. 2008). People with RRMS typically develop SPMS between 35-50 years of age (Confavreux & Vukusic 2006). However, the severity of RRMS does not affect the subsequent disease progression of SPMS (Leray et al. 2010). Furthermore, not all people with RRMS go on to develop SPMS (Goldenberg 2012; Vukusic & Confavreux 2003). Factors that influence the development of SPMS continue to be highly debated in the literature (Langer-Gould et al. 2006; Rovaris et al. 2006). Some studies have found that the duration between the first and second episodes of disability may be predictive of the onset of SPMS (Trojano et al. 1995; Vukusic & Confavreux 2003), whilst others did not (Eriksson et al. 2003). Age of onset may too be a predictor, with people who develop MS at an older age being more likely to develop SPMS earlier in the disease (Alroughani et al. 2015; Eriksson et al. 2003; Trojano et al. 1995; Vukusic & Confavreux 2003). Finally, some studies (Alroughani et al. 2015; Eriksson et al. 2003; Vukusic & Confavreux 2003) have found that males develop SPMS sooner than females, whilst others did not (Bergamaschi et al. 2001; Trojano et al. 1995). Treatment during the RRMS phase can decrease the likelihood of SPMS occurring, however does not impact the time till conversion to SPMS or the subsequent severity of disease progression (Coret et al. 2018). The average age of onset for the third MS phenotype, primary progressive (PPMS), is also between 35-50 years old (Confavreux & Vukusic 2006). PPMS affects approximately 10% of people with MS and is characterised by gradually worsening symptoms from the onset of the disease, with no remission periods (Goldenberg 2012; Lublin & Reingold 1996). Although PPMS may appear initially distinct from RRMS and SPMS and responds differently to treatment, the incidence of both subtypes within one family suggests a genetic or causal link common to both (Weiner 2009). Interestingly, one study found that men who later went on to develop PPMS up to 20 years later show significantly lower cognitive performance at ages 18-19, suggesting cognitive dysfunction occurs far earlier than typical symptom onset in this MS subtype (Cortese et al. 2016). Finally, 5% of people with MS present with the rarest form of MS, relapsing-progressive (RPMS), where symptoms get progressively worse with additional periods of even greater disability (Goldenberg 2012).

1.2.3. Genetic & Environmental Risk Factors

There is an element of genetic susceptibility to MS, with 15-20% of people with MS having a family history of the disease (Compston & Coles 2002). A variety of genetic factors may influence an individual's susceptibility to MS. Of these, the most prevalent genetic risk factor is variation in the human leukocyte antigen of the major histocompatibility complex (MHC) on chromosome 6p21 (Patsopoulos 2018), but as of 2015, there was a total of 110 polymorphisms associated with increased risk of MS discovered outside of the MHC (Hollenbach & Oksenberg 2015). Nevertheless, a universal genetic link has not yet been identified for the disease.

Whilst genetic susceptibility conveys increased risk of developing MS, it is becoming increasingly understood that environmental risk factors play a critical role (Pugliatti et al. 2008). Populations who live further from the equator have a higher incidence rate of MS (Acheson et al. 1960; Simpson et al. 2011). This suggests a key role of sunlight exposure for reducing the risk of developing MS. Perhaps correspondingly, vitamin D deficiency has been linked with an increased risk of developing MS (Holick 2004), with both vitamin D and ultraviolet (UV) radiation being shown to have protective effects against the development of the disease (Lucas et al. 2015). Nevertheless, some countries, such as Italy, actually show an inverse gradient effect, suggesting that though sun exposure may confer some risk, it is not a universal risk factor for developing MS (O’Gorman et al. 2012). Within Australia specifically, areas with lower UV exposure (van der Mei et al. 2001) and more southern regions (Hammond et al. 1988) are associated with increased MS incidences, suggesting there may be a latitude gradient within the Australian population.

Viral infections may convey an increased risk of developing MS, in particular infection with the Epstein-Barr Virus (Bjornevik et al. 2022; Marrie 2004). Other viruses that have been proposed to confer an increased risk to MS include human herpesvirus 6, MS-associated human endogenous retroviruses, and coronaviruses (Gilden 2005; Giovannoni et al. 2006).

Smoking may increase the chance of developing MS (Pugliatti et al. 2008), with some studies showing that those with a history of smoking have twice the risk of developing the disease (Riise et al. 2003). Obesity has been proposed to confer risk of developing MS (Hedström et al. 2016). Interestingly, adults with higher body fat have lower levels of circulating vitamin D (Parikh et al. 2004), so it is possible that there may be an interrelationship between body mass, vitamin D and MS risk. Overall, it is becoming increasingly understood that given the multitude and heterogeneity of both environmental and genetic risk factors, many factors interact in any one patient to ultimately convey increased susceptibility to developing MS (Olsson et al. 2017).

1.2.4. Demyelination as a Hallmark of MS

1.2.4.1. Oligodendroglia and Myelin

To provide necessary context for demyelinating diseases such as MS, it is important firstly to understand basic oligodendroglia and myelin biology. Oligodendrocytes are the myelinating cells of the CNS. Mature myelinating oligodendrocytes are generated from the differentiation and maturation of OPCs (Figure 1.3). However, it is important to note that using single-cell ribonucleic acid (RNA) sequencing, twelve distinct subpopulations of oligodendroglial cells have been identified, characterised on a continuum from OPCs to mature oligodendrocytes (Marques et al. 2016).

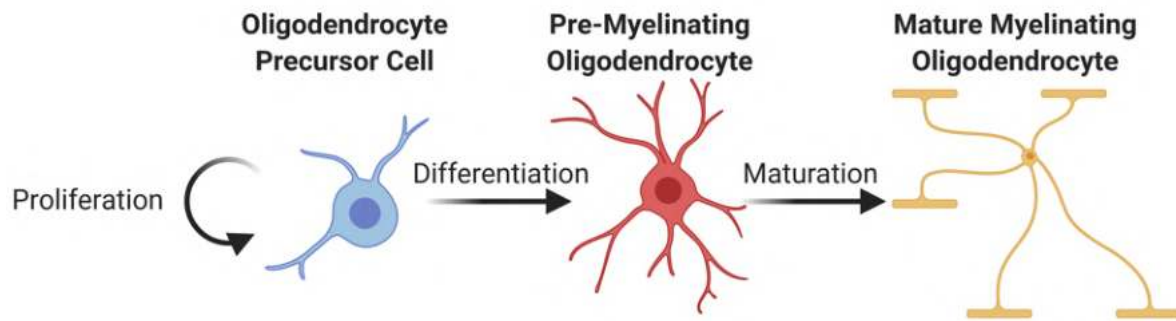


Figure 1.3. The oligodendroglial lineage. The oligodendroglial lineage can be broadly subdivided into three cellular stages; oligodendrocyte precursor cells (OPCs), pre-myelinating oligodendrocytes and mature myelinating oligodendrocytes. Pre-myelinating oligodendrocytes are formed by the differentiation of OPCs, and these pre-myelinating cells then go on to mature into myelinating oligodendrocytes. OPCs act as a proliferating progenitor pool for the production of oligodendrocytes, whilst also playing various roles within the CNS in their immature state. Original illustration created using BioRender.com.

General oligodendroglial markers include oligodendrocyte transcription factor 2 (Olig2) and SRY-related HMG-box 10 (SOX10), which are expressed to varying degrees throughout the oligodendrocyte lineage (Miron et al. 2011). Mature oligodendrocytes can be identified using immunohistochemical markers such as adenomatous polyposis coli (CC1) (Lin Xiao et al. 2016) and aspartoacylase (ASPA) (Moffett et al. 2011), as well as through their expression of myelin-related proteins such as proteolipid protein (PLP), myelin basic protein (MBP), myelin-associated glycoprotein (MAG) and myelin oligodendrocyte glycoprotein (MOG) (Levine et al. 2001; Miron et al. 2011). OPCs can be identified primarily by their expression of PDGFR α (Pringle et al. 1992) and the NG2 proteoglycan (Zhu et al. 2008). Unlike other oligodendrocyte lineage markers, both PDGFR α and NG2 are downregulated as OPCs differentiate and mature into myelinating oligodendrocytes (Rivers et al. 2008). Numerous OPC markers are expressed on other cell types, for example NG2 is expressed on pericytes (Ozerdem et al. 2002). Therefore colocalisation of these markers with another OPC or early oligodendroglial marker is required for specific visualisation of these cells.

Myelin is formed as oligodendrocytes extend and wrap their membranous processes around axons (Bradl & Lassmann 2010). Myelin is extremely lipid rich, comprised primarily of cholesterol, phospholipids, galactolipids and plasmalogens (Norton & Poduslo 1973), with these lipids in turn having an affinity for and binding myelin-associated proteins (Nave & Werner 2014). Sheath structure consists of compacted double bilayers of myelin, with the myelin-related proteins, predominantly MBP, essentially sealing the membranous bilayers together (Min et al. 2009). Mature myelin is comprised of up to 160 layers of compacted lamellae that can be visualised as interperiodic lines (Hildebrand et al. 1993). Oligodendrocytes myelinate axons with a variety of diameters (0.4-

1.2 μ m) (Nave & Werner 2014), with a singular oligodendrocyte possessing the capacity to supply up to 50 myelin segments across different axons (Richter-Landsberg 2008). Myelin's highly segmented structure allows it to facilitate correct neuronal signalling (Aggarwal et al. 2011; Figure 1.4). The enhanced saltatory conduction of action potentials on myelinated axons results in the conduction of signals 20 to 100 times faster than by unmyelinated axons of a similar diameter (Nave & Werner 2014). Though it's been long established that myelin thickness is proportional to the diameter of the ensheathed axon (Donaldson & Hoke 1905), it was recently discovered that both axonal diameter and the corresponding myelin thickness can vary considerably along the length of an axon (Giacci *et al.*, 2018a).

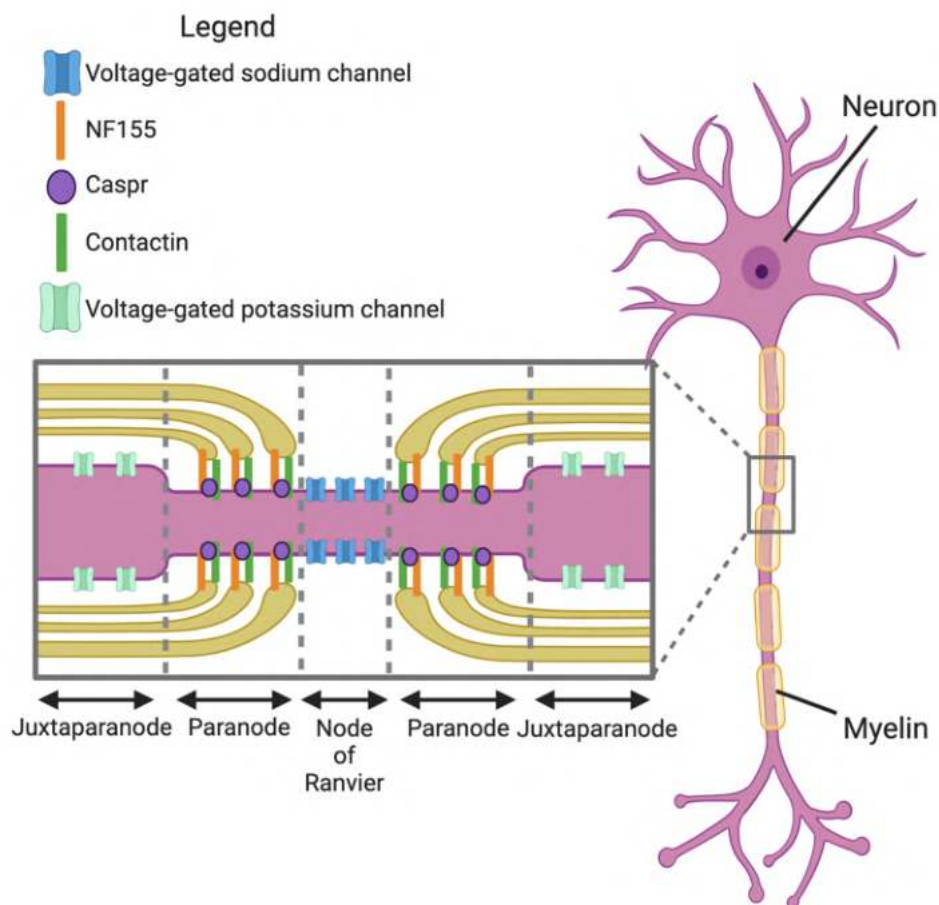


Figure 1.4. Structure of the myelin sheath. Oligodendrocytes wrap their processes around axons to create the myelin sheath and allow for saltatory conduction of axon potentials. The myelin sheath has four distinct sections. The internode is the long stretch of myelin that covers the axon. The gaps in the myelin are called the nodes of Ranvier, which are sites of action potential propagation *via* clusters of voltage-gated sodium channels. Directly adjoining the node is the paranode. The paranode is comprised of loops of myelin lamellae anchored to the axon *via* the paranodal junction, which consists of contactin, neurofascin 155 and contactin-associated protein (Caspr). The multifaceted roles of the paranode including anchoring the myelin lamellae to the axon to prevent stretch damage to myelin, segregating nodal sodium and juxtaparanodal potassium channels, and permitting only certain nutrients to diffuse in and out of the internodal periaxonal space. The juxtaparanode exists between the paranode and internode and contains a large volume of voltage gated potassium channels to maintain resting membrane potential. Distribution of nodal/paranodal components adapted from Edgar and Sibille 2012. Original illustration created using BioRender.com.

Other than acting to provide myelin for axons, oligodendrocytes play a variety of other roles within the CNS. For example, oligodendrocytes can act as immunomodulatory cells. Oligodendrocytes actively participate in the inflammatory process by expressing various factors, including cytokines and chemokines, antigen presenting molecules, and extracellular matrix proteins (Zeis et al. 2016). A specific disease-associated immunomodulatory oligodendrocyte phenotype can be observed using single-nucleus RNA sequencing in human MS tissue, suggesting that a subpopulation of oligodendrocytes also actively contribute to inflammatory MS disease processes (Pandey et al. 2022). Furthermore, neuron-oligodendrocyte interactions are also critical for axonal integrity, aside from the supportive role of myelination itself. Partial ablation of oligodendrocytes can cause degeneration of axons even without extensive demyelination (Oluich et al. 2012). Loss of oligodendrocyte-specific proteins such as PLP and 2',3'-cyclic nucleotide-3'-phosphodiesterase (CNPase) can also cause axonal swelling and degeneration despite a lack of change to myelin structure (Griffiths et al. 1998; Lappe-Siefke et al. 2003). This suggests that oligodendrocytes themselves have a multifaceted role in neuronal maintenance. One potential mechanism for this is the secretion of trophic factor exosomes by oligodendrocytes, which neurons then uptake to improve their own metabolic activity (Frühbeis et al. 2013). Oligodendrocytes also provide metabolites to neurons *via* monocarboxylate transporters and cytoplasmic channels, acting as further metabolic support for promoting neuronal survival (Philips & Rothstein 2017). Interactions between oligodendrocytes and neurons are adaptive and plastic, with neural signalling itself stimulating oligodendrogenesis and increases in myelin thickness (Gibson et al. 2014).

OPCs are glial cells that act as the progenitor cell population for oligodendrocytes. OPCs comprise between 8-9% and 2-3% of the total number of brain cells in adult white matter and grey matter respectively and are the major proliferating cells in the CNS (Dawson *et al.*, 2003). The earliest embryonic forebrain OPCs originate in the medial ganglionic eminence and anterior entopeduncular area, followed by a second wave of OPC generation from the lateral and caudal ganglionic eminences (Kessaris et al. 2006). A third wave of OPCs are generated in the dorsal subventricular zone and project radially through the corpus callosum and cortex (Kessaris et al. 2006). These developmental OPCs occupy the brain and spinal cord to form oligodendrocytes to myelinate the CNS postnatally, with a small proportion remaining as an immature, quiescent and proliferating population into adulthood (Dawson et al. 2003). If any of these OPC sources are ablated by diphtheria toxin, the remaining OPCs proliferate to generate the normal number of oligodendrocytes in the adult brain, and the mice survive with a normal behavioural phenotype (Kessaris et al. 2006), suggesting early functional homogeneity of this cell type.

OPCs are also called polydendrocytes, as increasing evidence is suggesting they are multipotential cells (Nishiyama et al. 2009). A subset of OPCs may possess the ability to differentiate

into astrocytes (Raff et al. 1983; Tanner et al. 2011), although it is contested as to whether this occurs naturally *in vivo* (Rivers et al. 2008; Zhu et al. 2008). In the adult mouse piriform cortex, OPCs can give rise to pyramidal glutamatergic neurons (Guo et al. 2010).

Many OPCs do not go on to differentiate into oligodendrocytes, instead remaining in a proliferative state (Fernandez-Castaneda & Gaultier 2016), with lower oligodendrocyte generation occurring in grey matter than white matter (Dimou et al. 2008). The morphology of OPCs changes between grey and white matter, however within regions, OPC morphology is thought to be homogenous (Dawson *et al.*, 2003). The functional homogeneity of OPCs has been contested, with differences in differentiation, proliferation, gene expression, growth factor profile, and electrophysiological properties observed (Clarke et al. 2012; Káradóttir et al. 2008; Mallon et al. 2002; Mason & Goldman 2002; Psachoulia et al. 2009). Recent work has shown that the expression of ion channels by OPCs become heterogeneous with age and the region analysed (Spitzer et al. 2019).

Other than acting as a progenitor pool for oligodendrocyte generation, OPCs also play various roles within the CNS. OPCs can migrate throughout the CNS to sites of injury to modulate the inflammatory response. Ablation of OPCs can cause excessive neuroinflammation, indicating that OPCs may suppress inflammation within a healthy system (Nakano et al. 2017). Following injury, OPCs become hypertrophic and contribute to the formation of the glial scar that prevents regeneration of the CNS (Hackett & Lee 2016). Deletion of signalling pathways in OPCs activated by pro-inflammatory cytokines secreted by peripheral T-cells, results in decreased expression of inflammatory genes (Kang et al. 2013). Furthermore, in MS lesions, a subtype of OPCs expressing MHC II have the ability to activate T-cells as well as directly phagocytose myelin themselves (Falcão et al. 2018).

Parenchymal OPCs also play a critical role in neuronal signalling. These OPCs contain a variety of voltage-gated ion channels and neurotransmitter receptors (Yang et al. 2013), and have direct synaptic contacts with neurons, in particular glutamatergic (Bergles et al. 2000) and GABAergic neurons (Lin & Bergles 2004). Some OPCs even modulate neuronal activity by initiating action potentials (Ttir et al. 2008). However, the underlying function of neuron-OPC signalling is currently unclear.

Some OPCs colocalise and interact with blood vessels, whilst others reside solely in the brain parenchyma; however, functional differences between perivascular and parenchymal OPCs remain to be investigated (Maki 2017). It's important to note that single-cell RNA sequencing has suggested that the PDGFR α ⁺ cells that line blood vessels may actually be a population distinct from OPCs (Marques et al. 2016). Nevertheless, OPCs with an intermediate phenotype have been observed, whereby they are both simultaneously perivascular and parenchymal (Maki et al. 2015). This suggests

that there are not distinct subpopulations but perhaps a spectrum based on association with the vasculature. More work is clearly needed to characterise this particular cellular subpopulation. The role of perivascular OPCs at the BBB will be discussed further in Chapter 5 of this thesis.

1.2.4.2. Demyelinated Plaques

The key hallmark of MS is demyelinated plaques (Noseworthy et al. 2000), or areas of the brain in which axons have lost the myelin sheath, in both the white and grey matter (Kutzelnigg & Lassmann 2006) (Figure 1.5).

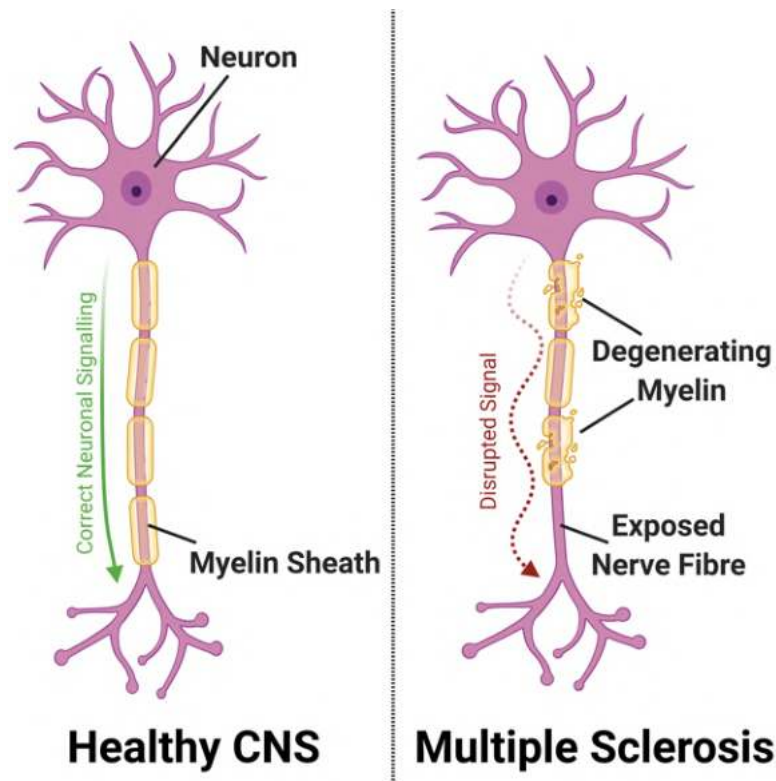


Figure 1.5. Demyelination in MS. Within a healthy CNS, the axons of neurons are wrapped in a myelin sheath by oligodendrocytes to facilitate correct neuronal signalling. However, within demyelinated lesions in MS brains, this myelin sheath is degraded and degenerates, which can leave nerve fibres exposed, and ultimately results in a disrupted neuronal signal which impedes overall function. Original illustration created using BioRender.com.

In white matter, the formation of new demyelinated lesions often occurs in the acute and/or relapsing phase of disease progression (Cotton et al. 2003). Once the disease is chronic and progressive, there is more generalised atrophy of white matter, associated with neurodegeneration and axonal loss following lesion formation (Miller et al. 2002). In grey matter, lesions form predominantly as continuations from the white matter plaques or as separate subpial demyelinated lesions (Lassmann et al. 2007). These lesions are characterised as band-like, extending down through the cortex to the deeper layers of cortical tissue, usually through layers I-IV (Kutzelnigg et al. 2005).

However, there is no association between the extent of white matter and grey matter demyelination, which suggests they are independent of each other (Bö et al. 2007).

Heterogeneity is an added complexity to understanding the pathophysiology of demyelination as there are four main types of early MS lesions (Figure 1.6). Therefore, it is likely that potential therapeutics may need to be combinatorial to target not only inflammatory pathways for pattern I and II lesions but also the observed oligodendroglipathy in pattern III and IV lesions. It's important to note though that once MS progression has advanced to a more established stage, this initial heterogeneity may disappear, with lesions becoming more homogenous between people with MS (Breij et al. 2008).

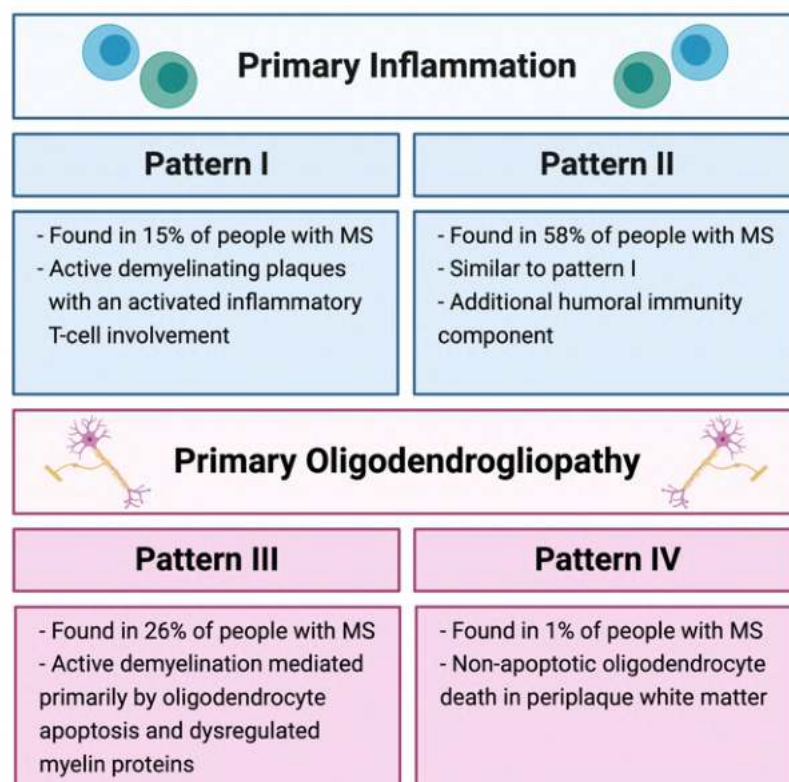


Figure 1.6. Four main types of early human MS lesions. In brief, pattern I lesions are found in 15% of people with MS and are characterised by active demyelinating plaques with an activated inflammatory T-cell involvement. Pattern II lesions are found in 58% of people with MS, and are similar to pattern I, but with an additional humoral immunity component. Pattern III lesions are found in 26% of people with MS and are characterised by active demyelination mediated primarily by oligodendrocyte apoptosis and dysregulated myelin proteins. Pattern IV lesions are rare and only found in 1% of people with MS, and are characterised by non-apoptotic oligodendrocyte death in periplaque white matter. Pattern I and II type lesions are mediated predominantly *via* inflammatory mechanisms and patterns III and IV are mediated by primary oligodendroglipathy. Based on information presented in Jarius et al. 2017; Lucchinetti et al. 2000; Popescu et al. 2013. Original illustration created using BioRender.com.

1.2.4.3. Normal Appearing White Matter

Within the brains of people with MS is normal appearing white matter, or white matter that has not become part of a demyelinated plaque (Allen et al. 2001). However, this normal appearing white matter still shows significant degenerative changes compared to healthy controls (Moll et al. 2011). Regions of normal appearing white matter display astrocyte and microglial activation, demyelination and axonal loss (Ludwin 2006), with varying degrees of BBB permeability (Cramer et al. 2018; Moll et al. 2011). Genes associated with innate CNS inflammation are upregulated in normal appearing white matter, and there is minimal peripheral immune cell involvement, suggesting a pivotal role for innate CNS-mediated damage (Zeis et al. 2007).

1.2.4.4. Remyelination and Shadow Plaques

Remyelination occurs as new myelin sheaths are formed on previously demyelinated axons, and resulting from OPCs undergoing differentiation into mature, myelinating oligodendrocytes (Höftberger & Lassmann 2018). The extent of remyelination is highly variable between people with MS and often depends on their subtype of MS, with the greatest remyelination occurring in people with RRMS (Patrikios et al. 2006). People who have RRMS often experience partial and/or complete remyelination during their recovery phase, however the myelin provided during remyelination is often thinner and shorter (Albert et al. 2007; Coman et al. 2006; Duncan et al. 2017). People with progressive forms of MS also experience some level of remyelination, with shadow plaques appearing in all MS disease states (Mahad et al. 2015). Shadow plaques are previously demyelinated plaques that have been completely remyelinated, however these areas are more likely to undergo another demyelinating insult than normal appearing white matter (Bramow et al. 2010).

In MS this remyelination mechanism is impaired and ultimately fails (Olsen & Akirav 2015). Several reasons have been postulated as to why remyelination fails in MS, such as the formation of a glial scar and extensive axonal damage leaving neurons unable to be ensheathed by myelin (Olsen & Akirav 2015). Additionally, increased numbers of undifferentiated OPCs and pre-myelinating oligodendrocytes halted in an undifferentiated state occur within MS lesions, suggesting a decreased ability of early-stage oligodendroglia to differentiate into mature remyelinating oligodendrocytes (Chang et al. 2002; Kuhlmann et al. 2008). Pre-existing mature oligodendrocytes have recently been discovered to possess remyelinating capabilities (Duncan et al. 2018; Nave & Ehrenreich 2019; Yeung et al. 2019), however remyelination is still impaired in active demyelinating MS lesions despite the presence of mature oligodendrocytes (Heß et al. 2020).

1.2.5. *Human MS Pathophysiology*

1.2.5.1. “Outside-In” Hypothesis

There are two prevailing theories of early human MS pathophysiology, the “inside-out” and “outside-in” hypotheses. MS has traditionally been considered an autoimmune disease, whereby

primary peripheral autoimmune cell inflammation results in a secondary myelin degradation within the CNS, in what is now known as the “outside-in” hypothesis (Titus et al. 2020). These peripheral cells include CD4⁺ and CD8⁺ T-cells, and autoreactive B cells, which are myelin-reactive and become activated by myelin antigens, the process of which is poorly understood but may be due to a leaky BBB (Dendrou et al. 2015). These cells then enter the brain parenchyma, releasing pro-inflammatory molecules that result in additional BBB opening (Hemmer et al. 2015). Once inside the CNS, these peripheral immune cells attack the myelin sheath, resulting in further dissemination of myelin proteins and thus activation of additional myelin-reactive immune cells (McFarland & Martin 2007). Peripheral immune cells release pro-inflammatory molecules which activate CNS resident phagocytes, microglia and macrophage cells, further mediating damage to myelin and oligodendrocytes (Dendrou et al. 2015; Friese & Fugger 2007) (Figure 1.7).

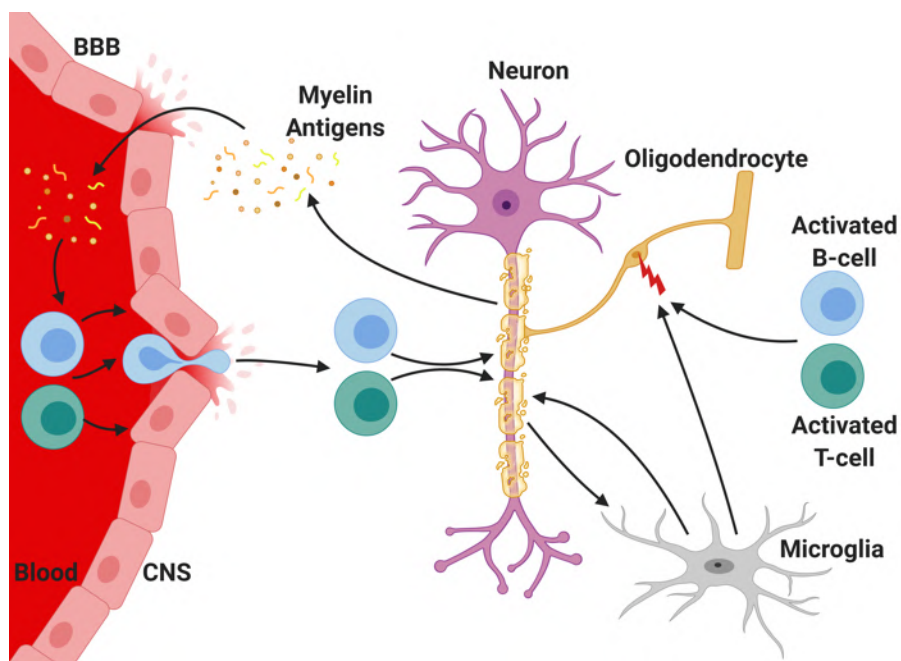


Figure 1.7. Peripheral immune cell-mediated damage to oligodendrocytes and myelin. Peripheral immune cells, including myelin-reactive T-cells and B-cells, become activated by myelin antigens in the periphery. These cells release inflammatory factors, such as cytokines, which increase permeability of the BBB and subsequently enter the brain parenchyma. Then the peripheral immune cells attack oligodendrocytes and their myelin, and both the degenerating myelin and the peripheral immune cells activate the CNS resident innate immune cells, microglia and macrophages. The degeneration of myelin results in the dissemination of myelin proteins through the breached BBB, which further propagates the activation of peripheral immune cells. Note: the BBB is comprised of a variety of cells, including endothelial cells, astrocytes, pericytes, and OPCs. Original illustration created using BioRender.com.

However, whilst many myelin antigens have been found in the cerebrospinal fluid of people with MS, studies are yet to discover a universal autoantigen (Archelos et al. 1998; Kennel De March et al. 2003; Lemus et al. 2018; Möller et al. 1989) and how the peripheral immune cells are initially

activated by myelin antigens is currently unknown. Furthermore, lesions with severe oligodendroglipathy that do not have any infiltration of peripheral inflammatory cells have been observed (Barnett & Prineas 2004). Therefore, the immune aspect of the disease may be secondary to neurodegeneration in some lesions, especially pattern III and IV lesions (Hauser & Oksenberg 2006), and whilst there is a strong immune component in MS, it's becoming increasingly agreed that the disease cannot be regarded as simply autoimmune (Lemus et al. 2018).

1.2.5.2. “Inside-Out” Hypothesis

Early stage lesions and normal appearing MS white matter can feature oligodendrocyte death and innate phagocyte activation without peripheral immune cell infiltration, which suggests peripheral immune activation may be a secondary mechanism of damage, particularly in pattern III lesions (Barnett & Prineas 2004). Therefore, an alternative hypothesis for the mechanism of damage that leads to the degeneration observed in MS lesions has been proposed, referred to as the “inside-out” hypothesis (Titus et al. 2020). In this alternative theory, it's thought that the primary pathophysiology begins with degeneration of oligodendrocytes, which is then followed by inflammatory processes activated as a result of the shedding of myelin antigens during this primary cytodegeneration (Stys et al. 2012). Microglia and macrophages, the innate phagocytes of the CNS, may be initially activated by primary degeneration of myelin (Hemmer et al. 2015). There is then interplay between activated innate CNS phagocytes and peripheral immune cells, as microglia and macrophages can present internalised myelin antigens to myelin-reactive T-cells, resulting in activation of the peripheral immune response (Cash et al. 1993). These activated peripheral immune cells then migrate to the CNS, resulting in further demyelination (Stinissen & Hellings 2008). Microglia and macrophages are also the major source of ROS in MS lesions (Fischer et al. 2012), which creates an environment that promotes oxidative stress in the surrounding cells, particularly oligodendrocytes and OPCs, which may result in self-propagating damage (Luo et al. 2017). Oxidative stress and its specific effects on oligodendroglia will be further discussed from Section 1.4.2 to Section 1.4.6.3. Additionally, given phenotypic subpopulations of both oligodendrocytes and OPCs are known to play important immunomodulatory and proinflammatory roles in MS lesions, oligodendroglia themselves are also likely contributors to early innate CNS inflammation (Falcão et al. 2018; Pandey et al. 2022; Psenicka et al. 2021).

1.2.6. *Current Therapeutic Strategies for MS*

Currently, clinically available therapies for MS are focused on immunomodulation and immunosuppression (Gilgun-Sherki et al. 2004; Trapp & Nave 2008). For example, interferon β is an immunomodulatory first-line therapy that has a plethora of effects, including inhibiting the inflammatory cytokine interferon- γ (Revel et al. 1995) and inhibiting T-cell activation (Markowitz 2007). Another first-line treatment is glatiramer acetate, which works by promoting an anti-

inflammatory helper T-cell phenotype, increasing the expression of anti-inflammatory cytokines (Aharoni et al. 2003; Hestvik et al. 2008). Often a combinatorial therapy will be used (Gold 2008), however drugs that have greater immunosuppressant effects tend to be second-line therapies due to their tendency to have more severe side effects than immunomodulatory alternatives (Aharoni 2010). Nevertheless, the current available therapies only slow disease development, are not preventative, and are of limited effect when administered during the progressive phase (Lassmann et al. 2007). It is thus likely that these immune-focused therapies may need to work concomitantly with an oligodendrocyte or myelin specific therapy to complementarily target multiple aspects of the disease. Still, despite growing support in the literature for the “inside-out” hypothesis of MS pathophysiology, there are not yet any treatments currently approved for clinical use that directly target oligodendrocytes or myelin (Yakimov et al. 2019). Therefore, though there are some promising therapeutic compounds that have been identified for promoting OPC differentiation and myelin repair within pre-clinical studies, some of which are currently in the clinical trials phase of development, it’s vital that the damage mechanisms underlying the degeneration of oligodendrocytes and myelin in MS are further investigated to allow for discovery of new alternative avenues of therapy for MS (Gacem & Nait-Oumesmar 2021).

1.2.7. The Cuprizone Model of Demyelinating Disease

Given the complexity of MS, animal models are needed to illuminate unknown mechanisms of demyelination and degeneration. There is currently no universal animal model used to study MS pathophysiology. Rather, there are multiple animal models, including but not limited to; (1) experimental autoimmune encephalomyelitis (EAE), (2) Theiler’s murine encephalomyelitis virus (TMEV) infection, (3) injected lysolecithin lesions, and (4) cuprizone-induced demyelination (for review, see Procaccini *et al.*, 2015).

Though EAE is the most commonly used animal model of MS, it investigates MS pathology caused by “outside-in” primary autoimmunity and only indirectly induces changes within the CNS itself *via* activating peripheral inflammation (Sriram & Steiner 2005; Wekerle & Kurschus 2006). To instead examine CNS degeneration in line with the “inside-out” MS hypothesis, the cuprizone model of demyelination is most appropriate (Gharagozloo et al. 2022). Cuprizone intoxication directly causes oligodendrocyte degeneration and demyelination without the influence of initial autoimmune inflammation, which closely resembles the primary oligodendropathy observed in some MS lesion subtypes (Zirngibl et al. 2022). Therefore, in order to probe early oxidative stress and other CNS intrinsic damage mechanisms, the cuprizone model will be the focus of this thesis.

1.2.7.1. Mechanism of Cuprizone Toxicity

The cuprizone model is a toxin-based technique to produce demyelination that is similar to the demyelination that occurs within the brains of people with MS. Cuprizone (or N,N'-

Bis(cyclohexylideneamino)oxamide) is a copper chelator that is orally delivered to rodents to produce oligodendrocyte death, active gliosis and demyelination *via* mitochondrial dysfunction (Kipp et al. 2009; Matsushima & Morell 2001; Torkildsen et al. 2008).

In brief, cuprizone administration results in: increased mitochondrial production of superoxide anions (Praet et al. 2014); a reduction in copper-dependent cytochrome *c* oxidase and monoamine oxidase activity (Matsushima & Morell 2001); decreased copper-zinc superoxide dismutase (Zhang et al. 2008) and glutathione antioxidant activity (Biancotti et al. 2008); and inhibition of the electron transport chain complex IV (Acs et al. 2013). These mechanisms ultimately result in mitochondrial injury and oxidative stress. Oligodendrocytes are especially vulnerable to cuprizone-mediated mitochondrial dysfunction (Acs et al. 2013), causing apoptosis of these cells (Matsushima & Morell 2001) and subsequent loss of myelin (Praet et al. 2014). This mitochondrial dysfunction results in endoplasmic reticulum stress (Fischbach et al. 2019; Xu et al. 2005; Yu et al. 2017), causing a further downregulation of myelin proteins (Gudi et al. 2011) and reduced myelin lipid synthesis (Praet et al. 2014). Copper deficiency also causes demyelination in humans (Jaiser & Winston 2010; Prodan et al. 2002; Stys et al. 2012). Dysfunction of the mitochondrial electron transport chain complex IV within oligodendrocytes is known to occur in type III active MS lesions (Mahad et al. 2008). However, simultaneously administering copper supplementation alongside cuprizone administration does not completely counteract cuprizone toxicity (Carlton 1967), which suggests that there may be additional copper-independent pathways of oligodendroglial damage activated by cuprizone (Zatta et al. 2005). Despite copper homeostasis disruption being postulated to play a role in MS pathogenesis, this dysregulation has not yet been fully elucidated (Stys et al. 2012). The copper chelating effect of cuprizone also induces iron dyshomeostasis, causing a ferroptosis-mediated depletion of myelin and oligodendrocytes (Jhelum et al. 2020). One study has suggested that the effects of cuprizone may be independent of copper chelation altogether, but instead associate with a Schiff base formation binding with the amino acid metabolism coenzyme pyridoxal 5'-phosphate, disrupting oligodendrocyte metabolism (Taraboletti et al. 2017). Regardless of its mechanism of action, cuprizone is a well-established and validated model for examining demyelination that is not directly related to peripheral inflammation and autoimmunity (Procaccini et al. 2015).

1.2.7.2. Cuprizone Pathophysiology Within the Corpus Callosum

The most commonly analysed area of the brain in the cuprizone model is the corpus callosum, particularly the caudal corpus callosum. In this area, one of the earliest observable pathologies is oligodendrocyte apoptosis, which occurs as early as 48 hours after commencing cuprizone administration (Buschmann et al. 2012; Krauspe et al. 2015). The number of IBA1+ microglial cells within the corpus callosum increases by 48 hours of cuprizone intoxication (Krauspe et al. 2015).

Also after 48 hours of cuprizone exposure, mRNA expression of various genes associated with mature oligodendrocytes are down-regulated, whilst genes associated with other cell types, particularly microglia/macrophages but also astrocytes, endothelial cells and OPCs, are up-regulated (Krauspe et al. 2015). By 3 days of cuprizone exposure, there is a significant increase in the level of Evans blue dye extravasation and a decrease in the expression of tight junction markers in the corpus callosum, suggesting early BBB dysfunction (Shelestak et al. 2020). The presence and role of BBB hyperpermeability in both MS and the cuprizone model will be discussed further in Chapter 5. By 4 days of cuprizone exposure, the density of mature oligodendrocytes are slightly but significantly decreased, and by 1 week the density of mature oligodendrocytes are decreased approximately six-fold (Fischbach et al. 2019). Also by the end of the first week, microglia are highly activated (Shelestak et al. 2020). Astrocytes display morphological changes as early as a week into cuprizone toxicity, with astrocyte density significantly increasing by 3 weeks (Hiremath et al. 1998; Zhan et al. 2020). By 3 weeks, OPCs accumulate within the corpus callosum, particularly caudally, to function as a progenitor pool for the differentiation and maturation of new myelinating oligodendrocytes (Mason et al. 2000; Xing et al. 2014). Demyelination is histologically detectable by 3 weeks of cuprizone intoxication (Zhan et al. 2020), with the number of oligodendrocytes depleting even further at this time point (Fischbach et al. 2019). By 4 weeks of intoxication, there are significant neurochemical alterations observable *via* proton magnetic resonance spectroscopy, such as a decrease in the ratios of N-acetylaspartate and N-acetylaspartylglutamate, total choline, glutamate, and glucose when compared to total creatine, as well as an increase in the ratio of taurine to total creatine (Orije et al. 2015). After 4.5 weeks of cuprizone exposure, the density of NG2⁺ cells, which is possibly indicative of OPCs although this population captures other cell types including pericytes, is beginning to decrease (Gudi et al. 2009). By 5 weeks, demyelination is severe and almost complete within the corpus callosum (acute demyelination; Gudi et al. 2009). Furthermore, acute axonal injury can be visualised in the corpus callosum by this time, observed as accumulations of amyloid precursor protein (APP)⁺ spheroids and other synaptic proteins such as vesicular glutamate transporter 1 (VGluT1), resulting from a disruption in anterograde axonal transport (Höflich et al. 2016). However, by 5 weeks of cuprizone, the number of mature oligodendrocytes has actually begun to increase, although the density still remains significantly lower compared to healthy controls (Fischbach et al. 2019). After 5 weeks of cuprizone, the re-expression of myelin protein genes is evident. By 6 weeks, PLP staining returns to the corpus callosum and the number of mature oligodendrocytes is not significantly different to controls, suggesting early remyelination despite continuing cuprizone intoxication (Baxi et al. 2017; Gudi et al. 2009). Therefore, if demyelination is being studied, it is common practice for researchers to cease cuprizone administration following 5 weeks exposure at the latest, to limit the confounding factor of initial remyelination. If administration of cuprizone is

continued, by 12 weeks of intoxication PLP staining of the corpus callosum is again reduced (chronic demyelination; Skripuletz et al. 2011). When cuprizone is fed continuously for 11 weeks, there are significant changes in 81 differential metabolites, in particular those associated with phospholipids and therefore myelin structure (Zhao et al. 2021). There is also a large alteration at this timepoint in metabolites involved in phosphatidylinositol 3-kinase (PI3K) / protein kinase B (AKT) signalling, mammalian target of rapamycin (mTOR) signalling, and extracellular signal-regulated kinase (ERK) / mitogen-activated protein kinase (MAPK) signalling, all of which are signalling pathways associated with oxidative stress mechanisms (Zhao et al. 2021).

Complete removal of cuprizone feed following acute demyelination results in spontaneous remyelination of the brain, with nearly 50% re-expression of myelin proteins one-week post-cuprizone withdrawal (Skripuletz et al. 2011). At 6 weeks remyelination following a 6 week acute cuprizone insult, the number of mature oligodendrocytes is significantly higher than controls, suggesting there is a far greater rate of oligodendrogenesis and an overactivation of compensatory repair mechanisms following cuprizone intoxication (Baxi et al. 2017). Similarly, at this 6 week remyelination timepoint following 6 weeks of cuprizone, all neurochemical alterations and metabolic differences observed during the intoxication period are returned to levels not different to control mice (Orije et al. 2015). Removal of cuprizone following chronic demyelination also results in remyelination; however, the process is comparatively delayed (Lindner et al. 2009). Interestingly, even at 28 weeks after an acute 5 week cuprizone insult, there is a continued significant loss of callosal axons but no difference in the density of neuronal cell bodies, and APP+ axons were still detectable despite these axons being remyelinated (Manrique-Hoyos et al. 2012). Neuronal pathology is associated with decreases in locomotor function compared to control animals at this timepoint which suggests that there is a continuing progressive degeneration of axons long after withdrawal of cuprizone (Manrique-Hoyos et al. 2012).

It is important to note that the susceptibility of the corpus callosum is not homogenous, with the vulnerability to cuprizone exposure varying in different regions of the corpus callosum. In the rostral corpus callosum, the lateral parts are more susceptible to cuprizone intoxication than the medial, whilst in the caudal regions the midline is most vulnerable to demyelination (Zhan et al. 2020). Furthermore, demyelination is more pronounced in the caudal corpus callosum than in the rostral, making the medial caudal corpus callosum the callosal area most susceptible to cuprizone (Steelman et al. 2012). Additionally, this sequence of pathophysiological events is specific to cuprizone delivered to C57Bl6 mice at a 0.2% dosage. Delivering cuprizone to alternate strains of rodents (Vega-Riquer et al. 2019), or at higher or lower doses (Hiremath et al. 1998), results in varying degrees of pathology and does not follow the specific timeline presented above.

1.2.7.3. Pathophysiology in Other Brain Regions

Cuprizone is also effective at demyelinating other brain regions. For example, for those wanting to look more specifically at cortical grey matter changes, there has been a plethora of work regarding the cortical response to cuprizone. Some additional brain regions that are often analysed are the anterior commissure, hippocampus, basal ganglia, brainstem, cerebellum, hypothalamus, thalamus, optic tract, among others (Skripuletz et al. 2011; Vega-Riquer et al. 2019). However, it is important to note that not all brain regions are similarly susceptible to cuprizone intoxication, with some areas less affected, and each region generally has its own slightly modified timeline of cuprizone pathophysiology (Vega-Riquer et al. 2019; Zhan et al. 2020). Therefore, selection of region of interest is crucial in studies utilising cuprizone, and accurate reporting of region is critical in reproducibility of work. For the work presented in this thesis, there will be a particular focus on the corpus callosum as a region of interest, to maximise comparability to existing literature.

1.2.7.4. Behavioural Changes in the Cuprizone Model

The cuprizone model also induces many behavioural and functional features similar to those experienced by people living with MS. Function can be assessed in the cuprizone model through a variety of measures, with the more widely utilised behavioural assays including the Rotarod test to assess motor deficits and the open field test to assess locomotor activity and determine the presence of anxiety in response to a novel environment (Faizi et al. 2016; Franco-Pons et al. 2007). There is a large discrepancy between some of the most highly prevalent MS symptoms, such as fatigue, and the proportion of publications utilising cuprizone that actually characterise these symptoms in the cuprizone model (Figure 1.8; Sen et al. 2019). Therefore, many of the symptomatic changes observed in MS have not been widely investigated following cuprizone intoxication and more studies are required to determine the extent to which the behavioural symptoms observed during and after cuprizone administration mimics symptoms observed in MS.

Outcome Measure	Multiple Sclerosis		Cuprizone	
	Direction of Change	% MS Population	Direction of Change	% Cuprizone Publications
Motor Function	↓	80%	↓	32%
Pain	↑	29-86%	↑	4%
Fatigue	↑	75%	×	1%
Cognition	↓	40-65%	↓	29%
Visual Function	↓	50%	↓	1%
Depression	↑	50%	×	1%
Sleep	↓	50%	-	0%
Anxiety	↑	35%	↑	30%

Figure 1.8. Comparison of behavioural and functional symptomology in MS and in the cuprizone model of demyelinating disease. The frequency of symptomatic presentation in MS was based on clinical prevalence whereas the percentage of cuprizone publications were measured by the proportion of studies that have been published utilising the cuprizone model that have assessed each specific outcome measure. Symbols: ↑, increase; ↓, decrease; X, no differences observed; -, outcome not yet assessed. Figure based on information reviewed in Sen *et al.*, 2019. Original illustration created using BioRender.com.

1.2.7.5. Limitations of the Cuprizone Model

Though the cuprizone model is useful for investigating intrinsic CNS changes in MS, it is still important to recognise potential limitations. Though demyelination in the spinal cord is common in people with MS (Moccia *et al.* 2019), the demyelinating result of cuprizone is almost entirely confined to the brain and has minimal effect on the spinal cord (Herder *et al.* 2011; Sen *et al.* 2020). Remyelination following acute cuprizone withdrawal is more complete than the repair observed in human brains, especially compared to more progressive and chronic forms of MS (Lassmann & Bradl 2016). Researchers need to be mindful of these disparities when selecting cuprizone exposure as their model of MS. The wider contention around the underlying mechanisms of cuprizone toxicity can also sometimes limit the ability to draw clear parallels with human MS pathophysiology (Gudi *et al.* 2014). The potential for inconsistent oral cuprizone consumption both within and between studies, as well as the sex-dependent and strain-dependent differences in cuprizone-induced pathology, can increase the variability of obtained results within the literature (Paton *et al.* 2022; Vega-Riquer *et al.* 2019).

The cuprizone model is also not just a model used specifically for studying MS, as cuprizone toxicity is additionally a model of schizophrenia. Like MS, schizophrenia is characterised by damage to the myelin sheath and decreased oligodendrocyte density (Davis et al. 2003; Flynn et al. 2003; Uranova et al. 2001), as well as increased microglial density (van Berckel et al. 2008; van Kesteren et al. 2017) and T-cell activation (Debnath 2015; Drexhage et al. 2011). Cuprizone administered mice show cognitive deficits similar to those with schizophrenia, such as spatial deficits, decreased sensory gating and decreased social interaction (Herring & Konradi 2011; Xu et al. 2009). When mice given cuprizone are treated with antipsychotic medication, there is an attenuation of non-motor behavioural deficits and myelin damage (Xu et al. 2010). Though there may indeed be a biological link between MS and schizophrenia (Andreassen et al. 2015), this broader applicability of this model to multiple pathologies may potentially limit the translation of pre-clinical findings.

1.3. Neurotrauma

1.3.1. Introducing “Damage mechanisms to oligodendrocytes and white matter in central nervous system injury: The Australian context”

Neurotrauma is the damage caused by an external mechanical force acting upon the CNS (Kobeissy 2015). The most prevalent type of neurotrauma is TBI (Khan et al. 2003), defined as a change to neurological functioning as a result of a blunt or penetrating force to the head (Bruns & Hauser 2003). Neurotrauma follows a similar pathogenesis to MS, with injury resulting in disruption to myelin structure and demyelination (Dong et al. 2009; Payne et al. 2011; Szymanski et al. 2013). Therefore, there may be potential common mechanisms of damage between MS lesions and traumatic injuries to the CNS. Prior to delving further into these common mechanisms between the two conditions, it is important to understand fully the complexities of the aetiology and pathophysiology of neurotrauma.

To address this, a co-first author review on the effects of neurotrauma on white matter is presented below and has been published as:

Warnock, A.*, **Toomey L.M.***, Wright, A.J., Fisher, K., Won, Y., Anyaegbu, C., and Fitzgerald, M. 2020. Damage mechanisms to oligodendrocytes and white matter in central nervous system injury: The Australian context. *Journal of Neurotrauma* 37, 739-769. doi.org/10.1089/neu.2019.6890

* *Equal contribution*

Damage Mechanisms to Oligodendrocytes and White Matter in Central Nervous System Injury: The Australian Context

Andrew Warnock,^{1,*} Lillian M. Toomey,^{1,2,*} Alexander J. Wright,¹ Katherine Fisher,³ Yerim Won,³ Chidozie Anyaegbu,¹ and Melinda Fitzgerald^{1,2}

Abstract

Traumatic brain injury (TBI) and spinal cord injury (SCI) present a significant contribution to the global disease burden. White matter tracts are susceptible to both the physical forces of trauma and cascades of pathological secondary degeneration. Oligodendrocytes, the myelinating cells of the central nervous system (CNS), and their precursors are particularly vulnerable cell populations and their disruption results in a loss of white matter, dysmyelination, and poor myelin repair. White matter aberrations in TBI and SCI can be visualized *in vivo* using a number of magnetic resonance imaging (MRI)-based modalities. Recent advances in diffusion MRI allow researchers to investigate subtle abnormalities in white matter microstructure and connectivity, resting state networks, and metabolic perturbations associated with injury. Damage to oligodendroglia underlies white matter aberrations and occurs as a result of glutamate excitotoxicity, intracellular calcium ion (Ca^{2+}) overload, and oxidative damage to lipids, proteins, and DNA. Structural changes to myelin include myelin decompaction, loosening of myelin lamellae, and disruption to the node of Ranvier complex. Neuronal and functional loss accompany dysmyelination together with an increase in astro- and microgliosis. Remyelination is often partial, and more work is needed to understand deficits in remyelination post-injury to develop strategies to both protect and repair myelin and thereby preserve function. This review covers disruptions to oligodendrocyte function and white matter tract structure in the context of TBI and SCI, with an emphasis on Australian contributions in recognition of the International Neurotrauma Symposium held in Melbourne, Australia in 2020.

Keywords: dysmyelination; magnetic resonance imaging; oligodendrocytes; oligodendrocyte precursor cells; oxidative damage; white matter

Introduction

INJURY TO THE CENTRAL NERVOUS SYSTEM (CNS) is a global health concern, with 27 million individuals suffering from traumatic brain injury (TBI) and approximately one million new cases of spinal cord injury (SCI) per year.^{1,2} The main causes of TBI and SCI are falls, motor vehicle accidents, assault, and conflict-related blast injuries.^{1–3} Unsurprisingly, conflict-affected countries have the highest incidence rates of TBI and SCI.² The economic impact of CNS injury is significant in developed nations, with the lifetime burden of TBI costing up to \$4.8 million per person in severe cases and exceeding \$9 million for patients with tetraplegia following SCI.^{4,5} TBI has also been found to have an epidemiological association with Alzheimer's disease and Parkinson's disease, and thus may carry an even greater socioeconomic burden.^{6,7} Individuals at most risk for CNS injury are young adult males and the elderly.^{1,8}

TBI can be classified along a continuum of mild to severe, with a substantially worse prognosis in severe cases (30–40% mortality). However, the vast majority of TBI cases (70–90%) are mild (mTBI).⁹ Clinically, mTBI has been defined as ≤ 30 min loss of consciousness; ≤ 24 h of transient amnesia, confusion, or disorientation; and a Glasgow Coma Scale (GCS) score between 13 and 15.^{9,10} The acute symptoms of mTBI include vestibular and oculomotor dysregulation, sleep disturbances, and emotional dysregulation and tend to resolve within weeks of injury.^{11,12}

However, patients suffering from mTBI can have deficits in memory and executive function as well as cognitive impairment persisting for months to years post-injury.^{11,13,14} Patients exposed to repeated mTBI have a worse prognosis, with successive hits exacerbating inflammation and yielding significantly greater long-term cognitive deficits.¹⁵ Sports persons and military personnel are at particular risk for repeated injury, along with subsequent

¹Curtin Health Innovation Research Institute, Curtin University, Bentley, Western Australia, Australia.

²Perron Institute for Neurological and Translational Science, Nedlands, Western Australia, Australia.

³School of Human Sciences, The University of Western Australia, Perth, Western Australia, Australia.

*The first two authors contributed equally.

neurodegenerative conditions that may include chronic traumatic encephalopathy (CTE), sleep disorders, and neuroendocrine disease.^{3,16} Prognosis is substantially worse in severe TBI, with 38% mortality in younger patients,¹⁷ and 74% for patients older than 55 years.¹⁸ Persisting somatic symptoms years after injury include headaches, impaired balance, and motor disability. However somatic symptoms are less frequent than cognitive complaints, with 60–70% of patients presenting with memory and concentration deficits at 8-year follow-up.¹⁹ In pediatric severe TBI, long-term social development is perturbed compared with mTBI and healthy peers, leading to family dysfunction and poorer caregiver mental health.²⁰

Neurotrauma comprises two components: the primary or mechanical damage, and the biochemical cascade known as secondary degeneration.²¹ Secondary degeneration is a self-propagating series of metabolic and structural changes, associated with increased intracellular calcium ions (Ca²⁺), that results in oxidative stress and apoptotic cell death of initially undamaged tissue.²² Because the initial insult is often unavoidable, treatments for functional recovery after TBI focus heavily on limiting secondary injury.²³

Patients with TBI and SCI are treated on a symptom-based approach, with priority given to reducing intracranial pressure (ICP), hemorrhagic complications, and edema.¹ Cerebral edema following TBI remains the most significant predictor of adverse outcome, with altered cerebral perfusion pressures leading to secondary ischemic injury.²⁴ Utilization of ICP monitoring reduces mortality rates in patients with severe TBI.²⁵ Decompression surgeries to correct raised ICP have mixed success, with reduced disability observed in pediatric patients but worsened neurological outcomes reported in adult patients.²⁶ Despite evidence in animal models for the use of osmotic transport devices to reduce edema,²⁷ craniectomy is still required for implantation and the surgery procedure itself may exacerbate injury.²⁴ Barbiturates are administered to 20% of patients with severe TBI to reduce ICP in the absence of surgical intervention. However, despite reducing ICP in 69% of patients, European studies indicate that barbiturate administration has no significant effect on outcome at any stage following injury.²⁸ In patients suffering from mTBI, treatments have little efficacy and patient education on the likely resolution of symptoms and the value of adherence to follow-up is currently considered one of the most effective approaches in regards to ameliorating persistent symptoms.²⁹ Despite extensive neurotrauma research, there is no effective pharmacological treatment currently available for preservation of white matter following injury.³⁰

Diffuse axonal injury (DAI) is a form of CNS injury following TBI that typically manifests in around 10% of patients, but is far more common (44.9%) in cases of severe TBI.^{31,32} DAI frequently affects the corpus callosum, brainstem, and white/gray matter tissue interface. The Adams DAI injury classification utilizes both clinical presentation and identification of lesions to diagnose three grades of severity, ranging from microscopic white matter changes (Grade 1) to severe focal lesions (Grade 3).³¹ A subset of DAI and an injury often observed in animal models is traumatic axonal injury (TAI), wherein damaged axons are dispersed among normal appearing axons in white matter tracts.³³ White matter injury can also manifest as demyelination or dysmyelination, wherein myelin structure is perturbed.³⁴ White matter is particularly vulnerable to mechanical injury, with studies indicating a greater inflammatory response and secondary degeneration compared with gray and cortical tissues following TBI and SCI.^{35,36} White matter vulnerability following trauma has been extensively characterized with various magnetic resonance imaging (MRI) techniques, which provide insight into structural, metabolic, and connectivity changes in the brain.^{37–39} The cellular mechanisms behind this selective

vulnerability have been explored using animal models, with evidence suggesting that specific predilection of oligodendrocytes to oxidative damage underlies white matter injury.^{40–43} This review focuses on white matter injury by first providing background on oligodendroglia and myelin, assessing macroscopic structural changes to white matter following trauma and then describing what is known of the cellular changes in oligodendroglia following injury. The review describes white matter injury through the lens of oligodendrocyte damage, as these cells are particularly vulnerable and critical to myelin integrity. In celebration of the International Neurotrauma Symposium being held in Australia in 2020, the review features Australian research where appropriate.

Oligodendroglia

Collectively known as oligodendroglia, oligodendrocyte precursor cells (OPCs) and their progeny, oligodendrocytes, are one of the most abundant cell types in the CNS. In the adult rodent brain, OPCs and oligodendrocytes comprise approximately 5% and 20% of total brain cells, respectively.^{44,45} OPCs are the main proliferative cell type of the CNS and are typically identified by their expression of the neuron glia antigen-2 (NG2), platelet-derived growth factor receptor alpha (PDGFR α) and/or oligodendrocyte transcription factor 2 (Olig2).⁴⁶ Lineage tracing of embryonic OPC development in mammals has shown that 80% of OPCs in the CNS arise from neuroepithelial progenitor cells located in the motor neuron progenitor (pMN), ventral midline region of the brain and spinal cord.⁴⁷ Dorsally derived OPCs, which originate from radial glia, constitute the remaining 20%.⁴⁸

Once generated, OPCs proliferate as they migrate laterally, dorsally, and ventrally from the midline, distributing evenly to various white and gray matter regions of the CNS.⁴⁹ Upon reaching their destination, OPCs can undergo two additional stages of differentiation, initially becoming immature oligodendrocytes that express markers such as O4 and ectonucleotide pyrophosphatase/phosphodiesterase 6 (ENPP6).⁵⁰ Following this, oligodendrocytes mature progressively to express transcription factors and proteins including myelin regulatory factor (MyRF), NK6 homeobox 2 (NKX6.2), myelin basic protein (MBP), and the myelin proteolipid protein (PLP) that form myelin.⁵⁰ Myelin is a multi-layer lipid structure that ensheathes axons, thereby increasing the speed of electrical signal transmission across the CNS and providing structural support to neurons.^{51,52} OPCs and oligodendrocytes have historically been considered homogenous cell populations.⁵³ However, accumulating evidence suggests that oligodendroglia are heterogenous, comprising various subpopulations with diverse characteristics, gene transcription profiles, and functions.⁵⁰

Oligodendroglia diversity

OPCs derived from different embryonic regions produce oligodendrocytes that preferentially populate different regions across the adult CNS.⁵⁴ Indeed, oligodendrocytes originating from the ventral region of a developing mouse brain mainly populate the anterior commissure, pre-optic tract, and the lateral olfactory tract, whereas their dorsally derived counterparts predominantly localize to the cortex and corpus callosum.^{48,54} Further, dorsally and ventrally derived oligodendrocytes preferentially myelinate dorsal and ventral regions of the adult CNS, respectively,⁴⁸ despite having a similar ability to generate mature oligodendrocytes.⁵⁵ Characteristic differences also exist between OPCs in white and gray matter, with the former having a fourfold faster rate of proliferation and a higher proclivity for maturing into myelinating oligodendrocytes.^{44,52,56}

With respect to transcriptional heterogeneity, single-cell RNA profiling of oligodendroglia in different regions of the mouse adult CNS identified 12 transcriptionally distinct subpopulations, comprising OPCs, differentiation-committed OPCs, newly formed oligodendrocytes (NFOL), myelin-forming oligodendrocytes (MFOL), and mature oligodendrocytes (MOL).⁵⁷ In contrast to OPCs, differentiation-committed OPCs lack PDGFR α and NG2 but express genes such as sex-determining region y-box (SOX) 6, Neu4 and Bmp4 that keep oligodendrocytes undifferentiated. NFOL are distinguishable from MFOL by their expression of genes associated with early stages of differentiation (such as Tcf7l2 and contactin-associated-protein [Caspr]) and downregulation of genes involved in myelin formation, including myelin oligodendrocyte protein (MOG), proteolipid protein 1 (PLP1), and oplalin. MOL express genes associated with late oligodendrocyte differentiation and myelin formation simultaneously. Whereas OPCs and differentiation-committed OPCs were found to be transcriptionally homogenous, two populations of NFOL (NFOL1 and NFOL2) and MFOL (MFOL1 and MFOL2) and six populations of MOL (MOL1 to MOL6) with distinct gene expression profiles have been identified.⁵⁵

These subpopulations differed in spatial distribution within the regions of the CNS analyzed (i.e., amygdala, corpus callosum, cortex, zona incerta, dentate gyrus, striatum, dorsal horn, hippocampus, hypothalamus, and substantia nigra/ventral tegmental area; SN/VTA). NFOL1 and NFOL2 were found in every region investigated except the corpus callosum, where NFOL2 was absent. MOL subpopulations varied in region specificity, with some populations, such as MOL5, being present throughout the regions, whereas others were enriched in particular regions; for example, MOL2 were abundant in the spinal cord but almost absent in the brain.⁵⁵

Although the functional implications of the transcriptional heterogeneity and spatial preferences of oligodendroglia are still unclear, a recent study suggested that MOL subpopulations may fulfil distinct regenerative functions, as MOL2 were depleted at the site of SCI and, in contrast, MOL5/6 increased their contribution to lineage repopulation and thus remyelination.⁵⁵ The development of different oligodendroglia subpopulations and their progression from OPCs to mature myelinating oligodendrocytes is tightly regulated by complex interactions between several transcription, post-transcription, translation, and post-translation factors.

Molecular control of oligodendroglia development

During embryonic development of the CNS, distinct molecular mechanisms control the production of dorsally and ventrally derived OPCs. Sonic hedgehog (SHH) signaling induces ventral OPC specification by driving NKX6.1, NKX6.2, NKX2.2, and Olig2 transcription in neural stem cells.⁵⁸ By contrast, dorsal OPC generation is regulated in a SHH-independent manner by Dbx1 and Ascl1 transcription factors and fibroblast growth factor and bone morphogenetic protein (BMP) signaling.⁴⁸ As OPCs migrate from their birthplace to populate the CNS, a complex network of transcriptional and translational changes coordinate to mediate OPC differentiation. Calcineurin, a calcium-dependent phosphatase, was recently identified as a key initiator of OPC differentiation.⁵⁹ Triggered by an increase in intracellular Ca²⁺ levels, calcineurin dephosphorylates the nuclear factor of activated T cells, cytoplasmic 2 (NFATC2) protein, resulting in its activation. In turn, activated NFATC2 interacts with SOX 10 transcription factor to allow Olig2 and NKX2.2 co-expression, which is a prerequisite for OPC differentiation.^{60,61} Numerous transcription factors have been re-

ported to play a role in oligodendrocyte differentiation over the years, including nuclear receptors such as retinoid X receptors, vitamin D receptors, and peroxisome proliferator-activated receptors that contribute to oligodendrocyte formation and myelination.⁶² However, Olig2, SOX10, NKX2.2, zincfinger protein 24 (ZFP24), and MyRF are widely recognized as the main regulators of full oligodendrocyte differentiation and myelination.⁶² SOX10 plays a central role in this process, binding and directly activating several genes involved in oligodendrocyte maturation, including MyRF, which mediates terminal differentiation of immature premyelinating oligodendrocytes.^{60,61} In addition, SOX10 induces expression of NKX2.2 and Olig2, the latter of which activates ZFP24 to generate myelin transcripts.⁶⁰

Genes involved in lipid and cholesterol synthesis are also associated with myelination of mature oligodendrocytes.⁶³ The transcription factors sterol regulatory element binding proteins (SREBPs) have been reported to control the supply of fatty acids for myelin formation through the mammalian target of rapamycin (mTOR) signaling pathway.^{63,64}

Oligodendrocyte development can also be regulated epigenetically. At the OPC stage of lineage progression, the transcription factors and histone-modifying enzymes that respond to extracellular stimuli are mainly inhibitory, preventing differentiation.⁶⁵ Long noncoding RNAs (lncRNAs) are approximately 200 nucleotides long, and regulate gene expression but lack protein-coding potential.⁶⁶ Oligodendrocyte-specific lncRNAs such as lncOL1 and lnc158 can downregulate inhibitors of histone deacetylase activity and heterochromatin formation to promote expression of oligodendrocyte differentiation genes.^{67,68} MicroRNAs (miRNAs) are another subgroup of ncRNA that have been shown to regulate myelination in oligodendrocytes. They are short nucleotides (20–25 nucleotides long) generated by enzymatic cleavage of long transcripts.⁶⁹ Numerous miRNAs with a role in oligodendrocyte development have been identified and reviewed in the literature.⁶² Of note, a recent study showed that oligodendrocyte-specific miRNA-219 and miRNA-338 collaborate to downregulate negative regulators of oligodendrocyte myelination including the transcription factors SOX6 and ETS variant 5.⁷⁰ In addition, miRNA-219 represses expression of proteins such as PDGFR α that maintain OPCs in their progenitor state, thereby promoting oligodendrocyte differentiation.⁷⁰

After oligodendrocytes are generated, myelination is triggered by the downregulation of precursor proteins such as PDGFR α and transcription of MyRF and its target proteins, which are essential for myelin formation, including MBP, PLP1, myelin-associated glycoprotein (MAG), cyclic nucleotide phosphodiesterase (CNP), and MOG.⁷¹ Myelinating oligodendrocytes use their expanded network of processes to make stable contact with neighboring axons, enveloping segments of the neuron body with myelin sheaths.^{72,73} The structure and function of myelin is central to white matter composition and physiology as white matter is mainly made up of myelinated axons.

Myelin structure and function

Myelin has a very high lipid content, comprising phospholipids, galactolipids, and plasmalogens⁷⁴ that have an affinity for, and bind, myelin-specific proteins.⁷² The myelin sheath consists of compacted double bilayers of myelin, with myelin proteins, particularly MBP, acting as an adhesive between the bilayer membranes.⁷⁵ Once matured, myelin can consist of up to 160 layers of membranous, compacted lamellae that can be visualized as interperiodic lines using electron microscopy. This myelin sheath allows for saltatory conduction of action potentials and refined neural signaling,⁷⁶ with

myelinated axons conducting signals at a speed 20 to 100 times that of unmyelinated axons of similar diameter. It has long been known that the thickness of the myelin sheath is proportional to the diameter of the axon⁷⁷; however, it was recently discovered that both axonal diameter and the corresponding myelin thickness can vary along the length of a single axon.⁷⁸

Myelin has a highly segmented structure to facilitate neuronal signaling.⁷⁹ The myelin sheath produced by mature oligodendrocytes along an axon comprises multiple myelin segments, called internodes, separated by unmyelinated regions called nodes.⁸⁰ Oligodendrocytes myelinate axons of all diameters above $\sim 0.4 \mu\text{m}$,⁷² and a single oligodendrocyte can provide up to 50 internodes of myelin on different axons.⁸¹ The length of internodes and processes of an oligodendrocyte limits its ability to myelinate the same axon twice.⁵¹

The spaces between internodes are referred to as nodes of Ranvier.⁸² Localized at the node of Ranvier are specialized sodium channels that facilitate and propagate action potential signaling.⁸³ Thermosensitive and mechanosensitive K2P potassium channels (TREK-1 and TRAAK) are clustered at the nodes of Ranvier and are the principal drivers of rapid action potential repolarization.⁸⁴ Directly adjacent to the node is the paranode, which consists of loops of myelin lamellae that are anchored to axons via the paranodal junction, which comprises contactin, neurofascin 155, and Caspr.⁸⁵ The paranode has multi-faceted roles in maintaining saltatory conduction; including (1) segregating nodal sodium and juxtapanodal potassium channels; (2) stabilizing and attaching the myelin sheath to the axon to prevent myelin damage from stretch stressors; and (3) allowing only specific nutrients to diffuse into and out of the internodal peri-axonal space.⁸⁶ The juxtapanode, which lies between the paranode and the internode, contains a high concentration of voltage-gated potassium channels,⁸³ although the function of these specific to their juxtapanode location is currently unclear.⁸²

Neuron-oligodendrocyte interaction is integral for axonal integrity. In addition to their well-established function of ensuring fast action potential propagation and axonal insulation, oligodendrocytes supply neurons with nutrients.⁸⁷ Oligodendrocytes transfer energy metabolites including pyruvate and lactate to neurons, through cytoplasmic channels and monocarboxylate transporters, allowing fast adenosine tri-phosphate (ATP) synthesis. Further, oligodendrocytes contribute to the maintenance of axon integrity and survival of neurons by producing neuroprotective and trophic factors such as ciliary neurotrophic factor (CNTF), insulin-like growth factor-1 (IGF-1), and glial cell line-derived neurotrophic factor.⁸⁸ Indeed, partial ablation of oligodendrocytes causes axonal degeneration, even in the absence of widespread demyelination.⁸⁹ Loss of oligodendrocyte-specific proteins such as PLP and CNPase results in axonal swelling and degeneration, even if myelin structure remains normal.^{90,91} These seminal studies confirm that oligodendrocytes play multiple roles in neuronal maintenance. A further means of interaction is the release of trophic factor exosomes from oligodendrocytes, which are taken up by neurons and improve their metabolic activity.⁹² In addition, oligodendrocyte-neuron interactions are adaptive and plastic, with neural signaling promoting oligodendrogenesis and increased myelin thickness.⁹³⁻⁹⁶

Other than acting as a pool of progenitors for oligodendrocytes, OPCs play multi-faceted roles in the CNS. Ablation of OPCs results in excessive inflammation, suggesting OPCs may suppress neuroinflammation in a healthy system.⁹⁷ It has recently been discovered that peri-vascular OPCs wrap their processes around blood vessels in the brain and may be partly responsible for regulating and modulating the neurovascular unit.⁹⁸

Specifically, OPCs play a role in maintaining blood-brain barrier (BBB) integrity via communication with cerebral endothelial cells,⁹⁹ including via transforming growth factor (TGF)- β signaling. OPCs located around blood vessels secrete TGF- β 1, which activates the mitogen-activated protein kinase (MEK)/extracellular signal-regulated kinases (ERK) pathway in cerebral endothelial cells, increasing expression of tight-junction proteins and protecting BBB integrity.¹⁰⁰ In turn, cerebral endothelial cells have been found to release growth factors such as brain-derived neurotrophic factor and basic fibroblast growth factor, which promote the survival and proliferation of OPCs, both of which are significantly decreased following stroke.^{101,102} This trophic coupling between the cerebral endothelium and neighboring OPCs has been dubbed the oligovascular niche.¹⁰² *In vitro* studies have also shown that astrocytes can support OPCs, via MEK/ERK and PI3K/Akt signaling,¹⁰³ and OPCs and pericytes could potentially secrete factors to support each other.¹⁰⁴ Further, within the developing brain, OPCs secrete hypoxia-induced factor to promote angiogenesis of the CNS vasculature.¹⁰⁵

Etiology of White Matter Injury

The etiology of white matter injury is complex, heterogeneous, and its magnitude relates specifically to the nature of the primary injury.¹⁵ White matter pathology manifests in a wide array of symptoms and presentations depending on the nature and timing of injury as well as stage of disease progression.¹⁵ Generally, injury from the acute mechanical forces manifests as cortical focal lesions at the site of impact and the contrecoup region. More subtly, diffuse white matter injury can include myelin decompaction or unfurling of the myelin sheath, and TAI. Wallerian degeneration can take place following injury: an immune-mediated response where primary discrete axonal injury spreads distally leading to irreversible fragmentation distant from the injury site.^{106,107} Oligodendrocytes are unable to clear myelin debris, leading to a prolonged and gradual reduction of myelin and long-term deposition of a glial scar.¹⁰⁸

In TBI, injury also results from both linear and rotational acceleration and impact deceleration forces on the brain. The brain's complex gyrencephalic structure and inhomogeneous tissue properties contribute to a non-linear dynamical behavior of deep white matter during trauma. Consequently, deep white matter tracts are particularly susceptible to injury, including: the corpus callosum, brainstem, thalamus, hippocampus, and the white/gray matter tissue interface.¹⁰⁹ Rotational direction-specific vulnerabilities exist due to the arrangement of fibers in these white matter tracts of the brain,¹¹⁰ and as a result of the anisotropic effects of axonal arrangement, deep white matter tracts are particularly susceptible to TAI.¹⁰⁹

Resultant insults include mechanical damage from shearing, tearing, or stretching of axons, neurons, glia, and blood vessels.^{15,107} Tearing of axonal tau-microtubule bonds by external mechanical forces damages the cytoskeleton, affecting axonal transport, ion flux, and initiating secondary axonal degeneration.¹¹¹ The initial injury may result in additional pathologies such as hemorrhage or cerebral edema; however, these complications only occur in approximately 10% of mTBI cases and could be considered "complicated" mTBI.¹ In SCI, raised intrathecal pressure due to edema or hemorrhage exacerbates the effect of secondary degeneration leading to deleterious functional outcomes.¹¹² Axons adjacent to the injury site are vulnerable to secondary damage due to the release of toxic factors by injured neurons and glia,

associated with an inflammatory immune response.^{113,114} The inflammatory immune response is greater in white matter compared with gray matter in both the brain and spinal cord, indicating a differential degree of secondary degeneration following injury.³⁵ Secondary degeneration is characterized by myriad reactive metabolic pathways, including astrocyte reactivity, microglial and macrophage activation and infiltration, glutamate and ATP induced excitotoxicity, intracellular Ca²⁺ overload, mitochondrial dysfunction, oxidative stress, and apoptotic cell death and dysmyelination.²² Oligodendrocyte and OPCs are particularly vulnerable to these degenerative processes, and their death is associated with chronic dysmyelination after injury;³⁴ this phenomenon will be addressed in greater detail in sections below.

Models of CNS injury

For the mechanisms of white matter degeneration following CNS injury to be studied, it is important to utilize reliable animal models of injury. Animal models can be employed to replicate human TBI and SCI, and experimental models can be amended to study specific facets of heterogeneous pathologies, allowing mechanisms to be studied in a rigorous and controlled manner.^{115,116} Rodent models of injury are typically employed by researchers as they are cost and time effective; however, many translational challenges exist due to inter-species differences in neurometabolism, lifespan, and anatomy.¹¹⁶ Animal models of SCI include spinal contusion and compression, which best simulate the biomechanics and pathology of human injury.¹¹⁵ Most SCI models use a thoracic injury site as opposed to cervical, as the thoracic SCI model tends to be more reproducible, has a lower risk of mortality, and permits the study of secondary white matter deficits.¹¹⁵ Prominent models of TBI include: blast injury models, fluid-percussion injury (FPI), controlled cortical impact (CCI) models, and closed-head weight-drop models.^{117–119} Additionally, TAI can be induced in mice using closed-skull stereotaxic impactors delivering single or repeated mTBI to study microstructural changes with electron microscopy and observe long-term behavioral changes.^{120–122}

Although all of the aforementioned models robustly elicit an inflammatory response and white matter injury, FPI and CCI models (which require the animal to be stationary) fail to mimic the human head kinematics following TBI.^{15,116} The closed-head impact model of engineered rotational acceleration (CHIMERA) is a recent innovation that allows highly reproducible and accurate mTBI delivery.¹²³ The CHIMERA model induces DAI, behavioral changes, and energy dose-dependent increases in axonal damage.¹²⁴ Closed-head weight-drop models have also been employed in recent years, as they approximate the angular and rotational forces of human TBI and allow study of repeated TBI.^{15,116,125} White matter reductions and demyelination are observed in the corpus callosum in the closed-head weight-drop model; therefore it remains an appropriate method to replicate human pathology.¹⁵ A caveat of the rodent model is that there is proportionally less cerebrospinal fluid (CSF) as compared with humans; therefore rotational effects are not necessarily comparable.^{126,127} Angular acceleration forces are reduced in rodent brains due to their small physical size; therefore white matter injury may be reduced and less clinically relevant. Large animals have a higher white-to-gray matter ratio due to their gyrencephalic structure, and therefore are better suited for translational validation of novel discoveries in rodent models.¹²⁷

In many models of neurotrauma, it is challenging to distinguish between primary and secondary damage, as there is often no clearly defined margin between tissue damaged by the initial insult and

spared tissue.¹²⁸ Partial optic nerve transection is an established and useful model for investigating secondary degeneration of a white matter tract that features a primary injury of a penetrating nature that does not mechanically damage adjacent tissue.¹²⁹ In the model, the right dorsal optic nerve is partially transected, which allows for spatial separation between primary and secondary injuries.¹²⁹ The partial optic nerve transection model results in transient disruption of the BBB, which can be a useful feature for proof of principle investigations into secondary degeneration of white matter with a transiently open BBB.¹³⁰ The optic nerve stretch model allows for the study of wallerian degeneration often seen in CTE.¹³¹ The stretch model and the transection model differ as the stretch model analyzes distal injured axons, whereas in the partial transection model uninjured axons ventral to the injury site are analyzed for secondary degeneration.

Imaging to Detect Changes to White Matter

Computerized tomography (CT) scans are the primary clinical diagnostic tool employed following TBI and SCI,^{132,133} and total emergency room usage of CT has increased by 330% in recent years.¹³⁴ Although CT scans are critical and effective for detecting macroscopic lesions, edema, and hemorrhage, 90% of scans are negative for clinically relevant brain injury.¹³⁵ CT scans therefore lack the sensitivity to detect the more subtle, diffuse changes that occur following TBI such as TAI. CT scans have robust efficacy in detecting bone fractures, which are a correlate of worse outcomes following severe TBI.¹³⁶ Micro CT also provides a promising avenue to study microstructural changes in trabeculae of rodent skulls following TBI, allowing inferences to be made in regards to damage from repeated TBI.¹³⁷ Although CT scans following SCI have robust efficacy in detecting fractures, early collar removal following negative CT scans may lead to further injury,¹³⁸ and follow-up magnetic resonance imaging (MRI) scans are recommended in obtunded blunt trauma patients.¹³⁹ MRI has significantly greater sensitivity in detecting white matter lesions following mTBI compared with CT; therefore it remains the imaging modality of choice when researching structural correlates of clinical outcomes.^{140,141}

Detecting lesions and volume changes

MRI is a reliable tool that can provide high-resolution images allowing for the detection of white matter lesions, detected as changes in iron and fluids due to hemorrhages and swelling in the brain. In a blinded study in the acute phase of TBI or minor stroke (<48 h post-injury), clinicians were able to accurately discriminate TBI from acute minor stroke: MRI-facilitated detection of vascular abnormalities in 54% of patients with TBI, whereas only 14% of patients had positive vascular findings using CT.¹⁴² Hyperintense white matter lesions can be detected following TBI using T2-weighted fluid-attenuated inversion recovery (FLAIR) sequences. FLAIR nullifies body fluids during acquisition, therefore suppressing CSF effects on image contrast and allowing peri-ventricular hyperintensities and meningeal focal enhancements common in TBI to be detected with greater accuracy.^{142,143} Presentations of lesions following TBI are heterogeneous. Although the number and volume of lesions correlates with adverse outcomes,¹⁴⁴ the presence of white matter hyperintensities and microhemorrhagic lesions in mTBI are uncommon and do not necessarily predict persisting symptoms.^{145,146}

However, in cases of moderate and severe TBI, microhemorrhages are an independent predictor of disability (GCS-extended

score ≤ 6 ; odds ratio = 2.5) in the absence of axonal injury. Therefore, caution should be taken when interpreting lesion data, as microhemorrhages have a significant role in TBI.¹⁴⁷ Additionally, T2-weighted MRI may be limited in its utility as lesions do not often appear in the acute phase following mTBI, but are more often detected at 6 month follow-up in cases of persisting symptoms.¹⁴⁸ However, in cases of severe TBI, lesions referred to by the authors as TAI in FLAIR sequences in the corpus callosum and the brainstem are predictors of reduced functional outcomes at 12 month follow-up.¹⁴⁹ Nevertheless, lesion presence alone does not provide sufficient prognostic clinical value.

Brain volume changes provide insight into gross structural changes to white matter in the brain. Reductions in cortical thickness provide an indication of widespread atrophy in patients with severe TBI and these changes are associated with deficits in declarative memory and auditory verbal learning.¹⁵⁰ Cortical thinning is exacerbated in patients with repeated mTBI and veterans exposed to blast injuries following mTBI.^{151,152} Despite cortical thickness reductions often taking place in tandem with reductions in white matter integrity,¹⁵⁰ changes to white matter integrity can take place independent of cortical thinning.¹⁵³ Widespread atrophy is also inferred by total brain volume reductions, with patients with severe TBI having on average a 4% reduction in brain volume at 12 months post-injury, indicative of long-term TAI.¹⁵⁴ Additionally, atrophy is greatest in white matter compared with gray matter.^{155,156} Regional brain volume reductions have been observed in the white matter of the anterior cingulate,¹⁵⁶ brainstem, thalamus, and corpus callosum.¹⁵⁴ In SCI, white matter volume loss is prevalent in the corticospinal tract, although gray matter atrophy appears to be more robustly evident compared with healthy controls.¹⁵⁷ Additionally, ventricular enlargement and CSF volume increases may serve as a surrogate marker of ascending neurodegeneration following SCI.¹⁵⁸ Taken together, it is clear that brain volume changes provide clinically relevant insight into longitudinal atrophy of both white and gray matter.

DTI connectivity changes

White matter fasciculi can be accurately mapped and characterized using diffusion tensor imaging (DTI) techniques. DTI utilizes the anisotropic nature of water displacement in white matter to derive values such as fractional anisotropy (FA), which characterizes diffusion anisotropy differences between intensity limits of zero and one. In highly organized white matter tracts, FA values are high (~ 0.8) due to diffusion approaching unity along white matter tracts and diffusion in all directions perpendicular to tracts. In gray matter, FA values generally vary (~ 0.10 – 0.25) depending on the structure of the region concerned.¹⁵⁹ In CSF, FA values approach zero as water diffusivity is equal in all directions.¹⁶⁰ Mean diffusivity (MD) is another common measurement and quantifies mean diffusion in each direction as opposed to FA, which quantifies the total magnitude of diffusion along axonal fibers. FA is calculated as a ratio of axial diffusivity (AD) and radial diffusivity (RD), which describe the magnitude of water diffusion parallel and perpendicular to the tract, respectively.¹⁶¹ In cervical SCI, mean FA values are reduced at the site of injury and mean MD values are increased, compared with healthy controls. The decrease in FA value may reflect a decreased degree of myelination in the tracts or increased cell density, whereas higher MD may be indicative of white matter tract disorganization or fluid edema.¹⁶²

Diffusion basis spectrum imaging (DBSI) is a novel technique that shows promise in elucidating underlying pathology behind

diffusion metric changes.¹⁶³ DBSI allows quantification of white matter tract density, as well as residual axon and myelin integrity and axonal volume while accounting for vasogenic edema. The DBSI technique has been validated in a traumatic SCI study in mice, wherein co-existing pathologies were identified non-invasively and then correlated with post-mortem histology markers.¹⁶³ Clinically, a decrease in FA values is also seen at the thoracic level below the injury site,¹⁶⁴ and persists in ascending tracts into cerebral white matter tracts, with reduced FA and increased MD in the corpus callosum, corona radiata, cingulate gyrus, and the thalamic radiation years post-injury.¹⁶⁵ White matter disruption is worse in patients with cervical compared with thoracic injury, and time since injury is negatively correlated with FA values in some brain regions.¹⁶⁵ These DTI changes are consistent with wallerian degeneration, with discrete white matter injury in the spinal cord causing demyelination and structural disorganization distal to the injury site.^{106,164,165}

Unlike SCI, DTI findings from TBI studies lack clinical consensus and are far more heterogeneous.¹⁶¹ An extensive review by Asken and colleagues¹⁶⁶ postulates that variability in the changes in FA and MD values after injury are attributable to different characteristics of the study populations and comparative control groups.^{166,167} In the acute phase of mTBI, FA values increase and MD values decrease in the days following injury. Specifically, FA values have been seen to increase in the corpus callosum,¹⁶⁸ fimbria, and the internal capsule.¹⁶⁹ These FA and MD changes are believed to be due to axonal cytotoxic edema in the initial phases of white matter degeneration following injury.^{168–170}

Axonal swelling can occur due to interruption of axonal transport and subsequent accumulation of transported materials, or it can manifest in axonal bulbs following complete axonal disconnection.¹⁷¹ In a rodent CCI study, acutely increased FA in the genu corpus callosum was accompanied by decreased RD and MD, with no changes in AD observed. The changes in FA observed using DTI were unable to be detected by anatomical MRI or hematoxylin and eosin staining.¹⁶⁸ FA decreases in the contralateral cortex, thalamus, and hippocampus at 7 days have also been observed in a recent Australian study following CCI in rodents, validated by cross-sectional histopathology.¹⁷² Accompanying acute injury in rodents, increased FA values have been associated with increased expression of tumor necrosis factor α (TNF- α) and a reduction in MBP staining. This supports the hypothesis that increased FA values immediately following injury are a result of cytotoxic processes affecting myelin integrity and therefore diffusivity along white matter tracts.¹⁶⁹ Wright and associates recently observed similar changes in DTI measures associated with changes to telomere length. Repeated mTBI resulted in reduced telomere lengths and these changes were associated with reductions in AD and RD.¹⁷³

An inverse pattern is observed in mTBI as time passes, wherein FA values decrease and MD values increase.^{174,175} Multiple injuries in animal models exacerbate changes in diffusivity metrics and are also associated with hypoconnectivity in the hippocampus, brainstem, and cerebellum. Interestingly, rats exposed to a single mTBI display hyperconnectivity between brain regions, suggesting an adaptive response to injury.¹⁷⁵ A similar finding was observed following single CCI, wherein the brain was connectively promiscuous post-injury in the thalamus and cortex, perhaps reflecting circuit reorganization.¹⁷⁶ Following repeated mTBI in mice, no changes in FA are observed acutely, but after 6 weeks FA is significantly reduced in the corpus callosum compared with sham animals. This corpus callosum FA reduction occurred in tandem with microglial activation detected by post-mortem immunohistochemistry, with activation peaking at 7 days post-injury.¹⁷⁴

Whereas DTI can be used to detect chronic white matter aberrations, the many changes in the tissue and cells within voxels may contribute to changes in DTI measures in ways not yet fully understood. The temporal inversion of FA values is reflected in the clinical findings of DTI. A longitudinal study of DTI metrics found FA values decreased from the acute phase following mTBI (<7 day) to the subacute phase (8 days to rehabilitation discharge). The variability of FA values in the acute phase means that DTI is more likely to be useful as a prognostic tool subacutely.¹⁷⁷ MD values are higher in athletes who have received multiple concussions compared with those who have had single or no concussions, in the absence of any major neuroanatomical differences.¹⁷⁸

In severe chronic TBI patients, increased FA values in the splenium of the corpus callosum have been associated with better performance in social inference tests. Despite a number of gray matter abnormalities, the changes in the corpus callosum were those most implicated in functional deficits in these TBI patients.¹⁷⁹ In combat veterans who suffered TBI while deployed, those with higher FA values and lower MD values have a greater likelihood of returning to work post-deployment.¹⁸⁰ In terms of long-term prognosis, higher FA values in the corpus callosum in the acute phase following injury are associated with higher disability rating scores. Whereas in the subacute period, higher FA values in the splenium correlate with lower disability rating scores.¹⁷⁷

Some brain regions, such as the internal capsule and the fronto-occipital fasciculus, show recovery from a transient reduction in FA values. Increased FA values at 1 month follow-up are positively associated with better performance on cognitive information processing speed at initial assessment. However, continued loss of integrity is observed in the corpus callosum, forceps major, and anterior corona radiata at 3 months, and these regions may serve as an objective biomarker of pathology that can predict persisting post-concussion symptoms (PPCS).¹⁸¹ Hiraad and co-workers¹⁸² used accelerometers and DTI imaging on college football players and tracked head impacts across a competitive season in conjunction with an mTBI cohort of patients. FA in the midbrain was reduced post-season compared with pre-season, as was the case for the right midbrain in the mTBI patients. Reductions in midbrain white matter integrity in the football players were related to the amount of rotational acceleration sustained as opposed to linear acceleration,¹⁸² and this is consistent with previous biomechanical models of TBI.^{109,110} Serum-based tau, a marker of axonal injury and BBB integrity, was inversely correlated with midbrain FA values in the mTBI patients.¹⁸²

FA and MD metrics can also be used to add structural insight to neuropsychological outcomes in TBI patients. In a recent Australian study,¹⁸³ patients with severe TBI had widespread white matter pathology in the corpus callosum, longitudinal fasciculi, corticospinal, brainstem, and cerebellar tracts. Diffuse white matter integrity disruption in these patients, particularly changes in the thalamus and fornix, was associated with social information processing deficits.¹⁸³ Diffusion tensor techniques can also be applied to derive individual patient structural connectomes, in which cognitive associations can be explored. Mishra and associates¹⁸⁴ created a structural connectome using average FA values and brain atlas-defined nodes to assess differences between cognitively impaired and non-impaired professional fighters. White matter reorganization in the hippocampus, precuneus, and insula was detected due to repeated head injury in fighters exhibiting cognitive decline.¹⁸⁴ Recent work¹⁸⁵ in white matter plasticity used DTI techniques as well as myelin water fraction and longitudinal relaxation rate R_1 to assess subtle changes in myelination and connectivity in healthy subjects

following working memory training. The study highlighted the sensitivity of the R_1 measure in detecting myelin remodeling following working memory training, which occurred in conjunction with changes in FA and RD parameters.¹⁸⁵ Given R_1 values may be more specific in detecting changes in oligodendrocytes.¹⁸⁶ Future studies could employ this measure to assess white matter regeneration following cognitive rehabilitation in TBI patients.

Novel methods for increased sensitivity

The diffusion tensor model faces a number of limitations that restrict its sensitivity in detecting microstructural changes in white matter pathology. One of these limitations lies in the fact that DTI assumes a single fiber orientation and is confounded at regions of "crossing" fibers. This can be overcome by analyzing apparent fiber density (AFD), utilizing a DWI post-processing technique known as constrained spherical deconvolution. In a recent rodent FPI study conducted by Wright and colleagues, DTI and AFD measures were both able to detect white matter changes in the corpus callosum: a uniformly orientated tract. However, DTI was unable to detect any changes in the corticospinal tract, whereas there was an observed reduction in AFD in the same animals.¹⁶⁷ Tract weighted imaging (TWI) is a novel technique that utilizes constrained spherical deconvolution to better characterize the fiber orientation distribution in regions of interest, allowing characterization of tract density, curvature, and length as additional measures that may be more sensitive to white matter pathology.¹⁸⁷ Using TWI in an awake closed-head model of injury, Australian researchers¹⁸⁸ found that tract density is significantly increased in the fimbria and contralateral external capsule following injury. Additionally, TWI detected changes between sham and TBI group at day 1 post-injury, whereas DTI metrics only detected changes at 7 days.¹⁸⁸

Another inherent limitation of DTI is that it applies a Gaussian distribution model to tissue using a normative distribution. In reality, the complexity of brain tissue means that water diffusion deviates significantly from this pattern.¹⁸⁹ As an example, when oligodendrocyte apoptosis occurs in combination with vasogenic edema, the result is enhanced diffusivity across axons. This pathological state results in a discrepancy between RD and histological outcomes.¹⁹⁰

Diffusion kurtosis imaging (DKI) is a non-Gaussian distribution measure that accounts for tissue heterogeneity and provides improved characterization of white matter integrity. Common DKI parameters include: mean kurtosis (MK) and mean kurtosis tensor (MKT), which reflect the average diffusion in all directions; and axial kurtosis (AK) and radial kurtosis (RK), which quantify diffusion along the axial or radial direction of the diffusion ellipsoid, respectively.¹⁸⁹ In a rat CCI study utilizing both DTI and DKI techniques *in vivo*, animals were imaged acutely (>2h) and subacutely (7 days) post-injury.¹⁹¹ In the acute phase, both DTI and DKI parameters detected differences in the injury versus sham animals. FA increased in the hippocampus and the ipsilateral cortex and MD decreased across all regions. However, at subacute testing most DTI changes had returned to baseline with the exception being a reduction in FA in the ipsilateral cortex. DKI measures were able to distinguish changes in both white and gray matter microstructure at the subacute period, with an increase in MK observed.¹⁹¹ In addition to being more sensitive than DTI metrics in this study, kurtosis abnormalities scaled inversely with distance from impact site, therefore providing some discriminatory power to injury severity.¹⁹¹ However, at longer time-points post-injury (42 days), it was found that DKI metrics did not provide additional sensitivity for detection of abnormalities in the corpus callosum compared with DTI metrics.¹⁷⁴

Similar to DTI metrics, a time-dependent biphasic response has been observed in MK values following injury, whereby MK values initially decrease following injury and later reverse 7 days following injury. This biphasic change in MK values is believed to represent a shift from cytotoxic to vasogenic edema.¹⁵⁹ Another confounding factor pertains to astrocyte activity following injury, as increases in FA can be falsely interpreted as remyelinating processes when in reality they reflect glial scar formation.¹⁹² Increases in MK have been associated with astrogliosis,¹⁹¹ and occur in tandem with higher density of microglia and astrocytes.¹⁹³ A recent Australian study¹⁹⁴ used a longitudinal rodent weight-drop design and assessed both DTI and DKI metrics. The study commended the sensitivity of both diffusion metrics; however, it highlighted that kurtosis measures were highly sensitive to changes in astrocyte markers at 3 months. Additionally, axial measures were not changed to the same degree as RK and RD metrics in the injury group. Therefore it is postulated that axonal integrity is maintained and the radial diffusivity changes may reflect cellular aggregations from glia, although these changes may also be due to demyelination.¹⁹⁴ However, a recent clinical mTBI study found that AK values were positively correlated with working memory deficits, indicating axonal perturbations.¹⁹⁵ Previous rodent work has also found correlations between DKI parameters and neuron loss, microglia activation, and myelin disruption. In addition, changes in MK values in the ipsilateral cortex and hippocampus are associated with deficits in cognitive function.¹⁹⁶

Advances in diffusion imaging techniques allow neuronal projections, known as neurites, to be imaged *in vivo*. The model used is known as neurite orientation dispersion and density imaging (NODDI), and estimates the microstructural complexity including dendrites and axons.¹⁹⁷ When NODDI is employed in conjunction with traditional DTI metrics, greater insight into the pathophysiological underpinnings of injury can be achieved. Repeated mTBI in martial arts athletes results in decreased FA, an increase in orientation dispersion index (ODI), and increased intracellular volume fraction (V_{IC}), therefore inferring a potential role of edema in traumatic injury.¹⁹⁸ In concussed athletes, increased FA and decreased MD was detected alongside increased V_{IC} and decreased ODI. The increase in neurite density and coherence of neurites in the white matter of sports-concussed athletes likely reflect an adaptive reparative response to injury, especially given the lack of functional impairment present.¹⁹⁹ In contrast, in a study conducted in athletes who suffered mTBI, reduced FA occurred concurrently with a reduction in V_{IC} , in the absence of any significant changes in ODI at 7 days post-injury. These changes may be associated with glial-mediated edema and the initiation of a neuroinflammatory response to injury. In athletes scanned after being given medical clearance to return to play, ODI was increased in individuals with elevated symptoms at initial consultation. Therefore, the change in neurite geometry may reflect a longitudinal response to injury, and may be a sensitive measure of clinically asymptomatic neuroplastic changes in the brain.²⁰⁰ A study comparing patients with mTBI with orthopedic trauma controls observed decreased FA and increased MD in anterior tracts at 2 weeks post-injury, with a concomitant elevated free water fraction (FISO) in white matter regions indicative of vasogenic edema. However, at 6-month follow-up, no significant differences were detected in DTI metrics, despite a longitudinal decrease in white matter neurite density on NODDI. Additionally, associations were found between ODI and FISO and rate and magnitude of functional improvement within the mTBI group.²⁰¹ In summary, NODDI augments the sensitivity of existing DTI metrics and further studies are warranted to explore its prognostic and research value.

Resting state and connectivity changes

Patients suffering trauma also have changes to functional connectivity within the brain that can be mapped and quantified using MRI-driven techniques analyzing the default mode network (DMN). The DMN spans the hippocampus, precuneus, cingulum, inferior parietal lobe, and the orbital frontal, medial prefrontal, lateral temporal, lateral parietal, cingulate, and parahippocampal cortices^{202–204} and is activated during rest or self-reflective periods but suppressed during attention or goal-oriented tasks.^{202,205,206} The DMN is suspected to be involved in integrating multi-modal information and evaluating the cognitive and homeostatic environment, and is connected by white matter tracts across the brain. However, its exact function is still unknown.²⁰³ The DMN is frequently used to characterize resting-state connectivity changes in neurological disorders, but has only recently been applied to examining functional outcomes of mTBI.^{205,207} A reduction in resting state functional connectivity (rs-FC) within the DMN during the acute stage of mTBI injury has been demonstrated,²⁰² consistent with significant reductions in rs-FC in more severe TBI populations shortly after injury.^{208,209}

Considerable variability exists in DMN rs-FC reductions in patients with mTBI during the subacute stage of injury across studies. These inconsistencies may be attributed to differing times of observation post-injury, heterogeneous inclusion criteria, and the innate differences in patients' rate of recovery.²¹⁰ Patients with mTBI have rs-FC within the DMN at the chronic stage of injury.^{202,210,211} Interestingly, patients with mTBI at the chronic stage have increased rs-FC between the DMN and the task positive network (TPN).²⁰² Additionally, there is increased rs-FC between the TPN and the medial prefrontal cortex (MPFC) and dorsal posterior cingulate cortex (dPCC) nodes of the DMN, with concomitant increases in rs-FC between the DMN and the left dorso-lateral prefrontal cortex (L-DLPFC).²⁰² An increase in rs-FC between the DMN and dorsal anterior cingulate cortex (ACC) and bilateral insula has been observed at both chronic²⁰² and subacute stages.²¹² The bilateral insula is part of the salience network (SN),²¹³ and is sometimes co-activated with the TPN.²¹⁴ This increased connectivity between the DMN and regions of the SN led to suggestions that there is a demand for the SN to modulate the activity of the disrupted DMN following mTBI,²⁰² and that the increased modulation is a possible cause of increased cognitive fatigue seen in patients with mTBI.²¹⁵ The changes in functional connectivity were found to persist for up to 6 months post-injury and likely reflect DAI in white matter.²⁰²

Cerebral blood flow (CBF) in the brain is also altered upon mTBI.²⁰² Imbalances between resting arterial spin labeling (ASL) perfusion within the DMN and TPN are found at the chronic stage,²⁰² leading to suggestions that recovery from mTBI is a highly dynamic mechanism that involves CBF changes to balance out the basal activity of the two networks.²⁰² The altered CBF allocation to the two networks may also contribute to the cognitive fatigue,²¹⁵ and attentional deficits seen in patients with mTBI.²¹⁶

Patients suffering from persistent post-concussive symptoms (PPCS) fail to maintain innate balance between perfusion to the DMN and TPN.²⁰² An increase in resting perfusion in the TPN nodes is seen in patients suffering from PPCS,²⁰² and patients with PPCS were unable to uphold network perfusion patterns comparably with non-PPCS mTBI and control participants. Therefore, it has been suggested that during the initial stages of injury, it may be possible to use network perfusion patterns to determine which patients will develop PPCS.²⁰² However, the relevant data involved two groups of patients with mTBI of varying ages and changes in

perfusion may be due to the age difference,²⁰² further confounded by the fact that older patients are at greater risk for developing PPCS.²¹⁷

Following mTBI, common complaints include cognitive fatigue, headaches, and emotional and vestibular dysregulation.^{11,12,218} Children may also experience mood changes, sleeping difficulties, and concentration and memory issues.²¹⁹ Despite this, neuropsychological tests rarely detect differences in objective performance on working memory tasks in children after mTBI.²¹⁸ Children and adolescents represent the population that is most at risk for incurring an mTBI,²²⁰ hence the Australian Barlow group including the KidStim Laboratory, focus on mTBI in children.²¹⁸ Working memory is described by the Barlow group as the ability to hold recent information and transiently manage it for goal-directed behaviors.²¹⁸ Working memory-related cortical activation is decreased in children who have not recovered from mTBI at 1 month post-injury.²¹⁸ Additionally, similar regions of cortical hypoactivation have been found in children 41 days post-injury.²²¹ However, other studies have demonstrated hyperactivation in cortical areas.^{222–225} These inconsistent findings are possibly the result of heterogeneous memory tasks, inconsistent inclusion criteria, and differing age ranges between studies.²¹⁸ Although the Barlow group found there to be similar working memory-related cortical activation and neurocognition in patients with mTBI and healthy controls, children showing signs of PPCS demonstrated greater inhibition of the DMN and hypoactivation in the DLPFC during the working memory task, compared with children showing no sign of PPCS post-injury.²¹⁸ Despite these changes, no performance differences were detected.²¹⁸ Resting-state data therefore provide an insight into internodal activity and a useful platform to characterize changes post-injury; however, more research is needed to achieve accurate prognostic value.

Metabolic changes

In addition to structural and functional aberrations in white matter following injury, a number of metabolic changes reflective of gliosis or pathology can be detected using magnetic resonance spectroscopy techniques. Magnetic resonance spectroscopy has been used to detect reductions in ratios of *N*-acetylaspartic acid (NAA), choline (Cho), and creatine (Cr) in the genu of the corpus callosum following mTBI in athletes regardless of number of hits.³⁹ Athletes recovering from their first mTBI showed the greatest alteration in NAA/Cho and NAA/Cr ratios, perhaps indicative of a tolerance effect with further hits.³⁹ Decreases in NAA/Cr ratios have been observed in the thalamus in mTBI patients with impaired cognitive function, and an increase in thalamic Cho/Cr ratio was evident in mTBI patients with self-reported sensory symptoms.²²⁶ However, the NAA/Cho and NAA/Cr ratios do not differ with the severity of symptoms.²²⁷ A substantial literature explores the relationship between metabolite changes in the brain following TBI, including in white matter. These have been extensively reviewed,^{228,229} and will not be covered further here.

Quantitative susceptibility mapping (QSM) is a novel imaging technique that allows *in vivo* measurement of magnetic biomarkers (iron) and high concentrations of Ca²⁺.^{230,231} The technique has displayed sensitivity in detecting changes in neurodegenerative disease, such as Parkinson's disease²³⁰ and Alzheimer's disease,²³² and has been used in TBI research.^{233,234} Iron deposition in the cortex has been associated with cognitive decline, and is believed to induce oxidative stress and a pro-inflammatory response.²³² Abnormal accumulation of iron in white matter can be caused as a result of microhemorrhage following TBI,²³³ and in patients with severe TBI, iron oxide targeting P-selectin microparticles can be

used to identify endothelial activation in the cortex and hippocampus.²³⁵ In a susceptibility-weighted imaging study in patients with chronic mTBI, abnormal iron depositions were detected in the hippocampus, thalamus, and the splenium of the corpus callosum at 6 months post-injury. Additionally, iron accumulations in the right substantia nigra are positively associated with cognitive impairments in patients with mTBI.²³⁶

More recently, QSM has been utilized in a FPI rodent model to visualize thalamic Ca²⁺ influx in severe TBI, repeated mTBI, and single mTBI. No calcifications were detected 1 week post-injury; however, at 4 weeks calcifications were detected in all injury severities. The repeated mTBI group had the largest calcification volumes, a higher prevalence of calcifications compared with control and sham animals, and calcium increases in repeated hits were associated with neurological disability.²³⁴ Another novel technique is flortaucipir positron emission tomography (PET), which allows the study of tau pathology in relation to TAI. Flortaucipir PET allows for *in vivo* detection of abnormal tau in neurofibrillary tangles, which traditionally has been used as a marker of pathology in post-mortem Alzheimer's disease tissue. In patients who received a single moderate TBI, flortaucipir binding was increased many years after injury compared with healthy controls. This increase in flortaucipir binding was associated with the presence of TAI, and with CSF markers of neurodegeneration T-tau and P-tau.²³⁷ Future analysis of biomarkers and metabolites may provide insight into subtle changes in white matter in patients with TBI.

Detection of Cell-Specific White Matter Pathologies

Glutamate excitotoxicity and changes in calcium ions and reactive species

In addition to the primary mechanical insult, white matter injury induces a cascade of molecular changes within neuroglia that can be detected using biochemical and imaging based methods. Glutamate-induced excitotoxicity is a prolonged or excessive exposure to glutamate that ultimately results in neuronal and glial cell death.^{238,239} In normal physiology, glutamate is rapidly removed from synapses by glutamic acid reuptake systems on glial cells and neurons.²⁴⁰ Reuptake prevents a buildup of glutamate within synapses, sustaining glutamate levels at approximately 0.6 μmol/L.²⁴¹ However, after neurotrauma the concentration of extracellular glutamate can increase to up to 5 μmol/L.²⁴¹ Following TBI in humans, the levels of glutamate in the CSF are increased, and remain higher 1 week following injury, with these levels correlated with injury severity.²⁴² Further, by 2 days following a moderate midline FPI, tonic glutamate levels are increased by 178% in the striatum and 256% in the dentate gyrus.²⁴³

Glutamate excitotoxicity has also been implicated in white matter damage following SCI.²⁴⁴ Glutamate elevation following injury is caused by: 1) Ca²⁺-dependent excitotoxic release of glutamate from axons; 2) dysfunctional astrocytic and neuronal glutamate reuptake and recycling; 3) ATP-dependent P2X₇ receptor-mediated astrocytic glutamate release; 4) spillage from adjacent injured cells and; 5) glutamate release from activated microglia, associated with an inflammatory response.^{241,245–247} In addition, there is a positive feedback mechanism associated with glutamatergic excitotoxic insult. Glutamate interacts with *N*-methyl-D-aspartate (NMDA) and α -amino-3-hydroxy-5-methyl-4-isoxazolepropionic acid (AMPA) receptors to increase the expression of inflammatory cytokines and chemokines.²⁴⁸ These toxins stimulate nearby microglia and astrocytes to release more glutamate and inflammatory factors into the extracellular space, exacerbating excitotoxic

insult.²⁴⁹ However, increased extracellular glutamate alone cannot induce the full spectrum of toxic effects observed following CNS injury.²⁵⁰

Intracellular Ca^{2+} overload activates apoptotic cellular mechanisms and has been coined the "final common pathway of cell death."²⁵¹ After neurotrauma, there is an immediate rise in extracellular Ca^{2+} levels due to spillage from injured and inflamed cells, and release from intra-axonal Ca^{2+} stores.²⁵² Using ^{45}Ca autoradiography following a lateral FPI, there is a marked increase in ^{45}Ca accumulation, even in areas of the brain without gross morphological damage, showing that Ca^{2+} flux plays a critical role in TBI pathology.²⁵³ Ca^{2+} rapidly enters neuroglia through a variety of channels and receptors, including AMPA receptors, NMDA receptors, voltage-gated calcium channels (VGCCs), and P2X_7 receptors,²⁵⁴ as well as through membrane pores created by the shearing force during the initial mechanical insult.²⁵⁵

Increased intracellular Ca^{2+} is self-propagating, due to Ca^{2+} -induced release of Ca^{2+} from intracellular stores, such as the endoplasmic reticulum, as well as reversal of the $\text{Na}^+/\text{Ca}^{2+}$ exchanger, which then pumps additional Ca^{2+} into the cell.²⁵⁶⁻²⁵⁸ Changes in Ca microdomains are also apparent in optic nerve vulnerable to secondary degeneration, detected using nanoscale secondary ion mass spectroscopy.²⁵⁹ Following neurotrauma, oligodendrocytes and OPCs are particularly vulnerable to intracellular Ca^{2+} overload,⁴⁰

partially because they contain higher concentrations of P2X_7 receptors and AMPA receptors than neurons and other glial cells.^{260,261} Therefore, more receptors are activated after injury, leading to greater Ca^{2+} influx when compared with cells that have a lower concentration of these receptors.²⁶² Further, oligodendrocytes and OPCs do not have the capacity for receptor-mediated desensitization of AMPA receptors when overstimulated, thus increasing their risk of Ca^{2+} -mediated damage.²⁶³ Once Ca^{2+} has entered cells, it mediates a variety of downstream pathways, including mitochondrial dysfunction and oxidative stress, ultimately resulting in apoptotic cell death and the spread of secondary degeneration,²⁶⁴ with oligodendrocytes being particularly vulnerable.

Oligodendrocyte susceptibility to oxidative stress

Increased intracellular Ca^{2+} accumulates in mitochondria, resulting in an increase in mitochondrial and cytoplasmic production of reactive oxygen species (ROS) and reactive nitrogen species (RNS),¹³⁰ as shown in Figure 1.

Following intracellular Ca^{2+} influx, Ca^{2+} accumulates inside the mitochondria via the mitochondrial permeability transition.²⁶⁶ Mitochondrial protein phosphatase then dephosphorylates cytochrome c oxidase, reducing allosteric ATP-inhibition and increasing the mitochondrial membrane potential.²⁶⁷ As ATP synthesis increases

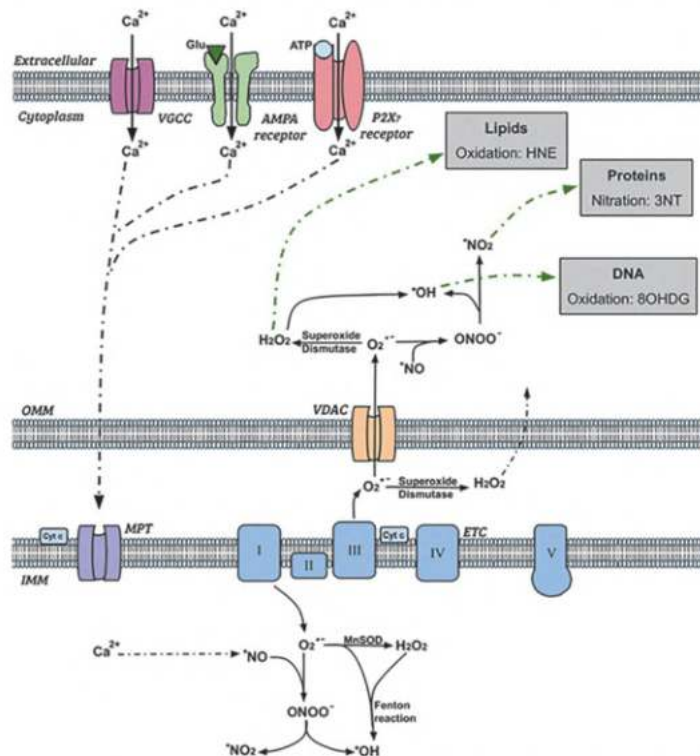


FIG. 1. Schematic diagram showing intracellular production and effect of reactive oxygen species during secondary degeneration. Reactions shown are indicative of processes and are not balanced equations. Not all possible reactions are shown. ETC, electron transport chain; MPT, mitochondrial permeability transition; OMM/IMM, outer/inner mitochondrial membrane; VDAC, voltage dependent anion channel. Adapted from O'Hare Doig et al.²⁶⁵

through the Krebs cycle, electrons are leaked at complexes I and III of the electron transport chain on the inner mitochondrial membrane, resulting in the increased formation of the superoxide anion ($O_2^{\bullet-}$).^{268,269} Superoxide dismutases reduce $O_2^{\bullet-}$ to hydrogen peroxide (H_2O_2), and the iron-catalyzed Fenton reaction further dismutates H_2O_2 into hydroxyl radicals (OH^{\bullet}).^{270,271} OPC vulnerability is heightened by increased baseline intracellular iron levels,²⁷² as increased intracellular iron is associated with increased ROS production via iron-facilitated Fenton reactions.²⁷³

Our team has demonstrated that at 1 and 3 days post-injury, there is an increase in H_2O_2 following a partial optic nerve injury.²⁶⁵ Nitric oxide (*NO) is enzymatically synthesized by inducible nitric oxide synthase (iNOS), and reacts with $O_2^{\bullet-}$ to produce peroxynitrate ($ONOO^{\bullet}$).²⁷⁴ $ONOO^{\bullet}$ can then be further reduced to form OH^{\bullet} and nitrogen dioxide (*NO_2).²⁷⁵ $O_2^{\bullet-}$ can travel from the mitochondria into the cytoplasmic space through voltage-dependent anion channels on the outer mitochondrial membrane, resulting in elevated ROS outside of the mitochondria.²⁷⁶ Further, H_2O_2 is membrane permeable, and so can diffuse out of the mitochondria into the cytosol.²⁷⁷ Within the cytoplasm and nucleus, these ROS oxidize DNA and lipid structures, and nitrate proteins, causing cellular damage and apoptosis.²⁶⁴ OH^{\bullet} also deprotonates lipids and proteins, causing a self-propagating cycle of oxidative damage.²⁷⁰

Our team has shown that following a partial optic nerve transection, the immunoreactivity of carboxymethyl-lysine (CML), an advanced glycation end-product as a marker of oxidative stress increases significantly post-injury in areas of nerve vulnerable to secondary degeneration, colocalized with Olig1+ oligodendroglial cells.¹³⁰ When animals were treated with a combination of ion channel inhibitors aimed to reduce Ca^{2+} influx through AMPA receptors, P2X₇ receptors, and VGCCs, the immunointensity of CML decreased to normal levels, suggesting increased advanced glycation end-products in this model are at least in part a result of Ca^{2+} -dependent mechanisms.¹³⁰

In a normal, uninjured system, ROS and RNS are detoxified by antioxidants, such as glutathione peroxidase (GPx1), heme oxygenase-1 (HO-1), and manganese superoxide dismutase (MnSOD), preventing a buildup of free radicals within cells.⁷⁸ Cells respond to increased production of ROS and RNS by increasing production of antioxidants; with research from our team showing a significant increase in MnSOD immunoreactivity in the optic nerve as early as 5 min after partial transection, colocalized within astrocytes.^{278,279} By 3 days following injury, there is a significant increase in GPx1, often colocalized within CC1+ oligodendrocytes, with a significant increase in HO-1 by 7 days post-injury, predominantly colocalized in ionized calcium-binding adaptor molecule (Iba1) positive microglia.²⁶⁵ Following two repeated closed-head weight-drop mTBIs in rats, MnSOD immunoreactivity increases 11 days post-injury.²⁸⁰ When a combination of ion channel inhibitors to limit Ca^{2+} entry via AMPA receptors, P2X₇ receptors, and VGCC is used following repeated mTBI, MnSOD immunoreactivity decreased, indicating modulating Ca^{2+} influx is key to limiting this antioxidant response.²⁸⁰ At both 1 and 14 days post-injury following a spinal cord contusion in rats, the level of MnSOD is significantly increased, with a similar increase in copper zinc superoxide dismutase (CuZnSOD) and GPx1 at 14 days post-injury.²⁸¹

When the rate of ROS and RNS generation becomes greater than the rate at which antioxidants can counterbalance, cells are unable to prevent the damaging effects of these free radicals and undergo oxidative and nitrosative stress.²⁴⁹ OPCs have lower concentrations of endogenous antioxidants, such as GPx1 and MnSOD and are thus particularly vulnerable.^{272,282} Glutathione prevents cell apoptosis by conjugating 4-hydroxynonenal (HNE), a by-product of

lipid peroxidation, and suppressing the toxic activity of 12-lipoxygenase.^{283,284} Therefore, lower levels of glutathione are correlated with an increased risk of oxidative damage to lipids.²⁸⁵ Further, when OPCs are engineered to overexpress the antioxidant MnSOD, there is an observable decrease in apoptosis.²⁸⁶

Mitochondrial oxidative stress also induces endoplasmic reticulum (ER) stress.²⁸⁷ ER stress results in unfolded proteins,²⁸⁸ and if the stress persists for an extended period, it can result in cell death.²⁸⁹ Further, in periods of stress, the ER releases large quantities of Ca^{2+} , which in turn increase the production of ROS/RNS in the mitochondria.²⁸⁷ Our research has shown that mitochondria in both axons and glia develop subtle structural changes following injury, with increased autophagic profiles demonstrating susceptibility of mitochondria to secondary degenerative processes.²⁹⁰

Oligodendrocyte vulnerability to oxidative stress is further exacerbated by its role in maintaining the myelin sheath.²⁸² The maintenance of myelin requires large amounts of energy, and involves catalyzing the production of lipids.²⁹¹ One by-product of these reactions is ROS; therefore, there is an intracellular accumulation of ROS within oligodendrocytes, amplifying oxidative stress mechanisms.²⁸²

Lipid peroxidation following injury

Lipid peroxidation, the process where ROS "steal" electrons from a cell's membranous lipid bilayer, is an important downstream mechanism of oxidative stress.²⁹² ROS attack the carbon to carbon double bonds of lipids, in particular of polyunsaturated fatty acids, as well as glycolipids, phospholipids, and to a lesser extent cholesterol.²⁹³ This attack on lipids results in the formation of toxic aldehydes, such as HNE.²⁹⁴ Further, iron plays a key role in ROS-mediated lipid peroxidation and enhances cytokine-mediated mitochondrial and membrane damage.^{81,295} Therefore, during secondary degeneration, OPCs not only produce more ROS but have greater ROS-mediated cell damage than other neuroglia due to their increased intracellular iron levels.²⁷² HNE mediates cell damage by binding to and disrupting membrane transport systems, including impairing glutamate reuptake in astrocytes.^{296,297} Therefore, the production of HNE by lipid peroxidation causes a positive feedback for glutamate excitotoxicity and exacerbates the cycle of cell damage.²⁹⁸

Our team has shown overall increased levels of HNE from 3 days after partial injury to the optic nerve,²⁶⁵ with a significant increase in HNE within the OPC and mature oligodendrocyte populations at this time.⁴³ When a combination of three ion channel inhibitors targeting AMPA receptors, P2X₇ receptors, and VGCCs was delivered acutely following the injury, OPCs were preserved when HNE decreased. The protection was associated with improvements in visual function, suggesting that limiting lipid peroxidation may aid in maintaining the number of OPCs following injury.⁴² Following a clip-compression-induced SCI, there is a biphasic increase in lipid peroxidation as shown by malondialdehyde assays, with the first peak at 4 h post-injury, and the second increase at 24 h to 5 days post-injury.²⁹⁹ In a model of repeated mTBI, our team has also shown increased lipid peroxidation in cortical neurons, demonstrating that oligodendroglia are not the only cell type vulnerable to lipid peroxidation.³⁰⁰ Further, following TBI in humans, circulating plasma levels of HNE increase compared with control patients.³⁰¹

Protein nitration following injury

Nitrosative stress also has a neurodestructive effect, mediating further lipid peroxidation, as well as protein nitration.^{302,303} Protein nitration occurs when a nitro group is added into the structure of a

protein,³⁰⁴ and primarily occurs as the reaction between $\cdot\text{NO}$ or $\cdot\text{NO}_2$ and the amino acid tyrosine, to form 3-nitrotyrosine (3-NT).³⁰⁵ Immunointensity of 3-NT, a protein nitration indicator, is significantly increased in a diffuse distribution 3 days following partial injury to the optic nerve.⁴² Further analysis using NanoSIMS technology shows that 3-NT is increased at 3 days within mature oligodendrocytes, NG2+ cells, Olig2+ cells, β III tubulin+ axons, and paranodes, with no structure selectively vulnerable to damage.⁴³ In addition, following a moderate diffuse closed-head injury, 3-NT immunoreactivity increased at 48 h post-injury.³⁰⁶ This suggests that the nitrosative pathways also contribute to the cellular damage observed in secondary degeneration.

Oxidative DNA damage following injury

DNA is highly vulnerable to oxidative damage, and there are a variety of mechanisms through which free radicals mediate DNA damage during oxidative stress, one of which is nucleobase modification.²⁴⁹ These DNA lesions can have extremely detrimental effects, by either altering the genetic code or by acting as a block during DNA replication.³⁰⁷ DNA is highly vulnerable to oxidative damage, as ROS, particularly $\bullet\text{OH}$, can mediate hydroxylation of DNA nucleic acid bases.²⁴⁹ This process converts deoxyguanosine to 8-hydroxy-2-deoxyguanosine (8OHdG), through a spontaneous transversion mutation, altering DNA structure.³⁰⁸ Our team has shown that by 24 h following partial optic nerve injury, 8OHdG is significantly increased in the ventral optic nerve white matter, and this is associated with apoptotic cell death.^{265,309} However, in our closed-head weight-drop model of repeated mTBI, there is no increase in 8OHdG immunoreactivity in a range of brain regions, with either 1, 2, or 3 injuries at 3 months following injury,³¹⁰ or with two injuries at 11 days post-injury.²⁸⁰ More work is needed to assess the acute time course of 8OHdG immunointensity in this model.

Going on to define the cellular specificity of the changes, we have shown that oligodendroglial cells are significantly more likely to succumb to oxidative 8OHdG DNA damage following neurotrauma compared with other neuroglial cells and structures.⁴³ Three days following the optic nerve injury, both OPCs and oligodendrocytes had increased levels of 8OHdG DNA damage.⁴³ Newly derived oligodendrocytes exhibited significantly more DNA damage than pre-existing oligodendrocytes, suggesting newly differentiated cells are more vulnerable to oxidative damage.⁴³ The DNA-damaged oligodendrocytes were more likely than non-DNA-damaged oligodendrocytes to become apoptotic.⁴³ However, newly derived oligodendrocytes were less likely to be apoptotic than pre-existing oligodendrocytes.⁴³ Thus, despite their increased susceptibility to DNA damage, newly derived oligodendrocytes are less vulnerable to apoptotic cell death than their pre-existing oligodendrocyte counterparts.⁴³ Interestingly, by 28 days after injury, these newly derived oligodendrocytes are still less likely to be apoptotic, but they also have decreased expression of MyRF.⁴³ This suggests that newly derived DNA damaged oligodendrocytes are more likely to survive following injury but have a reduced myelination capacity.⁴³ Therefore the ability for remyelination is compromised following oxidative damage due to neurotrauma and may lead to poor repair of damaged myelin.⁴³

Changes in numbers of oligodendroglia following injury

It has been widely reported, including in Australian research, that following experimentally induced TBI and SCI there is a loss of oligodendrocytes.^{40,41,311–314} However, some studies have not

detected oligodendrocyte death,¹²⁰ perhaps indicating differential responses of these cells depending on injury severity or mode.

We have shown that following partial injury to the optic nerve white matter,⁴³ using Olig2 together with NG2 as markers for OPCs, the number of OPCs remains similar to control at 1 and 3 days after injury.³¹⁵ However, OPC densities significantly decline from 7 days to 3 months, which is not attributable to optic nerve swelling.³¹⁵ At 3 days post-injury, OPCs proliferate more than controls.³¹⁵ At 1 and 3 days post-injury, the density of CC1+/Olig2+ immature oligodendrocytes decreases; however, by 3 days there is an increase in the density of CC1+/Olig2- mature oligodendrocytes, indicating differentiation of a subset of surviving immature oligodendrocytes.³¹⁵ By labeling dying oligodendroglia with the cell death marker TUNEL, it was found that an increase in TUNEL+ staining occurred across the oligodendroglial lineage by 7 days following injury, with a significant increase in OPC cell death sustained at 1 month post-injury.³¹³ This suggests that despite acute proliferation, there is an overall chronic depletion in the OPC population.^{43,315}

Similarly, following a contusion SCI, numbers of BrdU+/NG2+ OPCs increase, with proliferation of OPCs tripling in the first week following injury.³¹³ However, within the first 7 days following injury, the total number of OPCs decreases, demonstrating an overall reduction of this cellular population despite the proliferative response.³¹³

Change in the OPC population may be slightly different following TBI. Using an FPI model, the number of OPCs increases in white matter tracts from 2 days to 21 days following injury,⁴¹ quantified based upon use of Olig2 or Tcf4 individually to indicate OPCs. Further, although BrdU+/PLP+ newly derived oligodendrocytes are rare in the corpus callosum, they are significantly higher in number following a CCI than sham injury.¹²⁰ Finally, in another study utilizing a CCI, immunoreactivity of the OPC marker NG2, quantified by optical density measurements, peaks at 1 to 4 days following injury in the corpus callosum.³¹⁶ Taken together these studies suggest that OPC populations increase in response to injury in white matter following TBI. In the first few days following a moderate to severe TBI in humans, oligodendrocytes are lost with a concomitant increase in the number of OPCs.³¹⁷ Despite these findings, it is possible that variability exists in number of oligodendroglia depending on the type of white matter injury.

Axonal loss and neuronal damage following injury

Neuronal loss both within and around the injury site is a hallmark of white matter injury.³¹⁸ In TBI, neural degeneration has been observed within minutes following injury,³¹⁹ featuring the degenerative cascade of TAI.³³ Certain areas of white matter are more vulnerable to TAI, such as the corpus callosum and the brainstem.^{171,320} Staal and Vickers found that *in vitro* unmyelinated axons are more vulnerable to stretch injury than myelinated axons.³²¹ Further, unmyelinated fibers in the corpus callosum are more selectively vulnerable to damage than myelinated axons *in vivo*.³²² Following injury, increased intracellular Ca^{2+} within neurons results in damage to the axonal cytoskeleton and impairments to axonal transport via activation of degenerative enzymes and cysteine proteases such as caspase-3 and the Ca^{2+} -dependent neutral protease calpain.³²³ Caspase-3 cleaves proteins associated with DNA repair, contributing to the DNA damage observed following injury.³²⁴ The damage cascade results in accumulation of axonal transport proteins within the axon, DNA fragmentation, and axonal swelling, with affected neurons eventually undergoing

either apoptotic or necrotic cell death, impairing function.³²⁵ In addition, DNA damage from ROS enhances post-traumatic neuronal death following injury.³²⁶

The partial optic nerve transection model has allowed specific insight into the changes to axons and their parent somata vulnerable to secondary degeneration in a white matter tract. We have shown that at 24 h after injury, retinal ganglion cell somata show increased c-jun expression, associated with pro-apoptotic mechanisms.²⁷⁸ By 3 days after injury, poly (ADP-ribose) polymerase (PARP) is up-regulated in axons in the ventral optic nerve, implicating necrosis as an additional pathway to cellular demise.³²⁷ There is also decreased axonal stability at 1 day following PT, shown through decreased acetylated tubulin expression.⁴² Further, there are no changes in the ratio of Ca²⁺-independent phosphorylated Tau/panTau at [S²⁶²], whereas there is increased Ca²⁺-dependent phosphorylated Tau isoforms at this time.⁴²

When treated with a combination of ion channel inhibitors that reduce Ca²⁺ influx through AMPA receptors, P2X₇ receptors, and VGCCs, the ratio of phosphorylation of both [S²⁹⁶] and [T²⁰⁵] relative to total Tau decreases significantly at 3 day post-injury compared with injured untreated controls.⁴² The ion channel inhibitor combination also ameliorates acetylated tubulin immunoreactivity.⁴² Conversely, NogoA immunoreactivity decreases in the ventral optic nerve with injury but increases when animals were treated with the ion channel inhibitor combination. However, changes to NogoA did not appear to be a driver of therapeutic benefit following ion channel inhibitor administration, and the functional significance of changes to NogoA remain unclear. At 3 months following the optic nerve injury, β -III tubulin immunointensity is decreased, indicative of loss of axonal integrity and axonal death.¹⁵⁰ Indeed, by 3 months after injury, the number of axons in the ventral optic nerve has decreased by 30.7%.³⁴ The ion channel inhibitor combination protects β -III tubulin immunoreactivity 3 months post-injury, associated with preservation of myelin and improvements in visual function.¹³⁰ There is also a significant decrease in retinal ganglion cell densities in the central retina both 1 and 3 months after these injuries, which suggests retrograde damage to cell bodies along axons.³²⁸ Taken together the data indicate that loss of neurons is associated with Ca²⁺ dysregulation, oxidative stress mechanisms, and dysmyelination, and likely contributes to a decrease in function.^{42,150}

These degenerative changes to neurons and their axons are not limited to the optic nerve injury model. Following mTBI with TAI, degenerating axons are apparent with electron microscopy at 3 days through to 6 weeks post-injury, with swollen mitochondria, either abnormally high or low cytoplasmic density, and vesicle accumulation.¹²⁰ Unmyelinated axon density decreases in the corpus callosum following a moderate FPI, with diameter decreasing from 3 to 7 days post-injury and recovering at 15 days.³²⁹ In a TAI study utilizing compound action potentials evoked in the corpus callosum, it was found that the amplitude of myelinated axons was decreased up to 3 days post-FPI but recovered to control levels by 7 days. Whereas the unmyelinated axonal amplitude did not recover, therefore a differential vulnerability was observed.³²² Following a single-impact open-head weight-drop TBI, axons are damaged, with a concomitant decrease in conduction velocities across the corpus callosum.³³⁰ However, there is no increase in TUNEL+ neurons in white matter following a FPI, which suggests neurons are less vulnerable to apoptotic cell death than oligodendroglia.³³¹

Tau hyperphosphorylation is a driver of neurodegeneration as it results in a disruption of microtubules and may result in interrupted axonal transport and therefore decreased synaptic transmission.³³²

The Corrigan team at the University of Adelaide (Collins-Praino and colleagues³³³) have shown that regardless of whether rats receive a single moderate to severe TBI or three mTBIs, the level of AT180 tau phosphorylation has a biphasic pattern, with an initial spike at 24 h following injury, which returns to baseline before increasing again at 3 months post-injury. Further, levels of protein phosphatase 2Ac (PP2Ac) decrease at both 24 h and 3 months following injury, hypothesized to demonstrate a loss of PP2A phosphatase activity.³³³ Overall, this indicates that tauopathy and tau phosphorylation may be a significant feature of neurodegeneration following both repeated mTBIs and more moderate to severe single TBIs.

Axonal loss is also a hallmark of SCI. By 1 week following a contusion SCI, only 13% of axons remained in the degenerated core of the dorsal column at the injury site.³³⁴ Axons swelled, with the axoplasm becoming dense, followed by myelin detaching from the axon.³³⁴ Axons subsequently degenerated, leaving a microcyst inside a slowly disappearing myelin sheath.³³⁴

The amyloid- β (A β) peptide is derived from amyloid precursor protein (APP), with the aggregation of A β believed to play a role in Alzheimer's disease pathogenesis.³³⁵ Aggregation of A β is evident following severe TBI in humans,³³⁶ so it is not surprising that there is an epidemiological association between TBI and Alzheimer's disease later in life.⁶ The Vickers team have recently shown (Collins and associates³³⁷) that 30 days following a lateral FPI in the APP/PS1 transgenic model of Alzheimer's disease in mice, the aggregation response of A β is dependent on the state of amyloidosis at time of injury, with pre-plaque mice showing increased A β deposition in the cortex, and mice with established amyloidosis showing decreased total A β deposition. More work is needed to determine the A β response in white matter following injury. The functions of APP are manifold, including roles in neuronal and synaptic processes.³³⁸ The Vink team has shown (McAteer and co-workers³³⁹) that following repeated mTBI, there are increases in APP immunoreactivity at 12 weeks post-injury. However, APP derivatives can mediate both neurotoxic and neuroprotective effects. Indeed, the team in South Australia (Corrigan and colleagues³⁴⁰) has gone on to show that if APP is knocked out in mice, there is increased cortical and hippocampal cell loss, axonal injury, and decreased behavioral deficits following diffuse mTBI, suggesting upregulation of APP plays a neuroprotective role.³⁴⁰ Exogenous treatment with the APP derivative sAPP α prevents deficits in APP knockout mice after injury.³⁴¹ Together with Roberto Cappai, the team have shown (Plummer and associates³⁴²) that this neuroprotective effect of APP is mediated by residues 96-110 in the heparin-binding site in the growth-factor like domain (D1) of sAPP α , with APP96-110 having a neuroprotective effect following focal CCI. Intravenous administration of APP96-110 30 min after a moderate to severe diffuse impact-acceleration TBI results in reduced motor deficits, and decreased axonal injury and neuroinflammation in the corpus callosum at 3 days following injury.³⁴³ Further, when APP96-110 is administered intravenously 5 h post-injury, there are improvements in motor deficits and axonal injury in the corpus callosum.³⁴³ Therefore, APP96-110 may be a potential therapeutic option to limit axonal injury in white matter following TBI.

Dysmyelination and myelin structural changes

The myelin sheath is predominantly lipid-based, which means it is highly vulnerable to oxidative stress and lipid peroxidation,³⁴⁴ resulting in widespread dysmyelination following white matter

injury.^{15,345,346} Demyelination is a destructive process whereby the myelin sheath becomes abnormal in structure, associated with a loss of function due to reduced conduction of neural signals.³⁴⁷ A hallmark feature of demyelination is myelin decompaction. Myelin decompaction occurs when the myelin lamellae separate and the paranodal loops detach and split, associated with increased intracellular Ca^{2+} , as shown in Figure 2.³⁴⁸

Oxidative stress disrupts both the integral myelin sheath proteins, and the proteins between the surfaces of the myelin lamellae.^{351,352} We have shown that from 5 min following partial optic nerve injury, generalized increases in MBP immunofluorescence are observed in the ventral optic nerve, indicative of myelin degradation and increased immunoreactivity of MBP.²⁷⁸ However, by 3 months following injury, MBP immunoreactivity is decreased, suggesting long-term myelin loss.³⁴ In a rat model of TBI, MBP becomes proteolyzed in a calpain-mediated manner, contributing to lost integrity of the myelin sheath and demyelination.³⁵³ MBP has also been found to be elevated in the CSF following severe TBI in humans.³⁵⁴

Luxol fast blue (LFB) staining is a frequently used indicator of myelin integrity. Following a CCI, LFB staining reveals lesions within the corpus callosum from 1 day to 3 months after injury.³⁵⁵ At 1 year following a parasagittal FPI in rats, abnormal LFB staining is observed in the corpus callosum, with a decrease in LFB

staining in the ipsilateral cerebral peduncle compared with sham animals, indicating loss of myelin.³⁵⁶ At 24 h and 2 days following a contusion SCI, LFB staining is considerably decreased in the dorsal column at the middle of the injury site, with more granular staining visible in the ventrolateral white matter; by 10 weeks post-injury, a thick rim of LFB staining is apparent surrounding the injury site.³⁴⁴

Given the optic nerve is a highly myelinated white matter tract, the partial transection model has proved useful for studying changes to myelin structure following injury. We have used electron microscopy to demonstrate a significant increase in the proportion of axons with decompacted myelin in the ventral optic nerve at 3 months after injury,³⁵⁷ associated with lipid peroxidation and oxidative stress as described above.³⁵⁸ At 6 months, loosening of the myelin sheath is widespread throughout the nerve, with myelin thickness significantly increased at this time-point, likely due to the loosening.³⁴ The number of intraperiodic lines surrounding myelinated axons also increases at 6 months post-injury, suggesting oligodendrocytes may be wrapping more layers of myelin around axons in an attempt at repair.³⁴

In SCI, the necrotic core of the injury is surrounded by a rim of demyelinated axons.³⁵⁹ After a contusive SCI, the number of demyelinated axons peaks at 1 day following injury, and starts to resolve by 7–14 days, before then increasing again up to 450 days post-injury.³⁶⁰ Following a chronic clip compression injury of the rat thoracic spinal cord, the myelin is thinner in the injured dorsal column, associated with reduced action potential amplitudes in affected axons.³⁶¹

Following mTBI with TAI, electron microscopy has revealed an increase in double-layered myelin,¹²⁰ which can occur as myelin degenerates around injured axons.³⁶² We have shown that in normally myelinated axons myelin thickness in the corpus callosum is not significantly altered with up to three repeated mTBIs.³¹⁰ However, more work is needed to quantify demyelination, myelin decompaction, and loosening at various time-points following TBI at the electron microscopy level.

Demyelination severely disrupts the myelin node/paranode complex. The nodal sodium channels and the paranodal protein, Caspr, diffuse along the axon, increasing the size of the node and paranode respectively.³⁶³ Our team has shown that at 1 day following partial optic nerve injury, there is a significant increase in both the paranodal gap length and the proportion of atypical nodal complexes, and these changes are maintained at 3 months after injury.³⁶⁴ After closed-skull impact, paranodes were either shortened or absent with a concomitant increase in heminodes.³³⁰ Following closed-head weight-drop mTBI, the length of the paranode, the node of Ranvier, and the proportion of atypical nodal complexes in the corpus callosum increases.²⁸⁰ Interestingly, inhibiting VGCCs, P2X_7 receptors, and AMPA receptors results in improvements in both the length of the node as well as the proportion of atypical nodal complexes in both the optic nerve and mTBI models, indicating increased intracellular Ca^{2+} is a key mediator of myelin integrity at the node of Ranvier.^{42,280,365}

Demyelination after injury is associated with higher axonal susceptibility to excitotoxic insult,³⁶⁶ evidenced by a significant decrease in axonal density associated with demyelination both 1 and 3 months after partial optic nerve injury.³⁵⁷ It is therefore not surprising that demyelination is associated with a loss of visual tracking behavior after partial optic nerve injury at both acute and chronic timepoints.^{42,130} Abnormal myelination at a single internode can be sufficient to block neural signal transduction for an entire axon.³⁴⁴ White matter damage has also been associated with functional deficits following experimental models of TBI, with

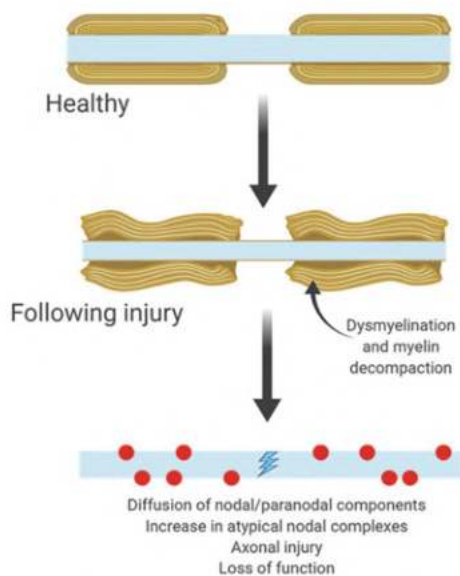


FIG. 2. Characteristics of demyelination and myelin decompaction. Following CNS injury, myelin structures succumb to oxidative stress and lipid peroxidation. This results in paranodal splitting, myelin retraction and decompaction, Ca^{2+} influx, and cytoskeletal alterations to the nodal complex. Diffusion of nodal components results in impaired saltatory conduction along nerves, resulting in axonal injury and/or loss. As irregular myelin repair is attempted by newly myelinating oligodendrocytes, the number of atypical nodal complexes increases. Red circles represent nodal and paranodal components. CNS, central nervous system. Figure created with BioRender.com; modified from Podbielska et al.³⁵⁰

deficits dependent on the location and severity of the injury.^{367,368} Therefore, limiting the extent of myelin damage, both by attenuating demyelination and promoting successful remyelination following injury, may result in improved functional outcomes.

Inflammation and gliosis

Myelin degradation is both a cause and consequence of inflammation, as shown in animal models of multiple sclerosis where myelin debris regulates microglial activation.³⁶⁹ Along with infiltrating macrophages, activated microglia secrete numerous cytokines, chemokines, ROS, and growth factors, affecting nearby cells.³⁷⁰ Proinflammatory chemokines further recruit immune cells to the injury site, exacerbating damage,^{371,372} with depletion of microglia following a moderate FPI resulting in a therapeutic effect on neuronal loss early post-injury.³⁷³ However, microglia have pleiotropic responses to injury, and can also mediate anti-inflammatory responses depending on environmental cues and exposure to specific cytokines.³⁷⁴ In SCI, it has recently been discovered that microglia form a "microglial scar," without which functional outcomes after injury are worsened.³⁷⁵ From 3 days after partial transection to the optic nerve, we have shown that Iba1+ microglia and ED1+ macrophages become activated and their numbers increase in ventral nerve vulnerable to secondary degeneration and remotely in the brain.^{278,376}

The Corrigan team have shown (Collins-Praino and associates³⁷⁷) that following a single diffuse impact-acceleration mTBI, there is an acute increase in Iba1+ cells in the hippocampus at 6 days, which resolves chronically by 3 months post-injury. The finding built upon earlier demonstrations of a significant increase in cortical microglial activation at 24 h following three impact acceleration diffuse mTBIs, and a significant increase following both one and three injuries at 12 weeks.³³⁹ Meanwhile, we have shown in a closed-head weight-drop model of repeated mTBI that microglia in the corpus callosum remain hypertrophic after two injuries at 3 months,³¹⁰ but only after one injury in cortex, suggesting repeated mTBI may cause more chronic microglial activation in white matter tracts. From 3 days following mTBI with TAI, there is an increase in microglial activation in the corpus callosum, persisting through to 6 weeks post-injury.^{120,378}

Further, following a closed-skull impact TBI with TAI, astrogliosis also significantly increases up to 6 weeks post-injury in the corpus callosum where axons are damaged.¹²⁰ To form a barrier around the injury site, reactive astrocytes become hypertrophic, their processes become interlaced, and these cells show an increased expression of glial fibrillary acidic protein (GFAP).³⁷⁹ We have shown that by 24 h after partial optic nerve transection, astrocytes display a hypertrophic morphology, with a significant increase in both the width of astrocytic processes and number of minor astrocytic processes.²⁷⁸ Neurotrauma can activate at least two different types of astrocyte reactivity, A1 and A2,³⁸⁰ nomenclature that mimics the M1/M2 macrophage/microglia terminology.³⁸¹ However, as with macrophages and microglia,³⁸¹ it is likely that astrocyte reactivity is a spectrum of various phenotypes, rather than distinct reactive states.³⁸⁰ In particular, A1 astrocytes have been associated with neuroinflammation, whereas A2 astrocytes have been associated with the production of reparative trophic factors.³⁸⁰

Following injury, it appears that there may be a mixture of these phenotypes present. Ablation of proliferating reactive astrocytes following a moderate TBI resulted in inflammation and neural degeneration,³⁸² suggesting the importance of astrocytes in the reparative response. Further, following white matter ischemic injury, astrocytes promote OPC differentiation and oligodendrocyte gener-

ation by secreting BDNF, a mechanism that may occur within traumatic injuries.³⁸³ However, reactive astrocytes also release inhibitory growth factors, cytokines, ROS, and glutamate that exacerbate injury and may have a detrimental effect on overall function.^{384–387} Recent data have shown that within the cortex, the astrocytic marker GFAP and A1 astrocyte phenotype marker C3 are upregulated from 8 h following both rat FPI and mouse CCI, with the microglial marker Iba1 increased at 24 h following injury. A peak was reached in both models 72 h after injury, suggesting astrocytes may become reactive prior to microglial activation.³⁸⁸ However, it is important to note that not all GFAP+ astrocytes were C3+, suggesting there may be a mix of reactive astrocyte phenotypes present following injury.³⁸⁸

These mechanisms may also be at play within the white matter following injury. In LFP TBI, reactive astrocytes are found 1 day post-injury in the subcortical white matter tracts, continuing at least until 1 month post-injury.³⁸⁹ At both 24 h and 12 months following a repeated closed-head injury, astrogliosis increases, but when only a single injury is administered, there is no increase in astrocyte reactivity at 24 h and only a mild elevation at 12 months.¹²² However, at 24 months post-injury, a single mTBI produced mild astrogliosis, which was more severe following repeated injuries.¹²¹ However, in our closed-head weight-drop model of repeated mTBI in rat, we find no astrogliosis with either one, two, or three injuries 3 months post-injury in the corpus callosum.³¹⁰ However, more research is needed to determine whether microglia and astrocytes have beneficial or detrimental effects following CNS injury.

Remyelination

Remyelination occurs when the normal myelin sheath is restored to demyelinated axons, allowing saltatory conduction, promoting axonal survival and improving function.³⁹⁰ Once a mature oligodendrocyte has myelinated a series of axons, it is traditionally thought to be relatively unable to remyelinate additional axons.³⁹¹ Instead, new oligodendrocytes must be generated for remyelination, with OPCs as the main source of remyelinating oligodendrocytes.³⁴⁹ Schwann cells may also contribute to remyelination, as OPCs possess the ability to differentiate into Schwann cells in the context of CNS demyelination.³⁹²

Recent work using single-cell transcriptomics as well as a ¹⁴C-based birth dating techniques in human multiple sclerosis tissue has revealed that mature oligodendrocytes may in fact possess the capacity to remyelinate additional axonal segments.^{393–395} However, the ability of mature oligodendrocytes to provide myelin to demyelinated axons has not yet been investigated following neurotrauma. Nevertheless, reduced generation of new myelinating oligodendrocytes from OPCs following injury is associated with decreased function following injury.³¹³ Further, transplantation of OPCs following SCI results in remyelination and functional recovery.³⁹⁶ Therefore, preserving and encouraging proliferation and differentiation of OPCs after injury is likely to be associated with improved functional outcomes after neurotrauma.

OPCs rely on factors released by microglia and astrocytes to switch from a quiescent to a regenerative phenotype.⁷³ Whereas normal astrocytes create a facilitatory environment for OPC differentiation, once activated, astrogliosis can inhibit differentiation and maturation of OPCs.³⁹⁷ However, blocking astrocyte scar formation inhibits axonal regeneration following a severe crush SCI in mice, suggesting that astrocytes also play a crucial role in recovery following injury.³⁹⁸ The effect of microglial cells on OPC differentiation depends on the balance of pro-inflammatory or anti-inflammatory phenotypes, with a switch from pro-inflammatory

toward anti-inflammatory coinciding with commencement of remyelination.^{399–401} Macrophages may also play a role in oligodendrogenesis following injury, as depletion of these cells delayed remyelination and OPC recruitment after lysocleithin-induced spinal cord demyelination.⁴⁰² Myelin proteins inhibit OPC differentiation, therefore MBP degradation may act as a further barrier to OPC differentiation as it is released into the extracellular space from damaged sheaths.^{403,404} However, microglia are in part responsible for the clearance of myelin debris, thus regulating oligodendrogenesis through myelin phagocytosis.⁴⁰⁵ Further, neural activity from the premotor cortex enhances OPC proliferation, differentiation into oligodendrocytes, and myelination.⁹³ Collaborative Australian research has shown that under normal conditions, increased neural activity leads to axons being myelinated with thicker myelin than axons with less neural activity,⁴⁰⁶ which may also be relevant to remyelination following white matter injury.

In demyelinating disease, remyelinated fibers are often characterized by thinner myelin sheaths than would be expected based on axonal diameter.⁴⁰⁷ However, Australian researcher Kaylene Young and colleagues discovered that myelination is an ongoing adult phenomenon, with evidence for myelin remodeling by adult-born oligodendrocytes, which made shorter and thinner myelin, but more internodes of myelin than early-born oligodendrocytes.⁵² This suggests that thinner myelin typical of remyelination may be a characteristic of adult myelination, rather than remyelination itself.

Our team has shown that the number of intraperiodic lines increase chronically following partial optic nerve injury, suggesting oligodendrocytes may be forming new layers of myelin; however, this was not associated with improvement in visual function.³⁴ However,

unlike in demyelinating disease, thicker myelin sheaths were observed, which was posited to be due to loosening of the myelin lamellae.³⁴ Following a contusion SCI, newly formed oligodendrocytes and Schwann cells remyelinated axons, and these myelin internodes were significantly shorter than in control mice,⁴⁰⁸ and elongated over 6 months post-injury.⁴⁰⁸ At most time-points tested, myelin thickness was not different in injured animals compared with controls.⁴⁰⁸ Therefore, long-term following SCI, remyelinated sheaths were neither thinner nor shorter than myelin in control mice.⁴⁰⁸

Following an open-head weight-drop TBI, conduction velocity along axons in the corpus callosum was partially restored by 2 weeks post-injury, alongside concomitant increased synthesis of myelin membranes, suggesting remyelination had occurred.³³⁰ Following mTBI with TAI, myelin thickness was reduced at 1, 2, and 6 weeks post-injury, following an earlier increase in the number of newly generated oligodendrocytes at 3 days post-injury.¹²⁰ However, more work is needed to determine the extent and pattern of remyelination in various models of white matter injury.

Conclusion

White matter injury is a key pathology that contributes to functional loss following neurotrauma of all etiologies. Evolving technologies are revealing the subtleties of structural changes in white matter tracts and the underlying causative biochemical and cellular disruptions (Fig. 3). Models including partial optic nerve transection are allowing an examination of contributing cellular dynamics in tissue exclusively vulnerable to secondary degeneration (summarized in Table 1). The next step will be to use this

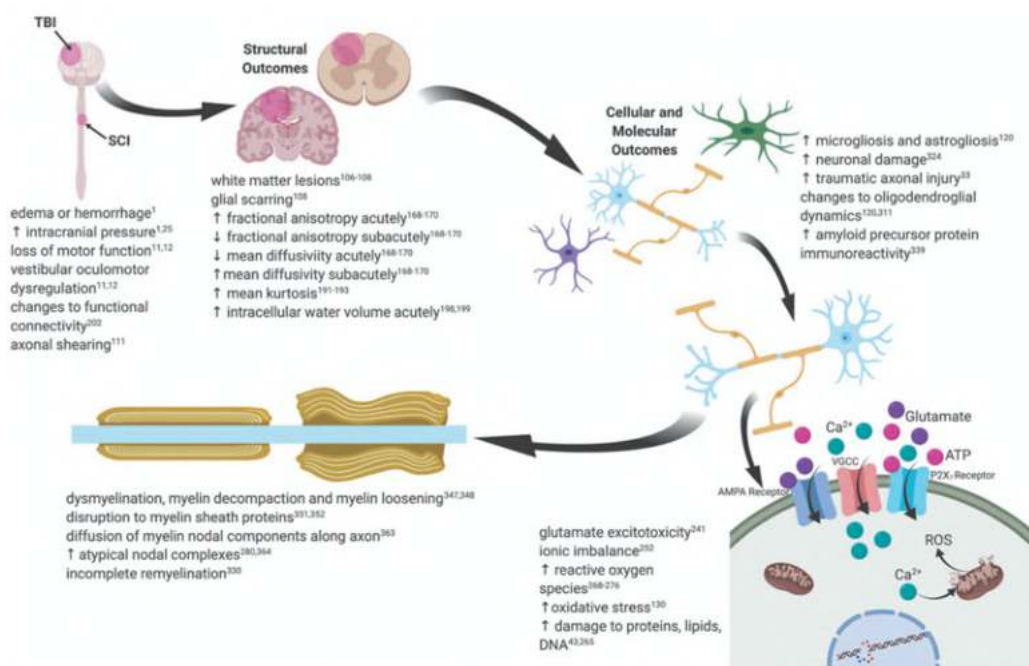


FIG. 3. Schematic illustration of structural and molecular mechanisms of white matter damage in central nervous system injury. Note: Traumatic brain injuries represented are non-penetrating. Figure created with BioRender.com.

TABLE 1. SUMMARY OF CELLULAR AND PATHOPHYSIOLOGICAL CHANGES REPORTED BY THE FITZGERALD TEAM IN RAT MODELS OF CNS INJURY

Partial optic nerve transection		Day 1	Day 3	Day 7	Day 11/14	Day 28	3 months	6 months	
Cells and pathophysiology affected	Neurons, nerves and function	↑ Ptau/panTau ratio ⁴² ● Acetylated tubulin ⁴² ↓ Nogo A ⁴² ●	● c-Jun+ RGCs ²⁷⁸ ↑ Acetylated tubulin ⁴² ↓ Nogo A ⁴² ↑ Iba1+ microglia ²⁷⁸ ↑ ED1+ microglia/Macs ²⁷⁸ ●	↑ Ptau/panTau ratio ⁴² ● Normal acetylated tubulin ⁴² Normal Nogo A ⁴² ↑ Iba1+ microglia ⁴¹⁰ ↑ ED1+ microglia/Macs ⁴¹⁰ ↑ iNOS ³⁷⁶ ↑ Arg1 ³⁷⁶ ↑ CD11b+ cells ³⁷⁶ ↑ CD45+ cells ³⁷⁶ ●	● RGC death ³²⁷ ●	● Normal axon diameter ³⁵⁷ ● ↓ Visual function ³⁶⁴ ● Iba1+ microglia ^{376,410} ● ED1+ microglia/Macs ⁴¹⁰ ● ↑ Arg1 ³⁷⁶ ● ↑ CD11b cells ³⁷⁶ ●	● Normal axon diameter ³⁵⁷ ● ↓ Visual function ³⁶⁴ ● Iba1+ microglia ^{376,410} ● ED1+ microglia/Macs ⁴¹⁰ ● ↑ Arg1 ³⁷⁶ ● ↑ CD11b cells ³⁷⁶ ●	↑ Axon diameter ^{34,357} ● ↓ Visual function ³⁶⁴ ● Nerve swells ³⁴ ●	↑ Axon diameter ³⁴ ● Nerve shrinks ³⁴ ●
	Immune cells	●	●	●	●	●	●	●	●
Astrocytes	● Hypertrophy ²⁷⁸ ↑ MnSOD in astrocytes ²⁷⁸ ●	● Hypertrophy ²⁷⁸ ↑ MnSOD in astrocytes ²⁷⁸ ●	● Hypertrophy ²⁷⁸ ↑ MnSOD in astrocytes ²⁷⁸ ●	●	●	●	●	●	●
Oxidative stress/damage	↑ DCF ³⁶⁴ , ↑ H ₂ O ₂ ; ↑ HOCl IS ³⁶⁵ ↓ Catalase activity ²⁷⁹ ↑ CML ³⁶⁴ in astrocytes ²⁷⁹ ↑ GluR1 ⁴⁰⁹ ↑ Mitochondrial area/autophagy ²⁹⁰ ↑ 8OHdG ²⁶⁵ ●	●	↑ DHE ²⁶⁵ ↑ Cyto. C Oxidase ³⁶⁴ ↑ CML ³⁶⁴ ●	●	●	●	●	●	
Myelin and matrix	●	●	●	●	●	●	●	●	
	↑ MnSOD in astrocytes and RGC ²⁷⁸ ↓ Ca microdomains ²⁵⁹ ↓ Atypical nodes ³⁴ ↑ Paranode length ³⁶⁴ ↑ Node length ³⁶⁴	↑ Ca microdomains ⁵⁹ ↓ Atypical nodes ³⁶⁴ ↑ Paranode length ³⁶⁴ ↑ Node length ³⁶⁴	●	●	●	●	●	●	

(continued)

TABLE 1. (CONTINUED)

Cells and pathophysiology affected	Day 1	Day 3	Day 7	Day 11/14	Day 28	3 months	6 months	
Pre-myelinating oligodendrocytes	•	↑ O4+ cells ⁴³ ↑ O4+ prolif. ⁴³ ↑ HNE in non-prolif. O4+ cells ⁴³	↑ O4+ cells ⁴³ ↑ O4+ prolif. ⁴³ # HNE in O4+ cells ⁴³	•	# O4+ cells ⁴³ ↑ O4+ prolif. ⁴³ # HNE in O4+ cells ⁴³	•	•	
Mature oligodendrocytes	↑ CCI+ Olig2+ cells ³¹⁵ # CCI+ Olig2- cells ³¹⁵ # CCI+ Olig2+ Ki67+ ³¹⁵	↑ CCI+ Olig2+ cells ³¹⁵ ↑ CCI+ Olig2- cells ³¹⁵ ↑ CCI+ Olig2+ Ki67+ ³¹⁵ ↑ CCI+ Olig2- cells ³¹⁵ ↑ 3NT, HNE & SOHDG in pre-existing and newly derived CCI+ cells ⁴³ # CCI+ cell death ³¹⁵	↑ CCI+ Olig2+ cells ³¹⁵ # CCI+ Olig2- cells ^{315,45} ↑ CCI+ Olig2+ Ki67+ ³¹⁵ # 3NT & SOHDG, but ↑ HNE, in newly derived CCI+ cells ⁴³ ↑ CCI+ cell death ³¹⁵	•	# CCI+ Olig2+ cells ³¹⁵ # CCI+ Olig2- cells ³¹⁵ ↑ CCI+ cells ³¹⁵ # CCI+ Olig2+ Ki67+ ³¹⁵ ↑ newly derived CCI+ cells ⁴³ # 3NT, HNE & SOHDG in CCI+ cells ⁴³ # CCI+ cell death ³¹⁵	# CCI+ Olig2+ cells ³¹⁵ # CCI+ Olig2- cells ³¹⁵ # CCI+ Olig2+ Ki67+ ³¹⁵	•	•
<i>Single and repeated mTBI</i>								
Cells and pathophysiology affected	Day 1	Day 3	Day 7	Day 11/14	Day 28	3 months	6 months	
Neurons and function	•	2x mTBI: ↓ MWM ³⁰⁰ 1x mTBI: ↓ foot faults beam walk ³⁰⁰ 3x mTBI - impact over lambda & bregma:	•	2x mTBI: ↓ MWM ^{300}} 2x mTBI: ↑ time beam walk ^{300}} 2x mTBI: ↑ Ibal+ resident microglia density in CC ^{300}}	•	•	1 and 2x mTBI: ↓ MWM ^{310}} • 1x mTBI: ↑ Ibal+ resident microglia size in cortex 2x mTBI: ↑ Ibal+ resident microglia size in CC ^{310}}	•
Immune cells	•	↓ Ibal+ resident microglia ^{300}}	•	•	•	•	•	

(continued)

TABLE 1. (CONTINUED)

Single and repeated mTBI	Day 1	Day 3	Day 7	Day 11/14	Day 28	3 months	6 months
<i>Cells and pathophysiology affected</i>							
Oxidative stress/damage	•	2x mTBI - impact over lambda: ↑ HNE in cortex ³⁰⁰ 3x mTBI - impact over bregma ↑ HNE in cortex ³⁰⁰	•	2x mTBI: ↑ MnSOD cortex and dentate gyrus ²⁸⁰	•	•	•
Myelin	•	3x mTBI impact over bregma ↑ MBP in cortex ³⁰⁰	•	2x mTBI: ↑ Atypical nodes in CC ²⁸⁰	•	2x mTBI: altered G ratio at post hoc level in CC ³¹⁰	•
	•	•	•	2x mTBI: ↑ Paranode length in CC ²⁸⁰	•	•	•
	•	•	•	2x mTBI: ↑ Node length in CC ²⁸⁰	•	•	•

Increases in cells means increase in cell number unless otherwise specified. "Normal" denotes return to sham-injured control level following elevation or deficit. Increases in oxidative stress indicators (HNE, 3NT, 8OHdG, GPx1, MnSOD, CML, DHE, and Cyto. C Oxidase) means increase in intensity or area of immunoreactivity. Cellular changes following partial optic nerve transection were assessed in the ventral optic nerve directly under injury site unless otherwise indicated.

Symbols: ↑, Increase relative to sham-injured control; ↓, Decrease relative to sham-injured control; •, Cells/pathophysiology were not assessed at this time-point; #, no change in; 1x, 2x, and 3x, indicate the cumulative number of mTBI delivered at 24-h intervals.

Arg1, Arginase-1; BBB, Blood-brain barrier; CML, carboxymethyl lysine; CC, corpus callosum; CNS, central nervous system; Cyto. C oxidase, cytochrome C oxidase; DCF, dichlorofluorescein; DHE, dihydroethidium; GPx1, glutathione peroxidase-1; GluR1, glutamate receptor 1; 8OHdG, 8-hydroxy-2'-deoxyguanosine; HNE, 4-hydroxynonenal; iNOS, inducible nitric oxide synthase; IS, injury site; Macs, macrophages; MBP, myelin basic protein; MyRF, myelin regulatory factor; MnSOD, manganese superoxide dismutase; mTBI, mild traumatic brain injury; MBP, myelin basic protein; MWM, performance on the Morris water maze; 3NT, 3-nitrotyrosine; OPC, oligodendrocyte progenitor cells; RGC, retinal ganglion cell; TUNEL, terminal deoxynucleotidyl transferase dUTP nick end labelling; vs, compared with.

information to design intervention strategies to minimize the oxidative damage associated with demyelination, preserve myelin, and promote remyelination where required, and in so doing preserve axonal and behavioral function.

Funding Information

The work was supported by the National Health and Medical Research Council of Australia (APP1160691).

Author Disclosure Statement

No competing financial interests exist.

References

- Dewan, M.C., Rattani, A., Gupta, S., Baticulon, R.E., Hung, Y.C., Panchak, M., Agrawal, A., Adeleye, A.O., Shrimo, M.G., Rubiano, A.M., Rosenfeld, J. V., and Park, K.B. (2019). Estimating the global incidence of traumatic brain injury. *J. Neurosurg.* 130, 1080–1097.
- James, S.L., Theadom, A., Ellenbogen, R.G., Bannick, M.S., Montjoy-Venning, W., Lucchesi, L.R., Abbasi, N., Abdulkader, R., Niguse Abraha, H., Adsuar, J.C., Afarideh, M., Agrawal, S., Ahmadi, A., Beshir Ahmed, M., Nidhal Aichour, A., Aichour, I., Taki Eddine Aichour, M., Olusola Akinyemi, R., Akseer, N., Alahdab, F., Alebel, A., Alghnam, S.A., Abdulqadir Ali, B., Alsharif, U., Altirkawi, K., Liliana Andrei, C., Anjomshoa, M., Ansari, H., Geleto Ansha, M., Abelardo Antonio, C.T., Christopher Yaw Appiah, S., Ariani, F., Gebremedhin Asefa, N., Weldegebreal Asgedom, S., Atique, S., Awasthi, A., Paulina Ayala Quintanilla, B., Ayuk, T.B., Azzopardi, P.S., Badali, H., Badawi, A., Balalla, S., Banstola, A., Lyn Barker-Collo, S., Winfried BÄ, T., Bedi, N., Behzadifar, M., Behzadifar, M., Begashaw Bekele, B., Bekele Belachew, A., Abebe Belay, Y., Bennett, D.A., Bensenor, I.M., Berhane, A., Beuran, M., Bhalla, A., Bhaumik, S., Bhutta, Z.A., Biadgo, B., Biffino, M., Bijani, A., Bililign, N., Birungi, C., Boufous, S., Brazinova, A., Brown, A.W., Car, M., Cã, R., Carrero, J.J., Carvalho, L., Castaã, C.A., Chaiah, Y., Paula Champs, A., Chang, J.-C., Choi, J.-Y.J., Christopher, D.J., Cooper, C., Stephen Crowe, C., Dandona, L., Dandona, R., Daryani, A., Virgil Davitoliu, D., Girma Degefa, M., Teklemariam Demoz, G., Deribe, K., Djalalinia, S., Phuc Do, H., Teye Doku, D., Drake, T.M., Dubey, M., Dubljanin, E., El-Khatib, Z., Ofori-Asenso, R., Eskandarieh, S., Esteghamati, A., Esteghamati, S., Faro, A., Farzadfar, F., et al. (2019). Global, regional, and national burden of traumatic brain injury and spinal cord injury, 1990–2016: a systematic analysis for the Global Burden of Disease Study 2016. *Lancet Neurol.* 18, 56–87.
- Lindquist, L.K., Love, H.C., and Elbogen, E.B. (2017). Traumatic brain injury in Iraq and Afghanistan veterans: new results from a national random sample study. *J. Neuropsychiatry Clin. Neurosci.* 29, 254–259.
- Khan, F., Amatya, B., Judson, R., Elmalik, A., and Galea, M.P. (2016). Factors associated with long-term functional and psychological outcomes in persons with moderate to severe traumatic brain injury. *J. Rehabil. Med.* 48, 442–448.
- Initiative, T.V.N. (2009). The economic cost of spinal cord injury and traumatic brain injury in Australia Report by Access Economics Pty Limited for The Victorian Neurotrauma Initiative. Rep. by Access Econ. Vic. Neurotrauma Initiat., 31.
- Johnson, V.E., Stewart, W., and Smith, D.H. (2010). Traumatic brain injury and amyloid- β pathology: a link to Alzheimer's disease? *Nat. Rev. Neurosci.* 11, 361.
- Impellizzeri, D., Campolo, M., Bruschetta, G., Crupi, R., Cordaro, M., Paterniti, I., Cuzzocrea, S., and Esposito, E. (2016). Traumatic brain injury leads to development of Parkinson's disease related pathology in mice. *Front. Neurosci.* 10, 458.
- Corrigan, J.D., Selassie, A.W., and Orman, J.A. (2010). The epidemiology of traumatic brain injury. *J. Head Trauma Rehabil.* 25, 72–80.
- Maas, A.I.R., Menon, D.K., Adelson, P.D., Andelic, N., Bell, M.J., Belli, A., Bragge, P., Brazinova, A., Büki, A., Chesnut, R.M., Citerio, G., Coburn, M., Cooper, D.J., Crowder, A.T., Czeiter, E., Czornyka, M., Diaz-Arastia, R., Dreier, J.P., Duhaime, A.-C., Ercole, A., van Essen, T.A., Feigin, V.L., Gao, G., Giacino, J., Gonzalez-Lara, L.E., Gruen, R.L., Gupta, D., Hartings, J.A., Hill, S., Jiang, J., Ketharanathan, N., Kompanje, E.J.O., Lanyon, L., Laureys, S., Lecky, F., Levin, H., Lingsma, H.F., Maegele, M., Majdan, M., Manley, G., Marsteller, J., Mascia, L., McFadyen, C., Mondello, S., Newcombe, V., Palotie, A., Parizel, P.M., Peul, W., Piercy, J., Polinder, S., Puybasset, L., Rasmussen, T.E., Rossaint, R., Smielewski, P., Söderberg, J., Stanworth, S.J., Stein, M.B., von Steinbüchel, N., Stewart, W., Steyerberg, E.W., Stocchetti, N., Synnot, A., Te Ao, B., Tenovuo, O., Theadom, A., Tibboel, D., Videtta, W., Wang, K.K.W., Williams, W.H., Wilson, L., Yaffe, K., Adams, H., Agnoletti, V., Allanson, J., Amrein, K., Andaluz, N., Anke, A., Antoni, A., van As, A.B., Audibert, G., Azaševac, A., Azouvi, P., Azzolini, M.L., Baciu, C., Badenes, R., Barlow, K.M., Bartels, R., Bauerfeind, U., Beauchamp, M., Beer, D., Beer, R., Belda, F.J., Bellander, B.-M., Bellier, R., Benali, H., Benard, T., Beqiri, V., Beretta, L., et al. (2017). Traumatic brain injury: integrated approaches to improve prevention, clinical care, and research. *Lancet Neurol.* 16, 987–1048.
- Andriessen, T.M.J.C.J.C., Horn, J., Franschman, G., van der Naalt, J., Haitsma, I., Jacobs, B., Steyerberg, E.W., and Vos, P.E. (2011). Epidemiology, severity classification, and outcome of moderate and severe traumatic brain injury: a prospective multicenter study. *J. Neurotrauma* 28, 2019–2031.
- Broadway, J.M., Rieger, R.E., Campbell, R.A., Quinn, D.K., Mayer, A.R., Yeo, R.A., Wilson, J.K., Gill, D., Fratzke, V., and Cavanagh, J.F. (2019). Executive function predictors of delayed memory deficits after mild traumatic brain injury. *Cortex* 120, 240–248.
- Ling, H., Hardy, J., and Zetterberg, H. (2015). Neurological consequences of traumatic brain injuries in sports. *Mol. Cell. Neurosci.* 66, 114–122.
- Vakil, E., Greenstein, Y., Weiss, I., and Shtein, S. (2019). The effects of moderate-to-severe traumatic brain injury on episodic memory: a meta-analysis. *Neuropsychol. Rev.* 29, 270–287.
- Norman, R.S., Shah, M.N., and Turkstra, L.S. (2019). Brain injury reaction time and cognitive-linguistic performance in adults with mild traumatic brain injury. *Brain Inj.* 33, 1173–1183.
- Fehily, B., and Fitzgerald, M. (2017). Repeated mild traumatic brain injury: potential mechanisms of damage. *Cell Transplant.* 26, 1131–1155.
- Saunders, L., Selassie, A.W., Hill, E.G., Nicholas, J.S., Horner, M.D., Corrigan, J.D., and Lackland, D.T. (2009). A population-based study of repetitive traumatic brain injury among persons with traumatic brain injury. *Brain Inj.* 23, 866–872.
- Turgeon, A.F., Lauzier, F., Zarychanski, R., Fergusson, D.A., Léger, C., McIntyre, L.A., Bernard, F., Rigamonti, A., Burns, K., Griesdale, D.E., Green, R., Scales, D.C., Meade, M.O., Savard, M., Shemilt, M., Paquet, J., Gariépy, J.L., Lavoie, A., Reddy, K., Jichici, D., Paggiarello, G., Zygun, D., and Moore, L. (2017). Prognostication in critically ill patients with severe traumatic brain injury: the TBI-Prognosis multicentre feasibility study. *BMJ Open* 7, e013779.
- Hukkelhoven, C.W.P.M., Steyerberg, E.W., Rampen, A.J.J., Farace, E., Habbema, J.D.F., Marshall, L.F., Murray, G.D., and Maas, A.I.R. (2003). Patient age and outcome following severe traumatic brain injury: an analysis of 5600 patients. *J. Neurosurg.* 99, 666–673.
- Ruet, A., Bayen, E., Jourdan, C., Ghout, I., Meaud, L., Lalanne, A., Pradat-Diehl, P., Nelson, G., Charanton, J., Aegerter, P., Vallat-Azouvi, C., and Azouvi, P. (2019). A detailed overview of long-term outcomes in severe traumatic brain injury eight years post-injury. *Front. Neurol.* 10, 120.
- Ryan, N.P., van Bijnen, L., Catroppa, C., Beauchamp, M.H., Crossley, L., Hearn, S., and Anderson, V. (2016). Longitudinal outcome and recovery of social problems after pediatric traumatic brain injury (TBI): contribution of brain insult and family environment. *Int. J. Dev. Neurosci.* 49, 23–30.
- Werner, C., and Engelhard, K. (2007). Pathophysiology of traumatic brain injury. *Br. J. Anaesth.* 99, 4–9.
- Dong, X.-X., Wang, Y., and Qin, Z.-H. (2009). Molecular mechanisms of excitotoxicity and their relevance to pathogenesis of neurodegenerative diseases. *Acta Pharmacol. Sin. Acta Pharmacol. Sin.* 30, 379–387.
- Doan, N., Patel, M., Doan, H., Janich, K., Nguyen, H.S., and Shabani, S. (2016). Traumatic brain injury. *Int. J. Phys. Med. Rehabil.* 4, 120–121.
- Donkin, J.J., and Vink, R. (2010). Mechanisms of cerebral edema in traumatic brain injury: therapeutic developments. *Curr. Opin. Neurol.* 23, 293–299.
- Atali, A.S., Fowler, R.A., Mainprize, T.G., Scales, D.C., Kiss, A., De Mestral, C., Ray, J.G., and Nathens, A.B. (2013). Intracranial pressure monitoring in severe traumatic brain injury: results from the

- american college of surgeons trauma quality improvement program. *J. Neurotrauma* 30, 1737–1746.
26. Quintard, H., Lebourdon, X., Staccini, P., and Ichai, C. (2015). Decompression surgery for severe traumatic brain injury (TBI): a long-term, single-centre experience. *Anaesth. Crit. Care Pain Med.* 34, 79–82.
 27. McBride, D.W., Szu, J.L., Hale, C., Hsu, M.S., Rodgers, V.G.J., and Binder, D.K. (2014). Reduction of cerebral edema after traumatic brain injury using an osmotic transport device. *J. Neurotrauma* 31, 1948–1954.
 28. Majdan, M., Mauritz, W., Wilbacher, I., Brazinova, A., Rusnak, M., and Leitgeb, J. (2013). Barbiturates use and its effects in patients with severe traumatic brain injury in five European countries. *J. Neurotrauma* 30, 23–29.
 29. Borg, J., Holm, L., Peloso, P.M., Cassidy, J.D., Carroll, L.J., von Holst, H., Paniak, C., and Yates, D. (2004). Non-surgical intervention and cost for mild traumatic brain injury: results of the WHO Collaborating Centre Task Force on Mild Traumatic Brain Injury. *J. Rehabil. Med. Suppl.*, 76–83.
 30. Kwon, B.K., Okon, E., Hillyer, J., Mann, C., Baptiste, D., Weaver, L.C., Fehlings, M.G., and Tetzlaff, W. (2011). A systematic review of non-invasive pharmacologic neuroprotective treatments for acute spinal cord injury. *J. Neurotrauma* 28, 1545–1588.
 31. Maxwell, W.L., and Graham, D.I. (2003). Diffuse axonal injury (DAI), in: *Encyclopedia of the Neurological Sciences*. Elsevier, pps. 10–12.
 32. Vieira, R. de C.A., Paiva, W.S., De Oliveira, D.V., Teixeira, M.J., De Andrade, A.F., and De Sousa, R.M.C. (2016). Diffuse axonal injury: epidemiology, outcome and associated risk factors. *Front. Neurol.* 7, 178.
 33. Hill, C.S., Coleman, M.P., and Menon, D.K. (2016). Traumatic axonal injury: mechanisms and translational opportunities. *Trends Neurosci.* 39, 311–324.
 34. Payne, S.C., Bartlett, C.A., Harvey, A.R., Dunlop, S.A., and Fitzgerald, M. (2012). Myelin sheath decompaction, axon swelling, and functional loss during chronic secondary degeneration in rat optic nerve. *Investig. Ophthalmol. Vis. Sci.* 53, 6093–6101.
 35. Batchelor, P.E., Tan, S., Wills, T.E., Porritt, M.J., and Howells, D.W. (2008). Comparison of inflammation in the brain and spinal cord following mechanical injury. *J. Neurotrauma* 25, 1217–1225.
 36. Braun, M., Vaibhav, K., Saad, N.M., Fatima, S., Vender, J.R., Baban, B., Hoda, M.N., and Dhandapani, K.M. (2017). White matter damage after traumatic brain injury: a role for damage associated molecular patterns. *Biochim. Biophys. Acta - Mol. Basis Dis.* 1863, 2614–2626.
 37. Charraud, S., Zahr, N., Sullivan, E. V., and Pfefferbaum, A. (2010). MR diffusion tensor imaging: a window into white matter integrity of the working brain. *Neuropsychol. Rev.* 20, 209–225.
 38. Riedy, G., Senseney, J.S., Liu, W., Ollinger, J., Sham, E., Krapiva, P., Patel, J.B., Smith, A., Yeh, P.H., Graner, J., Nathan, D., Caban, J., French, L.M., Harper, J., Eskay, V., Morissette, J., and Oakes, T.R. (2016). Findings from structural MR imaging in military traumatic brain injury. *Radiology* 279, 207–215.
 39. Johnson, B., Gay, M., Zhang, K., Neuberger, T., Horowitz, S.G., Hallett, M., Sebastianelli, W., and Slobounov, S. (2012). The use of magnetic resonance spectroscopy in the subacute evaluation of athletes recovering from single and multiple mild traumatic brain injury. *J. Neurotrauma* 29, 2297–2304.
 40. Lotocki, G., Vaccari, J. de R., Alonso, O., Molano, J.S., Nixon, R., Dietrich, W.D., and Bramlett, H.M. (2011). Oligodendrocyte vulnerability following traumatic brain injury in rats: effect of moderate hypothermia. *Ther. Hypothermia Temp. Manag.* 1, 43–51.
 41. Flygt, J., Djupsjö, A., Lenne, F., and Marklund, N. (2013). Myelin loss and oligodendrocyte pathology in white matter tracts following traumatic brain injury in the rat. *Eur. J. Neurosci.* 38, 2153–2165.
 42. O'Hare Doig, R.L., Chiha, W., Giacci, M.K., Yates, N.J., Bartlett, C.A., Smith, N.M., Hodgetts, S.L., Harvey, A.R., and Fitzgerald, M. (2017). Specific ion channels contribute to key elements of pathology during secondary degeneration following neurotrauma. *BMC Neurosci.* 18, 62.
 43. Giacci, M.K., Bartlett, C.A., Smith, N.M., Iyer, K.S., Toomey, L.M., Jiang, H., Guagliardo, P., Kilburn, M.R., and Fitzgerald, M. (2018). Oligodendroglia are particularly vulnerable to oxidative damage after neurotrauma in vivo. *J. Neurosci.* 38, 6491–6504.
 44. Dawson, M.R.L., Politò, A., Levine, J.M., and Reynolds, R. (2003). NG2-expressing glial progenitor cells: an abundant and widespread population of cycling cells in the adult rat. *CNS* 24, 476–488.
 45. Valério-Gomes, B., Guimarães, D.M., Szczupak, D., and Lent, R. (2018). The absolute number of oligodendrocytes in the adult mouse brain. *Front. Neuroanat.* 12, 90.
 46. Emery, B., and Lu, Q.R. (2015). Transcriptional and epigenetic regulation of oligodendrocyte development and myelination in the central nervous system. *Cold Spring Harb. Perspect. Biol.* 7, a020461.
 47. Bergles, D.E., and Richardson, W.D. (2016). Oligodendrocyte development and plasticity. *Cold Spring Harb. Perspect. Biol.* 8, a020453.
 48. Tripathi, R.B., Clarke, L.E., Burzomato, V., Kessar, N., Anderson, P.N., Attwell, D., and Richardson, W.D. (2011). Dorsally and ventrally derived oligodendrocytes have similar electrical properties but myelinate preferred tracts. *J. Neurosci.* 31, 6809–6819.
 49. Walsh, D.M., Röth, P.T., Holmes, W.R., Landman, K.A., Merson, T.D., and Hughes, B.D. (2016). Is cell migration or proliferation dominant in the formation of linear arrays of oligodendrocytes? *J. Theor. Biol.* 406, 17–30.
 50. Foerster, S., Hill, M.F.E., and Franklin, R.J.M. (2019). Diversity in the oligodendrocyte lineage: plasticity or heterogeneity? *Glia* 67, 1797–1805.
 51. Walsh, D.M., Merson, T.D., Landman, K.A., and Hughes, B.D. (2016). Evidence for cooperative selection of axons for myelination by adjacent oligodendrocytes in the optic nerve. *PLoS One* 11, e0165673.
 52. Young, K.M., Psachoulia, K., Tripathi, R.B., Dunn, S.J., Cossell, L., Attwell, D., Tohyama, K., and Richardson, W.D. (2013). Oligodendrocyte dynamics in the healthy adult CNS: evidence for myelin remodeling. *Neuron* 77, 873–885.
 53. Soreq, L., Rose, J., Soreq, E., Hardy, J., Trabzuni, D., Cookson, M.R., Smith, C., Ryten, M., Patani, R., and Ule, J. (2017). Major shifts in glial regional identity are a transcriptional hallmark of human brain aging. *Cell Rep.* 18, 557–570.
 54. Crawford, A.H., Tripathi, R.B., Richardson, W.D., and Franklin, R.J.M. (2016). Developmental origin of oligodendrocyte lineage cells determines response to demyelination and susceptibility to age-associated functional decline. *Cell Rep.* 15, 761–773.
 55. Floriddia, E.M., Zhang, S., Brugger, D. van Santos, J.P.G. dos, Alunkö, M., Förster, S., Tripathi, R.B., Richardson, W.D., Franklin, R.J.M., and Castelo-Branco, G. (2019). Specific oligodendrocyte populations have differential spatial distribution and susceptibility to injury. *bioRxiv*, 580985.
 56. Dimou, L., Simon, C., Kirchhoff, F., Takebayashi, H., and Gotz, M. (2008). Progeny of Olig2-expressing progenitors in the gray and white matter of the adult mouse cerebral cortex. *J. Neurosci.* 28, 10434–10442.
 57. Marques, S., Zeisel, A., Codeluppi, S., Van Bruggen, D., Falcão, A.M., Xiao, L., Li, H., Häring, M., Hochgerner, H., Romanov, R.A., Gyllberg, D., Muñoz-Manchado, A.B., La Manno, G., Lönnberg, P., Floriddia, E.M., Rezayee, F., Erboms, P., Arenas, E., Hjerling-Lefler, J., Harkany, T., Richardson, W.D., Linnarsson, S., and Castelo-Branco, G. (2016). Oligodendrocyte heterogeneity in the mouse juvenile and adult central nervous system. *Science* 352, 1326–1329.
 58. Sanchez, M.A., and Armstrong, R.C. (2018). Postnatal sonic hedgehog (Shh) responsive cells give rise to oligodendrocyte lineage cells during myelination and in adulthood contribute to remyelination. *Exp. Neurol.* 299, 122–136.
 59. Weider, M., Starost, L.J., Groll, K., Küspert, M., Sock, E., Wedel, M., Fröb, F., Schmitt, C., Baroti, T., Hartwig, A.C., Hillgärtner, S., Piefke, S., Fadler, T., Ehrlich, M., Ehlert, C., Stehling, M., Albrecht, S., Jabali, A., Schöler, H.R., Winkler, J., Kuhlmann, T., and Wegner, M. (2018). Nfat/calcineurin signaling promotes oligodendrocyte differentiation and myelination by transcription factor network tuning. *Nat. Commun.* 9, 899.
 60. Liu, Z., Hu, X., Cai, J., Liu, B., Peng, X., Wegner, M., and Qiu, M. (2007). Induction of oligodendrocyte differentiation by Olig2 and Sox10: evidence for reciprocal interactions and dosage-dependent mechanisms. *Dev. Biol.* 302, 683–693.
 61. Hornig, J., Fröb, F., Vogl, M.R., Hermans-Borgmeyer, I., Tamm, E.R., and Wegner, M. (2013). The transcription factors Sox10 and Myrf define an essential regulatory network module in differentiating oligodendrocytes. *PLoS Genet.* 9, e1003907.
 62. Elbaz, B., and Popko, B. (2019). Molecular control of oligodendrocyte development. *Trends Neurosci.* 42, 263–277.

63. Camargo, N., Goudriaan, A., van Deijk, A.L.F., Otte, W.M., Brouwers, J.F., Lodder, H., Gutmann, D.H., Nave, K.A., Dijkhuizen, R.M., Mansvelter, H.D., Chrast, R., Smit, A.B., and Verheijen, M.H.G. (2017). Oligodendroglial myelination requires astrocyte-derived lipids. *PLoS Biol.* 15, e1002605.
64. Figlia, G., Gerber, D., and Suter, U. (2018). Myelination and mTOR. *Glia* 66, 693–707.
65. Koreman, E., Sun, X., and Lu, Q.R. (2018). Chromatin remodeling and epigenetic regulation of oligodendrocyte myelination and myelin repair. *Mol. Cell. Neurosci.* 87, 18–26.
66. Wei, C.W., Luo, T., Zou, S.S., and Wu, A.S. (2018). The role of long noncoding RNAs in central nervous system and neurodegenerative diseases. *Front. Behav. Neurosci.* 12, 175.
67. He, D., Wang, J., Lu, Y., Deng, Y., Zhao, C., Xu, L., Chen, Y., Hu, Y.C., Zhou, W., and Lu, Q.R. (2017). lncRNA functional networks in oligodendrocytes reveal stage-specific myelination control by an lncOL1/Suz12 complex in the CNS. *Neuron* 93, 362–378.
68. Li, Y., Guo, B., Yang, R., Xiao, Z., Gao, X., Yu, J., Li, S., and Luo, Y. (2018). A novel long noncoding RNA lnc158 promotes the differentiation of mouse neural precursor cells into oligodendrocytes by targeting nuclear factor- κ B. *Neuroreport* 29, 1121–1128.
69. O'Brien, J., Hayder, H., Zayed, Y., and Peng, C. (2018). Overview of microRNA biogenesis, mechanisms of actions, and circulation. *Front. Endocrinol. (Lausanne)* 9, 402.
70. Zhao, X., He, X., Han, X., Yu, Y., Ye, F., Chen, Y., Hoang, T.N., Xu, X., Mi, Q.S., Xin, M., Wang, F., Appel, B., and Lu, Q.R. (2010). MicroRNA-mediated control of oligodendrocyte differentiation. *Neuron* 65, 612–626.
71. Mitew, S., Hay, C.M., Peckham, H., Xiao, J., Koenning, M., and Emery, B. (2014). Mechanisms regulating the development of oligodendrocytes and central nervous system myelin. *Neuroscience* 276, 29–47.
72. Nave, K.-A., and Werner, H.B. (2014). Myelination of the nervous system: mechanisms and functions. *Annu. Rev. Cell Dev. Biol.* 30, 503–533.
73. Bradl, M., and Lassmann, H. (2010). Oligodendrocytes: biology and pathology. *Acta Neuropathol.* 119, 37–53.
74. Norton, W.T., and Poduslo, S.E. (1973). Myelination in rat brain: changes in myelin composition during brain maturation. *J. Neurochem.* 21, 759–73.
75. Min, Y., Kristiansen, K., Boggs, J.M., Husted, C., Zasadzinski, J.A., and Israelachvili, J. (2009). Interaction forces and adhesion of supported myelin lipid bilayers modulated by myelin basic protein. *Proc. Natl. Acad. Sci. U. S. A.* 106, 3154–9.
76. Baumann, N., and Pham-Dinh, D. (2017). Biology of oligodendrocyte and myelin in the mammalian central nervous system. *Physiol. Rev.* 81, 871–927.
77. Donaldson, H., and Hoke, G.W. (1905). On the areas of the axis cylinder and medullary sheath as seen in cross sections of the spinal nerves of vertebrates. *J. Comp. Neurol. Psychol.* 15, 1–16.
78. Fraga, C.G., Shigenaga, M.K., Park, J.W., Degan, P., and Ames, B.N. (1990). Oxidative damage to DNA during aging: 8-Hydroxy-2'-deoxyguanosine in rat organ DNA and urine. *Proc. Natl. Acad. Sci. U. S. A.* 87, 4533–4537.
79. Aggarwal, S., Yurlova, L., and Simons, M. (2011). Central nervous system myelin: structure, synthesis and assembly. *Trends Cell Biol.* 21, 585–593.
80. Hildebrand, C., Remahl, S., Persson, H., and Bjartmar, C. (1993). Myelinated nerve fibres in the CNS. *Prog. Neurobiol.* 40, 319–384.
81. Richter-Landsberg, C. (2008). The cytoskeleton in oligodendrocytes. *J. Mol. Neurosci.* 35, 55–63.
82. Arancibia-Carcamo, I., and Attwell, D. (2014). The node of Ranvier in CNS pathology. *Acta Neuropathol.* 128, 161–175.
83. Rasband, M.N., and Trimmer, J.S. (2001). Developmental clustering of ion channels at and near the node of Ranvier. *Dev. Biol.* 236, 5–16.
84. Kanda, H., Ling, J., Tomomura, S., Noguchi, K., Matalon, S., and Gu, J.G. (2019). TREK-1 and TRAAK are principal K⁺ channels at the nodes of Ranvier for rapid action potential conduction on mammalian myelinated afferent nerves. *Neuron* 104, 960–971.
85. Pedraza, L., Huang, J.K., and Colman, D.R. (2001). Organizing principles of the axoglial apparatus. *Neuron* 30, 335–344.
86. Rosenbluth, J. (2009). Multiple functions of the paranodal junction of myelinated nerve fibers. *J. Neurosci. Res.* 87, 3250–3258.
87. Philips, T., and Rothstein, J.D. (2017). Oligodendroglia: metabolic supporters of neurons. *J. Clin. Invest.* 127, 3271–3280.
88. Wilkins, A., Majed, H., Layfield, R., Compston, A., and Chandran, S. (2003). Oligodendrocytes promote neuronal survival and axonal length by distinct intracellular mechanisms: a novel role for oligodendrocyte-derived glial cell line-derived neurotrophic factor. *J. Neurosci.* 23, 4967–4974.
89. Oluich, L.-J., Stratton, J.A.S., Lulu Xing, Y., Ng, S.W., Cate, H.S., Sah, P., Windels, F., Kilpatrick, T.J., and Merson, T.D. (2012). Targeted ablation of oligodendrocytes induces axonal pathology independent of overt demyelination. *J. Neurosci.* 32, 8317–8330.
90. Griffiths, I., Klugmann, M., Anderson, T., Yool, D., Thomson, C., Schwab, M.H., Schneider, A., Zimmermann, F., McCulloch, M., Nadon, N., and Nave, K.A. (1998). Axonal swellings and degeneration in mice lacking the major proteolipid of myelin. *Science* 280, 1610–1613.
91. Lappe-Siefke, C., Goebbels, S., Gravel, M., Nicksch, E., Lee, J., Braun, P.E., Griffiths, I.R., and Nave, K.A. (2003). Disruption of Cnp1 uncouples oligodendroglial functions in axonal support and myelination. *Nat. Genet.* 33, 366–374.
92. Frühbeis, C., Fröhlich, D., Kuo, W.P., and Krämer-Albers, E.-M. (2013). Extracellular vesicles as mediators of neuron-glia communication. *Front. Cell. Neurosci.* 7, 182.
93. Gibson, E.M., Purger, D., Mount, C.W., Goldstein, A.K., Lin, G.L., Wood, L.S., Inema, I., Miller, S.E., Bieri, G., Zuchero, J.B., Barres, B.A., Woo, P.J., Vogel, H., and Monje, M. (2014). Neuronal Activity Promotes Oligodendrogenesis and Adaptive Myelination in the Mammalian Brain NIH Public Access. *Science* 344, 1252304.
94. Foster, A.Y., Bujalka, H., and Emery, B. (2019). Axoglial interactions in myelin plasticity: evaluating the relationship between neuronal activity and oligodendrocyte dynamics. *Glia*, 2038–2049.
95. Jang, M., Gould, E., Xu, J., Kim, E.J., and Kim, J.H. (2019). Oligodendrocytes regulate presynaptic properties and neurotransmission through BDNF signaling in the mouse brainstem. *Elife* 8, pii: e42156.
96. Hughes, A.N., and Appel, B. (2019). Oligodendrocytes express synaptic proteins that modulate myelin sheath formation. *Nat. Commun.* 10, 4125.
97. Nakano, M., Tamura, Y., Yamato, M., Kume, S., Eguchi, A., Takata, K., Watanabe, Y., and Kataoka, Y. (2017). NG2 glial cells regulate neuroimmunological responses to maintain neuronal function and survival. *Sci. Rep.* 7, 42041.
98. Maki, T. (2017). Novel roles of oligodendrocyte precursor cells in the developing and damaged brain. *Clin. Exp. Neuroimmunol.* 8, 33–42.
99. Miyamoto, N., Pham, L.D.D., Seo, J.H., Kim, K.W., Lo, E.H., and Arai, K. (2014). Crosstalk between cerebral endothelium and oligodendrocyte. *Cell. Mol. Life Sci.* 71, 1055–1066.
100. Seo, J.H., Maki, T., Maeda, M., Miyamoto, N., Liang, A.C., Haya-kawa, K., Pham, L.D.D., Suwa, F., Taguchi, A., Matsuyama, T., Ihara, M., Kim, K.W., Lo, E.H., and Arai, K. (2014). Oligodendrocyte precursor cells support blood-brain barrier integrity via TGF- β signaling. *PLoS One* 9, e103174.
101. Arai, K., and Lo, E.H. (2009). Oligovascular signaling in white matter stroke. *Biol. Pharm. Bull.* 32, 1639–1644.
102. Arai, K., and Lo, E.H. (2009). An oligovascular niche: cerebral endothelial cells promote the survival and proliferation of oligodendrocyte precursor cells. *J. Neurosci.* 29, 4351–4355.
103. Arai, K., and Lo, E.H. (2010). Astrocytes protect oligodendrocyte precursor cells via MEK/ERK and PI3K/Akt signaling. *J. Neurosci. Res.* 88, 758–763.
104. Maki, T., Maeda, M., Uemura, M., Lo, E.K., Terasaki, Y., Liang, A.C., Shindo, A., Choi, Y.K., Taguchi, A., Matsuyama, T., Takahashi, R., Ihara, M., and Arai, K. (2015). Potential interactions between pericytes and oligodendrocyte precursor cells in perivascular regions of cerebral white matter. *Neurosci. Lett.* 597, 164–169.
105. Yuen, T.J., Silbereis, J.C., Griveau, A., Chang, S.M., Daneman, R., Fancy, S.P.J., Zahed, H., Maltepe, E., and Rowitch, D.H. (2014). Oligodendrocyte-encoded HIF function couples postnatal myelination and white matter angiogenesis. *Cell* 158, 383–396.
106. Gaudet, A.D., Popovich, P.G., and Ramer, M.S. (2011). Wallerian degeneration: gaining perspective on inflammatory events after peripheral nerve injury. *J. Neuroinflammation* 8, 110.
107. Armstrong, R.C., Mierzwa, A.J., Marion, C.M., and Sullivan, G.M. (2016). White matter involvement after TBI: clues to axon and myelin repair capacity. *Exp. Neurol.* 275, 328–333.
108. Buss, A., Brook, G.A., Kakulas, B., Martin, D., Franzen, R., Schoenen, J., Noth, J., and Schmitt, A.B. (2004). Gradual loss of

- myelin and formation of an astrocytic scar during Wallerian degeneration in the human spinal cord. *Brain* 127, 34–44.
109. Abderezaei, J., Zhao, W., Grijalva, C.L., Fabris, G., Ji, S., Laksari, K., and Kurt, M. (2019). Nonlinear dynamical behavior of the deep white matter during head impact. *Phys. Rev. Appl.* 12, 14058.
 110. Sullivan, S., Eucker, S.A., Gabrieli, D., Bradfield, C., Coats, B., Maltese, M.R., Lee, J., Smith, C., and Margulies, S.S. (2015). White matter tract-oriented deformation predicts traumatic axonal brain injury and reveals rotational direction-specific vulnerabilities. *Bio-mech. Model. Mechanobiol.* 14, 877–896.
 111. De Rooij, R., and Kuhl, E. (2018). Physical biology of axonal damage. *Front. Cell. Neurosci.* 12, 144.
 112. Leonard, A. V., Thornton, E., and Vink, R. (2015). The relative contribution of edema and hemorrhage to raised intrathecal pressure after traumatic spinal cord injury. *J. Neurotrauma* 32, 397–402.
 113. Gonzalez, R., Glaser, J., Liu, M.T., Lane, T.E., and Keirstead, H.S. (2003). Reducing inflammation decreases secondary degeneration and functional deficit after spinal cord injury. *Exp. Neurol.* 184, 456–463.
 114. Li, H.-Y., Ruan, Y.-W., Ren, C.-R., Cui, Q., and So, K.-F. (2014). Mechanisms of secondary degeneration after partial optic nerve transection. *Neural Regen. Res.* 9, 565–74.
 115. Sharif-Alhoseini, M., Khormali, M., Rezaei, M., Safdarian, M., Hajghadery, A., Khalatbari, M.M., Safdarian, M., Meknatkhan, S., Rezvan, M., Chalangari, M., Derakhshan, P., and Rahimi-Movaghar, V. (2017). Animal models of spinal cord injury: a systematic review. *Spinal Cord* 55, 714–721.
 116. Shultz, S.R., McDonald, S.J., Vonder Haar, C., Meconi, A., Vink, R., van Donkelaar, P., Taneja, C., Iverson, G.L., and Christie, B.R. (2017). The potential for animal models to provide insight into mild traumatic brain injury: translational challenges and strategies. *Neurosci. Biobehav. Rev.* 76, 396–414.
 117. DeWitt, D.S., Perez-Polo, R., Hulsebosch, C.E., Dash, P.K., and Robertson, C.S. (2013). Challenges in the development of rodent models of mild traumatic brain injury. *J. Neurotrauma* 30, 688–701.
 118. Thompson, H.J., Lifshitz, J., Marklund, N., Grady, M.S., Graham, D.L., Hovda, D.A., and McIntosh, T.K. (2005). Lateral fluid percussion brain injury: a 15-year review and evaluation. *J. Neurotrauma* 22, 42–75.
 119. Ma, X., Aravind, A., Pfister, B.J., Chandra, N., and Haorah, J. (2019). Animal models of traumatic brain injury and assessment of injury severity. *Mol. Neurobiol.* 56, 5332–5345.
 120. Mierzwa, A.J., Marion, C.M., Sullivan, G.M., McDaniel, D.P., and Armstrong, R.C. (2015). Components of myelin damage and repair in the progression of white matter pathology after mild traumatic brain injury. *J. Neuropathol. Exp. Neurol.* 74, 218–232.
 121. Mouzon, B.C., Bachmeier, C., Ojo, J.O., Acker, C.M., Ferguson, S., Paris, D., Ait-Ghezala, G., Crynen, G., Davies, P., Mullan, M., Stewart, W., and Crawford, F. (2018). Lifelong behavioral and neuropathological consequences of repetitive mild traumatic brain injury. *Ann. Clin. Transl. Neurol.* 5, 64–80.
 122. Mouzon, B., Bachmeier, C., Ojo, J., Acker, C., Ferguson, S., Crynen, G., Davies, P., Mullan, M., Stewart, W., and Crawford, F. (2019). Chronic white matter degeneration, but no tau pathology at one-year post-repetitive mild traumatic brain injury in a tau transgenic model. *J. Neurotrauma* 36, 576–588.
 123. Namjoshi, D.R., Cheng, W.H., McInnes, K.A., Martens, K.M., Carr, M., Wilkinson, A., Fan, J., Robert, J., Hayat, A., Crompton, P.A., and Wellington, C.L. (2014). Merging pathology with biomechanics using CHIMERA (Closed-Head Impact Model of Engineered Rotational Acceleration): a novel, surgery-free model of traumatic brain injury. *Mol. Neurodegener.* 9, 55.
 124. Namjoshi, D.R., Cheng, W.H., Bashir, A., Wilkinson, A., Stukas, S., Martens, K.M., Whyte, T., Abebe, Z.A., McInnes, K.A., Crompton, P.A., and Wellington, C.L. (2017). Defining the biomechanical and biological threshold of murine mild traumatic brain injury using CHIMERA (Closed Head Impact Model of Engineered Rotational Acceleration). *Exp. Neurol.* 292, 80–91.
 125. Kane, M.J., Angoa-Pérez, M., Briggs, D.I., Viano, D.C., Kreipke, C.W., and Kuhn, D.M. (2012). A mouse model of human repetitive mild traumatic brain injury. *J. Neurosci. Methods* 203, 41–9.
 126. Dai, J.X., Ma, Y., Bin, L., N.Y., Cao, J., and Wang, Y. (2018). Large animal models of traumatic brain injury. *Int. J. Neurosci.* 128, 243–254.
 127. Sorby-Adams, A.J., Vink, R., and Turner, R.J. (2018). Large animal models of stroke and traumatic brain injury as translational tools. *Am. J. Physiol. Regul. Integr. Comp. Physiol.* 315, R165–R190.
 128. Blair, M., Pease, M.E., Hammond, J., Valenta, D., Kielczewski, J., Levkovitch-Verbin, H., and Quigley, H. (2005). Effect of glatiramer acetate on primary and secondary degeneration of retinal ganglion cells in the rat. *Investig. Ophthalmology Vis. Sci.* 46, 884.
 129. Levkovitch-Verbin, H., Quigley, H.A., Martin, K.R.G., Zack, D.J., Pease, M.E., and Valenta, D.F. (2003). A model to study differences between primary and secondary degeneration of retinal ganglion cells in rats by partial optic nerve transection. *Investig. Ophthalmology Vis. Sci.* 44, 3388.
 130. Smith, N.M., Gachulinova, I., Ho, D., Bailey, C., Bartlett, C.A., Norret, M., Murphy, J., Buckley, A., Rigby, P.J., House, M.J., St. Pierre, T., Fitzgerald, M., Iyer, K.S., and Dunlop, S.A. (2016). An unexpected transient breakdown of the blood brain barrier triggers passage of large intravenously administered nanoparticles. *Sci. Rep.* 6, 335–344.
 131. Maxwell, W.L., Bartlett, E., and Morgan, H. (2015). Wallerian degeneration in the optic nerve stretch-injury model of traumatic brain injury: a stereological analysis. *J. Neurotrauma* 32, 780–790.
 132. Coles, J.P. (2007). Imaging after brain injury. *Br. J. Anaesth.* 99, 49–60.
 133. Sharwood, L.N., Dhaliwal, S., Ball, J., Burns, B., Flower, O., Joseph, A., Stanford, R., and Middleton, J. (2018). Emergency and acute care management of traumatic spinal cord injury: a survey of current practice among senior clinicians across Australia. *BMC Emerg. Med.* 18, 57.
 134. Baloesu, C. (2018). Diagnostic imaging in emergency medicine: how much is too much? *Ann. Emerg. Med.* 72, 637–643.
 135. Stiell, I.G., Clement, C.M., Grimshaw, J.M., Brison, R.J., Rowe, B.H., Lee, J.S., Shah, A., Brehaut, J., Holroyd, B.R., Schull, M.J., McKnight, R.D., Eisenhauer, M.A., Dreyer, J., Letovsky, E., Rutledge, T., MacPhail, I., Ross, S., Perry, J.J., Ip, U., Lesiuk, H., Bennett, C., and Wells, G.A. (2010). A prospective cluster-randomized trial to implement the Canadian CT Head Rule in emergency departments. *CMAJ* 182, 1527–1532.
 136. Tseng, W.C., Shih, H.M., Su, Y.C., Chen, H.W., Hsiao, K.Y., and Chen, I.C. (2011). The association between skull bone fractures and outcomes in patients with severe traumatic brain injury. *J. Trauma* 71, 1611–1614.
 137. McColl, T.J., Brady, R.D., Shultz, S.R., Lovick, L., Webster, K.M., Sun, M., McDonald, S.J., O'Brien, T.J., and Semple, B.D. (2018). Mild traumatic brain injury in adolescent mice alters skull bone properties to influence a subsequent brain impact at adulthood: a pilot study. *Front. Neurol.* 9, 372.
 138. Gebauer, G., Osterman, M., Harrop, J., and Vaccaro, A. (2012). Spinal cord injury resulting from injury missed on CT scan: the danger of relying on CT alone for collar removal. *Clin. Orthop. Relat. Res.* 470, 1652–1657.
 139. Fisher, B.M., Cowles, S., Matulich, J.R., Evanson, B.G., Vega, D., and Dissanaike, S. (2013). Is magnetic resonance imaging in addition to a computed tomographic scan necessary to identify clinically significant cervical spine injuries in obtunded blunt trauma patients? *Am. J. Surg.* 206, 987–994.
 140. Lee, H., Wintermark, M., Gean, A.D., Ghajar, J., Manley, G.T., and Mukherjee, P. (2008). Focal lesions in acute mild traumatic brain injury and neurocognitive outcome: CT versus 3T MRI. *J. Neurotrauma* 25, 1049–1056.
 141. Buttram, S.D.W., Garcia-Filion, P., Miller, J., Youssfi, M., Brown, S.D., Dalton, H.J., and Adelson, P.D. (2015). Computed tomography vs magnetic resonance imaging for identifying acute lesions in pediatric traumatic brain injury. *Hosp. Pediatr.* 5, 79–84.
 142. Chiara Ricciardi, M., Bokkers, R.P.H., Butman, J.A., Hammoud, D.A., Pham, D.L., Warach, S., and Latour, L.L. (2017). Trauma-specific brain abnormalities in suspected mild traumatic brain injury patients identified in the first 48 hours after injury: a blinded magnetic resonance imaging comparative study including suspected acute minor stroke patients. *J. Neurotrauma* 34, 23–30.
 143. Narayana, P.A. (2017). White matter changes in patients with mild traumatic brain injury: MRI perspective. *Concussion* 2, CNC35.
 144. Smitherman, E., Hernandez, A., Stavinoha, P.L., Huang, R., Kermie, S.G., Diaz-Arrastia, R., and Miles, D.K. (2016). Predicting outcome after pediatric traumatic brain injury by early magnetic resonance imaging lesion location and volume. *J. Neurotrauma* 33, 35–48.
 145. van der Horn, H.J., de Haan, S., Spikman, J.M., de Groot, J.C., and van der Naalt, J. (2018). Clinical relevance of microhemorrhagic lesions in subacute mild traumatic brain injury. *Brain Imaging Behav.* 12, 912–916.

146. Jarrett, M., Tam, R., Hernández-Torres, E., Martin, N., Perera, W., Zhao, Y., Shahinfard, E., Dadachanji, S., Taunton, J., Li, D.K.B., and Rauscher, A. (2016). A prospective pilot investigation of brain volume, white matter hyperintensities, and hemorrhagic lesions after mild traumatic brain injury. *Front. Neurol.* 7, 11.
147. Griffin, A.D., Turtzo, L.C., Parikh, G.Y., Tolpygo, A., Lodato, Z., Moses, A.D., Nair, G., Perl, D.P., Edwards, N.A., Dardzinski, B.J., Armstrong, R.C., Ray-Chaudhury, A., Mitra, P.P., and Latour, L.L. (2019). Traumatic microbleeds suggest vascular injury and predict disability in traumatic brain injury. *Brain* 142, 3550–3564.
148. Einarsen, C.E., Moen, K.G., Häberg, A.K., Eikenes, L., Kvistad, K.A., Xu, J., Moe, H.K., Tollefsen, M.H., Vik, A., and Skandsen, T. (2019). Patients with mild traumatic brain injury recruited from both hospital and primary care settings: a controlled longitudinal magnetic resonance imaging study. *J. Neurotrauma* 36, 3172–3182.
149. Moen, K.G., Brezova, V., Skandsen, T., Häberg, A.K., Folvik, M., and Vik, A. (2014). Traumatic axonal injury: the prognostic value of lesion load in corpus callosum, brain stem, and thalamus in different magnetic resonance imaging sequences. *J. Neurotrauma* 31, 1486–1496.
150. Palacios, E.M., Sala-Llonch, R., Junque, C., Fernandez-Espejo, D., Roig, T., Tormos, J.M., Bargallo, N., and Vendrell, P. (2013). Long-term declarative memory deficits in diffuse TBI: correlations with cortical thickness, white matter integrity and hippocampal volume. *Cortex* 49, 646–657.
151. List, J., Ott, S., Bukowski, M., Lindenberg, R., and Flöel, A. (2015). Cognitive function and brain structure after recurrent mild traumatic brain injuries in young-to-middle-aged adults. *Front. Hum. Neurosci.* 9, 228.
152. Clark, A.L., Merritt, V.C., Bigler, E.D., Bangen, K.J., Werhane, M., Sorg, S.F., Bondi, M.W., Schiehser, D.M., and Delano-Wood, L. (2018). Blast-exposed veterans with mild traumatic brain injury show greater frontal cortical thinning and poorer executive functioning. *Front. Neurol.* 9, 873.
153. Stricker, N.H., Salat, D.H., Foley, J.M., Zink, T.A., Kellison, I.L., McFarland, C.P., Grande, L.J., McGlinchey, R.E., Milberg, W.P., and Leritz, E.C. (2013). Decreased white matter integrity in neuropsychologically defined mild cognitive impairment is independent of cortical thinning. *J. Int. Neuropsychol. Soc.* 19, 925–937.
154. Sidaros, A., Skimminge, A., Liptrot, M.G., Sidaros, K., Engberg, A.W., Herning, M., Paulson, O.B., Jernigan, T.L., and Rostrup, E. (2018). Blast-exposed veterans with mild traumatic brain injury show greater frontal cortical thinning and poorer executive functioning. *Front. Neurol.* 9, 873.
155. Cole, J.H., Jolly, A., De Simon, S., Bourke, N., Patel, M.C., Scott, G., and Sharp, D.J. (2018). Spatial patterns of progressive brain volume loss after moderate-severe traumatic brain injury. *Brain* 141, 822–836.
156. Zhou, Y., Kierans, A., Kenul, D., Ge, Y., Rath, J., Reaume, J., Grossman, R.I., and Lui, Y.W. (2013). Mild traumatic brain injury: longitudinal regional brain volume changes. *Radiology* 267, 880–890.
157. Wang, W., Tang, S., Li, C., Chen, J., Li, H., Su, Y., and Ning, B. (2019). Specific brain morphometric changes in spinal cord injury: a voxel-based meta-analysis of white and gray matter volume. *J. Neurotrauma* 36, 2348–2357.
158. Seif, M., Ziegler, G., and Freund, P. (2018). Progressive ventricles enlargement and cerebrospinal fluid volume increases as a marker of neurodegeneration in patients with spinal cord injury: a longitudinal magnetic resonance imaging study. *J. Neurotrauma* 35, 2941–2946.
159. Soni, N., Mohamed, A.Z., Kurniawan, N.D., Borges, K., and Nasrallah, F. (2019). Diffusion magnetic resonance imaging unveils the spatiotemporal microstructural gray matter changes following injury in the rodent brain. *J. Neurotrauma* 36, 1306–1317.
160. Assaf, Y., and Pasternak, O. (2008). Diffusion tensor imaging (DTI)-based white matter mapping in brain research: a review. *J. Mol. Neurosci.* 34, 51–61.
161. Winkowski, P.J., Sabisz, A., Naumczyk, P., Jodzio, K., Szurowska, E., and Szarmach, A. (2018). Understanding the physiopathology behind axial and radial diffusivity changes: what do we know? *Front. Neurol.* 9, 92.
162. D'souza, M.M., Choudhary, A., Poonia, M., Kumar, P., and Khushu, S. (2017). Diffusion tensor MR imaging in spinal cord injury. *Injury* 48, 880–884.
163. Lin, T.H., Sun, P., Hallman, M., Hwang, F.C., Wallendorf, M., Ray, W.Z., Spees, W.M., and Song, S.K. (2019). Noninvasive quantification of axonal loss in the presence of tissue swelling in traumatic spinal cord injury mice. *J. Neurotrauma* 36, 2308–2315.
164. Petersen, J.A., Wilm, B.J., Von Meyenburg, J., Schubert, M., Seifert, B., Najafi, Y., Dietz, V., and Kollias, S. (2012). Chronic cervical spinal cord injury: DTI correlates with clinical and electrophysiological measures. *J. Neurotrauma* 29, 1556–1566.
165. Guo, Y., Gao, F., Liu, Y., Guo, H., Yu, W., Chen, Z., Yang, M., Du, L., Yang, D., and Li, J. (2019). White matter microstructure alterations in patients with spinal cord injury assessed by diffusion tensor imaging. *Front. Hum. Neurosci.* 13, 11.
166. Asken, B.M., DeKosky, S.T., Clugston, J.R., Jaffee, M.S., and Bauer, R.M. (2018). Diffusion tensor imaging (DTI) findings in adult civilian, military, and sport-related mild traumatic brain injury (mTBI): a systematic critical review. *Brain Imaging Behav.* 12, 585–612.
167. Wright, D.K., Johnston, L.A., Kershaw, J., Ordidge, R., O'Brien, T.J., and Shultz, S.R. (2017). Changes in apparent fiber density and track-weighted imaging metrics in white matter following experimental traumatic brain injury. *J. Neurotrauma* 34, 2109–2118.
168. Hoogenboom, W.S., Rubin, T.G., Ye, K., Cui, M.-H., Branch, K.C., Liu, J., Branch, C.A., and Lipton, M.L. (2019). Diffusion tensor imaging of the evolving response to mild traumatic brain injury in rats. *J. Exp. Neurosci.* 13, 117906951985862.
169. Herrera, J.J., Bockhorst, K., Kondraganti, S., Stertz, L., Quevedo, J., and Narayana, P.A. (2017). Acute white matter tract damage after frontal mild traumatic brain injury. *J. Neurotrauma* 34, 291–299.
170. Bazarian, J.J., Zhong, J., Blyth, B., Zhu, T., Kavcic, V., and Peterson, D. (2007). Diffusion tensor imaging detects clinically important axonal damage after mild traumatic brain injury: a pilot study. *J. Neurotrauma* 24, 1447–1459.
171. Johnson, V.E., Stewart, W., and Smith, D.H. (2013). Axonal pathology in traumatic brain injury. *Exp. Neurol.* 246, 35–43.
172. Soni, N., Mohamed, A.Z., Kurniawan, N.D., Borges, K., and Nasrallah, F. (2019). Diffusion magnetic resonance imaging unveils the spatiotemporal microstructural gray matter changes following injury in the rodent brain. *J. Neurotrauma* 36, 1306–1317.
173. Wright, D.K., O'Brien, T.J., Mychasiuk, R., and Shultz, S.R. (2018). Telomere length and advanced diffusion MRI as biomarkers for repetitive mild traumatic brain injury in adolescent rats. *NeuroImage Clin.* 18, 315–324.
174. Yu, F., Shukla, D.K., Armstrong, R.C., Marion, C.M., Radowski, K.L., Selwyn, R.G., and Dardzinski, B.J. (2017). Repetitive modeling of mild traumatic brain injury produces cortical abnormalities detectable by magnetic resonance diffusion imaging, histopathology, and behavior. *J. Neurotrauma* 34, 1364–1381.
175. Kulkarni, P., Morrison, T.R., Cai, X., Iriah, S., Simon, N., Sabrick, J., Neuroth, L., and Ferris, C.F. (2019). Neuroanatomical changes following single or repetitive mild TBI. *Front. Syst. Neurosci.* 13, 34.
176. Harris, N.G., Verley, D.R., Gutman, B.A., Thompson, P.M., Yeh, H.J., and Brown, J.A. (2016). Disconnection and hyper-connectivity underlie reorganization after TBI: a rodent functional connectomic analysis. *Exp. Neurol.* 277, 124–138.
177. Edlow, B.L., Copen, W.A., Izzy, S., Bakhadirov, K., van der Kouwe, A., Glenn, M.B., Greenberg, S.M., Greer, D.M., and Wu, O. (2016). Diffusion tensor imaging in acute-to-subacute traumatic brain injury: a longitudinal analysis. *BMC Neurol.* 16, 2.
178. Terry, D.P., Mewborn, C.M., and Miller, L.S. (2019). Repeated sport-related concussion shows only minimal white matter differences many years after playing high school football. *J. Int. Neuropsychol. Soc.* 25, 950–960.
179. McDonald, S., Rushby, J.A., Dalton, K.I., Allen, S.K., and Parks, N. (2018). The role of abnormalities in the corpus callosum in social cognition deficits after traumatic brain injury. *Soc. Neurosci.* 13, 471–479.
180. Ware, J.B., Biester, R.C., Whipple, E., Robinson, K.M., Ross, R.J., and Nucifora, P.G. (2016). Combat-related mild traumatic brain injury: association between baseline diffusion-tensor imaging findings and long-term outcomes. *Radiology* 280, 212–219.
181. Yin, B., Li, D.D., Huang, H., Gu, C.H., Bai, G.H., Hu, L.X., Zhuang, J.F., and Zhang, M. (2019). Longitudinal changes in diffusion tensor imaging following mild traumatic brain injury and correlation with outcome. *Front. Neural Circuits* 13, 28.
182. Hirad, A.A., Bazarian, J.J., Merchant-Borna, K., Garcea, F.E., Heilbronner, S., Paul, D., Hintz, E.B., van Wijngaarden, E., Schifitto, G., Wright, D.W., Espinoza, T.R., and Mahon, B.Z. (2019). A common neural signature of brain injury in concussion and subconcussion. *Sci. Adv.* 5, eaau3460.

183. McDonald, S., Dalton, K.I., Rushby, J.A., and Landin-Romero, R. (2019). Loss of white matter connections after severe traumatic brain injury (TBI) and its relationship to social cognition. *Brain Imaging Behav.* 13, 819–829.
184. Mishra, V.R., Sreenivasan, K.R., Zhuang, X., Yang, Z., Cordes, D., Banks, S.J., and Bernick, C. (2019). Understanding white matter structural connectivity differences between cognitively impaired and nonimpaired active professional fighters. *Hum. Brain Mapp.* 40, 5108–5122.
185. Metzler-Baddeley, C., Foley, S., De Santis, S., Charron, C., Hampshire, A., Caeyenberghs, K., and Jones, D.K. (2017). Dynamics of white matter plasticity underlying working memory training: multimodal evidence from diffusion MRI and relaxometry. *J. Cogn. Neurosci.* 29, 1509–1520.
186. Caeyenberghs, K., Metzler-Baddeley, C., Foley, S., and Jones, D.K. (2016). Dynamics of the human structural connectome underlying working memory training. *J. Neurosci.* 36, 4056–4066.
187. Tournier, J.D., Calamante, F., Gadian, D.G., and Connelly, A. (2004). Direct estimation of the fiber orientation density function from diffusion-weighted MRI data using spherical deconvolution. *Neuroimage* 23, 1176–1185.
188. Wortman, R.C., Meconi, A., Neale, K.J., Brady, R.D., McDonald, S.J., Christie, B.R., Wright, D.K., and Shultz, S.R. (2018). Diffusion MRI abnormalities in adolescent rats given repeated mild traumatic brain injury. *Ann. Clin. Transl. Neurol.* 5, 1588–1598.
189. Steven, A.J., Zhuo, J., and Melhem, E.R. (2014). Diffusion kurtosis imaging: an emerging technique for evaluating the microstructural environment of the brain. *Am. J. Roentgenol.* 202, W26–W33.
190. Joong, H.K., Loy, D.N., Liang, H.F., Trinkaus, K., Schmidt, R.E., and Song, S.K. (2007). Noninvasive diffusion tensor imaging of evolving white matter pathology in a mouse model of acute spinal cord injury. *Magn. Reson. Med.* 58, 253–260.
191. Zhuo, J., Xu, S., Proctor, J.L., Mullins, R.J., Simon, J.Z., Fiskum, G., and Gullapalli, R.P. (2012). Diffusion kurtosis as an in vivo imaging marker for reactive astrogliosis in traumatic brain injury. *Neuroimage* 59, 467–477.
192. Budde, M.D., Janes, L., Gold, E., Turtzo, L.C., and Frank, J.A. (2011). The contribution of gliosis to diffusion tensor anisotropy and tractography following traumatic brain injury: validation in the rat using Fourier analysis of stained tissue sections. *Brain* 134, 2248–2260.
193. Wang, M.L., Yu, M.M., Yang, D.X., Liu, Y.L., Wei, X.E., and Li, W.B. (2018). Longitudinal microstructural changes in traumatic brain injury in rats: a diffusional kurtosis imaging, histology, and behavior study. *Am. J. Neuroradiol.* 39, 1650–1656.
194. Braeckman, K., Descamps, B., Pieters, L., Vral, A., Caeyenberghs, K., and Vanhove, C. (2019). Dynamic changes in hippocampal diffusion and kurtosis metrics following experimental mTBI correlate with glial reactivity. *NeuroImage Clin.* 21, 101669.
195. Chung, S., Wang, X., Fieremans, E., Rath, J.F., Amorapanth, P., Foo, F.-Y.A., Morton, C.J., Novikov, D.S., Flanagan, S.R., and Lui, Y.W. (2019). Altered relationship between working memory and brain microstructure after mild traumatic brain injury. *Am. J. Neuroradiol.* 40, 1438–1444.
196. Wang, M.L., Yu, M.M., Yang, D.X., Liu, Y.L., Wei, X.E., and Li, W.B. (2018). Diffusion kurtosis imaging characterizes brain microstructural changes associated with cognitive impairment in a rat model of chronic traumatic brain injury. *Neuroscience* 392, 180–189.
197. Zhang, H., Schneider, T., Wheeler-Kingshott, C.A., and Alexander, D.C. (2012). NODDI: practical in vivo neurite orientation dispersion and density imaging of the human brain. *Neuroimage* 61, 1000–1016.
198. Mayer, A.R., Ling, J.M., Dodd, A.B., Meier, T.B., Hanlon, F.M., and Klimaj, S.D. (2017). A prospective microstructure imaging study in mixed-martial artists using geometric measures and diffusion tensor imaging: methods and findings. *Brain Imaging Behav.* 11, 698–711.
199. Churchill, N.W., Caverzasi, E., Graham, S.J., Hutchison, M.G., and Schweizer, T.A. (2017). White matter microstructure in athletes with a history of concussion: comparing diffusion tensor imaging (DTI) and neurite orientation dispersion and density imaging (NODDI). *Hum. Brain Mapp.* 38, 4201–4211.
200. Churchill, N.W., Caverzasi, E., Graham, S.J., Hutchison, M.G., and Schweizer, T.A. (2019). White matter during concussion recovery: comparing diffusion tensor imaging (DTI) and neurite orientation dispersion and density imaging (NODDI). *Hum. Brain Mapp.* 40, 1908–1918.
201. Palacios, E., Owen, J.P., Yuh, E.L., Wang, M.B., Vassar, M.J., Ferguson, A.R., Diaz-Arrastia, R., Giacino, J.T., Okonkwo, D.O., Robertson, C.S., Stein, M.B., Temkin, N., Jain, S., McCreary, M., Donald, C.L., Mac, Manley, G.T., Mukherjee, P., and Investigators, T.-T. (2018). The evolution of white matter microstructural changes after mild traumatic brain injury: a longitudinal DTI and NODDI study. *bioRxiv*, 345629.
202. Sours, C., Zhuo, J., Roys, S., Shanmuganathan, K., and Gullapalli, R.P. (2015). Disruptions in resting state functional connectivity and cerebral blood flow in mild traumatic brain injury patients. *PLoS One* 10, e0134019.
203. Lu, H., Zou, Q., Gu, H., Raichle, M.E., Stein, E.A., and Yang, Y. (2012). Rat brains also have a default mode network. *Proc. Natl. Acad. Sci. U. S. A.* 109, 3979–3984.
204. Palacios, E.M., Sala-Llonch, R., Junque, C., Roig, T., Tormos, J.M., Bargallo, N., and Vendrell, P. (2013). Resting-state functional magnetic resonance imaging activity and connectivity and cognitive outcome in traumatic brain injury. *JAMA Neurol.* 70, 845–851.
205. Hillary, F.G., Slocumb, J., Hills, E.C., Fitzpatrick, N.M., Medaglia, J.D., Wang, J., Good, D.C., and Wylie, G.R. (2011). Changes in resting connectivity during recovery from severe traumatic brain injury. *Int. J. Psychophysiol.* 82, 115–123.
206. Chuang, K.H., and Nasrallah, F.A. (2017). Functional networks and network perturbations in rodents. *Neuroimage* 163, 419–436.
207. Venkatesan, U.M., Dennis, N.A., and Hillary, F.G. (2015). Chronology and chronicity of altered resting-state functional connectivity after traumatic brain injury. *J. Neurotrauma* 32, 252–264.
208. Mayer, A.R., Mannell, M.V., Ling, J., Gasparovic, C., and Yeo, R.A. (2011). Functional connectivity in mild traumatic brain injury. *Hum. Brain Mapp.* 32, 1825–1835.
209. Johnson, B., Zhang, K., Gay, M., Horowitz, S., Hallett, M., Sebastianelli, W., and Slobounov, S. (2012). Alteration of brain default network in subacute phase of injury in concussed individuals: resting-state fMRI study. *Neuroimage* 59, 511–518.
210. Zhou, Y., Milham, M.P., Lui, Y.W., Miles, L., Reaume, J., Sodickson, D.K., Grossman, R.L., and Ge, Y. (2012). Default-mode network disruption in mild traumatic brain injury. *Radiology* 265, 882–892.
211. Bonnelle, V., Leech, R., Kinnunen, K.M., Ham, T.E., Beckmann, C.F., de Boissezon, X., Greenwood, R.J., and Sharp, D.J. (2011). Default mode network connectivity predicts sustained attention deficits after traumatic brain injury. *J. Neurosci.* 31, 13442–13451.
212. Sours, C., Zhuo, J., Janowich, J., Aarabi, B., Shanmuganathan, K., and Gullapalli, R.P. (2013). Default mode network interference in mild traumatic brain injury: a pilot resting state study. *Brain Res.* 1537, 201–215.
213. Seeley, W.W., Menon, V., Schatzberg, A.F., Keller, J., Glover, G.H., Kenna, H., Reiss, A.L., and Greicius, M.D. (2007). Dissociable intrinsic connectivity networks for salience processing and executive control. *J. Neurosci.* 27, 2349–2356.
214. Fox, M.D., Snyder, A.Z., Vincent, J.L., Corbetta, M., Van Essen, D.C., and Raichle, M.E. (2005). The human brain is intrinsically organized into dynamic, anticorrelated functional networks. *Proc. Natl. Acad. Sci. U. S. A.* 102, 9673–9678.
215. Ponsford, J. (2013). Factors contributing to outcome following traumatic brain injury. *NeuroRehabilitation* 32, 803–815.
216. Maruishi, M., Miyatani, M., Nakao, T., and Muranaka, H. (2007). Compensatory cortical activation during performance of an attention task by patients with diffuse axonal injury: a functional magnetic resonance imaging study. *J. Neurol. Neurosurg. Psychiatry* 78, 168–173.
217. Schönberger, M., Ponsford, J., Reutens, D., Beare, R., and O'Sullivan, R. (2009). The relationship between age, injury severity, and MRI findings after traumatic brain injury. *J. Neurotrauma* 26, 2157–2167.
218. Khetani, A., Rohr, C.S., Sojoudi, A., Bray, S., and Barlow, K.M. (2019). Alteration in Cerebral Activation during a Working Memory Task after Pediatric Mild Traumatic Brain Injury: A Prospective Controlled Cohort Study. *J. Neurotrauma* 36, 3274–3283.
219. Blinman, T.A., Houseknecht, E., Snyder, C., Wiebe, D.J., and Nance, M.L. (2009). Postconcussive symptoms in hospitalized pediatric patients after mild traumatic brain injury. *J. Pediatr. Surg.* 44, 1223–1228.
220. Centers for Disease Control and Prevention. (2014). Traumatic brain injury in the United States: Fact sheet. *CDC Inj. Cent. Get Facts*, 2009–2011.

221. Keightley, M.L., Singh Saluja, R., Chen, J.K., Gagnon, I., Leonard, G., Petrides, M., and Ptito, A. (2014). A functional magnetic resonance imaging study of working memory in youth after sports-related concussion: Is it still working? *J. Neurotrauma* 31, 437–451.
222. Lovell, M.R., Pardini, J.E., Welling, J., Collins, M.W., Bakal, J., Lazar, N., Roush, R., Eddy, W.F., and Becker, J.T. (2007). Functional brain abnormalities are related to clinical recovery and time to return-to-play in athletes. *Neurosurgery* 61, 352–359.
223. Pardini, J.E., Pardini, D.A., Becker, J.T., Dunfee, K.L., Eddy, W.F., Lovell, M.R., and Welling, J.S. (2010). Postconcussive symptoms are associated with compensatory cortical recruitment during a working memory task. *Neurosurgery* 67, 1020–1027.
224. Krivitzky, L.S., Roebuck-Spencer, T.M., Roth, R.M., Blackstone, K., Johnson, C.P., and Gioia, G. (2011). Functional magnetic resonance imaging of working memory and response inhibition in children with mild traumatic brain injury. *J. Int. Neuropsychol. Soc.* 17, 1143–1152.
225. Westfall, D.R., West, J.D., Bailey, J.N., Arnold, T.W., Kersey, P.A., Saykin, A.J., and McDonald, B.C. (2015). Increased brain activation during working memory processing after pediatric mild traumatic brain injury (mTBI). *J. Pediatr. Rehabil. Med.* 8, 297–308.
226. Sours, C., George, E.O., Zhuo, J., Roys, S., and Gullapalli, R.P. (2015). Hyper-connectivity of the thalamus during early stages following mild traumatic brain injury. *Brain Imaging Behav.* 9, 550–563.
227. Belli, A., Davies, D., Su, Z., Bentley, C., Hammond, D., Grey, M., Pietro, V., Di, Hill, L., and Evans, S. (2017). Do NAA/CHO and NAA/CR ratios as measure by 1h MR spectroscopy differ between symptomatic and non-symptomatic concussed athletes in the early post injury period? *Br. J. Sports Med.* 51, A4.3–A5.
228. Banoei, M.M., Casault, C., Metwally, S.M., and Winston, B.W. (2018). Metabolomics and biomarker discovery in traumatic brain injury. *J. Neurotrauma* 35, 1831–1848.
229. Stovell, M.G., Yan, J.L., Sleigh, A., Mada, M.O., Carpenter, T.A., Hutchinson, P.J.A., and Carpenter, K.L.H. (2017). Assessing metabolism and injury in acute human traumatic brain injury with magnetic resonance spectroscopy: Current and future applications. *Front. Neurol.* 8, 642.
230. Pelzer, E.A., Florin, E., and Schnitzler, A. (2019). Quantitative Susceptibility Mapping and Resting State Network Analyses in Parkinsonian Phenotypes—A Systematic Review of the Literature. *Front. Neural Circuits* 13 50.
231. Wang, Y., Spincemaille, P., Liu, Z., Dimov, A., Deh, K., Li, J., Zhang, Y., Yao, Y., Gillen, K.M., Wilman, A.H., Gupta, A., Tsiouris, A.J., Kovanlikaya, I., Chiang, G.C.Y., Weinsaft, J.W., Tanenbaum, L., Chen, W., Zhu, W., Chang, S., Lou, M., Kopell, B.H., Kaplitt, M.G., Devos, D., Hirai, T., Huang, X., Korogi, Y., Shtilbans, A., Jahng, G.H., Pelletier, D., Gauthier, S.A., Pitt, D., Bush, A.I., Brittenham, G.M., and Prince, M.R. (2017). Clinical quantitative susceptibility mapping (QSM): biometal imaging and its emerging roles in patient care. *J. Magn. Reson. Imaging* 46, 951–971.
232. Ayton, S., Wang, Y., Diouf, I., Schneider, J.A., Brockman, J., Morris, M.C., and Bush, A.I. (2019). Brain iron is associated with accelerated cognitive decline in people with Alzheimer pathology. *Mol. Psychiatry*. doi: 10.1038/s41380-019-0375-7 [Epub ahead of print].
233. Nisenbaum, E.J., Novikov, D.S., and Lui, Y.W. (2014). The presence and role of iron in mild traumatic brain injury: an imaging perspective. *J. Neurotrauma* 31, 301–307.
234. Schweser, F., Kyyriäinen, J., Preda, M., Pitkänen, A., Toffolo, K., Poulsen, A., Donahue, K., Levy, B., and Poulsen, D. (2019). Visualization of thalamic calcium influx with quantitative susceptibility mapping as a potential imaging biomarker for repeated mild traumatic brain injury. *Neuroimage* 200, 250–258.
235. Vegliante, G., Tolomeo, D., Drieu, A., Rubio, M., Micotti, E., Moro, F., Vivien, D., Forloni, G., Ali, C., and Zanier, E.R. (2019). Longitudinal molecular magnetic resonance imaging of endothelial activation after severe traumatic brain injury. *J. Clin. Med.* 8, 1134.
236. Lu, L., Cao, H., Wei, X., Li, Y., and Li, W. (2015). Iron deposition is positively related to cognitive impairment in patients with chronic mild traumatic brain injury: assessment with susceptibility weighted imaging. *Biomed Res. Int.* 2015, 1–7.
237. Gorgoraptis, N., Li, L.M., Whittington, A., Zimmerman, K.A., Maclean, L.M., McLeod, C., Ross, E., Heslegrave, A., Zetterberg, H., Passchier, J., Matthews, P.M., Gunn, R.N., McMillan, T.M., and Sharp, D.J. (2019). In vivo detection of cerebral tau pathology in long-term survivors of traumatic brain injury. *Sci. Transl. Med.* 11, pii: eaaw1993.
238. Doble, A. (1999). The role of excitotoxicity in neurodegenerative disease: implications for therapy. *Pharmacol. Ther.* 81, 163–221.
239. Guerriero, R.M., Giza, C.C., and Rotenberg, A. (2015). Glutamate and GABA imbalance following traumatic brain injury. *Curr. Neurol. Neurosci. Rep.* 15, 27–47.
240. Nicholls, D., and Attwell, D. (1990). The release and uptake of excitatory amino acids. *Trends Pharmacol. Sci.* 11, 462–468.
241. Mark, L.P., Prost, R.W., Ulmer, J.L., Smith, M.M., Daniels, D.L., Strottmann, J.M., Brown, W.D., and Hance-Bey, L. (2001). Pictorial review of glutamate excitotoxicity: fundamental concepts for neuroimaging. *Am. J. Neuroradiol.* 22, 1813–1824.
242. Hong, Z., Xinding, Z., Tianlin, Z., and Liren, C. (2001). Excitatory amino acids in cerebrospinal fluid of patients with acute head injuries. *Clin. Chem.* 47, 1458–1462.
243. Hinzman, J.M., Thomas, T.C., Burmeister, J.J., Quintero, J.E., Huettl, P., Pomerleau, F., Gerhardt, G.A., and Lifshitz, J. (2010). Diffuse brain injury elevates tonic glutamate levels and potassium-evoked glutamate release in discrete brain regions at two days post-injury: an enzyme-based microelectrode array study. *J. Neurotrauma* 27, 889–899.
244. Park, E., Velumian, A.A., and Fehlings, M.G. (2004). The role of excitotoxicity in secondary mechanisms of spinal cord injury: a review with an emphasis on the implications for white matter degeneration. *J. Neurotrauma* 21, 754–774.
245. Barger, S.W., Goodwin, M.E., Porter, M.M., and Beggs, M.L. (2007). Glutamate release from activated microglia requires the oxidative burst and lipid peroxidation. *J. Neurochem.* 101, 1205–1213.
246. Duan, S., Anderson, C.M., Keung, E.C., Chen, Y., Chen, Y., and Swanson, R.A. (2003). P2X7 receptor-mediated release of excitatory amino acids from astrocytes. *J. Neurosci.* 23, 1320–1328.
247. Katayama, Y., Kawamata, T., Tamura, T., Hovda, D.A., Becker, D.P., and Tsubokawa, T. (1991). Calcium-dependent glutamate release concomitant with massive potassium flux during cerebral ischemia in vivo. *Brain Res.* 558, 136–140.
248. Allen, N.J., and Attwell, D. (2001). A chemokine-glutamate connection. *Nat. Neurosci.* 4, 676–678.
249. Farooqui, A.A., Ong, W.Y., and Horrocks, L.A. (2008). Neurochemical aspects of excitotoxicity. Springer: New York.
250. Schwartz, M. (2004). Optic nerve crush: protection and regeneration. *Brain Res. Bull.* 62, 467–471.
251. Tymianski, M., and Tator, C.H. (1996). Normal and abnormal calcium homeostasis in neurons: a basis for the pathophysiology of traumatic and ischemic central nervous system injury. *Neurosurgery* 38, 1176–1195.
252. Wolf, J.A., Stys, P.K., Lusardi, T., Meaney, D., and Smith, D.H. (2001). Traumatic axonal injury induces calcium influx modulated by tetrodotoxin-sensitive sodium channels. *J. Neurosci.* 21, 1923–1930.
253. Fineman, I., Hovda, D.A., Smith, M., Yoshino, A., and Becker, D.P. (1993). Concussive brain injury is associated with a prolonged accumulation of calcium: a ⁴⁵Ca autoradiographic study. *Brain Res.* 624, 94–102.
254. Stirling, D.P., Cummins, K., Wayne Chen, S.R., and Stys, P. (2014). Axoplasmic reticulum Ca²⁺ release causes secondary degeneration of spinal axons. *Ann. Neurol.* 75, 220–229.
255. Weber, J.T. (2012). Altered calcium signaling following traumatic brain injury. *Front. Pharmacol.* 3, 60.
256. Andriessen, T.M.J.C., Jacobs, B., and Vos, P.E. (2010). Clinical characteristics and pathophysiological mechanisms of focal and diffuse traumatic brain injury. *J. Cell. Mol. Med.* 14, 2381–2392.
257. Kapoor, R., Davies, M., Blaker, P.A., Hall, S.M., and Smith, K.J. (2003). Blockers of sodium and calcium entry protect axons from nitric oxide-mediated degeneration. *Ann. Neurol.* 53, 174–180.
258. Staal, J.A., Dickson, T.C., Gasperini, R., Liu, Y., Foa, L., and Vickers, J.C. (2010). Initial calcium release from intracellular stores followed by calcium dysregulation is linked to secondary axotomy following transient axonal stretch injury. *J. Neurochem.* 112, 1147–1155.
259. Lozić, I., Bartlett, C.A., Shaw, J.A., Iyer, K.S., Dunlop, S.A., Kilburn, M.R., and Fitzgerald, M. (2014). Changes in subtypes of Ca microdomains following partial injury to the central nervous system. *Metallomics* 6, 455–464.
260. Matute, C., Torre, I., Pérez-Cerdá, F., Pérez-Samartín, A., Alberdi, E., Etxebarria, E., Arranz, A.M., Ravid, R., Rodríguez-Antigüedad,

- A., Sánchez-Gómez, M., and Domercq, M. (2007). Neurobiology of disease P2X7 receptor blockade prevents ATP excitotoxicity in oligodendrocytes and ameliorates experimental autoimmune encephalomyelitis. *J. Neurosci.* 27, 9525–9533.
261. Borges, K., Ohlemeyer, C., Trotter, J., and Kettenmann, H. (1994). AMPA/kainate receptor activation in murine oligodendrocyte precursor cells leads to activation of a cation conductance, calcium influx and blockade of delayed rectifying K⁺ channels. *Neuroscience* 63, 135–149.
262. Itoh, T., Beesley, J., Itoh, A., Cohen, A.S., Kavanaugh, B., Coulter, D.A., Grinspan, J.B., and Pleasure, D. (2002). AMPA glutamate receptor-mediated calcium signaling is transiently enhanced during development of oligodendrocytes. *J. Neurochem.* 81, 390–402.
263. Yamaya, Y., Yoshioka, A., Saiki, S., Yuki, N., Hirose, G., and Pleasure, D. (2002). Type-2 astrocyte-like cells are more resistant than oligodendrocyte-like cells against non-N-methyl-D-aspartate glutamate receptor-mediated excitotoxicity. *J. Neurosci. Res.* 70, 588–598.
264. Birben, E., Murat, U., Md, S., Sackesen, C., Erzurum, S., and Kalayci, O. (2012). Oxidative stress and antioxidant defense. *WAO J.* 5, 9–19.
265. O'Hare Doig, R.L., Bartlett, C.A., Maghzal, G.J., Lam, M., Archer, M., Stocker, R., and Fitzgerald, M. (2014). Reactive species and oxidative stress in optic nerve vulnerable to secondary degeneration. *Exp. Neurol.* 261, 136–146.
266. Adam-Vizi, V., and Starkov, A.A. (2010). Calcium and mitochondrial reactive oxygen species generation. *J. Alzheimer's Dis.* 20, 413–426.
267. Lee, I., Bender, E., and Kadenbach, B. (2002). Control of mitochondrial membrane potential and ROS formation by reversible phosphorylation of cytochrome c oxidase. *Mol. Cell. Biochem.* 234–235, 63–70.
268. Görlach, A., Bertram, K., Hudecova, S., and Krizanova, O. (2015). Calcium and ROS: a mutual interplay. *Redox Biol.* 6, 260–271.
269. Lenaz, G. (2001). The mitochondrial production of reactive oxygen species: mechanisms and implications in human pathology. *Life* 52, 159–164.
270. Lehtinen, M.K., and Bonni, A. (2006). Modeling oxidative stress in the central nervous system. *Curr. Mol. Med.* 6, 871–81.
271. Guo Dong Mao, Thomas, P.D., Lopaschuk, G.D., and Poznansky, M.J. (1993). Superoxide dismutase (SOD)-catalase conjugates. Role of hydrogen peroxide and the Fenton reaction in SOD toxicity. *J. Biol. Chem.* 268, 416–420.
272. Thorburne, S.K., and Juurlink, B.H. (1996). Low glutathione and high iron govern the susceptibility of oligodendroglial precursors to oxidative stress. *J. Neurochem.* 67, 1014–1022.
273. Land, E.T. (1990). Free radicals in biology and medicine. *Int. J. Radiat. Biol.* 58, 725–725.
274. Turrens, J.F. (2003). Mitochondrial formation of reactive oxygen species. *J. Physiol.* 552, 335–344.
275. Beckman, J.S., and Koppenol, W.H. (1996). Nitric oxide, superoxide, and peroxynitrite: the good, the bad, and the ugly. *Am. J. Physiol. Cell Physiol.* 271, 1424–1437.
276. Kowaltowski, A.J., De Souza-Pinto, N.C., Castilho, R.F., and Vercesi, A.E. (2009). Mitochondria and reactive oxygen species. *Free Radic. Biol. Med.* 47, 333–343.
277. Nordberg, J., and Arnér, E.S.J. (2001). Reactive oxygen species, antioxidants, and the mammalian thioredoxin system. *Free Radic. Biol. Med.* 31, 1287–1312.
278. Fitzgerald, M., Bartlett, C.A., Harvey, A.R., and Dunlop, S.A. (2010). Early events of secondary degeneration after partial optic nerve transection: an immunohistochemical study. *J. Neurotrauma* 27, 439–452.
279. Wells, J., Kilburn, M.R., Shaw, J.A., Bartlett, C.A., Harvey, A.R., Dunlop, S.A., and Fitzgerald, M. (2012). Early in vivo changes in calcium ions, oxidative stress markers, and ion channel immunoreactivity following partial injury to the optic nerve. *J. Neurosci. Res.* 90, 606–618.
280. Mao, Y., Black, A.M.B., Milbourn, H.R., Krakonja, S., Nesbit, M., Bartlett, C.A., Fehily, B., Takechi, R., Yates, N.J., and Fitzgerald, M. (2018). The effects of a combination of ion channel inhibitors in female rats following repeated mild traumatic brain injury. *Int. J. Mol. Sci.* 19, 3408.
281. Vaziri, N.D., Lee, Y.S., Lin, C.Y., Lin, V.W., and Sindhu, R.K. (2004). NAD(P)H oxidase, superoxide dismutase, catalase, glutathione peroxidase and nitric oxide synthase expression in subacute spinal cord injury. *Brain Res.* 995, 76–83.
282. Bernardo, A., Bianchi, D., Magnaghi, V., and Minghetti, L. (2009). Peroxisome proliferator-activated receptor-gamma agonists promote differentiation and antioxidant defenses of oligodendrocyte progenitor cells. *J. Neuropathol. Exp. Neurol.* 68, 797–808.
283. Kruman, I., Bruce-Keller, A.J., Bredesen, D., Waeg, G., and Mattson, M.P. (1997). Evidence that 4-hydroxynonenal mediates oxidative stress-induced neuronal apoptosis. *J. Neurosci.* 17, 5089–5100.
284. Li, Y., Maher, P., and Schubert, D. (1997). A role for 12-lipoxygenase in nerve cell death caused by glutathione depletion. *Neuron* 19, 453–463.
285. Husain, J., and Juurlink, B.H. (1995). Oligodendroglial precursor cell susceptibility to hypoxia is related to poor ability to cope with reactive oxygen species. *Brain Res.* 698, 86–94.
286. Butts, B., Houde, C., and Mehmet, H. (2008). Maturation-dependent sensitivity of oligodendrocyte lineage cells to apoptosis: implications for normal development and disease. *Cell Death Differ.* 15(7), 1178–1186.
287. Cao, S.S., and Kaufman, R.J. (2014). Endoplasmic reticulum stress and oxidative stress in cell fate decision and human disease. *Antioxid. Redox Signal.* 21, 396–413.
288. Hetz, C., and Saxena, S. (2017). ER stress and the unfolded protein response in neurodegeneration. *Nat. Rev. Neurol.* 13, 477–491.
289. Xu, C., Bailly-Maitre, B., and Reed, J.C. (2005). Endoplasmic reticulum stress: cell life and death decisions. *J. Clin. Invest.* 115, 2656–2664.
290. Cummins, N., Bartlett, C.A., Archer, M., Bartlett, E., Hemmi, J.M., Harvey, A.R., Dunlop, S.A., and Fitzgerald, M. (2013). Changes to mitochondrial ultrastructure in optic nerve vulnerable to secondary degeneration in vivo are limited by irradiation at 670 nm. *BMC Neurosci.* 14, 98.
291. Dewar, D., Underhill, S.M., and Goldberg, M.P. (2003). Oligodendrocytes and ischemic brain injury. *J. Cereb. Blood Flow Metab.* 23, 263–274.
292. Ischiropoulos, H., Beckman, J.S., Bieganski, R., Lansbury, P., and Ischiropoulos, H. (2003). Oxidative stress and nitration in neurodegeneration: cause, effect, or association? *J. Clin. Invest.* 111, 163–169.
293. Ayala, A., Muñoz, M.F., and Argüelles, S. (2014). Lipid peroxidation: production, metabolism, and signaling mechanisms of malondialdehyde and 4-hydroxy-2-nonenal. *Oxid. Med. Cell. Longev.* 2014, 360438.
294. Zhong, H., and Yin, H. (2015). Role of lipid peroxidation derived 4-hydroxynonenal (4-HNE) in cancer: focusing on mitochondria. *Redox Biol.* 4, 193–199.
295. Braugher, J.M., Duncan, L.A., and Chase, R.L. (1986). The involvement of iron in lipid peroxidation. Importance of ferric to ferrous ratios in initiation. *J. Biol. Chem.* 261, 10282–10289.
296. Blanc, E.M., Keller, J.N., Fernandez, S., and Mattson, M.P. (1998). 4-hydroxynonenal, a lipid peroxidation product, impairs glutamate transport in cortical astrocytes. *Glia* 22, 149–160.
297. Rothstein, J.D., Dykes-Hoberg, M., Pardo, C.A., Bristol, L.A., Jin, L., Kuncl, R.W., Kanai, Y., Hediger, M.A., Wang, Y., Schielke, J.P., and Welty, D.F. (1996). Knockout of glutamate transporters reveals a major role for astroglial transport in excitotoxicity and clearance of glutamate. *Neuron* 16, 675–686.
298. Mark, R., Lovell, M., Markesbery, W., Uchida, K., and Mattson, M. (1997). A role for 4-hydroxynonenal, an aldehydic product of lipid peroxidation, in disruption of ion homeostasis and neuronal death induced by amyloid beta-peptide. *J. Neurochemistry* 68, 255–264.
299. Christie, S.D., Comeau, B., Myers, T., Sadi, D., Purdy, M., and Mendez, I. (2008). Duration of lipid peroxidation after acute spinal cord injury in rats and the effect of methylprednisolone: laboratory investigation. *Neurosurg. Focus* 25, E5.
300. Yates, N.J., Lydiard, S., Fehily, B., Weir, G., Chin, A., Bartlett, C.A., Alderson, J., and Fitzgerald, M. (2017). Repeated mild traumatic brain injury in female rats increases lipid peroxidation in neurons. *Exp. Brain Res.* 235, 2133–2149.
301. Halstrom, A., MacDonald, E., Neil, C., Arendts, G., Fatovich, D., and Fitzgerald, M. (2017). Elevation of oxidative stress indicators in a pilot study of plasma following traumatic brain injury. *J. Clin. Neurosci.* 35, 104–108.
302. Abdul-Muneer, P.M., Schuetz, H., Wang, F., Skotak, M., Jones, J., Gorantla, S., Zimmerman, M.C., Chandra, N., and Haorah, J. (2013).

- Induction of oxidative and nitrosative damage leads to cerebrovascular inflammation in an animal model of mild traumatic brain injury induced by primary blast. *Free Radic. Biol. Med.* 60, 282–291.
303. Abdul-Muneer, P.M., Chandra, N., and Haorah, J. (2014). Interactions of oxidative stress and neurovascular inflammation in the pathogenesis of traumatic brain injury. *Mol. Neurobiol.* 51, 966–979.
 304. Corpas, F.J., Chaki, M., Leterrier, M., and Barroso, J.B. (2009). Protein tyrosine nitration: a new challenge in plants. *Plant Signal. Behav.* 4, 920–923.
 305. Radi, R. (2013). Protein tyrosine nitration: biochemical mechanisms and structural basis of functional effects. *Acc. Chem. Res.* 46, 550–559.
 306. Hall, E.D., Detloff, M.R., Johnson, K., and Kupina, N.C. (2004). Peroxynitrite-mediated protein nitration and lipid peroxidation in a mouse model of traumatic brain injury. *J. Neurotrauma* 21, 9–20.
 307. Laval, J., Jurado, J., Saparbaev, M., and Sidorkina, O. (1998). Antimitogenic role of base-excision repair enzymes upon free radical-induced DNA damage. *Mutat. Res.* 402, 93–102.
 308. Valavanidis, A., Vlachogianni, T., and Fiotakis, C. (2009). 8-hydroxy-2-deoxyguanosine (8-OHdG): a critical biomarker of oxidative stress and carcinogenesis. *J. Environ. Sci. Heal.* 27, 120–139.
 309. Fraga, C.G., Shigenaga, M.K., Park, J.-W., Degant, P., and Amest, B.N. (1990). Oxidative damage to DNA during aging: 8-hydroxy-2'-deoxyguanosine in rat organ DNA and urine. *Med. Sci.* 87, 4533–4537.
 310. Fehily, B., Bartlett, C.A., Lydiard, S., Archer, M., Milbourn, H., Majimbi, M., Hemmi, J.M., Dunlop, S.A., Yates, N.J., and Fitzgerald, M. (2019). Differential responses to increasing numbers of mild traumatic brain injury in a rodent closed-head injury model. *J. Neurochem.* 149, 660–678.
 311. Dent, K.A., Christie, K.J., Bye, N., Basrai, H.S., Turbic, A., Habgood, M., Cate, H.S., and Turnley, A.M. (2015). Oligodendrocyte birth and death following traumatic brain injury in adult mice. *PLoS One* 10, e0121541.
 312. Shuman, S.L., Bresnahan, J.C., and Beattie, M.S. (1997). Apoptosis of microglia and oligodendrocytes after spinal cord contusion in rats. *J. Neurosci. Res.* 50, 798–808.
 313. McTigue, D.M., Wei, P., and Stokes, B.T. (2001). Proliferation of NG2-positive cells and altered oligodendrocyte numbers in the contused rat spinal cord. *J. Neurosci.* 21, 3392–3400.
 314. Crowe, M.J., Bresnahan, J.C., Shuman, S.L., Masters, J.N., and Beattie, M.S. (1997). Apoptosis and delayed degeneration after spinal cord injury in rats and monkeys. *Nat. Med.* 3, 73–76.
 315. Payne, S.C., Bartlett, C.A., Savigni, D.L., Harvey, A.R., Dunlop, S.A., and Fitzgerald, M. (2013). Early proliferation does not prevent the loss of oligodendrocyte progenitor cells during the chronic phase of secondary degeneration in a CNS white matter tract. *PLoS One* 8, e65710–65720.
 316. Chen, S., Pickard, J.D., and Harris, N.G. (2003). Time course of cellular pathology after controlled cortical impact injury. *Exp. Neurol.* 182, 87–102.
 317. Flygt, J., Gumucio, A., Ingelsson, M., Skoglund, K., Holm, J., Alafuzoff, I., and Marklund, N. (2016). Human traumatic brain injury results in oligodendrocyte death and increases the number of oligodendrocyte progenitor cells. *J. Neuropathol. Exp. Neurol.* 75, 503–515.
 318. Donnelly, D.J., and Popovich, P.G. (2008). Inflammation and its role in neuroprotection, axonal regeneration and functional recovery after spinal cord injury. *Exp. Neurol.* 209, 378–388.
 319. Raghupathi, R. (2004). Cell death mechanisms following traumatic brain injury. *Brain Pathol.* 14, 215–222.
 320. Cloots, R.J.H., Van Dommelen, J.A.W., Kleiven, S., and Geers, M.G.D. (2013). Multi-scale mechanics of traumatic brain injury: predicting axonal strains from head loads. *Biomech. Model. Mechanobiol.* 12, 137–150.
 321. Staal, J.A., and Vickers, J.C. (2011). Selective vulnerability of non-myelinated axons to stretch injury in an in vitro co-culture system. *J. Neurotrauma* 28, 841–847.
 322. Reeves, T.M., Phillips, L.L., and Povlishock, J.T. (2005). Myelinated and unmyelinated axons of the corpus callosum differ in vulnerability and functional recovery following traumatic brain injury. *Exp. Neurol.* 196, 126–137.
 323. Rami, A. (2003). Ischemic neuronal death in the rat hippocampus: the calpain-calpastatin-caspase hypothesis. *Neurobiol. Dis.* 13, 75–88.
 324. Clark, R.S.B., Kochanek, P.M., Watkins, S.C., Chen, M., Dixon, C.E., Seidberg, N.A., Melick, J., Loeffert, J.E., Nathaniel, P.D., Jin, K.L., and Graham, S.H. (2001). Caspase-3 mediated neuronal death after traumatic brain injury in rats. *J. Neurochem.* 74, 740–753.
 325. Gennarelli, T.A., Thibault, L.E., and Graham, D.I. (1998). Diffuse axonal injury: an important form of traumatic brain damage. *Neuroscientist* 4, 202–215.
 326. Shaikh, A.Y., Ezekiel, U.R., Liu, P.K., and Hsu, C.Y. (1998). Ischemic neuronal apoptosis: a view based on free radical-induced DNA damage and repair. *Neurosci.* 4, 88–95.
 327. Fitzgerald, M., Payne, S.C., Bartlett, C.A., Evill, L., Harvey, A.R., and Dunlop, S.A. (2009). Secondary retinal ganglion cell death and the neuroprotective effects of the calcium channel blocker lomerizine. *Investig. Ophthalmol. Vis. Sci.* 50, 5456–5462.
 328. Selt, M., Bartlett, C.A., Harvey, A.R., Dunlop, S.A., and Fitzgerald, M. (2010). Limited restoration of visual function after partial optic nerve injury: a time course study using the calcium channel blocker lomerizine. *Brain Res. Bull.* 81, 467–471.
 329. Reeves, T.M., Smith, T.L., Williamson, J.C., and Phillips, L.L. (2012). Unmyelinated axons show selective rostrocaudal pathology in the corpus callosum after traumatic brain injury. *J. Neuropathol. Exp. Neurol.* 71, 198–210.
 330. Marion, C.M., Radowski, K.L., Cramer, N.P., Galdzicki, Z., and Armstrong, R.C. (2018). Experimental traumatic brain injury identifies distinct early and late phase axonal conduction deficits of white matter pathophysiology, and reveals intervening recovery. *J. Neurosci.* 38, 8723–8736.
 331. Conti, A.C., Raghupathi, R., Trojanowski, J.Q., and McIntosh, T.K. (1998). Experimental brain injury induces regionally distinct apoptosis during the acute and delayed post-traumatic period. *J. Neurosci.* 18, 5663–5672.
 332. Collins-Praino, L.E., and Corrigan, F. (2017). Does neuroinflammation drive the relationship between tau hyperphosphorylation and dementia development following traumatic brain injury? *Brain. Behav. Immun.* 60, 369–382.
 333. Collins-Praino, L., Gutschmidt, D., Sharkey, J., and Arulsamy, A. (2018). Temporal changes in tau phosphorylation and related kinase and phosphatases following two models of traumatic brain injury. *J. Neuroinflammation Neurodegener. Dis.* 2, 1–13.
 334. Ek, C.J., Habgood, M.D., Dennis, R., Dziegielewska, K.M., Mallard, C., Wheaton, B., and Saunders, N.R. (2012). Pathological changes in the white matter after spinal contusion injury in the rat. *PLoS One* 7, e43484.
 335. Shoji, M., Golde, T.E., Ghiso, J., Cheung, T.T., Estus, S., Shaffer, L.M., Cai, X.D., McKay, D.M., Tintner, R., Frangione, B., and Younkin, S.G. (1992). Production of the Alzheimer amyloid β protein by normal proteolytic processing. *Science* 258, 126–129.
 336. Ikonomic, M.D., Uryu, K., Abrahamson, E.E., Ciallella, J.R., Trojanowski, J.Q., Lee, V.M.-Y., Clark, R.S., Marion, D.W., Wisniewski, S.R., and DeKosky, S.T. (2004). Alzheimer's pathology in human temporal cortex surgically excised after severe brain injury. *Exp. Neurol.* 190, 192–203.
 337. Collins, J.M., King, A.E., Woodhouse, A., Kirkcaldie, M.T.K., and Vickers, J.C. (2019). Age moderates the effects of traumatic brain injury on beta-amyloid plaque load in APP/PS1 mice. *J. Neurotrauma* 36, 1876–1889.
 338. Müller, U.C., and Zheng, H. (2012). Physiological functions of APP family proteins. *Cold Spring Harb. Perspect. Med.* 2, a006288.
 339. McAteer, K.M., Corrigan, F., Thornton, E., Turner, R.J., and Vink, R. (2016). Short and long term behavioral and pathological changes in a novel rodent model of repetitive mild traumatic brain injury. *PLoS One* 11, e0160220.
 340. Corrigan, F., Vink, R., Blumbergs, P.C., Masters, C.L., Cappai, R., and Van Den Heuvel, C. (2012). Characterisation of the effect of knockout of the amyloid precursor protein on outcome following mild traumatic brain injury. *Brain Res.* 1451, 87–99.
 341. Corrigan, F., Vink, R., Blumbergs, P.C., Masters, C.L., Cappai, R., and Van Den Heuvel, C. (2012). SAPPz rescues deficits in amyloid precursor protein knockout mice following focal traumatic brain injury. *J. Neurochem.* 122, 208–220.
 342. Corrigan, F., Thornton, E., Roisman, L.C., Leonard, A.V., Vink, R., Blumbergs, P.C., Van Den Heuvel, C., and Cappai, R. (2014). The neuroprotective activity of the amyloid precursor protein against traumatic brain injury is mediated via the heparin binding site in residues 96–110. *J. Neurochem.* 128, 196–204.

343. Plummer, S.L., Corrigan, F., Thornton, E., Woenig, J.A., Vink, R., Cappai, R., and Den Heuvel, C. Van. (2018). The amyloid precursor protein derivative, APP96-110, is efficacious following intravenous administration after traumatic brain injury. *PLoS One* 13, e0190449.
344. Baumann, N., and Pham-Dinh, D. (2001). Biology of oligodendrocyte and myelin in the mammalian central nervous system. *Physiol. Rev.* 81, 871–927.
345. Smith, P.M., and Jeffery, N.D. (2006). Histological and ultrastructural analysis of white matter damage after naturally-occurring spinal cord injury. *Brain Pathol.* 16, 99–109.
346. Toomey, L.M., Bartlett, C.A., Gavriel, N., McGonigle, T., Majimbi, M., Gopalasingam, G., Rodger, J., and Fitzgerald, M. (2019). Comparing modes of delivery of a combination of ion channel inhibitors for limiting secondary degeneration following partial optic nerve transection. *Sci. Rep.* 9, 15297.
347. McDonald, J.W., and Belegu, V. (2006). Demyelination and remyelination after spinal cord injury. *J. Neurotrauma* 23, 345–359.
348. Maxwell, W.L. (2013). Damage to myelin and oligodendrocytes: a role in chronic outcomes following traumatic brain injury? *Brain Sci.* 3, 1374–1394.
349. Dong, X.X., Wang, Y., and Qin, Z.H. (2009). Molecular mechanisms of excitotoxicity and their relevance to pathogenesis of neurodegenerative diseases. *Acta Pharmacol. Sin.* 30, 379–387.
350. Podbielska, M., Banik, N.L., Kurowska, E., and Hogan, E.L. (2013). Myelin recovery in multiple sclerosis: The challenge of remyelination. *Brain Sci.* 3, 1282–1324.
351. Bongarzone, E., Pasquini, J., and Soto, E. (1995). Oxidative damage to proteins and lipids of CNS myelin produced by in vitro generated reactive oxygen species. *J. Neurosci. Res.* 41, 213–221.
352. Ravera, S., Bartolucci, M., Cuccarolo, P., Litamè, E., Illaricio, M., Calzia, D., Degan, P., Morelli, A., and Panfoli, I. (2015). Oxidative stress in myelin sheath: the other face of the extramitochondrial oxidative phosphorylation ability. *Free Radic. Res.* 49, 1156–1164.
353. Liu, M.C., Akle, V., Zheng, W., Kitlen, J., O'Steen, B., Larner, S.F., Dave, J.R., Tortella, F.C., Hayes, R.L., and Wang, K.K.W. (2006). Extensive degradation of myelin basic protein isoforms by calpain following traumatic brain injury. *J. Neurochem.* 98, 700–712.
354. Papa, L., Robertson, C.S., Wang, K.K.W., Brophy, G.M., Hannay, H.J., Heaton, S., Schmalzfuss, I., Gabrielli, A., Hayes, R.L., and Robicsek, S.A. (2015). Biomarkers improve clinical outcome predictors of mortality following non-penetrating severe traumatic brain injury. *Neurocrit. Care* 22, 52–64.
355. Glushakova, O.Y., Johnson, D., and Hayes, R.L. (2014). Delayed increases in microvascular pathology after experimental traumatic brain injury are associated with prolonged inflammation, blood-brain barrier disruption, and progressive white matter damage. *J. Neurotrauma* 31, 1180–1193.
356. Bramlett, H.M., and Dietrich, W.D. (2002). Quantitative structural changes in white and gray matter 1 year following traumatic brain injury in rats. *Acta Neuropathol.* 103, 607–614.
357. Payne, S.C., Bartlett, C.A., Harvey, A.R., Dunlop, S.A., and Fitzgerald, M. (2011). Chronic swelling and abnormal myelination during secondary degeneration after partial injury to a central nervous system tract. *J. Neurotrauma* 28, 1077–1088.
358. Haider, L., Fischer, M.T., Frischer, J.M., Bauer, J., Höftberger, R., Botond, G., Esterbauer, H., Binder, C.J., Witztum, J.L., and Lassmann, H. (2011). Oxidative damage in multiple sclerosis lesions. *Brain* 134, 1914–1924.
359. Waxman, S.G. (1989). Demyelination in spinal cord injury. *J. Neurol. Sci.* 91, 1–14.
360. Totouli, M.O., and Keirstead, H.S. (2005). Spinal cord injury is accompanied by chronic progressive demyelination. *J. Comp. Neurol.* 486, 373–383.
361. Nashmi, R., and Fehlings, M.G. (2001). Changes in axonal physiology and morphology after chronic compressive injury of the rat thoracic spinal cord. *Neuroscience* 104, 235–251.
362. Armstrong, R.C., Mierzwa, A.J., Sullivan, G.M., and Sanchez, M.A. (2016). Myelin and oligodendrocyte lineage cells in white matter pathology and plasticity after traumatic brain injury. *Neuropharmacology* 110, 654–659.
363. Rasband, M.N., Kagawa, T., Park, E.W., Ikenaka, K., and Trimmer, J.S. (2003). Dysregulation of axonal sodium channel isoforms after adult-onset chronic demyelination. *J. Neurosci. Res.* 73, 465–470.
364. Szymanski, C.R., Chiha, W., Morellini, N., Cummins, N., Bartlett, C.A., O'Hare Doig, R.L., Savigni, D.L., Payne, S.C., Harvey, A.R., Dunlop, S.A., and Fitzgerald, M. (2013). Paranode Abnormalities and Oxidative Stress in Optic Nerve Vulnerable to Secondary Degeneration: Modulation by 670 nm Light Treatment. *PLoS One* 8, e66448.
365. Toomey, L.M., Bartlett, C.A., Majimbi, M., Gopalasingam, G., Rodger, J., and Fitzgerald, M. (2018). Comparison of ion channel inhibitor combinations for limiting secondary degeneration following partial optic nerve transection. *Exp. Brain Res.* 237, 161–171.
366. Pitt, D., Gonzales, E., Cross, A.H., and Goldberg, M.P. (2010). Demyelinated axons in shiverer mice are highly vulnerable to α -amino-3-hydroxy-5-methylisoxazole-4-propionic acid (AMPA) receptor-mediated toxicity. *Brain Res.* 1309, 146–154.
367. Mychasiuk, R., Hehar, H., Candy, S., Ma, I., and Esser, M.J. (2016). The direction of the acceleration and rotational forces associated with mild traumatic brain injury in rodents affect behavioural and molecular outcomes. *J. Neurosci. Methods* 257, 168–178.
368. Fujimoto, S.T., Longhi, L., Saatman, K.E., and McIntosh, T.K. (2004). Motor and cognitive function evaluation following experimental traumatic brain injury. *Neurosci. Biobehav. Rev.* 28, 365–378.
369. Clarner, T., Diederichs, F., Berger, K., Denecke, B., Gan, L., van der Valk, P., Beyer, C., Amor, S., and Kipp, M. (2012). Myelin debris regulates inflammatory responses in an experimental demyelination animal model and multiple sclerosis lesions. *Glia* 60, 1468–1480.
370. Anderson, A.J. (2002). Mechanisms and pathways of inflammatory responses in CNS trauma: spinal cord injury. *J. Spinal Cord Med.* 25, 70–79.
371. Lucas, S.M., Rothwell, N.J., and Gibson, R.M. (2006). The role of inflammation in CNS injury and disease. *Br. J. Pharmacol.* 147, 232–240.
372. Potts, M.B., Koh, S.E., Whetstone, W.D., Walker, B.A., Yoneyama, T., Claus, C.P., Manvelyan, H.M., and Noble-Haesslein, L.J. (2006). Traumatic injury to the immature brain: inflammation, oxidative injury, and iron-mediated damage as potential therapeutic targets. *NeuroRx* 3, 143–153.
373. Wang, C., Zhao, C., Liu, W., Huang, X., Deng, Y., Jiang, J., and Li, W. (2019). Depletion of microglia attenuates dendritic spine loss and neuronal apoptosis in the acute stage of moderate traumatic brain injury in mice. *J. Neurotrauma* 36, 1–12.
374. Kigerl, K.A., Gensel, J.C., Ankeny, D.P., Alexander, J.K., Donnelly, D.J., and Popovich, P.G. (2009). Identification of two distinct macrophage subsets with divergent effects causing either neurotoxicity or regeneration in the injured mouse spinal cord. *J. Neurosci.* 29, 13435–13444.
375. Bellver-Landete, V., Bretheau, F., Mailhot, B., Vallières, N., Lesard, M., Janelle, M.E., Vernoux, N., Tremblay, M.E., Fuehrmann, T., Shoichet, M.S., and Lacroix, S. (2019). Microglia are an essential component of the neuroprotective scar that forms after spinal cord injury. *Nat. Commun.* 10, 518.
376. Smith, N.M., Giacci, M.K., Gough, A., Bailey, C., McGonigle, T., Black, A.M.B., Clarke, T.O., Bartlett, C.A., Swaminathan Iyer, K., Dunlop, S.A., and Fitzgerald, M. (2018). Inflammation and blood-brain barrier breach remote from the primary injury following neurotrauma. *J. Neuroinflammation* 15, 201.
377. Collins-Praino, L.E., Arulsamy, A., Katharesan, V., and Corrigan, F. (2018). The effect of an acute systemic inflammatory insult on the chronic effects of a single mild traumatic brain injury. *Behav. Brain Res.* 336, 22–31.
378. Sullivan, G.M., Mierzwa, A.J., Kijpaisalratana, N., Tang, H., Wang, Y., Song, S.K., Selwyn, R., and Armstrong, R.C. (2013). Oligodendrocyte lineage and subventricular zone response to traumatic axonal injury in the corpus callosum. *J. Neuropathol. Exp. Neurol.* 72, 1106–1125.
379. McGraw, J., Hiebert, G.W., and Steeves, J.D. (2001). Modulating astrogliosis after neurotrauma. *J. Neurosci. Res.* 63, 109–115.
380. Liddel, S.A., and Barres, B.A. (2017). Reactive astrocytes: production, function, and therapeutic potential. *Immunity* 46, 957–967.
381. Ransohoff, R.M. (2016). A polarizing question: do M1 and M2 microglia exist. *Nat. Neurosci.* 19, 987–991.
382. Myer, D.J., Gurkoff, G.G., Lee, S.M., Hovda, D.A., and Sofroniew, M. V. (2006). Essential protective roles of reactive astrocytes in traumatic brain injury. *Brain* 129, 2761–2772.
383. Miyamoto, N., Maki, T., Shindo, A., Liang, A.C., Maeda, M., Egawa, N., Itoh, K., Lo, E.K., Lok, J., Ihara, M., and Arai, K. (2015). Astrocytes promote oligodendrogenesis after white matter damage via brain-derived neurotrophic factor. *J. Neurosci.* 35, 14002–14008.

384. Brambilla, R., Bracchi-Ricard, V., Hu, W.H., Frydel, B., Bramwell, A., Karmally, S., Green, E.J., and Bethea, J.R. (2005). Inhibition of astroglial nuclear factor κ B reduces inflammation and improves functional recovery after spinal cord injury. *J. Exp. Med.* 202, 145–156.
385. Hamby, M.E., Hewett, J.A., and Hewett, S.J. (2006). TGF- β 1 potentiates astrocytic nitric oxide production by expanding the population of astrocytes that express NOS-2. *Glia* 54, 566–577.
386. Sofroniew, M.V. (2009). Molecular dissection of reactive astrogliosis and glial scar formation. *Trends Neurosci.* 32, 638–647.
387. Takano, T., Kang, J., Jaiswal, J.K., Simon, S.M., Lin, J.H.-C., Yu, Y., Li, Y., Yang, J., Dienel, G., Zielke, H.R., and Nedergaard, M. (2005). Receptor-mediated glutamate release from volume sensitive channels in astrocytes. *Proc. Natl. Acad. Sci. U. S. A.* 102, 16466–16471.
388. Clark, D.P.Q., Perreau, V.M., Shultz, S.R., Brady, R.D., Lei, E., Dixit, S., Taylor, J.M., Beart, P.M., and Boon, W.C. (2019). Inflammation in traumatic brain injury: roles for toxic α 1 astrocytes and microglial–astrocytic crosstalk. *Neurochem. Res.* 44, 1410–1424.
389. Hill, S.J., Barbarese, E., and McIntosh, T.K. (1996). Regional heterogeneity in the response of astrocytes following traumatic brain injury in the adult rat. *J. Neuropathol. Exp. Neurol.* 55, 1221–1229.
390. Franklin, R.J.M., and Ffrench-Constant, C. (2008). Remyelination in the CNS: from biology to therapy. *Nat. Rev. Neurosci.* 9, 839–855.
391. Watkins, T.A., Emery, B., Mulinyawe, S., and Barres, B.A. (2008). Distinct stages of myelination regulated by γ -secretase and astrocytes in a rapidly myelinating CNS coculture system. *Neuron* 60, 555–569.
392. Zawadzka, M., Rivers, L.E., Fancy, S.P.J., Zhao, C., Tripathi, R., Jamen, F., Young, K., Goncharevich, A., Pohl, H., Rizzi, M., Rowitch, D.H., Kessler, N., Suter, U., Richardson, W.D., and Franklin, R.J.M. (2010). CNS-resident glial progenitor/stem cells produce schwann cells as well as oligodendrocytes during repair of CNS demyelination. *Cell Stem Cell* 6, 578–590.
393. Arundine, M., and Tymianski, M. (2003). Molecular mechanisms of calcium-dependent neurodegeneration in excitotoxicity. *Cell Calcium* 34, 325–337.
394. Yeung, M.S.Y., Djelloul, M., Steiner, E., Bernard, S., Salehpour, M., Possnert, G., Brundin, L., and Frisén, J. (2019). Dynamics of oligodendrocyte generation in multiple sclerosis. *Nature* 566, 538–542.
395. Nave, K.A., and Ehrenreich, H. (2019). Time to revisit oligodendrocytes in multiple sclerosis. *Nat. Med.* 25, 364–366.
396. Keirstead, H.S., Nistor, G., Bernal, G., Totoiu, M., Cloutier, F., Sharp, K., and Steward, O. (2005). Human embryonic stem cell-derived oligodendrocyte progenitor cell transplants remyelinate and restore locomotion after spinal cord injury. *J. Neurosci.* 25, 4694–4705.
397. Wang, Y., Cheng, X., He, Q., Zheng, Y., Kim, D.H., Whittemore, S.R., and Cao, Q.L. (2011). Astrocytes from the contused spinal cord inhibit oligodendrocyte differentiation of adult oligodendrocyte precursor cells by increasing the expression of bone morphogenetic proteins. *J. Neurosci.* 31, 6053–6058.
398. Anderson, M.A., Burda, J.E., Ren, Y., Ao, Y., O’Shea, T.M., Kawaguchi, R., Coppola, G., Khakh, B.S., Deming, T.J., and Sofroniew, M.V. (2016). Astrocyte scar formation AIDS central nervous system axon regeneration. *Nature* 532, 195–200.
399. Miron, V.E., Boyd, A., Zhao, J.W., Yuen, T.J., Ruckh, J.M., Shadrach, J.L., Van Wijngaarden, P., Wagers, A.J., Williams, A., Franklin, R.J.M., and Ffrench-Constant, C. (2013). M2 microglia and macrophages drive oligodendrocyte differentiation during CNS remyelination. *Nat. Neurosci.* 16, 1211–1218.
400. Pang, Y., Campbell, L., Zheng, B., Fan, L., Cai, Z., and Rhodes, P. (2010). Lipopolysaccharide-activated microglia induce death of oligodendrocyte progenitor cells and impede their development. *Neuroscience* 166, 464–475.
401. Taylor, D.L., Pirianov, G., Holland, S., McGinnity, C.J., Norman, A.L., Reali, C., Diemel, L.T., Gveric, D., Yeung, D., and Mehmet, H. (2010). Attenuation of proliferation in oligodendrocyte precursor cells by activated microglia. *J. Neurosci. Res.* 88, 1632–1644.
402. Kotter, M.R., Zhao, C., Van Rooijen, N., and Franklin, R.J.M. (2005). Macrophage-depletion induced impairment of experimental CNS remyelination is associated with a reduced oligodendrocyte progenitor cell response and altered growth factor expression. *Neurobiol. Dis.* 18, 166–175.
403. Kotter, M.R., Li, W.W., Zhao, C., and Franklin, R.J.M. (2006). Myelin impairs CNS remyelination by inhibiting oligodendrocyte precursor cell differentiation. *J. Neurosci.* 26, 328–332.
404. Astradsson, A., Cooper, O., Vinuela, A., and Isacson, O. (2008). Recent advances in cell-based therapy for Parkinson disease. *Neurosurg. Focus* 24, E6.
405. Miron, V.E. (2017). Microglia-driven regulation of oligodendrocyte lineage cells, myelination, and remyelination. *J. Leukoc. Biol.* 101, 1103–1108.
406. Mitew, S., Gobius, I., Fenlon, L.R., McDougall, S.J., Hawkes, D., Xing, Y.L., Bujalka, H., Gundlach, A.L., Richards, L.J., Kilpatrick, T.J., Merson, T.D., and Emery, B. (2018). Pharmacogenetic stimulation of neuronal activity increases myelination in an axon-specific manner. *Nat. Commun.* 9, 306.
407. Ludwin, S.K., and Maitland, M. (1984). Long-term remyelination fails to reconstitute normal thickness of central myelin sheaths. *J. Neurol. Sci.* 64, 193–198.
408. Powers, B.E., Sellers, D.L., Lovelett, E.A., Cheung, W., Aalami, S.P., Zapertov, N., Maris, D.O., and Horner, P.J. (2013). Remyelination reporter reveals prolonged refinement of spontaneously regenerated myelin. *Proc. Natl. Acad. Sci. U. S. A.* 110, 4075–4080.
409. Challenor, M., O’Hare Doig, R., Fuller, P., Giacci, M., Bartlett, C., Wale, C.H., Cozens, G.S., Hool, L., Dunlop, S., Swaminathan Iyer, K., Rodger, J., and Fitzgerald, M. (2015). Prolonged glutamate excitotoxicity increases GluR1 immunoreactivity but decreases mRNA of GluR1 and associated regulatory proteins in dissociated rat retinae in vitro. *Biochimie* 112, 160–171.
410. Fitzgerald, M., Bartlett, C.A., Evill, L., Rodger, J., Harvey, A.R., and Dunlop, S.A. (2009). Secondary degeneration of the optic nerve following partial transection: the benefits of lomerizine. *Exp. Neurol.* 219, 219–230.

Address correspondence to:

Melinda Fitzgerald, PhD

Perron Institute for Neurological and Translational Science

Sarich Neuroscience Research Institute Building

8 Verdun Street

Nedlands, Western Australia 6009

Australia

E-mail: lindy.fitzgerald@curtin.edu.au

1.3.2. Partial Optic Nerve Transection Model

Neurotrauma is similar to MS in its complexity and heterogeneity, with no one animal model able to accurately replicate the full spectrum of biomechanical forces and physiological changes associated with a traumatic injury to the CNS (O'Connor et al. 2011). Consequently, there is no gold standard model for TBI. As discussed above by the review in section 1.3.1, there are a variety of commonly used models of TBI, including, but not limited to; (1) controlled cortical impact, (2) fluid percussion injury, and (3) closed-head weight-drop model. However, these models result in an injury where it is difficult to disentangle primary from secondary injury. When interested in understanding secondary degeneration, it becomes imperative to utilise models that have the ability to distinguish between primary and secondary injury.

The optic nerve is an ideal structure to assess secondary degeneration to white matter following injury as it is an easily accessible white matter tract and the extent of damage can be precisely controlled by the size of the transection (Bartlett & Fitzgerald 2018). The partial optic nerve transection model is particularly useful for differentiating the various secondary degenerative processes that occur following injury to the CNS from the primary injury site. In other models of neurotrauma, it is difficult to discriminate between the initially axotomised and spared tissue (Bartlett & Fitzgerald 2018; Levkovitch-Verbin et al. 2003). In a partial optic nerve transection, the dorsal aspect of the optic nerve is cut to a depth of 200µm, about 1mm behind the right retina (Bartlett & Fitzgerald 2018), leaving the ventral aspect vulnerable solely to secondary degeneration (**Error! Reference source not found.**). The observed secondary damage even spreads as far into the brain as the superior colliculus *via* the visual pathways, to elicit a remote degenerative response to injury (Smith et al. 2018). Many of the structural, cellular and biochemical changes that occur following a partial transection have already been studied in detail by the Fitzgerald team (Fitzgerald et al. 2009; Fitzgerald et al. 2010a; Giacci et al. 2018b; O'Hare Doig et al. 2014, 2017; Payne et al. 2012; Savigni et al. 2013; Smith et al. 2018; Szymanski et al. 2013; Toomey et al. 2018; Wells et al. 2012). Therefore, the partial optic nerve model is employed throughout this thesis to examine the mechanisms of secondary degeneration following neurotrauma.

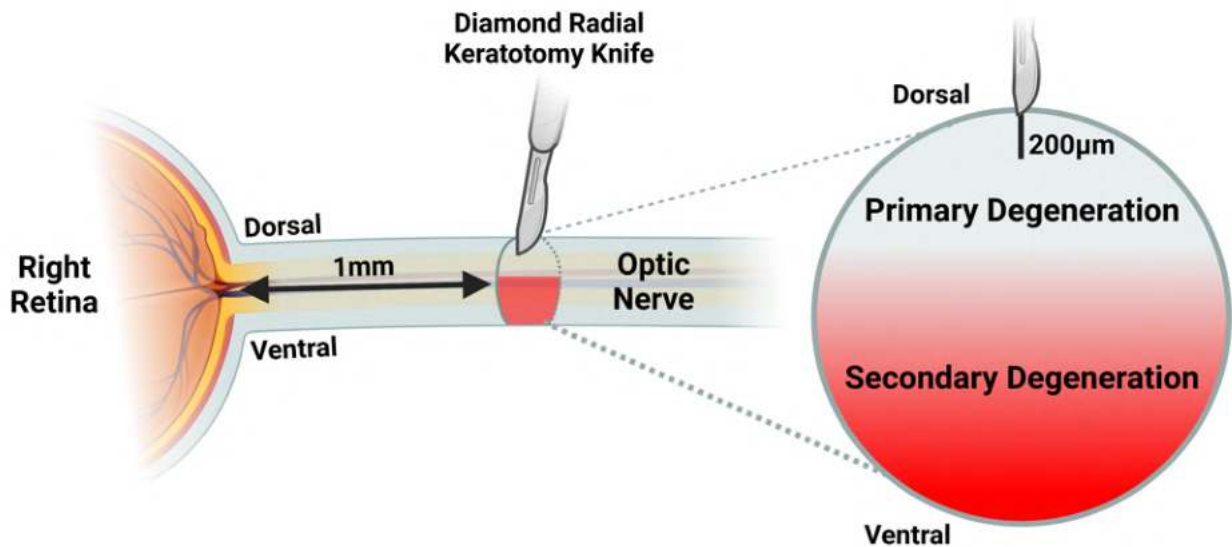


Figure 1.9. Schematic of a partial optic nerve transection. The dorsal aspect of the right optic nerve is transected to a depth of 200µm, about 1mm behind the retina, using a diamond radial keratotomy knife. This allows for the spatial segregation between the primary injury on the dorsal aspect of the nerve and secondary degeneration on the ventral aspect. Original illustration created using BioRender.com.

1.4. Common Mechanisms of Damage In MS and Neurotrauma

1.4.1. Overview of Common Mechanisms

Though MS and neurotrauma are two different conditions, both share common mechanisms of damage. In particular, oxidative stress plays a central role in the pathophysiology of both disorders. Therefore, it may be possible to translate knowledge obtained regarding either one and apply it to the understanding of the other. This third and final key component of the literature review chapter will therefore focus predominantly on the common mechanism of oxidative damage in these two disorders. It should be noted that for clarity, brevity and relevance to the remainder of the work presented in this thesis, particular attention will be provided towards mechanisms proven active within humans in MS and neurotrauma, as well as within both the cuprizone and partial optic nerve transection models for these respective neurological conditions.

1.4.2. Oxidative Burst

A central and unifying contributor to damage in both MS lesions and neurotrauma is oxidative stress. Oxidative stress occurs when the production of ROS increases and overwhelms the ability of antioxidants to detoxify ROS' potential damaging effects (Cornelius et al. 2013). There are two main pathways for increased ROS production, activation of oxidative burst enzymes and mitochondrial dysfunction (Fischer et al. 2012). Nicotinamide adenine dinucleotide phosphate hydrogen (NADPH) oxidase is an oxidative burst enzyme with the capacity for large-scale production of superoxide radicals by the reduction of molecular oxygen (Babior 2004).

As discussed in Section 1.2.5.2, microglia are the major source of ROS in MS plaques (Fischer et al. 2012). NADPH oxidase activity in microglia has been implicated in oxidative stress mechanisms for a variety of neurodegenerative diseases, including Parkinson's and Alzheimer's disease (Infanger et al. 2006). Therefore, it is perhaps unsurprising that microglial NADPH-mediated oxidative burst has been shown to be central in the production of ROS in MS lesions, particularly in the initiating stages of plaque formation (Fischer et al. 2012). There may be two phases to microglial activation in MS lesions, with microglia in pre-demyelinating lesions in particular displaying increased ROS production (Marik et al. 2007). Overall, it can be suggested that oxidative burst may be an initiating event in MS lesions.

NADPH has been shown to play an integral role in secondary degeneration following TBI, exhibiting a potentially biphasic activation pattern (Angeloni et al. 2015; Zhang et al. 2012). Up to 1 hour following a controlled cortical impact TBI, NADPH oxidase activation is significantly increased, with a neuronal origin (Zhang et al. 2012). The second peak of NADPH oxidase activity occurs from 24 to 96 hours following TBI, and is associated with microglial activation (Dohi et al. 2010; Zhang et al. 2012). However, another study found that NADPH activation increases dependent on time with a sole peak between 12 and 24 hours following injury (Ansari et al. 2014). Nevertheless, even at 1 year following a controlled cortical impact, NADPH oxidase is still highly expressed by chronically activated microglial cells (Loane et al. 2014).

Following a partial optic nerve transection, there is increased myeloperoxidase activity from macrophages in the dorsal optic nerve by 24 hours after injury (O'Hare Doig et al. 2014), which is also involved in oxidative burst and ROS generation mechanisms (Davies & Hawkins 2020). Myeloperoxidase is expressed by macrophages in cerebral white matter plaques in human MS brains, significantly associated with demyelination (Gray et al. 2008), suggesting a central role for this enzyme in both conditions.

1.4.3. Glutamate Excitotoxicity and Changes in Ca²⁺ Dynamics

Another driver of oxidative damage is glutamate excitotoxicity and ionic Ca²⁺ disturbances. Following neurotrauma, extracellular glutamate increases up to 5µmol/L from a baseline level of approximately 0.6µmol/L (Mark et al. 2001). After TBI in humans, the concentration of glutamate in the cerebrospinal fluid is increased and remains elevated at 1 week post-injury, with glutamate concentration correlated to injury severity (Hong et al. 2001). At 2 days following a moderate TBI in rodents, tonic glutamate levels are raised by 178% and 256% in the striatum and dentate gyrus respectively (Hinzman et al. 2010). Rise in glutamate is caused by a variety of pathological mechanisms including: (1) Ca²⁺-mediated axonal release of glutamate; (2) impaired glutamate reuptake and recycling by neurons and astrocytes; (3) adenosine triphosphate (ATP)-mediated glutamate release by astrocytes; (4) release of glutamate from injured and dying cells and; (5) release

of glutamate from activated microglia (Barger et al. 2007; Duan et al. 2003; Katayama et al. 1991; Mark et al. 2001). Ultimately, excess of glutamate released into the extracellular space causes the surrounding cells to experience prolonged exposure to glutamate which can result in cell death of originally healthy tissue in a process called glutamate excitotoxicity (Doble 1999; Guerriero et al. 2015).

Glutamate excitotoxicity is also a mechanism at play within demyelinating disease, with glutamate levels increasing significantly in the brains of people with MS (Cianfoni et al. 2007; Srinivasan et al. 2005). There are multiple causes for this elevated glutamate within demyelinating lesions, including increased glutamate release by activated inflammatory cells such as microglia, macrophages and leukocytes, as well as by astrocytes and demyelinated axons (Rajda et al. 2017). Glutamate receptors are also overexpressed (Newcombe et al. 2008), with concurrent deficits in glutamate reuptake in both cortical (Vercellino et al. 2007) and white matter lesions (Pitt et al. 2003), in particular within oligodendrocytes (Pitt et al. 2003). The release of proinflammatory cytokines in MS lesions increases glutamatergic synaptic transmission, causing excitotoxicity and subsequent synaptopathy (Mandolesi et al. 2015). There are also abnormalities observed in the enzymes involved in glutamate homeostasis, including decreases in glutamine synthetase and glutamate-dehydrogenase activity (Rajda et al. 2017). Similarly, upregulated glutaminase expression, a glutamate-producing enzyme, is associated with oligodendrocyte and axonal damage within human MS white matter (Werner et al. 2001).

Activation of glutamatergic receptors on cells results in influx of Ca^{2+} into the intracellular space (Arundine & Tymianski 2003), which leads to opening of voltage-gated Ca^{2+} channels (VGCCs; Verkhratsky & Kettenmann 1996), ultimately causing an influx of Ca^{2+} into cells. However, increased extracellular glutamate alone does not produce the neurotoxic levels of Ca^{2+} seen following neurotrauma (Schwartz 2004). After injury, there is an immediate increase in extracellular Ca^{2+} due to release from injured and dying cells, as well as release from the Ca^{2+} stores in axons (Wolf et al. 2001). Using ^{45}Ca autoradiography following TBI in rodents, there is a significant increase in ^{45}Ca accumulation, even in brain regions without gross damage, indicating the critical role of Ca^{2+} flux in TBI pathology (Fineman et al. 1993). Ca^{2+} then enters cells *via* a myriad of channels and receptors, and through membranous pores created by the shearing force of the initial injury (Stirling et al. 2014; Weber 2012). Similarly, Ca^{2+} dyshomeostasis may play a more direct role in MS (Enders et al. 2020). For example, Ca^{2+} enters axons within MS lesions *via* nanoruptures on the axonal plasma membrane independently from any glutamate-dependent mechanisms to drive axon degeneration (Witte et al. 2019).

Once inside cells, Ca^{2+} induces Ca^{2+} release from intracellular stores, including those in the endoplasmic reticulum, resulting in the reversal of the sodium ion (Na^+)/ Ca^{2+} exchanger on the cell

surface, which then pumps more Ca^{2+} in from the extracellular space (Andriessen et al. 2010; Kapoor et al. 2003; Staal et al. 2010). Following a partial optic nerve transection, there is a decrease in the size and intensity of subcellular Ca^{2+} microdomains, such as within intracellular organelles, and an increase in punctate Ca^{2+} , which perhaps reflects the release of Ca^{2+} from these internal stores into the cytosol (Lozić et al. 2014; Wells et al. 2012).

1.4.4. Mitochondrial Dysfunction

Once inside neuroglia, Ca^{2+} accumulates inside the mitochondria, resulting in mitochondrial dysfunction, increased production of ROS, release of cytochrome c into the cytosol, and subsequent cellular apoptosis (Adam-Vizi & Starkov 2010; Giorgi et al. 2012). Excitotoxicity and mitochondrial dysfunction have been observed in MS lesions (Fischer et al. 2012; Gonsette 2008; Su et al. 2013). Deficits in complex IV of the electron transport chain have been identified in pattern III MS lesions in oligodendrocytes, astrocytes and neurons (Mahad et al. 2008), and are associated with increased production of ROS (Ziabreva et al. 2010). Furthermore, deficits have been identified in complexes I and III in neurons in MS lesions (Dutta et al. 2006).

Mitochondrial deficits have also been observed following neurotrauma; with mitochondrial dysfunction evident at 24 and 48 hours following a mild closed head injury in the cortex and hippocampus of mice (Hubbard et al. 2019). Mitochondrial structure, including mitochondrial shape and autophagic profiles, and the activity of citric acid cycle enzymes are altered at various acute timepoints following a partial optic nerve transection (Cummins et al. 2013). Increased ROS creates a feed-forward loop of further ROS production (Vasquez-Vivar et al. 2000), which ultimately results in self-propagating oxidative injury.

1.4.5. Oxidative Stress

During normal cellular respiration ROS and reactive nitrogen species (RNS) are detoxified by antioxidants to prevent damage to cells (Sies 1997). In injured or diseased systems, the level of free radical production is greater than that which can be counterbalanced by antioxidants, meaning the cell is in a state of oxidative stress (Farooqui et al. 2008). Oxidative stress impacts a variety of biological structures and functions, causing lipid peroxidation, protein nitration and DNA damage (Abdul-Muneer et al. 2014; Farooqui et al. 2008; Ischiropoulos & Beckman 2003; Di Pietro et al. 2014). In lipid peroxidation, free radicals essentially steal an electron from lipids (Ischiropoulos & Beckman 2003). ROS, especially hydroxyl radicals, target the carbon-carbon double bonds of unsaturated lipids, particularly polyunsaturated fatty acids, as well as glycolipids, phospholipids, and to a lesser degree cholesterol (Ayala et al. 2014). This reaction causes the formation of toxic aldehydes, including 4-hydroxynonenal (HNE) (Zhong & Yin 2015). Protein nitration arises when a nitro group is added into a protein structure (Corpas et al. 2009), and mainly occurs through the reaction of either nitric oxide or nitrogen dioxide with the amino acid tyrosine, forming 3-

nitrotyrosine (3-NT) (Radi 2013). There are many ways in which oxidative damage can occur to DNA, which will be further discussed in Section 1.4.6.

Mitochondrial oxidative stress can cause endoplasmic reticulum stress (Cao & Kaufman 2014). Endoplasmic reticulum stress results in unfolded proteins (Schröder & Kaufman 2005), and if this stress continues for a prolonged period it also can induce cell death (Xu et al. 2005). During times of stress, the endoplasmic reticulum releases a large amount of Ca^{2+} , which in turn increases the production of mitochondrial ROS/RNS (Cao & Kaufman 2014).

The enzymes involved in ROS production (Fischer et al. 2012; Gray et al. 2008; Liu et al. 2001), as well as markers of lipid peroxidation and DNA damage (Haider et al. 2011), are increased within active MS lesions. Furthermore, increased markers of nitrosative stress in oligodendrocytes have been observed in MS, with nitrosative damage detected in astrocytes and macrophages (Jack et al. 2007). Proteins involved in antioxidant detoxification of ROS are increased within MS lesions (van Horssen et al. 2010). Increased expression of markers of oxidative stress have been identified in the cerebrospinal fluid (Dore-Duffy et al. 1991) and blood (Fiorini et al. 2013; Miller et al. 2012) of people with MS. In MS, oxidative stress damages the BBB and myelin structures and activates innate inflammatory cells (Gilgun-Sherki et al. 2004). Activated microglia and macrophages also produce large quantities of ROS/RNS, thus propagating oxidative damage (Ohl et al. 2016). ROS activate T-cells and thus may additionally play a role in activating peripheral immunity (Secchi et al. 2015). Intrinsically to the model, cuprizone-induced demyelination is associated with increased ROS and oxidative stress (Gopalasingam et al. 2019; Praet et al. 2014). However, the cell-specific consequences of oxidative damage in animal models of demyelinating disease and MS are yet to be fully elucidated.

The mechanisms of oxidative stress have also been explored both in humans and in a variety of animal models of neurotrauma, as discussed in depth in the review article presented in Section 1.3 of this chapter. Following a partial optic nerve transection, an early role of oxidative damage has been identified, with the majority of assessed oxidative stress outcomes and changes occurring within the first seven days after injury in this model (Cummins et al. 2013; Fitzgerald et al. 2009; Fitzgerald, Bartlett, Harvey, et al. 2010; O'Hare Doig et al. 2017; O'Hare Doig et al. 2014; Savigni et al. 2013; Szymanski et al. 2013; Wells et al. 2012). However, it is important to note that oxidative stress has not yet been comprehensively assessed chronically in this particular model. Nevertheless, when combined with the positive detection of oxidative markers in humans, the literature to date indicates that oxidative stress is a key mechanism of damage following neurotrauma.

1.4.6. Oxidative DNA Damage

There are a range of mechanisms through which free radicals can cause DNA damage under oxidative stress conditions, including nucleobase modifications, tandem base modifications, abasic

sites, inter-strand cross-links, intra-strand cross-links, DNA adducts, single-strand breaks and double-strand breaks (Cadet & Davies 2017). The forthcoming section will focus on nucleobase modifications, single-strand breaks and double-strand breaks as they pertain most to the remainder of the thesis (Figure 1.10).

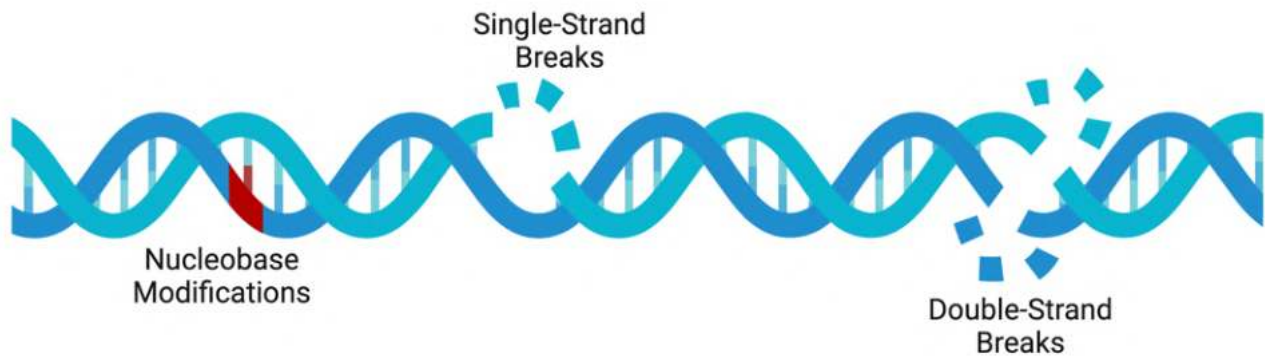


Figure 1.10. Relevant forms of oxidative DNA damage. Damage to DNA occurs under oxidative stress conditions *via* detrimental reactions between DNA structural components and ROS. This thesis focuses on three main types of oxidative DNA damage: nucleobase modifications, single-strand breaks and double-strand breaks. Original illustration created using BioRender.com.

1.4.6.1. Nucleobase Modifications and Base Excision Repair

Nucleobase modifications can result in exceptionally detrimental effects, by either modifying the genetic code or by acting as a block during DNA replication (Laval et al. 1998). Of the common nucleic bases, guanine possesses the lowest redox potential causing it to be highly vulnerable to ROS-mediated damage (Prabhulkar & Li 2010). The main by-product of guanine oxidation is 8-oxoguanine (8-OxoG) (Aguiar et al. 2013). Failure to eliminate 8-OxoG prior to DNA replication can cause a transverse mutation and mismatched based pairs. As 8-OxoG is functionally able to mimic a thymidine base it can become paired with adenosine (David et al. 2007). Furthermore, 8-OxoG when present during replication can create double-strand DNA breaks, which can be detrimental to cell survival (Aguiar et al. 2013). 8-OxoG also has a higher oxidation potential than guanine itself, making it vulnerable to additional oxidative damage (Kanvah & Schuster 2006). 8-OxoG is oxidised to 8-hydroxy-2-deoxyguanosine (8OH DG), the deoxyriboside form of 8-OxoG (Farooqui et al. 2008; Kanvah & Schuster 2006; Valavanidis et al. 2009). Similar to 8-OxoG, 8OH DG can result in guanine-cytosine to thymine-adenine transverse mutations (Valavanidis et al. 2009). Both 8-OxoG and 8OH DG have been well utilised in the literature as markers of oxidative DNA damage specifically and total oxidative stress (Arnett et al. 2005).

In active MS lesions, there is a significant build-up of 8OH DG DNA lesions, primarily within apoptotic oligodendrocytes, and to a smaller extent in astrocytes and innate inflammatory cells (Haider et al. 2011). A recent study from the Fitzgerald laboratory demonstrated a significant increase

in the level of 8OHdG DNA damage in the cuprizone model of demyelination, particularly colocalised within OPCs (Gopalasingam et al. 2019, Appendix B). Overall oligodendroglial susceptibility to DNA damage will be discussed further in Section 1.4.6.3. However, the potential effects of DNA damage specific to oligodendroglia in the cuprizone model is currently unknown.

Another recent study performed in the Fitzgerald laboratory discovered that oligodendroglia are significantly more vulnerable to developing oxidative 8OHdG DNA damage following a partial optic nerve transection compared to other neuroglial cells and structures (Giacci et al., 2018b). By 24 hours following a partial optic nerve transection, there was a significant increase in 8OHdG immunointensity in the ventral optic nerve, which extended out to 3 days post-injury (O'Hare Doig et al. 2017; O'Hare Doig et al. 2014). From as early as 15 minutes after a rodent controlled cortical impact mild TBI, 8OHdG lesions were present in the ipsilateral cortex (Mendez et al. 2004). However, following 1, 2 or 3 weight drop injuries to model repeated mild TBI, there were no increases in 8OHdG immunoreactivity at 3 months post-injury (Fehily et al. 2019). Following 2 closed head weight drop hits, at 11 days following injury, there was also no difference in the level of 8OHdG in the middle cortex, the hilus of the dentate gyrus or the splenium of the corpus callosum (Mao et al. 2018). More work is needed to determine whether there is 8OHdG DNA damage at other timepoints following single and repeated mild TBI. Additionally, older rats experience comparatively more 8OHdG DNA damage post-injury than younger rats, which suggests that aged brains may be more vulnerable to oxidative DNA damage (Itoh et al. 2013).

Both 8-OxoG and 8OHdG DNA lesions are primarily removed *via* short-patch base excision repair (Fortini et al. 1999; Prabhulkar & Li 2010) (Figure 1.11). Base excision repair is carried out by glycosylase enzymes to repair smaller DNA lesions to maintain genomic integrity (Krokan & Bjørå 2013). These enzymes function to excise the damaged base from the DNA strand (Jacobs & Schär 2012). There are eleven known glycosylases, and the appropriate one for each base excision repair is specific to the damaged nucleobase (Jacobs & Schär 2012), with the primary glycosylase for both 8-OxoG and 8OHdG being 8-oxoguanine glycosylase (OGG1) (Nishimura 2001; Torres-Gonzalez et al. 2014). Successful base excision repair can eliminate the potential genomic instability and even apoptosis caused by mismatched base pairs (Kaina et al. 2001; Nickson & Parsons 2014).

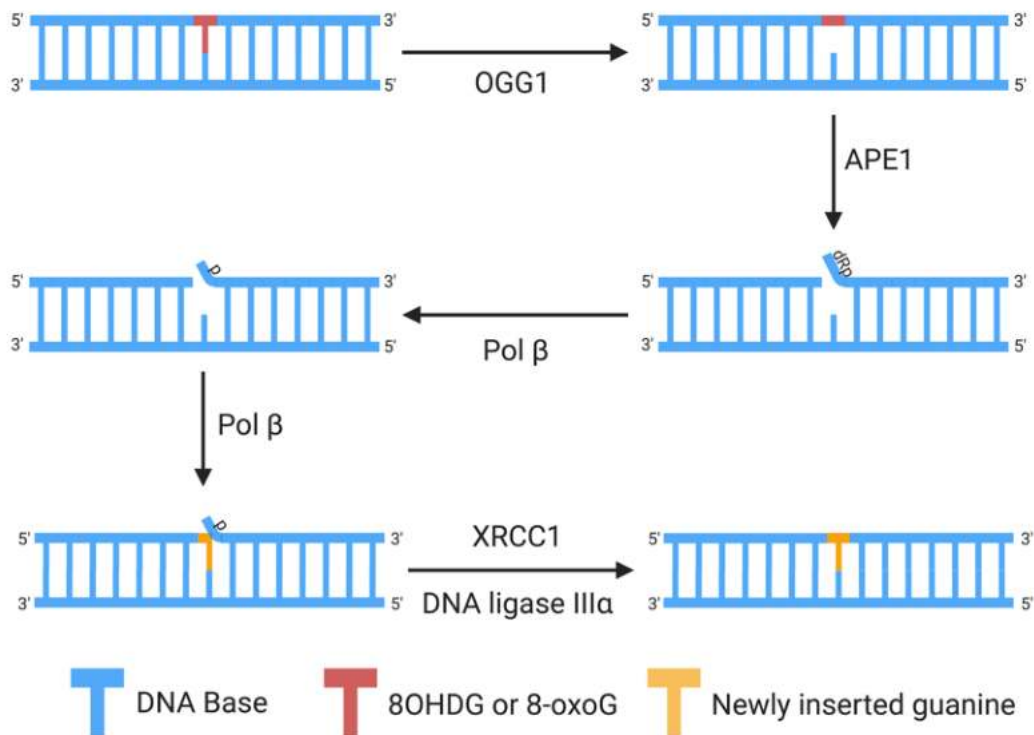


Figure 1.11. Mechanism of base excision repair to remove 8OHdG and 8-oxoG from DNA for maintaining genomic integrity. OGG1 excises the damaged 8OHdG or 8-oxoG nucleobase from the strand to create a temporary abasic site. This is cleaved by apurinic/apyrimidinic endonuclease-1 (APE1) to create a single-stranded DNA break flanked by 5'dRP and 3'hydroxyl ends. DNA polymerase β (Pol β) then cleaves the 5'dRP end and inserts a new guanine base. Finally, the strand is repaired by a complex of X-ray cross-complementing protein-1 (XRCC1) and DNA ligase III α . Information modified from Nickson and Parsons 2014. Original illustration created using BioRender.com.

This base excision repair mechanism may be specifically compromised in MS. People with a polymorphism of the reparative OGG1 gene have a significantly increased risk of developing MS (Karahalil et al. 2015). Furthermore, repair may be compromised in MS due to higher iron concentrations (Stephenson et al. 2014). As oligodendrocytes die, they release iron into the extracellular space, which leads to iron depositions in active MS lesions (Hametner et al. 2013). Iron overload has been shown to compromise key base excision repair enzymes (Li et al. 2009), which suggests that in MS, base excision repair may be further reduced. Altogether, this suggests that both genetic alterations in the base excision repair pathway and increased oxidative damage to DNA may play a role in the oligodendrocyte death observed in MS lesions.

There has not yet been specific investigations into changes base excision repair glycosylase enzymes following neurotrauma (Davis & Vemuganti 2021). However, other enzymes involved in base excision repair have been studied. APE1 expression is reduced in the ipsilateral cortex and hippocampus following a severe controlled cortical impact, inversely correlated with oxidative damage (Lewén et al. 2001). Similarly, following a cold injury-induced brain trauma, there is a

reduction in the expression of XRCC1 in the lesion area (Fujimura et al. 2000). Therefore, it may be that this reparative mechanism also falters following neurotrauma.

1.4.6.2. Single- and Double-Strand DNA Breaks and Repair

Free radicals have also been shown to cause more severe forms of DNA damage, such as single- and double-strand breaks. Sufficient DNA base or deoxyribose damage can result in a single-strand break (Woodbine et al. 2011). Peroxynitrite free radicals target DNA to cause single-strand breaks (Miljković & Spasojević 2013; Szabo & Ohshima 1997), which can result in localised denaturation and thereby increase the probability of a double-strand break (Sharma et al. 2016). Furthermore, if two single-strand breaks occur in nearby regions of the DNA strand, a double-strand break can occur (Woodbine et al. 2011). Hydroxyl radicals can also cause double-strand breaks (Sharma et al. 2016; Su et al. 2006).

Double-strand breaks are highly detrimental to cell survival, often initiating apoptosis or resulting in gene inactivation if left unrepaired (Barzilai & Yamamoto 2004). Cells do possess a reparative DNA damage response mechanism for double-strand breaks, and the pathway chosen to repair a particular section of DNA damage is crucial to maintaining genomic integrity (Panier & Boulton 2014). Following double-strand breaks, there are two main pathways for DNA repair, non-homologous end-joining and homologous recombination (Lieber 2010). The majority of double-strand breaks caused by exogenous factors, including ROS, are repaired *via* non-homologous end-joining (Delacôte & Lopez 2008). This is because these breaks usually occur outside of S phase of the cell cycle, or when there is no homology donor in close proximity, as required for homologous recombination (Lieber 2010). All DNA contains inactive DNA repair molecules, such as ataxia-telangiectasia mutated serine/threonine kinase (ATM). Once a double-strand break occurs, ATM is activated by phosphorylation (Bakkenist & Kastan 2003). Activated ATM phosphorylates a plethora of DNA damage response molecules, including the histone variant H2AX, which becomes γ H2AX (Savic et al. 2009). Phosphorylation of H2AX initiates ubiquitylation and SUMOylation pathways that recruit mediator proteins, including p53-binding protein 1 (53BP1) (Maréchal & Zou 2013). 53BP1 rapidly accumulates around the damage site and prevents resection of the double-strand break, preserving the double-strand break ends and promoting non-homologous end-joining over homologous recombination (Panier & Boulton 2014).

Using γ H2AX as a marker of DNA damage in human brains following mild TBI, it has been demonstrated that in some cases DNA damage is restricted to the ependymal lining of the ventricles, but in others it had spread to oligodendrocytes and astrocytes (Schwab et al. 2019). DNA damage repair genes are also predominantly downregulated following human mild TBI, suggesting inefficient DNA repair mechanisms (Schwab et al. 2019). Similar to nucleobase modifications, older rodents are also more susceptible to single-strand breaks following neurotrauma (Itoh et al. 2013). Furthermore,

polymorphisms in genes involved in the non-homologous end-joining damage response occur in people with MS, which means that repair of the more severe double-strand breaks may also be compromised in demyelinating disease (Briggs et al. 2010). However, the effects of reduced DNA strand break repair and/or increased DNA damage in either neurotrauma or MS, particularly to oligodendroglial cells, are relatively unknown.

1.4.6.3. Oligodendroglial Susceptibility to Oxidative DNA Damage

Work from a number of research teams, including the Fitzgerald laboratory, has revealed that both oligodendrocytes and OPCs are especially vulnerable to oxidative DNA damage, particularly in neurotrauma, but also potentially in MS (Husain and Juurlink, 1995; Thorburne and Juurlink, 1996; Juurlink, Thorburne and Hertz, 1998; Giacci et al., 2018b; Gopalasingam et al., 2019). One reason for this is the higher concentration of P2X₇ receptors and α -amino-3-hydroxy-5-methyl-4-isoxazolepropionic acid (AMPA) receptors on oligodendrocytes and OPCs compared to other neuroglia (Borges et al. 1994; Matute et al. 2007). Intracellular Ca²⁺ overload facilitated by these Ca²⁺-permeable receptor subtypes is a known cause of oxidative damage (Arundine & Tymianski 2003; Frantseva et al. 2002; Stirling & Stys 2010). Mature oligodendrocytes are also particularly vulnerable due to the continuous high energy consumption involved in maintaining the myelin sheath by catalysing the myelin lipids (Bernardo et al. 2009; Dewar et al. 2003). One prominent by-product of this process is ROS, which is not efficiently detoxified during periods of oxidative stress (Uberti et al. 1999), ultimately resulting in an increased intracellular accumulation of free radicals within oligodendrocytes (Bernardo et al. 2009). Furthermore, OPCs have higher intracellular iron than other neuroglia, which is associated with increased susceptibility to ROS, as iron is involved in many intracellular and mitochondrial oxidative pathways, including Fenton reactions and lipid peroxidation (Braugher et al. 1986; Halliwell & Gutteridge 1989; Thorburne & Juurlink 1996). OPCs also have lower levels of antioxidants such as manganese superoxide dismutase (MnSOD) and glutathione than other glial cells and neurons, which scavenge and detoxify ROS (Bernardo et al. 2009; Butts et al. 2008; Thorburne & Juurlink 1996). Mature oligodendrocytes have been shown to be more susceptible to oxidative DNA damage than microglia and astrocytes following 1 week of cuprizone toxicity (Luo et al. 2020). Within the Fitzgerald laboratory, we have demonstrated a heightened vulnerability of OPCs to oxidative DNA damage at 3 days following a partial optic nerve transection and after 3 weeks exposure to cuprizone (Giacci et al., 2018b; Gopalasingam et al., 2019). Therefore, this thesis will focus on 8OHdG DNA damage to OPCs specifically, given this heightened vulnerability.

1.5. Concluding Remarks

MS is a chronic inflammatory demyelinating disease that is increasingly acknowledged to be multifaceted and complex, with not only an autoimmune component driving disease processes, but

also primary oligodendrocyte death and innate phagocyte activation occurring even in the absence of peripheral immune cell infiltration. Current immunomodulatory treatments only slow disease progression rather than halt it completely, suggesting therapeutics that are more effective in targeting innate CNS damage are required to improve the quality of life for those living with MS. Neurotrauma is a neurological condition that shares similar mechanisms of damage with MS such as oxidative stress, and for which there are currently no effective treatments available. To facilitate rapid advancement of knowledge and potentially assist in the development of effective treatments for both of these disorders, it is important to deepen the understanding of mechanistic commonalities between MS and neurotrauma.

This thesis is therefore comprised of three primary aims:

Aim One: To demonstrate the generalisability of a combinatorial ion channel inhibitor treatment for ameliorating pathology in models of MS & neurotrauma

Aim Two: To establish the framework & commence initial experiments investigating shared mechanisms of oxidative damage to oligodendroglia in models of MS & neurotrauma

Aim Three: To determine whether oxidative DNA damage to perivascular OPCs and pericytes at the BBB is associated with increased BBB permeability in models of both MS and neurotrauma.

The thesis aims are addressed in the form of three overarching series. Series One presents work conducted utilising a combinatorial ion channel inhibitor treatment in models of MS and neurotrauma, comprising of one chapter. Series Two focusses on the initial work completed to investigate common mechanisms of oxidative damage between demyelinating disease and neurotrauma, comprising of two chapters. Meanwhile, Series Three concentrates more specifically on the research performed to assess the relationship between oxidative stress and BBB dysfunction in both demyelinating disease and neurotrauma, comprising of three chapters. The literature pertaining specifically to the BBB is reviewed in Chapter 5 to provide the necessary context for the remainder of the third series. The thesis closes with Chapter 8, which discusses the outcomes presented throughout this thesis within the context of the wider literature. This chapter also presents future targets for additional research to enhance the understanding of commonalities in damage mechanisms between the two neurological disorders and foster the development of future effective therapies for both MS and neurotrauma to ultimately improving the quality of life for those living with these conditions. An overview of the upcoming thesis structure is presented in Figure 1.12.

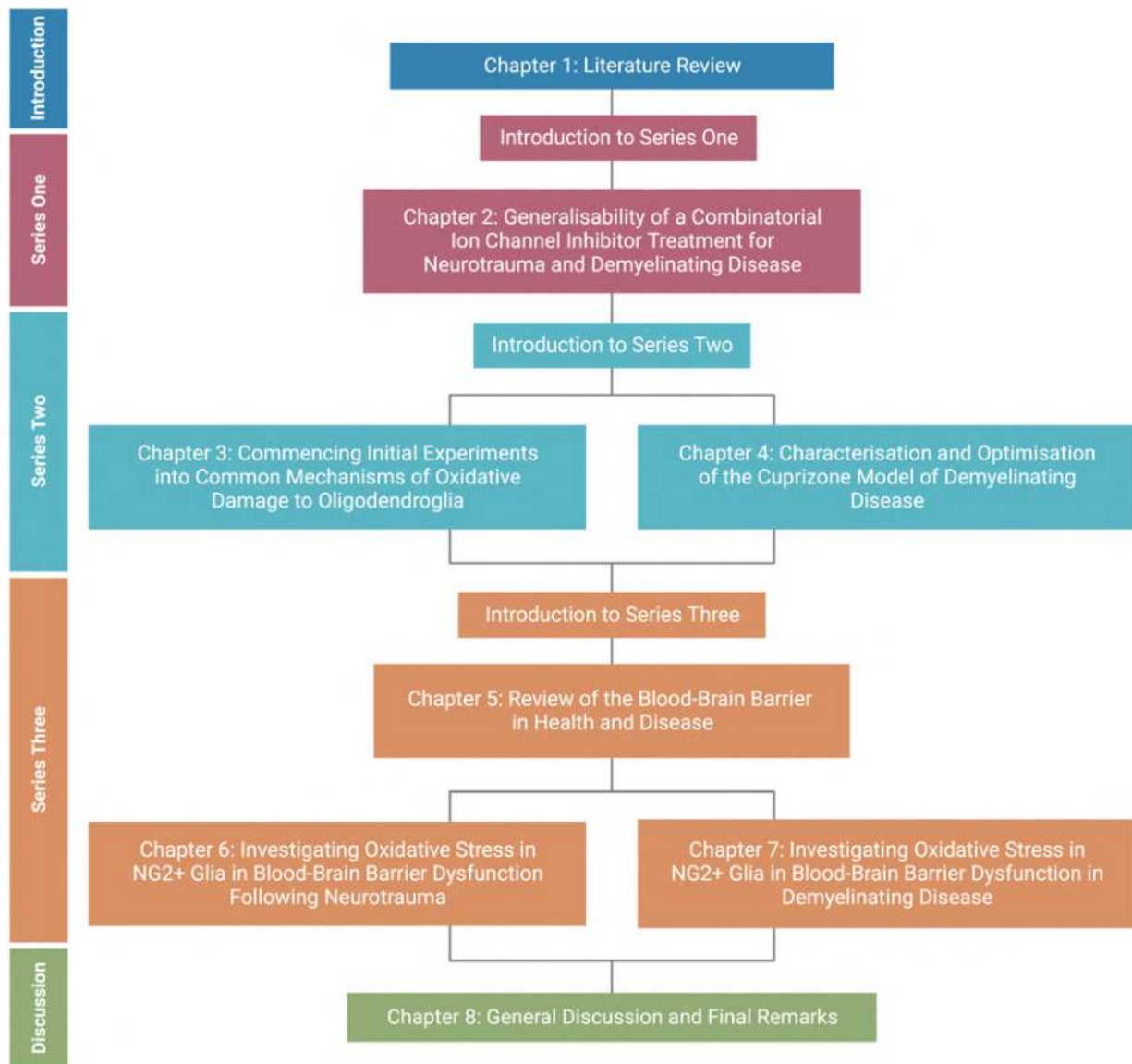


Figure 1.12. Flow diagram of the forthcoming thesis structure. The thesis chapters are presented in the form of three overarching series. Series One focuses on the generalisability of a combinatorial ion channel inhibitor treatment for neurotrauma and demyelinating disease, and comprises of Chapter 2. Series Two centres on establishing the methodological framework for investigating common mechanisms of damage between demyelinating disease and neurotrauma. Chapter 3 presents research completed to assess the effects of oxidative damage to the oligodendroglial lineage in demyelinating disease. However, due to the observed limited efficacy of the utilised cuprizone within this study, Chapter 4 then presents a published methodological article comparing the effects of powdered and pelleted cuprizone to optimise the model for future studies. Series Three concentrates more specifically on the role of oxidative stress in BBB dysfunction for both neurological conditions. Chapter 5 presents an additional short literature review on the BBB in health and disease to provide the necessary context for the remainder of this series. Chapter 6 and Chapter 7 focuses on research completed to date to investigate oxidative stress to perivascular NG2+ glia at the BBB in neurotrauma and demyelinating disease respectively. The thesis then concludes with Chapter 8, which discusses the entire collection of research outputs presented throughout and explores directions for additional future research.

Introduction to Series One

The first aim of this thesis focusses on the generalisability of a combinatorial ion channel inhibitor treatment for neurotrauma and demyelinating disease. This aim is addressed in Series One, comprising of Chapter 2, which describes research that utilised a combinatorial ion channel inhibitor treatment for neurotrauma and MS. This chapter encompasses research presented in two published papers that I contributed to during my candidature. Both studies utilised a combination of lomerizine, YM872 and BBG to limit excess Ca^{2+} influx into cells. The core data presented in this chapter is from a cohort of rats used in an experiment designed to assess whether the combinatorial ion channel inhibitor treatment was mediating an anti-inflammatory effect in the periphery, when systemically delivered following a partial optic nerve transection. This work built upon the results from an earlier experimental series conducted prior to candidature that compared the effects of local and systemic delivery of the combinatorial treatment on cellular changes following optic nerve injury. Significant improvements in myelin node/paranode structure with the ion channel inhibitor combination was observed post-injury in the earlier cohort but this was not accompanied by an effect of treatment on local inflammation. The further experiments conducted during candidature assessed whether peripheral inflammation was affected by either locally or systemically administered inhibitors. Blood cytokine and chemokine profiles were unchanged with either treatment modality, suggesting that the combinatorial therapy does not mediate its effect *via* modifying the immune response, but may instead directly act on the myelin sheath. Data from both cohorts were combined to form a single journal article that was published in *Scientific Reports*. However, only the work completed during candidature is described in detail within the chapter itself, with the full published version of the corresponding paper provided in Appendix A.

Similar outcomes were also observed in a parallel study that I contributed to during candidature, which was published in *Multiple Sclerosis and Related Disorders* (as presented in Appendix B). This work utilised systemic delivery of the ion channel inhibitor combination in the cuprizone model and resulted in preservation of myelin nodal structures with treatment, comparable to the outcomes observed in the previously described neurotrauma study. The demonstration of significant improvements in myelin outcomes in both studies suggests that similar Ca^{2+} -associated mechanisms mediate the nodal structure abnormalities in the two conditions. The efficacy of the ion channel inhibitor treatment for preserving myelin structure across models of both neurotrauma and demyelinating disease thus further established that common mechanisms do exist in the underlying pathology between the two conditions and that translating knowledge may expedite the development of therapeutics for both.

Chapter 2. Generalisability of a Combinatorial Ion Channel Inhibitor Treatment for Neurotrauma and Demyelinating Disease

2.1. Delivery of a Combinatorial Ion Channel Inhibitor Treatment

As discussed in Chapter 1, Ca^{2+} dyshomeostasis plays an important role in the pathophysiology of both neurotrauma and MS, making Ca^{2+} dynamics a significant therapeutic target for both disorders. Given Ca^{2+} can enter neuroglia *via* a myriad of channels and receptors, it is important to use a combinatorial treatment to target multiple routes for cellular Ca^{2+} entry. One such therapy that has been previously developed within the Fitzgerald laboratory is an ion channel inhibitor combination that targets VGCCs (Hara et al. 1999), AMPA receptors (Takahashi et al. 2002) and P2X_7 receptors (Jiang et al. 2000).

The first inhibitor of the combination is lomerizine, which is an orally administered treatment that blocks T-type and L-Type VGCCs (Hara et al. 1999). Lomerizine is a stable drug with few known side effects (Ren et al. 2014) that is primarily used clinically as an anti-migraine treatment. As lomerizine is highly lipid soluble and has a small molecular size, it is BBB permeable and is also highly selective for the CNS (Yamada et al. 1997). Studies using lomerizine have previously demonstrated neuroprotective effects in a variety of pathologies, including following a partial optic nerve transection (Fitzgerald et al. 2009; Karim et al. 2006; Selt et al. 2010; Yamada et al. 1997).

The combination also included YM872, which is a potent competitive AMPA receptor antagonist (Takahashi et al. 2002). Though YM872 is highly hydrophilic, it is presumed to cross the BBB given it demonstrates neuroprotective effects when administered systemically (Atsumi et al. 2003; Furukawa et al. 2003; Takahashi et al. 2002; Takahashi & Wei 1998). The effectiveness of YM872 is in part mediated by preventing initial Ca^{2+} -dependent cellular depolarisation, which indirectly inhibits VGCCs, N-methyl-D-aspartate (NMDA) receptor activation, and the reversal of the $\text{Na}^+/\text{Ca}^{2+}$ exchanger (Takahashi et al. 2002; Takahashi & Wei 1998; Wang et al. 2006).

Initial work assessing the efficacy of a combinatorial ion channel inhibitor treatment used oxATP to inhibit P2X_7 receptors. These previous studies utilised the partial optic nerve model of neurotrauma and found that when used in isolation, lomerizine, YM872 and oxATP had limited effects on secondary degeneration at a 3 month timepoint (Savigni et al. 2013). Conversely, when all three ion channel inhibitors were used in combination, the biggest therapeutic effect was observed, with myelin pathology, oxidative stress and behavioural disturbances significantly ameliorated (Savigni et al. 2013). Beneficial effects have also been observed at an acute 3 day timepoint, with the combinatorial treatment of lomerizine, YM872 and oxATP demonstrating significant improvements in myelin structure, oxidative stress, axonal integrity and density of OPCs (O'Hare Doig et al. 2017).

These early studies utilising the ion channel inhibitor combination delivered the treatment locally, *via* subcutaneously implanted osmotic mini-pumps, primarily due to the inability of oxATP to cross the BBB (O'Hare Doig et al. 2017; Savigni et al. 2013). However, invasive local administration of therapeutics is clinically limited, as it requires multiple costly surgeries for both implantation and extraction of the drug delivery device, which in turn increases risk of additional damage and/or infection (Dash & Cudworth 1998). Moreover, these drug delivery devices can only remain implanted for short periods, which may not align with optimal treatment durations (Dash & Cudworth 1998). For the preclinical evaluations of the combinatorial ion channel inhibitor treatment, the locally delivered YM872 and oxATP were only able to be administered for up to 2 weeks *via* the implanted osmotic mini-pumps, whilst the orally administered lomerizine was delivered for up to 3 months (Savigni et al. 2013).

Though systemic delivery routes are more clinically applicable for administering therapeutics, systemically delivered drugs need to be capable of crossing the BBB in order to treat CNS injuries. There are many methods through which the bioavailability of a treatment into the brain can be improved, such as by utilising nanoparticles or peptidomimetics (Kasinathan et al. 2015). However, the easiest method to achieve a combinatorial treatment designed for systemic delivery was to simply substitute oxATP with the BBB-permeable alternative BBG.

BBG is an analogue of FD&C blue dye No. 1 that was FDA approved for use in humans in 2019 (Borzelleca et al. 1990; FDA 2019; Wong et al. 2011). As well as being a non-competitive, reversible and selective P2X₇ inhibitor, BBG is also BBB permeable making it highly suitable for systemic delivery (Jiang et al. 2000; Wong et al. 2011). BBG has previously induced therapeutic effects in a multitude of neuropathologies (Kimbler et al. 2012; Peng et al. 2009; Ridderstrom & Ohlsson 2014; Wang et al. 2015). Indeed, we have previously demonstrated that the BBB-permeable combination of lomerizine, YM872 and BBG was at least as effective at preventing secondary degeneration after a partial optic nerve transection as the original combination that incorporated oxATP (Toomey et al. 2018). However, both treatments were delivered locally to ensure an accurate comparison of efficacy. During my candidature, I have been contributed to two separate studies that successfully utilised this combinatorial treatment of ion channel inhibitors when systemically delivered in both the partial optic nerve transection model of neurotrauma (Toomey et al. 2019; Appendix A) and in the cuprizone model of demyelinating disease (Gopalasingam et al. 2019; Appendix B).

2.2. Comparing Local and Systemic Delivery of a Combinatorial Ion Channel Inhibitor Treatment for Limiting Peripheral Cytokines and Chemokines Following Neurotrauma

2.2.1. Data Obtained Prior to Candidature

Prior to commencing this doctoral degree, I had already completed research delivering the ion channel inhibitor combination systemically in the partial optic nerve transection model. This work found that the combinatorial treatment was just as effective at significantly preserving myelin structure following systemic delivery as when delivered locally at the injury site (Toomey et al. 2019). Though there was a small significant effect of injury on local inflammation, there was no effect of treatment on local inflammatory cell densities, regardless of the delivery route employed. There was also no effect of either injury or treatment on the density of oligodendroglial cells.

This research was completed as part of my Honours degree but was later combined with the forthcoming work that was completed during my candidature to form a journal article published in *Scientific Reports*. The work undertaken during my doctoral degree comprised of an additional cohort of forty-eight rats to extend the assessment of the inflammatory response to include peripheral cytokine responses. Given the peripheral nature of systemic delivery, we had hypothesised that the systemically delivered ion channel inhibitor combinations may have mediated a therapeutic anti-inflammatory effect prior to reaching the injury site, whilst still in the circulatory system. Since a portion of the work presented within this paper has already been submitted for a prior qualification, only the work completed during candidature has been described in detail below, with the full published version of the corresponding paper available in Appendix A.

2.2.2. Rationale for Luminex Analysis

Cytokines and chemokines are integral components of both intercellular and intracellular inflammatory signalling pathways (Giavedoni 2005). These proteins regulate the immune response by recruiting inflammatory cells to sites of injury and infection, and by triggering numerous cellular activities, such as phagocytosis, cell adhesion and apoptosis (Ramesh et al. 2013). Given this important role of cytokine and chemokine signalling in inflammation, I examined the effect of the ion channel inhibitor combination on the expression of these proteins in the circulatory system to indicate the peripheral immune response.

Blood cytokine expression profiling using Luminex technology is a well-established method for analysing the peripheral inflammatory response across many disease and injury states (Bruce et al. 2019; Djoba Siawaya et al. 2008; Lu et al. 2017; Mukhamedshina et al. 2017; Patten et al. 2022; Vuolo et al. 2015). The Luminex system is a bench-top flow cytometer that discriminates up to one hundred different antigens simultaneously based on coupled beads (Giavedoni 2005). Each bead is

dyed with a specific ratio of red (658nm) and infrared (712nm) fluorophores to create a unique detectable spectral signature and is designed to covalently bond to an analyte of interest *via* capture antibodies (DuPont et al. 2005). An additional biotin-based detection antibody is also used in combination with streptavidin-phycoerythrin to quantify the amount of analyte bound to each bead (Giavedoni 2005). The multiplexing abilities of a Luminex analysis significantly enhances the quantification capacity of the assay when compared to alternative analysis methods, such as enzyme-linked immunosorbent assays (ELISA) and complement-dependent cytotoxicity assays, whilst still maintaining a high degree of sensitivity (DuPont et al. 2005; Katalinic et al. 2017; Vignali 2000). Luminex assays require as little as 25µL of sample per well (Djoba Siawaya et al. 2008), which significantly expands the screening output capacity to allow researchers to perform several multiplex assays on relatively small sample volumes. Therefore, the Luminex assay was considered to be most appropriate to determine the peripheral expression of various cytokine and chemokine proteins within extracted plasma samples.

2.2.3. Study Design and Procedures

2.2.3.1. Experimental Groups and Treatment Delivery Strategy

Adult, female PVG rats were obtained from the Animal Resource Centre (Murdoch, Western Australia) and housed with *ad libitum* access to water and food under a 12-hour light/dark cycle. All experimental procedures were approved by the University of Western Australia Animal Ethics Committee (RA3/100/1485) and were performed in accordance with the NHMRC of Australia Code of Practice for Use of Animals for Scientific Purposes.

There were six experimental groups (Figure 2.1) comprised of: a normal group (n = 8); an injured, systemically delivered vehicle group (n = 8); an injured, systemically delivered ion channel inhibitor combination treatment group (n = 8); an injured, locally delivered vehicle group (n = 8); an injured, ion channel inhibitor combination treated group (n = 8) and a sham injured, locally delivered vehicle group (n = 8). The normal group acted as the uninjured control for the systemic delivery groups whilst the sham group acted as the uninjured control for the local delivery groups. All experimental groups received either vehicle treatment or ion channel inhibitor treatment, except for the normal group, which did not receive any treatment. Treatment was delivered for 3 days post-surgery before immediate tissue collection.

		Treatment					
		No Treatment	Systemic Delivery		Local Delivery		
			Vehicle	Treated	Vehicle	Treated	
Injury	No Injury	Normal (n = 8)			Sham (n = 8)		
	Injured		Systemic Vehicle (n = 8)	Systemic Treated (n = 8)	Local Vehicle (n = 8)	Local Treated (n = 8)	

Figure 2.1. Experimental groups for the additional combinatorial ion channel inhibitor treatment cohort.

Lomerizine (30mg/kg, LKT Labs) was orally administered mixed into a soft butter vehicle twice a day, with an 8 hours interval. Lomerizine feeding commenced approximately 5 hours after the partial optic nerve transection, when animals had recovered from the anaesthetic, and continued twice daily until the end of experiment. The corresponding vehicle treatment was an equivalent volume of soft butter administered as a control oral treatment.

For local delivery of the ion channel inhibitors, BBG (540µM, Sigma-Aldrich) and YM872 (240µM, LKT Laboratories) were dissolved in phosphate buffered solution (PBS) and delivered *via* surgically implanted osmotic mini-pumps at a rate of 0.5µL/hour for the duration of the experimental period. These concentrations were consistent with previous studies where efficacy had been demonstrated (Savigni et al. 2013; Toomey et al. 2018). Both the sham uninjured and the injured, locally delivered vehicle control groups received PBS vehicle *via* the implanted osmotic mini-pump.

For systemic delivery, BBG (45 mg/kg, Sigma-Aldrich) and YM872 (20 mg/kg, LKT Laboratories) were again dissolved in PBS but were instead administered *via* two 1mL intraperitoneal injections. One injection occurred 2 hours post-surgery, with the other injection given in the afternoon 2 days later, a day prior to end of experiment. A delay of 2 hours following injury for systemic injections was chosen as this is when treatment is indicated to be most successful following rodent TBI, whilst still being clinically relevant for the predicted time delay in humans (Koob et al. 2008). The doses of both systemically administered BBG and YM872 were chosen based on previous studies (Cervetto et al. 2013; Diaz-Hernandez et al. 2012; Takahashi et al. 2002; Toomey et al. 2018). The injured, vehicle treated control group received an equal volume of PBS *via* intraperitoneal injection. The treatment strategies for the three ion channel inhibitors is summarised below (Figure 2.2).

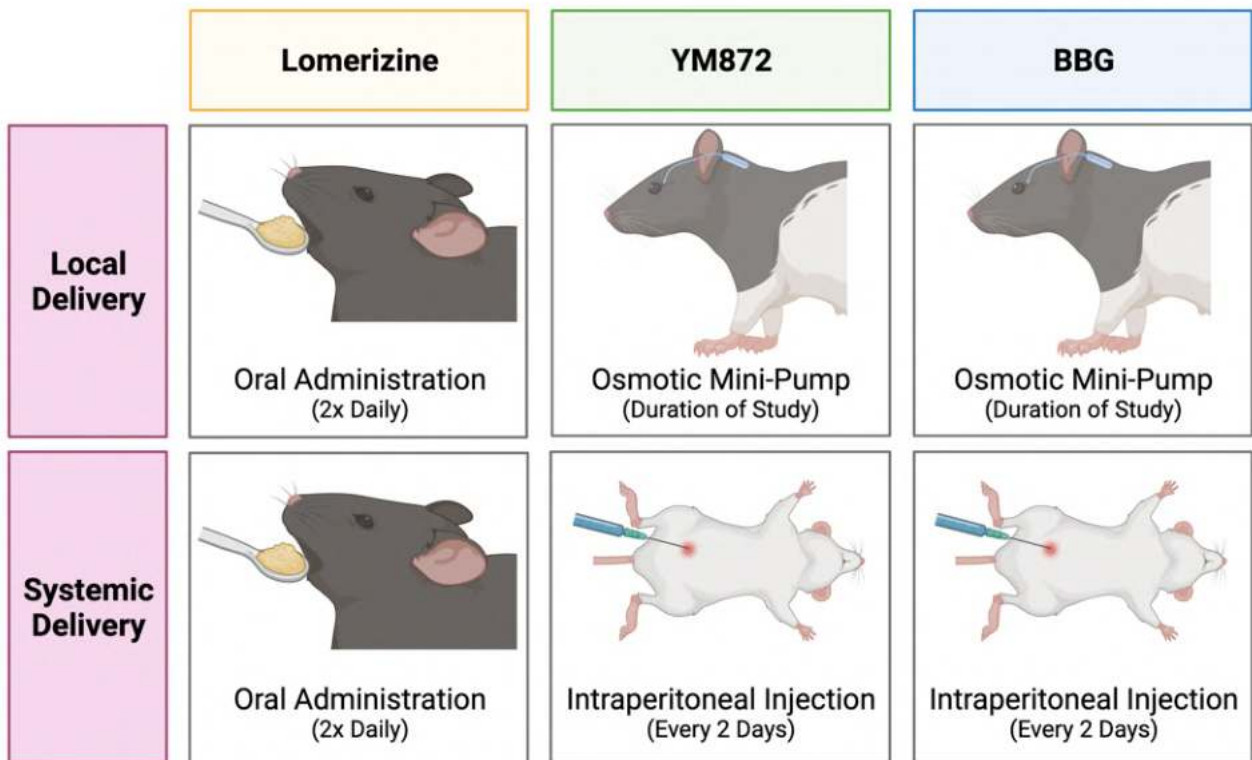


Figure 2.2. Ion channel inhibitor treatment strategy. Lomerizine was orally delivered twice a day regardless of overall drug delivery method. For local delivery, YM872 and BBG were delivered by implanted osmotic mini-pumps for the duration of the study. For systemic delivery, YM872 and BBG were administered *via* an intraperitoneal injection twice during the study. One injection was delivered 2 hours post-surgery and the second dose was delivered 2 days later, a day prior to the end of the experiment. Original illustration created using BioRender.com.

2.2.3.2. Priming Osmotic Mini-Pumps

The Alzet osmotic mini-pumps were primed a day prior to surgical implantation to commence their start-up gradient to ensure a sufficient rate flow following insertion. The polyvinylchloride catheter tubing (5.9mm diameter, Alzet) was cut into 5cm lengths and superglued to the flow moderator tip. Once the catheters were attached, the flow moderators were sterilised with 70% ethanol solution in a petri dish. Sequential ethanol and PBS were flushed through the catheter. The catheter was then filled with either the ion channel inhibitor solution or PBS vehicle. The mini-pumps were also filled with 200 μ L of either the ion channel inhibitor solution or vehicle PBS using the supplied filling tubes. The flow moderators were then inserted into the pumps and the pumps placed upright into a saline bath and incubated at 37°C overnight.

2.2.3.3. Surgical Procedures

Prior to any procedures, the surgical sites were shaved and then triple swabbed with 10% w/v povidone-iodine (Betadine) solution and 70% ethanol. Partial optic nerve transections were then performed by Mrs Carole Bartlett as described in Bartlett & Fitzgerald (2018), under Ketamine (Ketamil, 50 mg/kg, Troy Laboratories) and Xylazine (Ilium Xylazil, 10 mg/kg, Troy Laboratories)

anaesthesia that was delivered *via* intraperitoneal injection. In brief, the skin covering the skull behind the right eye was cut and retracted forwards to give surgical access to the orbit. About 1mm behind the right eye, the parenchyma of the optic nerve was exposed by making a longitudinal incision in the sheath with fine iridectomy scissors. The dorsal aspect of the nerve was then lesioned to a depth of approximately 200µm using a diamond radial keratotomy knife (Geuder). The lachrymal glands were carefully placed back and the skin sutured closed, before the animals were taken for postoperative care. Throughout the surgery, caution was taken to ensure that the optic nerve was not stretched and the major ophthalmic blood vessels were not injured. Immediately post-surgery, rats were administered analgesia (2.8 mg/kg carprofen, Norbrook) and 1mL sterile PBS *via* subcutaneous injections. Sham injury included all surgical procedures aside from the cut in the sheath and the partial optic nerve transection.

Implantation of the osmotic mini-pumps was performed as previously described (Savigni et al. 2013). To create a small cavity in which to house the pump capsule, the connective tissue between the head and the right shoulder was separated prior to the partial optic nerve transection. The pump body was positioned within the created pocket and the connective tissue on to the temporal ridge of the skull was scraped away to expose the bone. The pump capsule was then secured with cyanoacrylate superglue. A slight incision was subsequently made in the connective tissue on the bony margin of the eye socket and partially into the lateral muscle. Directly following injury, the tubing of the pump was trimmed and arranged so that the fluid dispersing catheter directly targeted the injury site, before being secured on the lateral bone surface using cyanoacrylate glue. An initial quantity of 1µL of either the treatment or vehicle solution was directly applied to the injured nerve, before proceeding with the remainder of the surgery.

2.2.3.4. Collection of Blood Samples

At 3 days post-injury, the rats were euthanised with pentobarbitone sodium (160 mg/kg, Delvet). Immediately following euthanasia, blood samples were acquired *via* aortic cardiac puncture using a heparinised syringe. The blood was dispensed into heparinised tubes and spun at 3000rpm at 4°C for 10 minutes in a centrifuge. Plasma and serum were then separated and both were stored at -80°C ready for subsequent Luminex analysis. The entire experimental design for this cohort is summarised in Figure 2.3.

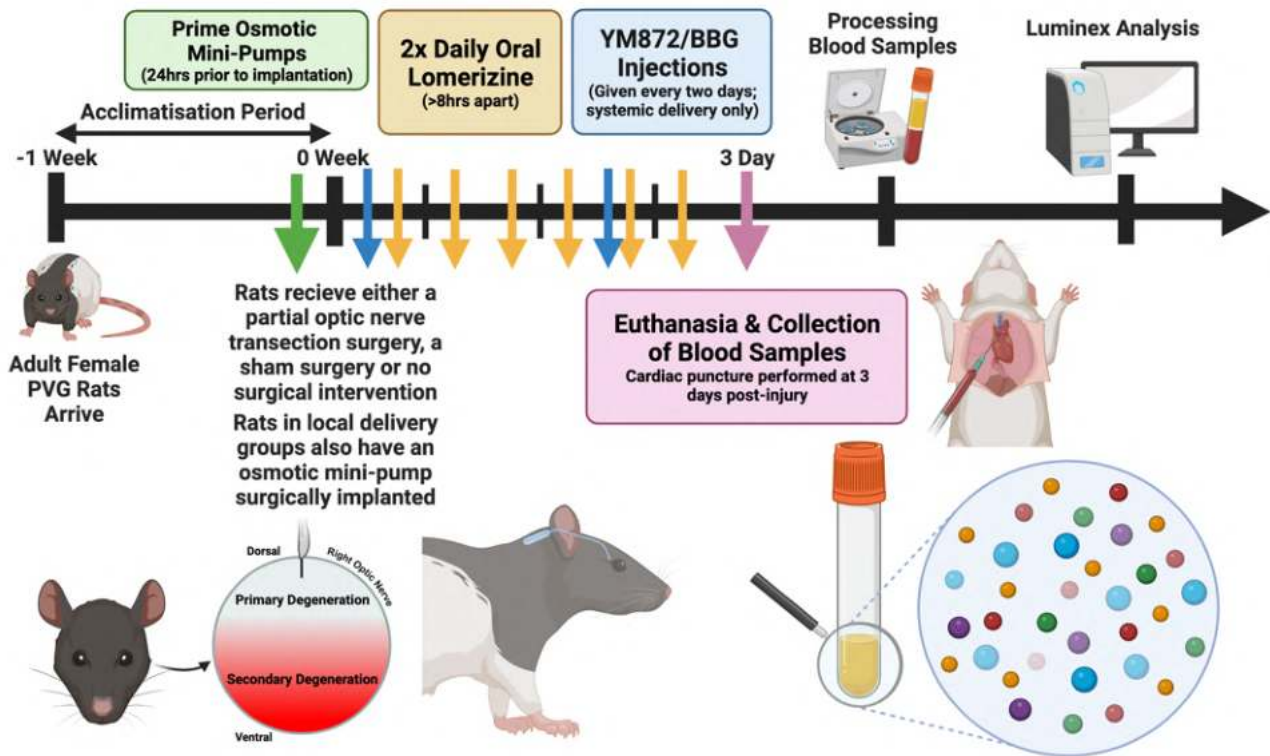


Figure 2.3. Experimental design for the additional combinatorial ion channel inhibitor treatment cohort. Adult female PVG rats ($n = 8/\text{group}$, total $n = 48$) underwent either a partial optic nerve surgery, a sham surgery or no surgical intervention. Rats being administered local treatments were surgically implanted with an osmotic mini-pump. Following 3 days of either local or systemic ion channel inhibitor or vehicle treatment, the rats were euthanised and blood samples collected *via* cardiac puncture for subsequent Luminex analysis. Original illustration created using BioRender.com.

2.2.3.5. Luminex Assay

The concentration of 22 cytokine and chemokines (IL-1 α , IL-1 β , IL-2, IL-4, IL-5, IL-6, IL-10, IL-12p70, IL-13, IL-17A, G-CSF (granulocyte-colony stimulating factor), GM-CSF (granulocyte-macrophage colony-stimulating factor), TNF α (tumour necrosis factor α), IFN γ (interferon gamma), IP-10 (interferon gamma-induced protein 10), Gro- α (growth-regulated oncogene α), MCP (monocyte chemoattractant protein) -1, MCP-3, MIP (macrophage inflammatory protein) -1 α , MIP-2, RANTES (regulated on activation normal T-cell expressed and secreted), and Eotaxin) were assessed in the collected plasma samples using a Cytokine and Chemokine 22-Plex Rat ProcartaPlexTM Panel (Invitrogen; Figure 2.4). Due to the space limitations of the 96-well plate, samples of $n = 6/\text{group}$ were selected using random sampling from the overall cohort of $n = 8/\text{group}$ and analysed in duplicate, together with duplicates of the supplied seven antigen standards and two blank wells. The plate was read on a Bio-Plex 200 system and the corresponding Bio-Plex Manager software automatically plotted the standard curve for each analyte using either a 4- or 5-parameter logistic model as appropriate. The cytokine and chemokine concentrations in each sample were then calculated based on the generated standard curves.



Figure 2.4. Luminex assay protocol for use on rat plasma samples. This protocol was conducted in line with manufacturer’s instructions and was completed over 2 consecutive days to allow for overnight incubation with samples and standards to increase sensitivity. The plate was analysed on the Luminex machine immediately following the application of streptavidin-phycoerythrin (SAPE) and the subsequent washes. Original illustration created using BioRender.com.

2.2.4. Effect of the Combinatorial Treatment on Plasma Cytokine and Chemokine Concentrations

Fifteen of the analytes (IL-1 α , IL-1 β , IL-2, IL-4, IL-5, IL-6, IL-10, IL-12p70, IL-13, IL-17A, G-CSF, CM-CSF, TNF α , IFN γ , MIP-2) were below the detection limit of the Luminex assay and were therefore excluded from the data analysis; data not shown. There were no significant differences between groups for the plasma concentrations of Eotaxin ($F = 1.478$, $df = 5$, Figure 2.5A), Gro- α ($F = 0.917$, $df = 5$, Figure 2.5B), IP-10 ($F = 1.023$, $df = 5$, Figure 2.5C), MCP-1 ($F = 0.507$, $df = 5$, Figure 2.5D), MIP-1 α ($F = 0.722$, $df = 5$, Figure 2.5F), or RANTES ($F = 1.089$, $df = 5$, Figure 2.5G).

Of the analytes above the detection limit, significant differences between groups were found for the analyte MCP-3 ($F = 8.084$, $df = 5$, Figure 2.5E). There was no effect of injury on MCP-3 concentration compared to the uninjured controls (systemic $p = 0.999$, local $p = 0.467$), and neither mode of delivery of the ion channel inhibitor combination altered MCP-3 concentration relative to their respective vehicle treated injured controls (systemic $p = 1.000$, local $p = 0.846$). However, the systemically delivered ion channel inhibitor combination did cause a significant decrease in MCP-3 concentration compared to local delivery ($p = 0.005$). Though there was no difference between groups for the two injured vehicle treated groups ($p = 0.151$), there was an observed significant difference in MCP-3 concentration between the two uninjured control groups ($p = 0.005$). This observed increase in MCP-3 concentration for both the sham uninjured group and locally delivered ion channel inhibitor group compared to their respective systemic delivery counterparts therefore likely reflects inflammation resulting from the implantation of the osmotic mini-pump.

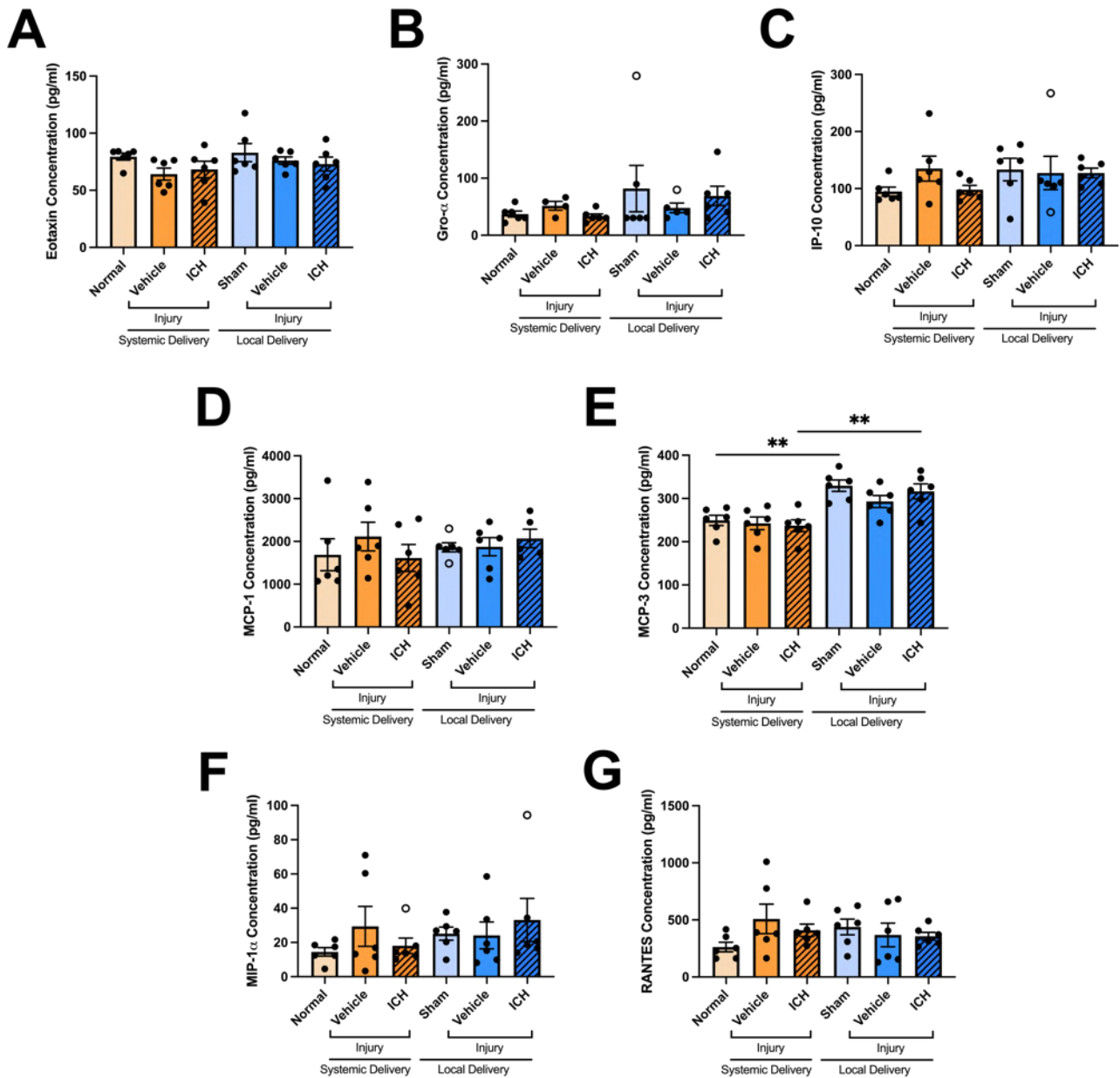


Figure 2.5. Effect of injury and combinatorial ion channel inhibitor treatment on the plasma concentration of cytokine and chemokine analytes. Concentration of Eotaxin (A), Gro- α (B), IP-10 (C), MCP-1 (D), MCP-3 (E), MIP-1 α (F), and RANTES (G) in the plasma of uninjured normal; sham injured, local vehicle treated animals; injured, systemic and local vehicle treated animals; and systemic and local ion channel inhibitor treated animals 3 days after partial optic nerve transection. Graphs display individual data points, overlaid on a bar displaying the mean \pm SEM. $n = 5-6$ rats per group. Outlier values as determined by the Tukey Outlier Detection Model were not excluded from analyses but are indicated by hollow data points on the graph. Abbreviations: ICH, ion channel inhibitor combinatorial treatment. Significant differences are indicated by $**p \leq 0.01$. Data values are as presented in Toomey et al. 2019, Appendix A.

2.2.5. Study Conclusions

The absence of an effect of treatment on peripheral inflammation, combined with the observed lack of an effect on local inflammatory cell densities in the previous cohort, suggests that the ion channel inhibitor combination does not act by attenuating either the local or peripheral immune

response post-injury. Instead it may be that the observed improvements in myelin outcomes within the study were due to the ion channel inhibitor combination acting on the myelin sheath directly. Additionally, the lack of a discernible increase in the peripheral immune in response to the partial optic nerve transection itself highlights the physically small nature of the injury compared to the size of the nerve and CNS of the animal, with the expression of inflammatory molecules typically highly dependent on the size and severity of injury (Patterson & Holahan 2012). However, it may also be that the window of opportunity to detect many of the cytokine and chemokine analytes had passed by the three day timepoint. Had peripheral inflammation been assessed closer to the time of injury, it is possible that significant changes in these molecules may have been detected. The heightened peripheral inflammation associated with the implantation of local delivery devices, even compared to the injury itself, further reinforces the necessity for systemic delivery of therapeutics bound for clinical translation. This research demonstrates the efficacy of the ion channel inhibitor treatment when delivered systemically. Therefore, this clinically relevant and BBB permeable combinatorial pharmacotherapy may be suitable for treating milder forms of neurotrauma, such as concussion, where the full extent and duration of BBB dysfunction is still unclear (Romeu-Mejia et al. 2019).

2.3. Utilising the Combinatorial Ion Channel Inhibitor Treatment in Demyelinating Disease

In a parallel study, mice were systemically treated with the ion channel inhibitor combination alongside 3 weeks of pelleted cuprizone administration to induce early demyelination. Given the close alignment of the study with my field of candidature and my interest in the work, I contributed to the dissemination of the outcomes by interpreting data, writing the manuscript, creating figures and performing final editorial changes. The study demonstrated that the ion channel inhibitor treatment reduced several aspects of cuprizone induced pathology (Gopalasingam et al. 2019; Appendix B). Most notably though, there was a similar preservation of myelin nodal structures as in the neurotrauma study described above in Section **Error! Reference source not found.**, which suggests that the structural abnormalities seen in the myelin node/paranode complex for the two conditions are underpinned by similar Ca^{2+} -related mechanisms (Figure 2.6).

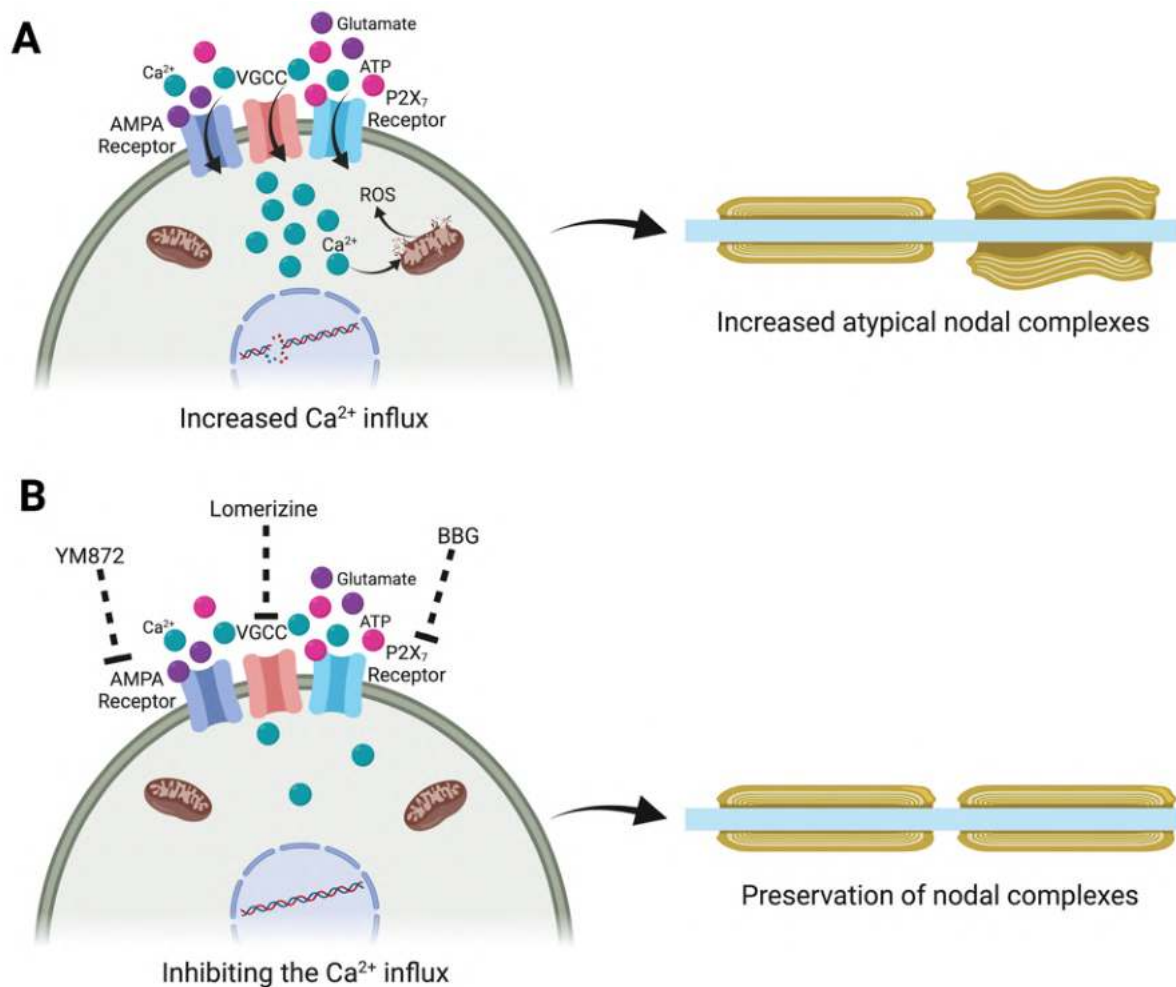


Figure 2.6. Effect of combinatorial ion channel inhibitor treatment on myelin outcomes. (A) Both MS and neurotrauma are associated with increased Ca²⁺ influx into cells and increased atypical myelin nodal complexes. (B) The systemically administered combinatorial ion channel inhibitor treatment comprised of YM872, lomerizine and BBG targeted AMPA receptors, VGCCs and P2X₇ receptors respectively to limit excessive Ca²⁺ influx. The treatment preserved the structure of myelin nodal complexes in models of both neurotrauma and demyelinating disease, indicating that disruption to nodal structure is mediated by similar Ca²⁺-dependent mechanisms in the two disorders. Original illustration created using BioRender.com.

2.4. Concluding Remarks

The observed generalisability of the ion channel inhibitor treatment for preserving myelin structure in models of both neurotrauma and demyelinating disease supports the notion presented throughout this thesis that common mechanisms exist in the underlying pathology between the two neurological conditions. By unifying our understanding of the two disease states, it may allow us to translate the knowledge obtained regarding either disorder and apply it to the other. This approach would facilitate the rapid advancement of knowledge to aid the development of effective therapeutic strategies for both of these disorders, such as with the combinatorial ion channel inhibitor treatment. Thus, this early work established the initial framework and provided justification to commence further experiments to investigate shared mechanisms of damage between neurotrauma and MS.

Introduction to Series Two

This second series of chapters (Chapters 3 and 4) aimed to establish the framework & commence experiments investigating shared mechanisms of oxidative damage to oligodendroglia in models of MS & neurotrauma. Chapter 3 presents the initial work performed to assess the role of oxidative DNA damage on cell cycling and the myelination capacity of oligodendroglia in the context of demyelinating disease. However, during the early stages of analysis for the behavioural, phenotypical and histological outcomes within this cohort, it became apparent that the cuprizone pellets that has been utilised had not effectively induced demyelinating disease. It is critical that mice are consistently given a 0.2% dose of cuprizone within their feed to generate reproducible and reliable demyelination. It was believed that during the manufacturing and pelleting process, the cuprizone was becoming deactivated. Limited literature suggested powdered cuprizone may be more effective at inducing demyelinating disease than a pelleted formulation (Hochstrasser et al. 2017). Therefore, given the efficacy issues of the cuprizone pellets, it was decided that a direct comparison between cuprizone feed formulations was required to ensure optimal cuprizone delivery.

Chapter 4 presents a comparative study which was performed to assess the efficacy of both powdered and pelleted cuprizone formulations at an early 3 week timepoint, using an alternative supplier of cuprizone pellets. This work found that cuprizone pellets were more effective than cuprizone powder at inducing demyelinating disease pathology across numerous outcomes including gliosis, neuroinflammation, oxidative stress, oligodendrocyte density and demyelination, particularly within the caudal corpus callosum. These findings were published in *Scientific Reports*. This work suggested that the pellets that were utilised for the initial cuprizone cohort were manufactured incorrectly, and so we were therefore confident in utilising pelleted cuprizone from a new supplier for future studies to induce demyelinating pathology. However, given the time constraints of the degree, the continuation of my contribution to the larger scale collaborative study presented in Chapter 3 was no longer able to form a sizeable part of this thesis. Nevertheless, the additional contributions I made to further the progression of this research is briefly detailed at the conclusion of the chapter.

Chapter 3. Commencing Initial Experiments into Common Mechanisms of Oxidative Damage to Oligodendroglia

This chapter describes an initial cohort of mice that was completed to assess the role of oxidative damage to oligodendroglia in demyelinating disease. Though the pelleted cuprizone used did not effectively induce demyelinating disease, this chapter provides the necessary context for the research presented in the remainder of Series Two.

3.1. Initial Cohort Rationale

In the original research plan for this thesis, the second aim was to investigate the effects of oxidative damage to the DNA of oligodendrocytes and OPCs in demyelinating disease within the cuprizone model. This aim was primarily based on two core studies that had utilised models of neurotrauma and Alzheimer's disease to analyse the effects of oxidative DNA damage to oligodendroglia (Giacci et al. 2018b, Tse et al. 2018). Taken together, this research suggested that DNA damaged pre-existing oligodendrocytes were aberrantly re-entering the cell cycle and undergoing cell apoptosis resulting in demyelination, whilst the reparative mechanism of OPCs to differentiate and produce myelin was itself compromised which may in turn impair remyelination (Figure 3.1). Therefore, as part of a larger collaborative study that also encompassed neurotrauma and Alzheimer's disease, we aimed to determine whether oxidative damage to oligodendroglia had comparable effects in a model of demyelinating disease. Using similar methods to our previous study that had employed cuprizone to model demyelinating disease (Gopalasingam et al. 2019; Chapter 2, Appendix B), a large scale cohort study was performed by delivering 0.2% cuprizone to mice in the form of pre-made pellets from the supplier Envigo for varying durations of time to simulate early demyelinating mechanisms. The outcomes of this cohort were to be compared to neurotrauma and Alzheimer's disease as part of the larger collaborative study to unify our understanding of oxidative oligodendroglial damage across disease states.

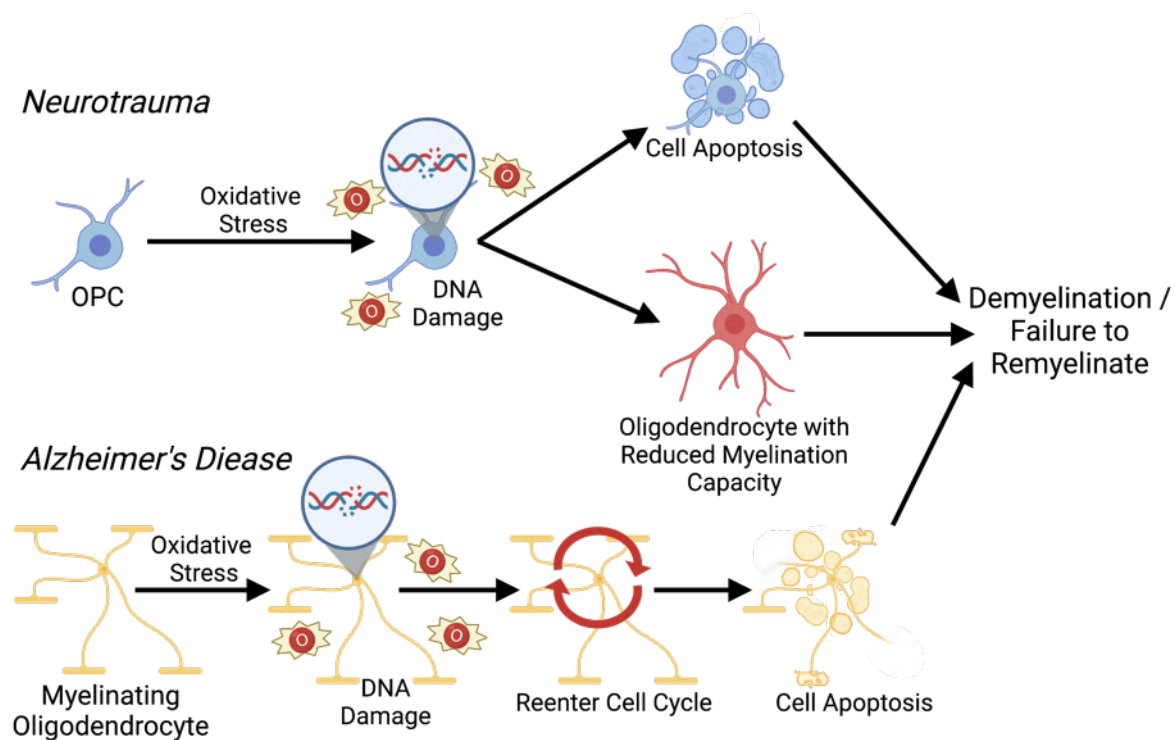


Figure 3.1. The effect of oxidative DNA damage to oligodendroglia in models of neurotrauma and Alzheimer's disease. When OPCs become oxidatively DNA damaged with 8OHdG nucleobase modifications following neurotrauma, some OPCs became immediately apoptotic following injury, whilst others differentiate into mature oligodendrocytes that have a reduced myelination capacity. Furthermore, these newly derived DNA damaged oligodendrocytes are less likely to undergo cell apoptosis than pre-existing DNA damaged oligodendrocytes. When pre-existing post-mitotic myelinating oligodendrocytes are DNA damaged with double-strand breaks in a mouse model of Alzheimer's disease, cell apoptosis is preceded by aberrant re-entry into the cell cycle. This dual mechanism of oxidative DNA damage to both OPCs and mature myelinating oligodendrocytes may be a contributing factor for both promoting demyelination and inhibiting remyelination. Based on Giacci et al. 2018b and Tse et al. 2018. Original illustration created using BioRender.com.

3.2. Initial Cuprizone Cohort

3.2.1. Study Design and Animal Procedures

An experimental cohort of ninety-six 8 week old male C57Bl/6J mice was obtained from the Animal Resource Centre (Murdoch, Western Australia). Male mice were specifically chosen for this study to facilitate direct comparisons with the existing MS literature. A vast majority of cuprizone studies utilise male mice, with one review finding that 84% of cuprizone papers use male C57Bl/6J mice (Sen et al. 2019). Female C57Bl/6J mice also trend towards less severe demyelination compared to male mice at the early 3 week timepoint of cuprizone administration, with no sex-differences present by 5 weeks (Taylor et al. 2010). Since this study was particularly interested in early mechanisms of oxidative damage, any delay in the onset of demyelination could preclude observable pathology and thus male mice were a more appropriate choice. The mice were housed under a 12 hour light/dark cycle and had *ad libitum* access to both food and water. All interventions and assessments were performed during the light phase of their 12 hour light/dark cycle. Procedures were

in accordance with the principles of the NHMRC and approved by the Animal Ethics Committee of The University of Western Australia (RA/3/100/1613) and the Animal Ethics Committee of Curtin University (ARE2019-4). Mice were given a 1 week acclimatisation period to the experimental holding location prior to commencement of the study. There were eight cuprizone administered and age-matched control groups at four different timepoints (n = 12/group), including mice that received cuprizone for 1, 2 or 3 weeks, and another group that received cuprizone for the full 3 weeks prior to withdrawing the cuprizone for a further week to allow for initial remyelination (a 3+1 week timepoint). Since we had previously successfully induced demyelination using pre-made 0.2% cuprizone pellets from the supplier Envigo (Gopalasingam et al. 2019; Appendix B), the same method was employed here. These pellets were made using the Envigo Teklad Global 18% Protein Rodent Diet as a base diet and then adding 0.2% cuprizone to form cuprizone-containing pellets. Mice were housed three per cage and pelleted feed was changed every two-three days, as per standard protocols (Steelman et al. 2012). Mice were also weighed daily throughout the experimental period to ensure there was no excessive weight loss due to cuprizone intoxication. Animal weights will be discussed in more detail in Section 3.2.2. To label cells actively undergoing the cell cycle, 5'Ethynyl-2-deoxyuridine (EdU, 20mg/kg, Invitrogen) was administered *via* intraperitoneal injection twice a day for 3 days prior to euthanasia, with a minimum of an 8 hour interval between injections. A day prior to euthanasia, mice underwent three behavioural assessments; the Rotarod test, the open field test, and the optokinetic nystagmus test (see Section 3.2.3). At the end of the experimental period, mice were euthanised with pentobarbitone sodium (160mg/kg, Delvet) and perfused transcardially with 0.9% saline followed by 4% paraformaldehyde (Sigma-Aldrich). Brains were dissected and immersed in 4% paraformaldehyde overnight. They were then transferred into 15% sucrose (Chem Supply), 0.1% sodium azide (Sigma-Aldrich) in PBS for cryoprotection and longer-term storage prior to subsequent cryosectioning and tissue analysis. The experimental design for this initial cuprizone cohort was as shown in Figure 3.2.

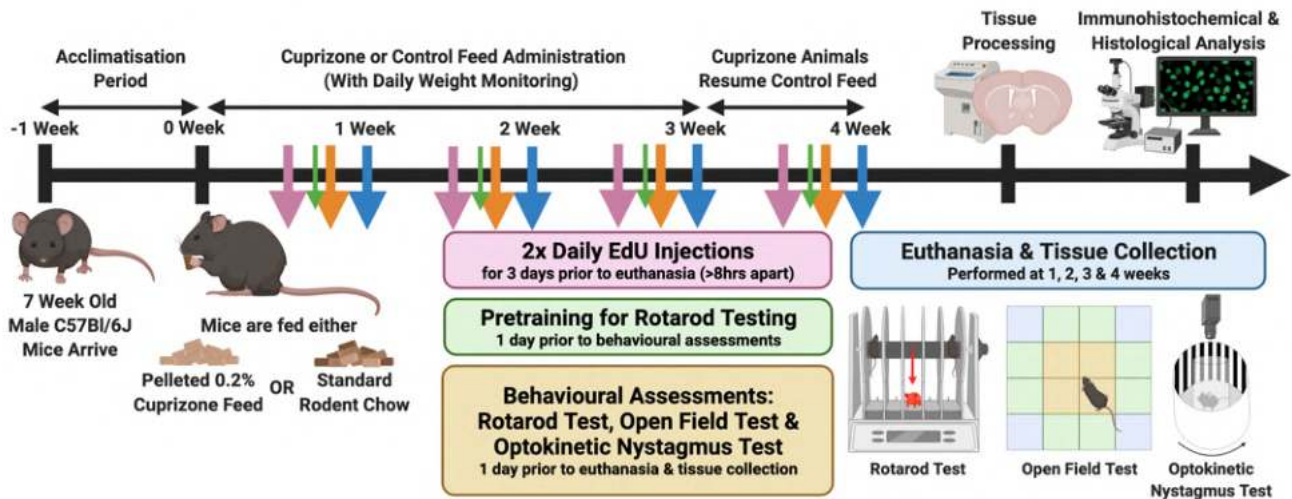


Figure 3.2. Experimental design for the initial cuprizone cohort. There were four groups receiving pelleted 0.2% cuprizone feed with four age-matched groups receiving standard rodent chow ($n = 12/\text{group}$, total $n = 96$). Cuprizone was delivered for either 1, 2 or 3 weeks to assess early demyelination, and there was an additional group given cuprizone for the full 3 weeks and then given standard rodent chow for a further 1 week to allow initial remyelination to occur (3+1 week). Mice were 8 weeks of age at the commencement of the experimental period. EdU (20mg/kg) was administered *via* intraperitoneal injection twice per day for 3 days prior to euthanasia, with a minimum of an 8 hour interval between injections. A day prior to euthanasia and tissue collection, behavioural assessments were performed, with the pretraining period for the Rotarod test occurring a day prior to this. Following euthanasia and tissue collection, the collected brains were cryosectioned and analysed. Original illustration created using BioRender.com.

3.2.2. Animal Weights

Both cuprizone and control animals were weighed daily throughout the experimental period, always using the same weight scales and at a consistent time of day. The body weights of the cuprizone-fed mice over time were then compared to their relative control groups using two-way repeated measures ANOVAs with Bonferroni *post-hoc* tests to detect differences between the groups at each individual timepoint (Figure 3.3). Within the 1 week timepoint group, there was a significant interaction effect between the administration of cuprizone and time on body weight ($F(7,154) = 5.35$, $p \leq 0.0001$; Figure 3.3A). However, further *post-hoc* analysis revealed that there was only a significant difference in body weight between cuprizone and control mice on the fifth day of cuprizone administration ($p = 0.03$), and not at any other time during the experimental period ($p > 0.05$). For the 2 week timepoint groups, there was also a significant interaction effect between the administration of cuprizone and time ($F(14,308) = 5.77$, $p \leq 0.0001$; Figure 3.3B). *Post-hoc* analysis discovered no differences between cuprizone and control mice on any day during the first week of cuprizone intoxication in these mice, but there were significant differences between the two groups at days 8, 10, 12, 13 and 14 ($p \leq 0.05$). Furthermore, though there was again a significant interaction

effect for both the 3 week ($F(21,462) = 2.76, p \leq 0.0001$; Figure 3.3C) and 3+1 week ($F(28,616) = 4.09, p \leq 0.0001$; Figure 3.3D) timepoint groups, there were no significant differences in body weight between cuprizone and control mice at any individual timepoints within these groups ($p > 0.05$). Therefore, when looking at this cohort as a whole, there was no sustained or reliable weight loss detected across any of the timepoint groups. It is generally expected that if cuprizone is actively inducing demyelinating pathology then mice will lose up to approximately 10% of their body weight within the first week of cuprizone administration (Steelman et al. 2012), an effect which was not observed in this study. The presence of some significant weight loss in the mice fed cuprizone for 2 weeks indicates that the cuprizone feed may have been partially effective at producing pathology. However, the lack of substantial weight loss across the four cuprizone-treated groups compared to the relative controls was an initial indication that the cuprizone pellets may not be efficacious in inducing the desired demyelinating effect.

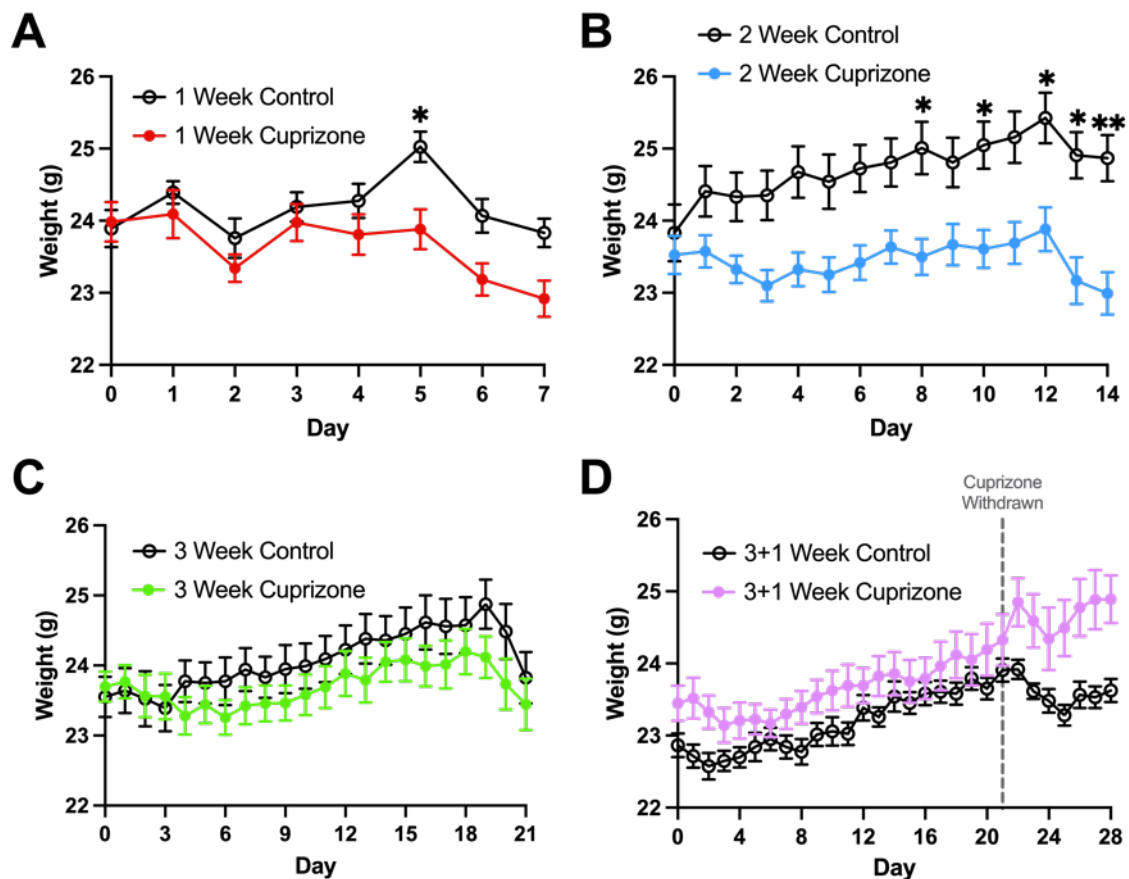


Figure 3.3. Effect of cuprizone on animal weights. Cuprizone was delivered for either 1, 2 or 3 weeks, with an additional group given cuprizone for the full 3 weeks and then allowed a further 1 week for initial remyelination to occur (3+1 week). Each cuprizone group had a relative, age-matched control group. $n = 12$ mice per group. Animals were weighed daily to assess weight loss throughout cuprizone or control feed administration. (A) Animal weights were compared between those fed cuprizone feed and control feed over 1 week (A), 2 weeks (B) or 3 weeks (C), as well as over a 3 week cuprizone administration followed by a 1 week remyelination period (D), to determine the effect of cuprizone intoxication on animal weight. Graph displays mean \pm SEM. Significant differences as determined by *post-hoc* analysis are indicated by * $p \leq 0.05$, ** $p \leq 0.01$.

3.2.3. Behavioural Assessments

A day prior to the end of the experimental period, three behavioural tests were performed to assess a variety of potential functional deficits, with the Rotarod test, the open field test and the optokinetic nystagmus test employed to measure changes in motor coordination, locomotor activity and response to a novel environment, and visual reflexes respectively (Figure 3.4).

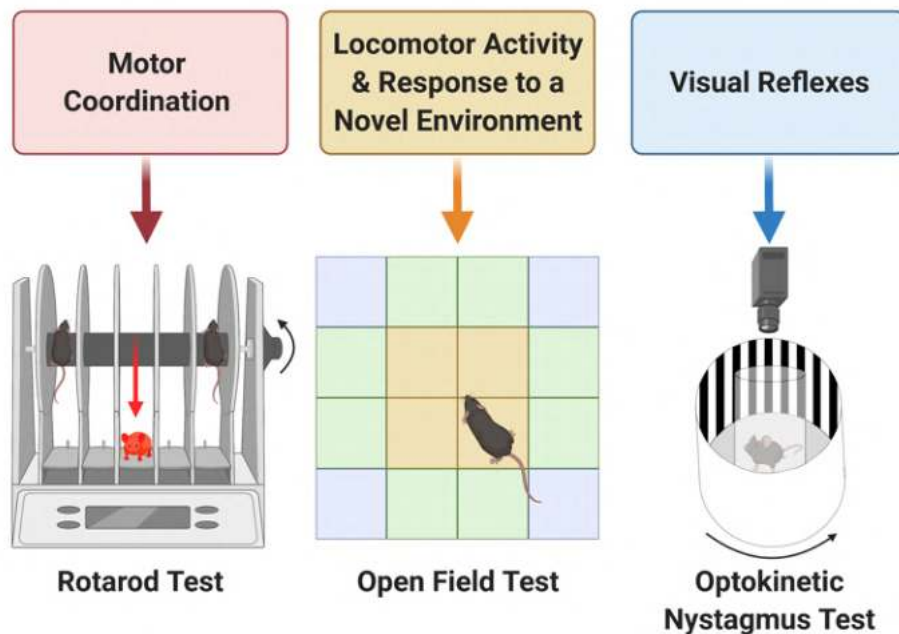


Figure 3.4. Schematic of behavioural tests performed. Behavioural assessments were performed one day prior to end of the experimental period to determine the presence of a range of behavioural deficits. Original illustration created using BioRender.com.

All behavioural assessments were performed in a restricted access room within the animal care facility to reduce transport anxiety and all mice had been exposed and habituated to the investigator carrying out the behavioural testing *via* repeated handling prior to the assessment day. 70% ethanol solution was used to clean and decontaminate all behavioural equipment in between mice to minimise any olfactory cues to the subsequent mice. Graphpad PRISM 9 software was used for data analysis and graphical illustration, with two-way ANOVAs with Tukey's *post-hoc* tests performed across all eight groups for each behavioural outcome measure.

3.2.3.1. Rotarod Test

Firstly, to assess motor coordination, the Rotarod test was employed. The Rotarod apparatus consists of a motor-driven 3cm diameter cylinder, which rotates at an accelerating speed of 4rpm to 40rpm. In line with previous studies (Mandillo et al. 2008; Mandillo et al. 2014), animals were pre-trained to stay on the Rotarod apparatus one day prior to testing. Rotarod pre-training consisted of three consecutive trials at least 10 minutes apart. During the first trial, the rod was kept stationary and the animals had to remain on the rod for 60 seconds. For the second and third trials, the rod was

rotated at 4rpm for 60 seconds each. The following day, the mice underwent an additional three trials for the testing period. Each trial consisted of placing the mouse on the rod whilst the rod accelerated from 4 to 40rpm over 300 seconds, with neurological deficit indicated by the inability to remain on the rotating rod. Each trial took place at least 15 minutes apart, and the three trials were then analysed both individually and when averaged. Only three mice were placed on the Rotarod at once so that there were empty lanes between them, to prevent the behaviour of one mouse influencing the others. Using this protocol, no differences were observed between cuprizone and control groups at trial one ($F(3,88) = 0.04, p > 0.05$; Figure 3.5A), trial two ($F(3,88) = 0.58, p > 0.05$; Figure 3.5B), or trial three ($F(3,88) = 1.07, p > 0.05$; Figure 3.5C), nor in the trial average ($F(3,88) = 0.72, p > 0.05$; Figure 3.5D).

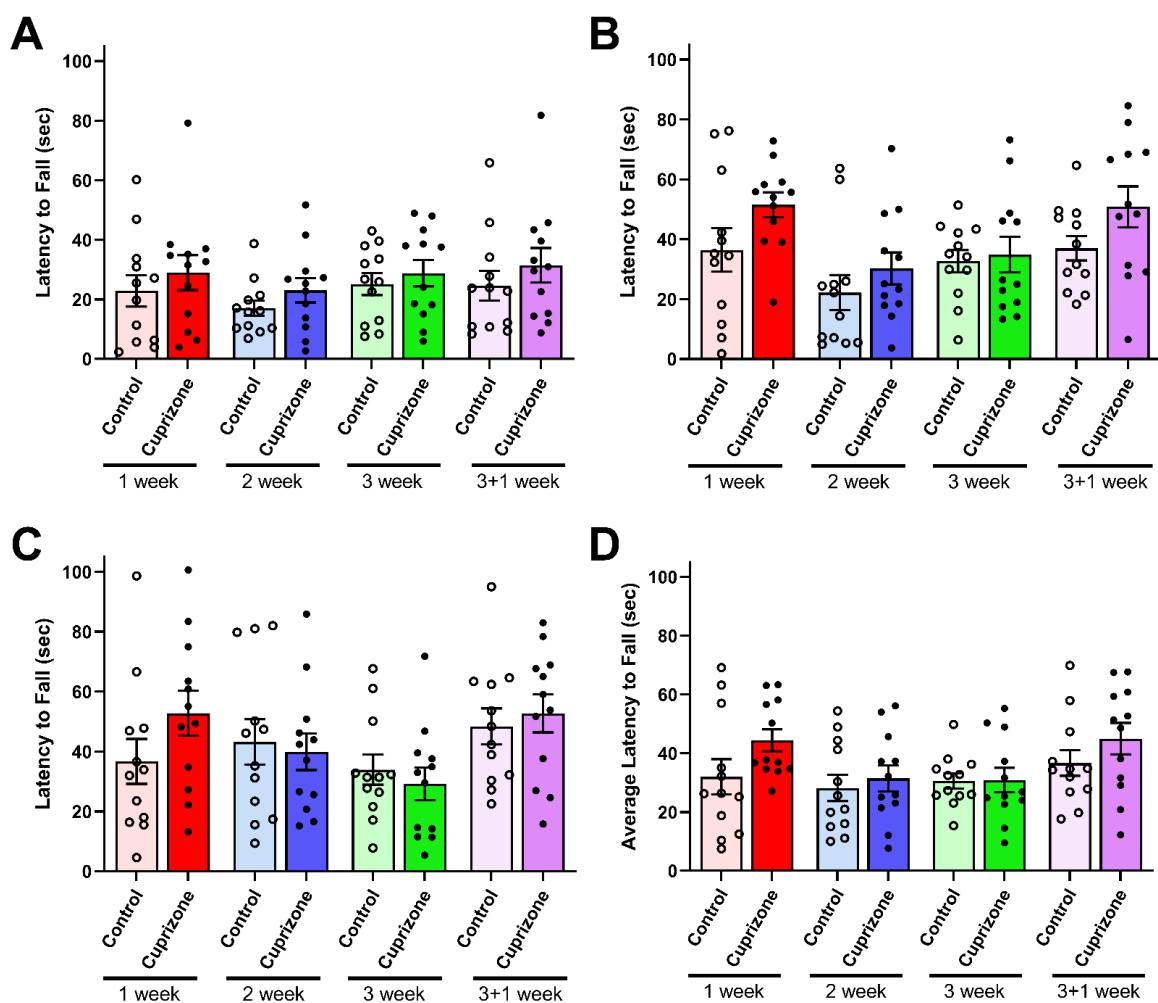


Figure 3.5. Effects of cuprizone administration on Rotarod test outcomes. Cuprizone was delivered for either 1, 2 or 3 weeks, with an additional group given cuprizone for the full 3 weeks and then allowed a further 1 week for initial remyelination to occur (3+1 week). Each cuprizone group had a relative, age-matched control group. No significant differences were found by a two-way ANOVA in the latency to fall off the Rotarod in trial one (A), trial two (B), or trial three (C), nor within the trial average (D). Graphs display individual data points, overlaid on a bar displaying the mean \pm SEM. $n = 12$ mice per group.

Whilst analysing the one and two week Rotarod data during the period of completing the animal procedures, I noticed that the data were broadly distributed and I felt that this high degree of variability might mask potential differences between groups. Therefore, when conducting the 3 week and 3+1 week timepoints, an additional training and testing period was added on the day of behavioural assessments. In brief, the original protocol was performed to completion to attain a complete original data set that could be used for a full analysis across all timepoints. Additional training was then completed, whereby the mice were placed on the rod again for a total of 5 minutes whilst the rod was rotating at 4rpm. Following completion of this additional training for all of the mice, the original testing period was repeated, with the mice undergoing an additional three trials for the second testing period. Again, each trial consisted of placing the mouse on the rod whilst the rod accelerated from 4 to 40rpm over 300 seconds, with each trial taking place at least 15 minutes apart. Similarly, the three trials were then analysed both individually and when averaged. However, despite the extra training and additional testing periods, there were no significant differences in the latency to fall off the apparatus between cuprizone and control groups at trial one ($F(1,44) = 0.06, p > 0.05$; Figure 3.6A), trial two ($F(1,44) = 0.28, p > 0.05$; Figure 3.5B), or trial three ($F(1,44) = 0.17, p > 0.05$; Figure 3.6C), nor in the trial average ($F(1,44) = 0.29, p > 0.05$; Figure 3.6D). Therefore, it was concluded that no gross deficit in motor coordination was evident within this cohort.

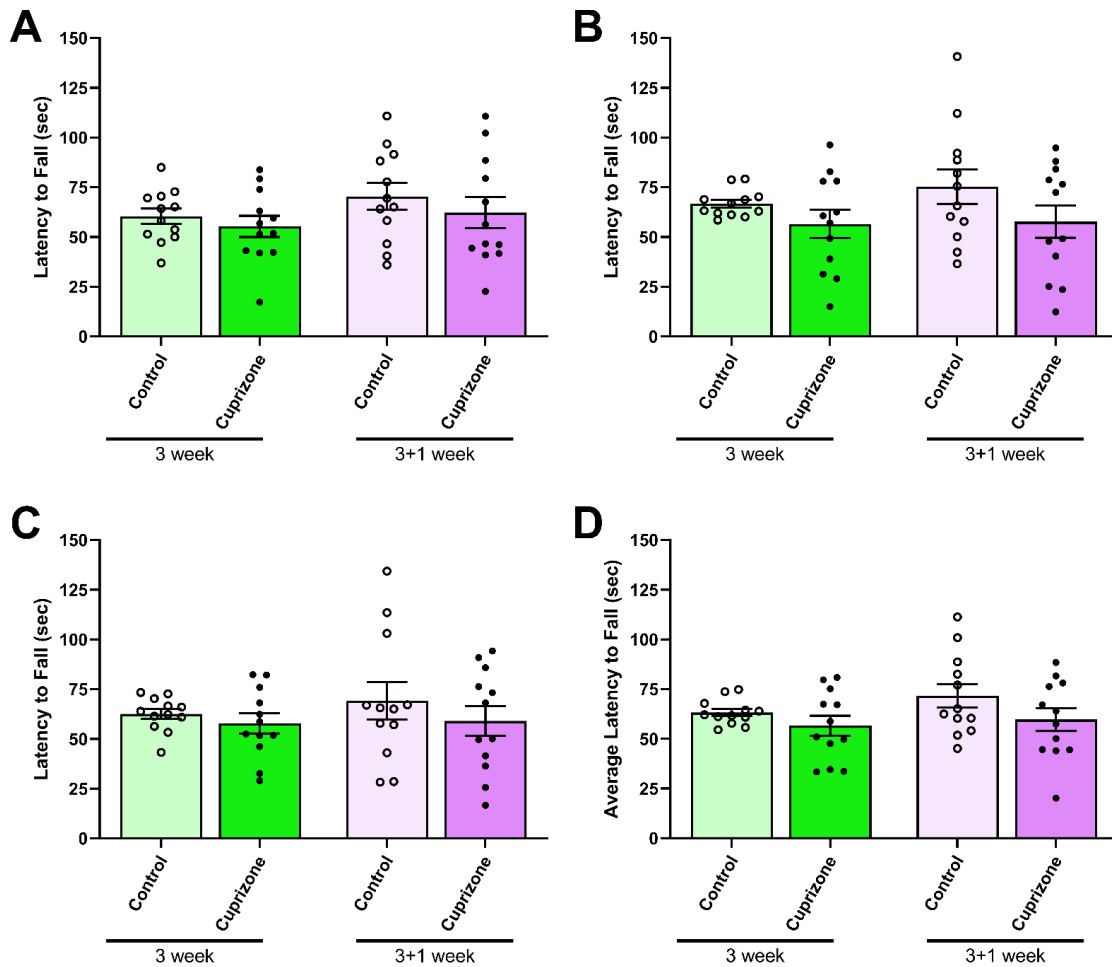


Figure 3.6. Effects of cuprizone administration on Rotarod test outcomes with a revised protocol. Cuprizone was delivered for 3 weeks, with another group given cuprizone for the full 3 weeks and then allowed a further 1 week for initial remyelination to occur (3+1 week). Each cuprizone group had a relative, age-matched control group. No significant differences were found by a two-way ANOVA in the latency to fall off the Rotarod in trial one (A), trial two (B), or trial three (C), nor within the trial average (D), despite additional training and testing periods. Graphs display individual data points, overlaid on a bar displaying the mean \pm SEM. $n = 12$ mice per group.

3.2.3.2. Open Field Test

To assess locomotor activity and response to a novel environment, the open field test was used. Following habituation to the testing room for a minimum of 30 minutes prior to testing, individual mice were placed inside a white 36cm x 36cm square box and were allowed to roam freely for 10 minutes. The behaviour of the animals was recorded using a Logitech C920 webcam placed directly overhead of the box. The investigator was out of view of the animal to prevent any influence on their behavioural activity. The mice were then manually removed from the apparatus and returned to their home cages. The number of faecal boli left in the chamber was manually recorded and analysed as a measure of anxiety. However, no differences were observed in the number of faecal

boli produced by the mice over the 10 minute testing period across any groups, suggesting no change in anxiety levels with cuprizone administration ($F(3,88) = 0.18, p > 0.05$; Figure 3.7A).

Any-Maze video tracking software was used to automate analysis of the footage obtained by accurately tracking the movement of each mouse. Firstly, following software recognition of the body of each mouse and calibration of the dimensions of the open field apparatus, the total distance travelled was quantified. However, the total distance travelled did not change with the administration of cuprizone across any timepoints ($F(3,88) = 1.10, p > 0.05$; Figure 3.7B). The testing apparatus was subsequently divided into twelve quadrants artificially overlaid onto the footage obtained to allow for more detailed examination of individual animal behaviour. These quadrants were then grouped into three key zones for further analysis; the centre zone, the thigmotaxis zone, and the corner zones (Figure 3.7D). Mice have been previously found to display more centre zone activity when cuprizone is delivered for 3 weeks (Franco-Pons et al. 2007), therefore the distance each mouse travelled in the centre zone relative to the total distance travelled was initially analysed. However, no significant differences were observed for distance travelled in the centre zone across any timepoint ($F(3,88) = 0.70, p > 0.05$; Figure 3.7C). Further sub-analyses for additional parameters again found no significant differences between any of the groups (data not shown). Thus, it was concluded that this cohort of mice did not display any of the expected behavioural deficits, and the efficacy of the cuprizone pellets that were delivered was further questioned.

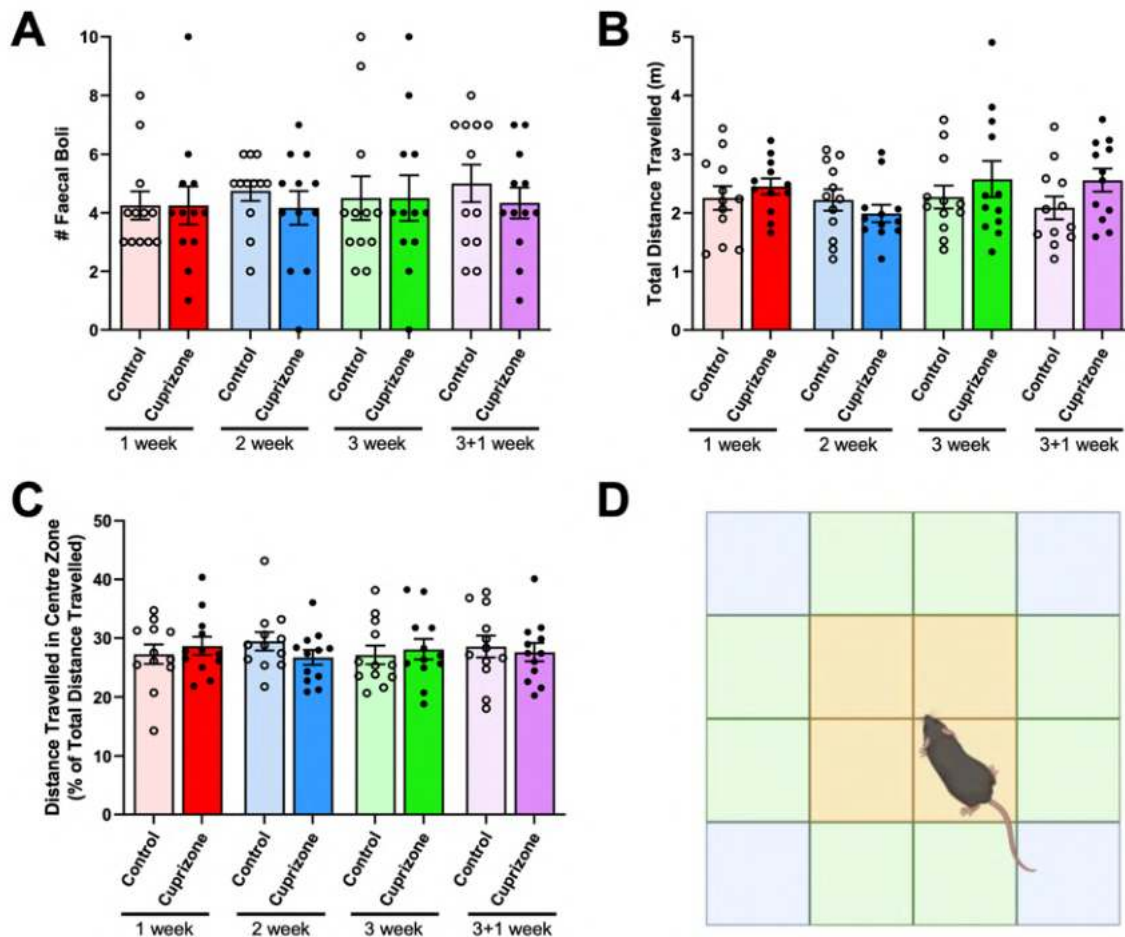


Figure 3.7. Effects of cuprizone administration on open field test outcomes. Cuprizone was delivered for either 1, 2 or 3 weeks, with an additional group given cuprizone for the full 3 weeks and then allowed a further 1 week for initial remyelination to occur (3+1 week). Each cuprizone group had a relative, age-matched control group. No significant differences were found by a two-way ANOVA in the total number of faecal boli produced during the 10 minute testing period (A), total distance travelled inside the open field box (B), or in the distance travelled in the centre zone (C). (D) Representative image of the zone divisions during automated analysis, with centre zone displayed in yellow, thigmotaxis zone displayed as a combination of green and blue, and corners zone displayed in blue. Graphs display individual data points, overlaid on a bar displaying the mean \pm SEM. $n = 12$ mice per group. Schematic depicting division of testing area into quadrants is an original illustration created using BioRender.com.

3.2.3.3. Optokinetic Nystagmus Test

Finally, the optokinetic nystagmus test was utilised in accordance with an established protocol following partial optic nerve transection (Fitzgerald et al. 2009; Fitzgerald et al. 2010; Savigni et al. 2013; Toomey et al. 2018) to screen for changes in visual reflexes and function with cuprizone administration. In brief, each mouse was placed inside a glass cylinder on an illuminated round platform within a rotating drum. The drum had alternating black and white stripes at a 1cm thickness that were rotated in either a clockwise or anti-clockwise direction. To habituate the mouse to the apparatus, each mouse was allowed 2 minutes inside the cylinder without the drum rotating, followed

by 2 minutes with the drum rotating clockwise and then a further 2 minutes rotating anticlockwise. The mouse was then removed from the apparatus and returned to its home cage. This acclimatisation process was then completed for all animals, with the cylinder and platform cleaned and decontaminated with 70% ethanol in between each mouse. Once this process had been completed with all of the animals, the initial mouse was returned to the cylinder. The animal was allowed 1 minute to readjust to the apparatus, before an overhead video camera began recording. A further minute of rest was then filmed, to capture any visible signs of distress in the animals. It is important to note that all mice tested showed no signs of distress when inside the optokinetic drum and exhibited typical grooming behaviour during this period. The striped drum was then rotated for 2 minutes in an anticlockwise direction, with the responses to the movement of the stripes recorded. Subsequently, the animal was returned to its home cage once more, and this testing period was then performed for all of the mice. Due to the small binocular overlap in rodents, visual responses in unrestrained mice rely concomitantly on full head movements as well as more subtle eye movements for image stabilisation and visual acuity (Kretschmer et al. 2017; Walls 1942). Therefore, a normal optokinetic response is considered to have been observed when the mouse turns its head to follow the stripes as the drum is rotating. Responses can be categorised broadly into either a smooth pursuit, whereby the mouse tracks the rotation of the stripes in an elongated and smooth head turning movement, or a fast reset, which is a saccade-like rapid head movement to realign with a new stripe on the drum (Abdeljalil et al. 2005). However, given the insignificant outcomes of the other two behavioural assessments, the decision was made to abstain from actually analysing the footage obtained during the optokinetic nystagmus testing until there was confirmation that the model was indeed inducing demyelination in the mice.

3.2.4. Histological Tissue Analysis

Given the lack of any gross weight loss with cuprizone intoxication and the lack of significant differences with initial behavioural assessments, the decision was made to analyse a subset of the tissue to confirm the cuprizone was indeed inducing demyelinating disease pathology. Demyelination has previously been found to be significantly detectable by 3 weeks of cuprizone exposure (Matsushima & Morell 2001). Therefore, to best observe any potential demyelinating effect, half of the 3 week cuprizone group and the relevant age-matched controls were selected for tissue analysis utilising specific histological myelin stains. For this, the brains were fast frozen in OCT within moulds placed in isopentane cooled in a bath of liquid nitrogen. Tissue was subsequently coronally cryosectioned at -20 °C to a thickness of 20µm. Sections were then collected onto slides that were stored at -80°C until histological analyses commenced. It is important to note that due to freezing artefacts and technical issues with mountant, there were visible holes in the tissue and also air bubbles over the surface of the tissue respectively. However, these issues were subsequently resolved in later

work that will be presented in Section 3.3. Furthermore, these technical problems did not prevent analysis of tissue from proceeding as planned.

3.2.4.1. Luxol Fast Blue

Firstly, a Luxol Fast Blue stain was utilised to visualise the level of myelination in both the rostral and caudal medial corpus callosum (Kiernan 2013; Klüver & Barrera 1953). In brief, tissue sections were hydrated to 95% ethanol, before being placed in 0.1% Luxol Fast Blue solution (Acros Organics) for 14 hours at 56°C. Excess stain was rinsed off in 95% ethanol followed by distilled water. Slides were then differentiated in 0.05% lithium carbonate (Sigma-Aldrich) for 30 seconds, followed by 70% ethanol and rinsed in distilled water. This was repeated 4 times, before slides were placed in 100% ethanol for 5 minutes twice. Finally, slides were cleared in xylene for 5 minutes twice, and then coverslipped using Fluoromount (Invitrogen) and imaged on a Nikon DS-Fi3 microscope. However, in both the rostral and caudal corpus callosum, there was no observable difference in the level of myelination between 3 week control and 3 week cuprizone tissue (Figure 3.8).

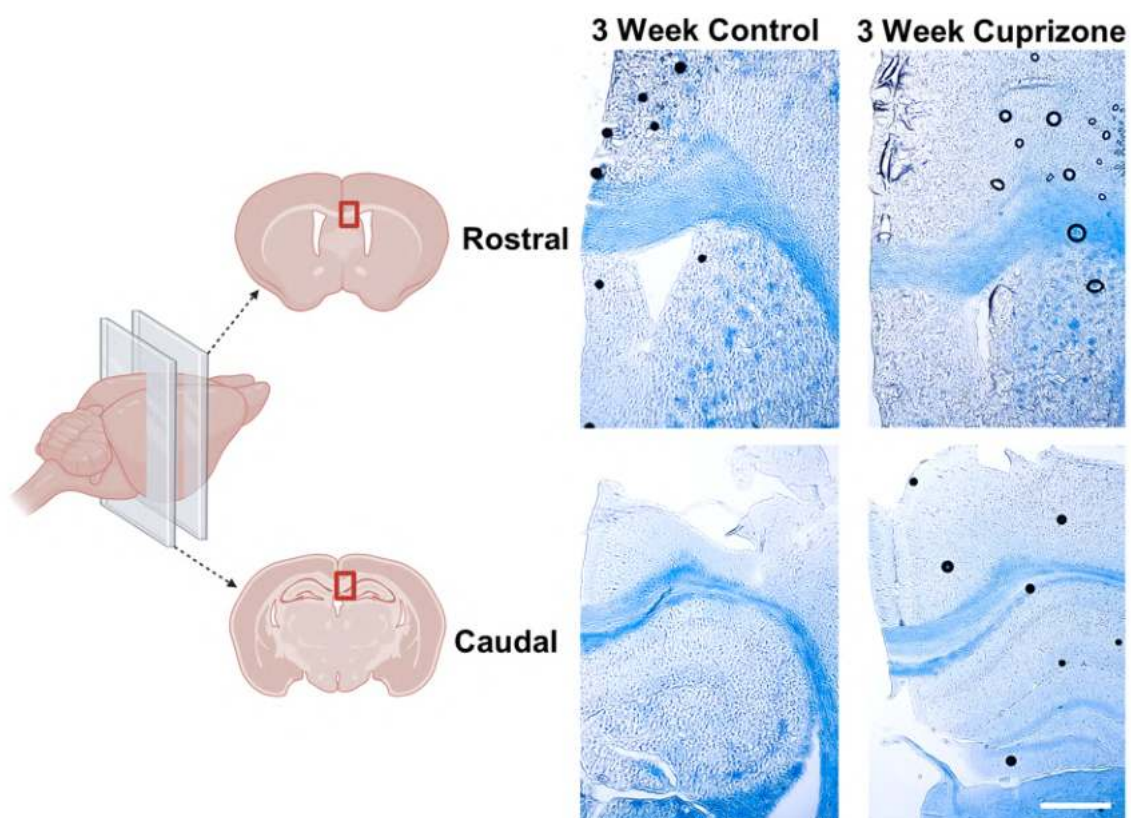


Figure 3.8. Histological assessments of myelin quality comparing 3 week control and cuprizone tissue using a Luxol Fast Blue stain. Cuprizone was delivered for 3 weeks and outcomes were compared with a relative, age-matched control group. No differences in myelination were observed in either the rostral and caudal medial corpus callosum. Representative images of Luxol Fast Blue stain; scale bar = 500µm. n = 6 mice per group. Brain schematic is an original illustration created using BioRender.com.

3.2.4.2. Myelin Black-Gold II

Although Luxol Fast Blue is a highly specific histological stain for myelin that is well-utilised in the literature (Largani et al. 2019; Morell et al. 1998; Noorzehi et al. 2018; Sun et al. 2006), it has a comparatively low resolution quality and contrast. Myelin Black-Gold II is a gold-based stain that can provide a much higher resolution for myelin detection down to a single fibre level, and is thus more sensitive to subtle changes in myelination than more traditional histological methods such as Luxol Fast Blue (Savaskan et al. 2009). Therefore, the Myelin Black-Gold II stain was also used to visualise the degree of myelination, in an effort to detect more subtle signs of potential demyelination. Sections were rehydrated in distilled water for 2 minutes, before incubating in 0.3% Myelin Black-Gold II solution (Merck Millipore) at 60°C for 38 minutes. Sections were rinsed twice in distilled water, before incubating in 1% sodium thiosulfate (ChemSupply) for 3 minutes at 60°C. Following three 2 minute rinses in distilled water, Cresyl Violet (Merck Millipore) was added and incubated for 3 minutes at room temperature. The sections were again rinsed three times for 2 minutes each, before being dehydrated using graded alcohols. Finally, slides were cleared in xylene for 2 minutes, coverslipped using Fluoromount (Invitrogen) and imaged on a Nikon DS-Fi3 microscope. Nevertheless, there were again no differences observed in the level of myelination between cuprizone-fed and control mice in either the rostral or caudal medial corpus callosum (Figure 3.9).

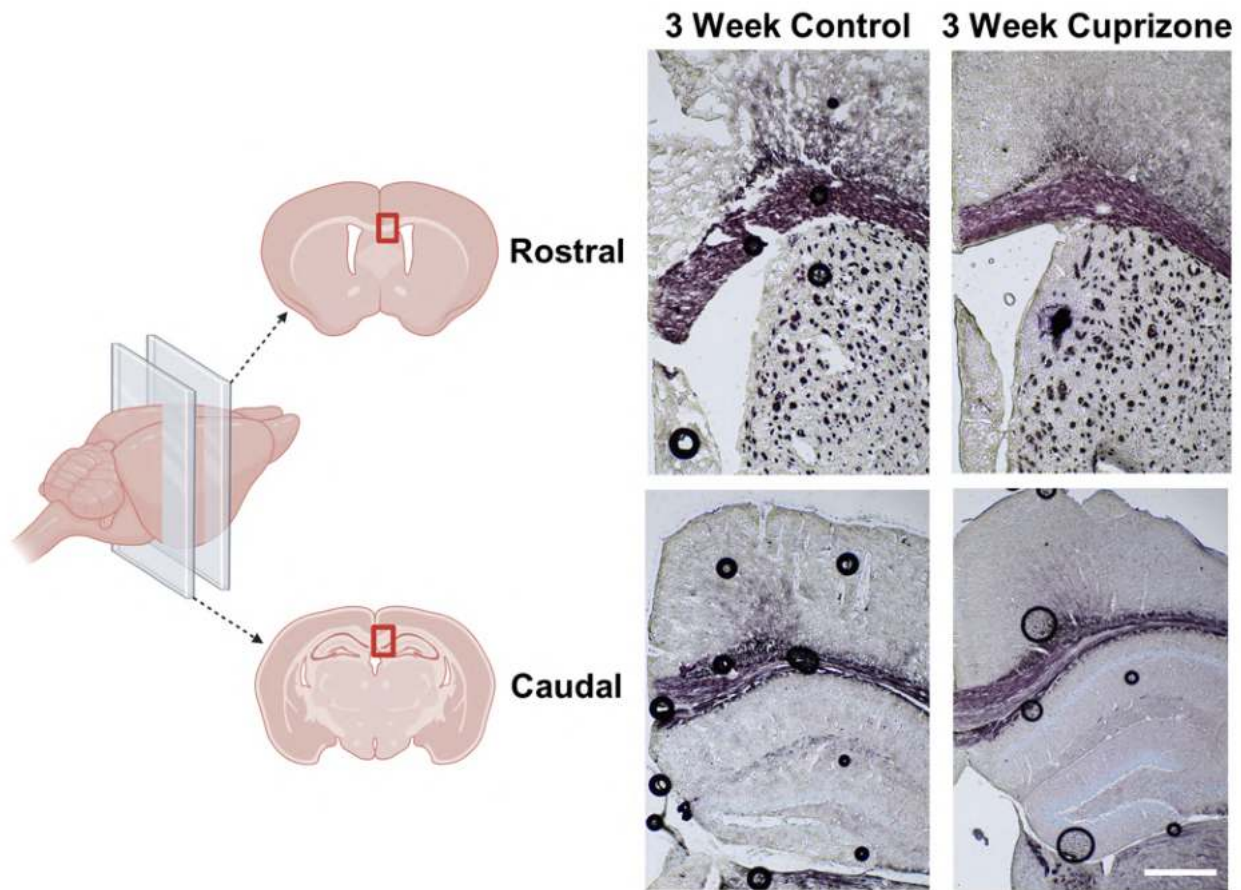


Figure 3.9. Histological assessments of myelin quality comparing 3 week control and cuprizone tissue using a Myelin Black-Gold II Stain. Cuprizone was delivered for 3 weeks and outcomes were compared with a relative, age-matched control group. No differences in myelination were observed in either the rostral and caudal medial corpus callosum. Representative images of Myelin Black-Gold II stain; scale bar = 500 μ m. n = 6 mice per group. Brain schematic is an original illustration created using BioRender.com.

3.2.5. Issues Regarding Efficacy of Cuprizone Pellets

The absence of a significant difference between the cuprizone and control groups in the outcomes described above suggested that the pelleted cuprizone wasn't effective at inducing demyelinating pathology in this cohort of mice. In order to perform research that is reproducible and comparable to the literature, it is vital that mice are consistently given 0.2% cuprizone in their feed to ensure reliable, consistent and robust demyelination. The lack of an effect of cuprizone in both histological and behavioural outcome measures signified that demyelination was not being reliably induced. In particular, the lack of change with cuprizone administration for any of the behavioural assessments performed was especially concerning. For example, for the open field test it is anticipated that by 3 weeks of cuprizone toxicity, the mice would be travelling significantly further within the centre zone of the apparatus and would also be producing fewer faecal boli due to decreased anxiety levels (Franco-Pons et al. 2007). This effect was not observed in this cohort. Similarly, mice have also been shown to display a reduced latency to fall off the rod in the Rotarod test after 3 weeks of

cuprizone treatment (de Rosa et al. 2019), which again was not observed. When combined with the lack of histologically observable demyelination, this suggests that the administered cuprizone wasn't effective at inducing demyelinating pathology in this cohort of mice.

It was decided to cease tissue analysis on this cohort until the issues with the cuprizone could be resolved. After contacting Envigo, the supplier of these cuprizone-containing pellets, it appeared that there may have been a batch issue affecting the efficacy of their cuprizone pellets. Furthermore, discussions with our collaborators as well as the literature suggested that powdered cuprizone rather than pelleted may be more reliable to induce demyelinating disease (Hochstrasser et al. 2017). Given the issues with cuprizone efficacy in our hands, a direct comparison between pelleted and powdered cuprizone was needed to decide which formulation to employ to address the aims of the main study. The designed study to compare powdered and pelleted cuprizone was conducted and will be presented in the upcoming Chapter 4.

3.3. Optimisation of Freezing Protocols

3.3.1. Rationale

As mentioned above, when cryosectioning and histologically staining the 3 week cuprizone and control tissue from the previous cohort, it was evident that there was tissue damage in the form of holes appearing throughout the tissue, which was suspected to be due to freezing artefacts during tissue processing. Therefore, prior to commencing the comparison between the two cuprizone formulations, it was important to ensure tissue was able to be analysed without methodological complications.

3.3.2. Confirming Freezing Issues

Firstly, it was necessary to confirm that the holes were due to issues surrounding freezing, rather than inadequate perfusions or other tissue processing issues. To perform the freezing method, block cut brains were placed into plastic moulds filled with optimal temperature compound (OCT, Scigen). These moulds were then placed into cooled isopentane in a bath of liquid nitrogen (Figure 3.10).

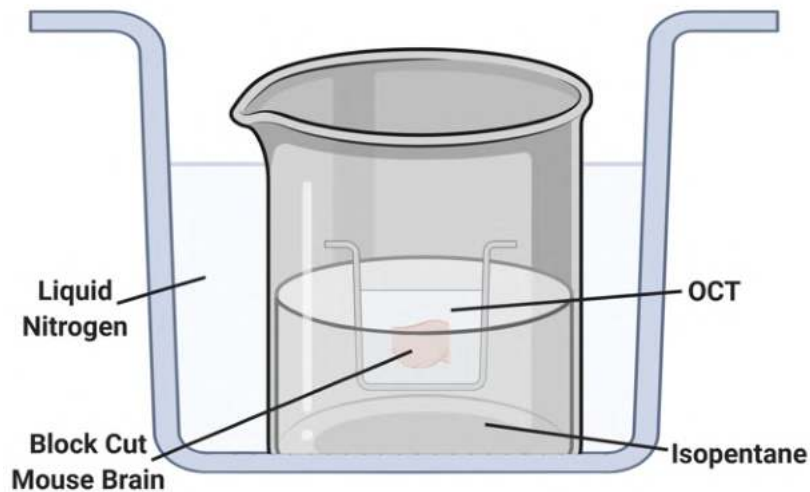


Figure 3.10. Freezing apparatus. Brains were embedded in a plastic mould filled with OCT. These moulds were placed in isopentane which was cooled in a bath of liquid nitrogen. Original illustration created using BioRender.com.

Using the 2 week tissue from the previous cohort, various durations of freezing time within the isopentane were compared, and it was found that the longer the tissue remained in the isopentane, the better the tissue quality, with shorter time in the isopentane producing holes within the tissue (Figure 3.11). A Myelin Black-Gold II stain and a Cresyl Violet counterstain was utilised to visualise tissue quality, performed as described in Section 3.2.4.2. The moulds were removed from the isopentane when the top surface of the OCT appeared solid and frozen, as an indicator that the mould was fully frozen inside. When the moulds were immersed in the isopentane for 210 seconds or 180 seconds in total, no holes were present within the tissue (Figure 3.11A-B). However, when the moulds were in the isopentane for shorter durations of 75 seconds or just 30 seconds, the tissue had an abundance of holes and tissue damage (Figure 3.11C-D), despite the OCT appearing fully frozen when observed. It is important to acknowledge that once the moulds were removed from the isopentane, they were placed in a -20°C freezer for a few hours before moving to the -80°C freezer for longer term storage. It is thus likely that although the top of the OCT had frozen on the shorter time points, the main body of the brain had probably not frozen fully within the centre of the mould. Therefore, upon placing the moulds into the -20°C freezer, both the OCT and the tissue located within the centre of the mould froze slowly, creating holes and other artefacts in the tissue due to the formation of crystals during the slower freezing process. Different freezing durations and methods were then trialled to optimise tissue quality and antigenicity.

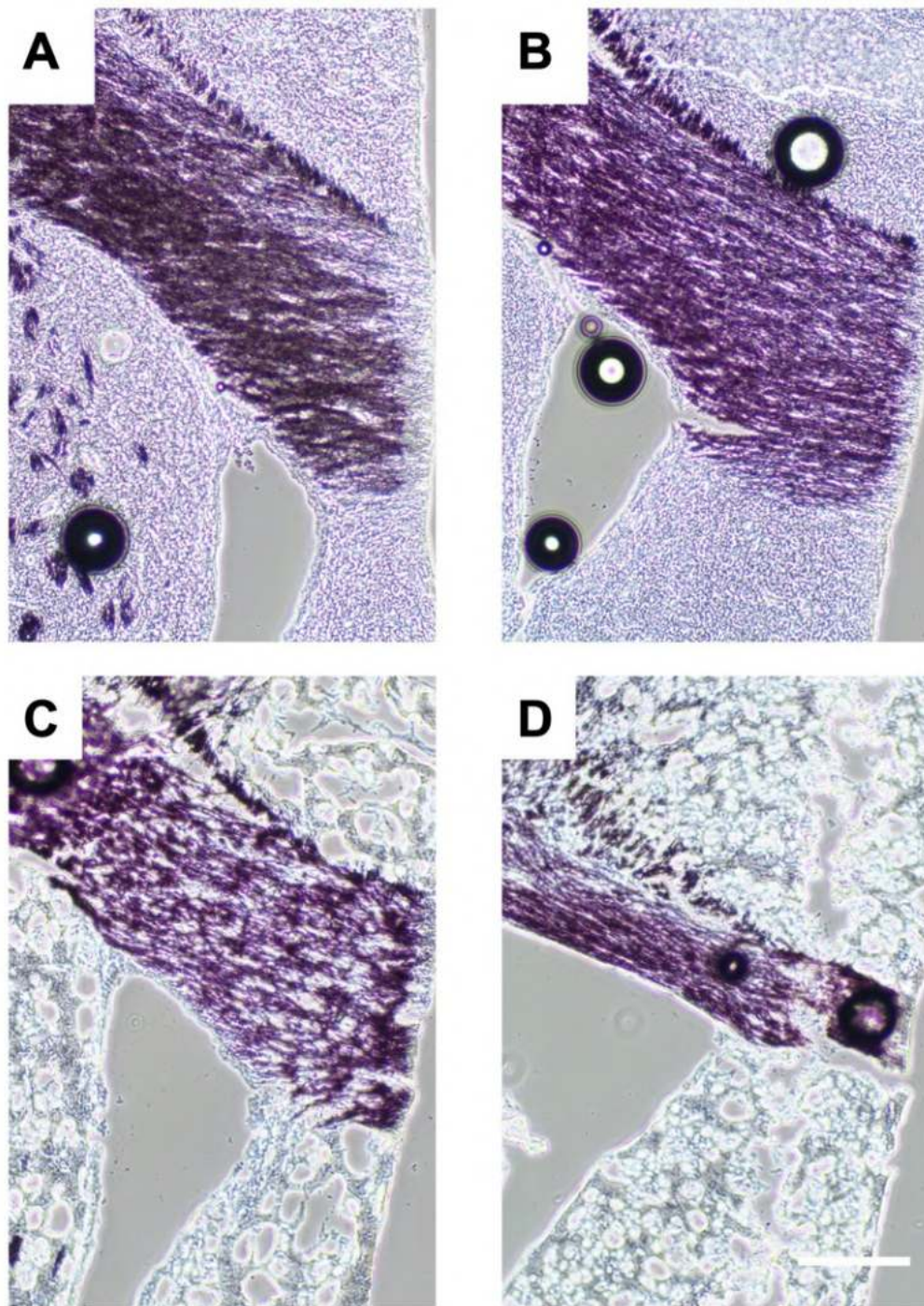


Figure 3.11. Comparison of different freezing times in a bath of isopentane. The moulds were placed in isopentane in a bath of liquid nitrogen for either 210 seconds (A), 180 seconds (B), 75 seconds (C), or 30 seconds (D). Brains were stained using Myelin Black-Gold II. Scale bar = 200 μ m.

3.3.3. Optimising Freezing Duration

Four different freezing methods were compared, with three different durations in isopentane, as well as comparing with brains embedded in OCT that were placed directly into the -80°C freezer, bypassing the fast freezing in cooled isopentane step. The freezing durations of the three isopentane groups were determined relative to the point in which the top of the OCT became opaque. A holder was constructed for the moulds to make sure that they were not accidentally fully submerged into the

isopentane at any point during the freezing process, to ensure a more reliable way to determine if the top of the OCT had fully frozen without the confounding factor of any unintentional direct contact with the cooled isopentane on that top surface. Therefore, moulds were initially removed from the isopentane once the top of the OCT became fully opaque, which was approximately 105 seconds after it was placed into the isopentane. The longer time required for the top of the OCT to freeze compared to the previous experiment presented in Section 3.3.2, indicates that keeping the moulds not fully submerged in the isopentane on the top of the OCT was a more reliable way to determine how frozen the mould may be inside, and prevent an earlier and more inaccurate frozen appearance on the top OCT surface. To trial longer freezing durations, the moulds were removed either 60 seconds after the top of the OCT became opaque or 120 seconds after the OCT became opaque. Importantly, instead of transferring to the -20°C freezer following the isopentane fast freezing, brains were placed on dry ice prior to being transferred and stored directly in the -80°C freezer, to further minimise the risk of a slow freeze process damaging the tissue. The resulting tissue was subsequently coronally cryosectioned at -20°C to a thickness of 20µm. Sections were then collected onto slides that were stored at -80°C until further histological and immunohistochemical analyses were commenced.

3.3.3.1. Impact of Freezing Duration on Tissue Quality

A portion of the sectioned tissue was stained using the Myelin Black-Gold II stain and Cresyl Violet counterstain to investigate tissue quality as previously described in Section 3.2.4.2. There was a slight methodological change to using dibutylphthalate polystyrene xylene (DPX; Lab Chem) as the coverslipping mounting media instead of Fluoromount (Invitrogen) to reduce the likelihood of any air bubbles appearing over the xylene cleared tissue. Interestingly, none of the freezing methods described above produced holes or any other tissue damage to the samples (Figure 3.12). This suggested that placing the moulds in the -20°C freezer following the fast freezing in the isopentane was indeed resulting in a slower secondary freezing process that caused the observed tissue damage.

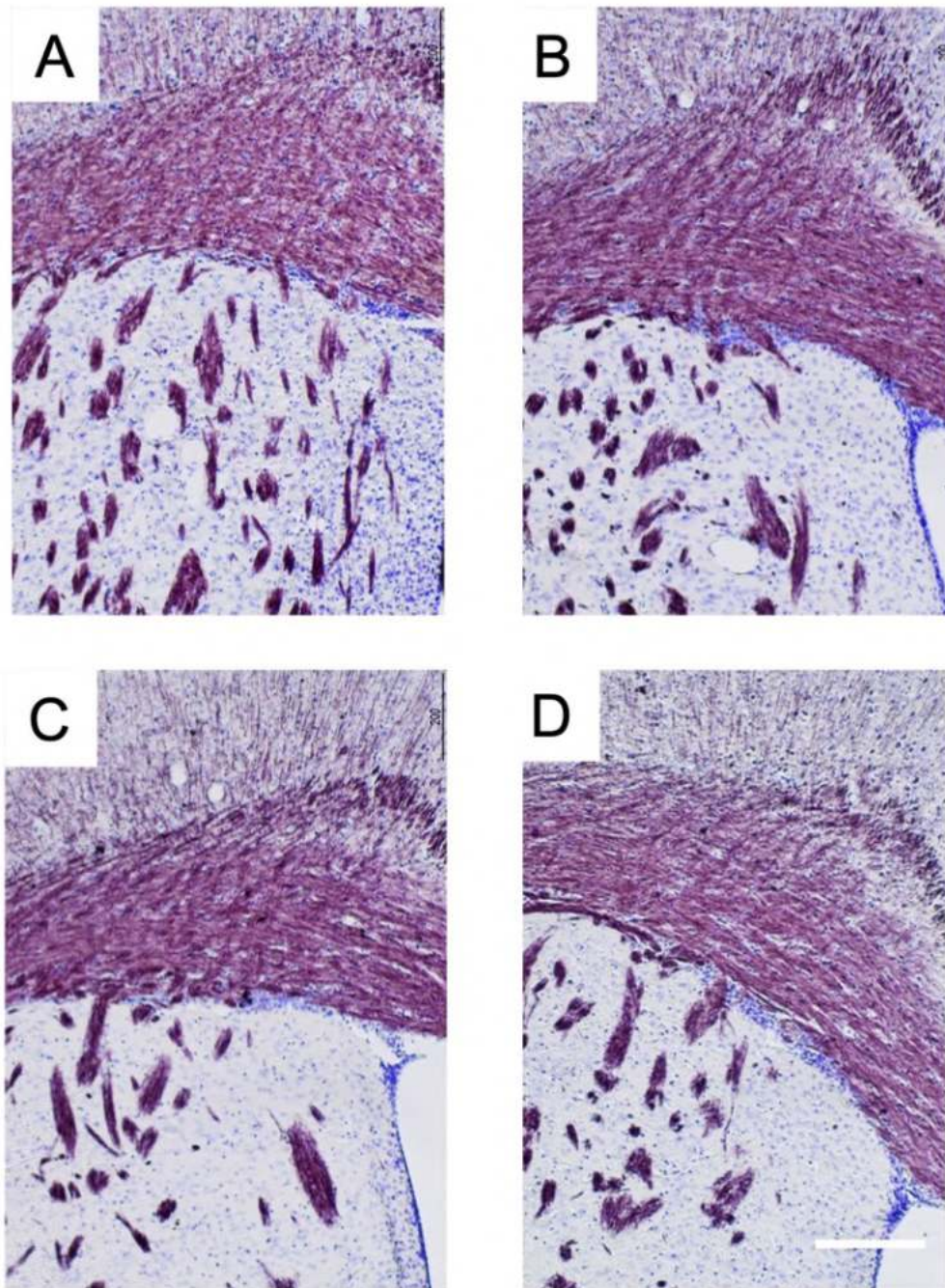


Figure 3.12. Comparison of different freezing times on tissue quality. The moulds were placed either (A) directly into the -80° freezer, or in isopentane in a bath of liquid nitrogen until either (B) the OCT turned opaque, (C) 60 seconds after the OCT turned opaque, or (D) 120 seconds after the OCT turned opaque. Scale bar = $200\mu\text{m}$.

3.3.3.2. Impact of Freezing Duration on Tissue Antigenicity

It is important that tissue quality is not only intact, but that antibodies are able to bind adequately to the desired antigens in order to conduct comprehensive immunohistochemical analyses. Therefore, in order to assess whether the antigenicity of the tissue was affected by the freezing durations, an immunohistochemistry experiment was performed. In brief, sections were washed in PBS, followed by a 5 minute incubation with PBS + 0.2% Triton-X 100 (Thermo-Fisher) + 5% normal donkey serum (Merck Millipore). Primary antibodies detecting astrocytes (anti-GFAP, 1:500,

Abcam, Ab33922, lot number GR148838-3), microglia (anti-IBA1, 1:500, Abcam, Ab5076, lot number GR3178800-2), and oligodendroglia (anti-Olig2, 1:500, R&D Systems, AF2418, lot number UPA0819111) were incubated overnight at 4°C diluted in PBS + 0.2% Triton-X 100 + 5% normal donkey serum. Antigenicity of the tissue was visualised following a 2 hour incubation at room temperature with the appropriate secondary antibodies (Invitrogen Alexa Fluor 488 or 555 at 1:400 in PBS) and a subsequent 10 minute incubation with Hoechst nuclear stain (1:1000, Invitrogen). Slides were coverslipped with Fluoromount (Invitrogen) and imaged using a Nikon Eclipse Ti2-E confocal microscope.

Differences in antigenicity between freezing methods were observed (Figure 3.13). The greatest difference between freezing methods was observed in the binding of GFAP and IBA1 antibodies, with more antigen binding occurring the longer the tissue was left in the isopentane after the OCT became opaque, and the lowest antigen binding occurring when moulds were simply placed in the -80°C freezer (Figure 3.13A-D). There were also subtle differences in the binding of Olig2 antibodies to the tissue, with more faintly positive staining appearing the longer the tissue was left in the isopentane (Figure 3.13E-H). However, the antigenicity of the tissue with the Olig2 antibody did not differ as considerably in comparison to the binding of GFAP and IBA1, indicating variance in the extent of changes to antigenicity for different antigens in the tissue. Nevertheless, based on both the intact tissue quality and the increased antigenicity of the tissue with increased freezing durations in the isopentane, it was decided to proceed with freezing the brain moulds within the cooled isopentane in a bath of liquid nitrogen until 120 seconds after the OCT became fully opaque.

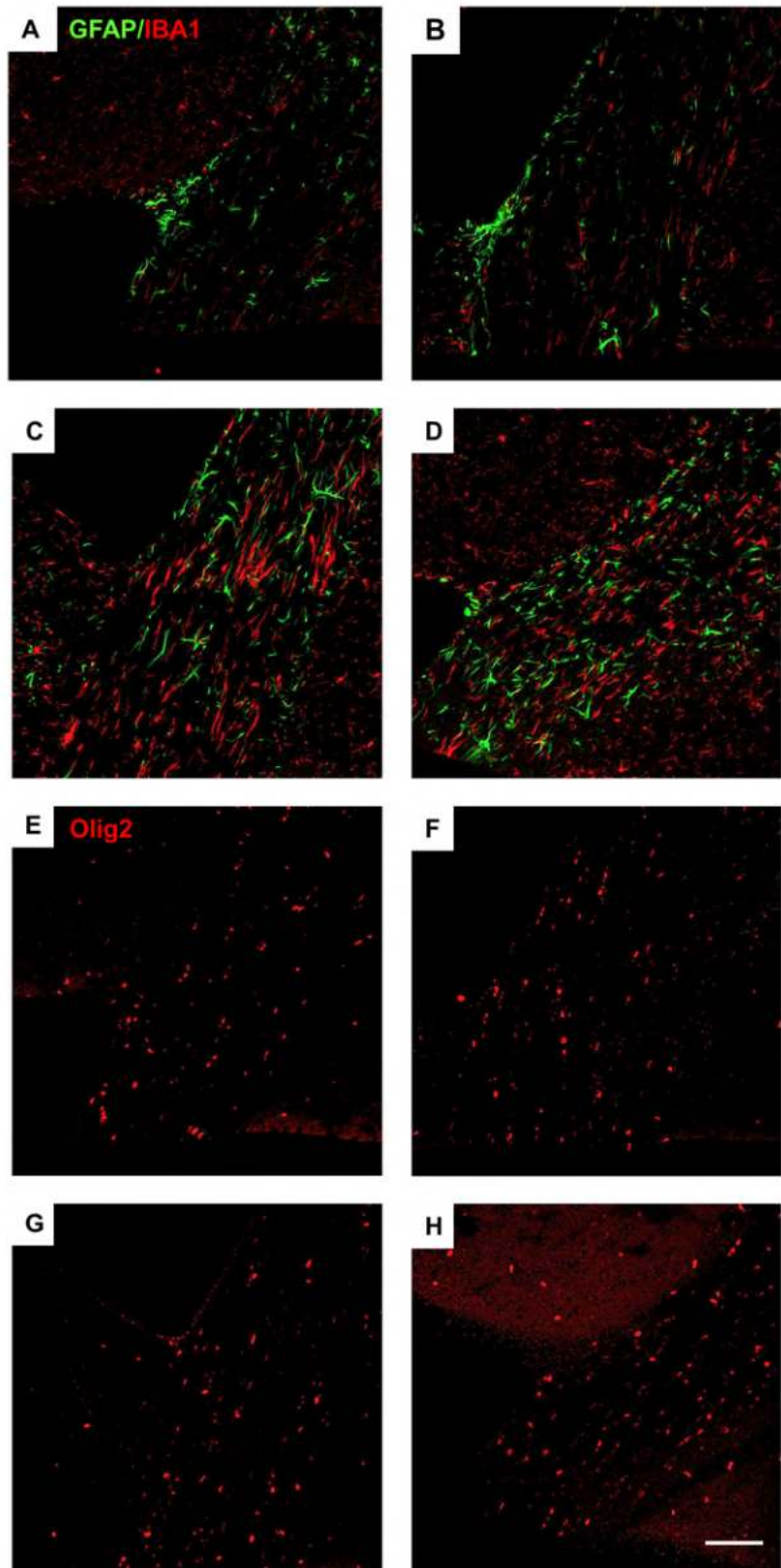


Figure 3.13. Comparison of different freezing methods on antigenicity. Antigenicity of GFAP and IBA1 (A-D) and Olig2 (E-H) were tested using various different freezing methods. The moulds were placed either directly into the -80° freezer (A,E), or in isopentane in a bath of liquid nitrogen until either the OCT turned opaque (B,F), 60 seconds after the OCT turned opaque (C,G), or 120 seconds after the OCT turned opaque (D,H). Scale bar = $100\mu\text{m}$.

3.4. Concluding Remarks

Within this chapter, the initial research performed to assess the role of oxidative damage to oligodendroglia in demyelinating disease was presented. However, the expected behavioural or phenotypical effects were not observed as a result of the cuprizone exposure, nor was there any demyelination present when a subset of the tissue was sectioned and histologically stained. It was thus decided that a direct comparison between pelleted and powdered cuprizone was needed to optimise the method of cuprizone delivery. Additionally, the optimisation of freezing protocols for mouse brain tissue were described in this chapter, conducted to ensure that the mouse tissue obtained throughout the rest of the thesis could be analysed without methodological complications from freezing artefacts.

Chapter 4. Characterisation and Optimisation of the Cuprizone Model of Demyelinating Disease

In order to perform research that is reproducible and comparable to the literature, as well as to ensure reliable demyelination, it is imperative that mice are consistently given 0.2% cuprizone in their feed. Given the ineffective induction of demyelinating disease in the cohort presented in Chapter 3, a study was designed to directly compare powdered and pelleted cuprizone formulations. Therefore, the next published paper of this thesis presents this data comparing the two methods of cuprizone administration.

4.1. Study Rationale

To my knowledge there had been only one study prior to this work that investigated the effectiveness of pelleted cuprizone in direct comparison with powdered cuprizone, which showed that cuprizone pellets were not as potent as powdered cuprizone to induce demyelinating disease (Hochstrasser et al. 2017). This study compared powdered and pelleted cuprizone at a 0.25% cuprizone dose (Hochstrasser et al. 2017), rather than the more commonly utilised 0.2% dosage (Hiremath et al. 1998), and employed a model centred more around remyelination, allowing 2 weeks of remyelination following an acute 3 week cuprizone exposure. Their analysis of the tissue did not include measures of oligodendroglial loss and astrogliosis. In the current study, a 0.2% dose of cuprizone was utilised, fed in both powdered and pelleted form, with appropriate control groups for both feed formulations, and a comprehensive analysis of the tissue was performed looking at a wide range of pathological hallmarks of cuprizone-mediated damage at a 3 week timepoint.

The 3 week timepoint was specifically chosen as this is when early demyelination should become observable in the corpus callosum, and a point at which gliosis, oxidative stress and oligodendroglial changes should already be established (Gudi et al. 2014) (Figure 4.1). The reliable appearance of this early demyelinating pathology is critical for our work, as we hypothesise that the oxidative stress associated initiating mechanisms of damage occur within the first few weeks of cuprizone administration. Furthermore, it had already been well established in the literature that by 5 weeks of administration of 0.2% cuprizone pellets, extensive demyelination has occurred (Danesh-Seta et al. 2021; Gonsalvez et al. 2019; Klein et al. 2018; Mazloumfard et al. 2020; Mohammadi-Rad et al. 2019; Ohgomori & Jinno 2019; Steelman et al. 2012; Tagge et al. 2016).

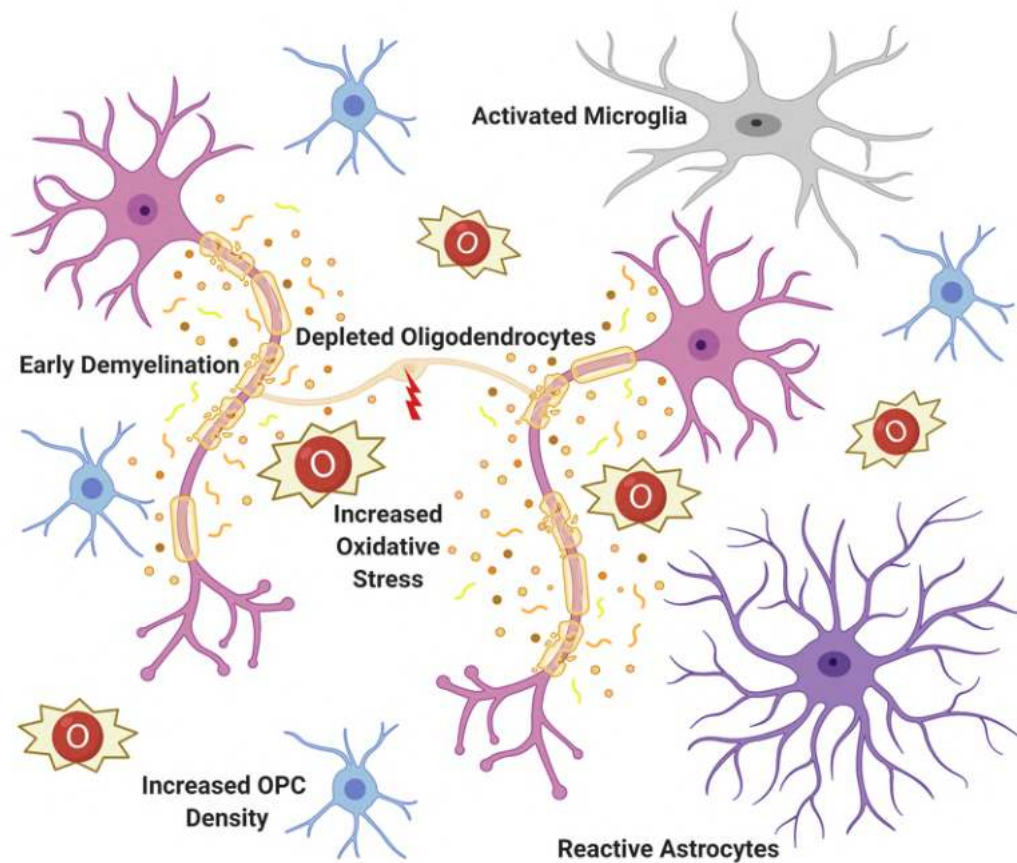


Figure 4.1. Expected demyelinating disease pathology within the corpus callosum following 3 weeks of cuprizone intoxication. By 3 weeks of cuprizone administration, early demyelination has become histologically detectable and there is a severe depletion of mature oligodendrocytes with a concomitant increase in the density of OPCs. Furthermore, by this timepoint reactive gliosis is well underway, with an increase in the density and hypertrophy of astrocytes, as well as high levels of microglial activation and oxidative stress. For more details on the expected time course and pathology of cuprizone intoxication, see Section 1.2.7.2. Original illustration created using BioRender.com.

4.2. Study Design and Animal Procedures

To directly compare the effects of powdered and pelleted cuprizone, an experiment was designed using forty-eight mice as illustrated in Figure 4.2. There were two cuprizone administration groups and two age-matched control groups ($n = 6/\text{group}$), with one group from each receiving their feed in a powdered form and one group in a pelleted form. Mice were provided equivalent amounts of either cuprizone or control feed throughout the study. Mice were weighed daily during the experimental period prior to being euthanased after 3 weeks of continuous feeding with either cuprizone or control feed. The tissue collected was then processed and immunohistochemically and histologically analysed. For this study, the pelleted cuprizone was made by a different supplier (Specialty Feeds) than in the previously presented cohorts from Chapters 2 and 3 (Envigo). These pellets were manufactured locally using the same batch of powdered cuprizone administered to the powdered cuprizone animals, with the aim to minimise variability between the two cuprizone groups. The feed formulation used as a base diet to create the cuprizone-containing pellets was the Specialty

Feeds Meat Free Rat and Mouse Diet, which was then utilised in either a powdered or pelleted form as the control diet to ensure nutritional similarity between delivered feeds.

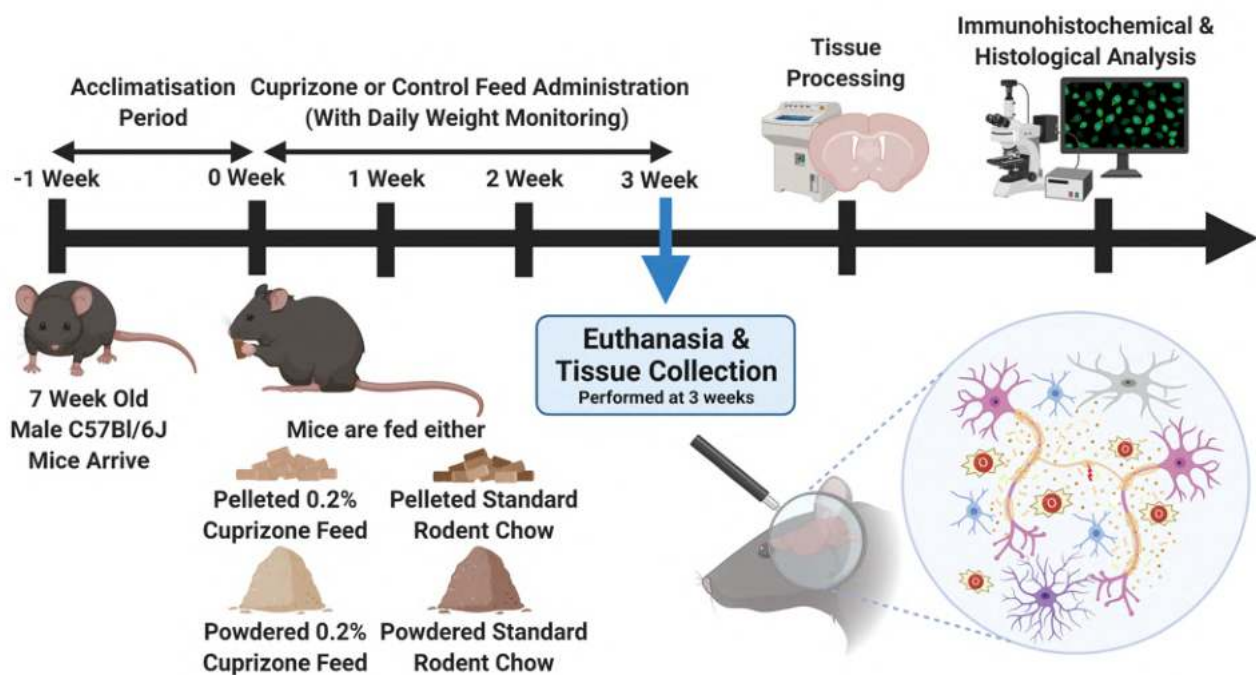


Figure 4.2. Experimental design for the direct comparison between powdered and pelleted cuprizone formulations. Two groups received 0.2% cuprizone for 3 weeks in either a powdered or pelleted formulation, and two age-matched control groups received either powdered or pelleted standard rodent chow (n = 6/group, total n = 24). Mice were 8 weeks of age at the commencement of the study and were weighed daily during the 3 week experimental period. Following euthanasia and tissue collection, the collected brains were cryosectioned and analysed for hallmarks of demyelinating disease pathology. Original illustration created using BioRender.com.

4.3. Optimisation of Immunohistochemistry

Since the majority of the research within the Fitzgerald laboratory to date had been performed on rat tissue, the immunohistochemical procedure had to be specifically optimised for use on the obtained mouse tissue. One of the key methodological differences between the rat and mouse protocols involved applying an unconjugated donkey anti-mouse immunoglobulin G (IgG) when utilising primary antibodies that were raised in mice to act as a mouse on mouse block. Though a similar step was included in the paper presented in Appendix B, that study utilised an unconjugated anti-mouse IgG2a antibody. This antibody solely reacted with the mouse IgG2a subclass, despite one of the three mouse antibodies used in that study having a IgG2b isotype. Therefore, it was instead more appropriate to switch to a broader unconjugated anti-mouse IgG H&L antibody that would block all of the heavy and light chains of mouse IgG subclasses. The utilisation of this broader unconjugated anti-mouse IgG H&L antibody for the forthcoming work ensured a more comprehensive mouse on mouse block to prevent cross-binding with all endogenous mouse IgG antigens when using primary

antibodies raised in mouse on the tissue, regardless of the primary antibody isotype. Another methodological difference was that all immunohistochemical experiments were performed with the tissue sections in 24 well plates rather than using tissue that had already been mounted onto slides to allow for double-sided antibody tissue penetration for more extensive antibody binding. Furthermore, an additional 30 minute incubation period at room temperature was included during the primary antibody incubation step prior to the well plates being transferred to 4°C overnight to also ensure maximal antibody binding. This modified protocol (Figure 4.3) proved highly optimal for mouse tissue and was therefore utilised for the forthcoming cuprizone paper.

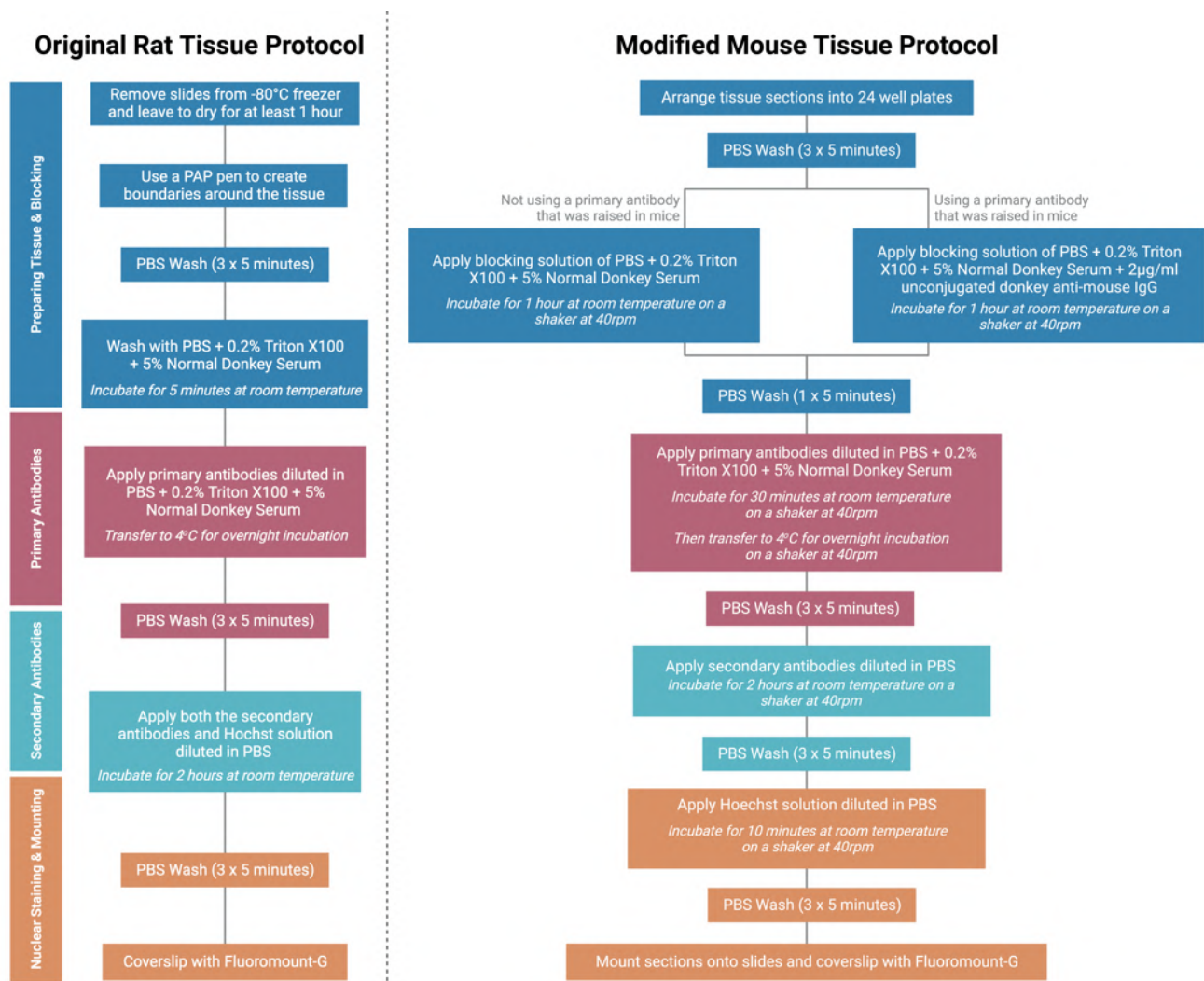


Figure 4.3. The modified immunohistochemistry protocol for use on mouse brain tissue sections. The original protocol had been typically utilised for rat tissue and is presented as described in previously published Fitzgerald group articles, including in Fitzgerald et al. 2010 and Toomey et al. 2019. The modified protocol has since been specifically optimised for mouse brain tissue and is as published in Toomey et al. 2021.

4.4. Study Outcomes

To determine the degree to which powdered and pelleted cuprizone induced pathology, various immunohistochemical and histological parameters were investigated, including oligodendrocyte loss, gliosis, oxidative stress and demyelination. Both the rostral and caudal medial corpus callosum were analysed, to investigate region specific changes in response to cuprizone feed formulation.

Within the rostral medial corpus callosum, the cuprizone-containing pellets were more efficacious than cuprizone powder at increasing the extent of astrogliosis, increasing microglial activation, inducing oxidative DNA damage and reducing the density of mature oligodendrocytes. However, the cuprizone powder was more potent at inducing oxidative protein nitration compared to the relative control feed. It is also important to note that within this rostral region, mice fed the control powder had a significantly decreased density of mature oligodendrocytes compared to those fed the control pellets, suggesting that there may be inherent metabolic differences between powdered and pelleted feed that particularly affects oligodendroglia. Previous studies have tended to either use a pelleted control for powdered cuprizone feed or not explicitly indicate the control feed formulation employed. In line with this, if the number of overall oligodendroglial cells as shown by positive Olig2 staining is compared between powdered cuprizone and pelleted control, rather than powdered control, the loss of oligodendroglia that has been reported in previous cuprizone studies at the 3 week timepoint becomes apparent. Therefore, this highlights the importance of using an appropriate control feed formulation to ensure a reliable comparison with mice administered cuprizone.

Within the caudal medial corpus callosum, cuprizone pellets were again more effective than cuprizone powder for inducing the desired demyelinating pathology compared to the relative controls, with the pelleted cuprizone group demonstrating increased astrogliosis, increased microglial activation, increased oxidative protein nitration and DNA damage, increased tissue swelling, decreased density of mature oligodendrocytes, and increased demyelination. The two feed formulations performed similarly for inducing changes to OPC dynamics.

Taken together, cuprizone pellets therefore performed either equal to or superior than cuprizone powder for inducing acute demyelinating disease compared to controls, particularly within the caudal corpus callosum. This regional specificity of cuprizone was in line with previous studies which have indicated a rostro-caudal pattern of demyelination in the medial corpus callosum with cuprizone intoxication (Steelman et al. 2012; Stidworthy et al. 2003; Wu et al. 2008; Xie et al. 2010).

Interestingly, the mice fed cuprizone powder lost a significant proportion of their body weight during cuprizone administration compared to those fed control powder, whereas those fed cuprizone pellets remained at an average body weight similar to controls. Thus, though weight loss during cuprizone intoxication has previously been considered to be indicative of the efficacy of the cuprizone

at inducing demyelinating disease (Steelman et al. 2012; Stidworthy et al. 2003), this study indicates that body weight may not be such a reliable proxy for cuprizone pathology. Instead, it is thought that the palatability of the cuprizone powder was reduced, resulting in an initially decreased consumption of this formulation and therefore a reduced or delayed onset of demyelinating disease. It is critical to note however that although the overall extent of cuprizone pathology was decreased in the powdered formulation group with demyelination not detectable in these mice, there was nevertheless a reduction in mature oligodendrocyte density. This loss of oligodendrocyte suggests that a degree of cuprizone intoxication did still occur and that a more extended administration period may have induced detectable demyelination. Nevertheless, the overall results of this study indicated that cuprizone pellets were a more efficacious cuprizone delivery method than cuprizone powder for inducing demyelinating disease at the early 3 week timepoint.

4.5. Introducing “Cuprizone feed formulation influences the extent of demyelinating disease pathology”

This study is presented below and has been published as:

Toomey L.M., Papini, M., Lins, B., Wright, A.J., Warnock, A., McGonigle, T., Bartlett, C.A., Hellewell, S.C., Anyaegbu, C., and Fitzgerald, M. 2021. Cuprizone feed formulation influences the extent of demyelinating disease pathology. *Scientific Reports*, 11(1), 1-16. doi.org/10.1038/s41598-021-01963-3



OPEN Cuprizone feed formulation influences the extent of demyelinating disease pathology

Lillian M. Toomey^{1,2}, Melissa Papini¹, Brittney Lins¹, Alexander J. Wright¹, Andrew Warnock¹, Terence McGonigle¹, Sarah C. Hellewell¹, Carole A. Bartlett¹, Chidozie Anyaegbu¹ & Melinda Fitzgerald^{1,2✉}

Cuprizone is a copper-chelating agent that induces pathology similar to that within some multiple sclerosis (MS) lesions. The reliability and reproducibility of cuprizone for inducing demyelinating disease pathology depends on the animals ingesting consistent doses of cuprizone. Cuprizone-containing pelleted feed is a convenient way of delivering cuprizone, but the efficacy of these pellets at inducing demyelination has been questioned. This study compared the degree of demyelinating disease pathology between mice fed cuprizone delivered in pellets to mice fed a powdered cuprizone formulation at an early 3 week demyelinating timepoint. Within rostral corpus callosum, cuprizone pellets were more effective than cuprizone powder at increasing astrogliosis, microglial activation, DNA damage, and decreasing the density of mature oligodendrocytes. However, cuprizone powder demonstrated greater protein nitration relative to controls. Furthermore, mice fed control powder had significantly fewer mature oligodendrocytes than those fed control pellets. In caudal corpus callosum, cuprizone pellets performed better than cuprizone powder relative to controls at increasing astrogliosis, microglial activation, protein nitration, DNA damage, tissue swelling, and reducing the density of mature oligodendrocytes. Importantly, only cuprizone pellets induced detectable demyelination compared to controls. The two feeds had similar effects on oligodendrocyte precursor cell (OPC) dynamics. Taken together, these data suggest that demyelinating disease pathology is modelled more effectively with cuprizone pellets than powder at 3 weeks. Combined with the added convenience, cuprizone pellets are a suitable choice for inducing early demyelinating disease pathology.

The cuprizone-induced animal model is a toxin-based method of producing demyelinating disease similar to that observed in the brains of people with MS. Cuprizone (or *bis*-cyclohexanone oxaldihydrazone) is a copper chelating agent that is orally administered to rodents to induce oligodendroglial death, glial cell activation and demyelination via mitochondrial dysfunction^{1–3}. Cuprizone induces mitochondrial injury and oxidative stress by increasing mitochondrial production of superoxide anions⁴, reducing copper-dependent cytochrome *c* oxidase and monoamine oxidase activity⁵, decreasing copper-zinc superoxide dismutase⁵ and glutathione⁶ antioxidant activity, and inhibiting electron transport chain complex IV⁷. Oligodendrocytes are particularly vulnerable to cuprizone-induced mitochondrial dysfunction⁷, resulting in apoptosis¹ and subsequent loss of myelin⁴. In addition, mitochondrial dysfunction in oligodendrocytes results in endoplasmic reticulum stress^{8–10}, causing further downregulation of myelin proteins¹¹ and reduced myelin lipid synthesis⁴. In humans, copper deficiency results in CNS demyelination^{12–14}. Furthermore, mitochondrial electron transport chain complex IV dysfunction in oligodendrocytes has been found in type III active MS lesions¹⁵. However, cuprizone may also induce its biological effects via copper-independent mechanisms¹⁶. Concomitant copper supplementation alongside cuprizone administration does not completely attenuate the observed degenerative effects¹⁷. Furthermore, it has been suggested that the effects of cuprizone on oligodendrocyte metabolism are related to a Schiff base formation binding with the amino acid metabolism coenzyme pyridoxal 5'-phosphate, and completely independent of copper chelation¹⁸.

¹Curtin Health Innovation Research Institute, Curtin University, Bentley WA 6102, Australia. ²Perron Institute for Neurological and Translational Science, Sarich Neuroscience Research Institute Building, 8 Verdun St, Nedlands, WA 6009, Australia. ✉email: lindy.fitzgerald@curtin.edu.au

A recent study has also discovered that the copper chelating action of cuprizone produces dysregulation of iron homeostasis, leading to ferroptosis-mediated loss of oligodendrocytes and myelin¹⁹.

Irrespective of its mechanism of action, cuprizone is a widely utilised and validated toxin for modelling CNS demyelination that is not directly associated with peripheral autoimmunity²⁰. Furthermore, cuprizone intoxication is a useful tool for studying the processes of remyelination, as withdrawal of cuprizone typically results in remyelination in the CNS of the intoxicated animal²¹, albeit at a significantly slower rate following chronic cuprizone intoxication²².

While cuprizone mainly affects oligodendrocyte myelination, indirect effects on other cell types in the CNS can be observed. For example, as early as 1 week into cuprizone intoxication, microglia are activated within both the cortex and the corpus callosum²³. Astrocytes exhibit morphological changes as early as 1 week, with numbers of astrocytes significantly increasing from 3 weeks of cuprizone administration²⁴. Also by 3 weeks, OPCs have accumulated in the corpus callosum, particularly in the caudal regions, ready to act as a progenitor pool for the differentiation and maturation of new oligodendrocytes^{25,26}.

The reliability and reproducibility of a cuprizone-induced model of demyelinating disease depends critically on the animals ingesting the full dose of cuprizone consistently in different studies. Traditionally, cuprizone has been delivered in powdered form mixed into ground rodent chow, but in recent years pelleted formulations of cuprizone that allow more convenient handling and feeding have become available. Despite some evidence suggesting that pelleted formulations of cuprizone can be less effective^{27,28}, the use of cuprizone in a pelleted form is growing in popularity, with many research groups successfully utilising the pelleted form at chronic timepoints^{29–36}. However, one study in particular noted that their cuprizone-containing pellets failed to induce demyelination despite toxicological analysis of the pellets confirming that they still contained active cuprizone²⁸. Another study has directly compared the potency of cuprizone pellets and powder and demonstrated that cuprizone powder was more effective at inducing demyelinating pathology than pellets at an equivalent dose of cuprizone²⁷. This study used a 0.25% dose of cuprizone, rather than the more commonly used 0.2% cuprizone dose²⁴ and included 2 weeks remyelination after the 3 week cuprizone administration²⁷. Effects of the different feed formulations on oligodendroglial death and astrogliosis were not assessed. Information on the effects of pelleted cuprizone at the early 3 week timepoint during demyelination is lacking. In the present study, we assessed the potency of pelleted and powdered cuprizone at an early demyelinating timepoint. 0.2% cuprizone was delivered in both powdered and pelleted form and outcomes were assessed following 3 weeks of cuprizone administration. Various cytochemical and immunohistochemical parameters, including oligodendroglial death, gliosis, oxidative stress and demyelination, were investigated to determine the extent to which powdered and pelleted cuprizone differ in their capacity to induce the hallmarks of cuprizone-intoxication in the CNS.

Results

Effects of cuprizone feed formulation on body weight. Following 3 weeks on diets of control powder, cuprizone-containing powder, control pellet or cuprizone-containing pellet, mice were assessed for weight loss, a widely recognised hallmark of cuprizone intoxication³⁴. Post-hoc analyses revealed that mice administered cuprizone powder had significantly lower body weight than those fed control powder from 7 days of cuprizone until the end of the study ($p < 0.05$; Fig. 1). However, mice fed cuprizone pellets did not have any significant differences in body weight compared to their control pellet counterparts at any timepoint ($p > 0.05$). There were no differences between cuprizone pellet and cuprizone powder ($p > 0.05$).

Effects of cuprizone feed formulation on inflammatory responses. Within the rostral corpus callosum the area of GFAP immunoreactivity, indicative of astrocyte reactivity, significantly increased when cuprizone was delivered in the form of pellets compared to control pelleted feed ($p < 0.0001$; Fig. 2a,c). Similarly, the area of GFAP immunoreactivity increased with powdered cuprizone delivery when compared to control powdered feed ($p = 0.0158$). There were no significant differences between control groups or cuprizone groups ($p = 0.999$ and $p = 0.144$ respectively). Within the caudal corpus callosum, mice fed pelleted cuprizone again had a significantly greater area of GFAP immunoreactivity than those fed control pellets ($p = 0.002$; Fig. 2b,c). However, in the caudal region of the corpus callosum, animals fed cuprizone in the form of powder did not have increased GFAP immunoreactivity when compared to those fed control powder ($p = 0.980$). When cuprizone was delivered in the form of pellets, there was a significantly greater area of GFAP immunoreactivity than when it was delivered in the form of powder ($p = 0.007$). There were no differences between the two control groups ($p = 0.998$).

Within the rostral corpus callosum, the area of IBA1 immunoreactivity, indicative of microglial activation, significantly increased when cuprizone was delivered in the form of pellets compared to control pelleted feed ($p = 0.0005$; Fig. 2d,f). There was also an increase in the area of IBA1 immunoreactivity when cuprizone was delivered as powder compared to control powdered feed ($p = 0.0095$). There were no differences between the two control groups ($p = 0.920$) or the two cuprizone groups ($p = 0.254$). Within the caudal corpus callosum, mice fed pelleted cuprizone had a significantly greater area of IBA1 immunoreactivity than those fed control pellets ($p < 0.0001$; Fig. 2e,f). It is worth noting that IBA1 immunoreactivity in these cuprizone pellet fed animals was considerably more pronounced in caudal than rostral corpus callosum (Fig. 2f). However in caudal corpus callosum there was no significant increase in the area of IBA1 immunoreactivity when cuprizone was delivered as powder compared to control powdered feed ($p = 0.9527$). Similarly to the findings with GFAP, when cuprizone was delivered in the form of pellets, there was significantly more IBA1 immunoreactivity than when it was delivered in the form of powder ($p < 0.0001$). There were no differences between the two control groups ($p > 0.999$).

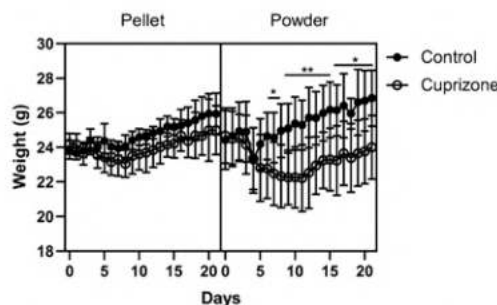


Figure 1. Effects of cuprizone feed formulation on animal weights. Animals were weighed daily to assess weight loss throughout cuprizone administration. Cuprizone was delivered in either pelleted or powdered form. $N = 6$ mice per group; graph displays mean weight \pm SEM. Significant differences are indicated by * $p \leq 0.05$, ** $p \leq 0.01$.

Effects of cuprizone feed formulation on oxidative stress. Within the rostral corpus callosum the area of 3-NT immunoreactivity, indicative of protein nitration, was not affected by delivery of cuprizone in the form of pellets ($p = 0.1929$, Fig. 3a,c). In contrast, the area of 3-NT significantly increased when cuprizone was delivered in the form of powder compared to control powdered feed ($p < 0.0001$). When cuprizone was delivered in the form of powder, there was a significantly greater area of 3-NT immunoreactivity than when it was delivered in the form of pellets ($p = 0.0008$). There were no differences between the two control groups ($p = 0.9897$). In contrast, within the caudal corpus callosum, mice fed pelleted cuprizone had a significantly greater area of 3-NT immunoreactivity than those fed control pellets ($p = 0.0002$; Fig. 3b,c). Similarly to the pattern of IBA1 immunoreactivity, 3-NT immunoreactivity was more pronounced caudally than rostrally (Fig. 3c). However there was no increase in the area of 3-NT immunoreactivity when cuprizone was delivered as powder compared to control powdered feed ($p = 0.2051$). When cuprizone was delivered in the form of pellets, there was a significantly greater area of 3-NT immunoreactivity than when it was delivered in the form of powder ($p = 0.0138$). There were no differences between the two control groups ($p = 0.9997$).

Within the rostral corpus callosum the area of 8OHdG immunoreactivity, indicative of oxidative DNA damage, significantly increased when cuprizone was delivered in the form of pellet compared to control pelleted feed ($p = 0.005$; Fig. 3d,f). However there was no significant difference when cuprizone was delivered as powder, compared to control powdered feed ($p = 0.2353$). There were no differences between the two control groups ($p = 0.9931$) or the two cuprizone groups ($p = 0.1679$). Within the caudal corpus callosum, mice fed pelleted cuprizone had a significantly greater area of 8OHdG immunoreactivity than those fed control pellets ($p < 0.0001$; Fig. 3e,f). There was also an increase in the area of 8OHdG immunoreactivity when cuprizone was delivered as powder compared to control powdered feed ($p = 0.0021$). There were no differences between the two control groups ($p > 0.9999$) or the two cuprizone groups ($p = 0.487$).

Effects of cuprizone feed formulation on tissue swelling. The area of the rostral corpus callosum was not significantly different between either of the two pellet groups ($p = 0.9462$; Fig. 4a,e) or powder groups ($p = 0.2868$). There was also no difference between the two control groups ($p = 0.1659$), but there was a significant increase in the size of the rostral corpus callosum when cuprizone was delivered as a powder compared to pellets ($p = 0.0122$). The area of the caudal corpus callosum was significantly larger in mice fed pelleted cuprizone than those fed control pellets ($p < 0.0001$; Fig. 4b,e). There was also an increase in the area of the caudal corpus callosum when cuprizone was delivered as powder compared to control powdered feed ($p = 0.0114$). There were no differences between the two control groups ($p = 0.0552$) or the two cuprizone groups ($p = 0.7506$).

To determine whether the enlarged corpus callosum was due to a general increase in cell density, the number of Hoechst+ cells per mm^2 was quantified. In the rostral ($p > 0.05$; Fig. 4c,e) and caudal ($p > 0.05$, Fig. 4d,e) corpus callosum there were no significant differences between groups. This suggests that variation in size of the corpus callosum is due to swelling, rather than increased cell density.

Effects of cuprizone feed formulation on oligodendroglia. Within the rostral corpus callosum the density of Olig2+ cells, broadly indicative of oligodendroglia, significantly decreased when cuprizone was delivered in the form of pellets compared to control pelleted feed ($p = 0.0001$; Fig. 5a,c,i). In contrast, cuprizone powder did not result in a significantly decreased density of Olig2+ cells, when compared to mice fed control powder ($p = 0.3723$). Interestingly, however, when powdered cuprizone was compared to pelleted control, the density of Olig2+ cells decreased in the caudal ($p < 0.0021$) and rostral ($p < 0.0001$) corpus callosum (Fig. 5a–d,i). When the control feed was delivered as a powder rather than as pellets, there was a significant decrease in the density of Olig2+ cells ($p < 0.0001$). There was no significant difference between the two cuprizone groups ($p = 0.2262$). Within the caudal corpus callosum, there were no differences between mice fed control pellets and cuprizone pellets ($p = 0.6126$; Fig. 5b,d,i), or those fed control powder and cuprizone powder ($p = 0.9609$). Again, control

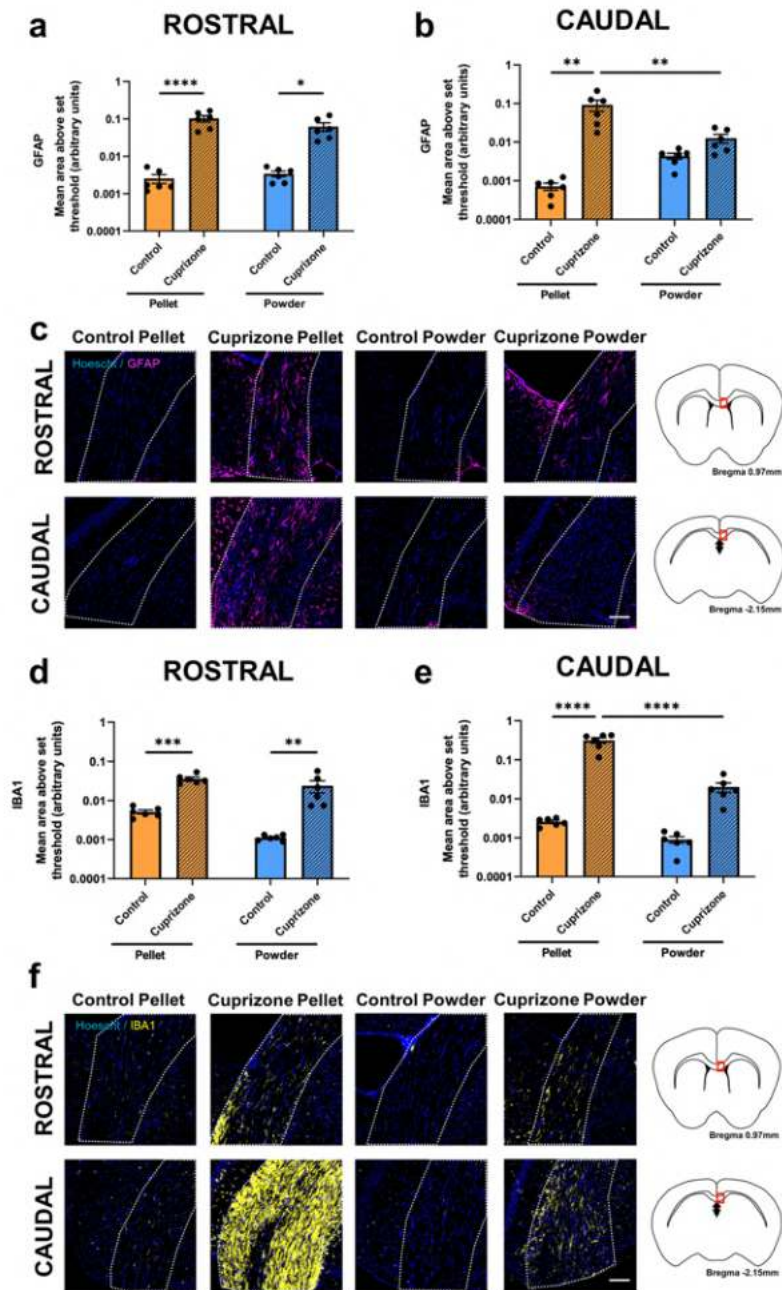


Figure 2. Effects of cuprizone feed formulation on glial reactivity. Area of immunointensity of GFAP in the rostral (a) and caudal (b) corpus callosum was assessed to determine the level of astrocyte reactivity. Area of immunointensity of IBA1 in the rostral (d) and caudal (e) corpus callosum was assessed to determine the level of microglial activation. N=6 mice per group, graphs display individual data points overlaid on a bar displaying the mean \pm SEM. Significant differences are indicated by * $p \leq 0.05$, ** $p \leq 0.01$, *** $p \leq 0.001$, **** $p \leq 0.0001$. Representative images of the area of GFAP (c) and IBA1 (f) immunoreactivity is shown, scale bars = 100 μ m. Area of the corpus callosum analysed is denoted by dotted lines. This area is indicated by the red box in the coronal overviews illustrating the rostral and caudal regions of the corpus callosum (c,f). The stereotaxic coordinates are indicated.

powder led to lower density of Olig2+ cells than in mice fed control pellets ($p=0.0007$), cuprizone powder also resulted in a lower density of Olig2+ cells than cuprizone pellet ($p=0.0332$).

To quantify OPCs, PDGFR α was utilised both alone, and in combination with Olig2³⁷. Within the rostral corpus callosum there were no significant differences in the density of PDGFR α + cells between any of the groups ($p>0.05$; Fig. 5a,e,i). Within the caudal corpus callosum, the number of PDGFR α + cells significantly increased when cuprizone was delivered as pellets compared to control pelleted feed ($p<0.0001$; Fig. 5b,f,i). Similarly, the number of PDGFR α + cells significantly increased when cuprizone was delivered in the form of powder compared to control powdered feed ($p=0.0005$). There was no difference between the two control groups ($p=0.9908$) or the two cuprizone groups ($p=0.2258$).

Similar to the analyses of PDGFR α + cells, there were no differences in density of Olig2+/PDGFR α + cells between any of the groups in rostral corpus callosum ($p>0.05$; Fig. 5a,g,i). Within the caudal corpus callosum, the density of Olig2+/PDGFR α + cells significantly increased when cuprizone was delivered as pellets compared to control pelleted feed ($p=0.0195$; Fig. 5b,h,i). Similarly, the number of Olig2+/PDGFR α + cells significantly increased when cuprizone was delivered in the form of powder compared to control powdered feed ($p=0.0272$). There was no difference between the two control groups ($p=0.9969$) or the two cuprizone groups ($p>0.9999$).

ASPA and CC1 were used to enumerate mature oligodendrocytes³⁸. Within the rostral corpus callosum there was a significant decrease in the density of ASPA+ cells when cuprizone was delivered as pellets compared to control pelleted feed ($p=0.0004$, Fig. 6a,c,g). However, there was no difference in ASPA+ cell density between mice fed control powder or cuprizone powder ($p=0.1851$). Interestingly, similar to the Olig2+ cell counts, there was a decrease in the density of ASPA+ cells in the control powder group compared to the control pelleted group ($p=0.0100$). There were no significant differences between the two cuprizone groups ($p=0.9017$). Within the caudal corpus callosum, there was a significant decrease in the density of ASPA+ cells with both cuprizone pellets ($p<0.0001$, Fig. 6b,d,g) and cuprizone powder ($p=0.0002$) compared to their relative control groups. There were no differences between control groups ($p=0.4154$) or the two cuprizone groups ($p=0.6206$).

Within the rostral corpus callosum there was no difference in CC1+ cell density between mice fed cuprizone pellet ($p=0.0536$, Fig. 6a,e,g) or cuprizone powder ($p=0.9875$) compared to their relative control groups. However, again there was a significant decrease in the density of CC1+ cells in mice fed control powder compared to those fed control pellets ($p=0.0182$). There were no differences between cuprizone groups ($p=0.8352$). Within the caudal corpus callosum, there was a significant decrease in density of CC1+ cells only when cuprizone was delivered as pellets ($p=0.0114$, Fig. 6b,f,g), and not when it was delivered as a powder ($p=0.6875$), compared to the relative control groups. There were no significant differences between control groups ($p=0.2943$) or cuprizone groups ($p=0.9423$). It is worth noting that the density of CC1+ cells was generally higher than the density of ASPA+ cells (Fig. 6a–d) and not all CC1+ cells were ASPA+ (Fig. 6g; yellow arrow).

Effects of cuprizone feed formulation on myelination. Utilising the histological stain Myelin Black-Gold II as a marker for myelination, there were no significant differences in the level of myelination within the rostral corpus callosum between groups ($p>0.05$, Fig. 7a,c,e). Within the caudal corpus callosum, there was a significant decrease in myelination only when cuprizone was delivered in the form of pellets ($p=0.0199$, Fig. 7b,d,e), and not when it was delivered as a powder ($p=0.1025$), compared to the relative control groups. There were no significant differences between control groups ($p=0.7038$) or cuprizone groups ($p=0.2659$). Note, the pink hue present in the control powder group was replicated across multiple staining runs and does not affect the analysis.

Discussion

Though the efficacy of cuprizone pellets has been debated^{27,28}, research has proven that at more chronic time-points cuprizone pellets can induce reliable demyelination^{29–35}. Therefore, in this study we investigated the extent that cuprizone pathology is dependent on feed formulation at an early 3 week timepoint. Across most of the outcome measures analysed, cuprizone pellets were generally better than cuprizone powder at inducing early demyelinating disease pathology compared to their relative controls, particularly in the caudal corpus callosum (Table 1). Cuprizone pellets are a more convenient route of cuprizone administration, as they can be commercially custom made and do not require daily replacement to ensure activity is not compromised by rodent urine. Cuprizone pellets also pose a lower inhalation risk to the researcher than powdered cuprizone.

In this study, mice were given equivalent quantities of cuprizone regardless of feed formulation, and feed was replenished in line with standard protocols^{34,39}, therefore it is likely that the observed differences between formulations is due to differences in consumption of the feed between different formulations. Weight loss in cuprizone-fed animals over the first week of administration is thought to be indicative that the drug is efficacious at producing demyelinating pathology^{34,40}. However, the more pronounced differences in astrocyte reactivity, microglial activation, oxidative stress, tissue swelling and demyelination within the cuprizone pellet group compared to their controls at 3 weeks, despite no significant weight loss, suggest that weight loss may not be a reliable proxy of the extent of demyelinating disease. Instead, the initial weight loss observed in mice fed the cuprizone powder despite reduced cuprizone pathology suggests that the weight loss was due to the mice not ingesting the powdered cuprizone feed. It is plausible that the addition of cuprizone to powdered chow changes the palatability of the feed⁴¹, but why this did not occur with the cuprizone pellets is currently unclear. Nevertheless, the current data suggest that reduced palatability and subsequent aversion to the powdered cuprizone by the mice may result in the animals initially not ingesting the powdered feed and thus having a reduced or perhaps a delayed effect of cuprizone at the 3 week timepoint. However, a time course comparison study would be needed to fully elucidate whether the reduced ingestion of the feed resulted in a delayed onset of cuprizone-induced pathology. Importantly, it is clear that cuprizone intoxication did take place with the powdered cuprizone, as ASPA+

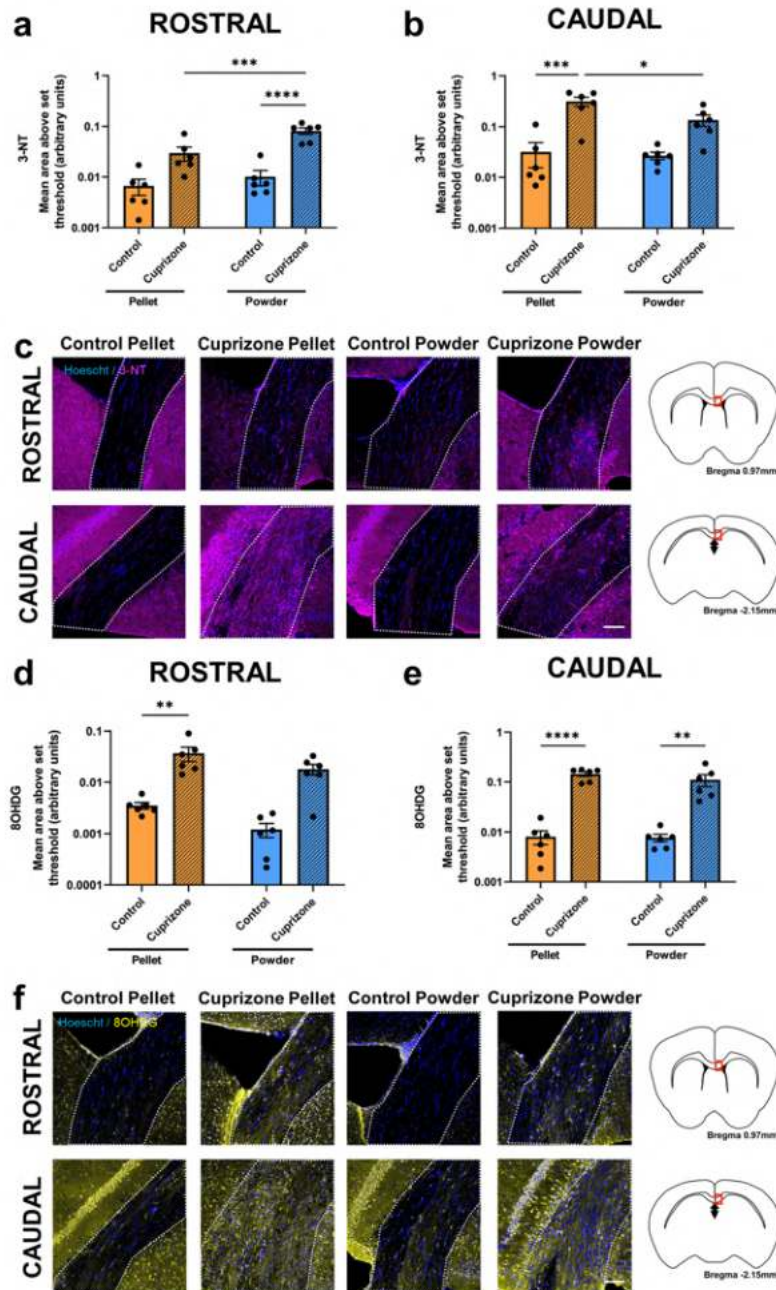


Figure 3. Effects of cuprizone feed formulation on oxidative stress. Area of immunointensity of 3-NT in the rostral (a) and caudal (b) corpus callosum was assessed to determine the level of protein nitration. Area of immunointensity of 8OHDG in the rostral (d) and caudal (e) corpus callosum was assessed to determine the level of oxidative DNA damage. N = 6 mice per group, graphs display individual data points overlaid on a bar displaying the mean \pm SEM. Significant differences are indicated by * $p \leq 0.05$, ** $p \leq 0.01$, *** $p \leq 0.001$, **** $p \leq 0.0001$. Representative images of the area of 3-NT (c) and 8OHDG (f) immunoreactivity are shown, scale bars = 100 μ m. Area of the corpus callosum analysed is denoted by dotted lines. This area is indicated by the red box in the coronal overviews illustrating the rostral and caudal regions of the corpus callosum (c,f). The stereotaxic coordinates are indicated.

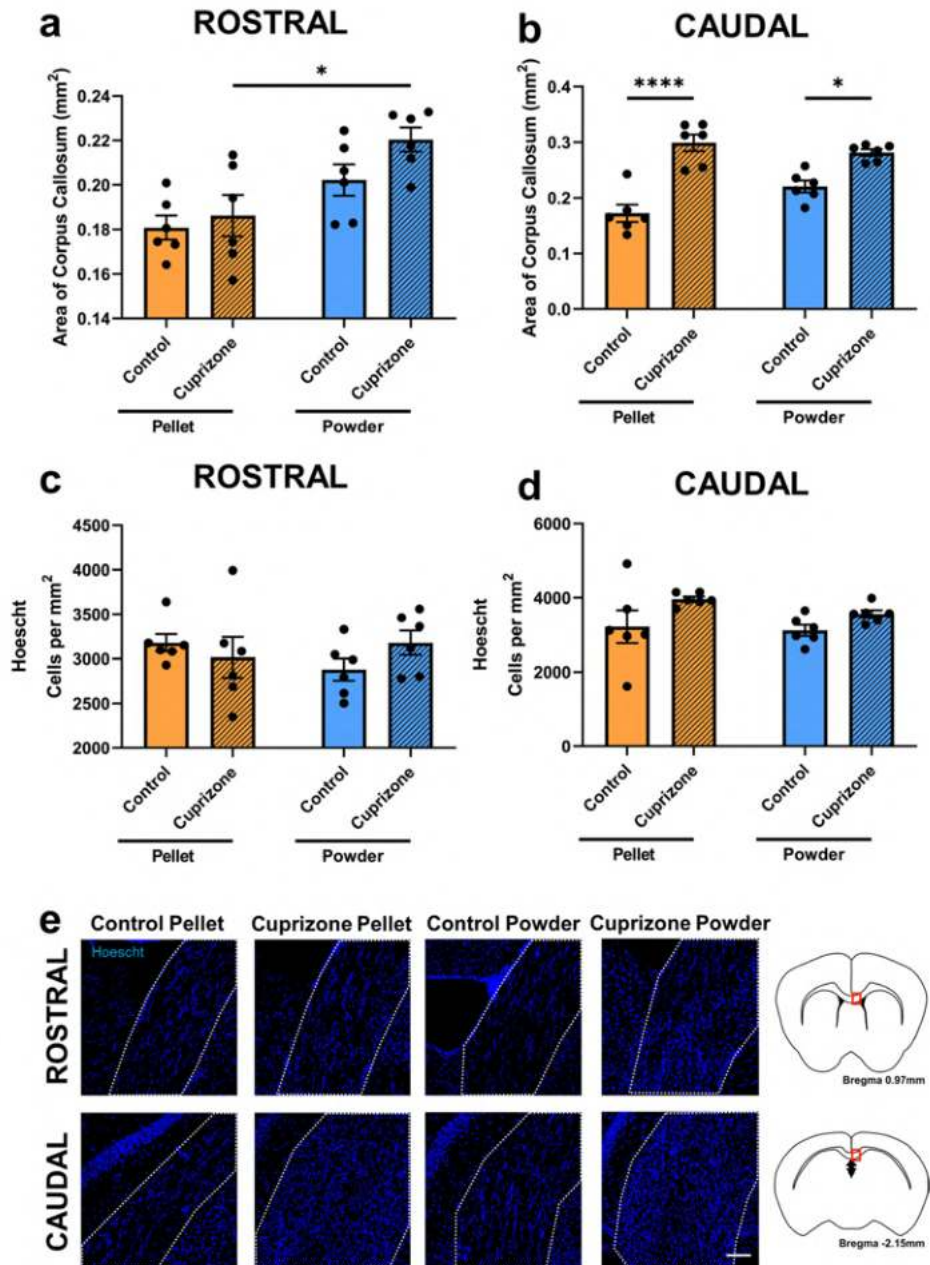


Figure 4. Effects of cuprizone feed formulation on tissue swelling. The area of the corpus callosum in the rostral (a) and caudal (b) areas was assessed. The density of Hoechst+ cells was also quantified in the rostral (c) and caudal (d) corpus callosum. N = 6 mice per group, graphs display individual data points overlaid on a bar displaying the mean ± SEM. Significant differences are indicated by * $p \leq 0.05$, ** $p \leq 0.01$, *** $p \leq 0.001$, **** $p \leq 0.0001$. Representative images Hoechst+ cells (e) is shown, scale bars = 100 μm . Area of the corpus callosum analysed is denoted by dotted lines. This area is indicated by the red box in the coronal overviews illustrating the rostral and caudal regions of the corpus callosum (e). The stereotaxic coordinates are indicated.

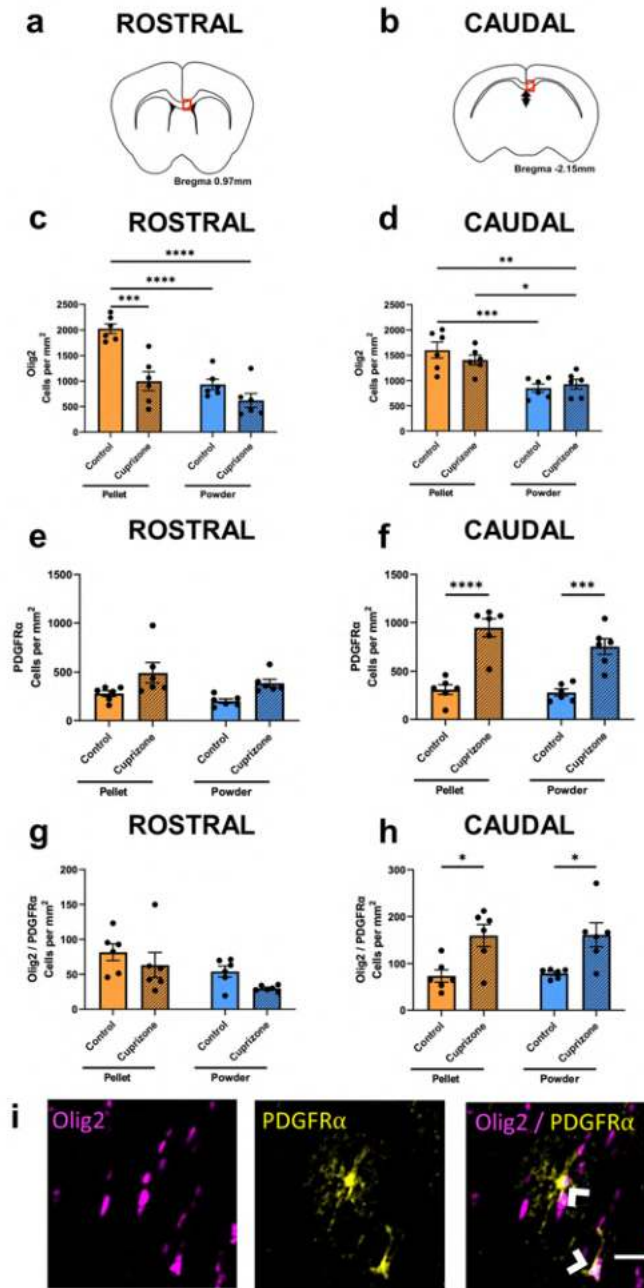


Figure 5. Effects of cuprizone feed formulation on densities of Olig2⁺, PDGFRα⁺ and Olig2⁺/PDGFRα⁺ cells. The area of the rostral and caudal corpus callosum analysed is denoted by the red box in the coronal illustrations of the brain (a,b). The density of Olig2⁺ cells (c,d), PDGFRα⁺ cells (e,f) and Olig2⁺/PDGFRα⁺ cells (g,h) were quantified in the rostral and caudal corpus callosum. N = 6 mice per group, graphs display individual data points overlaid on a bar displaying the mean ± SEM. Significant differences are indicated by *p ≤ 0.05, **p ≤ 0.01, ***p ≤ 0.001, ****p ≤ 0.0001. (i) Representative images of Olig2⁺, PDGFRα⁺ and Olig2⁺/PDGFRα⁺ cells, indicated with arrow heads; scale bar = 25 μm.

oligodendrocytes were reduced in the caudal corpus callosum with this formulation, relative to the appropriate control powdered feed. It has also been suggested that for effectively inducing demyelinating disease pathology via cuprizone, mice need to additionally intake the cuprizone powder through the skin and respiratory system²⁸. However, this does not occur when cuprizone pellets are delivered. Our current study suggests this may not be as central to the pathological action of cuprizone as previously thought.

It is also important to note that mice fed control powder had significantly fewer oligodendrocytes than those fed control pellets, particularly in the rostral corpus callosum. In addition, the density of Olig2+ cells were lower in the cuprizone powder fed mice compared to their cuprizone pellet fed counterparts. This may be due to abnormal energy metabolism as mice fed powdered food are known to develop hyperglycaemia and increases in epinephrine and other catecholamines⁴². Catecholamines can be toxic to oligodendrocytes when the protective effect of astrocytes is impaired⁴³, and astrocyte function is impaired under hyperglycaemic conditions⁴⁴. This interesting finding may have implications for remyelination studies, as mice fed powdered control chow may not be suitable controls for oligodendrocyte density. In line with this notion, the loss of oligodendroglia reported in previous studies at 3 weeks with powdered cuprizone^{45–48} only became apparent when we compared powdered cuprizone to pelleted control. As these earlier studies either used pelleted feed as control for powdered cuprizone or did not specify the formulation of their control feed, the seeming discrepancy in oligodendroglia loss between such studies and ours may relate to the formulation of control feed used to assess the effect of cuprizone. These data highlight the importance of using control feed in the same formulation as the cuprizone-containing feed to evaluate the effect of cuprizone. The effect of powdered feed on oligodendroglia should also be considered when designing remyelination studies, as a change to powdered control chow from powdered cuprizone diet may not reflect a full return to a healthy mature oligodendrocyte population that is able to remyelinate fully.

Both powder and pellets produced the well-known rostro-caudal pattern of demyelination, whereby the medial caudal region of the corpus callosum is more susceptible to cuprizone insult^{34,46,49,50}. Regionally specific susceptibility may be due to the proximity of the medial rostral corpus callosum to the subventricular zone, as neural precursor cells from the subventricular zone migrate into the proximal rostral corpus callosum by week 3 of cuprizone administration, where they can dampen the inflammatory response and differentiate into mature oligodendrocytes^{26,51–53}. It is important to note however that despite the midline being most susceptible to demyelination in the caudal regions, in the rostral corpus callosum the lateral areas are more susceptible to cuprizone intoxication³⁹. Since the lateral corpus callosum was not analysed in the current study, the effect of the cuprizone formulations on inducing demyelination in these regions may have been missed. Mice fed powdered cuprizone displayed greater within-group variability than those fed cuprizone pellets, perhaps due to variable intake of the powdered and possibly less palatable feed. The variability in certain outcomes in mice fed cuprizone powder may have been a factor in the lack of statistically significant differences compared to relative controls. Therefore, the reduced variability with mice fed cuprizone pellets is another advantage of the pelleted cuprizone technique.

When utilising animal models, it is critical that the features of the model are replicated across studies, including the time at which aspects of the pathology begin to become detectable. The most widely recognized hallmarks of cuprizone-induced toxicity are the loss of mature myelinating oligodendrocytes and demyelination. Death of oligodendrocytes occurs from around 2–7 days into cuprizone administration, and reduced oligodendrocyte density is still apparent at 3 weeks, whilst demyelination becomes detectable from around 3 weeks^{10,39,54}. The demyelination observed in this study in the cuprizone pellet group is in the early phase at 3 weeks, and a longer period of exposure to cuprizone of 5 weeks may have resulted in a more severe demyelinating effect³⁹. Indeed, at 5 weeks, powdered cuprizone has been found to be effective at inducing demyelinating pathology³⁹. The lack of significant demyelination observed with 3 weeks administration of cuprizone powder may reflect delayed cuprizone intake, rather than a complete lack of efficacy, given the significant loss of mature ASPA+ oligodendrocytes seen in this group. The lack of change in Olig2+ and CC1+ cell densities with powdered feed may reflect the contribution to cell densities of OPCs⁵⁵ and astrocytes⁵⁶ respectively. The demyelination and mature oligodendrocyte depletion observed with pelleted cuprizone indicates that the potency of cuprizone was not compromised by the copper contained in standard rodent chow. Moreover, our powdered feed contained the same amount of copper as the pelleted feed, allowing reliable interpretation of the effects of feed formulation on demyelination pathology. The observed oligodendropathy and demyelination were complemented by a robust inflammatory response. It is known that by 1 week of cuprizone administration, microglia are activated in the corpus callosum²³, with astrocytes showing morphological changes as early as 1 week and increasing in density by 3 weeks²⁴. In the current study, similar inflammatory changes were accompanied by increased immunoreactivity of oxidative stress markers for protein nitration and DNA damage, which we have previously demonstrated following 3 weeks of cuprizone administration⁵⁷. The higher protein nitration in rostral corpus callosum with powdered cuprizone compared to the caudal region is an interesting finding that warrants further mechanistic investigations. There is limited information available on the effects of cuprizone intoxication on protein nitration in the rostral and caudal corpus callosum. A plausible hypothesis is that high protein nitration is a response to cuprizone intoxication when the initial density of mature oligodendrocytes is low in the rostral region. Consistent with this hypothesis, we found that the density of mature oligodendrocytes in the rostral region was lower with control powder when compared to pelleted control. Future studies identifying the cell types and mechanisms responsible for high protein nitration in the rostral corpus callosum will allow better understanding of the regional differences with powdered and pelleted cuprizone. Given the lack of change in cell densities, the observed tissue swelling is likely to be due to increased water content and oedema, which has been found to occur as early as 3 days into cuprizone exposure and continue to at least 5 weeks⁵⁸. The reported reparative mechanism of OPC migration to—and proliferation in—the corpus callosum, particularly caudally, at 3 weeks of cuprizone administration^{25,26}, was also observed here. In sum, the pathological features we demonstrate (particularly when mice were fed cuprizone pellets) are consistent with the literature descriptions of the cuprizone-induced model of demyelinating disease when assessed at the later 5 week timepoint and beyond.

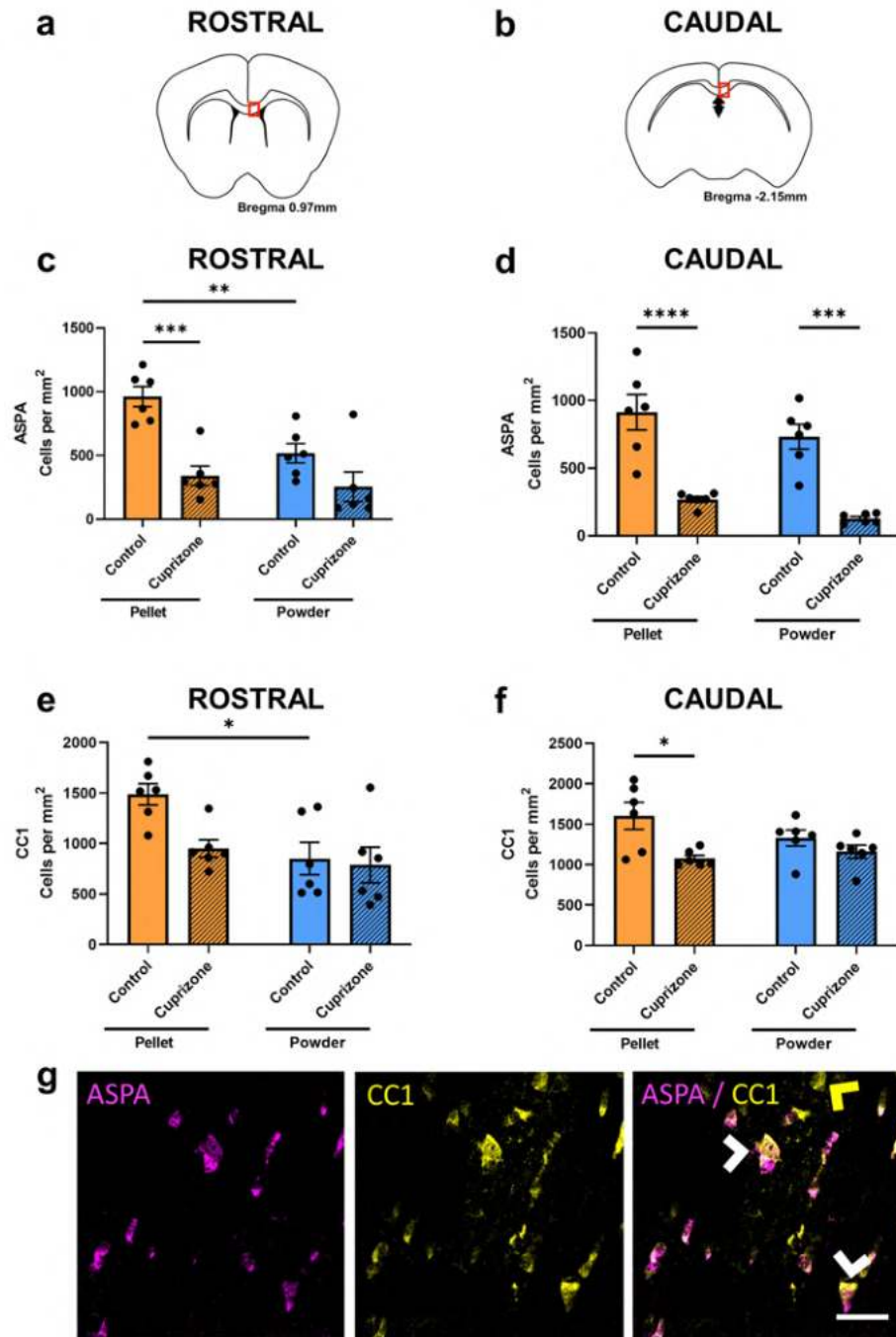


Figure 6. Effects of cuprizone feed formulation on densities of ASPA+ and CC1+ cells. The area of the rostral and caudal corpus callosum analysed is denoted by the red box in the coronal illustrations of the brain (a,b). The density of ASPA+ cells (c,d) and CC1+ cells (e,f) were quantified in the rostral and caudal corpus callosum. N=6 mice per group, graphs display individual data points overlaid on a bar displaying the mean \pm SEM. Significant differences are indicated by * $p \leq 0.05$, ** $p \leq 0.01$, *** $p \leq 0.001$, **** $p \leq 0.0001$. (g) Representative images of ASPA+ and CC1+ cells, indicated with white arrow heads; example ASPA-/CC1+ cell indicated with yellow arrow head; scale bar = 25 μ m.

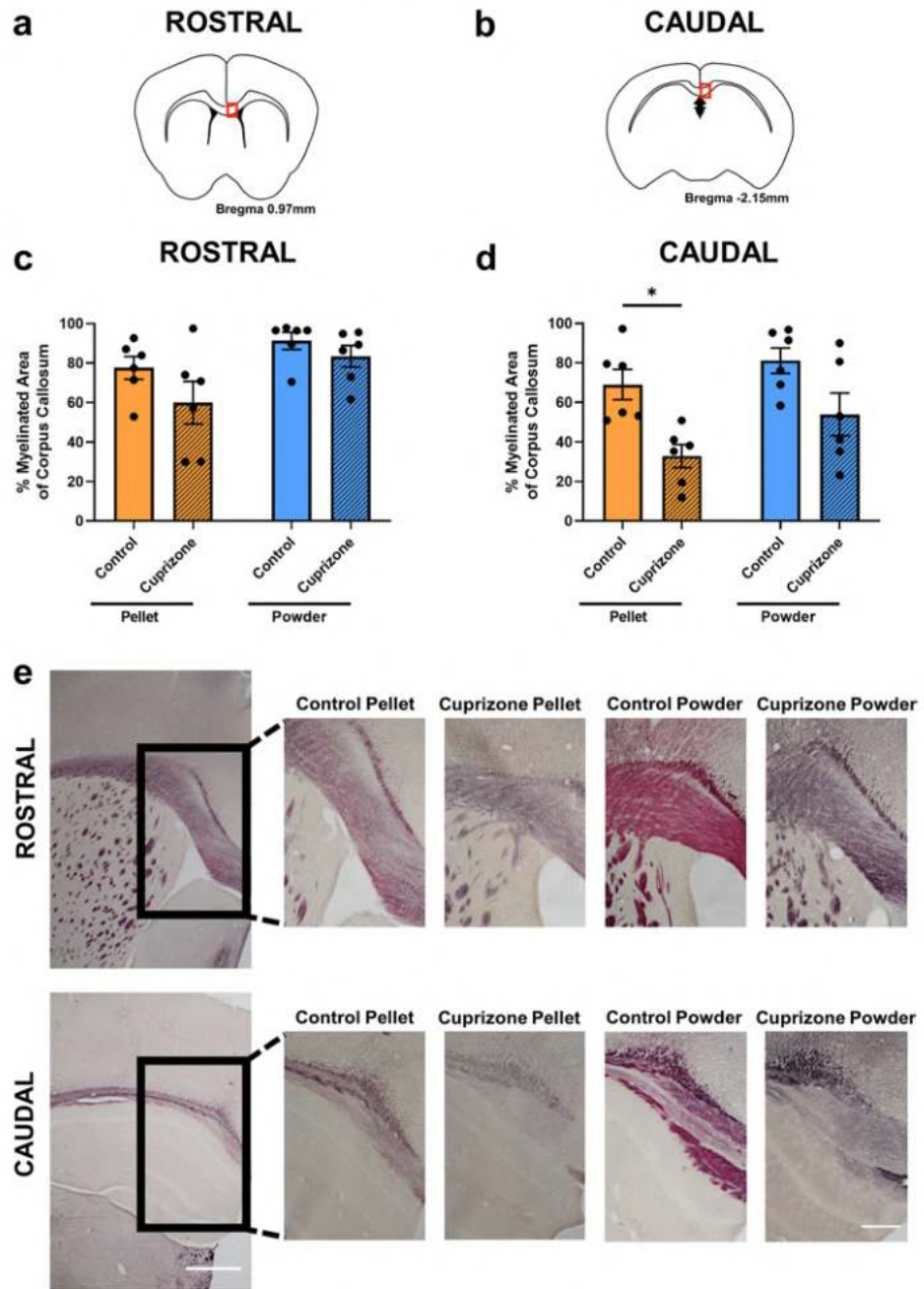


Figure 7. Effects of cuprizone feed formulation on demyelination. The area of the rostral and caudal corpus callosum analysed is denoted by the red box in the coronal illustrations of the brain (a,b). Percentage area of staining of Black-Gold II in the rostral (c) and caudal (d) corpus callosum was assessed to determine the level of myelination. N=6 mice per group, graphs display individual data points overlaid on a bar displaying the mean \pm SEM. Significant differences are indicated by * $p \leq 0.05$, ** $p \leq 0.01$, *** $p \leq 0.001$, **** $p \leq 0.0001$. (e) Representative images of the area of Black-Gold II for each group is shown, 4 \times images scale bar = 500 μ m; 10 \times images scale bar = 200 μ m.

Outcome measure	Cuprizone pellet relative to control pellet		Cuprizone powder relative to control powder		Cuprizone pellet relative to cuprizone powder		Control powder relative to control pellet	
	Rostral	Caudal	Rostral	Caudal	Rostral	Caudal	Rostral	Caudal
Astrocyte reactivity	↑↑	↑	↑	-	-	↑	-	-
Microglial activation	↑↑	↑↑	↑	-	-	↑↑	-	-
Protein nitration	-	↑↑	↑↑	-	↓↓	↑	-	-
DNA damage	↑	↑↑	-	↑	-	-	-	-
Area of corpus callosum	↓	↑↑	-	↑	-	-	-	-
Hoechst+ cells	-	-	-	-	-	-	-	-
Olig2+ cells	↓↓	-	-	-	-	↑	↓↓	↓↓
PDGFRα+ cells	-	↑↑	-	↑↑	-	-	-	-
Olig2+/PDGFRα+ cells	-	↑	-	↑	-	-	-	-
ASPA+ cells	↓↓	↓↓	-	↓↓	-	-	↓	-
CC1+ cells	-	↓	-	-	-	-	↓	-
Myelination	-	↓	-	-	-	-	-	-

Table 1. Summary of immunohistochemical and histological outcomes. Arrows ↑ and ↓ represent a statistically significant increase or decrease and - represents no significant difference. Single arrows represent p values of greater than 0.001 and less than 0.05, whilst double arrows represent p values ≤ 0.001.

Taken together, this study found that at a 3 week timepoint, cuprizone pellets were more efficacious than cuprizone powder at producing astrocyte reactivity, microglial activation, oxidative stress, tissue swelling, and a reduction in the density of mature oligodendrocytes and demyelination when compared to control feeds, particularly in the caudal corpus callosum. These results indicate that cuprizone pellets are a more effective method of delivering cuprizone than powdered feed to induce demyelinating disease pathology at this early 3 week demyelination timepoint.

Materials and methods

Animals and study design. Twenty-four 8 week old male C57Bl/6J mice were obtained from the Animal Resource Centre (Murdoch, Western Australia). The mice had ad libitum access to food and water and were housed under a 12 h light/dark cycle. All procedures were approved by the Animal Ethics Committee (AEC) of The University of Western Australia (RA/3/100/1613), with reciprocal approval from the AEC of Curtin University (ARE2019-4), and were performed in accordance with the principles of the National Health and Medical Research Council of Australia. This study is reported in accordance with the ARRIVE guidelines. Animal randomisation was achieved at a cage level by allocating animals to groups in the order in which they were received from the supplier. Animals were allowed a 1 week acclimatisation period to the experimental location prior to commencing the study. 0.2% cuprizone (ChemSupply) was delivered for 3 weeks either mixed into control powdered feed (Specialty Feeds, Perth, Western Australia) or as cuprizone-containing pellets (Specialty Feeds, Perth, Western Australia). The cuprizone-containing pellets were formed using cuprizone powder from the same batch as that delivered directly to the mice, to minimise any batch or supplier variability. Animals were given equivalent amounts of cuprizone, regardless of feed formulation. Mice fed the cuprizone pellets ate approximately 3–5 g of feed each per day, however the quantity of cuprizone powder consumed could not be determined as the mice were consistently urinating, defecating and digging around in the feed. Animals not receiving cuprizone were administered either control pellets with the same nutritional composition to the cuprizone-containing pellets (except cuprizone), or the control powder that the cuprizone powder was mixed into. The control powder was nutritionally the same as the control pellets.

The animals were divided into four experimental groups depending on feed type (N = 6/group); a control pellet group, a cuprizone pellet group, a control powder group, and a cuprizone powder group. 6 mice/group was chosen as power calculation (using G*Power Version 3.1⁵⁹) at α-level of 0.05 showed that it was sufficient for an 80% chance of detecting the published effect size of 2.02 for immunohistochemical measures of myelin and glia in the corpus callosum following cuprizone treatment⁶⁰. Animals were housed two animals per cage and were weighed daily, and if cuprizone-fed animals weighed less than 85% of their body weight at the start of the experimental period, they were weighed twice daily and their feed was supplemented with normal powdered chow until they returned to above the 85% threshold. One mouse fed cuprizone powder underwent this intervention; however, they were returned to cuprizone powdered feed 24 h after commencing diet supplementation due to substantial weight gain during this period. The level of myelination for this particular mouse was not found to be an outlier compared to the rest of the cuprizone powder group, as it was not 1.5 interquartile ranges outside of the 1st or 3rd quartiles as per Tukey's outlier detection model. Therefore, the data generated from this mouse was not removed from the data set and was included in all analyses. No further animals from either cuprizone feed groups required diet supplementation due to weight loss. Cuprizone powdered feed was changed daily³⁹, whilst pellets were changed every 2–3 days³⁸, as per standard protocols.

Tissue processing. Following the 3 weeks of cuprizone treatment, mice were euthanised using pentobarbitone sodium (160 mg/kg, Delvet), and transcardially perfused with 0.9% saline, followed by 4% paraformaldehyde (Sigma-Aldrich) in 0.1 M phosphate buffered solution pH 7.4. The brains were dissected and fixed overnight in 4% paraformaldehyde. The brains were transferred into 15% sucrose (ChemSupply) 0.1% sodium azide (Sigma-Aldrich) for cryoprotection and storage at 4 °C. Brains were cut down the midline into two hemispheres and block cut to isolate the region of the cortex that contained the corpus callosum. The right hemisphere was then embedded in a mould of optimal cutting temperature compound (OCT, Scigen) and fast frozen in isopentane in a bath of liquid nitrogen until 2 min after the OCT had turned opaque. Tissue was then cryosectioned coronally at -20 °C into 24 well plates (ThermoFisher Scientific) containing PBS 0.1% sodium azide at 25 µm thickness and stored at 4 °C until use.

Immunohistochemistry. Immunohistochemistry was performed within 24-well trays (ThermoFisher Scientific). Sections were washed with PBS three times, before being blocked in phosphate buffered saline (PBS) + 0.2% Triton X100 with 5% normal donkey serum (NDS) for 1 h at room temperature on a shaker at 40 revolutions per minute (rpm). When a primary antibody was to be used that was raised in mouse, an unconjugated donkey anti-mouse IgG (2 µg/ml, 1:1000, Abcam, Ab6707) was also included in the blocking solution. Following another wash with PBS, sections were incubated with primary antibodies recognising: activated resident microglia/macrophages (IBA1, 2 µg/ml, 1:500, Abcam, goat Ab5076); reactive astrocyte marker glial fibrillary acid protein (GFAP, 0.4 µg/ml, 1:500, Abcam, rabbit Ab33922); oxidative stress markers 3-nitrotyrosine (3-NT, 2 µg/ml, 1:500, Abcam, mouse Ab61392) and 8-hydroxy-2'-deoxyguanosine (8OHdG, concentration undetermined by manufacturer, 1:250, Novus Biologicals, goat NB600-1508); and oligodendroglial indicators oligodendrocyte transcription factor 2 (Olig2, 0.08 µg/ml, 1:250, R&D Systems, goat AF2418), platelet-derived growth factor receptor alpha (PDGFRα, 5 µg/ml, 1:200, ThermoFisher Scientific, rabbit PA5-16571), aspartoacylase (ASPA, 2 µg/ml, 1:500, EMD Millipore, rabbit ABN1698), and adenomatous polyposis coli (APC) clone (CC1, 0.2 µg/ml, 1:500, ThermoFisher Scientific, mouse MA1-25884). Primary antibodies were diluted in PBS + 0.2% Triton X100 with 5% NDS. Following a 30 min incubation with primary antibodies at room temperature on a shaker at 40 rpm, the well plates were transferred to 4 °C for overnight incubation on a shaker at 40 rpm. Sections were then washed three times before being incubated with secondary antibodies (1:400, species-specific Alexa Fluor 488, 555 or 647, Thermo Fisher Scientific), diluted in PBS for 2 h at room temperature on a shaker at 40 rpm. Finally, sections were washed another three times before being incubated with Hoechst 3342 (1:2000, Thermo Fisher Scientific) and washed another three times. Sections were then mounted onto slides using fine paintbrushes, and coverslipped with Fluoromount-G (Thermo Fisher Scientific).

Histology. Myelin Black-Gold II (Biosensis) was performed within 24-well plates (ThermoFisher Scientific) in line with the manufacturer's instructions. Staining of all sections was conducted in a single session. In brief, sections were washed with distilled water before being immersed in 1 × Black-Gold II solution and incubated at 65 °C for 14 min, until staining of the myelinated regions was becoming apparent. Following three washes with distilled water, sections were mounted onto slides and imaged within the same day.

Imaging and analysis. For immunohistochemical outcome measures, the rostral and caudal medial corpus callosum were visualised using a Nikon A1 confocal microscope (Nikon Corporation, Australia, Coherent Scientific), and a series of 13 images were taken at 0.5 µm increments along the z-axis at a magnification of 20× and a numerical aperture of 0.75. For histological Black-Gold II, the rostral and caudal corpus callosum were visualised at a single visual slice along the z-axis using a Nikon Eclipse Ts2 microscope (Nikon Corporation, Australia, Coherent Scientific), at a magnification of 20× and a numerical aperture of 0.25. The rostral corpus callosum was imaged at approximately 0.97 mm anterior to bregma and the caudal corpus callosum at approximately 2.15 mm posterior to bregma. Imaging for each outcome measure for each region of interest was performed in a single session with consistent microscope capture settings for all experimental groups.

The area of immunoreactivity of IBA1, GFAP, 3-NT, and 8OHdG were semi-quantified using Fiji/ImageJ software. In brief, a single visual slice was selected, and the total area of the corpus callosum was quantified. A threshold was set to distinguish positive immunofluorescence from background, and an intensity analysis was performed to determine the area of intensity above threshold within the region. The data were then normalised against the total area of the corpus callosum analysed. The area of the corpus callosum in a 20× image was also quantified using Fiji/ImageJ, by determining the area of the region of interest within the total image, based on Hoechst+ nuclei.

Hoechst+, Olig2+, PDGFRα+, Olig2+/PDGFRα+, ASPA+, and CC1+ cells were quantified using the ZEISS Zen Intellesis image analysis software, which uses deep learning to automatically identify cells of interest based on a range of features from the image, including pixel intensity and cell morphology⁶¹. Data are expressed per mm² to provide a cell density for the region of interest.

For Black-Gold II, analysis was performed similar to as previously described⁶². In brief, using Fiji/ImageJ software, the raw image was split into three channels as an RGB stack, with the green channel selected for analysis due to its high contrast. The corpus callosum was selected and the total area measured. A threshold was set to distinguish the myelin from demyelinated regions/grey matter, and the area of myelin positive pixels was quantified and normalised against the total area of the corpus callosum, determining the percentage myelination present.

Blinding to animal identity was not possible as investigators needed to evaluate the range of immunoreactivity across groups to determine intensity thresholds. Analyses were subsequently performed objectively using automated algorithms in the ZEISS Zen Intellesis and Fiji/ImageJ.

Statistical analyses. Graphpad PRISM 9 software was used for data analysis and illustration. A three-way repeated-measures ANOVA was used to analyse changes in animal weight over time. Sphericity was assessed using the Greenhouse–Geisser epsilon value in conjunction with the Greenhouse–Geisser adjustment, and sphericity was not assumed ($\epsilon < 0.75$). To detect changes between groups within timepoints, two-way ANOVAs were performed at each timepoint using Tukey's post-hoc test. For all other outcomes, two-way ANOVA with Tukey's post-hoc test was performed across all four groups. Statistical significances shown on graphs are hypothesis-driven and may not display all significant differences obtained. Specifically, only significant differences between the respective control and cuprizone groups are shown, as well as differences between the two cuprizone formulations and the two control feed formulations. Outliers were not removed for any of the outcome measures. *p* values in the text are for post hoc comparisons.

Data availability

The datasets generated during and/or analysed during the current study are available from the corresponding author on reasonable request.

Received: 13 July 2021; Accepted: 1 November 2021

Published online: 19 November 2021

References

- Matsushima, G. K. & Morell, P. The neurotoxicant, cuprizone, as a model to study demyelination and remyelination in the central nervous system. *Brain Pathol.* **11**, 107–116 (2001).
- Kipp, M. *et al.* The cuprizone animal model: New insights into an old story. *Acta Neuropathol.* **118**, 723–736 (2009).
- Torkildsen, Ø., Brunborg, L. A., Myhr, K. M. & Bø, L. The cuprizone model for demyelination. *Acta Neurol. Scand.* **117**, 72–76 (2008).
- Praet, J., Guglielmetti, C., Berneman, Z., Van der Linden, A. & Ponsaerts, P. Cellular and molecular neuropathology of the cuprizone mouse model: Clinical relevance for multiple sclerosis. *Neurosci. Biobehav. Rev.* **47**, 485–505 (2014).
- Zhang, Y. *et al.* Quetiapine alleviates the cuprizone-induced white matter pathology in the brain of C57BL/6 mouse. *Schizophr. Res.* **106**, 182–191 (2008).
- Biancotti, J. C., Kumar, S. & de Vellis, J. Activation of inflammatory response by a combination of growth factors in cuprizone-induced demyelinated brain leads to myelin repair. *Neurochem. Res.* **33**, 2615–2628 (2008).
- Acs, P., Selak, M. A., Komoly, S. & Kalman, B. Distribution of oligodendrocyte loss and mitochondrial toxicity in the cuprizone-induced experimental demyelination model. *J. Neuroimmunol.* **262**, 128–131 (2013).
- Yu, Q. *et al.* Strain differences in cuprizone induced demyelination. *Cell Biosci.* **7**, 59 (2017).
- Xu, C., Bailly-Maitre, B. & Reed, J. C. Endoplasmic reticulum stress: Cell life and death decisions. *J. Clin. Investig.* **115**, 2656–2664 (2005).
- Fischbach, F. *et al.* Cuprizone-induced graded oligodendrocyte vulnerability is regulated by the transcription factor DNA damage-inducible transcript 3. *Glia* **67**, 263–276 (2019).
- Gudi, V. *et al.* Spatial and temporal profiles of growth factor expression during CNS demyelination reveal the dynamics of repair priming. *PLoS One* **6**, e22623 (2011).
- Prodan, C. I., Holland, N. R., Wisdom, P. J., Burstein, S. A. & Bottomley, S. S. CNS demyelination associated with copper deficiency and hyperzincemia. *Neurology* **59**, 1453–1456 (2002).
- Jaiser, S. R. & Winston, G. P. Copper deficiency myelopathy. *J. Neurol.* **257**, 869–881 (2010).
- Stys, P. K., Zamponi, G. W., van Minnen, J. & Geurts, J. J. G. Will the real multiple sclerosis please stand up?. *Nat. Rev. Neurosci.* **13**, 507–514 (2012).
- Mahad, D., Ziabreva, I., Lassmann, H. & Turnbull, D. Mitochondrial defects in acute multiple sclerosis lesions. *Brain* **131**, 1722–1735 (2008).
- Zatta, P. *et al.* Copper and zinc dismetabolism in the mouse brain upon chronic cuprizone treatment. *Cell. Mol. Life Sci.* **62**, 1502–1513 (2005).
- Carlton, W. W. Studies on the induction of hydrocephalus and spongy degeneration by cuprizone feeding and attempts to antidote the toxicity. *Life Sci.* **6**, 11–19 (1967).
- Taraboletti, A. *et al.* Cuprizone intoxication induces cell intrinsic alterations in oligodendrocyte metabolism independent of copper chelation. *Biochemistry* **56**, 1518–1528 (2017).
- Jhelum, P. *et al.* Ferroptosis mediates cuprizone-induced loss of oligodendrocytes and demyelination. *J. Neurosci.* **40**, 9327–9341 (2020).
- Procaccini, C., De Rosa, V., Pucino, V., Formisano, L. & Matarese, G. Animal models of multiple sclerosis. *Eur. J. Pharmacol.* **759**, 182–191 (2015).
- Morell, P. *et al.* Gene expression in brain during cuprizone-induced demyelination and remyelination. *Mol. Cell. Neurosci.* **12**, 220–227 (1998).
- Lindner, M., Fokuhl, J., Linsmeier, F., Trebst, C. & Stangel, M. Chronic toxic demyelination in the central nervous system leads to axonal damage despite remyelination. *Neurosci. Lett.* **453**, 120–125 (2009).
- Shelestak, J. *et al.* Increased blood-brain barrier hyperpermeability coincides with mast cell activation early under cuprizone administration. *PLoS One* **15**, e0234001 (2020).
- Hiremath, M. M. *et al.* Microglial/macrophage accumulation during cuprizone-induced demyelination in C57BL/6 mice. *J. Neuroimmunol.* **92**, 38–49 (1998).
- Mason, J. L. *et al.* Mature oligodendrocyte apoptosis precedes IGF-1 production and oligodendrocyte progenitor accumulation and differentiation during demyelination/remyelination. *J. Neurosci. Res.* **61**, 251–262 (2000).
- Xing, Y. L. *et al.* Adult neural precursor cells from the subventricular zone contribute significantly to oligodendrocyte regeneration and remyelination. *J. Neurosci.* **34**, 14128–14146 (2014).
- Hochstrasser, T., Exner, G. L., Nyamoya, S., Schmitz, C. & Kipp, M. Cuprizone-containing pellets are less potent to induce consistent demyelination in the corpus callosum of C57BL/6 mice. *J. Mol. Neurosci.* **61**, 617–624 (2017).
- Hagemeyer, N. *et al.* Erythropoietin attenuates neurological and histological consequences of toxic demyelination in mice. *Mol. Med.* **18**, 628–635 (2012).
- Ohgomori, T. & Jinno, S. Cuprizone-induced demyelination in the mouse hippocampus is alleviated by phytoestrogen genistein. *Toxicol. Appl. Pharmacol.* **363**, 98–110 (2019).
- Klein, B. *et al.* Age influences microglial activation after cuprizone-induced demyelination. *Front. Aging Neurosci.* **10**, 278 (2018).
- Mohammadi-Rad, M., Ghasemi, N. & Aliomrani, M. Evaluation of apamin effects on myelination process in C57BL/6 mice model of multiple sclerosis. *Res. Pharm. Sci.* **14**, 424–431 (2019).

32. Gonsalvez, D. G. *et al.* Imaging and quantification of myelin integrity after injury with spectral confocal reflectance microscopy. *Front. Mol. Neurosci.* **12**, 275 (2019).
33. Mazloumfard, F., Mirian, M., Eftekhari, S.-M. & Aliomrani, M. Hydroxychloroquine effects on miR-155-3p and miR-219 expression changes in animal model of multiple sclerosis. *Metab. Brain Dis.* <https://doi.org/10.1007/s11011-020-00609-z> (2020).
34. Steelman, A. J., Thompson, J. P. & Li, J. Demyelination and remyelination in anatomically distinct regions of the corpus callosum following cuprizone intoxication. *Neurosci. Res.* **72**, 32–42 (2012).
35. Tagge, I. *et al.* Spatio-temporal patterns of demyelination and remyelination in the cuprizone mouse model. *PLoS One* **11**, 1–24 (2016).
36. Danesh-Seta, T., Emami, F., Nasr-Esfahani, M. H., Ghaedi, K. & Aliomrani, M. Bee venom-derived BBB shuttle and its correlation with oligodendrocyte proliferation markers in mice model of multiple sclerosis. *Neurotox. Res.* **1**, 3 (2021).
37. Kuhn, S., Gritti, L., Crooks, D. & Dombrowski, Y. Oligodendrocytes in development, myelin generation and beyond. *Cells* **8**, 1424 (2019).
38. Madhavarao, C. N. *et al.* Immunohistochemical localization of aspartoacylase in the rat central nervous system. *J. Comp. Neurol.* **472**, 318–329 (2004).
39. Zhan, J. *et al.* The cuprizone model: Dos and do nots. *Cells* **9**, 843 (2020).
40. Stidworthy, M. F., Genoud, S., Suter, U., Mantei, N. & Franklin, R. J. M. Quantifying the early stages of remyelination following cuprizone-induced demyelination. *Brain Pathol.* **13**, 329–339 (2003).
41. Kopanitsa, M. V. *et al.* Cognitive disturbances in the cuprizone model of multiple sclerosis. *Genes Brain Behav.* <https://doi.org/10.1111/gbb.12663> (2020).
42. Tsuchiya, M. *et al.* Long-term feeding on powdered food causes hyperglycemia and signs of systemic illness in mice. *Life Sci.* **103**, 8–14 (2014).
43. Noble, P. G., Antel, J. P. & Yong, V. W. Astrocytes and catalase prevent the toxicity of catecholamines to oligodendrocytes. *Brain Res.* **633**, 83–90 (1994).
44. Li, W. *et al.* Hyperglycemia alters astrocyte metabolism and inhibits astrocyte proliferation. *Aging Dis.* **9**, 674–684 (2018).
45. Clarner, T. *et al.* Myelin debris regulates inflammatory responses in an experimental demyelination animal model and multiple sclerosis lesions. *Glia* **60**, 1468–1480 (2012).
46. Norkute, A. *et al.* Cuprizone treatment induces demyelination and astrocytosis in the mouse hippocampus. *J. Neurosci. Res.* **87**, 1343–1355 (2009).
47. Groebe, A. *et al.* Cuprizone treatment induces distinct demyelination, astrocytosis, and microglia cell invasion or proliferation in the mouse cerebellum. *Cerebellum* **8**(3), 163–174 (2009).
48. Kipp, M. *et al.* BLBP-expression in astrocytes during experimental demyelination and in human multiple sclerosis lesions. *Brain Behav. Immun.* **25**, 1554–1568 (2011).
49. Wu, Q. Z. *et al.* MRI identification of the rostral-caudal pattern of pathology within the corpus callosum in the cuprizone mouse model. *J. Magn. Reson. Imaging* **27**, 446–453 (2008).
50. Xie, M. *et al.* Rostrocaudal analysis of corpus callosum demyelination and axon damage across disease stages refines diffusion tensor imaging correlations with pathological features. *J. Neuropathol. Exp. Neurol.* **69**, 704–716 (2010).
51. Brousse, B., Magalon, K., Durbec, P. & Cayre, M. Region and dynamic specificities of adult neural stem cells and oligodendrocyte precursors in myelin regeneration in the mouse brain. *Biol. Open* **4**, 980–992 (2015).
52. Butti, E. *et al.* Neural stem cells of the subventricular zone contribute to neuroprotection of the corpus callosum after cuprizone-induced demyelination. *J. Neurosci.* **39**, 5481–5492 (2019).
53. Brousse, B., Magalon, K., Daian, F., Durbec, P. & Cayre, M. Endogenous neural stem cells modulate microglia and protect from demyelination. *bioRxiv* <https://doi.org/10.1101/2020.06.18.158782> (2020).
54. Gudi, V., Gingele, S., Skripuletz, T. & Stangel, M. Glial response during cuprizone-induced de- and remyelination in the CNS: Lessons learned. *Front. Cell. Neurosci.* **8**, 73 (2014).
55. Valério-Gomes, B., Guimarães, D. M., Szczupak, D. & Lent, R. The absolute number of oligodendrocytes in the adult mouse brain. *Front. Neuroanat.* **12**, 90 (2018).
56. Bin, J. M., Harris, S. N. & Kennedy, T. E. The oligodendrocyte-specific antibody 'CC1' binds Quaking 7. *J. Neurochem.* **139**, 181–186 (2016).
57. Gopalasingam, G. *et al.* The effects of a combination of ion channel inhibitors on pathology in a model of demyelinating disease. *Mult. Scler. Relat. Disord.* **34**, 1–8 (2019).
58. Berghoff, S. A. *et al.* Blood-brain barrier hyperpermeability precedes demyelination in the cuprizone model. *Acta Neuropathol. Commun.* **5**, 94 (2017).
59. Faul, F., Erdfelder, E., Buchner, A. & Lang, A. G. Statistical power analyses using G*Power 3.1: Tests for correlation and regression analyses. *Behav. Res. Methods* **41**, 1149–1160 (2009).
60. Leicaj, M. L. *et al.* Changes in neurosteroidogenesis during demyelination and remyelination in cuprizone-treated mice. *J. Neuroendocrinol.* **30**, e12649 (2018).
61. Andrew, M. A quantified study of segmentation techniques on synthetic geological XRM and FIB-SEM images. *Comput. Geosci.* **22**, 1503–1512 (2018).
62. Denny, L. *et al.* Nalfurafine reduces neuroinflammation and drives remyelination in models of CNS demyelinating disease. *Clin. Transl. Immunol.* **10**, e1234 (2021).

Acknowledgements

The authors would like to thank Mr. Michael Nesbit of the Curtin Health Innovation Research Institute at Curtin University for helpful discussions about image analysis using the Zen Intellesis software, and Mr Parth Patel for assisting with the Zen Intellesis analysis.

Author contributions

M.F. and L.M.T. conceived and designed the study. Data collection was performed by L.M.T., M.P., B.L., A.J.W., A.W., T.M., C.A.B., S.C.H., and C.A. Data analyses were performed by L.M.T. and C.A. The first draft of the manuscript was written by L.M.T. and all authors reviewed drafts of the manuscript. All authors read and approved the final manuscript.

Funding

This work was supported by the National Health and Medical Research Fund (APP1160691). LT is supported by an MS Research Australia Postgraduate Scholarship and a Byron Kakulas Prestige Scholarship from the Perron Institute for Neurological and Translational Science.

Competing interests

The authors declare no competing interests.

Additional information

Correspondence and requests for materials should be addressed to M.F.

Reprints and permissions information is available at www.nature.com/reprints.

Publisher's note Springer Nature remains neutral with regard to jurisdictional claims in published maps and institutional affiliations.



Open Access This article is licensed under a Creative Commons Attribution 4.0 International License, which permits use, sharing, adaptation, distribution and reproduction in any medium or format, as long as you give appropriate credit to the original author(s) and the source, provide a link to the Creative Commons licence, and indicate if changes were made. The images or other third party material in this article are included in the article's Creative Commons licence, unless indicated otherwise in a credit line to the material. If material is not included in the article's Creative Commons licence and your intended use is not permitted by statutory regulation or exceeds the permitted use, you will need to obtain permission directly from the copyright holder. To view a copy of this licence, visit <http://creativecommons.org/licenses/by/4.0/>.

© The Author(s) 2021

4.6. Concluding Remarks and Continuing Experimental Work

Based on the data presented in the research paper above, cuprizone pellets are a reliable and more effective alternative to cuprizone powder for inducing acute demyelinating disease. Since the cuprizone pellets administered as part of the initial large scale cuprizone cohort described in Chapter 3 did not effectively produce demyelinating pathology, it is therefore highly likely that these pellets were manufactured incorrectly which resulted in a deactivation of the contained cuprizone. The potential causes for the discrepancy in the effectiveness of the two batches of cuprizone pellets will be discussed further in Chapter 8. Nevertheless, it appears that when manufactured correctly, cuprizone pellets are a reliable and more effective alternative to cuprizone powder for inducing demyelinating disease. Thus, we were confident in utilising cuprizone pellets in future studies, including the forthcoming work presented in this thesis, to induce demyelinating disease.

4.6.1. Additional Contributions to Ongoing Experimental Work

The optimised cuprizone model was used to assess the role of oxidative DNA damage in demyelinating disease, and enable comparisons to outcomes in models of neurotrauma and Alzheimer's Disease. Due to the time constraints of this degree and the large scale nature of this collaborative research, the additional contributions I have made to further the progression of this research no longer form a sizeable part of this thesis. Nevertheless, I assisted in organising the repeated cuprizone cohort and contributed substantially to the daily feeding schedule over the 3 weeks of cuprizone administration. Moreover, the methods and techniques I have established as presented throughout this chapter are expediting the acquisition of results. I have also contributed to the animal work for the neurotrauma component of this study. The neurotrauma cohort utilised both the partial optic nerve transection model and a closed head weight drop model of mTBI across four timepoints, ranging from 4 days to 10 months post-injury. I contributed to both pre- and post-operative care during surgeries, completed animal monitoring throughout the experimental periods, administered EdU injections, and performed the initial dissections to extract either the injured optic nerves or brains in over half of this cohort. I also helped to design the immunohistochemical combinations that are being used to analyse the obtained tissue.

Introduction to Series Three

This third series of chapters centres specifically on the role of oxidative stress and BBB dysfunction in both demyelinating disease and neurotrauma. The first chapter in this series (Chapter 5) is an additional short literature review to present the relevant context surrounding the BBB in health and disease. The structure and function of the BBB is discussed, before an examination of BBB dysfunction in the pathology of both demyelinating disease and neurotrauma. The role of oxidative stress in the loss of BBB integrity observed in both conditions is also reviewed, with a particular focus on perivascular OPCs and pericytes. The work presented throughout the remainder of Series Three investigates whether oxidative DNA damage to perivascular OPCs and pericytes causes dysfunction of these cells and whether this dysfunction is associated with increased BBB permeability in models of neurotrauma and demyelinating disease.

Chapter 6 investigates the role of oxidative stress in NG2⁺ glia (including pericytes and perivascular OPCs) at the BBB following neurotrauma. In this study, the partial optic nerve model of neurotrauma was employed to examine the relationship between oxidative stress, BBB dysfunction and cellular proliferation in both injured and control animals at one day post-injury. There was an increase in 8OHdG⁺ immunoreactivity indicating DNA damage in the ventral nerve vulnerable to secondary degeneration, as well as specifically within both NG2⁺ and PDGFR α ⁺ glia in this region. The presence of both DNA damaged pericytes and OPCs was qualitatively identified. In line with previous work conducted at this timepoint (Smith et al. 2016), there was significant breach of the BBB acutely post-injury and this BBB dysfunction was significantly and strongly correlated to the extent of oxidative DNA damage. Furthermore, the density of newly derived and proliferating cells with DNA damage in the ventral nerve increased with injury. The PDGFR α ⁺ population, which is primarily comprised of OPCs, was found to be the major proliferating, DNA damaged cell type at 1 day following injury to the optic nerve. This novel data provides valuable insights into oxidative stress within the optic nerve at an acute timepoint following neurotrauma and further highlights these damage mechanisms as a worthy target for future investigations. This work has since been published by the International Journal of Molecular Sciences, with the full version available in Appendix C.

Chapter 7 presents parallel research that has been commenced to investigate the role of oxidative stress in perivascular OPCs and pericytes at the BBB in demyelinating disease. This study utilises the cuprizone model of demyelinating disease at early timepoints, when the BBB has been shown to be dysfunctional. There is still additional work remaining for this study due to delays in tissue analysis from COVID-19 associated laboratory shutdowns and the corresponding time constraints of this doctoral degree. Therefore, the discussion of this study is confined to the experimental work completed to date together with detailed plans for the continuation of this research.

Chapter 5. Review of the Blood-Brain Barrier in Health and Disease

The BBB is compromised in both MS and neurotrauma; however, the underlying cause of this dysfunction is unclear in both conditions. This chapter provides an additional short literature review on the BBB in health and disease to provide the necessary context for the studies in Series Three and remainder of the thesis.

5.1. The Blood-Brain Barrier

5.1.1. Structure of the Cerebrovasculature

The human brain has high metabolic demand, representing over 20% of the total oxygen metabolism in the body (Watts et al. 2018). Blood acts to transport oxygen and nutrients to the brain, to remove carbon dioxide and other metabolic waste products, to carry hormonal signals between organs, and to regulate the peripheral immune response (Daneman & Prat 2015). Cerebral blood vessels carry blood between the heart and the brain. There are a multitude of cerebral artery types, based on the level of penetration into the brain parenchyma (Figure 5.1A). The blood circulation of the brain vasculature is supplied by the internal carotid and vertebral arteries, which form the circle of Willis at the base of the brain (Iadecola & Nedergaard 2007). These cerebral arteries branch into pial arteries, which are intracranial vessels on the surface of the brain within the leptomeninges or glia limitans, and are surrounded by cerebrospinal fluid (CSF) (Cipolla 2009; Zlokovic 2005). Pial vessels bifurcate into smaller penetrating arterioles that lie within the interstitial fluid filled Virchow-Robin space (Mohan et al. 2009). These penetrating arterioles form parenchymal or intracerebral arterioles which completely penetrate into the brain parenchyma and become almost entirely covered by astrocytic end-feet which form the glial limitans (Cipolla 2009; Coelho-Santos & Shih 2020). These arterioles give rise to the capillary network of the brain, with capillaries making up about 85% of the brain vasculature (Sweeney et al. 2018). This specialised microvasculature of the CNS is encased by the BBB, which acts to prevent toxic and pathogenic substances from entering the brain parenchyma from the blood and the periphery (Abbott et al. 2010). The BBB is comprised primarily of endothelial cells, astrocytes, neurons, pericytes, and perivascular OPCs, which interact to produce a highly regulated cellular barrier (Figure 5.1B) (Abbott et al. 2006). However, it's important to note that even within specific regions of the brain heterogeneity exists in BBB features between vessels and some areas of cerebral vasculature lack a BBB entirely, for example at the choroid plexus (Liebner et al. 2018).

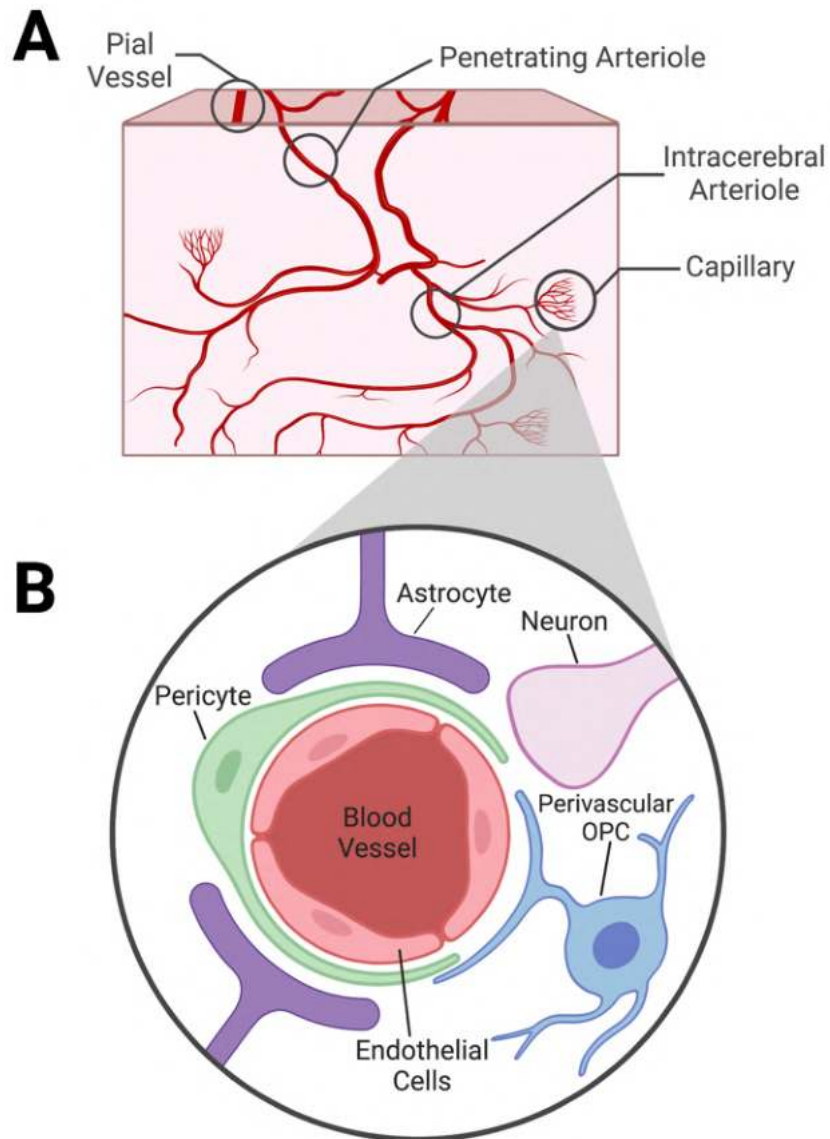


Figure 5.1. Structure and cellular components of the cerebrovasculature. (A) There are a multitude of cerebral artery types based on the level of penetration into the brain parenchyma, including pial vessels, penetrating and intracerebral arterioles and capillaries. The capillary network of the brain is encased by specialised perivascular cells at the BBB. (B) The vascular unit surrounding the BBB is primarily comprised of endothelial cells, pericytes, astrocytes, neurons and perivascular OPCs; which regulates cerebral blood flow and the passage of molecules into the brain parenchyma. Modified from Rustenhoven *et al.* 2017 and Coelho-Santos & Shih 2020. Original illustration created using BioRender.com.

5.1.2. Cells at the Blood-Brain Barrier

5.1.2.1. Endothelial Cells

Endothelial cells are simple squamous epithelial cells that line the walls of blood vessels, and control CNS homeostasis by regulating the passage of solutes, such as ions and nutrients, through physical and molecular barriers as well as through specific transporters (Daneman & Prat 2015). The endothelial cells that line cerebral blood vessels differ to those in the rest of the body as they are non-

fenestrated, they contain more tight junctions, and they rarely employ pinocytosis for the movement of substrates into the brain (Ballabh et al. 2004). Brain endothelial cells express two main types of transporters; efflux transporters (Löscher & Potschka 2005) and specific nutrient transporters (Mittapalli et al. 2010), which are highly controlled to limit what solutes can pass into the brain parenchyma. Endothelial cells contain several ion channels, which are involved in a plethora of molecular mechanisms, such as the release of vasoactive and haemostatic factors (Stamatovic et al. 2008). Endothelial cells are held together by tight junctions, which serve as a physical barrier to regulate CNS homeostasis. Tight junctions are comprised of integral transmembrane proteins, such as claudins and occludin, and membrane-associated cytoplasmic proteins (Luissint et al. 2012). Tight junctions act as a barrier of diffusion of solutes, ions and water through the paracellular space between endothelial cells (Sandoval & Witt 2008) as they form “kissing points” whereby membranes of adjacent endothelial cells are joined together (Bauer et al. 2014).

5.1.2.2. Astrocytes and Neurons

Astrocytes extend polarised processes that wrap around and ensheath blood vessels and neurons, with this neurovascular coupling allowing for blood flow and vessel diameter to be tightly regulated in response to neuronal activity (Gordon et al. 2011). This contact of an astrocyte with the vasculature forms an astrocytic end-foot, with every astrocyte having at least one contact with a blood vessel (Verkhatsky & Nedergaard 2018). Astrocytic connections to the vasculature allow for astrocytic regulation of endothelial cell properties, and the release of growth factors by astrocytes play important roles in the formation of tight junctions and polarisation of transporters (Abbott et al. 2006). Astrocytes also communicate with each other *via* gap junctions to create a coordinated functional syncytium which regulates the cerebrovasculature (Alvarez et al. 2013).

Neurons can directly modulate the neurovascular unit by the release of vasoactive substances to increase cerebral blood flow in response to heightened metabolic needs through functional hyperaemia (McConnell et al. 2017). However, activation of both excitatory and inhibitory neurons induces increases in cerebral blood flow, which means that neurovascular coupling can occur even when there is an overall decrease in neuronal activity (Kaplan et al. 2020).

5.1.2.3. Pericytes

Pericytes are another integral component of the BBB interface. Pericytes are a type of mural cell that envelop and spread their processes along the abluminal surface of the endothelial tube and are embedded in the basement membrane (Sims 1986). The basement membrane is a form of the extracellular matrix that is comprised of four major proteins: collagen IV, laminin, nidogen and perlecan (Xu et al. 2019). Pericytes have the ability to regulate capillary blood flow by controlling the diameter of the blood vessel through the employment of contractile proteins (Hall et al. 2014). Pericytes also play roles in angiogenesis, excreting factors for the extracellular matrix, wound healing

following injury, and regulating immune cell infiltration (Daneman & Prat 2015). Pericytes are essential for vessel stability and structural integrity (Ballabh et al. 2004), and pericyte loss is associated with microaneurysms (Lindahl et al. 1997). Furthermore, pericyte deficient mice show significant neurovascular uncoupling, resulting in a reduced oxygen supply going to the brain and subsequent metabolic stress, highlighting the importance of these cells at modulating the BBB and the neurovascular unit (Kisler et al. 2017). The role of pericytes and the effect on them following injury and disease will be further described throughout this brief review. Pericytes can be identified by their expression of markers such as NG2, platelet-derived growth factor receptor- β (PDGFR β), and CD13 (Smyth et al. 2018). However, pericytes are not the only NG2⁺ cells at the BBB interface, with OPCs also contributing to the vascular unit.

5.1.2.4. OPCs

Aside from acting as a progenitor pool for the generation of mature oligodendrocytes, OPCs are a heterogeneous population and play multifaceted roles within the brain, including involvement in maintaining BBB integrity (Maki 2017). There are three OPC phenotypes depending on their spatial location relative to the cerebrovasculature: (1) parenchymal OPCs that do not interact with the BBB, (2) perivascular OPCs that encase microvessels with their processes, and (3) intermediate OPCs that have processes that partially localise with the BBB (Maki et al. 2015). Perivascular OPCs positioned at the BBB wrap their fine processes around the microvasculature and play a role in the maintenance of BBB integrity through bidirectional signalling with cerebral endothelial cells (Miyamoto et al. 2014), with this coupling between endothelial cells and neighbouring OPCs called the oligovascular niche (Arai and Lo, 2009a). Endothelial cells produce PDGF-BB that binds to PDGFR α on perivascular OPCs, which may stimulate the release of TGF- β from OPCs (Kimura et al. 2020). It is known that OPCs located adjacent to blood vessels secrete TGF- β 1, which activates the mitogen-activated protein kinase (MEK) / ERK pathway in the cerebral endothelium, promoting tight junction protein expression and supporting BBB integrity (Seo et al. 2014). In turn, cerebral endothelial cells secrete growth factors, including brain-derived neurotrophic factor and basic fibroblast growth factor, to support OPC survival and proliferation (Arai and Lo, 2009a), both of which are negatively impacted following stroke (Arai and Lo, 2009b). Therefore, there is a self-propagating increase in BBB integrity through interactions between endothelial cells and OPCs, which may be disrupted during pathology. *In vitro*, oxidative stress to endothelial cells caused a disruption to their trophic coupling with OPCs, which consequently resulted in an inability of these endothelial cells to support OPCs (Arai and Lo, 2009). Furthermore, even low levels of oxidative stress that would not be enough to cause cell death may attenuate the level of endothelial cell-derived growth factors supporting OPCs, resulting in deficient trophic support to OPCs under disease states

(Egawa et al. 2016). However, the direct effect of oxidative stress on OPCs at the BBB is currently unknown, including in pathologies such as neurotrauma and MS.

Developmentally, OPC-endothelial cell interactions also regulate vascularisation of white matter by interacting with angiogenic tip cells (Chavali et al. 2020), which indicates a role for the interaction between these cell types from development through to a mature CNS. In addition, OPCs are associated with other cell types at the BBB besides endothelial cells. *In vitro* research has demonstrated that astrocytes can support OPCs *via* MEK/ERK and PI3K/Akt signalling (Arai & Lo 2010), suggesting that OPCs and astrocytes may support each other at the BBB. Pericytes and OPCs also colocalise at the vasculature, and *in vitro* experiments suggest they exchange soluble supportive factors that promote cell survival and proliferation (Maki et al. 2015). The interconnected interactions between OPCs and other cell types at the vasculature warrant further investigation. Moreover, it is important to note that mature oligodendrocytes themselves also play a role at the vasculature, and may mediate effects on BBB integrity in alternative pathways to OPC-dependent mechanisms (Kimura et al. 2020).

5.2. Blood-Brain Barrier Dysfunction

The BBB is controlled by a multitude of intercellular complex signalling pathways to ensure homeostasis is maintained within the neural environment (Daneman & Prat 2015). The BBB is relatively dynamic and can adapt in response to physiological signals from the periphery (Keaney & Campbell 2015). However, the overall functionality of the BBB relies on the function of every cellular component, with dysfunction of any particular cell ultimately contributing to a breakdown of BBB integrity. Loss of BBB integrity has been implicated in a wide range of CNS disorders, including both MS and neurotrauma. It is important to note that dysfunction of the BBB can take various forms, with the capacity for both disruptive and non-disruptive changes (Figure 5.2). Much of the research focus investigating the BBB in neuropathologies is primarily quantifying disruptive changes to the BBB. Non-disruptive changes, or changes solely to the function of the BBB rather than its structural anatomy, are also pathologically significant (Varatharaj & Galea 2017). However, it can be more difficult to detect and measure vascular changes when the BBB remains morphologically intact. Thus, the remainder of the thesis examines disruptive BBB changes in both MS and neurotrauma, but the potential contribution of non-disruptive changes to overall pathology also warrants further investigation in future studies.

Disruptive BBB Change	Non-Disruptive BBB Change
Change in anatomy	Change in function
Typically occurs at a histological level & shows visible change in structural architecture	Typically occurs at a molecular level & doesn't show visible change in structural architecture
Can be detected using inert tracers (ie. Evans blue)	Cannot be detected using inert tracers
Changes in permeability are not substance-specific	Changes in permeability are substance-specific
<u>Examples of disruptive changes:</u> Changes in the expression of tight junction proteins Degradation of glycocalyx Damage to endothelial cells Increased vesicular activity Breakdown of glia limitans Increased fenestration of capillaries Astroglial activation & changes to astrocytic end-feet	<u>Examples of non-disruptive changes:</u> Increased cytokine production Upregulation of endothelial receptors and transporters Increased cellular transmigration (ie. leukocytes) Pathogen neuroinvasion Subtle modulation of astrocytic function

Figure 5.2. Summary of differences between disruptive and non-disruptive changes to the BBB. Modified from Varatharaj & Galea 2017.

5.2.1. BBB Dysfunction in MS

A leading hallmark of MS lesions is hyperpermeability of the BBB. BBB dysfunction is often an early hallmark of the degeneration observed in those with MS, occurring in otherwise healthy looking tissue and preceding the onset of symptoms (Filippi et al. 1998; Spencer 2018; Vos et al. 2005). Using post-mortem tissue, tight junction proteins zonula occludens 1 (ZO-1) and occludin had abnormal expression in not only active lesions, but also at inflamed blood vessels in the normal appearing white matter (Plumb et al. 2006). These observed abnormalities in tight junction proteins can occur at all sizes of blood vessels, which suggests that no particular calibre of vessel is more susceptible to BBB dysfunction in MS (Kirk et al. 2003). Circulating pro-inflammatory cytokines in the blood and also within the CNS itself can cause dysfunction in BBB endothelial cells in MS brains (Minagar et al. 2006; Minagar et al. 2012). Across brain samples from people with RRMS, SPMS, and PPMS acquired at autopsy, leaky endothelial cells were present in normal appearing white matter and in active and chronic lesions as shown by endothelial cell dysferlin expression (Hochmeister et al. 2006). Furthermore, in active MS lesions, astrocytes become swollen and disruption occurs to astrocytic endfeet, resulting in sections of basal lamina without astrocytic encasing, ultimately associated with further BBB dysfunction (Brosnan & Raine 2013). Even chronic inactive lesions in both the RRMS and SPMS subtypes display detectable BBB leakage *via* gadolinium (Gd)-DPTA enhanced MRI, suggesting that BBB dysfunction is a continuing feature even in less active lesion sites (Soon et al. 2007). PPMS also displays ZO-1 tight junction abnormalities in both active and inactive white matter lesions (Leech et al. 2007). Dysregulation of tight junction proteins at the BBB in MS allows for progressive immune cell entry into the brain parenchyma as activated leukocytes

can bind to induced adhesion molecules on the inflamed endothelium to enter the brain parenchyma from the periphery (Grammas et al. 2011; Steinman 2001). In MS, endothelial cells may also de-differentiate towards mesenchymal cells upon inflammation, cumulating in cytoskeletal alterations and BBB dysfunction (Derada Troletti et al. 2019). In chronic PPMS, pericytes degenerate which is associated with leakage at the BBB (Claudio et al., 1995). Furthermore, in chronic active lesions within both early and late stage progressive MS, the pericyte marker PDGFR β localises significantly less with endothelial cells, potentially reflecting a detachment of pericytes from the vascular unit (Iacobaeus et al. 2017). In humans with MS, perivascular OPCs cluster around blood vessels in white matter lesions, particularly in active inflammatory areas (Niu et al. 2019). In a murine model, these perivascular clusters of OPCs secrete Wnt inhibitory factor 1, which disrupts endothelial cell tight junctions and displaces astrocytic endfeet, thus increasing BBB permeability and triggering inflammation (Niu et al. 2019).

Using weekly MRI scans to detect lesion initiation patterns in the white matter of people with RRMS, a subset of lesions were detected prior to observable BBB dysfunction (Guttmann et al. 2016). This finding was postulated to represent a type of MS disease progression analogous to pattern III lesions wherein parenchymal changes, including microglial activation, axonal degeneration and oligodendrocyte loss, precede activated peripheral autoimmune inflammation. However, it is important to note that to detect BBB dysfunction in this study the researchers used Gd-enhanced MRI which brings limitations, such as Gd dose-dependent detection by which increasing the dose of Gd increases the detection rate of BBB leakages (Filippi et al. 1995). An increase in the dose of Gd may reveal subtler alterations in BBB integrity associated with the observed parenchymal degeneration, which occur prior to the more extensive BBB breach that is typically associated with the adaptive inflammatory response.

Looking instead at cortical grey matter lesions, SPMS cortical blood vessels displayed abnormal tight junctions, whereas PPMS cortical blood vessels were not different from healthy controls (Leech et al. 2007). However, another study found no evidence of BBB dysfunction in cortical lesions when looking at serum leakage and tight junction protein expression (van Horssen et al. 2007). Fibrinogen depositions have been found in the motor cortex of people with progressive MS associated with a reduction in neuronal density, suggesting a degree of BBB dysfunction (Yates *et al.*, 2017). Therefore, it may be that the ultrastructural changes to the BBB in grey matter lesions are less pronounced and cortical BBB pathology is generally less severe than that detected in white matter lesions.

Traditionally, it was thought that there is no breach to the BBB during cuprizone administration (Bakker & Ludwin 1987; Kondo et al. 1987; McMahon et al. 2002). However, there is emerging evidence to suggest that the BBB may not be as intact following cuprizone administration

as once believed. A study in 2017 published in Nature Communications found that in C57BL/6N mice treated with cuprizone for 4 weeks, BBB permeability (as determined by the level of Evans Blue dye extravasation) significantly increased compared to mice fed control chow (Berghoff *et al.*, 2017a). The level of BBB dysfunction was less than that observed in EAE, which was hypothesised to have been the reason why it was not detected in previous studies (Berghoff *et al.*, 2017a). To characterise these alterations to the BBB following cuprizone administration, these researchers went on to investigate changes to the BBB at different stages of cuprizone disease progression (Berghoff *et al.*, 2017b). Following just 3 days of cuprizone administration, both brain oedema and increased extravasation of fluorescent vascular perfusion dyes were present, representing a breach of the BBB, and this damage progressively increased with time. In the first 5 days of cuprizone administration, various inflammatory factors of an astroglial origin, such as IL-1 β and tumour necrosis factor, were upregulated, and tight junction proteins, such as claudin-5 and occludin were downregulated. Furthermore, there were significantly increased levels of nitric oxide synthases, which suggests that nitrosative stress may play a role in BBB hyperpermeability. After the first 5 days, these factors only moderately changed for the remainder of the 5 weeks of cuprizone treatment. Given demyelination is not observable in the cuprizone model until about 3 weeks of cuprizone administration, this study demonstrated that BBB dysfunction preceded detectable levels of demyelination.

Another study looking specifically at early time points of cuprizone exposure found that the level of Evans Blue dye extravasation and the level of BBB permeability was highest at 3 days following cuprizone initiation, but continued out to 2 weeks to a lesser extent (Shelestak *et al.* 2020). The tight junction protein occludin was also significantly reduced in the corpus callosum at 3 days of cuprizone administration, preceding the onset of demyelination and gliosis. Mast cells were associated with this early BBB permeability, with higher densities of mast cells in both the cortex and corpus callosum at 3 days, alongside a concomitant decrease in mast cell granulation (Shelestak *et al.* 2020). Mast cells are located nearby the BBB and the factors they release upon activation, such as histamine, are associated with increasing BBB permeability by inducing endothelial cell endoplasmic reticulum stress (Tran *et al.* 2019). However, the contribution of other cell types to the BBB dysfunction observed in the cuprizone model is yet to be explored.

5.2.2. BBB Dysfunction in Neurotrauma

Following neurotrauma, BBB dysfunction has been shown in both animal models and human studies, however the extent of this dysfunction varies. In post-mortem human brains acutely following a severe fatal TBI, structural vascular alterations and irregularities in the surface of endothelial cells at blood vessels are widespread, particularly in the middle and deep capillary zones rather than the more superficial pial or subpial vessels, suggesting extensive breaches to the BBB in the cortex (Rodríguez-Baeza *et al.* 2003). Similarly, in post-mortem brains in those who survived for at least a

year following a moderate to severe TBI, significantly increased markers of BBB breach, such as fibrinogen and IgG, were found specifically throughout mid and deep cortical layers (Hay et al. 2015).

In milder cases of human TBI, the extent of BBB dysfunction is unclear and is generally determined *via* the presence of blood-based biomarkers. Creatine kinase BB is an enzyme indicative of BBB dysfunction if in the circulation in high amounts (Brayne et al. 1982), with the serum creatine kinase BB concentration increased in some people following mild TBI (23% of people), albeit far fewer people than following moderate to severe TBI (88% of people) (Skogseid et al. 1992). Acute increases in the serum level of the astrocytic protein S100 calcium-binding protein B (S100B) have also been found following mild TBIs and sub-concussive hits, and have been suggested to be indicative of disruption to the BBB (Marchi et al. 2013). However, there are a variety of confounding factors when analysing blood-based biomarkers following mild TBI, including individual variations in total blood volume, age, peripheral contributions to biomarker levels and potential impairments in renal function (Hier et al. 2021). Additionally, the timing of biomarker sampling is critical, with suboptimal timing of sample collection resulting in missed detection of elevations. The ideal sampling time varies for each biomarker. For example, S100B is ideally sampled within about the first 6 hours post-TBI to see any significant changes compared to uninjured controls, whereas neurofilament light (NF-L) can be accurately sampled for far longer, with sustained increases in serum NF-L levels found for at least the first 2 weeks post-injury (Thelin et al. 2017). Furthermore, given that biomarkers can enter the blood *via* other drainage pathways, such as the glymphatic system, instead of through a breach to the BBB, it is important to note that a comprehensive analysis of the pathways of biomarkers from the brain to the peripheral blood following a mild TBI is lacking (Hier et al. 2021). Thus, it is relatively unclear what the precise mode of entry is from the brain to the blood for these biomarkers and more definitive studies are necessary in this area to aid future understanding. Nevertheless, when patients are imaged utilising MRI with a Gd-based contrast agent within 6 hours following a mild TBI, up to half of those examined were found to have either a compromised BBB or blood-cerebrospinal fluid barrier at this acute stage (Turtzo et al. 2020).

In a variety of rodent models of mild TBI, varying degrees of changes to BBB integrity are evident. Increases in BBB permeability following a lateral controlled cortical impact has a biphasic pattern, with peaks at 4-6 hours and 3 days post-injury (Başkaya et al. 1997). Following a blast injury, there are increases in Evans blue extravasation with 24 hours post-injury with concomitant decreases in the expression of tight junction proteins at both 6 and 24 hours post-injury, associated with increased oxidative damage (Abdul-Muneer et al. 2013). By 3 days following a blast injury, increases in BBB permeability have resolved (Readnower et al. 2010). Conversely, other studies using cortical contusion have shown increased Evans blue extravasation continuing out to 10 days post-injury. Following both a controlled cortical impact and a closed head diffuse injury, BBB permeability, again

shown by Evans blue extravasation, increased immediately but resolved by 24 hours post-injury (Adelson et al. 1998). Another study that employed the weight drop model of TBI demonstrated that both single and repeated injuries did not result in increased BBB permeability (Deford et al. 2002). However, there are several limitations to using extravasating dyes to estimate BBB permeability (Saunders et al. 2008) which may have confounded interpretations. Following a closed head cerebral contusion, the passage of large molecules into the brain had resolved within 4-5 hours post-injury, whereas small molecules were still able to cross the BBB at 4 days post-injury (Habgood et al. 2007).

Following a partial optic nerve transection, there is disruption to the BBB directly at the injury site for days, with peak permeability as shown by Evans blue extravasation occurring at 3 days post-injury, and returning to levels not different to controls by 1 week post-injury (Smith et al. 2016) and 28 days after injury (Smith et al. 2018). In the ventral aspect of the optic nerve adjacent to the injury site there is substantial Evans blue extravasation at 1 day, peaking at 3 days post-injury (Smith et al. 2016). By 7 days post-injury, there are increased low-intensity and diffuse Evans blue extravasation in the ventral nerve, which resolves by 28 days post-injury (Smith et al. 2018). By 3 days following injury the observed breach in the BBB has progressed along the optic nerve towards the brain, as shown by increased Evans blue extravasation (Smith et al. 2016). There were additional changes in the immunoreactivity of fibrinogen at multiple points along the length of the optic tract up until 7 days post-injury (Smith et al. 2018). Interestingly, at 1 day post-injury there is already increased extravasation of Evans blue in the visual regions of the brain, namely the optic chiasm, optic tracts, lateral geniculate nucleus and superior colliculus (Smith et al. 2016), and at 14 days, the immunoreactivity of caveolin-1 at the third ventricle in the brain is significantly decreased (Smith et al. 2018). These findings suggest that remote breaches to the BBB can occur in other areas of the CNS axonally connected to the injury site and supports the notion of a transient alteration in BBB permeability remotely following a partial optic nerve transection. Altogether, although there is some contention in the literature, it is likely there is at least a transient breach to the BBB following a range of severities of neurotrauma.

5.3. The Blood-Brain Barrier and Oxidative Stress

As discussed in Chapter 1, oxidative stress is a known damage mechanism in both MS and neurotrauma. Oxidative stress has also been associated with BBB dysfunction in a variety of CNS diseases and injuries (Grammas et al. 2011). Correspondingly, oxidative stress has been linked to BBB dysfunction following neurotrauma, with increased ROS reducing the expression of tight junction proteins and increased leakage through the BBB following injury (Abdul-Muneer et al. 2014). Oxidative damage is also associated with the BBB tight junction abnormalities, increased leukocyte migration and overall BBB dysfunction observed in MS lesions (Ortiz et al. 2014).

Oxidative conditions can affect the perivascular cells that comprise the BBB. Cells at the BBB inherently have increased vulnerability to oxidative damage because ROS/RNS are used as signalling molecules at the vasculature under normal conditions and are therefore already fairly ubiquitous in perivascular regions. For example, nitric oxide is a signalling molecule for vasodilation from cerebral endothelial cells (Dawson & Snyder 1994). Thus, perivascular cells have a limited capacity to compensate for redox imbalances. Cerebral endothelial cells have a high concentration of mitochondria, the main cellular organelle responsible for the production of ROS, conveying a greater opportunity for oxidative stress to occur in these cells (Grammas et al. 2011). Mitochondrial stress in endothelial cells compromises BBB integrity by increasing permeability, increasing leukocyte trafficking and disrupting tight junctions (Doll et al. 2015). Astrocytes are known propagators of oxidative stress and exacerbate the levels of free radicals (Freeman & Keller 2012). When the levels of the antioxidant glutathione are decreased, the BBB becomes dysfunctional (Agarwal & Shukla 1999), which suggests that overall redox balance is critical for ensuring BBB integrity.

The two specific perivascular cells of interest for this thesis are pericytes and OPCs. Similar to OPCs, pericytes are known to be particularly susceptible to oxidative damage (Rinaldi et al. 2021). Oxidative DNA damage to pericytes due to cathepsin D deficiency has been previously shown to impair BBB integrity by increasing blood vessel diameter, causing hyperpermeability and allowing for the infiltration of peripheral immune cells (Okada et al. 2015). Since pericytes detach from the vascular unit in both MS (Iacobaeus et al. 2017) and neurotrauma (Dore-Duffy et al. 2000), the functional role of oxidative damage in this process is particularly interesting. Given that the overall population of OPCs is particularly vulnerable to oxidative DNA damage (Giacci et al. 2018), it is hypothesised that perivascular OPCs specifically are also similarly vulnerable to the effects of oxidative stress. However, the oligovascular niche is relatively unexplored in both conditions, and the direct effect of oxidative damage to OPCs at the BBB is currently unknown. OPCs and pericytes can also attach to each other and interact, with trophic coupling occurring between these two cell types (Maki et al., 2015). Thus, the interconnected interactions between OPCs and pericytes at the vasculature may be pathologically significant, particularly in the context of oxidative stress.

5.4. Concluding Remarks

Though the BBB is compromised in both MS and neurotrauma, the underlying cause of this dysfunction is not fully understood. However, oxidative stress has been implicated in the loss of BBB integrity observed in both conditions. The forthcoming work presented throughout the remainder of Series Three therefore investigates whether oxidative DNA damage to perivascular OPCs and pericytes causes dysfunction of these cells, to determine whether this was associated with increased BBB permeability in models of neurotrauma and MS.

Chapter 6. Investigating Oxidative Stress in NG2+ Glia in Blood-Brain Barrier Dysfunction Following Neurotrauma

This chapter focusses specifically on oxidative stress in NG2+ glia, primarily comprised of pericytes and perivascular OPCs, at the BBB following neurotrauma. As discussed in Chapter 5, there is a transient disruption to the BBB following a partial optic nerve transection, with substantial Evans blue extravasation at 1 day, peaking at 3 days post-injury (Smith et al. 2016). In order to assess early oxidative damage mechanisms that may contribute to BBB dysfunction, this study employed the partial optic nerve transection model and assessed outcomes at the acute 1 day timepoint. This chapter presents the experimental work performed to investigate the relationship between oxidative stress, BBB dysfunction and cellular proliferation following neurotrauma.

6.1. Tissue Analysis Pipeline Development

6.1.1. Rationale and Design of Immunohistochemical Analyses

Immunohistochemistry is a widely used technique for visually detecting and localising specific antigens within tissue samples (Magaki et al. 2019), with fluorescence-labelled antibodies conveying heightened sensitivity compared to other immunohistochemical antibodies (Moreno et al. 2022). A main advantage of this technique is that it facilitates identification of specific proteins within the spatial context of the tissue with an ability to semi-quantitatively compare the expression of the proteins of interest (Laurinavicius et al. 2016). Immunohistochemical analysis had also been widely utilised throughout the work presented in thesis thus far and is well established in the Fitzgerald laboratory.

A limitation of immunohistochemistry is the number of available fluorescent channels. Many multi-colour confocal microscopes work *via* lasers that provide excitation at different wavelengths with emission filters discriminating the signal from the various fluorescent channels. Due to the overlapping spectra of many fluorescent dyes, it is important to limit the number of fluorophore wavelengths used on a single sample to minimise the signal cross-talk between channels (Cardoso 2005). Spectral unmixing to allow for additional wavelength detection is possible, but this processing technique comes with caveats, including the possibilities of a decreased signal to noise ratio, an incomplete segregation of the fluorophore spectrums or interference from background autofluorescence (Zimmermann et al. 2014). Additionally, there is a limited number of commercially available antibodies that are raised in different species, with most antibodies raised in either goat, mouse or rabbit. If primary antibodies that were raised in the same species are used together, there is a high risk of the same secondary antibody binding to both primary antibodies and thus it is generally recommended to limit the simultaneous use of primary antibodies that were raised in the same species

(Mao et al. 2021). Staining a sample with four different fluorophores simultaneously is considered the optimal maximum to reduce the potential degree of spectral overlap and antibody cross-reactivity, with the ability to perform consecutive staining on two samples an alternative to maximise the available number of fluorescent channels (Jonkman et al. 2020). Therefore, four fluorescent channels (with wavelengths of 405nm, 488nm, 555nm and 647nm) were utilised for the forthcoming work (Figure 6.1).

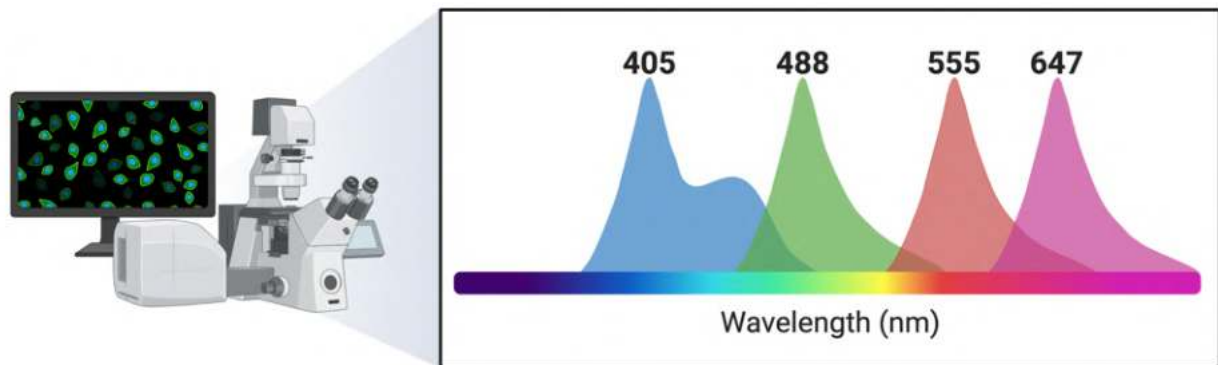


Figure 6.1. The detection of four fluorescent wavelengths by confocal laser scanning microscopy. To minimise spectral overlap and antibody cross-reactivity, samples were stained with four different fluorophores for use with confocal laser excitation wavelengths of 405nm, 488nm, 555nm and 647nm. Original illustration created using BioRender.com.

Since there were only four available channels, careful consideration was required to decide which antigens to detect simultaneously. Colocalisation of two immunohistochemical markers was required to positively identify many of the desired cell types. For example, colocalised expression of PDGFR α and Olig2 is used to specifically visualise OPCs, thus occupying two of the four available fluorescent channels. Given that the purpose of this work is to identify oxidatively damaged cells, a marker indicative of DNA damage is required in colocalisation with the cell specific identification markers, thus further limiting the number of additional markers that can be applied to the same section of tissue.

BBB breach is traditionally identified by the extravasation of tracing dyes, such as Evans blue. Previous work in the partial optic nerve transection model demonstrated a transient extravasation of Evans blue dye away from blood vessels in the first few days following injury, indicating an overt breach of the BBB at this early timepoint (Smith et al. 2016; Smith et al. 2018). However, since the Evans blue dye is injected *in vivo* prior to euthanasia, it cannot be applied to only a subset of tissue sections. The dye also fluoresces at a wavelength that would interfere with the 647nm channel for immunohistochemical analysis (Wang & Lai 2014), which would prevent that wavelength being employed to assess the other desired parameters in brain tissue. Therefore, detection of IgG was considered to be a more appropriate method to measure any breach to the BBB (Franke et al. 2021).

As BBB permeability increases, there is an observable influx of blood proteins and antibodies into the parenchyma, such as serum albumin and IgG (Acharya et al. 2013). By combining an antibody recognising IgG with the rat endothelial cell antigen-1 (RECA) marker to identify blood vessel endothelium, the degree of BBB breach can be determined by the association of parenchymal IgG with individual RECA+ blood vessels. However, since three of the four channels were already occupied by cell damage and cell type specific antibodies, the BBB specific combination had to be applied to an adjacent section.

The immunohistochemistry panels were designed to assess cell type specific damage and BBB dysfunction on consecutive tissue sections. The antibody combinations employed a colocalisation approach for cellular identification, alongside simultaneous staining for DNA damage and another cell status marker to indicate either proliferation or apoptosis. The extent of BBB dysfunction would be detected on an adjacent tissue section by immunohistochemically staining for blood vessel endothelial cells and perivascular IgG. To ensure accurate correlation of individual cells with specific blood vessels visualised in adjacent sections, blood vessel detection was included within one panel of adjacent sections. A summary of the immunohistochemical panels is presented below in Figure 6.2.

Assessing	Channel 1	Channel 2	Channel 3	Channel 4		
OPC Damage	OPCs (Olig2)	OPCs (PDGFR α)	DNA Damage (8OHdG)	Blood Vessels (RECA)	OR Proliferation (EdU)	OR Apoptosis (Caspase3)
BBB Dysfunction	Blood Vessels (RECA)	BBB Breach (IgG)				
Pericyte Damage	Pericyte (NG2)	Pericyte (PDGFR β)	DNA Damage (8OHdG)	Blood Vessels (RECA)	OR Proliferation (EdU)	OR Apoptosis (Caspase3)

Figure 6.2. Immunohistochemical panels designed to assess the role of oxidative damaged OPCs and pericytes at the BBB following neurotrauma. Each immunohistochemical experiment was designed to assess three adjacent sections, for OPC damage, BBB dysfunction and pericyte damage respectively. The fourth antibody used in the cell specific panels was designed to be interchanged to reflect the core research questions. Original illustration created using BioRender.com.

6.1.2. Initial ImageJ Analysis Pipeline

In order to ensure that the images were capable of answering the research questions, an image analysis pipeline was designed. The ImageJ analysis protocol below was developed to allow for the identification and mapping of DNA damage cells in relation to sites of BBB breach. (Figure 6.3). This technique allowed for the specific segregation of the overall ventral nerve and the perivascular and parenchymal regions therein. A perivascular region was defined as the area within a 10 μ m radius of a RECA⁺ blood vessel to capture the cells that directly neighbour and interact with the cerebrovasculature. For images without a RECA stain, the RECA signal from the immediately adjacent section was superimposed onto the image to allow for mapping of blood vessel locations. The parenchymal area was created as an inverse region of the selected perivascular areas to capture all cells that reside more than 10 μ m away from the vasculature within the ventral nerve. This method also involved creating a map of the breach status of each blood vessel using the associated extravasation of IgG to associate specific perivascular regions with BBB dysfunction. Finally, thresholding analyses were used to objectively define and measure cell identification markers and the associated levels of oxidative stress using the panels designed in Section 6.1.1.



Figure 6.3. ImageJ analysis pipeline developed to investigate the role of oxidative damaged OPCs and pericytes in BBB dysfunction following neurotrauma.

6.2. Study Design and Animal Procedures

To investigate the relationship between oxidative stress and BBB dysfunction at 1 day after a partial optic nerve transection, adult female PVG rats weighing approximately 180g were acquired from the Animal Resource Centre (Murdoch, Western Australia). The rats had *ad libitum* access to food and water, were housed under a 12-hour light/dark cycle and were given a 1 week acclimatisation period to the holding location prior to the commencement of the experimental period. The experimental cohort consisted of nineteen rats with two experimental groups, a control group that received a sham injury (n = 9) and an injured group that received a partial optic nerve transection (n = 10). The reduction in the number of sham control animals compared to injured animals is due to one rat being resistant to the anaesthesia required for surgical procedures and therefore omitted from the study. All procedures were in accordance with the principles of the NHMRC and approved by the Animal Ethics Committee of The University of Western Australia (RA/3/100/1485) and the Animal Ethics Committee of Curtin University (ARE2017-4).

Partial optic nerve transection was performed by Mrs Carole Bartlett as previously described (Chapter 2; Bartlett & Fitzgerald 2018), under Ketamine (Ketamil, 50mg/kg, Troy Laboratories) and Xylazine (Ilium Xylazil, 10mg/kg, Troy Laboratories) anaesthesia that was delivered *via* intraperitoneal injection. In this procedure, the dorsal aspect of the right optic nerve is cut to a depth of 200µm with a diamond radial keratotomy knife, at 1mm behind the eye. The sham uninjured control animals received all surgical procedures, apart from the cut in the sheath and the partial incision into the nerve. Post-operative analgesia consisted of a single subcutaneous injection of Carprofen (2.8mg/kg, Norbook Australia) alongside another subcutaneous injection of 1 mL sterile PBS directly following surgery for fluids maintenance. To label cells actively undergoing the cell cycle, EdU (20mg/kg, Invitrogen) was intraperitoneally administered twice, once immediately following surgical procedures during post-operative care and once the following morning at least 2 hours prior to euthanasia.

At 1 day following injury, tissue was collected and processed. Rats were euthanised with pentobarbitone sodium (160mg/kg, Delvet) and perfused transcardially with 0.9% saline followed by 4% paraformaldehyde (Sigma-Aldrich). The right optic nerves were dissected and immersed in 4% paraformaldehyde overnight, before being transferred to 15% sucrose (Chem Supply), 0.1% sodium azide (Sigma-Aldrich) in PBS for cryoprotection. The nerves were then embedded in OCT and cryosectioned transversely at 14µm. The resulting sections were collected onto Superfrost Plus glass microscope slides and stored at -80°C for subsequent immunohistochemical analysis. The entire experimental design for this cohort is summarised in Figure 6.4.

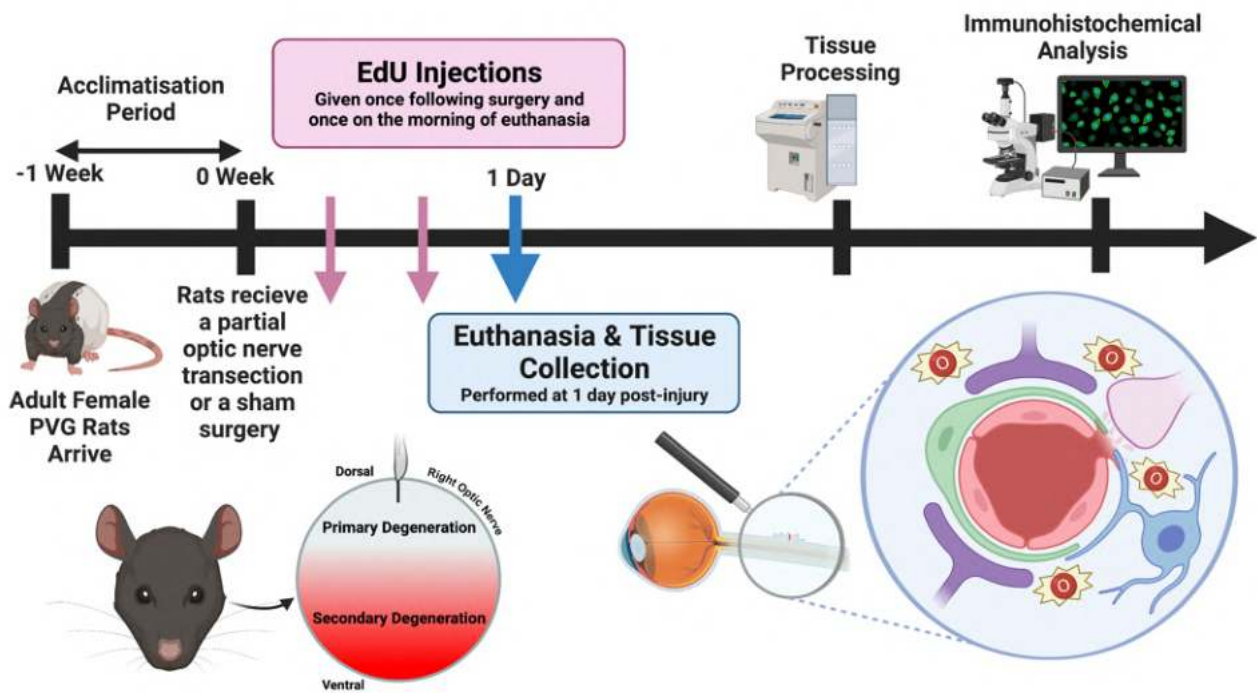


Figure 6.4. Experimental design for cohort investigating BBB dysfunction following a partial optic nerve transection. Adult female PVG rats underwent either a partial optic nerve transection ($n = 10$) or a sham surgery ($n = 9$) and were subsequently euthanised at 1 day post-injury to capture early BBB dysfunction. EdU (20mg/kg) was administered *via* intraperitoneal injection twice during the experimental period, once following surgical procedures and once on the morning of euthanasia. Following euthanasia and tissue collection at 1 day post-injury, the collected optic nerves were cryosectioned and analysed. Original illustration created using BioRender.com.

6.3. Variability in Blood Vessel Location and Morphology in the Optic Nerve

Prior to undertaking comprehensive analysis of the tissue using the protocols described in Section 6.1.1, it was imperative to ensure that the location of blood vessels could be accurately tracked between adjacent transverse sections. During cryosectioning, the optic nerves were embedded in groups of four to five and then sectioned at $14\mu\text{m}$ thickness with the adjacent sections of tissue placed onto neighbouring slides (Figure 6.5A). In doing so, the middle z plane of each section was theoretically $14\mu\text{m}$ apart from the adjacent section on either of the two neighbouring slides. Three adjacent slides for each group of nerves were immunohistochemically stained with the RECA antibody in line with established protocols (Fitzgerald *et al.*, 2010) to label all of the blood vessels of the optic nerve. Once imaged, the three RECA+ sections per animal were digitally superimposed to create a composite image (Figure 6.5B). However, following this overlaying process, it became clear that the blood vessels were moving location and significantly changing morphology across the three adjacent sections (Figure 6.5C).

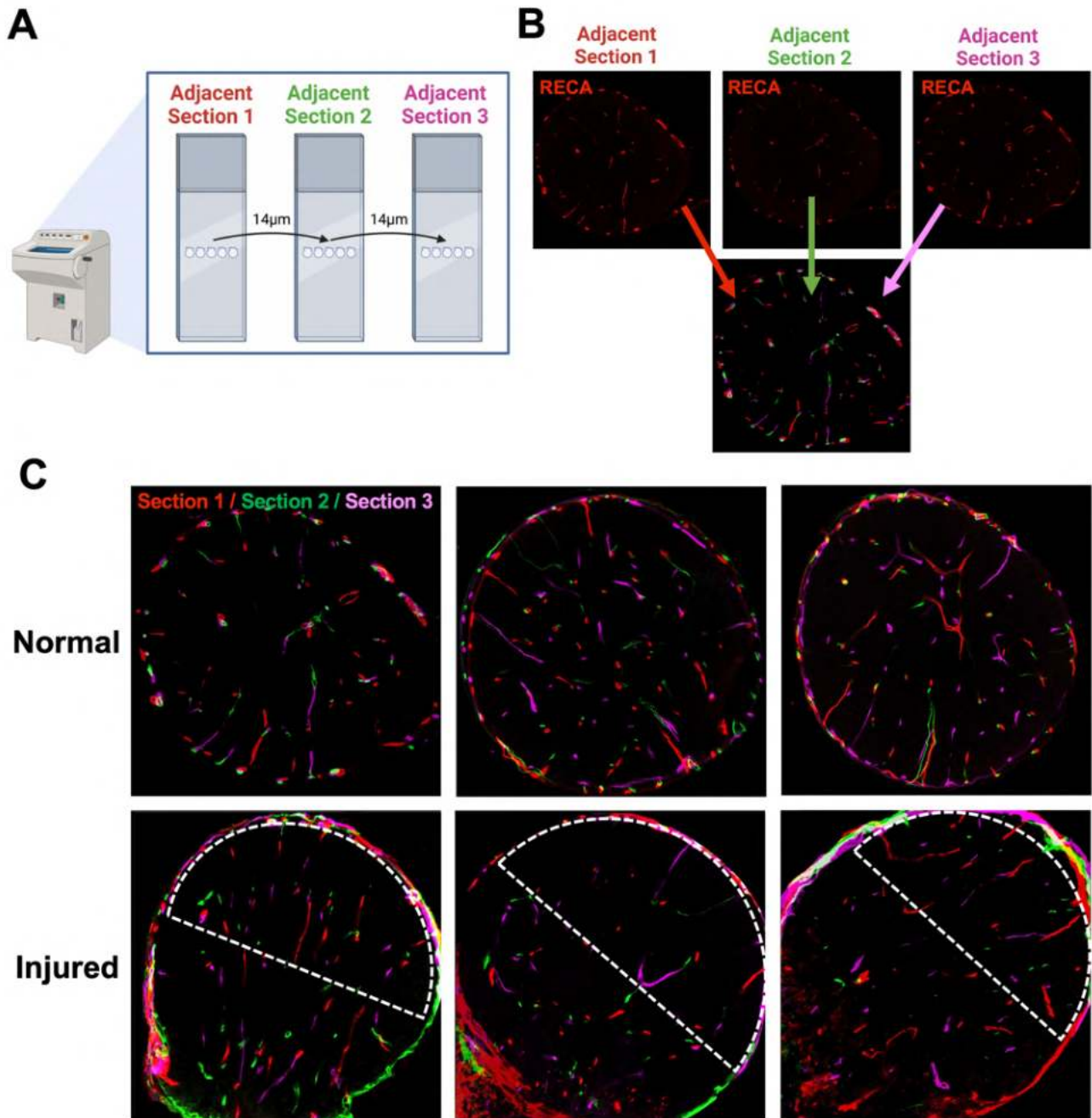


Figure 6.5. Representative images demonstrating the variability in blood vessel location and morphology across adjacent transverse sections of the optic nerve. (A) Adjacent sections were collected onto neighbouring slides to allow for an analysis of blood vessels throughout three continuous transverse sections of optic nerve. Original illustration created using BioRender.com (B) Three adjacent sections per animal were stained to detect blood vessels using an anti-RECA antibody, with the collected images digitally superimposed to create one composite image. (C) Representative images demonstrating that across three adjacent sections for both normal ($n = 3$) and injured animals ($n = 3$), the location and morphology of blood vessels significantly changed. $n = 5$ rats per group were analysed in total. For injured animals, the ventral aspect of the nerve vulnerable to secondary degeneration has been denoted with dotted lines.

While occasional blood vessels were conserved in location across sections, these vessels were typically located on the peripheral pial surface of the nerve, with the branching capillaries inside the nerve parenchyma showing the greatest degree of variability (Lessell 1974). The orientation of these parenchymal capillaries ranged from being positioned parallel to the nerve axis to a horizontal perpendicular orientation, with these vessels specifically being cut obliquely during cryosectioning. These perpendicular vessels were particularly variable, which may be due to their orientation inherently prevented them from being preserved across the adjacent transverse sections. The observed lateral movement in blood vessels was found in both injured and sham nerves, and thus was not a product of damage mechanisms but rather a general reflection of the complex branching of rat optic nerve capillaries. A key ramification of this observed blood vessel variability was that if perivascular cells were identified solely by overlaying a map of the locations of RECA+ blood vessels from an adjacent section, there would likely be a high degree of error. Therefore, it would not be accurate to overlay adjacent RECA+ images onto the images of cellular outcomes to determine the location of specific cells in relation to blood vessels.

It's also important to note that placing cellular outcomes markers over adjacent sections would also not have been suitable either due to the relative size of the cells compared to the section thickness. For example, OPC cell bodies have a diameter of only 6-8 μ m (Karasek et al. 2004), which means that an individual OPC is highly unlikely to span across adjacent 14 μ m thick sections. Hence, all antibodies regarding cellular identification and status were required to be within the one combination. Therefore, although performing an adjacent section analysis is an option for increasing the capacity to simultaneously detect multiple antigens, this type of analysis would not have been able to address the core research questions and it was necessary to modify the ImageJ analysis plan.

To investigate DNA damage to cells at the vasculature and in the parenchyma, the immunohistochemistry panel containing RECA, 8OHdG and the relevant cell identification markers was utilised. It was not possible to include an immunohistochemical analysis that encompassed both IgG and RECA to detect the ratio of breached and non-breached blood vessels as well as the markers required to identify DNA damaged double positive perivascular cells. Thus, the extent of IgG extravasation was examined in an adjacent section using RECA and IgG, but the degree of breach at the level of individual blood vessels would not be directly linked across the adjacent sections. Rather, the overall level of IgG extravasation from blood vessels would be statistically correlated to the degree of damage quantified separately in the adjacent section. Furthermore, due to the limitations of four colour immunohistochemistry, as described in Section 6.1.1, the role of DNA damage to OPCs and pericytes for cell proliferation and apoptosis would be analysed in the ventral nerve as a whole, without the inclusion of RECA to focus outcomes specifically to blood vessels.

6.4. Optimisation of Immunohistochemistry Protocols

There were initial delays in the immunohistochemical analysis for this study due to methodological setbacks, including lack of tissue adherence to the microscope slides, and the need to optimise techniques to minimise fluorescence cross-reactivity given the use of four colour immunohistochemistry. In collaboration with Dr. Chidozie Anyaegbu and Ms. Melissa Papini, the immunohistochemical protocol was systematically adjusted to accommodate for these issues and the resultant refined protocol is outlined (Figure 6.6).

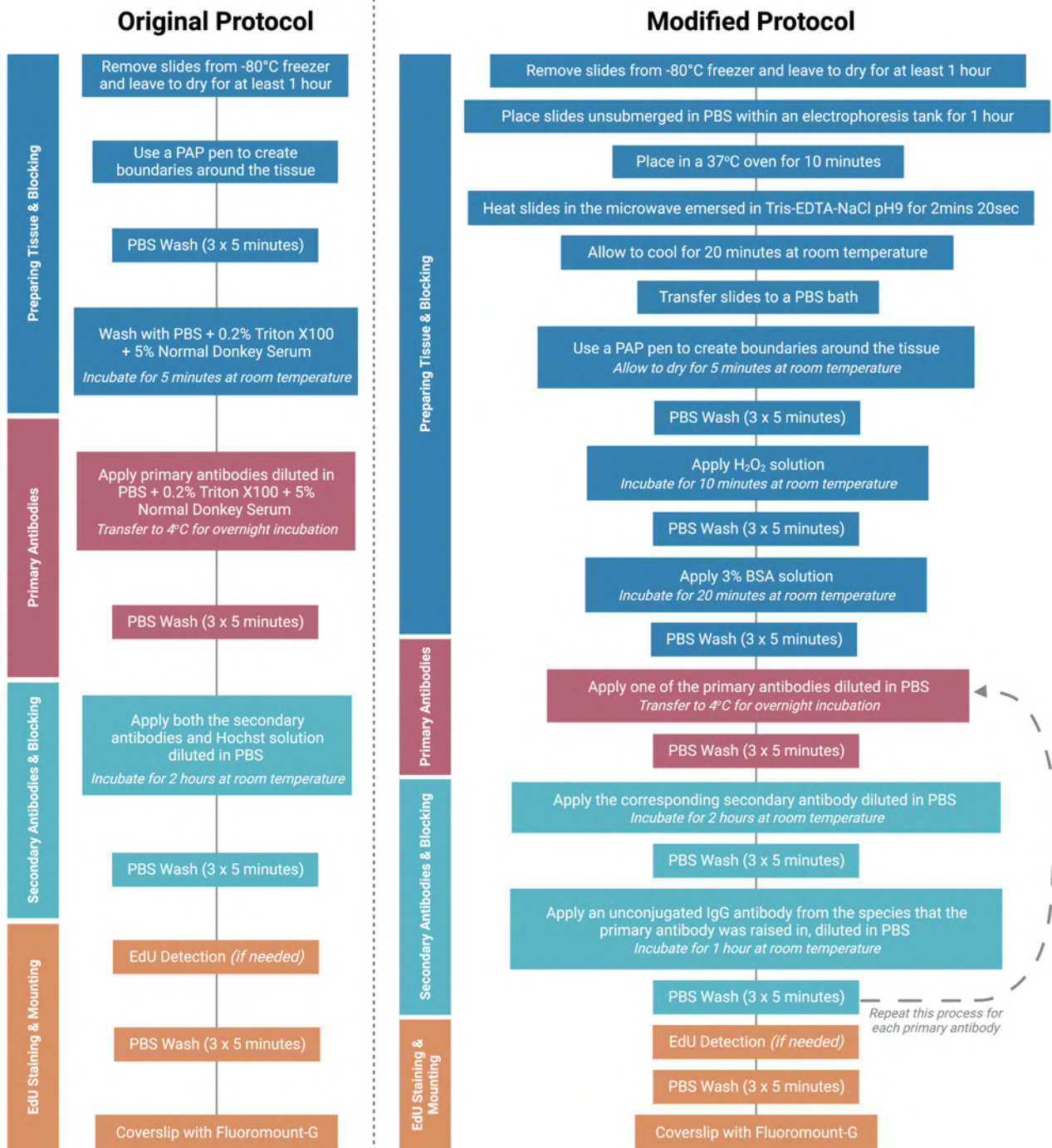


Figure 6.6. Modified immunohistochemistry protocol for use on rat optic nerve tissue sections. The original protocol was previously optimised for rat optic nerve and is presented as described in published Fitzgerald group articles, including in Fitzgerald *et al.*, 2010 and Toomey *et al.*, 2019. The modified protocol was optimised for four colour immunohistochemistry.

There were many modifications made to this protocol throughout the optimisation period, the first of which was initially placing the slides into an electrophoresis tank for 1 hour. This technique was developed by Ms. Melissa Papini to enable the microscope slides to be recharged to prevent tissue from detaching throughout the remainder of the protocol. Additionally, an antigen retrieval

step was included to maximise the immunohistochemistry signals. Citrate buffer and Tris-EDTA-NaCl were compared, with Tris-EDTA-NaCl better enhancing epitope binding.

To prevent non-specific binding, a variety of blocking techniques were compared including applying normal donkey serum, bovine serum albumin (BSA), hydrogen peroxide solution, Triton X-100 and background sniper for varying lengths of time (eg. 5 minutes, 20 minutes or 60 minutes). Following extensive trials of blocking combinations, the optimal technique to prevent non-specific binding was an application of hydrogen peroxide solution for 10 minutes followed by 3% BSA solution for 20 minutes. Similarly, it was critical to prevent cross-reactivity between antibodies. To minimise the degree of cross-binding, each primary and secondary antibody combination was applied separately. The order of this sequential application was also optimised to minimise unwanted binding. Following each secondary antibody application, an unconjugated IgG antibody from the species that primary antibody was raised in was applied to the tissue. This technique blocked the Fc & Fab regions of the preceding antibody to minimise cross-reactivity during the upcoming additional antibody incubations.

Other smaller modifications included allowing a 5 minute period following the application of the PAP pen boundary to allow the wax pen to fully dry on the slide and prevent an astrocytic-like staining pattern. Similarly, the concentrations of each primary and secondary antibody were optimised for the relevant channels. In particular, optimising antibodies for use in the 405nm channel was difficult as the 405 secondary antibodies had poor signal strength and thus required a high concentration for adequate antigen detection. Once the antibodies for each panel were optimised both in isolation and in combination using the above protocol, the immunohistochemical experiments were performed on the full cohort of tissue in collaboration with Ms. Melissa Papini.

6.5. Analysing Immunohistochemical Outcomes

For each analysis, the entire optic nerve was visualised and images captured at a 20x magnification using confocal microscopy, with a series of images taken at 0.5 μ m increments along the z axis. Imaging for each experiment was conducted with consistent microscope settings for all experimental groups. Upon imaging the three final immunohistochemical experiments, although some antibody staining was successful, many of the images demonstrated poor and inconsistent immunohistochemical staining for some markers. These issues typically manifested as a high degree of non-specific staining, significant cross-reactivity with other antibodies within the combination, the lifting of nerve sections from the slide resulting in uneven staining patterns, and/or simply the absence of any positive staining. Unfortunately, there was insufficient tissue remaining to repeat the immunohistochemical procedures. Any sections for which there was doubt regarding the staining

were excluded, leaving fewer outcomes available for analysis. Specifically, robust data were available for antibodies detecting 8OHdG, NG2, PDGFR α , IgG and EdU.

Since a more generalised approach to analysing outcomes was now required, the analysis pipeline was again modified. The area of the ventral nerve was segmented and quantified with ImageJ software. The mean area and intensity of immunoreactivity for IgG and 8OHdG were semi-quantified using the single most in focus visual slice within the z stack. An immunointensity threshold for each was determined to distinguish positive signal from background before an intensity analysis determined the area and intensity above the set threshold within the ventral nerve. Area above threshold measurements were then normalised to the total area of the ventral nerve. To assess the levels of DNA damage specifically within NG2⁺ glia and PDGFR α ⁺ glia, additional representative thresholds were set to identify positive NG2 and PDGFR α immunointensity respectively, with the intensity of 8OHdG then also measured solely within the identified glia. Finally, the density of EdU⁺ cells were counted within the ventral nerve, normalised against the total ventral area and expressed as the mean number of cells/mm². The presence of EdU⁺ 8OHdG⁺ cells were determined by the colocalisation of EdU⁺ cells with 8OHdG immunointensity above the set threshold. Similarly, EdU⁺ cells were categorised into colocalised PDGFR α ⁺ and PDGFR α ⁻ subpopulations using the aforementioned representative threshold for identifying PDGFR α ⁺ glia. The PDGFR α ⁺ and PDGFR α ⁻ subpopulations were further categorised *via* the colocalised presence of 8OHdG DNA damage.

Resulting data were analysed using GraphPad PRISM 9 software. All outcome measures relating to 8OHdG and EdU satisfied the assumption of normality according to a Kolmogorov–Smirnov test and thus either a t-test, two-way ANOVA with Tukey’s *post-hoc* or three-way ANOVA with Tukey’s *post-hoc* were used as appropriate. However, the area of IgG immunointensity did not satisfy the assumption of normality according to a Kolmogorov–Smirnov test and thus the non-parametric Mann-Whitney test was used to assess the statistical difference between sham and injury for this outcome measure. A Spearman’s correlation was used to assess the relationship between IgG and either 8OHdG or EdU as this statistical analysis is most compatible with monotonic relationships between two variables, as opposed to the Pearson’s correlation which best assesses linear relationships. Outliers were not removed for any outcome measures. Reductions in final n’s reflect loss of tissue from slides during the immunohistochemical analyses or the exclusion of sections that had become damaged during tissue processing and analysis in a way that precluded reliable quantification of outcomes.

6.6. Investigating the Relationship Between Oxidative Stress, BBB Dysfunction and Cellular Proliferation in Neurotrauma

6.6.1. Effect of Injury on the Level of Oxidative DNA Damage

The effect of a partial optic nerve transection on oxidative DNA damage as indicated by 8OHdG immunoreactivity in the ventral nerve was assessed (Figure 6.7). Both the mean area ($t(4.448) = 17, p = 0.0004$, Figure 6.7A) and mean intensity ($t(4.197) = 17, p = 0.0006$, Figure 6.7B) of 8OHdG immunoreactivity significantly increased with injury compared to sham controls. When NG2+ glia were specifically analysed, the mean intensity of 8OHdG also significantly increased compared to the sham group ($t(2.161) = 15, p = 0.0472$, Figure 6.7C). The NG2+ population is primarily comprised of pericytes and OPCs, with additional colocalised markers, such as PDGFR β , required for more accurate cell type specific identification. Although the immunoreactivity of PDGFR β was not consistent enough to perform a quantitative analysis specific to pericytes or OPCs, a qualitative assessment indicated that both NG2+/PDGFR β + pericytes and other NG2+/PDGFR β -glia, likely to be OPCs, experience 8OHdG+ DNA damage post-injury (Figure 6.7E). Correspondingly, there was an observed significant increase with injury in the mean intensity of 8OHdG within PDGFR α + glia, which likely predominantly reflects the OPC population ($t(3.992) = 17, p = 0.0009$, Figure 6.7D). Thus, additional work is needed to determine the relative contribution of pericytes and OPCs to this overall 8OHdG+/NG2+ population. Further work can also determine the level of 8OHdG in perivascular compared to parenchymal NG2+ glia, which will deepen understanding of the pathology of BBB breach following neurotrauma. Nevertheless, these results indicate that OPCs, and perhaps also pericytes, are oxidative DNA damaged at 1 day post-injury.

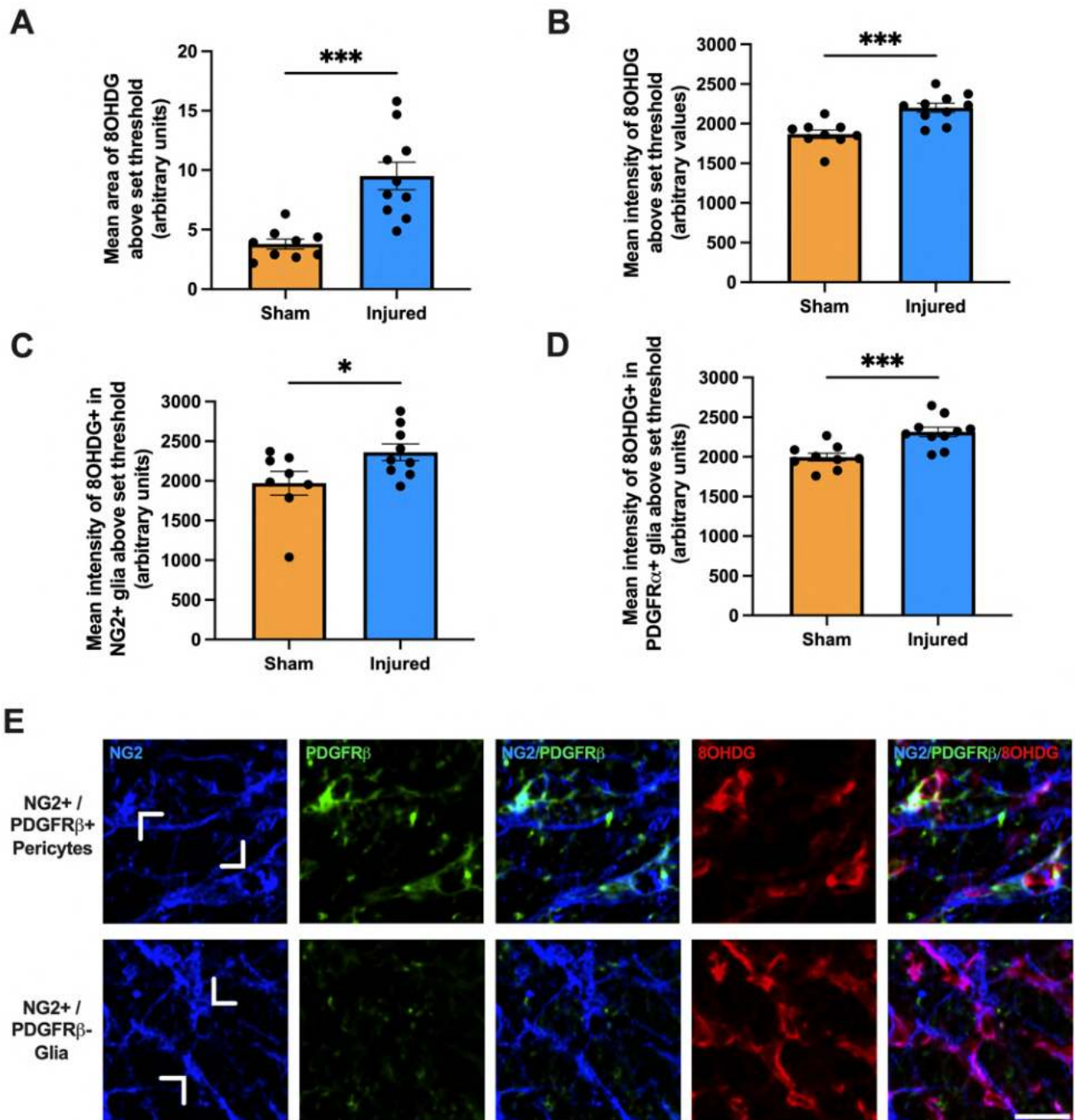


Figure 6.7. Effects of injury for oxidative DNA damage within the ventral nerve. Area (A) and mean intensity (B) of 8OHDG immunointensity within the ventral nerve was assessed to determine the level of oxidative DNA damage following a partial optic nerve transection. The mean intensity of 8OHDG was specifically quantified inside NG2+ glial cells (C) and PDGFR α + glia (D) in the ventral nerve. Graphs display individual data points overlaid on a bar displaying the mean \pm SEM. $n = 8-10$ rats per group. Statistical analysis by t-tests. Significant differences are indicated by * $p \leq 0.05$, *** $p \leq 0.001$. (E) Representative images of both NG2+/PDGFR β + pericytes and NG2+/PDGFR β - glia with 8OHDG+ DNA damage are shown, scale bar = 20 μ m.

6.6.2. Effect of Injury on BBB Integrity

Additionally, the effect of a partial optic nerve transection on BBB breach as indicated by the extravasation of IgG in the ventral nerve was assessed (Figure 6.8). The mean area of IgG immunoreactivity significantly increased with injury compared to sham controls ($Mdn_{sham} = 2.018$, $Mdn_{injured} = 0.00825$, $U = 0$, $p < 0.0001$, Figure 6.8A,C). A strong and significant positive monotonic relationship between the mean areas of IgG and 8OHdG immunoreactivities was observed ($r_s = 0.752$, $p = 0.0003$, Figure 6.8B), demonstrating that animals with increased DNA damage in the ventral optic nerve typically experience greater levels of BBB dysfunction in the same area. For the associated correlation scatterplot (Figure 6.8B,C), the mean area of IgG immunointensity has been plotted on a log scale to best illustrate the overall relationship between IgG and 8OHdG.

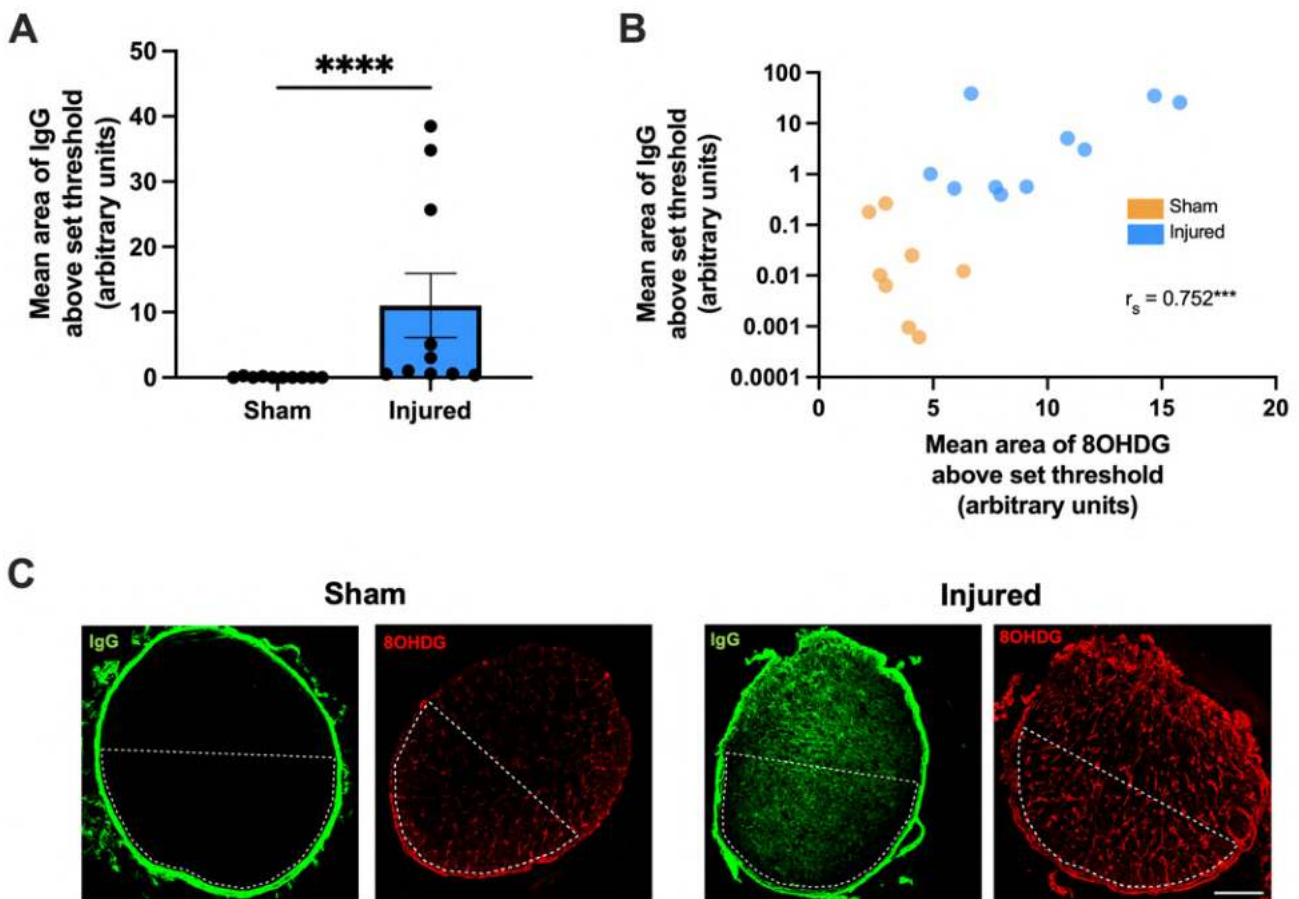


Figure 6.8. Effects of injury for BBB dysfunction and oxidative DNA damage within the ventral nerve. (A) Area of IgG immunointensity within the ventral nerve was assessed to determine the level of BBB breach following a partial optic nerve transection. Graph displays individual data points overlaid on a bar displaying the mean \pm SEM. Statistical analysis by Mann-Whitney test. (B) The area of IgG immunointensity was correlated to the area of 8OHdG using a Spearman's correlation, with the r_s value and corresponding p value displayed on the graph. Each data point on the graph represents an individual animal. $n = 8-10$ rats per group. Significant differences are indicated by $***p \leq 0.001$, $****p \leq 0.0001$. (C) Representative images of both 8OHdG and IgG immunoreactivity in sham and injured rats are shown. Area of the ventral nerve is denoted by dotted lines, scale bar = $100\mu m$.

6.6.3. Effect of Injury on Cellular Proliferation

The effect of a partial optic nerve transection on cellular proliferation as indicated by EdU+ staining in the ventral nerve was also assessed (Figure 6.9). The densities of EdU+ cells had a trend towards increasing with injury compared to sham controls, but this difference did not reach significance ($t(2.072) = 17$, $p = 0.0528$, Figure 6.9A). A weak but significant positive monotonic relationship between the mean area of IgG immunointensity and EdU+ densities was observed ($r_s = 0.466$, $p = 0.0446$, Figure 6.9B). EdU+ cells were then categorised based on colocalisation with 8OHdG and a two-way ANOVA was used to compare the densities of proliferating cells either with or without oxidative DNA damage ($F(1,34) = 2.947$, Figure 6.9C). A significant difference was observed by Tukey *post-hoc* comparisons in the density of EdU+ 8OHdG+ cells with injury compared to both EdU+ 8OHdG+ ($p = 0.0264$) and EdU+ 8OHdG- cells ($p = 0.0365$) for the sham group. There was no differences in the density of EdU+ 8OHdG- cells with injury compared to EdU+ 8OHdG- cells without injury ($p > 0.05$). The EdU+ population was then identified as either PDGFR α + or PDGFR α - glia and analysed using a two-way ANOVA ($F(1,36) = 1.457$, Figure 6.9D). Tukey *post-hoc* comparisons revealed a significant increase in the density of EdU+ PDGFR α + cells with injury compared to sham ($p = 0.0466$). No significant difference was observed in the density of EdU+ PDGFR α - cells with injury ($p > 0.05$). The EdU+ PDGFR α + and EdU+ PDGFR α - populations were further classified by the localisation with 8OHdG DNA damage and analysed *via* a three-way ANOVA with Tukey *post-hoc* comparisons ($F(1, 64) = 1.958$, Figure 6.9E,F). There was a significant increase with injury in the density of EdU+ PDGFR α + 8OHdG+ cells compared to sham ($p = 0.0115$). There was also a significant difference between the density of EdU+ PDGFR α + 8OHdG+ cells with injury compared to the density of both EdU+ PDGFR α + 8OHdG- cells ($p = 0.0021$) and EdU+ PDGFR α - 8OHdG+ cells ($p = 0.0115$) in sham animals. Interestingly, the density of EdU+ PDGFR α + 8OHdG+ cells were also significantly higher than EdU+ PDGFR α + 8OHdG- cells within injured animals ($p = 0.0033$). Due to poor immunohistochemical staining, a similar cell specific analysis was not able to be completed for either NG2+ or PDGFR β + cells. Nevertheless, a large proportion of proliferating cells belonged to the PDGFR α + cell population, which is primarily comprised of OPCs. Altogether, this suggests that OPCs are the major proliferating, DNA damaged cell type at 1 day following injury to the optic nerve.

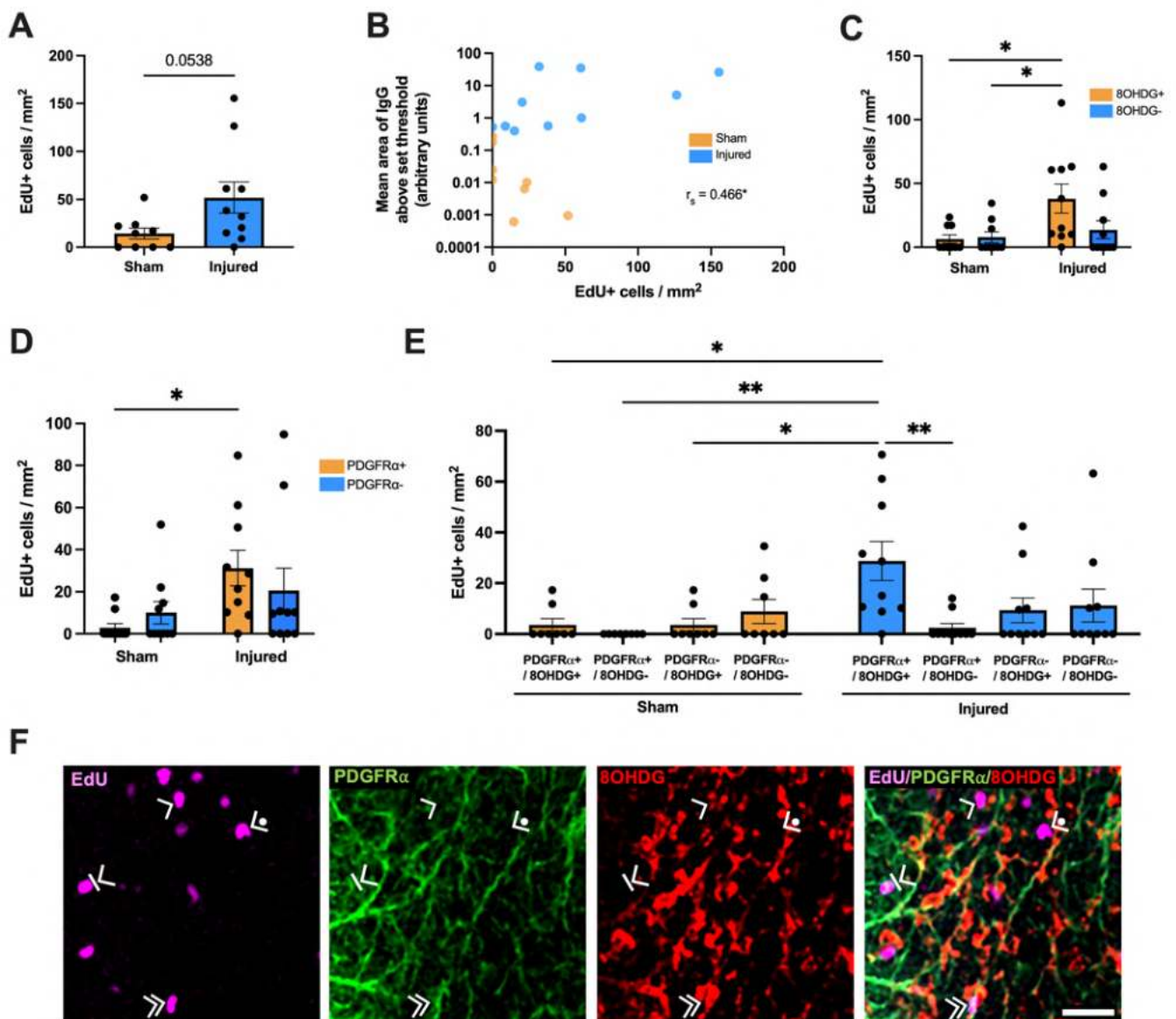


Figure 6.9. Effects of injury for cellular proliferation and oxidative DNA damage within the ventral nerve. (A) The density of EdU+ cells were quantified in the ventral optic nerve following a partial optic nerve transection. Statistical analysis by t-test. (B) The area of IgG immunointensity was correlated to the density of EdU+ cells using a Spearman's correlation, with the r_s value and corresponding p value displayed on the graph. The relative densities of EdU+ 8OHDG+ and EdU+ 8OHDG- cells (C) as well as EdU+ PDGFR α + and EdU+ PDGFR α - cells (D) were quantified. Statistical analysis by two-way ANOVA and Tukey *post-hoc* tests. (E) The relative densities of EdU+ cells colocalised with PDGFR α and 8OHDG were quantified. Statistical analysis by three-way ANOVA with Tukey *post-hoc* tests. All graphs display individual data points overlaid on a bar displaying the mean \pm SEM, except for (B) where each data point on the graph represents an individual animal. $n = 8-10$ rats per group. Significant differences are indicated by * $p \leq 0.05$, ** $p \leq 0.01$. (F) Representative images illustrating EdU+ PDGFR α + 8OHDG+ OPCs (indicated by >>), EdU+ PDGFR α + 8OHDG- OPCs (indicated by >|), EdU+ PDGFR α - 8OHDG+ cells (indicated by >), EdU+ PDGFR α - 8OHDG- cells (indicated by >•) are shown, scale bar = 25 μ m.

6.7. Concluding Remarks

This chapter presents the work performed to assess the role of oxidative damage to perivascular OPCs and pericytes at the BBB in neurotrauma. In this study, the partial optic nerve transection model of neurotrauma was employed at an acute 1 day timepoint. The observed increase in BBB dysfunction in the nerve 1 day post-injury in this cohort is in line with previous studies that have demonstrated increased Evans blue extravasation at the 1 day timepoint (Smith et al. 2016). In addition, this study has demonstrated that the 8OHdG+ DNA damage significantly increases in the ventral nerve. Increases in 8OHdG immunointensity were observed specifically within NG2+ glia at this early timepoint, with qualitative assessment of colocalisation between NG2 and PDGFR β suggesting that both pericytes and OPCs may be vulnerable to DNA damage following injury. In particular, the colocalisation of 8OHdG DNA damage with PDGFR α indicates a potential vulnerability of OPCs to DNA damage acutely post-injury. Importantly, the level of 8OHdG damage significantly correlated to the extent of IgG extravasation, suggesting a relationship between oxidative DNA damage and acute BBB breach. Furthermore, the density of newly derived and proliferating cells increased with injury, with a weak but significant correlation between IgG extravasation and the density of EdU+ cells. The proportion of newly derived and proliferating cells with DNA damage in the ventral nerve also increased with injury, suggesting that there may be a functional implication of DNA damage to cell cycling mechanisms. Finally, this study demonstrated that the PDGFR α + cell population, which is primarily comprised of OPCs, is the major proliferating, DNA damaged cell type at 1 day following injury to the optic nerve. Though additional research is needed to further probe the role of oxidative damage mechanisms in both BBB and cellular dysfunction, these preliminary novel results are valuable insights into the mechanisms underpinning secondary degeneration of the optic nerve at this acute timepoint following neurotrauma.

The work presented throughout this chapter has since been clarified and formed into a publication titled, "Secondary degeneration of oligodendrocyte precursor cells occurs as early as 24 hours after optic nerve injury in rats". This article focuses specifically on the role of early oxidative damage mechanisms to OPCs to highlight this cellular population as an important therapeutic target for limiting the progression of secondary degeneration following neurotrauma. The paper has been published by the International Journal of Molecular Sciences, with the full version available in Appendix C. The implications of these results in the context of the wider literature and the rest of the thesis are also discussed further within Chapter 8.

Chapter 7. Investigating Oxidative Stress in NG2+ Glia in Blood-Brain Barrier Dysfunction in Demyelinating Disease

Alongside assessing cellular damage related to BBB dysfunction in neurotrauma, this thesis aimed to assess whether similar mechanisms were operating in demyelinating disease, to identify common mechanisms of BBB damage. As discussed in Chapter 5, the initial disruption to BBB integrity during cuprizone toxicity also occurs very early in the disease pathology. Previous studies have demonstrated increased extravasation of fluorescent dyes in the corpus callosum occurring as early as 3 days into cuprizone administration, with a peak at 5 days that decreases again by 7 days (Berghoff et al. 2017; Shelestak et al. 2020). To capture this window of BBB dysfunction, the forthcoming study was designed to assess the cellular mechanisms that underpin early BBB dysfunction in the cuprizone model at 3, 5 and 7 days after commencement of pelleted cuprizone feed. The core goal of this study was to investigate the role of oxidative damage to perivascular OPCs and pericytes at the BBB in demyelinating disease. Due to the time constraints of candidature and the methodological difficulties already described, as well as the impact of COVID-19 associated laboratory shutdowns throughout the PhD program, there is still additional work remaining for this study. Therefore, this chapter presents the preliminary experimental work performed to date together with detailed plans for the continuation of this research.

7.1. Study Design and Animal Procedures

Forty-eight 8 week old male C57Bl/6J mice were divided into four groups (n=12/group), with mice fed cuprizone pellets for either 3, 5, or 7 days, and an additional age-matched control group given pelleted standard rodent chow for 5 days (Figure 7.1). Mice that were fed either the cuprizone or control feed for either 3 or 5 days were delivered directly to the experimental holding location from the Animal Resource Centre (Murdoch, Western Australia). However, due to the 14 day holding period restrictions at the animal facility, as well as the limited availability of days for animal delivery from the Animal Resource Centre, mice who were fed cuprizone for the entire 7 days were originally delivered to a separate nearby holding facility for 2 days prior to relocation to the experimental location. Nevertheless, all mice were given a full 1 week acclimatisation period to the experimental holding location prior to the commencement of the study.

		Timepoint		
		3 Day	5 Day	7 Day
Control			n = 12	
Cuprizone	n = 12	n = 12	n = 12	n = 12

Figure 7.1. Experimental groups for cohort investigating oxidative stress and BBB dysfunction in the cuprizone model of demyelinating disease. There were four experimental groups, including 3, 5 and 7 day cuprizone groups and a 5 day age-matched control group (n = 12/group, total n = 48).

The animals had *ad libitum* access to water and food, and were housed under a 12 hour light/dark cycle. Procedures were in accordance with the principles of the NHMRC and approved by both the Animal Ethics Committee of The University of Western Australia (RA/3/100/1613) and the Animal Ethics Committee of Curtin University (ARE2019-4). Given the successful induction of demyelinating disease when mice were administered cuprizone pellets rather than cuprizone powder in the paper presented in Chapter 4, the same intoxication technique was utilised in the current study. Cuprizone-fed mice were delivered 0.2% cuprizone (ChemSupply) in the form of pelleted feed (Specialty Feeds, Perth, Western Australia). Mice that did not receive pelleted cuprizone were instead given control pellets with the same nutritional composition to the cuprizone-containing pellets, with the exception of the addition of cuprizone. Animals were housed two per cage and pellets were changed every 1 to 3 days. To label cells actively undergoing the cell cycle, EdU (20mg/kg, Invitrogen) was administered *via* intraperitoneal injection twice in the day prior to euthanasia, with a minimum of an 8 hour interval between injections.

In accordance with animal ethics approval requirements, mice were weighed daily and if they weighed less than 85% of their original body weight at the commencement of the experimental period, their feed was supplemented with normal powdered chow. They were subsequently weighed twice daily until they returned to above the 85% weight threshold. No mice within the 5 day control group nor the 3 or 5 day cuprizone groups required diet supplementation due to substantive weight loss. However, within the 7 day cuprizone timepoint group, n = 7 mice required this dietary intervention for a single 24 hour period across the last 3 days of the experimental period. The impact of this diet supplementation on animal weights and potentially on the demyelinating pathology achieved will be further discussed in Section 7.2.

At the end of the experimental period, mice were euthanised with pentobarbitone sodium (160mg/kg, Delvet), prior to transcardial perfusion with 0.9% saline, followed by 4%

paraformaldehyde (Sigma-Aldrich) in 0.1M phosphate buffered solution pH 7.4. Subsequently, the brains were dissected and fixed overnight in 4% paraformaldehyde (Sigma-Aldrich), before being transferred into 15% sucrose (ChemSupply) 0.1% sodium azide (Sigma-Aldrich) for cryoprotection and storage at 4°C ready for further upcoming tissue processing. A summary timeline of the study is presented below in Figure 7.2.

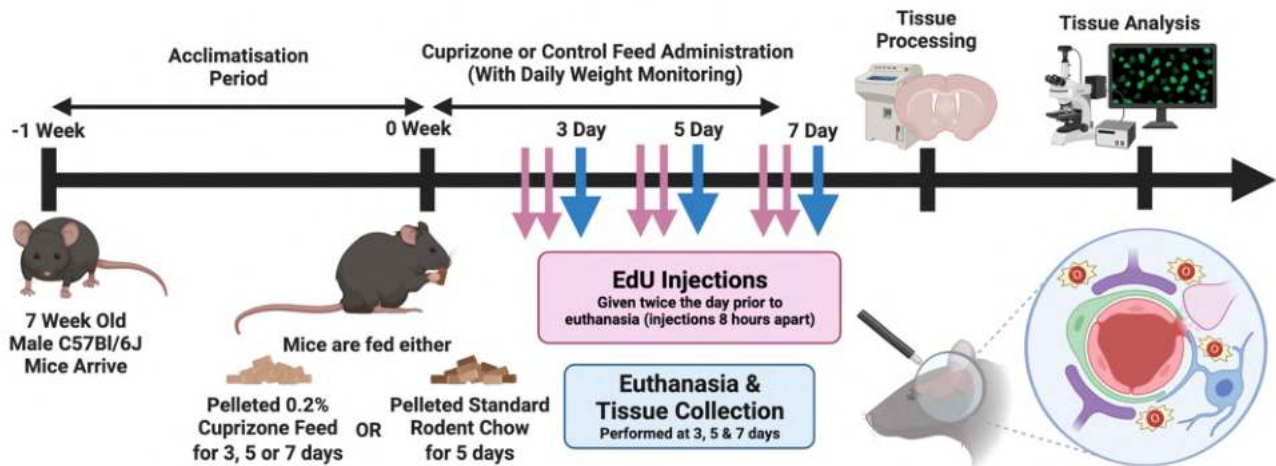


Figure 7.2. Experimental design for cohort investigating BBB dysfunction during cuprizone intoxication. There were three groups receiving pelleted 0.2% cuprizone feed for either 3, 5 or 7 days, with another age-matched group receiving pelleted standard rodent chow for 5 days ($n = 12/\text{group}$, total $n = 48$). Mice were 8 weeks of age at the commencement of the experimental period. EdU (20mg/kg) was administered *via* intraperitoneal injection twice in the day prior to euthanasia, with a minimum of an 8 hour interval between the injections. Following euthanasia and tissue collection at the end of the experimental period, the collected brains were cryosectioned and analysed. Original illustration created using BioRender.com.

7.2. Animal Weights

As with previous cuprizone cohorts, all of the cuprizone and control mice were weighed daily throughout the experimental period, always using the same weight scales and at a consistent time of day. The data obtained was then graphed and analysed using GraphPad PRISM software. To assess the effects of cuprizone consumption on animal weight, a two-way repeated measures ANOVA was performed comparing the daily weights from the 5 day control mice and the 5 day cuprizone mice ($F(5,110) = 24.35$; Figure 7.3A). Bonferroni *post-hoc* tests used to compare these two groups at each timepoint revealed that cuprizone-fed mice had significantly lower body weight than those fed control feed from 2 days of cuprizone exposure until the end of the 5 day period ($p < 0.05$). This is a contradictory finding to the results in the paper presented in Chapter 4, whereby mice fed cuprizone pellets did not have significant weight loss compared to those fed control pellets at any point over the 3 week experimental period. Furthermore, although statistical analysis was performed solely between the 5 day timepoint groups in the present study, the weight loss observed with cuprizone was consistently found with all cuprizone groups (Figure 7.3B). As mentioned in Section 7.1, for those

fed cuprizone for the full 7 days, seven out of the twelve mice in this group spent 24 hours on soft feed due to excessive weight loss of greater than 15% of their original weight as measured on day 0. This only occurred within the last 3 days of the experimental period, with one mouse going onto soft feed at day 4, five mice at day 5, and another one mouse at day 6. No mouse was given soft feed for more than one 24 hour period, and during this time they were temporarily individually housed before going back to their original cage upon returning to above the 15% weight loss threshold. The disproportionate quantity of mice who required soft feed at day 5 within this group and the subsequent weight gain that entailed, explains the average weight increase within this group on day 6.

To assess whether weight changes may have been due to reduced cuprizone consumption, the average feed consumed daily per mouse was assessed and differences between groups were analysed with a one-way ANOVA ($F(3) = 33.58$; Figure 7.3C). The analysis has been adjusted to exclude the period without cuprizone feed from the analysis for the seven mice from the 7 day cuprizone-fed group who spent 24 hours on soft feed. Tukey *post-hoc* tests found that there was a significant difference in daily feed consumption between all three of the cuprizone groups compared to the control group (3 day cuprizone group, $p < 0.0001$; 5 day cuprizone group, $p = 0.0007$; 7 day cuprizone group, $p < 0.0001$). Furthermore, the mice fed cuprizone for three days consumed a lower amount of cuprizone per day than those fed cuprizone for five ($p = 0.0004$) or seven days ($p = 0.0455$). There was no difference in average daily consumption between those fed cuprizone for five and seven days ($p = 0.1703$). Interestingly, when an unpaired t-test is used to compare the average daily feed consumption per mouse between those fed pelleted cuprizone and pelleted control in the first week of the experimental period only in the paper presented in Chapter 4, there is no significant difference between the two groups ($t(4) = 0.0875$, $p = 0.4308$; grey bars on Figure 7.3C).

The same cuprizone administration technique was utilised in the current study as in Chapter 4, with mice housed two per cage and pellets changed every 1 to 3 days. Despite the equivalent cuprizone feeding protocols, it was only within this cohort that mice administered cuprizone pellets ate significantly less feed than those fed control pellets over the first week of the experimental period. It may be that in this current cohort the lower body weights of cuprizone-fed animals compared to those fed control pellets is due to lower intake of feed, rather than due to any cuprizone-induced weight loss. A reduction in cuprizone consumption may potentially have affected the level of early demyelinating disease achieved in these animals. Any reduction in demyelinating pathology due to decreased consumption would also be further enhanced within the 7 day timepoint since more than half of the mice fed cuprizone in that group required a 24 hour diet supplementation period due to their substantive weight loss. It will thus be important to confirm the degree of cuprizone toxicity obtained within the current cohort prior to commencing further tissue analyses to ensure sufficient induction of pathology, especially given the acute nature of this study. It is also worth noting that the

lack of weight loss observed within the cohort in Chapter 3 was not associated with the absence of cuprizone toxicity. Though demyelinating disease was not successfully induced in the results described in that chapter, this was due to inactive cuprizone pellets rather than decreased feed consumption. Therefore, the impact of decreased cuprizone consumption in the current cohort should be considered independently of any inferences obtained from the results of Chapter 3.

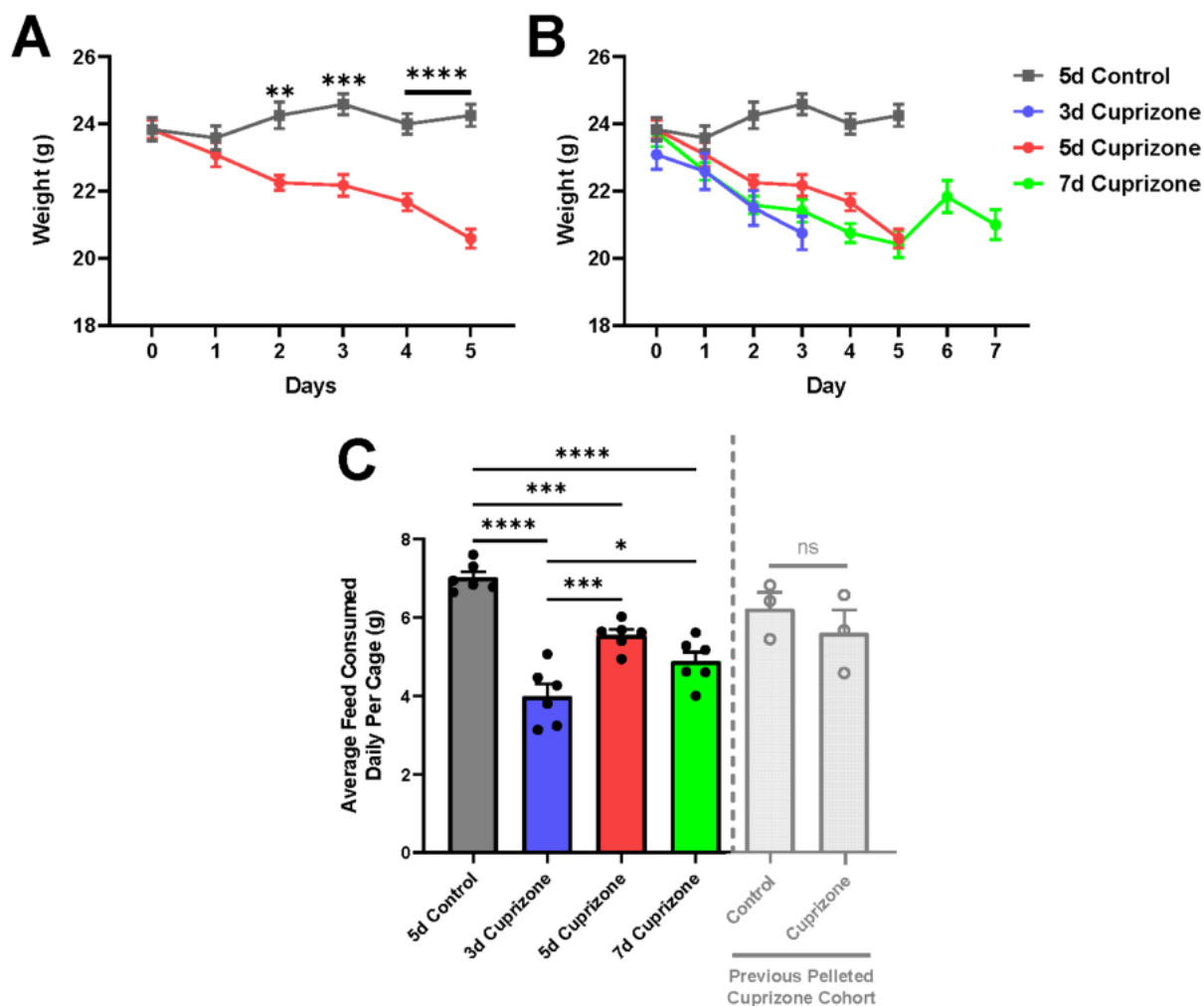


Figure 7.3. Effects of cuprizone intoxication and quantity of feed consumption on animal weights. Cuprizone pellets were delivered for 3, 5 or 7 days, and another group was fed control pellets for 5 days ($n = 12/$ group, total $n = 48$). Animals were weighed daily to assess weight loss throughout cuprizone administration. (A) Animal weights were compared for those fed cuprizone and control feeds across 5 days to determine the effect of cuprizone intoxication on animal weight. Graph displays mean \pm SEM. (B) Animal weights across time are displayed for all experimental groups to demonstrate the consistency of weight loss over time in cuprizone-fed mice. (C) Difference in the average feed consumed daily per cage of two mice during the experimental period was analysed between groups. For comparison, the quantity of feed consumed daily per cage for those fed either control or cuprizone pellets during the first week in the previous cuprizone cohort in the research paper from Chapter 4 has been presented in grey. Graph displays mean \pm SEM. Graph displays individual cage data points overlaid on a bar displaying the mean \pm SEM. Significant differences are indicated by $*p \leq 0.05$, $**p \leq 0.01$, $***p \leq 0.001$, $****p \leq 0.0001$.

7.3. Plans for Remaining Experimental Work

Due to the time constraints of this doctoral degree, tissue analysis from this cohort is yet to be conducted. However, I have produced detailed plans for the continuation of this study, as follows.

7.3.1. Initial Optimisation of Immunohistochemical Tissue Analysis

The original plan for this project was to perform immunohistochemistry in line with the tissue analysis performed in Chapter 6. All of the antibody combinations for this work had already been specifically devised to allow for the key research questions to be answered, utilising adjacent sections and similar combinations of antibodies as in the previous BBB work. During the previous immunohistochemical analyses on mouse tissue presented in Chapter 4, dilutions for many of the antibodies that would have been utilised for this study were optimised. Furthermore, whilst working on the neurotrauma BBB cohort, I also concurrently commenced optimising the protocols for the remaining antibodies for this study using spare mouse tissue. One example of this is the optimisation of the CD31 antibody (Figure 7.4). CD31 would have been used in these immunohistochemical panels as an equivalent alternative for RECA, which had been utilised in Chapter 6 to identify the endothelium of blood vessels. RECA is a very commonly used antibody for rat endothelial cells (Kitchen et al. 2020; Pizzo et al. 2018; Ülger et al. 2002; Uzunalli et al. 2021; Wang et al. 2021), but it is highly specific to rat tissue. Instead, antibodies recognising CD31 are most appropriate for detecting endothelial cells at the BBB in mouse tissue (Bernard-Patrzynski et al. 2019). Though CD31 is widely utilised for identifying the mouse endothelium, it is still important to note that CD31 is also diffusely expressed to a lesser extent by various immune cells, such as leukocytes (Muller 2003). Thus, it is critical to assess both morphology and immunointensity to ensure accurate identification of blood vessels using this marker.

To optimise the CD31 antibody, a range of primary antibody concentrations were employed, from 1:125 to 1:1000, whilst the concentration of the secondary antibody remained consistent at 1:400 (specific antibody details can be found in Figure 7.4C). When keeping the microscope settings consistent, a concentration dependent decrease in fluorescent signal was found as the CD31 antibody became more dilute, and no fluorescent signal was detected when the primary antibody was omitted for the secondary only control (Figure 7.4A). Given signal was still present at all tested antibody concentrations, the microscopy settings were optimised for the lower concentrations. When the laser power on the microscope was increased to detect the signal present in the lower concentrations, the 1:500 concentration of the CD31 antibody was deemed optimal (Figure 7.4B). This particular concentration still allowed for sufficient detection of the fluorescent signal, whilst not requiring a large quantity of the antibody to be used for each immunohistochemical experiment or requiring the laser power to be so amplified where it may risk bleaching the tissue whilst it is being imaged.

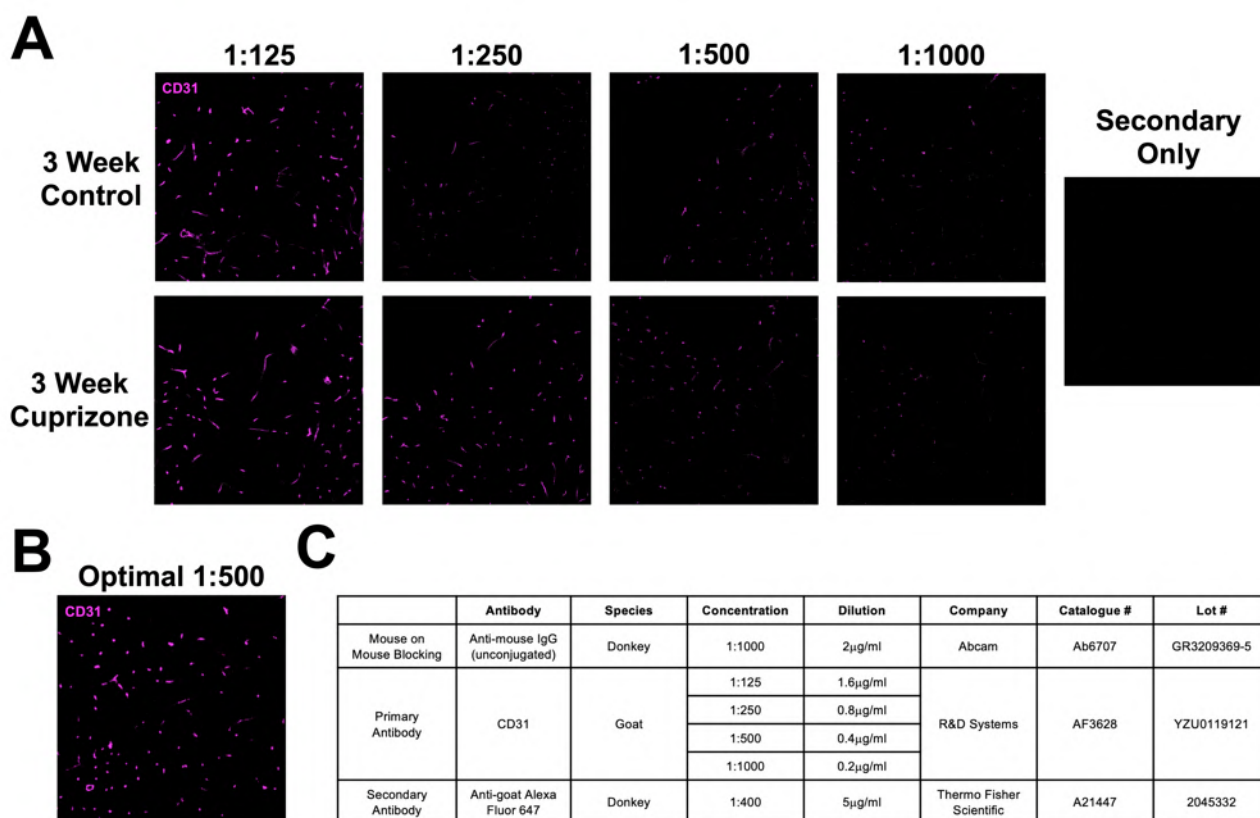


Figure 7.4. Optimisation of the CD31 primary antibody on mouse brain tissue. (A) When keeping microscope settings consistent, there was a concentration dependent decrease in fluorescent signal as the CD31 antibody became more dilute, with no signal detected when the CD31 antibody was omitted for a secondary only control. (B) When the microscope settings were adjusted for detecting the signal present in the lower concentrations, the 1:500 concentration of the CD31 antibody was the optimal antibody concentration. (C) The table presents the relevant information regarding the antibodies employed in this optimisation experiment.

As the work in Chapter 6 progressed it became apparent that immunohistochemistry may not be an optimal method of tissue analysis for this particular research. Though the tissue specific problems that arose in that study may not have impacted this mouse model counterpart, the issues surrounding the variability of blood vessels between adjacent sections and the limitations of four colour fluorescent microscopy remained. Therefore, an alternative method for tissue analysis was devised.

7.3.2. GeoMx Spatial Proteomic Analysis

One alternative to immunohistochemistry is GeoMx digital spatial profiling (DSP), which is an emerging method of multiplex proteomics that can detect over one hundred proteins simultaneously with preservation of spatial resolution (Figure 7.5). The multiplexing capacity of GeoMx DSP means that the scope of the study can be extended to include additional markers than were planned for the immunohistochemical analyses. Though GeoMx couldn't have been used within Chapter 6 as the technique is not yet validated for rat tissue, there are mouse tissue compatible assays available making it a suitable alternative technique for this work.

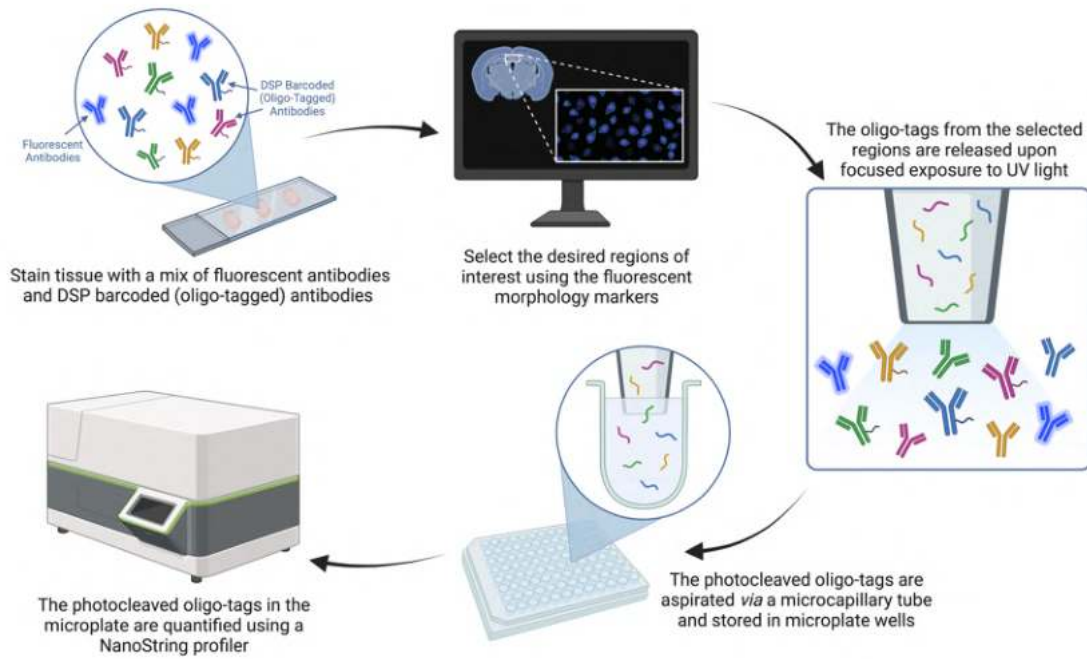


Figure 7.5. GeoMx spatial proteomics experimental workflow. Tissue is stained with a combination of fluorescent antibodies and DSP barcoded (oligo-tagged) antibodies. Desired regions of interest are selected based on the fluorescent signal. By quantifying the oligo-tags in specific regions of interest, protein targets can be identified and measured with spatial resolution. Original illustration created using BioRender.com.

A GeoMx panel has been designed that can investigate the role of oxidative damage to perivascular OPCs and pericytes during early cuprizone intoxication (Figure 7.6).

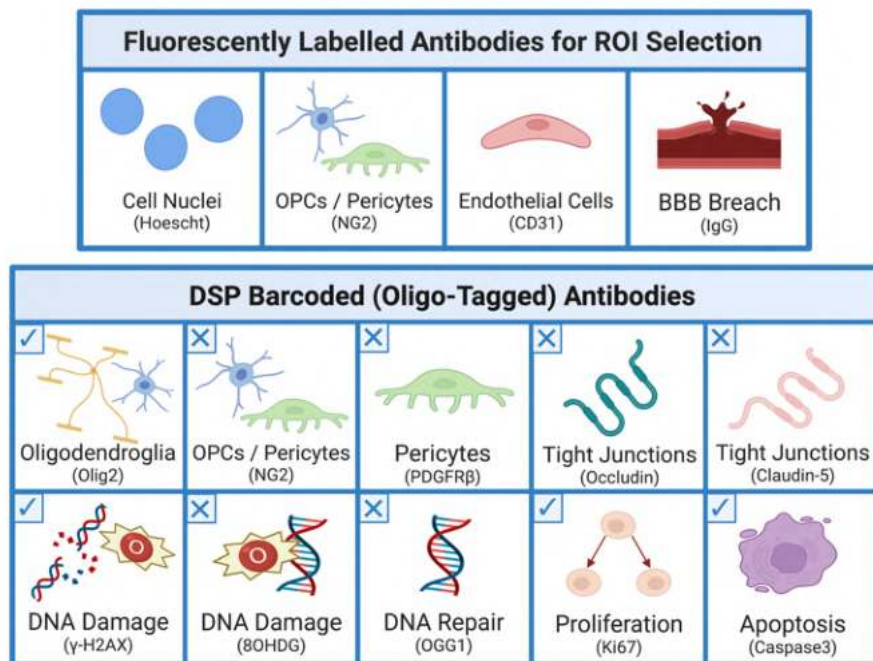


Figure 7.6. GeoMx panel designed to assess the role of oxidative damage to perivascular OPCs and pericytes during early cuprizone intoxication. The custom assay contains cell identification markers for OPCs and pericytes, cell

status markers and BBB status markers. Antibodies already included in existing GeoMx assays are indicated with ✓ and antibodies that would require custom barcoding are indicated with X. Original illustration created using BioRender.com.

Since the 405nm fluorescent channel was the most difficult channel to employ in Chapter 6, a Hoechst dye can be utilised within this channel for tissue navigation using patterns of cell nuclei. Digital cell segmentation based on fluorescent immunointensity can then create specific cellular regions of interest. For blood vessel identification, CD31 can be used as optimised above in Section 7.3.1. Since both OPCs and pericytes express NG2, NG2 can be used as a broad marker to initially indicate the presence of either cell type. The subsequent colocalised protein expression of NG2 with either Olig2 or PDGFR β will indicate the presence of either an OPC or a pericyte respectively. The relative distance of these two cellular subpopulations to the closest blood vessel can be determined to quantify detachment of these perivascular cells from the blood vessels.

An anti-mouse IgG antibody can be utilised to indicate serum protein extravasation as a marker of BBB dysfunction, similar to the approach taken in Chapter 6. Though early studies of cuprizone administration indicated no overt breach of the BBB with cuprizone (Bakker & Ludwin 1987; McMahan et al. 2002), both of these two studies did in fact observe mild but insignificant increases in IgG staining in the parenchyma adjacent to blood vessels. However, recent studies have found increased extravasation of fluorescent dyes as early as 3 days into cuprizone exposure (Shelestak et al. 2020). Given the substantial advancements in image analysis in the past 20, smaller changes in IgG immunoreactivity proximal to blood vessels are likely to now become apparent. More subtle changes in the tight junction proteins occludin and claudin-5 can also be detected within digitally segmented blood vessels to additionally indicate damage to the BBB.

Though in Chapter 6 the only antibody used to detect DNA damage was 8OHdG, the multiplexing ability of GeoMx profiling provides the capacity to form a more complete picture of the extent of oxidative damage. Antibodies detecting γ -H2AX, 8OHdG and OGG1 can be used to detect double-strand breaks, nucleobase modifications and base excision repair mechanisms respectively. Utilising these three antibodies simultaneously would allow quantification of the balance between both forms of DNA damage as well as a corresponding repair mechanism within each individual cell. This work can continue to utilise Caspase3 as a marker of apoptosis and Ki67 will be utilised to detect cell proliferation, in line with other previous work from the Fitzgerald laboratory (Payne et al. 2013). EdU cannot be detected using GeoMx so an additional separate immunohistochemical analysis that detects EdU could also be appropriate for quantification of cells in the S-phase of the cell cycle specifically (Buck et al. 2008). This entire planned GeoMx assay would therefore generate specific profiling datasets that would facilitate the necessary cell-specific analyses for answering the research questions.

7.4. Concluding Remarks

Within this chapter, the preliminary work performed to assess the role of oxidative damage to OPCs and pericytes at the BBB in demyelinating disease was presented. In this study, the cuprizone model of demyelinating disease was employed at acute timepoints when the BBB is known to be dysfunctional. The plan that I have generated for completing this work was also outlined. Though the research was unable to be completed during my candidature, the continuation of this work will hopefully yield interesting and novel results regarding the role of perivascular OPCs and pericytes in MS pathology and may also identify oxidative DNA damage to these cell types as a therapeutic target worthy of further investigation.

Chapter 8. General Discussion and Final Remarks

This thesis explored mechanisms of damage common to MS and neurotrauma. The relevant literature for both disorders was reviewed in-depth, including a published narrative review on damage to white matter following neurotrauma. The notion of common damage mechanisms was explored by the utilisation of a combinatorial ion channel inhibitor treatment in models of neurotrauma and MS. Similar improvements in myelin structure with this treatment in both models indicated that the observed myelin damage was in part mediated by similar Ca^{2+} -dependent mechanisms. In order to allow investigation of this pathology in demyelinating disease, the cuprizone model was optimised, with a pelleted cuprizone formulation found to be overall more effective at inducing early demyelinating disease pathology than the powdered cuprizone alternative. Finally, oxidative DNA damage was investigated at the BBB following neurotrauma, with a particular focus on NG2⁺ glia (comprised of OPCs and pericytes). There was a significant increase in the level of DNA damage both overall within the ventral nerve and more specifically within both NG2⁺ and PDGFR α ⁺ glia, with DNA damaged OPCs and pericytes qualitatively identified. A significant association was found between the level of oxidative damage and the extent of BBB dysfunction at 1 day post-injury. The density of newly derived and proliferating cells with DNA damage also increased with injury. Additionally, the PDGFR α ⁺ population, comprised primarily of OPCs, was identified as the major proliferating, DNA damaged cell type at 1 day following injury to the optic nerve. The initial experimental work completed to date and detailed plans for the continuation of parallel research into the BBB in demyelinating disease was also presented. Altogether, this thesis explored common mechanisms of damage in models of MS and neurotrauma and established the relevant framework to facilitate continuing research to compare the two disorders.

8.1. Translating Knowledge of Common Damage Mechanisms

As discussed throughout Chapter 1, both MS and neurotrauma are characterised by myelin degeneration, oxidative stress, microglial and macrophage activation, oligodendrocyte death, and BBB dysfunction. However, research that directly investigates common mechanisms between MS and neurotrauma is limited. Therefore, the overarching goal of this thesis was to investigate shared damage mechanisms and to hopefully identify therapeutic targets to expedite the development of effective treatment strategies for both of these disorders. Though methodological complications limited some avenues of investigation, this research has been successful in establishing the foundational framework for continuing research in this space.

Within the work discussed in Chapter 2, the same combinatorial ion channel treatment was effectively employed in models of both neurotrauma and MS. In the two studies, an improvement

was observed in the preservation of myelin node/paranode structures (Gopalasingam et al. 2019; Toomey et al. 2019). This similarity in therapeutic outcomes suggests that myelin damage in both models is mediated at least in part by similar Ca^{2+} mechanisms, with the lack of other consistent significant improvements following the partial optic nerve transection indicating that the combinatorial treatment was acting on the myelin sheath directly. Myelin degeneration is associated with the activation of P2X_7 receptors following injury (Matute 2008). AMPA receptors also exist along the myelin sheath (Fowler et al. 2003), with myelin abnormalities resulting in the additional exposure of sub-myelin VGCCs (Zhang & David 2015). One mechanism through which excessive intracellular Ca^{2+} influx can induce myelin degeneration is *via* increased Ca^{2+} -mediated calpain activation (Croall & Demartino 1991; Khorchid & Ikura 2002). Overactivation of calpain causes cleaving of myelin-related proteins (Fu et al. 2007; Shields et al. 1997), which is associated with retraction of paranodal myelin and redistribution of nodal, paranodal and juxtaparanodal components (Fu et al. 2009; Huff et al. 2011). By preventing multiple routes of entry for Ca^{2+} into the myelin sheath, the combinatorial ion channel inhibitor treatment may have limited this calpain-mediated pathway for myelin degeneration within both models. Furthermore, as discussed in Chapter 1, oligodendrocytes are particularly vulnerable to oxidative damage. This susceptibility is in part due to oligodendroglia containing higher concentrations of P2X_7 receptors and AMPA receptors than other cell types (Borges et al. 1994; Matute et al. 2007). Though oxidative damage does not always result in oligodendrocyte death, it is associated with node/paranode abnormalities (Szymanski et al. 2013). Therefore, the beneficial effects observed for myelin outcomes with the inhibitor treatment may also be due to preventing Ca^{2+} influx into the associated myelinating oligodendrocytes. The generalisability of the combinatorial treatment in preserving myelin structures in models of both neurotrauma and demyelinating disease initially supported the concept of common mechanisms within the underlying pathology between the two neurological conditions. Further discussion surrounding investigations into common damage mechanisms specifically at the BBB will be provided in Section 8.3, with the peripheral inflammation outcomes in the above neurotrauma cohort also discussed in Section 8.4.

8.2. Implications for Increased Efficacy of Cuprizone-Containing Pellets

8.2.1. Potential Variations Between the Two Suppliers of Cuprizone-Containing Pellets

Prior to discussing the implications of the increased efficacy of cuprizone-containing pellets, it is critical to consider the potential causes for the discrepancy in the effectiveness of the two batches of cuprizone pellets utilised throughout Series Two. Demyelinating disease was successfully induced with the Specialty Feeds pelleted cuprizone diet in Chapter 4, but the Envigo cuprizone pellets administered in Chapter 3 were ineffective and seemingly deactivated. It is possible that nutritional

differences in the base diets of the two types of cuprizone pellets may have influenced the efficacy of the cuprizone contained within them. However, the cuprizone-containing pellets used for previous work in the laboratory that were effective at inducing demyelinating disease (Gopalasingam *et al.*, 2019; see Appendix B) were also manufactured by Envigo using the same base diet, so it is unlikely that nutritional differences between base diets is responsible for the deactivation of the Envigo pellets.

It is far more probable that differences in the manufacturing process between suppliers is responsible for the observed decreases in cuprizone efficacy. Though the process of pelleting animal feed is relatively standard between manufacturers (Figure 8.1), issues in the generation of the cuprizone-containing pellets are likely to result in decreased potency.

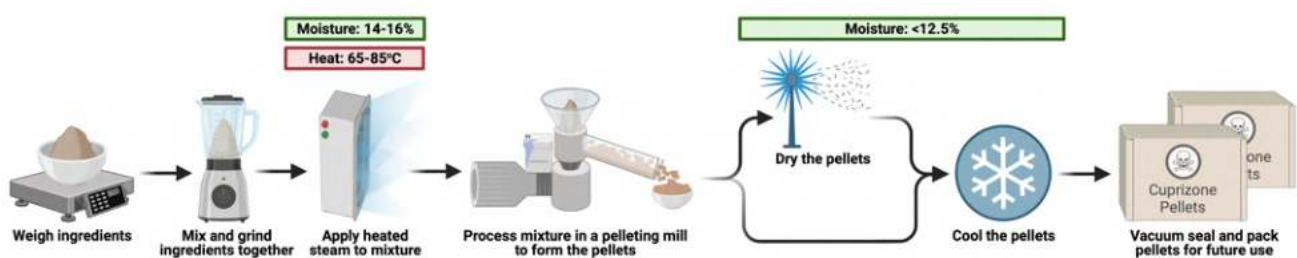


Figure 8.1 Workflow of the generalised feed pelleting process. Firstly, the feed ingredients are mixed and ground to the desired ratios and density. Heated steam is then applied to moisten the mixture to a 14-16% moisture content. The mixture is processed in a pellet mill before either being dried to less than 12.5% moisture and subsequently cooled or cooled without a drying step, depending on the created pellets water content. The pellets are then packed and vacuum sealed for future use. Figure based on Weiskirchen *et al.*, 2020. Original illustration created using BioRender.com.

Potential variability in feed exposure to heat and moisture as shown in the above manufacturing process (Figure 8.1) are the most likely causes of the observed discrepancies in pellet efficacy. It has been previously postulated that cuprizone-containing pellets may be less effective due to the heat needed for the pelleting process (Zhan *et al.* 2020). However, cuprizone that has been thermally pre-treated at a range of temperatures from 60°C - 121°C does not have reduced toxicity compared to cuprizone powder that was not heated (Heckers *et al.* 2017). The maximum tested temperature in that study far exceeds the peak temperature of 85°C reached during the pelleting process (Weiskirchen *et al.* 2020) and altogether suggests cuprizone is not as heat sensitive as perhaps was once thought. Interestingly though, although pure cuprizone is not degraded when mixed with water, when this cuprizone is mixed into a control chow to a 0.3% concentration and then exposed to water, there is a significant degradation of the cuprizone that worsens with increased water content (Zheng *et al.* 2021). Thus, in the presence of water cuprizone can react with other components of the control feed, which may ultimately result in cuprizone deactivation and the production of inefficacious pellets. As shown in Figure 8.1, the combined cuprizone and control chow mixture is typically meant to be exposed to a maximum of approximately 16% moisture during the pelleting

process (Weiskirchen et al. 2020), which would already result in around a 10% degradation of the contained cuprizone (Zheng et al. 2021). However, if the cuprizone and control mixture was mistakenly exposed to 50% water, this would result in a 60% degradation of the cuprizone. Consequently, if the manufacturers don't strictly control the exposure to water during the pelleting process and it inadvertently increases, this may result in batch to batch variability for the manufactured cuprizone-containing pellets. Therefore, the discrepancy observed in pellet effectiveness between the two manufactures utilised in Chapters 3 and 4 could have been due to poorly controlled exposure to water during the pelleting process and thus both feed manufacturers and future researchers should ensure that any feed containing cuprizone has had limited exposure to water wherever possible.

8.2.2. Implications of Increased Efficacy of a Pelleted Cuprizone Feed Formulation for the Cuprizone Literature and Future Studies

The paper presented in Chapter 4 demonstrated the significance of feed formulation for both cuprizone and control feed when assessing the extent of demyelinating disease in this model. Within the literature, there is little consistency between research groups in both the cuprizone and control feed formulations utilised, with the formulations used within studies sometimes not even reported in publications. Notably, this paper established that it is critical to use an optimal cuprizone formulation and to compare to a similarly formulated control feed, which will hopefully assist future researchers to improve and optimise their own study designs to best assess cuprizone-induced toxicity.

8.2.2.1. Importance of Control Feed Formulation

The study presented in Chapter 4 highlighted the importance of selecting an appropriate control feed formulation. Within the rostral corpus callosum, the density of mature oligodendrocytes were significantly lower in mice fed control powder than control pellets (Toomey et al. 2021). This difference was also reflected in the density of the overall oligodendroglial population, with mice fed control powder exhibiting a lower density of Olig2+ cells compared to control pellets in both the rostral and caudal regions (Toomey et al. 2021). Though cuprizone powder did cause a significant decrease in oligodendroglial density when compared with control pellets, the absence of a difference between cuprizone powder and control powder when looking at the density of the Olig2+ oligodendroglia population makes it difficult to discern the effectiveness of cuprizone powder and even indicates that the nature of the powdered feed itself was contributing to changes in oligodendroglial density regardless of the presence of cuprizone (Toomey et al. 2021). This is reinforced by the fact that a large proportion of cuprizone studies either use pelleted control feed for powdered cuprizone or simply do not specify the employed formulation of the control feed (Clarner et al. 2012; Groebe et al. 2009; Kipp et al. 2011; Norkute et al. 2009; Oveland et al. 2021; Pagnin et al. 2022; Plant et al. 2007; Shelestak et al. 2020; Wang et al. 2016; Zhan et al. 2021). This indicates

that discrepancies in the reduction of oligodendroglial density between our study and the existing powdered cuprizone literature may be in part due to the formulation of control feed used to assess the effect of the powdered cuprizone. These data highlight the importance of using control chow that is the same formulation as the employed cuprizone feed formulation to fully assess the toxic effect of cuprizone, and limit any potential confounding effects of the feed formulation on oligodendroglial dynamics. Furthermore, this effect of powdered feed is even more critical to consider for studies investigating remyelination. Mice fed powdered control feed may not be appropriate controls for oligodendrocyte density since a change from powdered cuprizone to powdered control may not reflect the return to a normal density of the oligodendroglial population if the nature of a powdered diet itself is also resulting in loss of oligodendrocytes. However, transitioning from powdered cuprizone to pelleted control would also confound results as it would be impossible to discern the relative contribution of cuprizone withdrawal and changing feed formulation to the repopulation of oligodendrocytes.

One potential reason for the decrease in oligodendroglial density in mice fed control powder could be abnormal changes to glucose metabolism. Mice continuously fed a standard powdered diet develop hyperglycaemia and decreased serum insulin levels, as well as increases in epinephrine and other catecholamines (Tsuchiya et al. 2014). Under hyperglycaemic conditions, astrocyte function can become impaired (Li et al. 2018), which renders oligodendrocytes highly vulnerable to the toxic effects of catecholamines (Noble et al. 1994). Hyperglycaemia also increases ROS production whilst simultaneously decreasing antioxidants (Muriach et al. 2014), and given oligodendroglia are particularly vulnerable to oxidative damage as discussed in Section 1.4.6.3, it may be that this hyperglycaemic oxidative insult may preferentially damage the oligodendrocyte lineage.

Gnawing and mastication behaviour reduces serum cortisol levels, indicating that chewing may actually ameliorate stress and anxiety in rodents (Ayada et al. 2002; Kubo et al. 2015). Thus perhaps unsurprisingly, consuming feed in a powdered form may also act as an emotional stressor for mice, with powdered feed resulting in increased serum levels of corticosterone (Tsuchiya et al. 2014). Interestingly, there have been multiple studies that suggest that increased psychological stress can result in decreases in oligodendrocyte gene expression in various white and grey matter areas (Banasr et al. 2007; Cathomas et al. 2019; Sibille et al. 2009).

Altogether, the differences observed between the two control feeds in this paper demonstrated the importance of selecting a control chow that is the same formulation as the cuprizone-containing feed. Furthermore, it reinforces the necessity for studies that are using cuprizone to investigate both de- and remyelination to transparently report the formulation of the control feed used.

8.2.2.2. Importance of Cuprizone-Containing Feed Formulation

The paper presented in Chapter 4 also highlighted the importance of selecting an appropriate cuprizone feed formulation, with demyelinating disease only being induced effectively in mice fed cuprizone pellets. A key hallmark of effective cuprizone intoxication is a decrease in the body weight of the mice fed cuprizone-containing feed (Steelman et al. 2012; Stidworthy et al. 2003). However, only the mice fed cuprizone powder significantly lost body weight compared to the relevant control group, despite the more pronounced pathology in those fed pelleted cuprizone (Toomey et al. 2021). This suggests that the weight loss observed in the mice fed cuprizone powder is likely due instead to the mice not ingesting the same amount of feed, despite the fact that all mice were provided equal amounts of cuprizone-containing or control feed in the cage regardless of formulation. As discussed in the paper itself, it is plausible that the addition of cuprizone alters the palatability of the feed (Kopanitsa et al. 2020), however why this did not also occur with pelleted cuprizone is unclear. Alternatively, given the mice were urinating in the powdered feed, it is also possible that the water content of their urine was also having a partial deactivation effect on the cuprizone, despite the powder being changed daily in line with standard protocols (Zhan et al. 2020). Nevertheless, a decreased cuprizone consumption with powdered cuprizone may have resulted in the observed reduction in pathology compared to those fed cuprizone pellets.

Mice fed cuprizone powder did display decreases in the density of mature oligodendrocytes in the caudal corpus callosum compared to those fed control powder, thus a degree of cuprizone intoxication did occur in these mice (Toomey et al. 2021). It's important to note that decreased density of mature oligodendrocytes is one of the earliest pathological hallmarks of cuprizone intoxication (Buschmann et al. 2012; Fischbach et al. 2019; Krauspe et al. 2015), therefore it may also be that the resulting pathology was simply delayed due to an early aversion to the feed. A time course comparison on the development of cuprizone pathology between the two feed formulations would help to elucidate this further. Interestingly, calorie restriction with concurrent cuprizone administration for 6 weeks has recently been discovered to decrease the accumulation of microglia in the corpus callosum, alter the inflammatory profile and polarisation of remaining microglial populations, decrease cellular apoptosis and ameliorate demyelination (Zarini et al. 2021). Thus if the mice fed cuprizone powder did indeed ingest a reduced quantity of the feed, this may have had a neuroprotective effect against the toxicity of the cuprizone itself.

It is worth noting that weight loss was also observed with these cuprizone pellets in the cohort presented in Chapter 7, associated with significantly decreased cuprizone consumption. It will be important to establish the degree of cuprizone toxicity obtained in this cohort to ensure sufficient induction of acute pathology prior to commencing extensive tissue analyses.

It has been previously suggested that for successful cuprizone intoxication to occur, cuprizone needs to be additionally adsorbed through the skin and respiratory system as well as through the digestive tract (Hagemeyer et al. 2012; Hochstrasser et al. 2017). Mice fed cuprizone pellets are not exposed to these additional adsorption routes compared to those fed cuprizone powder. Given the increased pathology in the mice fed cuprizone pellets (Toomey et al. 2021), this study indicates that these routes may not be as central to the mechanism of cuprizone intoxication as once thought.

This work looked exclusively at the rostral and caudal medial corpus callosum, but there are various other structures that would be worth analysing including the cortex, hippocampus, and subcortical regions like the thalamus. In particular though, the rostral lateral corpus callosum is more vulnerable to cuprizone intoxication than the corresponding medial region (Zhan et al. 2020). Thus, the analysis of the effect of cuprizone formulation in the paper presented in Chapter 4 may have potentially missed early demyelinating pathology in the rostral region and future studies should expand the analysed areas to further clarify the diverse applications of the model at this specific time point.

8.3. Oxidative DNA Damage and the Blood-Brain Barrier in MS and Neurotrauma

The third major aim of this thesis was to establish whether oxidative damage to perivascular OPCs and pericytes at the BBB is associated with increased BBB permeability in both MS and neurotrauma. It was hypothesised that oxidative DNA damage will occur to a greater extent in perivascular OPCs and pericytes associated with BBB dysfunction. The novel data generated in Chapter 6 demonstrated a relationship between oxidative stress, BBB dysfunction and cellular proliferation at 1 day following neurotrauma, with OPCs identified as the major proliferating, DNA damaged cell type acutely following injury.

8.3.1. Relationship Between Oxidative Stress and Blood-Brain Barrier Dysfunction

In line with previous work that assessed outcomes at 1 day following a partial optic nerve transection (O'Hare Doig et al. 2014), this study found significantly elevated levels of oxidative 8OHdG DNA damage in the ventral optic nerve vulnerable to secondary degeneration. Similarly, the observed increase in BBB dysfunction 1 day post-injury in this work corresponds with previous research that has demonstrated increased Evans blue extravasation at the 1 day timepoint (Smith et al. 2016). This study also uncovered a strong and significant positive monotonic relationship between the extent of oxidative DNA damage and BBB breach, with this correlation observed across animals in both the sham and injured groups. Oxidative stress has already been closely associated with BBB dysfunction in a variety of CNS diseases and injuries (Grammas et al. 2011), including MS (Ortiz et al. 2014) and neurotrauma (Abdul-Muneer et al. 2014; Kuriakose et al. 2019). However, the extent

of a direct relationship between oxidative stress and BBB breach had not been previously investigated within the partial optic nerve transection model of neurotrauma.

The functional significance of this observed relationship between oxidative damage and BBB dysfunction remains to be assessed. It will be important to determine whether oxidative damage is driving pathological mechanisms or if it is a by-product of them. For example, when the BBB is breached within MS lesions, the fibrinogen proteins that subsequently diffuse into the parenchyma activate microglia, which causes these microglia to secrete toxic factors that exacerbate demyelination and neuronal degeneration (Adams et al. 2007). It is therefore likely that BBB breach also directly results in increased levels of ROS, and thus there is a causality dilemma for oxidative damage and BBB dysfunction that will need to be investigated in future studies.

8.3.2. Cell Specific Oxidative DNA Damage

In this study, increases in oxidative DNA damage were not only observed within the overall ventral nerve, but also specifically within both NG2⁺ glia and PDGFR α ⁺ glia. OPCs and pericytes are the key cellular populations that express the NG2 marker (Smyth et al. 2018; Zhu et al. 2008). The qualitative assessment performed using PDGFR β colocalisation with NG2 to specifically identify pericytes indicated that both pericytes and OPCs experience DNA damage at this timepoint. Though PDGFR α can be expressed to varying degrees by cells throughout the CNS, it is most abundantly expressed by OPCs (Bergles & Richardson 2016). Therefore, the concurrent identification of both the NG2⁺ and PDGFR α ⁺ glial populations with significant levels of 8OHdG DNA damage also specifically supports the presence of oxidatively damaged OPCs.

The significant increase in 8OHdG DNA damage within OPCs highlights the heightened vulnerability of this cell type in particular to oxidative DNA damage. As previously noted, OPCs have already been shown to be especially vulnerable to DNA damage at 3 days following a partial optic nerve transection (Giacci *et al.*, 2018b), with this study extending this outcome back to the acute 1 day timepoint. At 7 days post-injury, there is an observable increase in TUNEL⁺ apoptotic OPC death (Payne et al. 2013), with a concomitant decrease in the immunointensity of 8OHdG within the remaining OPCs to levels not different to control animals (Giacci *et al.*, 2018b). This suggests that early DNA damage may contribute to loss of this cell type later in the pathological sequelae. The implications of the observed relationship between DNA damaged OPCs and increased proliferation will be further discussed in Section 8.3.3.

It may be that the observed DNA damaged OPC population modulated detrimental effects at the BBB. OPCs located at the vasculature have already been found to key play roles in compromising BBB integrity under pathological states, such as cerebral hypoperfusion (Seo et al. 2013) and MS (Girolamo et al. 2019; Niu et al. 2019). One potential mechanism through which oxidative damage to perivascular OPCs may mediate BBB dysfunction is by disrupting the balance of TGF- β 1 secretion

by OPCs. Perivascular OPCs secrete TGF- β 1 to activate the MEK/ERK pathway in endothelial cells at blood vessels, which increases expression of tight junction proteins and protects BBB integrity (Seo et al. 2014). Oxidative stress conditions are known to increase TGF- β 1 secretion in various cells (Liu & Desai 2015), and thus oxidative damage to OPCs may increase their production of TGF- β 1. Overexpression of TGF- β 1 has been found to increase BBB permeability by the upregulation of matrix metalloproteinase 9 and disruption of tight junction proteins (Behzadian et al. 2001; McMillin et al. 2015). Perivascular OPC-mediated damage to the BBB has also previously been associated with an increased expression of matrix metalloproteinase 9 (Seo et al. 2013). Therefore, it may be that oxidatively damaged OPCs oversecrete TGF- β 1, thus damaging BBB integrity. Future studies should thus determine the relative vulnerability of parenchymal and perivascular OPCs to oxidative DNA damage and elucidate any potential consequences of perivascular OPC damage for pathological BBB dysfunction.

A DNA damaged pericyte population was also qualitatively identified, with these damaged pericytes also potentially contributing to the observed loss of BBB integrity. Pericytes are known to be particularly susceptible to oxidative damage (Rinaldi et al. 2021). Oxidative DNA damage to pericytes due to cathepsin D deficiency has been previously shown to impair BBB integrity by increasing blood vessel diameter, causing hyperpermeability and allowing for the infiltration of peripheral immune cells (Okada et al. 2015). Additionally, pericytes are more vulnerable to apoptosis when exposed to high levels of hydrogen peroxide than endothelial cells (Zhou et al. 2013), with apoptosis of pericytes at blood vessels is associated with BBB dysfunction in a variety of CNS disorders (He et al. 2020). Interestingly, the oxidative damage mediated by hydrogen peroxide at blood vessels is specifically associated with heightened tyrosine nitration (Zhou et al. 2019). In the paper presented in Chapter 4, we observed increased levels of 3-NT within the caudal corpus callosum with the successful induction of cuprizone pathology with pelleted feed (Toomey et al. 2021). Thus, it may be that the observed nitrosative damage in that paper was reflective of the degree of pericyte damage and dysfunction, however the colocalisation of 3-NT with pericyte markers was not specifically analysed within this cohort. Pericytes can also propagate oxidative stress *via* the production of nitric oxide and superoxide radicals (Rustenhoven et al. 2017), providing a feed-forward loop for oxidative damage.

Pericyte detachment from the vascular unit is potentially a common feature of both MS and neurotrauma. Following TBI in mice, there is a rapid reduction in pericytes within the first 12 hours following injury, followed by a significant increase in pericytes and pericyte proliferation by 3 to 5 days post-injury (Zehendner et al. 2015). Pericytes can detach from the vascular wall following TBI, with approximately 40% of pericytes lifting away from the vasculature, which may compromise BBB integrity (Dore-Duffy et al. 2000). These pericytes migrate into the interstitial space partly to form a

portion of the fibrotic glial scar (Laredo et al. 2019). The detachment of pericytes from the vasculature may also play a role in angiogenesis, as this allows for endothelial cells to form vessel sprouts (Salehi et al. 2017). The pericytes that detach from the blood vessels following TBI remained ultrastructurally viable, whereas pericytes that remained at the BBB displayed ultrastructural changes indicative of apoptosis and degeneration (Dore-Duffy et al. 2000). Similarly, in chronic active MS lesions the attachment of PDGFR β ⁺ pericytes at the endothelium is diminished, which is posited to be a result of pericyte detachment (Iacobaeus et al. 2017). An examination of the role of oxidative damage in this detachment process for both MS and neurotrauma could potentially yield interesting results.

It is imperative that future studies assess the relevant contribution of both OPCs and pericytes to DNA damaged NG2⁺ glia following neurotrauma, with a particular focus on differentiating between the parenchymal and perivascular populations of these cells. It is important to note that these cell types do not exist in isolation, and cross-talk between OPCs and pericytes, as well as with other surrounding cells, is likely to also contribute to outcomes. For example, an overexpression of TGF- β 1 by perivascular OPCs as described above could trigger the production of ROS/RNS and other proinflammatory mediators by pericytes (Rustenhoven et al. 2016). Additionally, heterogeneity within both OPC (Beiter et al. 2022) and pericyte (Armulik et al. 2011; Rustenhoven et al. 2017) populations could convey varying degrees of susceptibility to oxidative damage.

The continuation of the work presented in Chapter 7 may elucidate some of these remaining questions. The multiplexed GeoMx assay would facilitate a more comprehensive investigation into the relationship between oxidative damage to both parenchymal and perivascular OPCs and pericytes with the dysfunction of corresponding blood vessels in the context of demyelinating disease. This analysis would also allow for a comparative assessment of the relative contribution of OPCs and pericytes within the overall NG2⁺ glial population for oxidative stress outcomes, which may help determine whether significant increases in DNA damaged NG2⁺ glia is solely driven by oxidative damage to OPCs. Though this technique is not yet able to be employed in rat tissue for assessment in the partial optic nerve transection model, any key findings discovered with this parallel cuprizone work could be validated in the future in additional mouse models of neurotrauma.

8.3.3. Relationship Between Oxidative Stress and Cell Proliferation

Another interesting finding of this work was that the density of proliferating DNA damaged cells significantly increased with injury, with no change in the density of proliferating cells without DNA damage as indicated by 8OHdG immunoreactivity. PDGFR α ⁺ glia were also identified as the major proliferating and DNA damaged cell type, with this PDGFR α ⁺ population likely to be comprised primarily of OPCs. This finding builds on previous work in this model which has shown that at 1 day post-injury approximately 54% of proliferating cells are NG2⁺ Olig2⁺ OPCs (Payne et al. 2013). Furthermore, this early injury-related proliferative response occurs prior to the onset of

OPC death at 7 days (Payne et al. 2013). Early proliferation also does not prevent a chronic depletion of OPCs, with OPC loss continuing out to 3 months post-injury (Payne et al. 2013). Combined with the observed significant increase in proliferation of oxidatively DNA damaged OPCs compared to OPCs without DNA damage in the injured nerve, this all suggests that proliferation could be an early indicator of OPC damage and dysfunction following neurotrauma. However, whether increased OPC proliferation is actively induced by DNA damage or whether already proliferating OPCs are inherently more vulnerable to oxidative damage mechanisms post-injury necessitates clarification.

As OPC's differentiate into mature oligodendrocytes post-injury, a peak ratio of proliferating to non-proliferating OPCs occurs at 3 days post-injury before these EdU+ OPCs differentiate through the stages of the oligodendroglial lineage towards becoming mature myelinating oligodendrocytes (Figure 8.2, Payne et al. 2013 Giacci et al. 2018b).

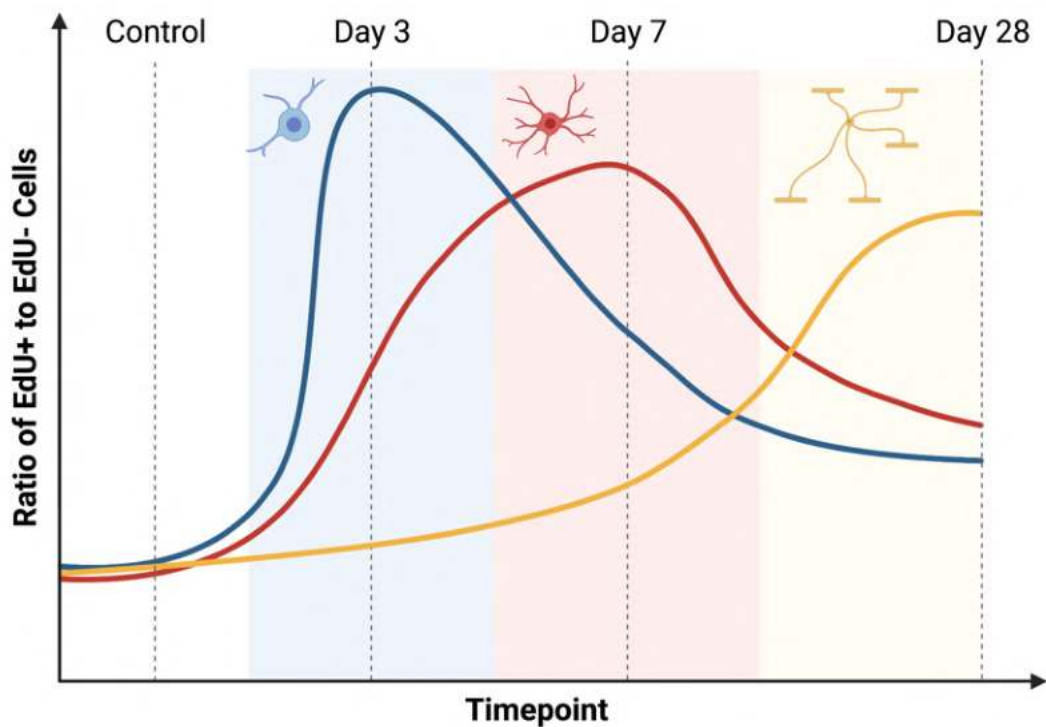


Figure 8.2 Schematic of the approximate relative ratios of proliferating and non-proliferating oligodendroglial cells in the ventral nerve following a partial optic nerve transection. Proliferating and newly derived oligodendroglial subpopulations can be distinguished using markers for proliferation, such as EdU. The relative ratios of EdU+ to EdU- cells for OPCs (blue), pre-myelinating oligodendrocytes (red) and mature myelinating oligodendrocytes (yellow) are schematically represented. Figure based on data presented in Giacci et al. 2018b. Original illustration created using BioRender.com.

It is also already known that at 3 days following a partial optic nerve transection, there is a specific subpopulation of newly derived mature oligodendrocytes that have increased levels of DNA damage compared to their pre-existing counterparts (Giacci et al. 2018b). It is highly likely that a proportion of the identified proliferating and DNA damaged OPC population at 1 day post-injury

may differentiate into mature oligodendrocytes at later timepoints. Furthermore, the subpopulation of DNA damaged, newly derived mature oligodendrocytes at 3 days following injury are less likely to become apoptotic than pre-existing oligodendrocytes, but demonstrate a decreased long term capacity for myelination (Giacci et al. 2018b). The decreased apoptosis of newly derived and proliferating oligodendrocytes suggests proliferation and differentiation may potentially have been protective against cell death associated with DNA damage post-injury. Nevertheless, the concurrent death of pre-existing oligodendrocytes alongside the reduced myelination capacity of newly derived, DNA damaged oligodendrocytes likely contributes to chronic deficits in myelination following neurotrauma.

There are also likely specific pathological implications of perivascular OPC proliferation. Following prolonged cerebral hypoperfusion in mice, OPCs proliferate and mediate BBB leakage and neutrophil infiltration *via* the release of matrix metalloproteinase 9 (Seo et al. 2013). In the EAE model of MS, the density of perivascular OPCs also increases and these cells are mostly associated with both breached blood vessels and vessels with tight junction abnormalities (Girolamo et al. 2019). In humans with MS, perivascular OPCs cluster around blood vessels in white matter lesions, particularly in active inflammatory areas (Niu et al. 2019). When looking at areas of focal demyelination in mice following lysolecithin lesioning, there was also an increased association of OPCs with blood vessels, with perivascular OPCs migrating along the vasculature towards demyelinated regions (Niu et al. 2019). These perivascular clusters of OPCs secrete Wnt inhibitory factor 1, which disrupts endothelial cell tight junctions and displaces astrocytic endfeet, thus increasing BBB permeability and triggering inflammation (Niu et al. 2019). However, the effect of oxidative stress on perivascular OPC proliferation is currently unknown.

Not all of the cells that are proliferating post-injury will be OPCs, with a variety of cells proliferating following neurotrauma, including astrocytes and microglia (Karve et al. 2016; Loane & Byrnes 2010). A proliferative response to injury has already been previously found within NG2+ Olig2- glia, likely to be pericytes. This NG2+ Olig2- cellular subtype represents approximately 5% of proliferating cells at the 1 day timepoint compared to 0% of proliferating cells within control tissue (Payne et al. 2013). CNS pericytes are multipotent and can differentiate in response to environmental stress into a wide variety of cells, such as astrocytes, immature oligodendrocytes, neurons, macrophages, and fibroblasts (Dore-Duffy et al. 2006). During differentiation, these pericytes exhibit markers of proliferation, and thus a proportion of the PDGFR α - proliferative population observed may also be comprised of differentiating pericytes. Given the heightened susceptibility of pericytes to oxidative DNA damage, it may be that there were subtle increases in the density of EdU+ 8OHdG+ pericytes post-injury. However, since this work was unable to specifically examine pericyte

proliferation and the observed PDGFR α - population encompassed a wide variety of cell types, it may be that a proliferative response of pericytes to injury specifically was missed.

The data does suggest that the majority of cellular proliferation acutely post-injury is driven by an oxidatively damaged OPC population. The continuation of the research commenced in Chapter 7 will likely aid in determining whether pericytes also undergo proliferation in association with oxidative damage, as well as potentially identify a similar proliferative response of DNA damaged OPCs in a model of demyelinating disease. Additionally, it will be important for future studies to further define the observed relationship between proliferation and oxidative damage, with the potential chronic functional implications of proliferating DNA damaged OPCs also warranting additional investigation.

8.4. Pathological Differences Between MS and Neurotrauma

It is also important to remain cognisant of the pathological differences between MS and neurotrauma. For example, the research presented in Chapter 2 found no effect of injury or the inhibitor combination on peripheral cytokine and chemokine concentrations (Toomey et al. 2019), which contrasts to changes in peripheral inflammation within MS. The lack of an observed peripheral immune response in response to injury in this study is likely in part reflective of the nature of a partial optic nerve transection injury, which at a depth of 14 μ m is a relatively small incision physically compared to the size of both the optic nerve and CNS of the animal. It may also be that the window of opportunity to detect change in the cytokine and chemokine analytes has passed by the 3 day timepoint (Patterson & Holahan 2012). It is worth noting that there was an observed increase in serum MCP-3 concentration following the partial optic nerve transection, but this was associated with the implantation of the local delivery devices rather than injury itself.

In humans who experience concussion, changes in blood cytokine and chemokine levels are transient, with one study showing the peripheral concentrations of these molecules returning to baseline levels within 48 hours after injury (Nitta et al. 2019). The assessed cytokines and chemokines from the study presented in Chapter 2 have also been specifically assessed following TBI in humans. For example, when analysing plasma IP-10 concentrations at 6 and 12 hours following hospital admission for either a moderate or severe TBI, IP-10 significantly decreases compared to healthy controls, but returns to normal levels by 24 hours after admission (Di Battista et al. 2016). Meanwhile, no differences have been detected in plasma IP-10 levels following mild TBI compared to controls, either immediately following hospital admission, or at three follow-up timepoints over the subsequent year (Chaban et al. 2020). Similarly there is a significant increase in the serum concentration of Gro- α (otherwise known as chemokine (C-X-C motif) ligand 1 or CXCL1) within the first 24 hours following hospital admission for severe TBI compared to healthy controls, with no differences

observed at this timepoint in cases of mild TBI (Chen et al. 2022). There is also a transient increase in plasma Eotaxin concentration post-injury, with elevations observed in the subacute phase following a sports-related mild TBI at around 4 days following injury and no differences observed compared to healthy controls when the athletes are medically cleared to return to play approximately 25 days post-injury (Di Battista et al. 2019).

This transient and severity-dependent nature of cytokines and chemokines following neurotrauma, particularly for milder injuries, is similar to other inflammatory blood-based biomarkers, such as S100b. With a relatively short half-life, kinetic modelling has found that serum S100b concentration peaks around 27 hours following severe TBI before rapidly decreasing (Ercole et al. 2016). When looking specifically at mild TBI, serum sampling for S100b should be performed and interpreted within the initial 6 hours post-injury to ensure that the window of opportunity for detection has not been missed (Thelin et al. 2016). It is also likely that changes to oxidative stress markers are similarly transient, with some rodent studies indicating that both the accumulation of oxidation products and antioxidant levels are acutely affected post-injury and then gradually resolve in a time-dependent manner (Ansari et al. 2008; Itoh et al. 2010; Petronilho et al. 2010). For example, increased oxidative damage to OPCs occurs acutely following a partial optic nerve transection, with a return to levels comparable to control animals at 7 and 28 days post-injury (Giacci *et al.*, 2018b). However, further work is needed to fully elucidate the time course of oxidative events following neurotrauma. Nevertheless, it is already established that suboptimal timing of sample collection can result in missed detection of changes in the concentration of inflammatory molecules post-injury.

It is difficult to accurately correlate the time course of biomarker fluctuations between rats and humans. Each day for an adult rat is usually thought to be approximately equivalent to just over a month for a human (Sengupta 2013). However, there isn't a universal conversion of time between rodents and humans following injury, with different pathological mechanisms possessing different temporal profiles (Agoston et al. 2019). Given inflammatory processes are thought to occur approximately 100 times faster in the rat than in humans (Agoston et al. 2019), it is highly likely that any transient increase in peripheral inflammation post-injury was missed by the 3 day timepoint within the study presented in Chapter 2. Had peripheral inflammation been assessed closer to the initial time of injury, it is feasible that significant changes in circulating cytokines and chemokines with both injury and potentially treatment may have been detected.

This absence of an observed peripheral immune response at 3 days following a partial optic nerve transection contrasts to the cuprizone model, where the peripheral cytokine immune response is known to progressively increase with continuing cuprizone-induced demyelination (Avşar et al. 2021). Likewise, cytokines and chemokines are known to play important roles in all MS subtypes, with a broad association between disease progression and increases in pro-inflammatory signalling

(Wang et al. 2018). Many markers of oxidative stress also show a comparable correlation to disease severity in MS, although some remain similarly elevated throughout continued disease progression compared to healthy controls (Adamczyk & Adamczyk-Sowa 2016). Therefore, though there is a similar severity-dependent expression of pro-inflammatory molecules for both MS and neurotrauma, increases in pro-inflammatory molecules are less transient in nature for MS pathology but rather continue to generally increase with disease progression.

Though BBB dysfunction is an early feature of both pathologies, there are mechanistic differences at the BBB between MS and neurotrauma. As discussed in Chapter 5, early disruptions to the BBB following neurotrauma are transient, particularly after mild injuries, and the BBB is eventually closed again through reparative mechanisms (Ziebell & Morganti-Kossmann 2010). BBB dysfunction is also often an early hallmark of the degeneration observed in MS lesions, occurring in otherwise healthy looking tissue and preceding the onset of symptoms (Filippi et al. 1998; Spencer 2018; Vos et al. 2005). BBB dysfunction is detectable in acute active, chronic active and chronic inactive MS lesions (Minagar & Alexander 2003; Soon et al. 2007), suggesting that BBB dysfunction continues throughout disease progression, even within less active lesion sites. Therefore, the reparative mechanisms that promote BBB repair following mild TBI are generally either ineffective or relatively absent in MS pathology. This difference in the mechanisms of BBB repair is also found within the relevant animal models. Following a partial optic nerve transection, peak BBB permeability occurs at 3 days post-injury, and returning to levels not different to controls from 1 week post-injury onwards (Smith et al. 2016; Smith et al. 2018). Meanwhile, in the cuprizone model, the level of BBB dysfunction is highest at 3 days after initiation of cuprizone toxicity (Shelestak et al. 2020), but still remains elevated by the 5 week timepoint (Berghoff *et al.*, 2017b). Future research should thus also investigate the underlying differences between BBB dysfunction in MS and neurotrauma to further elucidate therapeutic targets for promoting BBB repair.

These divergences between MS and neurotrauma pathological sequelae is likely underpinned by the core fundamental difference between the two disorders. MS is chronic condition with largely continual neurodegeneration that occurs gradually over many years. Meanwhile, neurotrauma has a sole initiating event that spurs both degenerative and reparative mechanisms concomitantly. Though there are secondary mechanisms that propagate the damage throughout the neighbouring tissue, another injury is required to induce additional areas of primary damage, unlike the persistent development of new demyelinated lesions as observed in people with MS. These discrepancies between the two disorders are highly pertinent and reinforces that though parallels can be drawn between the degeneration observed in the two neuropathologies, it is important to also remain cognisant of the differences as well.

8.5. Potential Therapeutic Strategies

The work presented in this thesis has demonstrated a promising therapeutic effect of a combinatorial ion channel inhibitor treatment in models of neurotrauma and demyelinating disease, as well as identified oxidative DNA damage to be a potentially worthy therapeutic target in both disorders. This forthcoming section will further discuss these possible avenues for effective therapeutic strategies and then discuss some important aspects of treatment development that require consideration.

8.5.1. Combinatorial Ion Channel Inhibitor Treatment

Throughout Chapter 2, a systemic combinatorial ion channel inhibitor treatment consisting of lomerizine, YM872 and BBG was employed to limit excess cellular Ca^{2+} (O'Hare Doig et al. 2016). This therapeutic combination ameliorated aspects of pathology in the partial optic nerve transection model (Toomey et al. 2019, Appendix A) and the cuprizone model (Gopalasingam et al. 2019, Appendix B). Research utilising the previous inhibitor combination of lomerizine, YM872 and oxATP were limited by the short implantation period of the osmotic mini-pumps, which likely didn't align with the optimal treatment durations (Dash & Cudworth 1998). However, even in these studies a 2 week period of local drug delivery improved outcomes by 3 months to a greater extent than was observed with just 3 days of delivery at an acute timepoint (O'Hare Doig et al. 2017; Savigni et al. 2013). These additional chronic improvements included further reductions in oxidative stress and the preservation of visual function following partial optic nerve transection (Savigni et al. 2013). With the development of the systemic treatment, this new combination of ion channel inhibitors could now be delivered continuously for a longer duration. Chronic administration of this therapeutic combination may result in greater longer term improvements in both of these models, including limiting oxidative damage. Therefore, future work should focus on both elucidating the inhibitor treatment's longer term effects on functional outcomes in both models and testing various treatment durations to establish an optimal therapeutic regime for chronic administration. Furthermore, the heightened peripheral inflammation, as demonstrated by plasma MCP-3 concentration, that was associated with the implantation of the local delivery device in Chapter 2 further reinforces the necessity for systemic delivery of therapeutics bound for clinical translation (Toomey et al. 2019, Appendix A).

It may be that the ion channel inhibitor combination could also improve BBB-related outcomes for both MS and neurotrauma. Elevated intracellular Ca^{2+} is associated with BBB dysfunction in ischemic conditions, with VGCC blockers known to ameliorate BBB damage (Rakkar & Bayraktutan 2016). This combinatorial treatment targets three separate pathways for intracellular Ca^{2+} influx, including VGCCs, and thus may confer a superior neuroprotective effect at the BBB. However, the effect of this combinatorial treatment for preventing BBB dysfunction in either

neurotrauma or MS has not yet been directly assessed. Thus, investigating the effect of the treatment for preserving BBB integrity is an important avenue for future research as demonstrated efficacy would provide further rationale for clinical translation of the inhibitor combination. Additionally, the effect of this combinatorial treatment on oxidative DNA damage to NG2⁺ glia specifically is not yet known. The observed colocalisation of 8OHdG within OPCs specifically during cuprizone administration alongside the preservation of OPC density with delivery of the ion channel inhibitor combination suggests that the treatment could potentially be mediating a protective effect against oxidative damage to OPCs (Gopalasingam et al. 2019, Appendix B). However, more work is needed to elucidate the presence of this potential therapeutic mechanism further.

It is worth noting that YM872 may have limited clinical application and an alternative AMPA receptor antagonist may be required. Though YM872 did progress to two different clinical trials for treating damage following ischemic stroke, both were terminated early due to inducing severe side effects in humans, such as hallucinations, catatonia and agitation (Farooqui 2010). Future studies should thus consider substituting YM872 with another AMPA receptor that is known to be clinically safe. One such alternative AMPA receptor antagonist is perampanel, which has already been approved for clinical use in over 55 countries (Tsai et al. 2018). Notably, both lomerizine (Imai et al. 2007) and BBG (FDA 2019) have already been approved for human clinical use. Nevertheless, although the inhibitor combination including YM872 provided proof of principle evidence for further investigation, additional work would be needed to ensure an adequate safety profile to utilise the combinatorial treatment in humans.

8.5.2. Anti-Oxidant Therapies

As discussed in Chapter 1, following a diagnosis of MS, people are typically commenced on immunomodulatory or immunosuppressant therapies, however these treatments only slow disease progression rather than halt it completely (Lassmann et al. 2007). Preventing oxidative stress has been previously identified as a therapeutic target in MS (Carvalho et al. 2014). Despite preliminary studies demonstrating beneficial effects following treatment with various antioxidant compounds in people with MS (Guan et al. 2018; Khalili et al. 2014; Miller et al. 2013; Monti et al. 2020; Pantzaris et al. 2013; Sanoobar et al. 2013; Sanoobar et al. 2014; Sanoobar et al. 2015), there are still no antioxidant therapies approved for clinical use for the condition. Likewise, there are currently limited pharmacological treatments clinically available for neurotrauma (Mohamadpour et al. 2019; Zibara et al. 2019). Similar to MS, there are ongoing investigations both preclinically and clinically to identify an effective antioxidant therapy for limiting neurodegeneration following traumatic injuries to the CNS (Hall et al. 2019; Rizwana & Agarwal 2022). Given oxidative damage appears likely to play a key role in exacerbating pathology in demyelinating disease and neurotrauma, this further emphasises oxidative stress as a therapeutic target worthy of further investigation.

8.5.2.1. Metformin

One potential therapeutic approach that could target oxidative DNA damage is metformin. Metformin, or 1,1-dimethylbiguanide hydrochloride, is an orally administered anti-diabetic drug that has been in use as a first-line therapy for patients with type 2 diabetes since 1958 (Scarpello and Howlett 2008; Wang *et al.* 2017). However, not only is metformin a potent antihyperglycemic agent, but it also acts as an anti-inflammatory and an antioxidant. Metformin has been shown to reduce 8OHdG oxidative DNA damage in multiple pathologies (Sova *et al.* 2013; Wang *et al.* 2017; Xu *et al.* 2018; Chen *et al.* 2019; Yang *et al.* 2020), as well as preventing other forms of oxidative DNA damage like double-strand breaks (Algire *et al.* 2012; Halicka *et al.* 2011; Na *et al.* 2013). When mice given cuprizone are treated with metformin, oxidative stress decreases alongside a concomitant reduction in microglial inflammation, which was associated with the preservation of oligodendrocytes and decreased demyelination (Abdi *et al.* 2021; Largani *et al.* 2019). Following a single TBI in mice, metformin treatment improved spatial learning and reduced neuroinflammation (DiBona *et al.* 2021). Similarly, in mice given a closed head TBI on 4 consecutive days in order to model repeated mild TBI, metformin treatment reduced damage to white matter, attenuated astrogliosis, limited the loss of hippocampal parvalbumin neurons, improved mitochondrial function and preserved motor and cognitive function (Underwood *et al.* 2021). Therefore, metformin has shown promising therapeutic effects preclinically for both neurotrauma and demyelinating disease, suggesting it may be a particularly useful treatment strategy for limiting damage in these pathologies.

8.5.3. *Important Considerations for Developments of Therapeutics*

There are important aspects of therapeutic development that need to be considered to develop effective and translatable treatments for both MS and neurotrauma. Given the nature of neurodegenerative diseases, the underlying damage can occur for years before a person with MS actually reaches the clinic. Therefore, this delay for treatment onset should be considered when trialling therapeutics preclinically. Similarly, it will be important that preclinical treatment schedules are employed that represent the delays for treatment in humans following neurotrauma. Many people who experience milder forms of neurotrauma, such as concussion, will typically wait for days or even weeks before seeking medical assistance (Kushner 1998). It is worth noting though that with increasing public awareness surrounding concussion, primarily through heightened media attention, the willingness to quickly report symptoms and seek help for milder injuries is improving (Patterson & Holahan 2012).

There is also a great deal of heterogeneity in both disorders, both between individuals and temporally within individuals. It is therefore vital that therapeutics are validated in multiple animal models to represent this heterogeneity (Friese *et al.* 2006). Employing preclinical models that utilise humanised rodents may also accelerate the translation of animal findings to the clinic (Dash *et al.*

2021). Additionally, future treatment strategies may need to consider a more personalised approach to reflect the variability both between and within individuals with MS and following neurotrauma. For example, specifically tailoring therapeutics at defined temporal intervals to reflect changes in identified inflammatory and degenerative profiles over time (Patterson & Holahan 2012).

It would also be valuable to test potential treatments in larger animal models prior to clinical translation, particularly for use following neurotrauma. Rodent brains do differ anatomically compared to humans, such as being lissencephalic rather than gyrencephalic and being overall far smaller in size. The sulci and gyri present on the human brain alters the biomechanics of neurotrauma, with a comparatively greater degree of injury occurring when a brain is gyrencephalic (Vink 2018). Similarly, smaller brains can also withstand greater acceleration and deceleration forces during impact and thus are more robust against the effects of injury (Finnie 2001). Larger animal models in pigs and sheep have already proven vital for illuminating mechanisms of damage following neurotrauma and are regarded as a useful screening tool for trialling new therapies prior to human clinical trials (Dai et al. 2018). When looking at models of demyelinating disease, most studies are performed in rodents. The visna virus can be used to model MS in sheep as it causes similar demyelinated plaques to those observed in human brains (Dal Canto & Rabinowitz 1982; Pachner 2011). However, this model is not well characterised, especially compared to the available rodent models for demyelinating disease, such as the cuprizone model or EAE. It is important to note though that rodents do have a lower ratio of white matter to grey matter than humans, and thus larger animals with a greater relative volume of white matter may provide additional relevant insights particularly into white matter pathology (Vink 2018).

8.6. Broader Clinical Applicability and Translatability

Animal models are widely used throughout scientific research to aid in furthering the understanding of disease pathophysiology and facilitate development of therapeutics. Due to their phylogenetic and physiological similarity to humans, combined with their comparatively enhanced ability to be housed and bred in highly controlled laboratory settings compared to other larger animals, rodents have long served as the ideal animals through which to investigate a plethora of human conditions (Perlman 2016). The capacity to manipulate, edit and mutate genes in the rodent genome, particularly in mice, to delve even deeper into disease mechanisms at the level of a singular gene has further increased the prevalence of rodents in animal research (Rosenthal & Brown 2007). Additionally, there is a great deal of similarity between the human and rodent cerebrovasculature, making rodent models useful tools in investigating changes to the cerebral blood supply and the BBB (Lee 1995). However, though there are many similarities between rodents and humans, there are many differences too that could potential limit the translatability of animal work. For example, mice

have higher rates of ROS production and are therefore more susceptible to oxidative damage than humans (Perlman 2016), which may be a confounding factor in the work presented in this thesis. Reinforcing this, though many attempts have been made to directly translate animal research into human studies, not all rodent work has been able to be accurately translated for clinical applicability to human conditions. Looking at the most highly cited (> 500 citations) articles using animal models published between 1980 to 2000 in the top seven scientific journals worldwide, only one third of these studies described treatments that were translated to humans in clinical randomised control trials, and only a tenth were subsequently approved for human use in the clinic (Hackam & Redelmeier 2006). Given that these studies were of considerably high impact, it's exceedingly likely that less cited animal research in less prominent journals will have an even poorer chance of clinical translatability (van der Worp et al. 2010). Thus, it is absolutely vital for animal models to accurately reflect human disorders as much as possible to increase the potential clinical applicability of these studies.

8.6.1. Cuprizone Model of Demyelinating Disease Compared to Human MS Pathology

MS is a multifaceted condition that appears to be entirely unique to humans (Ransohoff 2012). There are multiple forms of MS and even MS lesions themselves are extremely heterogenous, which has ultimately resulted in the underlying pathogenesis of this complex disorder remaining enigmatic despite extensive global research efforts. Given this considerable variability in clinical presentation of MS, as well as in lesion pathophysiology, there is consequently no gold standard for the optimal animal model for investigating MS aetiology.

The cuprizone model is an especially suitable model for investigating the mechanisms underpinning pattern III lesions in human MS brains (Ransohoff 2012) and for exploring the “inside-out” hypothesis as discussed in Section 1.2.5.2. In particular, cuprizone may be more useful than alternative animal models of demyelination for analysing initiating events early in lesion formation, particularly for this type of lesion (Sen et al. 2019). A key hallmark of pattern III MS lesions is active demyelination that is mediated primarily by oligodendrocyte apoptosis and dysregulated myelin proteins (Jarius et al. 2017; Lucchinetti et al. 2000; Popescu et al. 2013), which is mimicked in the development of cuprizone pathophysiology (Ransohoff 2012).

Many of the pathological hallmarks of progressive MS are also present in the cuprizone model, including focal white matter lesions, cortical and deep grey matter demyelination, degeneration and loss of oligodendrocytes, axonal damage, active gliosis, and oxidative stress (Zhan et al. 2020). Furthermore, the diffuse and considerably reduced pathological abnormalities found in some white matter areas of the brain after prolonged cuprizone intoxication, such as in the hippocampal fimbria region or the anterior commissure, presents similarly to normal appearing white matter in progressive MS (Kipp et al. 2017). Thus, when utilising these regions specifically, it allows

researchers to look specifically at the development and progression of normal appearing white matter pathology.

It's important to note though that the remyelination that occurs following withdrawal of cuprizone actually more closely resembles the spontaneous remyelination that can occur in people with RRMS (Vega-Riquer et al. 2019). This reparative remyelination mechanism is typically incomplete or relatively absent in more chronic MS lesions (Goldschmidt et al. 2009), and therefore the cuprizone model can also be utilised to help decipher the potential underlying mechanisms that promote remyelination following cessation of cuprizone, as well as to aid the development of therapeutics that stimulate this endogenous remyelination (Gingele et al. 2020). Thus, cuprizone is an animal model of demyelinating disease that has wide applicability to various aspects of the complex MS disease state making it particularly valuable for investigating and quantifying neurodegeneration.

The cuprizone model has traditionally been thought to not adequately address the contribution of BBB dysfunction or autoimmune T-cells to overall MS pathology, potentially limiting its clinical applicability (Kipp et al. 2017; Praet et al. 2014). However, as discussed in Chapter 5 it is now known that BBB permeability is indeed increased as early as 3 days into cuprizone exposure, likely due to a localised astroglial-derived inflammatory milieu that impairs BBB integrity, far preceding detectable demyelination (Berghoff et al. 2017). This increased hyperpermeability is associated with increased extravasation of fluorescent dyes from blood vessels, increased brain oedema, decreased expression of tight junction proteins, increased mast cell infiltration, and by 5 weeks of cuprizone, increased diffusivity of aquaporin 4 expression (Berghoff et al. 2017; Shelestak et al. 2020). Therefore, cuprizone administration does in fact induce disruption to the BBB which further promotes cuprizone as a clinically applicable model of MS.

The cuprizone model has been criticised for the lack of an autoimmune component similar to that observed in human MS pathophysiology, particularly within pattern I and II lesions (Nyamoya et al. 2017; Sutiwisesak et al. 2021). Research groups have thus begun utilising a combined animal model that employs both cuprizone and the autoimmune-centric EAE model to encompass the two discrete degenerative cascades into a singular model to better reflect the complex heterogeneity of MS lesions (Chrzanowski et al. 2019; Nack et al. 2019; Nedelcu et al. 2020; Rohr et al. 2020; R  ther et al. 2017; Yakimov et al. 2019). However, the EAE model is primarily dominated by the infiltration of CD4+ T-cells (Kuchroo et al. 2003), whilst the majority of MS lesions primarily have CD8+ T-cell infiltration (Babbe et al. 2000; Hauser et al. 1986; Kaddatz et al. 2021; Salou et al. 2015a; Salou et al. 2015b). Interestingly, this peripheral CD8+ T-cell inflammation in progressive MS is still pronounced but far less severe than in acute or relapsing forms of the disease, which may also in part underpin the lack of effectiveness of immunomodulatory therapies in the progressive MS subtypes

(Frischer et al. 2009; Machado-Santos et al. 2018). More recent research in the cuprizone model has revealed significant increases in the infiltration of T-cells, particularly CD8⁺ cytotoxic T-cells within the corpus callosum after acute (5 weeks) and chronic (11 weeks) cuprizone intoxication that were comparative to T-cell densities in progressive MS lesions (Kaddatz et al. 2021). Thus, the oligodendrocyte degeneration and neuroinflammation observed during cuprizone administration may in fact trigger secondary peripheral immune cell recruitment comparable to the autoimmune mechanisms present in progressive MS lesion pathology. It is also important to note that though the basic functions of mouse and human immune systems are relatively similar, there is still a considerable degree of difference, with many mechanisms and immune pathways differing between the two species, including in some of the pathways resulting in the activation of T-cells and in pro-inflammatory signalling (Bailey et al. 2013; Rydell-Törmänen & Johnson 2019). Therefore, the clinical applicability of mouse models must be carefully and critically evaluated for any potential divergences in the immune systems between species. Nevertheless, this newfound involvement of T-cell infiltration during cuprizone intoxication further supports the potential applicability of this model to human MS pathology, even without the addition of a concomitant EAE induction.

A potential further limitation of this model is the relative age of the mice administered cuprizone compared to humans with MS. The mice used for cuprizone intoxication began the experimental period at 8 weeks of age, which is roughly equivalent to a human age that is more closely aligned with the age of onset in paediatric MS (Alroughani & Boyko 2018; Dutta & Sengupta 2016). Given that the adult MS disease onset is approximately 30 years of age (Goodin 2014), this corresponds more accurately to a 6 month old mouse (Dutta & Sengupta 2016). Interestingly, when 6 month old mice are administered 0.2% cuprizone for either 5 or 6 weeks, demyelination is not detectable in the corpus callosum and in order to induce a demyelinating pathology similar to that seen for the 8 week old mice at these timepoints, mice need to be administered 0.4% cuprizone for 6.5 weeks (Gingele et al. 2020). Remyelination is also much slower and becomes stagnated at an incomplete level in aged mice compared to 8 week old mice. Oligodendrocyte repopulation is also less efficient (Gingele et al. 2020), and more comparable to the incomplete remyelination observed in progressive MS (Goldschmidt et al. 2009). Thus, the standardised use of 8 week old mice in cuprizone studies does not accurately correspond to the age of onset for adult human MS and therefore also may not precisely reflect the core pathophysiology of human MS, particularly in regards to potentially partial remyelination.

8.6.2. Partial Optic Nerve Transection Compared to Human Neurotrauma

Similar to MS, there are a multitude of animal models of neurotrauma that encompass different aspects of human pathology. Since a particular focus of this thesis was understanding the mechanisms underlying secondary degeneration, the partial optic nerve transection model was

utilised. As previously discussed, the partial optic nerve transection model is particularly useful for examining secondary damage mechanisms following injury to the CNS compared to other models of neurotrauma, such as the controlled cortical impact model, fluid percussion model and the closed head weight drop model, where it is difficult to distinguish between the initially axotomised and spared tissue (Bartlett & Fitzgerald 2018; Levkovitch-Verbin et al. 2003). The optic nerve is a relatively non-regenerative and easily accessible CNS white matter tract that is particularly useful for identifying mechanisms of damage following injury to the brain (Benowitz & Yin 2008). When the optic nerve is partially transected, it is straightforward to distinguish between the areas of primary and secondary damage following injury to the CNS and the extent of this damage can be precisely controlled by the size of the transection (Bartlett & Fitzgerald 2018). However, the partial transection injury is focal in nature. Many people who experience a mild TBI do not have a solely focal injury but rather present with more diffuse and widespread forms of damage, whereby primary and secondary injury interact to create a multifaceted and continually evolving disease process (Masel & DeWitt 2010; Sharp & Jenkins 2015). Therefore, the partial optic nerve transection model does not accurately represent the full spectrum of damage seen following trauma and cannot be considered a direct model of TBI *per se*. Another limitation of this model is that it cannot be used to assess the effect of repeated injury to the CNS, as once the optic nerve is transected, it is not clinically relevant to transect it again. The brain is more vulnerable to additional injury and prolonged deficits following additional head trauma (Blennow et al. 2012), and those who have sustained a mild TBI previously have a two to fivefold greater risk of experiencing a subsequent mild TBI (Bolton-Hall et al. 2019). Therefore, any mechanistic understanding obtained *via* utilising the partial transection model should also be assessed in other animal models that do allow for evaluation of the potentially accumulative damage that occurs following repeated mild TBIs, such as in the repeated closed head weight drop model (Fehily et al. 2019; Mao et al. 2018; Yates et al. 2017). Nevertheless, the partial optic nerve transection model is useful in furthering knowledge of the underlying damage and/or compensatory mechanisms present following neurotrauma, and when this insight is incorporated with data acquired in other animal models and clinical observations and outcomes, it will hopefully assist in developing a fuller picture of the neurological response to damage following injury to the CNS.

8.7. Final Concluding Remarks

The overarching aim of this thesis was to establish the relevant framework and commence investigation into shared damage mechanisms between MS and neurotrauma in order to facilitate rapid advancement of knowledge. Common damage mechanisms were initially explored *via* the utilisation of a combinatorial ion channel inhibitor treatment in models of neurotrauma and MS. The cuprizone model of demyelinating disease was also optimised, to facilitate further investigations into

the pathological mechanisms underpinning MS within our laboratory as well as within the wider scientific community. Finally, a relationship between oxidative DNA damage, BBB dysfunction and cellular proliferation was established in a model of neurotrauma, with OPCs identified as the major proliferating, DNA damaged cell type acutely following injury. A parallel study investigating oxidative damage and BBB dysfunction in a model of demyelinating disease was also commenced. The work described in this thesis has been published thus far within five papers, including a co-first author narrative review paper presented in Chapter 1 and a first author research paper presented in Chapter 4. Altogether, this thesis supported the notion that pathological similarities exist between MS and neurotrauma and that unifying our understanding of the two disorders may facilitate the development of effective treatments for both.

References

- Abbott, NJ, Patabendige, AAK, Dolman, DEM, Yusof, SR, & Begley, DJ 2010, 'Structure and function of the blood–brain barrier', *Neurobiology of Disease*, vol. 37, no. 1, pp. 13–25.
- Abbott, NJ, Rönnbäck, L, & Hansson, E 2006, 'Astrocyte–endothelial interactions at the blood–brain barrier', *Nature Reviews Neuroscience*, vol. 7, pp. 41–53.
- Abdeljalil, J, Hamid, M, Abdel-Mouttalib, O, Stéphane, R, Raymond, R, Johan, A, José, S, Pierre, C, & Serge, P 2005, 'The optomotor response: A robust first-line visual screening method for mice', *Vision Research*, vol. 45, pp. 1439–1446.
- Abdi, M, Pasbakhsh, P, Shabani, M, Nekoonam, S, Sadeghi, A, Fathi, F, Abouzaripour, M, Mohamed, W, Zibara, K, Kashani, IR, & Zendedel, A 2021, 'Metformin Therapy Attenuates Pro-inflammatory Microglia by Inhibiting NF- κ B in Cuprizone Demyelinating Mouse Model of Multiple Sclerosis', *Neurotoxicity Research*, vol. 39, no. 6, pp. 1732–1746.
- Abdul-Muneer, PM, Chandra, N, & Haorah, J 2014, 'Interactions of oxidative stress and neurovascular inflammation in the pathogenesis of traumatic brain injury', *Molecular Neurobiology*, vol. 51, no. 3, pp. 966–979.
- Abdul-Muneer, PM, Schuetz, H, Wang, F, Skotak, M, Jones, J, Gorantla, S, Zimmerman, MC, Chandra, N, & Haorah, J 2013, 'Induction of oxidative and nitrosative damage leads to cerebrovascular inflammation in an animal model of mild traumatic brain injury induced by primary blast', *Free Radical Biology and Medicine*, vol. 60, pp. 282–291.
- Acharya, NK, Levin, EC, Clifford, PM, Han, M, Tourtellotte, R, Chamberlain, D, Pollaro, M, Coretti, NJ, Kosciuk, MC, Nagele, EP, Demarshall, C, Freeman, T, Shi, Y, Guan, C, MacPhee, CH, Wilensky, RL, & Nagele, RG 2013, 'Diabetes and hypercholesterolemia increase blood-brain barrier permeability and brain amyloid deposition: Beneficial effects of the LpPLA2 inhibitor darapladib', *Journal of Alzheimer's Disease*, vol. 35, no. 1, pp. 179–198.
- Acheson, E, Bachrach, C, & Wright, F 1960, 'Some comments on the relationship of the distribution of multiple sclerosis to latitude, solar radiation and other variables', *Acta Psychiatr Scand Suppl.*, vol. 35, no. 147, pp. 132–47.
- Acs, P, Selak, MA, Komoly, S, & Kalman, B 2013, 'Distribution of oligodendrocyte loss and mitochondrial toxicity in the cuprizone-induced experimental demyelination model', *Journal of Neuroimmunology*, vol. 262, no. 1–2, pp. 128–131.
- Adam-Vizi, V & Starkov, AA 2010, 'Calcium and mitochondrial reactive oxygen species generation', *Journal of Alzheimer's Disease*, vol. 20, pp. 413–426.
- Adamczyk, B & Adamczyk-Sowa, M 2016, 'New Insights into the Role of Oxidative Stress Mechanisms in the Pathophysiology and Treatment of Multiple Sclerosis', *Oxidative Medicine and Cellular Longevity*, vol. 2016, pp. 1–18.

Adams, RA, Bauer, J, Flick, MJ, Sikorski, SL, Nuriel, T, Lassmann, H, Degen, JL, & Akassoglou, K 2007, 'The fibrin-derived γ 377-395 peptide inhibits microglia activation and suppresses relapsing paralysis in central nervous system autoimmune disease', *Journal of Experimental Medicine*, vol. 204, no. 3, pp. 571–582.

Adelson, PD, Whalen, MJ, Kochanek, PM, Robichaud, P, & Carlos, TM 1998, 'Blood brain barrier permeability and acute inflammation in two models of traumatic brain injury in the immature rat: A preliminary report', in *Intracranial Pressure and Neuromonitoring in Brain Injury*, pp.104–106. Springer Vienna, Vienna.

Agarwal, R & Shukla, GS 1999, 'Potential role of cerebral glutathione in the maintenance of blood-brain barrier integrity in rat.', *Neurochemical Research*, vol. 24, no. 12, pp. 1507–14.

Aggarwal, S, Yurlova, L, & Simons, M 2011, 'Central nervous system myelin: structure, synthesis and assembly', *Trends in Cell Biology*, vol. 21, no. 10, pp. 585–593.

Agoston, D V., Vink, R, Helmy, A, Risling, M, Nelson, D, & Prins, M 2019, 'How to Translate Time: The Temporal Aspects of Rodent and Human Pathobiological Processes in Traumatic Brain Injury', *Journal of Neurotrauma*, vol. 36, no. 11, p. 1724.

Aguiar, PHN, Furtado, C, Repolês, BM, Ribeiro, GA, Mendes, IC, Peloso, EF, Gadelha, FR, Macedo, AM, Franco, GR, Pena, SDJ, Teixeira, SMR, Vieira, LQ, Guarneri, AA, Andrade, LO, & Machado, CR 2013, 'Oxidative stress and DNA lesions: the role of 8-oxoguanine lesions in Trypanosoma cruzi cell viability.', *PLoS Neglected Tropical Diseases*, vol. 7, no. 6, p. e2279.

Aharoni, R 2010, 'Immunomodulatory drug treatment in multiple sclerosis', *Expert Review of Neurotherapeutics*, vol. 10, no. 9, pp. 1423–1436.

Aharoni, R, Kayhan, B, Eilam, R, Sela, M, & Arnon, R 2003, 'Glatiramer acetate-specific T cells in the brain express T helper 2/3 cytokines and brain-derived neurotrophic factor in situ', *Proceedings of the National Academy of Sciences*, vol. 100, no. 24, pp. 14157–14162.

Albert, M, Antel, J, Brück, W, & Stadelmann, C 2007, 'Extensive cortical remyelination in patients with chronic multiple sclerosis', *Brain Pathology*, vol. 17, no. 2, pp. 129–138.

Algire, C, Moiseeva, O, Deschênes-Simard, X, Amrein, L, Petruccelli, L, Birman, E, Viollet, B, Ferbeyre, G, & Pollak, MN 2012, 'Metformin reduces endogenous reactive oxygen species and associated DNA damage', *Cancer Prevention Research*, vol. 5, no. 4, pp. 536–543.

Allen, I V, Mcquaid, • S, Mirakhur, • M, Nevin, • G, Mcquaid, S, Nevin, G, & Sci, N 2001, 'Pathological abnormalities in the normal-appearing white matter in multiple sclerosis', *Neurological Science*, vol. 22, pp. 141–144.

Alroughani, R & Boyko, A 2018, 'Pediatric multiple sclerosis: a review', *BMC Neurology*, vol. 18, no. 1.

Alroughani, RA, Akhtar, S, Ahmed, SF, & Al-Hashel, JY 2015, 'Clinical predictors of disease

progression in multiple sclerosis patients with relapsing onset in a nation-wide cohort', *International Journal of Neuroscience*, vol. 125, no. 11, pp. 831–837.

Alusi, SH, Worthington, J, Glickman, S, & Bain, PG 2001, 'A study of tremor in multiple sclerosis', *Brain*, vol. 124, no. 4, pp. 720–730.

Alvarez, JI, Katayama, T, & Prat, A 2013, 'Glial influence on the blood brain barrier', *GLIA*, vol. 61, no. 12, pp. 1939–1958.

Amato, MP, Ponziani, G, Rossi, F, Liedl, CL, Stefanile, C, & Rossi, L 2001, 'Quality of life in multiple sclerosis: the impact of depression, fatigue and disability', *Multiple Sclerosis*, vol. 7, pp. 340–344.

Andreassen, OA, Harbo, HF, Wang, Y, Thompson, WK, Schork, AJ, Mattingsdal, M, Zuber, V, Bettella, F, Ripke, S, Kelsoe, JR, Kendler, KS, O'Donovan, MC, Sklar, P, McEvoy, LK, Desikan, RS, Lie, BA, Djurovic, S, & Dale, AM 2015, 'Genetic pleiotropy between multiple sclerosis and schizophrenia but not bipolar disorder: differential involvement of immune-related gene loci', *Molecular Psychiatry*, vol. 20, no. 2, pp. 207–214.

Andriessen, TMJC, Jacobs, B, & Vos, PE 2010, 'Clinical characteristics and pathophysiological mechanisms of focal and diffuse traumatic brain injury', *Journal of Cellular and Molecular Medicine*, vol. 14, no. 10, pp. 2381–2392.

Angeloni, C, Prata, C, Vieceli, F, Segal, D, Piperno, R, & Hrelia, S 2015, 'Traumatic Brain Injury and NADPH Oxidase: A Deep Relationship', *Oxidative Medicine and Cellular Longevity*, vol. 2015.

Ansari, MA, Roberts, KN, & Scheff, SW 2008, 'A Time Course of Contusion-Induced Oxidative Stress and Synaptic Proteins in Cortex in a Rat Model of TBI', *Journal of Neurotrauma*, vol. 25, no. 5, pp. 513–526.

Ansari, MA, Roberts, KN, & Scheff, SW 2014, 'A time course of NADPH-oxidase up-regulation and endothelial nitric oxide synthase activation in the hippocampus following neurotrauma', *Free Radical Biology and Medicine*, vol. 77, pp. 21–29.

Arai, K. & Lo, EH 2009, 'An oligovascular niche: Cerebral endothelial cells promote the survival and proliferation of oligodendrocyte precursor cells', *Journal of Neuroscience*, vol. 29, no. 14, pp. 4351–4355.

Arai, Ken & Lo, EH 2009, 'Oligovascular signaling in white matter stroke', *Biological & pharmaceutical bulletin*, vol. 32, no. 10, pp. 1639–44.

Arai, K & Lo, EH 2010, 'Astrocytes protect oligodendrocyte precursor cells via MEK/ERK and PI3K/Akt signaling', *Journal of Neuroscience Research*, vol. 88, pp. 758–763.

Archelos, JJ, Trotter, J, Previtali, S, Weigbrich, B, Toyka, K V, & Hartung, H-P 1998, 'Isolation and Characterization of an Oligodendrocyte Precursor-Derived Epitope in Multiple

Sclerosis B-Cell', *Annals of Neurology*, vol. 43, no. 1, pp. 15–24.

Armulik, A, Genové, G, & Betsholtz, C 2011, 'Pericytes: Developmental, Physiological, and Pathological Perspectives, Problems, and Promises', *Developmental Cell*, vol. 21, no. 2, pp. 193–215.

Arnett, SD, Osbourn, DM, Moore, KD, Vandaveer, SS, & Lunte, CE 2005, 'Determination of 8-oxoguanine and 8-hydroxy-2'-deoxyguanosine in the rat cerebral cortex using microdialysis sampling and capillary electrophoresis with electrochemical detection.', *Journal of Chromatography*, vol. 827, no. 1, pp. 16–25.

Arundine, M & Tymianski, M 2003, 'Molecular mechanisms of calcium-dependent neurodegeneration in excitotoxicity', *Cell Calcium*, vol. 34, pp. 325–337.

Atsumi, T, Hoshino, S, Furukawa, T, Kobayashi, S, Asakura, T, Takahashi, M, & Teramoto, A 2003, 'The glutamate AMPA receptor antagonist, YM872, attenuates regional cerebral edema and IgG immunoreactivity following experimental brain injury in rats', *Brain Edema XII. Acta Neurochirurgica Supplements*, vol. 86, pp. 305–307.

Avşar, T, Çelikyapi Erdem, G, Terzioğlu, G, & Tahir Turanlı, E 2021, 'Investigation of neuro-inflammatory parameters in a cuprizone induced mouse model of multiple sclerosis', *Turkish Journal of Biology*, vol. 45, no. 5, p. 644.

Ayada, K, Tadano, T, & Endo, Y 2002, 'Gnawing behavior of a mouse in a narrow cylinder: A simple system for the study of muscle activity, fatigue, and stress', *Physiology & Behavior*, vol. 77, no. 1, pp. 161–166.

Ayala, A, Muñoz, MF, & Argüelles, S 2014, 'Lipid peroxidation: production, metabolism, and signaling mechanisms of malondialdehyde and 4-hydroxy-2-nonenal', *Oxidative Medicine and Cellular Longevity*, vol. 2014, p. 360438.

Babbe, H, Roers, A, Waisman, A, Lassmann, H, Goebels, N, Hohlfeld, R, Friese, M, Schröder, R, Deckert, M, Schmidt, S, Ravid, R, & Rajewsky, K 2000, 'Clonal expansions of CD8(+) T cells dominate the T cell infiltrate in active multiple sclerosis lesions as shown by micromanipulation and single cell polymerase chain reaction', *The Journal of Experimental Medicine*, vol. 192, no. 3, pp. 393–404.

Babior, BM 2004, 'NADPH oxidase', *Current Opinion in Immunology*, vol. 16, no. 1, pp. 42–47.

Bailey, M, Christoforidou, Z, & Lewis, MC 2013, 'The evolutionary basis for differences between the immune systems of man, mouse, pig and ruminants', *Veterinary Immunology and Immunopathology*, vol. 152, no. 1–2, pp. 13–19.

Bakkenist, CJ & Kastan, MB 2003, 'DNA damage activates ATM through intermolecular autophosphorylation and dimer dissociation', *Nature*, vol. 421, no. 6922, pp. 499–506.

Bakker, DA & Ludwin, SK 1987, 'Blood-brain barrier permeability during Cuprizone-

induced demyelination Implications for the pathogenesis of immune-mediated demyelinating diseases', *Journal of the Neurological Sciences*, vol. 78, pp. 125–137.

Ballabh, P, Braun, A, & Nedergaard, M 2004, 'The blood-brain barrier: An overview: Structure, regulation, and clinical implications', *Neurobiology of Disease*, vol. 16, no. 1, pp. 1–13.

Banasr, M, Valentine, GW, Li, XY, Gourley, SL, Taylor, JR, & Duman, RS 2007, 'Chronic Unpredictable Stress Decreases Cell Proliferation in the Cerebral Cortex of the Adult Rat', *Biological Psychiatry*, vol. 62, no. 5, pp. 496–504.

Barger, SW, Goodwin, ME, Porter, MM, & Beggs, ML 2007, 'Glutamate release from activated microglia requires the oxidative burst and lipid peroxidation', *Journal of Neurochemistry*, vol. 101, no. 5, pp. 1205–1213.

Barnett, MH & Prineas, JW 2004, 'Relapsing and remitting multiple sclerosis: Pathology of the newly forming lesion', *Annals of Neurology*, vol. 55, no. 4, pp. 458–468.

Bartlett, C & Fitzgerald, M 2018, 'Partial Transection of Adult Rat Optic Nerve as a Model of Secondary Degeneration in the Central Nervous System', *BIO-PROTOCOL*, vol. 8, no. 24.

Barzilai, A & Yamamoto, K-I 2004, 'DNA damage responses to oxidative stress', *DNA Repair*, vol. 3, no. 8–9, pp. 1109–1115.

Başkaya, MK, Rao, AM, Doğan, A, Donaldson, D, & Dempsey, RJ 1997, 'The biphasic opening of the blood-brain barrier in the cortex and hippocampus after traumatic brain injury in rats', *Neuroscience Letters*, vol. 226, no. 1, pp. 33–36.

Di Battista, AP, Churchill, N, Rhind, SG, Richards, D, & Hutchison, MG 2019, 'Evidence of a distinct peripheral inflammatory profile in sport-related concussion', *Journal of Neuroinflammation*, vol. 16, no. 1, pp. 1–12.

Di Battista, AP, Rhind, SG, Hutchison, MG, Hassan, S, Shiu, MY, Inaba, K, Topolovec-Vranic, J, Neto, AC, Rizoli, SB, & Baker, AJ 2016, 'Inflammatory cytokine and chemokine profiles are associated with patient outcome and the hyperadrenergic state following acute brain injury', *Journal of Neuroinflammation*, vol. 13, no. 1, pp. 1–14.

Bauer, HC, Krizbai, IA, Bauer, H, & Traweger, A 2014, "'You shall not pass"- tight junctions of the blood brain barrier', *Frontiers in Neuroscience*, vol. 8, p. 392.

Baxi, EG, DeBruin, J, Jin, J, Strasburger, HJ, Smith, MD, Orthmann-Murphy, JL, Schott, JT, Fairchild, AN, Bergles, DE, & Calabresi, PA 2017, 'Lineage tracing reveals dynamic changes in oligodendrocyte precursor cells following cuprizone-induced demyelination', *Glia*, vol. 65, no. 12, pp. 2087–2098.

Behzadian, MA, Wang, XL, Windsor, LJ, Ghaly, N, & Caldwell, RB 2001, 'TGF-beta increases retinal endothelial cell permeability by increasing MMP-9: possible role of glial cells in endothelial barrier function - PubMed', *Investigative Ophthalmology & Visual Science*, vol. 42, no.

3, pp. 853–859.

Beiter, RM, Rivet-Noor, C, Merchak, AR, Bai, R, Johanson, DM, Slogar, E, Sol-Church, K, Overall, CC, & Gaultier, A 2022, 'Evidence for oligodendrocyte progenitor cell heterogeneity in the adult mouse brain', *Scientific Reports* 2022 12:1, vol. 12, no. 1, pp. 1–15.

Benedict, RHB, Wahlig, E, Bakshi, R, Fishman, I, Munschauer, F, Zivadinov, R, & Weinstock-Guttman, B 2005, 'Predicting quality of life in multiple sclerosis: accounting for physical disability, fatigue, cognition, mood disorder, personality, and behavior change', *Journal of the Neurological Sciences*, vol. 231, no. 1–2, pp. 29–34.

Benowitz, L & Yin, Y 2008, 'Rewiring the injured CNS: Lessons from the optic nerve', *Experimental Neurology*, vol. 209, no. 2, pp. 389–398.

van Berckel, BN, Bossong, MG, Boellaard, R, Kloet, R, Schuitemaker, A, Caspers, E, Luurtsema, G, Windhorst, AD, Cahn, W, Lammertsma, AA, & Kahn, RS 2008, 'Microglia Activation in Recent-Onset Schizophrenia: A Quantitative (R)-[11C]PK11195 Positron Emission Tomography Study', *Biological Psychiatry*, vol. 64, no. 9, pp. 820–822.

Bergamaschi, R, Berzuini, C, Romani, A, & Cosi, V 2001, 'Predicting secondary progression in relapsing-remitting multiple sclerosis: a Bayesian analysis.', *Journal of the Neurological Sciences*, vol. 189, no. 1–2, pp. 13–21.

Berghoff, SA, Düking, T, Spieth, L, Winchenbach, J, Stumpf, SK, Gerndt, N, Kusch, K, Ruhwedel, T, Möbius, W, & Saher, G 2017, 'Blood-brain barrier hyperpermeability precedes demyelination in the cuprizone model', *Acta Neuropathologica Communications*, vol. 5, no. 1, p. 94.

Berghoff, SA, Gerndt, N, Winchenbach, J, Stumpf, SK, Hosang, L, Odoardi, F, Ruhwedel, T, Böhler, C, Barrette, B, Stassart, R, Liebetanz, D, Dibaj, P, Möbius, W, Edgar, JM, & Saher, G 2017, 'Dietary cholesterol promotes repair of demyelinated lesions in the adult brain', *Nature Communications*, vol. 8.

Bergles, DE & Richardson, WD 2016, 'Oligodendrocyte development and plasticity', *Cold Spring Harbor Perspectives in Biology*, vol. 8, no. 2.

Bergles, DE, Roberts, JDB, Somogyi, P, & Jahr, CE 2000, 'Glutamatergic synapses on oligodendrocyte precursor cells in the hippocampus', *Nature*, vol. 405, no. 6783, pp. 187–191.

Bernard-Patrzynski, F, Lécuyer, MA, Puscas, I, Boukhatem, I, Charabati, M, Bourbonnière, L, Ramassamy, C, Leclair, G, Prat, A, & Roullin, VG 2019, 'Isolation of endothelial cells, pericytes and astrocytes from mouse brain', *PLOS ONE*, vol. 14, no. 12, p. e0226302.

Bernardo, A, Bianchi, D, Magnaghi, V, & Minghetti, L 2009, 'Peroxisome proliferator-activated receptor-gamma agonists promote differentiation and antioxidant defenses of oligodendrocyte progenitor cells.', *Journal of Neuropathology and Experimental Neurology*, vol. 68, no. 7, pp. 797–808.

Betts, CD, D'Mellow, MT, & Fowler, CJ 1993, 'Urinary symptoms and the neurological features of bladder dysfunction in multiple sclerosis.', *Journal of Neurology, Neurosurgery, and Psychiatry*, vol. 56, no. 3, pp. 245–50.

Biancotti, JC, Kumar, S, & de Vellis, J 2008, 'Activation of Inflammatory Response by a Combination of Growth Factors in Cuprizone-Induced Demyelinated Brain Leads to Myelin Repair', *Neurochemical Research*, vol. 33, no. 12, pp. 2615–2628.

Birben, E, Sahiner, UM, Sackesen, C, Erzurum, S, & Kalayci, O 2012, 'Oxidative stress and antioxidant defense', *World Allergy Organization Journal*, vol. 5, no. 1, pp. 9–19.

Bjornevik, K, Cortese, M, Healy, BC, Kuhle, J, Mina, MJ, Leng, Y, Elledge, SJ, Niebuhr, DW, Scher, AI, Munger, KL, & Ascherio, A 2022, 'Longitudinal analysis reveals high prevalence of Epstein-Barr virus associated with multiple sclerosis', *Science*, vol. 375, no. 6578, pp. 296–301.

Blennow, K, Hardy, J, & Zetterberg, H 2012, 'The Neuropathology and Neurobiology of Traumatic Brain Injury', *Neuron*, vol. 76, no. 5, pp. 886–899.

Bö, L, Geurts, JJG, van der Valk, P, Polman, C, & Barkhof, F 2007, 'Lack of Correlation Between Cortical Demyelination and White Matter Pathologic Changes in Multiple Sclerosis', *Archives of Neurology*, vol. 64, no. 1, p. 76.

Bolton-Hall, AN, Hubbard, WB, & Saatman, KE 2019, 'Experimental Designs for Repeated Mild Traumatic Brain Injury: Challenges and Considerations', *Journal of Neurotrauma*, vol. 36, pp. 1203–1221.

Borges, K, Ohlemeyer, C, Trotter, J, & Kettenmann, H 1994, 'AMPA/kainate receptor activation in murine oligodendrocyte precursor cells leads to activation of a cation conductance, calcium influx and blockade of delayed rectifying K⁺ channels', *Neuroscience*, vol. 63, no. 1, pp. 135–149. Available from: <https://linkinghub.elsevier.com/retrieve/pii/0306452294900124>. [13 April 2017].

Borzelleca, JF, Depukat, K, & Hallagan, JB 1990, 'Lifetime toxicity/carcinogenicity studies of FD & C Blue No. 1 (brilliant blue FCF) in rats and mice.', *Food and Chemical Toxicology*, vol. 28, no. 4, pp. 221–34.

Bradl, M & Lassmann, H 2010, 'Oligodendrocytes: Biology and pathology', *Acta Neuropathologica*, vol. 119, no. 1, pp. 37–53.

Bramow, S, Frischer, JM, Lassmann, H, Koch-Henriksen, N, Lucchinetti, CF, Sørensen, PS, & Laursen, H 2010, 'Demyelination versus remyelination in progressive multiple sclerosis', *Brain*, vol. 133, no. 10, pp. 2983–2998.

Braugher, J, Duncan, L, & Chase, R 1986, 'The involvement of iron in lipid peroxidation', *Journal of Biological Chemistry*, vol. 261, pp. 10282–10289.

Brayne, CE, Dow, L, Calloway, SP, & Thompson, RJ 1982, 'Blood creatine kinase isoenzyme

BB in boxers.’, *Lancet (London, England)*, vol. 2, no. 8311, pp. 1308–9.

Breij, ECW, Brink, BP, Veerhuis, R, Van Den Berg, C, Vloet, R, Yan, R, Dijkstra, CD, Van Der Valk, P, & Bö, L 2008, ‘Homogeneity of active demyelinating lesions in established multiple sclerosis’, *Annals of Neurology*, vol. 63, no. 1, pp. 16–25.

Briggs, FBS, Goldstein, BA, McCauley, JL, Zuvich, RL, De Jager, PL, Rioux, JD, Iverson, AJ, Compston, A, Hafler, DA, Hauser, SL, Oksenberg, JR, Sawcer, SJ, Pericak-Vance, MA, Haines, JL, & Barcellos, LF 2010, ‘Variation Within DNA Repair Pathway Genes and Risk of Multiple Sclerosis’, *American Journal of Epidemiology*, vol. 172, no. 2, pp. 217–224.

Brosnan, CF & Raine, CS 2013, ‘The astrocyte in multiple sclerosis revisited’, *GLIA*, vol. 61, no. 4, pp. 453–465.

Brownlee, WJ, Hardy, TA, Fazekas, F, & Miller, DH 2017, ‘Diagnosis of multiple sclerosis: progress and challenges’, *The Lancet*, vol. 389, no. 10076, pp. 1336–1346.

Bruce, M, Streifel, KM, Boosalis, CA, Heuer, L, González, EA, Li, S, Harvey, DJ, Lein, PJ, & Van De Water, J 2019, ‘Acute peripheral immune activation alters cytokine expression and glial activation in the early postnatal rat brain’, *Journal of Neuroinflammation*, vol. 16, no. 1, pp. 1–15.

Bruns, J & Hauser, WA 2003, ‘The Epidemiology of Traumatic Brain Injury: A Review’, *Epilepsia*, vol. 44, pp. 2–10.

Buck, SB, Bradford, J, Gee, KR, Agnew, BJ, Clarke, ST, & Salic, A 2008, ‘Detection of S-phase cell cycle progression using 5-ethynyl-2'-deoxyuridine incorporation with click chemistry, an alternative to using 5-bromo-2'-deoxyuridine antibodies’, *BioTechniques*, vol. 44, no. 7, pp. 927–929.

Buschmann, JP, Berger, K, Awad, H, Clarner, T, Beyer, C, & Kipp, M 2012, ‘Inflammatory response and chemokine expression in the white matter corpus callosum and gray matter cortex region during cuprizone-induced demyelination’, *Journal of Molecular Neuroscience*, vol. 48, no. 1, pp. 66–76.

Butts, BD, Houde, C, & Mehmet, H 2008, ‘Maturation-dependent sensitivity of oligodendrocyte lineage cells to apoptosis: Implications for normal development and disease’, *Cell Death and Differentiation*, vol. 15, no. 7, pp. 1178–1186.

Cadet, J & Davies, KJA 2017, ‘Oxidative DNA Damage & Repair: An Introduction’, *Free radical biology & medicine*, vol. 107, p. 2.

Cady, N, Peterson, SR, Freedman, SN, & Mangalam, AK 2020, ‘Beyond Metabolism: The Complex Interplay Between Dietary Phytoestrogens, Gut Bacteria, and Cells of Nervous and Immune Systems’, *Frontiers in Neurology*, vol. 11, p. 150.

Cao, SS & Kaufman, RJ 2014, ‘Endoplasmic reticulum stress and oxidative stress in cell fate decision and human disease.’, *Antioxidants & redox signaling*, vol. 21, no. 3, pp. 396–413.

Cardoso, MC 2005, 'Fluorescence Microscopy: Spectral Imaging vs. Filter-based Imaging', *Encyclopedic Reference of Genomics and Proteomics in Molecular Medicine*, pp. 583–586.

Carlton, WW 1967, 'Studies on the induction of hydrocephalus and spongy degeneration by cuprizone feeding and attempts to antidote the toxicity', *Life Sciences*, vol. 6, pp. 11–19.

Carvalho, AN, Lim, JL, Nijland, PG, Witte, ME, & Van Horsen, J 2014, 'Glutathione in multiple sclerosis: More than just an antioxidant?', *Multiple Sclerosis Journal*, vol. 20, no. 11, pp. 1425–1431.

Cash, E, Zhang, Y, & Rott, O 1993, 'Microglia present myelin antigens to T cells after phagocytosis of oligodendrocytes', *Cellular Immunology*, vol. 147, pp. 129–138.

Cathomas, F, Azzinnari, D, Bergamini, G, Sigrist, H, Buerge, M, Hoop, V, Wicki, B, Goetze, L, Soares, S, Kukulova, D, Seifritz, E, Goebbels, S, Nave, KA, Ghandour, MS, Seoighe, C, Hildebrandt, T, Leparc, G, Klein, H, Stupka, E, Hengerer, B, & Pryce, CR 2019, 'Oligodendrocyte gene expression is reduced by and influences effects of chronic social stress in mice', *Genes, Brain and Behavior*, vol. 18, no. 1, p. e12475.

Cervetto, C, Frattaroli, D, Maura, G, & Marcoli, M 2013, 'Motor neuron dysfunction in a mouse model of ALS: Gender-dependent effect of P2X7 antagonism', *Toxicology*, vol. 311, pp. 69–77.

Chaban, V, Clarke, GJB, Skandsen, T, Islam, R, Einarsen, CE, Vik, A, Damå, JK, Mollnes, TE, Hå, AK, & Pischke, SE 2020, 'Systemic Inflammation Persists the First Year after Mild Traumatic Brain Injury: Results from the Prospective Trondheim Mild Traumatic Brain Injury Study', *Journal of Neurotrauma*, vol. 37, pp. 2120–2130.

Chang, A, Tourtellotte, WW, Rudick, R, & Trapp, BD 2002, 'Premyelinating Oligodendrocytes in Chronic Lesions of Multiple Sclerosis', *New England Journal of Medicine*, vol. 346, no. 3, pp. 165–173.

Chavali, M, Ulloa-Navas, MJ, Pérez-Borredá, P, Garcia-Verdugo, JM, McQuillen, PS, Huang, EJ, & Rowitch, DH 2020, 'Wnt-Dependent Oligodendroglial-Endothelial Interactions Regulate White Matter Vascularization and Attenuate Injury', *Neuron*, vol. 108, no. 6, pp. 1130–1145.e5.

Chen, C, Kassan, A, Castañeda, D, Gabani, M, Choi, S-K, & Kassan, M 2019, 'Metformin prevents vascular damage in hypertension through the AMPK/ER stress pathway HHS Public Access', *Hypertens Res*, vol. 42, no. 7, pp. 960–969.

Chen, Y, Wang, Y, Xu, J, Hou, T, Zhu, J, Jiang, Y, Sun, Liying, Huang, C, Sun, Lulu, & Liu, S 2022, 'Multiplex Assessment of Serum Chemokines CCL2, CCL5, CXCL1, CXCL10, and CXCL13 Following Traumatic Brain Injury', *Inflammation*, pp. 1–12.

Chrzanowski, U, Bhattarai, S, Scheld, M, Clarner, T, Fallier-Becker, P, Beyer, C, Rohr, SO,

Schmitz, C, Hochstrasser, T, Schweiger, F, Amor, S, Horn-Bochtler, A, Denecke, B, Nyamoya, S, & Kipp, M 2019, 'Oligodendrocyte degeneration and concomitant microglia activation directs peripheral immune cells into the forebrain', *Neurochemistry International*, vol. 126, pp. 139–153.

Chwastiak, LA & Ehde, DM 2007, 'Psychiatric issues in multiple sclerosis.', *The Psychiatric clinics of North America*, vol. 30, no. 4, pp. 803–17.

Cianfoni, A, Niku, S, & Imbesi, SG 2007, 'Metabolite Findings in Tumefactive Demyelinating Lesions Utilizing Short Echo Time Proton Magnetic Resonance Spectroscopy', *American Journal of Neuroradiology*, vol. 28, pp. 272–277.

Cipolla, MJ 2009, '*Anatomy and Ultrastructure*' *The Cerebral Circulation*. Morgan & Claypool Life Sciences.

Clarke, LE, Young, KM, Hamilton, NB, Li, H, Richardson, WD, & Attwell, D 2012, 'Properties and fate of oligodendrocyte progenitor cells in the corpus callosum, motor cortex, and piriform cortex of the mouse', *Journal of Neuroscience*, vol. 32, no. 24, pp. 8173–8185.

Clarner, T, Diederichs, F, Berger, K, Denecke, B, Gan, L, van der Valk, P, Beyer, C, Amor, S, & Kipp, M 2012, 'Myelin debris regulates inflammatory responses in an experimental demyelination animal model and multiple sclerosis lesions', *Glia*, vol. 60, no. 10, pp. 1468–1480.

Coelho-Santos, V & Shih, AY 2020, 'Postnatal development of cerebrovascular structure and the neurogliovascular unit', *Wiley Interdisciplinary Reviews: Developmental Biology*, vol. 9, no. 2, p. e363.

Coman, I, Aigrot, MS, Seilhean, D, Reynolds, R, Girault, JA, Zalc, B, & Lubetzki, C 2006, 'Nodal, paranodal and juxtapanodal axonal proteins during demyelination and remyelination in multiple sclerosis', *Brain*, vol. 129, no. 12, pp. 3186–3195.

Compston, A & Coles, A 2002, 'Multiple sclerosis', *The Lancet*, vol. 359, no. 9313, pp. 1221–1231.

Confavreux, C & Vukusic, S 2006, 'Age at disability milestones in multiple sclerosis', *Brain*, vol. 129, no. 3, pp. 595–605.

Coret, F, Pérez-Miralles, FC, Gascón, F, Alcalá, C, Navarré, A, Bernad, A, Boscá, I, Escutia, M, Gil-Perotin, S, & Casanova, B 2018, 'Onset of secondary progressive multiple sclerosis is not influenced by current relapsing multiple sclerosis therapies.', *Multiple sclerosis Journal*, vol. 4, no. 2.

Cornelius, C, Crupi, R, Calabrese, V, Graziano, A, Milone, P, Pennisi, G, Radak, Z, Calabrese, EJ, & Cuzzocrea, S 2013, 'Traumatic Brain Injury: Oxidative Stress and Neuroprotection', *Antioxidants & Redox Signaling*, vol. 19, no. 8, pp. 836–853. Available from: <http://www.liebertpub.com/doi/10.1089/ars.2012.4981>. [4 May 2018].

Corpas, FJ, Chaki, M, Letierrier, M, & Barroso, JB 2009, 'Protein tyrosine nitration: a new

challenge in plants.’, *Plant signaling & behavior*, vol. 4, no. 10, pp. 920–3.

Cortese, M, Riise, T, Bjørnevik, K, Bhan, A, Farbu, E, Grytten, N, Hogenesch, I, Midgard, R, Smith Simonsen, C, Telstad, W, Ascherio, A, & Myhr, KM 2016, ‘Preclinical disease activity in multiple sclerosis: A prospective study of cognitive performance prior to first symptom’, *Annals of Neurology*, vol. 80, no. 4, pp. 616–624.

Cosman, F, Nieves, J, Komar, L, Ferrer, G, Herbert, J, Formica, C, Shen, V, & Lindsay, R 1998, ‘Fracture history and bone loss in patients with MS’, *Neurology*, vol. 51, no. 4, pp. 1161–1165.

Cotton, F, Weiner, HL, Jolesz, FA, & Guttman, CRG 2003, ‘MRI contrast uptake in new lesions in relapsing-remitting MS followed at weekly intervals.’, *Neurology*, vol. 60, no. 4, pp. 640–6.

Cramer, SP, Simonsen, HJ, Varatharaj, A, Galea, I, Frederiksen, JL, & Larsson, HB 2018, ‘Permeability of the blood–brain barrier predicts no evidence of disease activity at 2 years after natalizumab or fingolimod treatment in relapsing–remitting multiple sclerosis’, *Annals of Neurology*, vol. 83, no. 5, pp. 902–914.

Croall, DE & Demartino, GN 1991, ‘Calcium-activated neutral protease (calpain) system: Structure, function, and regulation’, *Physiological Reviews*, vol. 71, no. 3, pp. 813–847.

Cummins, N, Bartlett, CA, Archer, M, Bartlett, E, Hemmi, JM, Harvey, AR, Dunlop, SA, & Fitzgerald, M 2013, ‘Changes to mitochondrial ultrastructure in optic nerve vulnerable to secondary degeneration in vivo are limited by irradiation at 670 nm’, *BMC Neuroscience*, vol. 14, no. 1, p. 98.

Dai, JX, Ma, Y Bin, Le, NY, Cao, J, & Wang, Y 2018, ‘Large animal models of traumatic brain injury’, *International Journal of Neuroscience*, vol. 128, no. 3, pp. 243–254.

Dal Canto, MC & Rabinowitz, SG 1982, ‘Experimental models of virus-induced demyelination of the central nervous system’, *Annals of Neurology*, vol. 11, no. 2, pp. 109–127.

Daneman, R & Prat, A 2015, ‘The blood–brain barrier’, *Cold Spring Harbor Perspectives in Biology*, vol. 7, no. 1.

Danesh-Seta, T, Emami, F, Nasr-Esfahani, MH, Ghaedi, K, & Aliomrani, M 2021, ‘Bee Venom–Derived BBB Shuttle and its Correlation with Oligodendrocyte Proliferation Markers in Mice Model of Multiple Sclerosis’, *Neurotoxicity Research*, vol. 1, p. 3.

Dash, A & Cudworth, G 1998, ‘Therapeutic applications of implantable drug delivery systems’, *Journal of Pharmacological and Toxicological Methods*, vol. 40, no. 1, pp. 1–12.

Dash, PK, Gorantla, S, Poluektova, L, Hasan, M, Waight, E, Zhang, C, Markovic, M, Edagwa, B, Machhi, J, Olson, KE, Wang, X, Mosley, RL, Kevadiya, B, & Gendelman, HE 2021, ‘Humanized Mice for Infectious and Neurodegenerative disorders’, *Retrovirology* 2021 18:1, vol. 18, no. 1, pp. 1–17.

David, SS, O’Shea, VL, & Kundu, S 2007, ‘Base-excision repair of oxidative DNA damage.’,

Nature, vol. 447, no. 7147, pp. 941–50.

Davies, MJ & Hawkins, CL 2020, ‘The Role of Myeloperoxidase in Biomolecule Modification, Chronic Inflammation, and Disease’, <https://home.liebertpub.com/ars>, vol. 32, no. 13, pp. 957–981.

Davis, CK & Vemuganti, R 2021, ‘DNA damage and repair following traumatic brain injury’, *Neurobiology of Disease*, vol. 147, p. 105143.

Davis, KL, Stewart, DG, Friedman, JI, Buchsbaum, M, Harvey, PD, Hof, PR, Buxbaum, J, & Haroutunian, V 2003, ‘White Matter Changes in Schizophrenia’, *Archives of General Psychiatry*, vol. 60, no. 5, p. 443.

Dawson, MRL, Polito, A, Levine, JM, & Reynolds, R 2003, ‘NG2-expressing glial progenitor cells: An abundant and widespread population of cycling cells in the adult rat CNS’, *Molecular and Cellular Neuroscience*, vol. 24, pp. 476–488.

Dawson, TM & Snyder, SH 1994, ‘Gases as biological messengers: nitric oxide and carbon monoxide in the brain.’, *Journal of Neuroscience*, vol. 14, no. 9, pp. 5147–59.

Debnath, M 2015, ‘Adaptive Immunity in Schizophrenia: Functional Implications of T Cells in the Etiology, Course and Treatment’, *Journal of Neuroimmune Pharmacology*, vol. 10, no. 4, pp. 610–619.

Deford, SM, Wilson, MS, Rice, AC, Clausen, T, Rice, LK, Barabnova, A, Bullock, R, & Hamm, RJ 2002, ‘Repeated mild brain injuries result in cognitive impairment in B6C3F1 mice’, *Journal of Neurotrauma*, vol. 19, no. 4, pp. 427–438.

Delacôte, F & Lopez, BS 2008, ‘Importance of the cell cycle phase for the choice of the appropriate DSB repair pathway, for genome stability maintenance: the trans-S double-strand break repair model’, *Cell Cycle*, vol. 7, no. 1, pp. 33–38.

Dendrou, CA, Fugger, L, & Friese, MA 2015, ‘Immunopathology of multiple sclerosis’, *Nature Reviews Immunology*, vol. 15, no. 9, pp. 545–558.

Derada Troletti, C, Fontijn, RD, Gowing, E, Charabati, M, van Het Hof, B, Didouh, I, van der Pol, SMA, Geerts, D, Prat, A, van Horssen, J, Kooij, G, & de Vries, HE 2019, ‘Inflammation-induced endothelial to mesenchymal transition promotes brain endothelial cell dysfunction and occurs during multiple sclerosis pathophysiology’, *Cell Death and Disease*, vol. 10, no. 2, pp. 1–13.

Dewar, D, Underhill, SM, & Goldberg, MP 2003, ‘Oligodendrocytes and ischemic brain injury’, *Journal of Cerebral Blood Flow & Metabolism*, vol. 23, pp. 263–274.

Diaz-Hernandez, JI, Gomez-Villafuertes, R, León-Otegui, M, Hontecillas-Prieto, L, Del Puerto, A, Trejo, JL, Lucas, JJ, Garrido, JJ, Gualix, J, Miras-Portugal, MT, & Diaz-Hernandez, M 2012, ‘In vivo P2X7 inhibition reduces amyloid plaques in Alzheimer’s disease through GSK3 β and secretases’, *Neurobiology of Aging*, vol. 33, no. 8, pp. 1816–1828.

DiBona, VL, Shah, MK, Krause, KJ, Zhu, W, Vogtlewede, MM, Smith, DM, Crockett, DP, & Zhang, H 2021, 'Metformin reduces neuroinflammation and improves cognitive functions after traumatic brain injury', *Neuroscience Research*, vol. 172, pp. 99–109.

Dimou, L, Simon, C, Kirchhoff, F, Takebayashi, H, & Götz, M 2008, 'Progeny of Olig2-expressing progenitors in the gray and white matter of the adult mouse cerebral cortex.', *The Journal of neuroscience : the official journal of the Society for Neuroscience*, vol. 28, no. 41, pp. 10434–42.

Djoba Siawaya, JF, Roberts, T, Babb, C, Black, G, Golakai, HJ, Stanley, K, Bapela, NB, Hoal, E, Parida, S, van Helden, P, & Walzl, G 2008, 'An Evaluation of Commercial Fluorescent Bead-Based Luminex Cytokine Assays', *PLOS ONE*, vol. 3, no. 7, p. e2535.

Doble, A 1999, 'The role of excitotoxicity in neurodegenerative disease: Implications for therapy', *Pharmacological Therapies*, vol. 81, no. 3, pp. 163–221.

Dohi, K, Ohtaki, H, Nakamachi, T, Yofu, S, Satoh, K, Miyamoto, K, Song, D, Tsunawaki, S, Shioda, S, & Aruga, T 2010, 'Gp91phox (NOX2) in classically activated microglia exacerbates traumatic brain injury', *Journal of Neuroinflammation*, vol. 7, no. 1, p. 41.

Doll, DN, Hu, H, Sun, J, Lewis, SE, Simpkins, JW, & Ren, X 2015, 'Mitochondrial Crisis in Cerebrovascular Endothelial Cells Opens the Blood-Brain Barrier', *Stroke; a journal of cerebral circulation*, vol. 46, no. 6, p. 1681.

Donaldson, H & Hoke, GW 1905, 'On the areas of the axis cylinder and medullary sheath as seen in cross sections of the spinal nerves of vertebrates', *The Journal of Comparative Neurology and Psychology*, vol. 15, no. 1, pp. 1–16.

Dong, X-X, Wang, Y, & Qin, Z-H 2009, 'Molecular mechanisms of excitotoxicity and their relevance to pathogenesis of neurodegenerative diseases', *Acta Pharmacol Sin Acta Pharmacologica Sinica*, vol. 30, no. 30, pp. 379–387.

Dore-Duffy, P, Ho, SY, Donovan, C, Fieschi, C, & Levi, G 1991, 'Cerebrospinal fluid eicosanoid levels: endogenous PGD2 and LTC4 synthesis by antigen-presenting cells that migrate to the central nervous system.', *Neurology*, vol. 41, no. 2, pp. 322–4.

Dore-Duffy, P, Katychhev, A, Wang, X, & Van Buren, E 2006, 'CNS microvascular pericytes exhibit multipotential stem cell activity', *Journal of Cerebral Blood Flow and Metabolism*, vol. 26, no. 5, pp. 613–624.

Dore-Duffy, P, Owen, C, Balabanov, R, Murphy, S, Beaumont, T, & Rafols, JA 2000, 'Pericyte migration from the vascular wall in response to traumatic brain injury', *Microvascular Research*, vol. 60, no. 1, pp. 55–69.

Drexhage, RC, Hoogenboezem, TA, Cohen, D, Versnel, MA, Nolen, WA, van Beveren, NJM, & Drexhage, HA 2011, 'An activated set point of T-cell and monocyte inflammatory networks in recent-onset schizophrenia patients involves both pro- and anti-inflammatory forces', *International*

Journal of Neuropsychopharmacology, vol. 14, no. 6, pp. 746–755.

Duan, S, Anderson, C, Keung, E, Chen, Y, Chen, Y, & Swansosn, R 2003, ‘P2X7 receptor-mediated release of excitatory amino acids from astrocytes’, *Journal of Neuroscience*, vol. 23, no. 4, pp. 1320–1328.

Duncan, ID, Marik, RL, Broman, AT, & Heidari, M 2017, ‘Thin myelin sheaths as the hallmark of remyelination persist over time and preserve axon function’, *Proceedings of the National Academy of Sciences*, pp. 1–7.

Duncan, ID, Radcliff, AB, Heidari, M, Kidd, G, August, BK, & Wierenga, LA 2018, ‘The adult oligodendrocyte can participate in remyelination’, *Proceedings of the National Academy of Sciences of the United States of America*, vol. 115, no. 50, pp. E11807–E11816.

DuPont, NC, Wang, K, Wadhwa, PD, Culhane, JF, & Nelson, EL 2005, ‘Validation and comparison of luminex multiplex cytokine analysis kits with ELISA: Determinations of a panel of nine cytokines in clinical sample culture supernatants’, *Journal of Reproductive Immunology*, vol. 66, no. 2, pp. 175–191.

Dutta, R, Mcdonough, J, Yin, X, Peterson, J, Chang, A, Torres, T, Gudz, T, Macklin, WB, Lewis, DA, Fox, RJ, Rudick, R, Mirnics, K, & Trapp, BD 2006, ‘Mitochondrial Dysfunction as a Cause of Axonal Degeneration in Multiple Sclerosis Patients’, *Ann Neurol*, vol. 59, pp. 478–489.

Dutta, S & Sengupta, P 2016, ‘Men and mice: Relating their ages’, *Life Sciences*, vol. 152, pp. 244–248.

Edgar, N & Sibille, E 2012, ‘A putative functional role for oligodendrocytes in mood regulation’, *Translational Psychiatry*, vol. 2, no. 5, pp. e109–e109.

Edwards, LJ & Constantinescu, CS 2004, ‘A prospective study of conditions associated with multiple sclerosis in a cohort of 658 consecutive outpatients attending a multiple sclerosis clinic’, *Multiple Sclerosis Journal*, vol. 10, no. 5, pp. 575–581.

Egawa, N, Lok, J, & Arai, K 2016, ‘Mechanisms of cellular plasticity in cerebral perivascular region’, *Progress in Brain Research*, vol. 225, pp. 183–200.

Enders, M, Heider, T, Ludwig, A, & Kuerten, S 2020, ‘Strategies for neuroprotection in multiple sclerosis and the role of calcium’, *International Journal of Molecular Sciences*, vol. 21, no. 5.

Ercole, A, Thelin, EP, Holst, A, Bellander, BM, & Nelson, DW 2016, ‘Kinetic modelling of serum S100b after traumatic brain injury’, *BMC Neurology*, vol. 16, no. 1, pp. 1–8.

Eriksson, M, Andersen, O, & Runmarker, B 2003, ‘Long-term follow up of patients with clinically isolated syndromes, relapsing-remitting and secondary progressive multiple sclerosis’, *Multiple Sclerosis Journal*, vol. 9, no. 3, pp. 260–274.

Faizi, M, Salimi, A, Seydi, E, Naserzadeh, P, Kouhnavard, M, Rahimi, A, & Pourahmad, J

2016, 'Toxicity of cuprizone a Cu²⁺ chelating agent on isolated mouse brain mitochondria: a justification for demyelination and subsequent behavioral dysfunction', *Toxicology Mechanisms and Methods*, vol. 26, no. 4, pp. 276–283.

Falcão, AM, van Bruggen, D, Marques, S, Meijer, M, Jäkel, S, Agirre, E, Samudyata, Floriddia, EM, Vanichkina, DP, French-Constant, C, Williams, A, Guerreiro-Cacais, AO, & Castelo-Branco, G 2018, 'Disease-specific oligodendrocyte lineage cells arise in multiple sclerosis', *Nature Medicine*, vol. 24, no. 12, pp. 1837–1844.

Farooqui, AA 2010, *Neurochemical aspects of neurotraumatic and neurodegenerative diseases*. Springer, New York.

Farooqui, AA, Ong, W-Y, & Horrocks, LA 2008, *Neurochemical Aspects of Excitotoxicity*. Springer, New York.

FDA 2019, *Drug Approval Package: TISSUEBLUE, USA Food and Drug Administration (FDA)*.

Fehily, B, Bartlett, CA, Lydiard, S, Archer, M, Milbourn, H, Majimbi, M, Hemmi, JM, Dunlop, SA, Yates, NJ, & Fitzgerald, M 2019, 'Differential responses to increasing numbers of mild traumatic brain injury in a rodent closed-head injury model', *Journal of Neurochemistry*, vol. 149, pp. 660–678.

Fernandez-Castaneda, A & Gaultier, A 2016, 'Adult oligodendrocyte progenitor cells - Multifaceted regulators of the CNS in health and disease.', *Brain, behavior, and immunity*, vol. 57, pp. 1–7.

Filippi, M, Campi, A, Martinelli, V, Colombo, B, Yousry, T, Canal, N, Scotti, G, & Comi, G 1995, 'Comparison of triple dose versus standard dose gadolinium-DTPA for detection of MRI enhancing lesions in patients with primary progressive multiple sclerosis', *Journal of Neurology, Neurosurgery and Psychiatry*, vol. 59, no. 5, pp. 540–544.

Filippi, M, Rocca, MA, Ciccarelli, O, De Stefano, N, Evangelou, N, Kappos, L, Rovira, A, Sastre-Garriga, J, Tintorè, M, Frederiksen, JL, Gasperini, C, Palace, J, Reich, DS, Banwell, B, Montalban, X, & Barkhof, F 2016, 'MRI criteria for the diagnosis of multiple sclerosis: MAGNIMS consensus guidelines', *The Lancet Neurology*, vol. 15, no. 3, pp. 292–303.

Filippi, M, Rocca, MA, Martino, G, Horsfield, MA, & Comi, G 1998, 'Magnetization Transfer Changes in the Normal Appearing White Matter Precede the Appearance of Enhancing Lesions in Patients with Multiple Sclerosis', *Annals of Neurology*, vol. 43, pp. 809–814.

Fineman, I, Hovda, DA, Smith, M, Yoshino, A, & Becker, DP 1993, 'Concussive brain injury is associated with a prolonged accumulation of calcium: a⁴⁵Ca autoradiographic study', *Brain Research*, vol. 624, no. 1–2, pp. 94–102.

Finnie, JW 2001, 'Animal models of traumatic brain injury: a review', *Australian Veterinary*

Journal, vol. 79, no. 9, pp. 628–633.

Fiorini, A, Koudriavtseva, T, Bucaj, E, Coccia, R, Foppoli, C, Giorgi, A, Schininà, ME, Di Domenico, F, De Marco, F, & Perluigi, M 2013, 'Involvement of Oxidative Stress in Occurrence of Relapses in Multiple Sclerosis: The Spectrum of Oxidatively Modified Serum Proteins Detected by Proteomics and Redox Proteomics Analysis', *PLoS ONE*, vol. 8, no. 6, p. e65184.

Fischbach, F, Nedelcu, J, Leopold, P, Zhan, J, Clarner, T, Nellessen, L, Beißel, C, van Heuvel, Y, Goswami, A, Weis, J, Denecke, B, Schmitz, C, Hochstrasser, T, Nyamoya, S, Victor, M, Beyer, C, & Kipp, M 2019, 'Cuprizone-induced graded oligodendrocyte vulnerability is regulated by the transcription factor DNA damage-inducible transcript 3', *Glia*, vol. 67, no. 2, pp. 263–276.

Fischer, MT, Sharma, R, Lim, JL, Haider, L, Frischer, JM, Drexhage, J, Mahad, D, Bradl, M, van Horssen, J, & Lassmann, H 2012, 'NADPH oxidase expression in active multiple sclerosis lesions in relation to oxidative tissue damage and mitochondrial injury', *Brain*, vol. 135, no. 3, pp. 886–899.

Fitzgerald, M, Bartlett, CA, Evill, L, Rodger, J, Harvey, AR, & Dunlop, SA 2009, 'Secondary degeneration of the optic nerve following partial transection: The benefits of lomerizine', *Experimental Neurology*, vol. 216, pp. 219–230.

Fitzgerald, M, Bartlett, CA, Harvey, AR, & Dunlop, SA 2010, 'Early events of secondary degeneration after partial optic nerve transection: An immunohistochemical study', *Journal of Neurotrauma*, vol. 27, pp. 439–452.

Fitzgerald, M, Bartlett, CA, Payne, SC, Hart, NS, Rodger, J, Harvey, AR, & Dunlop, SA 2010, 'Near Infrared Light Reduces Oxidative Stress and Preserves function in CNS Tissue Vulnerable to Secondary Degeneration following Partial Transection of the Optic Nerve', *Journal of Neurotrauma*, vol. 27, pp. 2107–2119.

Flynn, SW, Lang, DJ, Mackay, AL, Goghari, V, Vavasour, IM, Whittall, KP, Smith, GN, Arango, V, Mann, JJ, Dwork, AJ, Falkai, P, & Honer, WG 2003, 'Abnormalities of myelination in schizophrenia detected in vivo with MRI, and post-mortem with analysis of oligodendrocyte proteins', *Molecular Psychiatry*, vol. 8, pp. 811–820.

Fortini, P, Parlanti, E, Sidorkina, OM, Laval, J, & Dogliotti, E 1999, 'The type of DNA glycosylase determines the base excision repair pathway in mammalian cells.', *Journal of Biological Chemistry*, vol. 274, no. 21, pp. 15230–6.

Fowler, J, McCracken, E, Dewar, D, & McCulloch, J 2003, 'Intracerebral injection of AMPA causes axonal damage in vivo', *Brain Research*, vol. 991, no. 1–2, pp. 104–112.

Franco-Pons, N, Torrente, M, Colomina, MT, & Vilella, E 2007, 'Behavioral deficits in the cuprizone-induced murine model of demyelination/remyelination', *Toxicology Letters*, vol. 169, no. 3, pp. 205–213.

Franke, M, Bieber, M, Stoll, G, & Schuhmann, MK 2021, 'Validity and Efficacy of Methods

to Define Blood Brain Barrier Integrity in Experimental Ischemic Strokes: A Comparison of Albumin Western Blot, IgG Western Blot and Albumin Immunofluorescence’, *Methods and Protocols*, vol. 4, no. 1.

Frantseva, M, Perez Velazquez, JL, Tonkikh, A, Adamchik, Y, & Carlen, PL 2002, ‘Neurotrauma/neurodegeneration and mitochondrial dysfunction’, *Progress in Brain Research*, vol. 137, pp. 171–176.

Freeman, LR & Keller, JN 2012, ‘Oxidative stress and cerebral endothelial cells: Regulation of the blood–brain-barrier and antioxidant based interventions’, *Biochimica et Biophysica Acta*, vol. 1822, no. 5, pp. 822–829.

Friese, MA & Fugger, L 2007, ‘T cells and microglia as drivers of multiple sclerosis pathology’, *Brain*, vol. 130, no. 11, pp. 2755–2757.

Friese, MA, Montalban, X, Willcox, N, Bell, JI, Martin, R, & Fugger, L 2006, ‘The value of animal models for drug development in multiple sclerosis’, *Brain*, vol. 129, no. 8, pp. 1940–1952.

Frischer, JM, Bramow, S, Dal-Bianco, A, Lucchinetti, CF, Rauschka, H, Schmidbauer, M, Laursen, H, Sorensen, PS, & Lassmann, H 2009, ‘The relation between inflammation and neurodegeneration in multiple sclerosis brains’, *Brain*, vol. 132, no. 5, pp. 1175–1189.

Frühbeis, C, Fröhlich, D, Kuo, WP, & Krämer-Albers, E-M 2013, ‘Extracellular vesicles as mediators of neuron-glia communication’, *Frontiers in Cellular Neuroscience*, vol. 7, p. 182.

Fu, Y, Sun, W, Shi, Y, Shi, R, & Cheng, JX 2009, ‘Glutamate excitotoxicity inflicts paranodal myelin splitting and retraction’, *PLoS ONE*, vol. 4, no. 8.

Fu, Y, Wang, H, Huff, TB, Shi, R, & Cheng, J-X 2007, ‘Coherent anti-Stokes Raman scattering imaging of myelin degradation reveals a calcium-dependent pathway in lyso-PtdCho-induced demyelination.’, *Journal of Neuroscience Research*, vol. 85, no. 13, pp. 2870–81.

Fujimura, M, Morita-Fujimura, Y, Noshita, N, Yoshimoto, T, & Chan, PH 2000, ‘Reduction of the DNA base excision repair protein, XRCC1, may contribute to DNA fragmentation after cold injury-induced brain trauma in mice’, *Brain Research*, vol. 869, no. 1–2, pp. 105–111.

Furukawa, T, Hoshino, S, Kobayashi, S, Asakura, T, Takahashi, M, Atsumi, T, & Teramoto, A 2003, ‘The glutamate AMPA receptor antagonist, YM872, attenuates cortical tissue loss, regional cerebral edema, and neurological motor deficits after experimental brain injury in rats’, *Journal of Neurotrauma*, vol. 20, no. 3, pp. 269–278.

Gacem, N & Nait-Oumesmar, B 2021, ‘Oligodendrocyte development and regenerative therapeutics in multiple sclerosis’, *Life*, vol. 11, no. 4, p. 327.

Gharagozloo, M, Mace, JW, & Calabresi, PA 2022, ‘Animal models to investigate the effects of inflammation on remyelination in multiple sclerosis’, *Frontiers in Molecular Neuroscience*, vol. 15, p. 571.

Ghasemi, N, Razavi, S, & Nikzad, E 2017, 'Multiple Sclerosis: Pathogenesis, Symptoms, Diagnoses and Cell-Based Therapy', *Cell Journal*, vol. 19, no. 1, p. 1.

Giacci, Marcus K., Bartlett, CA, Huynh, M, Kilburn, MR, Dunlop, SA, & Fitzgerald, M 2018, 'Three dimensional electron microscopy reveals changing axonal and myelin morphology along normal and partially injured optic nerves', *Scientific Reports*, vol. 8, no. 1, p. 3979.

Giacci, Marcus K, Bartlett, CA, Smith, NM, Iyer, KS, Toomey, LM, Jiang, H, Guagliardo, P, Kilburn, MR, & Fitzgerald, M 2018, 'Oligodendroglia Are Particularly Vulnerable to Oxidative Damage after Neurotrauma In Vivo', *The Journal of Neuroscience*, vol. 38, no. 29, pp. 6491–6504. Available from: <https://www.jneurosci.org/lookup/doi/10.1523/JNEUROSCI.1898-17.2018>.

Giavedoni, LD 2005, 'Simultaneous detection of multiple cytokines and chemokines from nonhuman primates using luminex technology', *Journal of Immunological Methods*, vol. 301, no. 1–2, pp. 89–101.

Gibson, EM, Purger, D, Mount, CW, Goldstein, AK, Lin, GL, Wood, LS, Inema, I, Miller, SE, Bieri, G, Zuchero, JB, Barres, BA, Woo, PJ, Vogel, H, & Monje, M 2014, 'Neuronal Activity Promotes Oligodendrogenesis and Adaptive Myelination in the Mammalian Brain NIH Public Access', *Science*, vol. 344, no. 6183, p. 1252304.

Gilden, DH 2005, 'Infectious causes of multiple sclerosis', *The Lancet Neurology*, vol. 4, no. 3, pp. 195–202.

Gilgun-Sherki, Y, Melamed, E, & Offen, D 2004, 'The role of oxidative stress in the pathogenesis of multiple sclerosis: The need for effective antioxidant therapy', *Journal of Neurology*, vol. 251, pp. 261–268.

Gingele, S, Henkel, F, Heckers, S, Moellenkamp, TM, Hümmert, MW, Skripuletz, T, Stangel, M, & Gudi, V 2020, 'Delayed Demyelination and Impaired Remyelination in Aged Mice in the Cuprizone Model', *Cells*, vol. 9, no. 4.

Giorgi, C, Baldassari, F, Bononi, A, Bonora, M, De Marchi, E, Marchi, S, Missiroli, S, Patergnani, S, Rimessi, A, Suski, JM, Wieckowski, MR, & Pinton, P 2012, 'Mitochondrial Ca(2+) and apoptosis.', *Cell Calcium*, vol. 52, no. 1, pp. 36–43.

Giovannoni, G, Cutter, GR, Lunemann, J, Martin, R, Münz, C, Sriram, S, Steiner, I, Hammerschlag, MR, & Gaydos, CA 2006, 'Infectious causes of multiple sclerosis', *The Lancet Neurology*, vol. 5, no. 10, pp. 887–894.

Girolamo, F, Errede, M, Longo, G, Annese, T, Alias, C, Ferrara, G, Morando, S, Trojano, M, De Rosbo, NK, Uccelli, A, & Virgintino, D 2019, 'Defining the role of NG2-expressing cells in experimental models of multiple sclerosis. A biofunctional analysis of the neurovascular unit in wild type and NG2 null mice', *PLoS ONE*, vol. 14, no. 3.

Gold, R 2008, 'Combination therapies in multiple sclerosis', *Journal of Neurology*, vol. 255,

no. S1, pp. 51–60.

Goldenberg, MM 2012, ‘Multiple sclerosis review.’, *Pharmacy and Therapeutics*, vol. 37, no. 3, pp. 175–84.

Goldschmidt, T, Antel, J, König, FB, Brück, W, & Kuhlmann, T 2009, ‘Remyelination capacity of the MS brain decreases with disease chronicity’, *Neurology*, vol. 72, no. 22, pp. 1914–1921.

Gonsalvez, DG, Yoo, S, Fletcher, JL, Wood, RJ, Craig, GA, Murray, SS, & Xiao, J 2019, ‘Imaging and Quantification of Myelin Integrity After Injury With Spectral Confocal Reflectance Microscopy’, *Frontiers in Molecular Neuroscience*, vol. 12, p. 275.

Gonsette, R 2008, ‘Oxidative stress and excitotoxicity: a therapeutic issue in multiple sclerosis?’, *Multiple Sclerosis*, vol. 14, pp. 22–34.

Goodin, DS 2014, ‘The epidemiology of multiple sclerosis: insights to disease pathogenesis’, *Handbook of Clinical Neurology*, vol. 122, pp. 231–266.

Gopalasingam, G, Bartlett, CA, McGonigle, T, Majimbi, M, Warnock, A, Ford, A, Gough, A, Toomey, LM, & Fitzgerald, M 2019, ‘The effects of a combination of ion channel inhibitors on pathology in a model of demyelinating disease’, *Multiple Sclerosis and Related Disorders*.

Gordon, GRJ, Howarth, C, & MacVicar, BA 2011, ‘Bidirectional control of arteriole diameter by astrocytes’, *Experimental Physiology*, vol. 96, no. 4, pp. 393–399.

Grammas, P, Martinez, J, & Miller, B 2011, ‘Cerebral microvascular endothelium and the pathogenesis of neurodegenerative diseases’, *Expert Reviews in Molecular Medicine*, vol. 13, p. e19. Available from: https://www.cambridge.org/core/product/identifier/S1462399411001918/type/journal_article. [31 October 2018].

Gray, E, Thomas, TL, Betmouni, S, Scolding, N, & Love, S 2008, ‘Elevated myeloperoxidase activity in white matter in multiple sclerosis’, *Neuroscience Letters*, vol. 444, no. 2, pp. 195–198.

Griffiths, I, Klugmann, M, Anderson, T, Yool, D, Thomson, C, Schwab, MH, Schneider, A, Zimmermann, F, McCulloch, M, Nadon, N, & Nave, K-A 1998, ‘Axonal swellings and degeneration in mice lacking the major proteolipid of myelin’, *Science*, vol. 280, pp. 1610–1613.

Groebe, A, Clarner, T, Baumgartner, W, Dang, J, Beyer, C, & Kipp, M 2009, ‘Cuprizone treatment induces distinct demyelination, astrocytosis, and microglia cell invasion or proliferation in the mouse cerebellum’, *Cerebellum*, vol. 8, no. 3, pp. 163–174.

Guan, J-Z, Guan, W-P, & Maeda, T 2018, ‘Vitamin E administration erases an enhanced oxidation in multiple sclerosis’, *Canadian Journal of Physiology and Pharmacology*, vol. 96, no. 11, pp. 1181–1183.

Gudi, V, Gingele, S, Skripuletz, T, & Stangel, M 2014, ‘Glial response during cuprizone-

induced de- and remyelination in the CNS: lessons learned', *Frontiers in Cellular Neuroscience*, vol. 8, p. 73.

Gudi, V, Moharreggh-Khiabani, D, Skripuletz, T, Koutsoudaki, PN, Kotsiari, A, Skuljec, J, Trebst, C, & Stangel, M 2009, 'Regional differences between grey and white matter in cuprizone induced demyelination', *Brain Research*, vol. 1283, pp. 127–138.

Gudi, V, Škuljec, J, Yildiz, Ö, Frichert, K, Skripuletz, T, Moharreggh-Khiabani, D, Voss, E, Wissel, K, Wolter, S, & Stangel, M 2011, 'Spatial and temporal profiles of growth factor expression during CNS demyelination reveal the dynamics of repair priming.', *PloS one*, vol. 6, no. 7, p. e22623.

Guerriero, RM, Giza, CC, & Rotenberg, A 2015, 'Glutamate and GABA imbalance following traumatic brain injury', *Current Neurology and Neuroscience Reports*, vol. 15, no. 5, pp. 27–47.

Guo, F, Maeda, Y, Ma, J, Xu, J, Horiuchi, M, Miers, L, Vaccarino, F, & Pleasure, D 2010, 'Pyramidal neurons are generated from oligodendroglial progenitor cells in adult piriform cortex', *Journal of Neuroscience*, vol. 30, no. 36, pp. 12036–12049.

Guttmann, CRG, Rousset, M, Roch, JA, Hannoun, S, Durand-Dubief, F, Belaroussi, B, Cavallari, M, Rabilloud, M, Sappey-Marinier, D, Vukusic, S, & Cotton, F 2016, 'Multiple sclerosis lesion formation and early evolution revisited: A weekly high-resolution magnetic resonance imaging study', *Multiple Sclerosis Journal*, vol. 22, no. 6, pp. 761–769.

Habgood, MD, Bye, N, Dziegielewska, KM, Ek, CJ, Lane, MA, Potter, A, Morganti-Kossmann, C, & Saunders, NR 2007, 'Changes in blood-brain barrier permeability to large and small molecules following traumatic brain injury in mice', *European Journal of Neuroscience*, vol. 25, no. 1, pp. 231–238.

Hackam, DG & Redelmeier, DA 2006, 'Translation of Research Evidence From Animals to Humans', *JAMA*, vol. 296, no. 14, pp. 1727–1732.

Hackett, AR & Lee, JK 2016, 'Understanding the NG2 Glial Scar after Spinal Cord Injury.', *Frontiers in Neurology*, vol. 7, p. 199.

Hagemeyer, N, Boretius, S, Ott, C, Von Streitberg, A, Welpinghus, H, Sperling, S, Frahm, J, Simons, M, Ghezzi, P, & Ehrenreich, H 2012, 'Erythropoietin attenuates neurological and histological consequences of toxic demyelination in mice', *Molecular Medicine*, vol. 18, no. 4, pp. 628–635.

Haider, L, Fischer, MT, Frischer, JM, Bauer, J, Hö, R, Botond, G, Esterbauer, H, Binder, CJ, Witztum, JL, & Lassmann, H 2011, 'Oxidative damage in Multiple Sclerosis lesions', *Brain*, vol. 134, pp. 1914–1924.

Halicka, HD, Zhao, H, Li, J, Traganos, F, Zhang, S, Lee, M, & Darzynkiewicz, Z 2011, 'Genome protective effect of metformin as revealed by reduced level of constitutive DNA damage signaling.', *Aging*, vol. 3, no. 10, pp. 1028–38.

Hall, CN, Reynell, C, Gesslein, B, Hamilton, NB, Mishra, A, Sutherland, BA, Oâ Farrell, FM, Buchan, AM, Lauritzen, M, & Attwell, D 2014, 'Capillary pericytes regulate cerebral blood flow in health and disease', *Nature*, vol. 508, no. 1, pp. 55–60.

Hall, ED, Wang, JA, Miller, DM, Cebak, JE, & Hill, RL 2019, 'Newer pharmacological approaches for antioxidant neuroprotection in traumatic brain injury', *Neuropharmacology*, vol. 145, pp. 247–258.

Halliwell, B & Gutteridge, J 1989, *Free Radicals in Biology and Medicine*. Clarendon Press, Oxford.

Hametner, S, Wimmer, I, Haider, L, Pfeifenbring, S, Bruck, W, & Lassmann, H 2013, 'Iron and Neurodegeneration in the Multiple Sclerosis Brain', *Annals of Neurology*, vol. 74, no. 6, pp. 848–861.

Hammond, SR, McLeod, JG, Millingen, KS, Stewart-Wynne, EG, English, D, Holland, JT, & McCall, MG 1988, 'The epidemiology of multiple sclerosis in three Australian cities: Perth, Newcastle and Hobart.', *Brain*, vol. 111, no. 1, pp. 1–25.

Hara, H, Shimazawa, M, Sasaoka, M, Yamada, C, Iwakura, Y, Sakai, T, Maeda, Y, Yamaguchi, T, Sukamoto, T, & Hashimoto, M 1999, 'Selective effects of lomerizine, a novel diphenylmethylpiperazine Ca²⁺ channel blocker, on cerebral blood flow in rats and dogs', *Clinical and Experimental Pharmacology and Physiology*, vol. 26, no. 11, pp. 870–876.

Hauser, SL, Bhan, AK, Gilles, F, Kemp, M, Kerr, C, & Weiner, HL 1986, 'Immunohistochemical analysis of the cellular infiltrate in multiple sclerosis lesions', *Annals of Neurology*, vol. 19, no. 6, pp. 578–587.

Hauser, SL & Oksenberg, JR 2006, 'The Neurobiology of Multiple Sclerosis: Genes, Inflammation, and Neurodegeneration', *Neuron*, vol. 52, no. 1, pp. 61–76.

Hay, JR, Johnson, VE, Young, AMH, Smith, DH, & Stewart, W 2015, 'Blood-Brain Barrier Disruption Is an Early Event That May Persist for Many Years After Traumatic Brain Injury in Humans', *Journal of Neuropathology & Experimental Neurology*, vol. 74, no. 12, pp. 1147–1157.

He, P, Talukder, MAH, & Gao, F 2020, 'Oxidative Stress and Microvessel Barrier Dysfunction', *Frontiers in Physiology*, vol. 11, p. 472.

Heckers, S, Held, N, Kronenberg, J, Skripuletz, T, Bleich, A, Gudi, V, & Stangel, M 2017, 'Investigation of Cuprizone Inactivation by Temperature', *Neurotoxicity research*, vol. 31, no. 4, pp. 570–577.

Hedström, A, Olsson, T, & Alfredsson, L 2016, 'Body mass index during adolescence, rather than childhood, is critical in determining MS risk', *Multiple Sclerosis Journal*, vol. 22, no. 7, pp. 878–883.

Hemmer, B, Kerschensteiner, M, & Korn, T 2015, 'Role of the innate and adaptive immune

responses in the course of multiple sclerosis', *The Lancet Neurology*, vol. 14, no. 4, pp. 406–419.

Herder, V, Hansmann, F, Stangel, M, Skripuletz, T, Baumgärtner, W, & Beineke, A 2011, 'Lack of cuprizone-induced demyelination in the murine spinal cord despite oligodendroglial alterations substantiates the concept of site-specific susceptibilities of the central nervous system', *Neuropathology and Applied Neurobiology*, vol. 37, no. 6, pp. 676–684.

Herring, NR & Konradi, C 2011, 'Myelin, copper, and the cuprizone model of schizophrenia.', *Frontiers in Bioscience*, vol. 3, pp. 23–40.

Heß, K, Starost, L, Kieran, NW, Thomas, C, Vincenten, MCJ, Antel, J, Martino, G, Huitinga, I, Healy, L, & Kuhlmann, T 2020, 'Lesion stage-dependent causes for impaired remyelination in MS', *Acta Neuropathologica*, vol. 140, no. 3, pp. 359–375.

Hestvik, A, Skorstad, G, Price, D, Vartdal, F, & Holmoy, T 2008, 'Multiple sclerosis: glatiramer acetate induces anti-inflammatory T cells in the cerebrospinal fluid', *Multiple Sclerosis Journal*, vol. 14, no. 6, pp. 749–758.

Hier, DB, Obafemi-Ajayi, T, Thimgan, MS, Olbricht, GR, Azizi, S, Allen, B, Hadi, BA, & Wunsch, DC 2021, 'Blood biomarkers for mild traumatic brain injury: a selective review of unresolved issues', *Biomarker Research 2021 9:1*, vol. 9, no. 1, pp. 1–17.

Hildebrand, C, Remahl, S, Persson, H, & Bjartmar, C 1993, 'Myelinated nerve fibres in the CNS', *Progress in Neurobiology*, vol. 40, no. 3, pp. 319–384.

Hinzman, JM, Thomas, TC, Burmeister, JJ, Quintero, JE, Huettl, P, Pomerleau, F, Gerhardt, GA, & Lifshitz, J 2010, 'Diffuse brain injury elevates tonic glutamate levels and potassium-evoked glutamate release in discrete brain regions at two days post-injury: an enzyme-based microelectrode array study.', *Journal of neurotrauma*, vol. 27, no. 5, pp. 889–99.

Hiremath, MM, Saito, Y, Knapp, GW, Ting, JPY, Suzuki, K, & Matsushima, GK 1998, 'Microglial/macrophage accumulation during cuprizone-induced demyelination in C57BL/6 mice', *Journal of Neuroimmunology*, vol. 92, no. 1–2, pp. 38–49.

Hochmeister, S, Grundtner, R, Bauer, J, Engelhardt, B, Lyck, R, Gordon, G, Korosec, T, Kutzelnigg, A, Berger, JJ, Bradl, M, Bittner, RE, & Lassmann, H 2006, 'Dysferlin Is a New Marker for Leaky Brain Blood Vessels in Multiple Sclerosis', *Journal of Neuropathology and Experimental Neurology*, vol. 65, no. 9, pp. 855–865.

Hochstrasser, T, Exner, GL, Nyamoya, S, Schmitz, C, & Kipp, M 2017, 'Cuprizone-Containing Pellets Are Less Potent to Induce Consistent Demyelination in the Corpus Callosum of C57BL/6 Mice', *Journal of Molecular Neuroscience*, vol. 61, no. 4, pp. 617–624.

Höflich, KM, Beyer, C, Clarner, T, Schmitz, C, Nyamoya, S, Kipp, M, & Hochstrasser, T 2016, 'Acute axonal damage in three different murine models of multiple sclerosis: A comparative approach', *Brain Research*, vol. 1650, pp. 125–133.

Höftberger, R & Lassmann, H 2018, 'Inflammatory demyelinating diseases of the central nervous system', in *Handbook of Clinical Neurology*, pp.263–283. Elsevier B.V.

Holick, MF 2004, 'Sunlight and vitamin D for bone health and prevention of autoimmune diseases, cancers, and cardiovascular disease', *The American Journal of Clinical Nutrition*, vol. 80, no. 6, pp. 1678S-1688S.

Hollenbach, JA & Oksenberg, JR 2015, 'The immunogenetics of multiple sclerosis: A comprehensive review.', *Journal of Autoimmunity*, vol. 64, pp. 13–25.

Hong, Z, Xinding, Z, Tianlin, Z, & Liren, C 2001, 'Excitatory Amino Acids in Cerebrospinal Fluid of Patients with Acute Head Injuries', *Clinical Chemistry*, vol. 47, no. 8, pp. 1458–1462.

van Horssen, J, Brink, BP, de Vries, HE, van der Valk, P, & Bø, L 2007, 'The Blood-Brain Barrier in Cortical Multiple Sclerosis Lesions', *Journal of Neuropathology & Experimental Neurology*, vol. 66, no. 4, pp. 321–328.

van Horssen, J, Drexhage, JAR, Flor, T, Gerritsen, W, van der Valk, P, & de Vries, HE 2010, 'Nrf2 and DJ1 are consistently upregulated in inflammatory multiple sclerosis lesions', *Free Radical Biology and Medicine*, vol. 49, no. 8, pp. 1283–1289.

Hubbard, WB, Joseph, B, Spry, M, Vekaria, HJ, Saatman, KE, & Sullivan, PG 2019, 'Acute Mitochondrial Impairment Underlies Prolonged Cellular Dysfunction after Repeated Mild Traumatic Brain Injuries', *Journal of Neurotrauma*, vol. 36, no. 8, pp. 1252–1263.

Huff, TB, Shi, Y, Sun, W, Wu, W, Shi, R, & Cheng, JX 2011, 'Real-Time CARS Imaging Reveals a Calpain-Dependent Pathway for Paranodal Myelin Retraction during High-Frequency Stimulation', *PLOS ONE*, vol. 6, no. 3, p. e17176.

Husain, J & Juurlink, BH 1995, 'Oligodendroglial precursor cell susceptibility to hypoxia is related to poor ability to cope with reactive oxygen species', *Brain Research*, vol. 698, pp. 86–94.

Iacobaeus, E, Sugars, R V., Törnqvist Andrén, A, Alm, JJ, Qian, H, Frantzen, J, Newcombe, J, Alkass, K, Druid, H, Bottai, M, Röyttä, M, & Le Blanc, K 2017, 'Dynamic Changes in Brain Mesenchymal Perivascular Cells Associate with Multiple Sclerosis Disease Duration, Active Inflammation, and Demyelination', *STEM CELLS Translational Medicine*, vol. 6, no. 10, pp. 1840–1851.

Iadecola, C & Nedergaard, M 2007, 'Glial regulation of the cerebral microvasculature', *Nature Neuroscience*, vol. 10, no. 11, pp. 1369–1376.

Imai, N, Konishi, T, Serizawa, M, & Okabe, T 2007, 'Do the Effects of Long-term Lomerizine Administration Differ with Age?', *Internal Medicine*, vol. 46, no. 10, pp. 683–684.

Infanger, DW, Sharma, R V, & Davisson, RL 2006, 'NADPH Oxidases of the Brain: Distribution, Regulation, and Function', *Antioxidants and Redox Signalling*, vol. 8, no. 9–10, pp. 1583–1596.

Ischiropoulos, H & Beckman, JS 2003, 'Oxidative stress and nitration in neurodegeneration: Cause, effect, or association?', *Journal of Clinical Investigation*, vol. 111, no. 2, pp. 163–169.

Itoh, T, Imano, M, Nishida, S, Tsubaki, M, Mizuguchi, N, Hashimoto, S, Ito, A, & Satou, T 2013, 'Increased apoptotic neuronal cell death and cognitive impairment at early phase after traumatic brain injury in aged rats', *Brain Structure and Function*, vol. 218, no. 1, pp. 209–220.

Itoh, T, Satou, T, Nishida, S, Tsubaki, M, Imano, M, Hashimoto, S, & Ito, H 2010, 'Edaravone protects against apoptotic neuronal cell death and improves cerebral function after traumatic brain injury in rats', *Neurochemical Research*, vol. 35, no. 2, pp. 348–355.

Jack, C, Antel, J, Brück, W, & Kuhlmann, T 2007, 'Contrasting potential of nitric oxide and peroxynitrite to mediate oligodendrocyte injury in multiple sclerosis', *Glia*, vol. 55, no. 9, pp. 926–934.

Jacobs, AL & Schär, P 2012, 'DNA glycosylases: in DNA repair and beyond', *Chromosoma*, vol. 121, no. 1, pp. 1–20.

Jaiser, SR & Winston, GP 2010, 'Copper deficiency myelopathy.', *Journal of Neurology*, vol. 257, no. 6, pp. 869–81.

Jarius, S, König, FB, Metz, I, Ruprecht, K, Paul, F, Brück, W, & Wildemann, B 2017, 'Pattern II and pattern III MS are entities distinct from pattern I MS: evidence from cerebrospinal fluid analysis', *Journal of Neuroinflammation*, vol. 14, no. 1, p. 171.

Jhelum, P, Santos-Nogueira, E, Teo, W, Haumont, A, Lenoël, I, Stys, PK, & David, S 2020, 'Ferroptosis mediates cuprizone-induced loss of oligodendrocytes and demyelination', *Journal of Neuroscience*, vol. 40, no. 48, pp. 9327–9341.

Jiang, L-H, Mackenzie, AB, North, RA, & Surprenant, A 2000, 'Brilliant Blue G selectively blocks ATP-gated rat P2X7 receptors', *Molecular Pharmacology*, vol. 58, pp. 82–88.

Jonkman, J, Brown, CM, Wright, GD, Anderson, KI, & North, AJ 2020, 'Tutorial: guidance for quantitative confocal microscopy', *Nature Protocols* 2020 15:5, vol. 15, no. 5, pp. 1585–1611.

Juurink, B, Thorburne, SK, & Hertz, L 1998, 'Peroxide-scavenging deficit underlies oligodendrocyte susceptibility to oxidative stress', *Glia*, vol. 22, no. 4, pp. 371–378.

Kaddatz, H, Joost, S, Nedelcu, J, Chrzanowski, U, Schmitz, C, Gingele, S, Gudi, V, Stangel, M, Zhan, J, Santrau, E, Greiner, T, Frenz, J, Müller-Hilke, B, Müller, M, Amor, S, van der Valk, P, & Kipp, M 2021, 'Cuprizone-induced demyelination triggers a CD8-pronounced T cell recruitment', *GLIA*, vol. 69, no. 4, pp. 925–942.

Kaina, B, Ochs, K, Grösch, S, Frizz, G, Lips, J, Tomicic, M, Dunkern, T, & Christmann, M 2001, 'BER, MGMT, and MMR in defense against alkylation-induced genotoxicity and apoptosis', *Progress in Nucleic Acid Research and Molecular Biology*, vol. 68, pp. 41–54.

Kang, Z, Wang, C, Zepp, J, Wu, L, Sun, K, Zhao, J, Chandrasekharan, U, Dicorleto, PE,

Trapp, BD, Ransohoff, RM, & Li, X 2013, 'Act1 mediates IL-17-induced EAE pathogenesis selectively in NG2 + glial cells', *Nat Neurosci*, vol. 16, no. 10, pp. 1401–1408.

Kanvah, S & Schuster, GB 2006, 'Oxidative damage to DNA: Inhibition of guanine damage', *Pure Appl. Chem*, vol. 78, no. 12, pp. 2297–2304.

Kaplan, L, Chow, BW, & Gu, C 2020, 'Neuronal regulation of the blood–brain barrier and neurovascular coupling', *Nature Reviews Neuroscience*, vol. 21, no. 8, pp. 416–432.

Kapoor, R, Davies, M, Blaker, PA, Hall, SM, & Smith, KJ 2003, 'Blockers of sodium and calcium entry protect axons from nitric oxide-mediated degeneration', *Annals of Neurology*, vol. 53, no. 2, pp. 174–180.

Káradóttir, R, Hamilton, NB, Bakiri, Y, & Attwell, D 2008, 'Spiking and nonspiking classes of oligodendrocyte precursor glia in CNS white matter', *Nature Neuroscience*, vol. 11, no. 4, pp. 450–456.

Karahalil, B, Orhan, G, & Ak, F 2015, 'The impact of detoxifying and repair gene polymorphisms and the levels of serum ROS in the susceptibility to multiple sclerosis', *Clinical Neurology and Neurosurgery*, vol. 139, pp. 288–294.

Karasek, M, Swiltosławski, J, & Zielińska, A 2004, 'Ultrastructure of the central nervous system: The basics', *Folia Neuropathol*, vol. 42, pp. B1–B9.

Karim, Z, Sawada, A, Kawakami, H, Yamamoto, T, & Taniguchi, T 2006, 'A new calcium channel antagonist, lomerizine, alleviates secondary retinal ganglion cell death after optic nerve injury in the rat', *Current Eye Research*, vol. 31, no. 3, pp. 273–283.

Karve, IP, Taylor, JM, & Crack, PJ 2016, 'The contribution of astrocytes and microglia to traumatic brain injury', *British Journal of Pharmacology*, vol. 173, no. 4, pp. 692–702.

Kasinathan, N, Jagani, H V, Alex, AT, Volety, SM, & Rao, JV 2015, 'Drug Delivery Strategies for drug delivery to the central nervous system by systemic route Strategies for drug delivery to the central nervous system by systemic route', *Drug Delivery*, vol. 22, no. 3, pp. 243–257.

Katalinic, N, Starcevi, A, Mavrincac, M, & Balen, S 2017, 'Complement-dependent cytotoxicity and Luminex technology for human leucocyte antigen antibody detection in kidney transplant candidates exposed to different sensitizing events', *Clinical Kidney Journal*, vol. 10, no. 6, p. 852.

Katayama, Y, Kawamata, T, Tamura, T, Hovda, DA, Becker, DP, & Tsubokawa, T 1991, 'Calcium-dependent glutamate release concomitant with massive potassium flux during cerebral ischemia in vivo', *Brain Research*, vol. 558, pp. 136–140.

Keaney, J & Campbell, M 2015, 'The dynamic blood–brain barrier', *The FEBS Journal*, vol. 282, no. 21, pp. 4067–4079.

Kennel De March, A, De Bouwerie, M, Kolopp-Sarda, MN, Faure, GC, Béné, MC, &

Bernard, CCA 2003, 'Anti-myelin oligodendrocyte glycoprotein B-cell responses in multiple sclerosis.', *Journal of Neuroimmunology*, vol. 135, no. 1–2, pp. 117–25.

Kessarlis, N, Fogarty, M, Iannarelli, P, Grist, M, Wegner, M, & Richardson, WD 2006, 'Competing waves of oligodendrocytes in the forebrain and postnatal elimination of an embryonic lineage', *Nature Neuroscience*, vol. 9, no. 2, pp. 173–179.

van Kesteren, CFMG, Gremmels, H, de Witte, LD, Hol, EM, Van Gool, AR, Falkai, PG, Kahn, RS, & Sommer, IEC 2017, 'Immune involvement in the pathogenesis of schizophrenia: a meta-analysis on postmortem brain studies.', *Translational psychiatry*, vol. 7, no. 3, p. e1075.

Khalili, M, Eghtesadi, S, Mirshafiey, A, Eskandari, G, Sanoobar, M, Sahraian, MA, Motevalian, A, Norouzi, A, Moftakhar, S, & Azimi, A 2014, 'Effect of lipoic acid consumption on oxidative stress among multiple sclerosis patients: A randomized controlled clinical trial', *Nutritional Neuroscience*, vol. 17, no. 1, pp. 16–20.

Khan, F, Baguley, I, & Cameron, I 2003, 'Rehabilitation after traumatic brain injury', *Medical Journal of Australia*, vol. 178, pp. 290–295.

Khorchid, A & Ikura, M 2002, 'How calpain is activated by calcium', *Nature Structural Biology*, vol. 9, no. 4, pp. 239–241.

Kiernan, JA 2013, 'Histochemistry of Staining Methods for Normal and Degenerating Myelin in the Central and Peripheral Nervous Systems', <http://dx.doi.org/10.1179/his.2007.30.2.87>, vol. 30, no. 2, pp. 87–106.

Kimble, DE, Shields, J, Yanasak, N, Vender, JR, Dhandapani, KM, & Kleinschnitz, C 2012, 'Activation of P2X7 promotes cerebral edema and neurological injury after traumatic brain injury in mice', *PLoS ONE*, vol. 7, no. 7.

Kimura, I, Dohgu, S, Takata, F, Matsumoto, J, Watanabe, T, Iwao, T, Yamauchi, A, & Kataoka, Y 2020, 'Oligodendrocytes upregulate blood-brain barrier function through mechanisms other than the PDGF-BB/PDGFR α pathway in the barrier-tightening effect of oligodendrocyte progenitor cells', *Neuroscience Letters*, vol. 715, p. 134594.

Kipp, M, Clarner, T, Dang, J, Sjeff, A, Ae, C, & Beyer, C 2009, 'The cuprizone animal model: new insights into an old story', *Acta Neuropathologica*, vol. 118, pp. 723–736.

Kipp, M, Gingele, S, Pott, F, Clarner, T, van der Valk, P, Denecke, B, Gan, L, Siffrin, V, Zipp, F, Dreher, W, Baumgartner, W, Pfeifenbring, S, Godbout, R, Amor, S, & Beyer, C 2011, 'BLBP-expression in astrocytes during experimental demyelination and in human multiple sclerosis lesions', *Brain, Behavior, and Immunity*, vol. 25, no. 8, pp. 1554–1568.

Kipp, M, Nyamoya, S, Hochstrasser, T, & Amor, S 2017, 'Multiple sclerosis animal models: a clinical and histopathological perspective', *Brain Pathology*, vol. 27, no. 2, pp. 123–137.

Kirk, J, Plumb, J, Mirakhor, M, & McQuaid, S 2003, 'Tight junctional abnormality in multiple

sclerosis white matter affects all calibres of vessel and is associated with blood-brain barrier leakage and active demyelination’, *Journal of Pathology*, vol. 201, no. 2, pp. 319–327.

Kisler, K, Nelson, AR, Rege, S V., Ramanathan, A, Wang, Y, Ahuja, A, Lazic, D, Tsai, PS, Zhao, Z, Zhou, Y, Boas, DA, Sakadžić, S, & Zlokovic, B V. 2017, ‘Pericyte degeneration leads to neurovascular uncoupling and limits oxygen supply to brain’, *Nature Neuroscience*, vol. 20, no. 3, pp. 406–416.

Kitchen, P, Salman, MM, Halsey, AM, Clarke-Bland, C, MacDonald, JA, Ishida, H, Vogel, HJ, Almutiri, S, Logan, A, Kreida, S, Al-Jubair, T, Winkel Missel, J, Gourdon, P, Törnroth-Horsefield, S, Conner, MT, Ahmed, Z, Conner, AC, & Bill, RM 2020, ‘Targeting Aquaporin-4 Subcellular Localization to Treat Central Nervous System Edema’, *Cell*, vol. 181, no. 4, pp. 784–799.e19.

Klein, B, Mrowetz, H, Barker, CM, Lange, S, Rivera, FJ, & Aigner, L 2018, ‘Age Influences Microglial Activation After Cuprizone-Induced Demyelination’, *Frontiers in Aging Neuroscience*, vol. 10, no. SEP, p. 278.

Klüver, H & Barrera, E 1953, ‘A Method for the Combined Staining of Cells and Fibers in the Nervous System’, *Journal of Neuropathology & Experimental Neurology*, vol. 12, no. 4, pp. 400–403.

Kobeissy, FH 2015, *Brain Neurotrauma: Molecular, Neuropsychological, and Rehabilitation Aspects*. CRC Press, Florida.

Kobelt, G, Berg, J, Lindgren, P, Fredrikson, S, & Jönsson, B 2006, ‘Costs and quality of life of patients with multiple sclerosis in Europe’, *J Neurol Neurosurg Psychiatry*, vol. 77, pp. 918–926.

Kondo, A, Nakano, T, & Suzuki, K 1987, ‘Blood-brain barrier permeability to horseradish peroxidase in twitcher and cuprizone-intoxicated mice’, *Brain Research*, vol. 425, no. 1, pp. 186–190.

Koob, AO, Colby, JM, & Borgens, RB 2008, ‘Behavioral recovery from traumatic brain injury after membrane reconstruction using polyethylene glycol’, *Journal of Biological Engineering*, vol. 2, no. 9.

Kopanitsa, M V., Lehtimäki, KK, Forsman, M, Suhonen, A, Koponen, J, Piipponiemi, TO, Kärkkäinen, A, Pavlidi, P, Shatillo, A, Sweeney, PJ, Merenlender-Wagner, A, Kaye, J, Orbach, A, & Nurmi, A 2020, ‘Cognitive disturbances in the cuprizone model of multiple sclerosis’, *Genes, Brain and Behavior*.

Krauspe, BM, Dreher, W, Beyer, C, Baumgartner, W, Denecke, B, Janssen, K, Langhans, CD, Clarner, T, & Kipp, M 2015, ‘Short-Term Cuprizone Feeding Verifies N-Acetylaspartate Quantification as a Marker of Neurodegeneration’, *Journal of Molecular Neuroscience*, vol. 55, no. 3, pp. 733–748.

Kretschmer, F, Tariq, M, Chatila, W, Wu, B, & Badea, TC 2017, 'The Mouse Visual System: Comparison of optomotor and optokinetic reflexes in mice', *Journal of Neurophysiology*, vol. 118, no. 1, p. 300.

Krokan, HE & Bjørå, M 2013, 'Base Excision Repair', *Cold Spring Harbor Perspectives in Biology*, vol. 3, no. 5, p. a012583.

Kubo, KY, Inuma, M, & Chen, H 2015, 'Mastication as a Stress-Coping Behavior', *BioMed Research International*, vol. 2015.

Kuchroo, VK, Anderson, AC, Waldner, H, Munder, M, Bettelli, E, & Nicholson, LB 2003, 'T Cell Response in Experimental Autoimmune Encephalomyelitis (EAE): Role of Self and Cross-Reactive Antigens in Shaping, Tuning, and Regulating the Autopathogenic T Cell Repertoire', *Annual Review of Immunology*, vol. 20, pp. 101–123.

Kuhlmann, T, Miron, V, Cuo, Q, Wegner, C, Antel, J, Bruck, W, & Brück, W 2008, 'Differentiation block of oligodendroglial progenitor cells as a cause for remyelination failure in chronic multiple sclerosis', *Brain*, vol. 131, no. 7, pp. 1749–1758.

Kuriakose, M, Younger, D, Ravula, AR, Alay, E, Rama Rao, K V., & Chandra, N 2019, 'Synergistic Role of Oxidative Stress and Blood-Brain Barrier Permeability as Injury Mechanisms in the Acute Pathophysiology of Blast-induced Neurotrauma', *Scientific Reports*, vol. 9, no. 1, pp. 1–12.

Kurtzke, JF 1983, 'Rating neurologic impairment in multiple sclerosis: An expanded disability status scale (EDSS)', *Neurology*, vol. 33, no. 11, pp. 1444–1452.

Kushner, D 1998, 'Mild traumatic brain injury: Toward understanding manifestations and treatment', *Archives of Internal Medicine*, vol. 158, no. 15, pp. 1617–1624.

Kutzelnigg, A & Lassmann, H 2006, 'Cortical demyelination in multiple sclerosis: A substrate for cognitive deficits?', *Journal of the Neurological Sciences*, vol. 245, no. 1–2, pp. 123–126.

Kutzelnigg, A, Lucchinetti, CF, Stadelmann, C, Brück, W, Rauschka, H, Bergmann, M, Schmidbauer, M, Parisi, JE, & Lassmann, H 2005, 'Cortical demyelination and diffuse white matter injury in multiple sclerosis', *Brain*, vol. 128, no. 11, pp. 2705–2712.

Langer-Gould, A, Popat, RA, Huang, SM, Cobb, K, Fontoura, P, Gould, MK, & Nelson, LM 2006, 'Clinical and Demographic Predictors of Long-term Disability in Patients With Relapsing-Remitting Multiple Sclerosis', *Archives of Neurology*, vol. 63, no. 12, p. 1686.

Lappe-Siefke, C, Goebbels, S, Gravel, M, Nicksch, E, Lee, J, Braun, PE, Griffiths, IR, & Nave, K-A 2003, 'Disruption of Cnp1 uncouples oligodendroglial functions in axonal support and myelination', *Nature Genetics*, vol. 33, no. 3, pp. 366–374.

Laredo, F, Plebanski, J, & Tedeschi, A 2019, 'Pericytes: Problems and Promises for CNS Repair', *Frontiers in Cellular Neuroscience*, vol. 13, p. 546.

Largani, SHH, Borhani-Haghighi, M, Pasbakhsh, P, Mahabadi, VP, Nekoonam, S, Shiri, E, Kashani, IR, & Zendejdel, A 2019, 'Oligoprotective effect of metformin through the AMPK-dependent on restoration of mitochondrial hemostasis in the cuprizone-induced multiple sclerosis model', *Journal of Molecular Histology*.

Lassmann, H & Bradl, M 2016, 'Multiple sclerosis: experimental models and reality', *Acta Neuropathologica* 2016 133:2, vol. 133, no. 2, pp. 223–244. Available from: <https://link.springer.com/article/10.1007/s00401-016-1631-4>. [8 February 2023].

Lassmann, H, Brück, W, & Lucchinetti, CF 2007, 'The Immunopathology of Multiple Sclerosis: An Overview', *Brain Pathology*, vol. 17, no. 2, pp. 210–218.

Laurinavicius, A, Plancoulaine, B, Herlin, P, & Laurinaviciene, A 2016, 'Comprehensive Immunohistochemistry: Digital, Analytical and Integrated', *Pathobiology*, vol. 83, no. 2–3, pp. 156–163.

Laval, J, Jurado, J, Sapparbaev, M, & Sidorkina, O 1998, 'Antimutagenic role of base-excision repair enzymes upon free radical- induced DNA damage', *Mutation Research*, vol. 402, no. 1–2, pp. 93–102.

Lee, RMKW 1995, 'Morphology of cerebral arteries', *Pharmacology and Therapeutics*, vol. 66, no. 1, pp. 149–173.

Leech, S, Kirk, J, Plumb, J, & McQuaid, S 2007, 'Persistent endothelial abnormalities and blood-brain barrier leak in primary and secondary progressive multiple sclerosis', *Neuropathology and Applied Neurobiology*, vol. 33, no. 1, pp. 86–98.

Lemus, HN, Warrington, AE, & Rodriguez, M 2018, 'Multiple Sclerosis Mechanisms of Disease and Strategies for Myelin and Axonal Repair', *Neurologic Clinics of NA*, vol. 36, pp. 1–11.

Leray, E, Yaouanq, J, Le Page, E, Coustans, M, Laplaud, D, Oger, J, & Edan, G 2010, 'Evidence for a two-stage disability progression in multiple sclerosis.', *Brain*, vol. 133, no. Pt 7, pp. 1900–13.

Lessell, S 1974, 'Capillaries of Rat Optic Nerve', *Archives of Ophthalmology*, vol. 91, pp. 308–310.

Levine, JM, Reynolds, R, & Fawcett, JW 2001, 'The oligodendrocyte precursor cell in health and disease', *Trends in Neurosciences*, vol. 24, no. 1, pp. 39–47.

Levkovitch-Verbin, H, Quigley, HA, Martin, KRG, Zack, DJ, Pease, ME, & Valenta, DF 2003, 'A model to study differences between primary and secondary degeneration of retinal ganglion cells in rats by partial optic nerve transection', *Investigative Ophthalmology & Visual Science*, vol. 44, no. 8, p. 3388.

Lewén, A, Sugawara, T, Gasche, Y, Fujimura, M, & Chan, PH 2001, 'Oxidative Cellular Damage and the Reduction of APE/Ref-1 Expression after Experimental Traumatic Brain Injury',

Neurobiology of Disease, vol. 8, no. 3, pp. 380–390.

Li, H, Swiercz, R, & Englander, EW 2009, 'Elevated metals compromise repair of oxidative DNA damage via the base excision repair pathway: implications of pathologic iron overload in the brain on integrity of neuronal DNA.', *Journal of Neurochemistry*, vol. 110, no. 6, pp. 1774–83.

Li, W, Choudhury, GR, Winters, A, Prah, J, Lin, W, Liu, R, & Yang, SH 2018, 'Hyperglycemia alters astrocyte metabolism and inhibits astrocyte proliferation', *Aging and Disease*, vol. 9, no. 4, pp. 674–684.

Lieber, MR 2010, 'The Mechanism of Double-Strand DNA Break Repair by the Nonhomologous DNA End-Joining Pathway', *Annual Review of Biochemistry*, vol. 79, no. 1, pp. 181–211.

Liebner, S, Dijkhuizen, RM, Reiss, Y, Plate, KH, Agalliu, D, & Constantin, G 2018, 'Functional morphology of the blood–brain barrier in health and disease', *Acta Neuropathologica* 2018 135:3, vol. 135, no. 3, pp. 311–336.

Lin, S & Bergles, DE 2004, 'Synaptic signaling between GABAergic interneurons and oligodendrocyte precursor cells in the hippocampus', *Nature Neuroscience*, vol. 7, no. 1, pp. 24–32.

Lin Xiao, Ohayon, D, McKenzie, IA, Sinclair-Wilson, A, Wright, JL, Fudge, AD, Emery, B, Li, H, & Richardson, WD 2016, 'Rapid production of new oligodendrocytes is required in the earliest stages of motor skill learning', *Nat Neurosci*, vol. 19, no. 9, pp. 1210–1217.

Lindahl, P, Johansson, BR, Leveen, P, & Betsholtz, C 1997, 'Pericyte loss and microaneurysm formation in PDGF-B-deficient mice', *Science*, vol. 277, no. 5323, pp. 242–245.

Lindner, M, Fokuhl, J, Linsmeier, F, Trebst, C, & Stangel, M 2009, 'Chronic toxic demyelination in the central nervous system leads to axonal damage despite remyelination', *Neuroscience Letters*, vol. 453, no. 2, pp. 120–125.

Liu, JS-H, Zhao, M-L, Brosnan, CF, & Lee, SC 2001, 'Expression of Inducible Nitric Oxide Synthase and Nitrotyrosine in Multiple Sclerosis Lesions', *The American Journal of Pathology*, vol. 158, no. 6, pp. 2057–2066.

Liu, RM & Desai, LP 2015, 'Reciprocal regulation of TGF- β and reactive oxygen species: A perverse cycle for fibrosis', *Redox Biology*, vol. 6, p. 565.

Loane, DJ & Byrnes, KR 2010, 'Role of Microglia in Neurotrauma', *Neurotherapeutics*, vol. 7, no. 4, pp. 366–377.

Loane, DJ, Kumar, A, Stoica, BA, Cabatbat, R, & Faden, AI 2014, 'Progressive neurodegeneration after experimental brain trauma: association with chronic microglial activation.', *Journal of neuropathology and experimental neurology*, vol. 73, no. 1, pp. 14–29.

Löscher, W & Potschka, H 2005, 'Blood-brain barrier active efflux transporters: ATP-binding cassette gene family', *NeuroRx*, vol. 2, no. 1, pp. 86–98.

Lozić, I, Bartlett, C, Shaw, I, Iyer, K, Dunlop, S, Kilburn, M, & Fitzgerald, M 2014, 'Changes in subtypes of Ca microdomains following partial injury to the central nervous system', *Metallomics*, vol. 6, no. 3, pp. 455–464.

Lu, Y, Ho, CS, Liu, X, Chua, AN, Wang, W, McIntyre, RS, & Ho, RC 2017, 'Chronic administration of fluoxetine and pro-inflammatory cytokine change in a rat model of depression', *PLoS ONE*, vol. 12, no. 10, p. e0186700.

Lublin, FD & Reingold, SC 1996, 'Defining the clinical course of multiple sclerosis: results of an international survey. National Multiple Sclerosis Society (USA) Advisory Committee on Clinical Trials of New Agents in Multiple Sclerosis.', *Neurology*, vol. 46, no. 4, pp. 907–11.

Lucas, RM, Byrne, SN, Correale, J, Ilschner, S, & Hart, PH 2015, 'Ultraviolet radiation, vitamin D and multiple sclerosis', *Neurodegenerative Disease Management*, vol. 5, no. 5, pp. 413–424.

Lucchinetti, C, Brück, W, Parisi, J, Scheithauer, B, Rodriguez, M, Lassmann, H, & Heterogeneity, LH 2000, 'Heterogeneity of Multiple Sclerosis Lesions: Implications for the Pathogenesis of Demyelination', *Annals of Neurology*, vol. 47, pp. 707–717.

Ludwin, SK 2006, 'The Pathogenesis of Multiple Sclerosis', *Journal of Neuropathology and Experimental Neurology*, vol. 65, no. 4, pp. 305–318.

Luissint, AC, Artus, C, Glacial, F, Ganeshamoorthy, K, & Couraud, PO 2012, 'Tight junctions at the blood brain barrier: Physiological architecture and disease-associated dysregulation', *Fluids and Barriers of the CNS*, vol. 9, no. 1, pp. 1–12.

Luo, C, Jian, C, Liao, Y, Huang, Q, Wu, Yuejuan, Liu, X, Zou, D, & Wu, Yuan 2017, 'The role of microglia in multiple sclerosis.', *Neuropsychiatric disease and treatment*, vol. 13, pp. 1661–1667.

Luo, M, Deng, M, Yu, Z, Zhang, Y, Xu, S, Hu, S, & Xu, H 2020, 'Differential Susceptibility and Vulnerability of Brain Cells in C57BL/6 Mouse to Mitochondrial Dysfunction Induced by Short-Term Cuprizone Exposure', *Frontiers in Neuroanatomy*, vol. 14, p. 30.

Machado-Santos, J, Saji, E, Tröscher, AR, Paunovic, M, Liblau, R, Gabriely, G, Bien, CG, Bauer, J, & Lassmann, H 2018, 'The compartmentalized inflammatory response in the multiple sclerosis brain is composed of tissue-resident CD8⁺ T lymphocytes and B cells', *Brain*, vol. 141, no. 7, pp. 2066–2082.

Magaki, S, Hojat, SA, Wei, B, So, A, & Yong, WH 2019, 'An Introduction to the Performance of Immunohistochemistry', *Methods in molecular biology (Clifton, N.J.)*, vol. 1897, p. 289.

Mahad, D, Ziabreva, I, Lassmann, H, & Turnbull, D 2008, 'Mitochondrial defects in acute multiple sclerosis lesions', *Brain*, vol. 131, no. 7, pp. 1722–1735.

Mahad, DH, Trapp, BD, & Lassmann, H 2015, 'Pathological mechanisms in progressive

multiple sclerosis', *The Lancet Neurology*, vol. 14, no. 2, pp. 183–193.

Maki, T 2017, 'Novel roles of oligodendrocyte precursor cells in the developing and damaged brain', *Clinical and Experimental Neuroimmunology*, vol. 8, no. 1, pp. 33–42.

Maki, T, Maeda, M, Uemura, M, Lo, EK, Terasaki, Y, Liang, AC, Shindo, A, Choi, YK, Taguchi, A, Matsuyama, T, Takahashi, R, Ihara, M, & Arai, K 2015, 'Potential interactions between pericytes and oligodendrocyte precursor cells in perivascular regions of cerebral white matter', *Neuroscience Letters*, vol. 597, pp. 164–169. Available from: <https://linkinghub.elsevier.com/retrieve/pii/S0304394015003468>.

Mallon, BS, Elizabeth Shick, H, Kidd, GJ, & Macklin, WB 2002, 'Proteolipid promoter activity distinguishes two populations of NG2-positive cells throughout neonatal cortical development', *Journal of Neuroscience*, vol. 22, no. 3, pp. 876–885.

Mandillo, S, Heise, I, Garbugino, L, Tocchini-Valentini, GP, Giuliani, A, Wells, S, & Nolan, PM 2014, 'Early motor deficits in mouse disease models are reliably uncovered using an automated home-cage wheel-running system: a cross-laboratory validation', *Disease Models and Mechanisms*, vol. 7, pp. 397–407.

Mandillo, S, Tucci, V, Hölter, SM, Meziane, H, Al Banchaabouchi, M, Kallnik, M, Lad, H V., Nolan, PM, Ouagazzal, AM, Coghill, EL, Gale, K, Golini, E, Jacquot, S, Krezel, W, Parker, A, Riet, F, Schneider, I, Marazziti, D, Auwerx, J, Brown, SDM, Chambon, P, Rosenthal, N, Tocchini-Valentini, G, & Würst, W 2008, 'Reliability, robustness, and reproducibility in mouse behavioral phenotyping: A cross-laboratory study', *Physiological Genomics*, vol. 34, no. 3, pp. 243–255.

Mandolesi, G, Gentile, A, Musella, A, Fresegna, D, De Vito, F, Bullitta, S, Sepman, H, Marfia, GA, & Centonze, D 2015, 'Synaptopathy connects inflammation and neurodegeneration in multiple sclerosis', *Nature Reviews Neurology* 2015 11:12, vol. 11, no. 12, pp. 711–724.

Manrique-Hoyos, N, Jürgens, T, Grønborg, M, Kreutzfeldt, M, Schedensack, M, Kuhlmann, T, Schrick, C, Brück, W, Urlaub, H, Simons, M, & Merkler, D 2012, 'Late motor decline after accomplished remyelination: Impact for progressive multiple sclerosis', *Annals of Neurology*, vol. 71, no. 2, pp. 227–244.

Mao, S, Xiong, G, Johnson, BN, Cohen, NA, & Cohen, AS 2021, 'Blocking Cross-Species Secondary Binding When Performing Double Immunostaining With Mouse and Rat Primary Antibodies', *Frontiers in Neuroscience*, vol. 15, p. 524.

Mao, Y, Black, A, Milbourn, H, Krakonja, S, Nesbit, M, Bartlett, C, Fehily, B, Takechi, R, Yates, N, & Fitzgerald, M 2018, 'The Effects of a Combination of Ion Channel Inhibitors in Female Rats Following Repeated Mild Traumatic Brain Injury', *International Journal of Molecular Sciences*, vol. 19, no. 11, p. 3408.

Marchi, N, Bazarian, JJ, Puvenna, V, Janigro, M, & Ghosh, C 2013, 'Consequences of

Repeated Blood-Brain Barrier Disruption in Football Players', *PLoS ONE*, vol. 8, no. 3, p. 56805.

Maréchal, A & Zou, L 2013, 'DNA damage sensing by the ATM and ATR kinases.', *Cold Spring Harbor Perspectives in Biology*, vol. 5, no. 9.

Marik, C, Felts, PA, Bauer, J, Lassmann, H, & Smith, KJ 2007, 'Lesion genesis in a subset of patients with multiple sclerosis: a role for innate immunity?', *Brain*, vol. 130, no. 11, pp. 2800–2815.

Mark, LP, Prost, RW, Ulmer, JL, Smith, MM, Daniels, DL, Strottmann, JM, Brown, WD, & Hacein-Bey, L 2001, 'Pictorial review of glutamate excitotoxicity: Fundamental concepts for neuroimaging', *American Journal of Neuroradiology*, vol. 22, pp. 1813–1824.

Markowitz, CE 2007, 'Interferon-beta: Mechanism of action and dosing issues', *Neurology*, vol. 68, no. Issue 24, Supplement 4, pp. S8–S11.

Marques, S, Zeisel, A, Codeluppi, S, Van Bruggen, D, Falcão, AM, Xiao, L, Li, H, Häring, M, Hochgerner, H, Romanov, RA, Gyllborg, D, Muñoz-Manchado, AB, La Manno, G, Lönnerberg, P, Floriddia, EM, Rezayee, F, Ernfors, P, Arenas, E, Hjerling-Leffler, J, Harkany, T, Richardson, WD, Linnarsson, S, & Castelo-Branco, G 2016, 'Oligodendrocyte heterogeneity in the mouse juvenile and adult central nervous system', *Science*, vol. 352, no. 6291, pp. 1326–1329.

Marrie, RA 2004, 'Environmental risk factors in multiple sclerosis aetiology', *The Lancet Neurology*, vol. 3, no. 12, pp. 709–718.

Masel, BE & DeWitt, DS 2010, 'Traumatic Brain Injury: A Disease Process, Not an Event', *Journal of Neurotrauma*, vol. 27, no. 8, pp. 1529–1540.

Mason, JL & Goldman, JE 2002, 'A2B5+ and O4+ cycling progenitors in the adult forebrain white matter respond differentially to PDGF-AA, FGF-2, and IGF-1', *Molecular and Cellular Neuroscience*, vol. 20, no. 1, pp. 30–42.

Mason, JL, Jones, JJ, Taniike, M, Morell, P, Suzuki, K, & Matsushima, GK 2000, 'Mature oligodendrocyte apoptosis precedes IGF-1 production and oligodendrocyte progenitor accumulation and differentiation during demyelination/remyelination', *Journal of Neuroscience Research*, vol. 61, no. 3, pp. 251–262.

Matsushima, GK & Morell, P 2001, 'The neurotoxicant, cuprizone, as a model to study demyelination and remyelination in the central nervous system', *Brain Pathology*, vol. 11, no. 1, pp. 107–16.

Matute, C 2008, 'P2X7 receptors in oligodendrocytes: A novel target for neuroprotection', *Molecular Neurobiology*, vol. 38, no. 2, pp. 123–128.

Matute, C, Torre, I, Pérez-Cerdá, F, Pérez-Samartín, A, Alberdi, E, Etxebarria, E, Arranz, AM, Ravid, R, Rodríguez-Antigüedad, A, Sánchez-Gómez, MV, & Domercq, M 2007, 'P2X7 receptor blockade prevents ATP excitotoxicity in oligodendrocytes and ameliorates experimental autoimmune encephalomyelitis', *Journal of Neuroscience*, vol. 27, no. 35, pp. 9525–9533.

Mazloumfard, F, Mirian, M, Eftekhari, S-M, & Aliomrani, M 2020, 'Hydroxychloroquine effects on miR-155-3p and miR-219 expression changes in animal model of multiple sclerosis', *Metabolic Brain Disease*, pp. 1–9.

McCabe, MP & McKern, S 2002, 'Quality of Life and Multiple Sclerosis: Comparison Between People with Multiple Sclerosis and People from the General Population', *Journal of Clinical Psychology in Medical Settings*, vol. 9, no. 4, pp. 287–295.

McConnell, HL, Kersch, CN, Woltjer, RL, & Neuwelt, EA 2017, 'The translational significance of the neurovascular unit', *Journal of Biological Chemistry*, vol. 292, no. 3, pp. 762–770.

McDonald, WI, Compston, A, Edan, G, Goodkin, D, Hartung, H-P, Lublin, FD, McFarland, HF, Paty, DW, Polman, CH, Reingold, SC, Sandberg-Wollheim, M, Sibley, W, Thompson, A, Van Den Noort, S, Weinshenker, BY, & Wolinsky, JS 2001, 'Recommended diagnostic criteria for multiple sclerosis: Guidelines from the international panel on the diagnosis of multiple sclerosis', *Annals of Neurology*, vol. 50, no. 1, pp. 121–127.

McFarland, HF & Martin, R 2007, 'Multiple sclerosis: a complicated picture of autoimmunity', *Nature Immunology*, vol. 8, no. 9.

McMahon, EJ, Suzuki, K, & Matsushima, GK 2002, 'Peripheral macrophage recruitment in cuprizone-induced CNS demyelination despite an intact blood-brain barrier', *Journal of Neuroimmunology*, vol. 130, no. 1–2, pp. 32–45.

McMillin, MA, Frampton, GA, Seiwel, AP, Patel, NS, Jacobs, AN, & DeMorrow, S 2015, 'TGFβ1 exacerbates blood-brain barrier permeability in a mouse model of hepatic encephalopathy via upregulation of MMP9 and downregulation of claudin-5', *Laboratory investigation; a journal of technical methods and pathology*, vol. 95, no. 8, p. 903.

van der Mei, Ingrid A F, Ponsonby, A-L, Blizzard, L, Dwyer, T, & Van Der Mei, I A F 2001, 'Regional Variation in Multiple Sclerosis Prevalence in Australia and Its Association with Ambient Ultraviolet Radiation', *Neuroepidemiology*, vol. 20, pp. 168–174.

Mendez, DR, Cherian, L, Moore, N, Arora, T, Liu, PK, & Robertson, CS 2004, 'Oxidative DNA Lesions in a Rodent Model of Traumatic Brain Injury', *The Journal of Trauma: Injury, Infection, and Critical Care*, vol. 56, no. 6, pp. 1235–1240.

Miljković, D & Spasojević, I 2013, 'Multiple sclerosis: molecular mechanisms and therapeutic opportunities.', *Antioxidants & redox signaling*, vol. 19, no. 18, pp. 2286–334.

Miller, DH, Barkhof, F, Frank, JA, Parker, GJM, & Thompson, AJ 2002, 'Measurement of atrophy in multiple sclerosis: pathological basis, methodological aspects and clinical relevance.', *Brain*, vol. 125, no. Pt 8, pp. 1676–95.

Miller, E, Walczak, A, Majsterek, I, & Kędziora, J 2013, 'Melatonin reduces oxidative stress

in the erythrocytes of multiple sclerosis patients with secondary progressive clinical course', *Journal of Neuroimmunology*, vol. 257, pp. 97–101.

Miller, E, Walczak, A, Saluk, J, Ponczek, MB, & Majsterek, I 2012, 'Oxidative modification of patient's plasma proteins and its role in pathogenesis of multiple sclerosis', *Clinical Biochemistry*, vol. 45, no. 1–2, pp. 26–30.

Min, Y, Kristiansen, K, Boggs, JM, Husted, C, Zasadzinski, JA, & Israelachvili, J 2009, 'Interaction forces and adhesion of supported myelin lipid bilayers modulated by myelin basic protein.', *Proceedings of the National Academy of Sciences of the United States of America*, vol. 106, no. 9, pp. 3154–9.

Minagar, A & Alexander, JS 2003, 'Blood-brain barrier disruption in multiple sclerosis', *Multiple Sclerosis*, vol. 9, pp. 540–549.

Minagar, A, Jy, W, Jimenez, JJ, & Steven Alexander, J 2006, 'Multiple sclerosis as a vascular disease', *Neurological Research*, vol. 28, no. 3, pp. 230–235.

Minagar, A, Maghzi, AH, Mcgee, JC, & Alexander, S 2012, 'Emerging roles of endothelial cells in multiple sclerosis pathophysiology and therapy', *Neurological Research*, vol. 34, no. 8, pp. 738–745.

Miron, VE, Kuhlmann, T, & Antel, JP 2011, 'Cells of the oligodendroglial lineage, myelination and remyelination', *Biochimica et Biophysica Acta*, vol. 1812, pp. 184–193.

Mittapalli, RK, Manda, VK, Adkins, CE, Geldenhuys, WJ, & Lockman, PR 2010, 'Exploiting nutrient transporters at the blood-brain barrier to improve brain distribution of small molecules', *Therapeutic Delivery*, vol. 1, no. 6, pp. 775–784.

Miyamoto, N, Pham, L-DD, Hae Seo, J, Kim, K-W, Lo, EH, & Arai, K 2014, 'Crosstalk between cerebral endothelium and oligodendrocyte', *Cell and Molecular Life Sciences*, vol. 71, no. 6, pp. 1055–1066.

Moccia, M, Ruggieri, S, Ianniello, A, Toosy, A, Pozzilli, C, & Ciccarelli, O 2019, 'Advances in spinal cord imaging in multiple sclerosis', *Therapeutic Advances in Neurological Disorders*, vol. 12. Available from: [/pmc/articles/PMC6477770/](https://pubmed.ncbi.nlm.nih.gov/31211111/). [8 February 2023].

Moffett, JR, Arun, P, Ariyannur, PS, Garbern, JY, Jacobowitz, DM, & Namboodiri, AMA 2011, 'Extensive aspartoacylase expression in the rat central nervous system', *GLIA*, vol. 59, no. 10, pp. 1414–1434.

Mohamadpour, M, Whitney, K, & Bergold, PJ 2019, 'The importance of therapeutic time window in the treatment of traumatic brain injury', *Frontiers in Neuroscience*, vol. 13, p. 7.

Mohammadi-Rad, M, Ghasemi, N, & Aliomrani, M 2019, 'Evaluation of apamin effects on myelination process in C57BL/6 mice model of multiple sclerosis', *Research in Pharmaceutical Sciences*, vol. 14, no. 5, pp. 424–431.

Mohan, S, Verma, A, Sitoh, Y-Y, & Kumar, S 2009, 'Virchow-Robin Spaces in Health and Disease', *The Neuroradiology Journal*, vol. 22, pp. 518–524.

Moll, NM, Rietsch, AM, Thomas, S, Ransohoff, AJ, Lee, J-C, Fox, R, Chang, A, Ransohoff, RM, & Fisher, E 2011, 'Multiple sclerosis normal-appearing white matter: pathology-imaging correlations.', *Annals of neurology*, vol. 70, no. 5, pp. 764–73.

Möller, JR, Johnson, D, Brady, RO, Tourtellotte, WW, & Quarles, RH 1989, 'Antibodies to myelin-associated glycoprotein (MAG) in the cerebrospinal fluid of multiple sclerosis patients.', *Journal of Neuroimmunology*, vol. 22, no. 1, pp. 55–61.

Monti, DA, Zabrecky, G, Leist, TP, Wintering, N, Bazzan, AJ, Zhan, T, & Newberg, AB 2020, 'N-acetyl Cysteine Administration Is Associated With Increased Cerebral Glucose Metabolism in Patients With Multiple Sclerosis: An Exploratory Study', *Frontiers in Neurology*, vol. 11, p. 88.

Morell, P, Barrett, C V., Mason, JL, Toews, AD, Hostettler, JD, Knapp, GW, & Matsushima, GK 1998, 'Gene expression in brain during cuprizone-induced demyelination and remyelination', *Molecular and Cellular Neurosciences*, vol. 12, no. 4–5, pp. 220–227.

Moreno, V, Smith, EA, & Piña-Oviedo, S 2022, 'Fluorescent Immunohistochemistry', in, *Immunohistochemistry and Immunocytochemistry*, pp.131–146. Humana Press Inc., New York, NY.

Mukhamedshina, YO, Akhmetzyanova, ER, Martynova, E V., Khaiboullina, SF, Galieva, LR, & Rizvanov, AA 2017, 'Systemic and local cytokine profile following spinal cord injury in rats: A multiplex analysis', *Frontiers in Neurology*, vol. 8, p. 581.

Muller, WA 2003, 'Leukocyte-endothelial-cell interactions in leukocyte transmigration and the inflammatory response', *Trends in Immunology*, vol. 24, no. 6, pp. 326–333.

Muriach, M, Flores-Bellver, M, Romero, FJ, & Barcia, JM 2014, 'Diabetes and the brain: Oxidative stress, inflammation, and autophagy', *Oxidative Medicine and Cellular Longevity*, vol. 2014.

Na, H-J, Park, J-S, Pyo, J-H, Lee, S-H, Jeon, H-J, Kim, Y-S, & Yoo, M-A 2013, 'Mechanism of metformin: Inhibition of DNA damage and proliferative activity in Drosophila midgut stem cell', *Mechanisms of Ageing and Development*, vol. 134, no. 9, pp. 381–390.

Nack, A, Brendel, M, Nedelcu, J, Daerr, M, Nyamoya, S, Beyer, C, Focke, C, Deussing, M, Hoornaert, C, Ponsaerts, P, Schmitz, C, Bartenstein, P, Rominger, A, & Kipp, M 2019, 'Expression of Translocator Protein and [18F]-GE180 Ligand Uptake in Multiple Sclerosis Animal Models', *Cells*, vol. 8, no. 2, p. 94.

Nakano, M, Tamura, Y, Yamato, M, Kume, S, Eguchi, A, Takata, K, Watanabe, Y, & Kataoka, Y 2017, 'NG2 glial cells regulate neuroimmunological responses to maintain neuronal function and survival', *Scientific Reports*, vol. 7, no. 1, p. 42041.

Nave, K-A & Ehrenreich, H 2019, 'Time to revisit oligodendrocytes in multiple sclerosis',

Nature Medicine.

Nave, K-A & Werner, HB 2014, 'Myelination of the Nervous System: Mechanisms and Functions', *Annual Review of Cell and Developmental Biology*, vol. 30, no. 1, pp. 503–533.

Nedelcu, J, Reinbach, C, Brendel, M, Rominger, A, Kaye, J, Behrangi, N, Jiangshan, Z, Schmitz, C, & Kipp, M 2020, 'Lacquinimod ameliorates secondary brain inflammation', *Neurobiology of Disease*, vol. 134, p. 104675.

Newcombe, J, Uddin, A, Dove, R, Patel, B, Turski, L, Nishizawa, Y, & Smith, T 2008, 'Glutamate receptor expression in multiple sclerosis lesions', *Brain Pathology*, vol. 18, no. 1, pp. 52–61.

Nickson, CM & Parsons, JL 2014, 'Monitoring regulation of DNA repair activities of cultured cells in-gel using the comet assay', *Frontiers in Genetics*, vol. 5.

Nishimura, S 2001, 'Mammalian Ogg1/Mmh gene plays a major role in repair of the 8-hydroxyguanine lesion in DNA', *Progress in Nucleic Acid Research and Molecular Biology*, vol. 68, pp. 107–123.

Nishiyama, A, Komitova, M, Suzuki, R, & Zhu, X 2009, 'Polydendrocytes (NG2 cells): multifunctional cells with lineage plasticity.', *Nature reviews. Neuroscience*, vol. 10, no. 1, pp. 9–22.

Nitta, ME, Savitz, J, Nelson, LD, Teague, TK, Hoelzle, JB, McCrea, MA, & Meier, TB 2019, 'Acute elevation of serum inflammatory markers predicts symptom recovery after concussion', *Neurology*, vol. 93, no. 5, p. e497.

Niu, J, Tsai, HH, Hoi, KK, Huang, N, Yu, G, Kim, K, Baranzini, SE, Xiao, L, Chan, JR, & Fancy, SPJ 2019, 'Aberrant oligodendroglial–vascular interactions disrupt the blood–brain barrier, triggering CNS inflammation', *Nature Neuroscience*, vol. 22, no. 5, pp. 709–718.

Noble, PG, Antel, JP, & Yong, VW 1994, 'Astrocytes and catalase prevent the toxicity of catecholamines to oligodendrocytes', *Brain Research*, vol. 633, no. 1–2, pp. 83–90.

Noorzehi, G, Pasbakhsh, P, Borhani-Haghighi, M, Kashani, IR, Madadi, S, Tahmasebi, F, Nekoonam, S, & Azizi, M 2018, 'Microglia polarization by methylprednisolone acetate accelerates cuprizone induced demyelination', *Journal of Molecular Histology*, vol. 49, no. 5, pp. 471–479.

Norkute, A, Hieble, A, Braun, A, Johann, S, Clarner, T, Baumgartner, W, Beyer, C, & Kipp, M 2009, 'Cuprizone treatment induces demyelination and astrogliosis in the mouse hippocampus', *Journal of Neuroscience Research*, vol. 87, no. 6, pp. 1343–1355.

Norton, WT & Poduslo, SE 1973, 'Myelination in rat brain: changes in myelin composition during brain maturation.', *Journal of Neurochemistry*, vol. 21, no. 4, pp. 759–73.

Nortvedt, MW, Riise, T, Myhr, KM, & Nyland, HI 1999, 'Quality of life in multiple sclerosis: measuring the disease effects more broadly.', *Neurology*, vol. 53, no. 5, pp. 1098–103.

Noseworthy, JH, Lucchinetti, C, Rodriguez, M, & Weinshenker, BG 2000, 'Multiple

Sclerosis', *New England Journal of Medicine*, vol. 343, no. 13, pp. 938–952.

Nyamoya, S, Schweiger, F, Kipp, M, & Hochstrasser, T 2017, 'Cuprizone as a model of myelin and axonal damage', *Drug Discovery Today: Disease Models*, vol. 25–26, pp. 63–68.

O'Connor, WT, Smyth, A, & Gilchrist, MD 2011, 'Animal models of traumatic brain injury: A critical evaluation', *Pharmacology and Therapeutics*, vol. 130, no. 2, pp. 106–113.

O'Gorman, C, Lucas, R, & Taylor, B 2012, 'Environmental risk factors for multiple sclerosis: a review with a focus on molecular mechanisms.', *International journal of molecular sciences*, vol. 13, no. 9, pp. 11718–52.

O'Hare Doig, R, Chiha, W, Giacci, M, Yates, N, Bartlett, C, Smith, N, Hodgetts, S, Harvey, A, & Fitzgerald, M 2017, 'Specific ion channels contribute to key elements of pathology during secondary degeneration following neurotrauma', *BMC Neuroscience*, vol. 18, no. 62.

O'Hare Doig, RL, Bartlett, CA, Maghzal, GJ, Lam, M, Archer, M, Stocker, R, & Fitzgerald, M 2014, 'Reactive species and oxidative stress in optic nerve vulnerable to secondary degeneration', *Experimental Neurology*, vol. 261, pp. 136–146. Available from: <https://linkinghub.elsevier.com/retrieve/pii/S0014488614001940>. [7 February 2017].

O'Hare Doig, RL, Bartlett, CA, Smith, NM, Hodgetts, SI, Dunlop, SA, Hool, L, & Fitzgerald, M 2016, 'Specific combinations of Ca²⁺ channel inhibitors reduce excessive Ca²⁺ influx as a consequence of oxidative stress and increase neuronal and glial cell viability in vitro', *Neuroscience*, vol. 339, pp. 450–462.

Offenbacher, H, Fazekas, F, Schmidt, R, Freidl, W, Flooh, E, Payer, F, & Lechner, H 1993, 'Assessment of MRI criteria for a diagnosis of MS.', *Neurology*, vol. 43, no. 5, pp. 905–9.

Ohgomori, T & Jinno, S 2019, 'Cuprizone-induced demyelination in the mouse hippocampus is alleviated by phytoestrogen genistein', *Toxicology and Applied Pharmacology*, vol. 363, pp. 98–110.

Ohl, K, Tenbrock, K, & Kipp, M 2016, 'Oxidative stress in multiple sclerosis: Central and peripheral mode of action', *Experimental Neurology*, vol. 277, pp. 58–67.

Okada, R, Wu, Z, Zhu, A, Ni, J, Zhang, J, Yoshimine, Y, Peters, C, Saftig, P, & Nakanishi, H 2015, 'Cathepsin D deficiency induces oxidative damage in brain pericytes and impairs the blood–brain barrier', *Molecular and Cellular Neuroscience*, vol. 64, pp. 51–60.

Olsen, JA & Akirav, EM 2015, 'Remyelination in multiple sclerosis: Cellular mechanisms and novel therapeutic approaches', *Journal of Neuroscience Research*, vol. 93, no. 5, pp. 687–696.

Olsson, T, Barcellos, LF, & Alfredsson, L 2017, 'Interactions between genetic, lifestyle and environmental risk factors for multiple sclerosis', *Nature Reviews Neurology*, vol. 13, no. 1, pp. 25–36.

Oluich, L-J, Stratton, JAS, Lulu Xing, Y, Ng, SW, Cate, HS, Sah, P, Windels, F, Kilpatrick,

TJ, & Merson, TD 2012, 'Targeted Ablation of Oligodendrocytes Induces Axonal Pathology Independent of Overt Demyelination', *Journal of Neuroscience*, vol. 32, no. 24, pp. 8317–8330.

Orije, J, Kara, F, Guglielmetti, C, Praet, J, Van der Linden, A, Ponsaerts, P, & Verhoye, M 2015, 'Longitudinal monitoring of metabolic alterations in cuprizone mouse model of multiple sclerosis using ¹H-magnetic resonance spectroscopy', *NeuroImage*, vol. 114, pp. 128–135.

Ortiz, GG, Pacheco-Moisés, FP, Macías-Islas, MÁ, Flores-Alvarado, LJ, Mireles-Ramírez, MA, González-Renovato, ED, Hernández-Navarro, VE, Sánchez-López, AL, & Alatorre-Jiménez, MA 2014, 'Role of the Blood-Brain Barrier in Multiple Sclerosis', *Archives of Medical Research*, vol. 45, no. 8, pp. 687–697.

Oveland, E, Ahmad, I, Lereim, RR, Kroksveen, AC, Barsnes, H, Guldbrandsen, A, Myhr, KM, Bø, L, Berven, FS, & Wergeland, S 2021, 'Cuprizone and EAE mouse frontal cortex proteomics revealed proteins altered in multiple sclerosis', *Scientific Reports 2021 11:1*, vol. 11, no. 1, pp. 1–16.

Ozerdem, U, Monosov, E, & Stallcup, WB 2002, 'NG2 Proteoglycan Expression by Pericytes in Pathological Microvasculature', *Microvascular Research*, vol. 63, no. 1, pp. 129–134.

Pachner, AR 2011, 'Experimental models of multiple sclerosis', *Current Opinion in Neurology*, vol. 24, no. 3, pp. 291–299.

Pagnin, M, Dekiwadia, C, Petratos, S, & Richardson, SJ 2022, 'Enhanced re-myelination in transthyretin null mice following cuprizone mediated demyelination', *Neuroscience Letters*, vol. 766, p. 136287.

Pandey, S, Shen, K, Lee, S-H, Shen, Y-AA, Wang, Y, Otero-García, M, Kotova, N, Vito, ST, Laufer, BI, Newton, DF, Rezzonico, MG, Hanson, JE, Kaminker, JS, Bohlen, CJ, Yuen, TJ, & Friedman, BA 2022, 'Disease-associated oligodendrocyte responses across neurodegenerative diseases', *Cell Reports*, vol. 40, no. 8, p. 111189.

Panier, S & Boulton, SJ 2014, 'Double-strand break repair: 53BP1 comes into focus', *Nature Reviews Molecular Cell Biology*, vol. 15, no. 1, pp. 7–18.

Pantzaris, MC, Loukaides, GN, Ntzani, EE, & Patrikios, IS 2013, 'A novel oral nutraceutical formula of omega-3 and omega-6 fatty acids with vitamins (PLP10) in relapsing remitting multiple sclerosis: a randomised, double-blind, placebo-controlled proof-of-concept clinical trial', *BMJ Open*, vol. 3, no. 4, p. e002170.

Parikh, SJ, Edelman, M, Uwaifo, GI, Freedman, RJ, Semega-Janneh, M, Reynolds, J, & Yanovski, JA 2004, 'The Relationship between Obesity and Serum 1,25-Dihydroxy Vitamin D Concentrations in Healthy Adults', *Journal of Clinical Endocrinology & Metabolism*, vol. 89, no. 3, pp. 1196–1199.

Paton, KF, Hong, S, Biggerstaff, A, & Kivell, BM 2022, 'Sex Differences in the Behavioural Aspects of the Cuprizone-Induced Demyelination Model in Mice', *Brain Sciences*, vol. 12, no. 12.

Patrikios, P, Stadelmann, C, Kutzelnigg, A, Rauschka, H, Schmidbauer, M, Laursen, H, Sorensen, PS, Brück, W, Lucchinetti, C, & Lassmann, H 2006, 'Remyelination is extensive in a subset of multiple sclerosis patients', *Brain*, vol. 129, no. 12, pp. 3165–3172.

Patsopoulos, NA 2018, 'Genetics of Multiple Sclerosis: An Overview and New Directions', *Cold Spring Harbor Perspectives in Medicine*, vol. 8.

Patten, KT, Valenzuela, AE, Wallis, C, Harvey, DJ, Bein, KJ, Wexler, AS, Gorin, FA, & Lein, PJ 2022, 'Hippocampal but Not Serum Cytokine Levels Are Altered by Traffic-Related Air Pollution in TgF344-AD and Wildtype Fischer 344 Rats in a Sex- and Age-Dependent Manner', *Frontiers in Cellular Neuroscience*, vol. 16, p. 182.

Patterson, ZR & Holahan, MR 2012, 'Understanding the neuroinflammatory response following concussion to develop treatment strategies', *Frontiers in Cellular Neuroscience*, vol. 6, no. 58, pp. 11–10.

Payne, SC, Bartlett, CA, Harvey, AR, Dunlop, SA, & Fitzgerald, M 2011, 'Chronic swelling and abnormal myelination during secondary degeneration after partial injury to a central nervous system tract', *Journal of Neurotrauma*, vol. 28, pp. 1077–1088.

Payne, SC, Bartlett, CA, Harvey, AR, Dunlop, SA, & Fitzgerald, M 2012, 'Myelin sheath decompaction, axon swelling, and functional loss during chronic secondary degeneration in rat optic nerve', *Investigative Ophthalmology and Visual Science*, vol. 53, no. 10, pp. 6093–6101.

Payne, SC, Bartlett, CA, Savigni, DL, Harvey, AR, Dunlop, SA, & Fitzgerald, M 2013, 'Early proliferation does not prevent the loss of oligodendrocyte progenitor cells during the chronic phase of secondary degeneration in a CNS white matter tract', *PLoS ONE*, vol. 8, no. 6, pp. 65710–65720.

Peng, W, Cotrina, ML, Han, X, Yu, H, Bekar, L, Blum, L, Takano, T, Tian, G-F, Goldman, SA, & Nedergaard, M 2009, 'Systemic administration of an antagonist of the ATP-sensitive receptor P2X7 improves recovery after spinal cord injury', *Proceedings of the National Academy of Sciences of the United States of America*, vol. 106, no. 30, pp. 12489–12493.

Perlman, RL 2016, 'Mouse models of human disease: An evolutionary perspective', *Evolution, Medicine, and Public Health*, vol. 2016, no. 1, p. 170.

Petronilho, F, Feier, G, De Souza, B, Guglielmi, C, Constantino, LS, Walz, R, Quevedo, J, & Dal-Pizzol, F 2010, 'Oxidative Stress in Brain According to Traumatic Brain Injury Intensity', *Journal of Surgical Research*, vol. 164, no. 2, pp. 316–320.

Philips, T & Rothstein, JD 2017, 'Oligodendroglia: metabolic supporters of neurons', *Journal of Clinical Investigation*, vol. 127, no. 9, pp. 3271–3280.

Di Pietro, V, Lazzarino, Giacomo, Amorini, AM, Tavazzi, B, D'Urso, S, Longo, S, Vagnozzi, R, Signoretti, S, Clementi, E, Giardina, B, Lazzarino, Giuseppe, & Belli, A 2014, 'Neuroglobin expression and oxidant/antioxidant balance after graded traumatic brain injury in the rat', *Free*

Radical Biology and Medicine, vol. 69, pp. 258–264.

Pitt, D, Nagelmeier, IE, Wilson, HC, & Raine, CS 2003, 'Glutamate uptake by oligodendrocytes: Implications for excitotoxicity in multiple sclerosis', *Neurology*, vol. 61, no. 8, pp. 1113–1120.

Pizzo, ME, Wolak, DJ, Kumar, NN, Brunette, E, Brunquell, CL, Hannocks, MJ, Abbott, NJ, Meyerand, ME, Sorokin, L, Stanimirovic, DB, & Thorne, RG 2018, 'Intrathecal antibody distribution in the rat brain: surface diffusion, perivascular transport and osmotic enhancement of delivery', *The Journal of physiology*, vol. 596, no. 3, pp. 445–475.

Plant, SR, Iocca, HA, Wang, Y, Cameron Thrash, J, O, BP, Arnett, HA, Fu, Y-X, Carson, MJ, & P-Y Ting, J 2007, 'Neurobiology of Disease Lymphotoxin Receptor (LtR): Dual Roles in Demyelination and Remyelination and Successful Therapeutic Intervention Using LtR-Ig Protein', *Journal of Neuroscience*, vol. 27, no. 28, pp. 7429–7437.

Plumb, J, McQuaid, S, Mirakhur, M, & Kirk, J 2006, 'Abnormal Endothelial Tight Junctions in Active Lesions and Normal-appearing White Matter in Multiple Sclerosis', *Brain Pathology*, vol. 12, no. 2, pp. 154–169.

Popescu, BFG, Pirko, I, & Lucchinetti, CF 2013, 'Pathology of multiple sclerosis: where do we stand?', *Continuum*, vol. 19, no. 4, pp. 901–21.

Prabhulkar, S & Li, C-Z 2010, 'Assessment of oxidative DNA damage and repair at single cellular level via real-time monitoring of 8-OHdG biomarker', *Biosensors and Bioelectronics*, vol. 26, no. 4, pp. 1743–1749.

Praet, J, Guglielmetti, C, Berneman, Z, Van der Linden, A, & Ponsaerts, P 2014, 'Cellular and molecular neuropathology of the cuprizone mouse model: Clinical relevance for multiple sclerosis', *Neuroscience & Biobehavioral Reviews*, vol. 47, pp. 485–505.

Prakash, R, Snook, E, Lewis, J, Motl, R, & Kramer, A 2008, 'Cognitive impairments in relapsing-remitting multiple sclerosis: a meta-analysis', *Multiple Sclerosis*, vol. 14, pp. 1250–1261.

Pringle, NP, Mudhar, HS, Collarini, EJ, & Richardson, WD 1992, 'PDGF receptors in the rat CNS: during late neurogenesis, PDGF alphareceptor expression appears to be restricted to glial cells of the oligodendrocyte lineage', *Development*, vol. 115, pp. 535–551.

Procaccini, C, De Rosa, V, Pucino, V, Formisano, L, & Matarese, G 2015, 'Animal models of Multiple Sclerosis', *European Journal of Pharmacology*, vol. 759, pp. 182–191.

Prodan, CI, Holland, NR, Wisdom, PJ, Burstein, SA, & Bottomley, SS 2002, 'CNS demyelination associated with copper deficiency and hyperzincemia.', *Neurology*, vol. 59, no. 9, pp. 1453–6.

Psachoulia, K, Jamen, F, Young, KM, & Richardson, WD 2009, 'Cell cycle dynamics of NG2 cells in the postnatal and ageing brain', *Neuron Glia Biology*, vol. 5, no. 3–4, pp. 57–67.

Psenicka, MW, Smith, BC, Tinkey, RA, & Williams, JL 2021, 'Connecting Neuroinflammation and Neurodegeneration in Multiple Sclerosis: Are Oligodendrocyte Precursor Cells a Nexus of Disease?', *Frontiers in Cellular Neuroscience*, vol. 15, p. 221.

Pugliatti, M, Harbo, H, Holmoy, T, Kampman, M, Myhr, K-M, Riise, T, & Wolfson, C 2008, 'Environmental risk factors in multiple sclerosis', *Acta Neurologica Scandinavica*, vol. 117, pp. 34–40.

Radi, R 2013, 'Protein Tyrosine Nitration: Biochemical Mechanisms and Structural Basis of its Functional Effects', *Accounts of Chemical Research*, vol. 46, no. 2, pp. 550–559.

Raff, MC, Miller, RH, & Noble, M 1983, 'A glial progenitor cell that develops in vitro into an astrocyte or an oligodendrocyte depending on culture medium.', *Nature*, vol. 303, no. 5916, pp. 390–6.

Rajda, C, Pukoli, D, Bende, Z, Majláth, Z, & Vécsei, L 2017, 'Excitotoxins, mitochondrial and redox disturbances in multiple sclerosis', *International Journal of Molecular Sciences*, vol. 18, no. 2, pp. 11–13.

Rakkar, K & Bayraktutan, U 2016, 'Increases in intracellular calcium perturb blood–brain barrier via protein kinase C-alpha and apoptosis', *Biochimica et Biophysica Acta: Molecular Basis of Disease*, vol. 1862, no. 1, pp. 56–71.

Ramesh, G, Maclean, AG, & Philipp, MT 2013, 'Cytokines and Chemokines at the Crossroads of Neuroinflammation, Neurodegeneration, and Neuropathic Pain', *Mediators of Inflammation*, vol. 2013, p. 20.

Ransohoff, RM 2012, 'Animal models of multiple sclerosis: the good, the bad and the bottom line', *Nature Neuroscience*, vol. 15, no. 8, p. 1074.

Readnower, RD, Chavko, M, Adeeb, S, Conroy, MD, Pauly, JR, McCarron, RM, & Sullivan, PG 2010, 'Increase in blood-brain barrier permeability, oxidative stress, and activated microglia in a rat model of blast-induced traumatic brain injury.', *Journal of Neuroscience Research*, vol. 88, no. 16, pp. 3530–3539.

Ren, Y, Liu, T, Song, G, Hu, Y, & Liang, J 2014, 'Determination of lomerizine in human plasma by liquid chromatography/tandem mass spectrometry and its application to a pharmacokinetic study', *Journal of Chromatography B*, vol. 947, pp. 96–102.

Revel, M, Chebath, J, Mangelus, M, Harroch, S, & Moviglia, GA 1995, 'Antagonism of interferon beta on interferon gamma: inhibition of signal transduction in vitro and reduction of serum levels in multiple sclerosis patients.', *Multiple Sclerosis*, vol. 1 Suppl 1, pp. S5-11.

Richter-Landsberg, C 2008, 'The Cytoskeleton in Oligodendrocytes', *Journal of Molecular Neuroscience*, vol. 35, no. 1, pp. 55–63.

Ridderstrom, M & Ohlsson, M 2014, 'Brilliant blue G treatment facilitates regeneration after

optic nerve injury in the adult rat.’, *Neuroreport*, vol. 25, no. 17, pp. 1405–1410.

Riise, T, Nortvedt, MW, & Ascherio, A 2003, ‘Smoking is a risk factor for multiple sclerosis.’, *Neurology*, vol. 61, no. 8, pp. 1122–4.

Rinaldi, C, Donato, L, Alibrandi, S, Scimone, C, D’angelo, R, & Sidoti, A 2021, ‘Oxidative Stress and the Neurovascular Unit’, *Life*, vol. 11, no. 8.

Rivers, LE, Young, KM, Rizzi, M, Jamen, F, Psachoulia, K, Wade, A, Kessaris, N, & Richardson, WD 2008, ‘PDGFRA/NG2 glia generate myelinating oligodendrocytes and piriform projection neurons in adult mice’, *Nature Neuroscience*, vol. 11, no. 12.

Rizwana, N & Agarwal, V 2022, ‘Antioxidant for Neurological Diseases and Neurotrauma and Bioengineering Approaches’, *Antioxidants*, vol. 11, no. 72, pp. 1–24.

Rodríguez-Baeza, A, Reina-De La Torre, F, Poca, A, Martí, M, & Garnacho, A 2003, ‘Morphological features in human cortical brain microvessels after head injury: a three-dimensional and immunocytochemical study’, *The anatomical record. Part A, Discoveries in molecular, cellular, and evolutionary biology*, vol. 273, no. 1, pp. 583–593.

Rohr, SO, Greiner, T, Joost, S, Amor, S, Valk, P van der, Schmitz, C, & Kipp, M 2020, ‘Aquaporin-4 Expression during Toxic and Autoimmune Demyelination’, *Cells*, vol. 9, no. 10.

Rolak, LA 2003, ‘Multiple sclerosis: it’s not the disease you thought it was.’, *Clinical medicine & research*, vol. 1, no. 1, pp. 57–60.

Romeu-Mejia, R, Giza, CC, & Goldman, JT 2019, ‘Concussion Pathophysiology and Injury Biomechanics’, *Current Reviews in Musculoskeletal Medicine*, vol. 12, no. 2, pp. 105–116.

de Rosa, V, Secondo, A, Pannaccione, A, Ciccone, R, Formisano, L, Guida, N, Crispino, R, Fico, A, Polishchuk, R, D’Aniello, A, Annunziato, L, & Boscia, F 2019, ‘D-Aspartate treatment attenuates myelin damage and stimulates myelin repair’, *EMBO Molecular Medicine*, vol. 11, no. 1.

Rosenthal, N & Brown, S 2007, ‘The mouse ascending: Perspectives for human-disease models’, *Nature Cell Biology*, vol. 9, no. 9, pp. 993–999.

Rovaris, M, Confavreux, C, Furlan, R, Kappos, L, Comi, G, & Filippi, M 2006, ‘Secondary progressive multiple sclerosis: current knowledge and future challenges’, *The Lancet Neurology*, vol. 5, no. 4, pp. 343–354.

Rustenhoven, J, Aalderink, M, Scotter, EL, Oldfield, RL, Bergin, PS, Mee, EW, Graham, ES, Faull, RLM, Curtis, MA, Park, TIH, & Dragunow, M 2016, ‘TGF-beta1 regulates human brain pericyte inflammatory processes involved in neurovasculature function’, *Journal of Neuroinflammation*, vol. 13, no. 1, pp. 1–15.

Rustenhoven, J, Jansson, D, Smyth, LC, & Dragunow, M 2017, ‘Brain Pericytes As Mediators of Neuroinflammation’, *Trends in Pharmacological Sciences*, vol. 38, no. 3, pp. 291–304.

Rüther, BJ, Scheld, M, Drey Mueller, D, Clarner, T, Kress, E, Brandenburg, LO,

Swartenbroekx, T, Hoornaert, C, Ponsaerts, P, Fallier-Becker, P, Beyer, C, Rohr, SO, Schmitz, C, Chrzanowski, U, Hochstrasser, T, Nyamoya, S, & Kipp, M 2017, 'Combination of cuprizone and experimental autoimmune encephalomyelitis to study inflammatory brain lesion formation and progression', *Glia*, vol. 65, no. 12, pp. 1900–1913.

Rydell-Törmänen, K & Johnson, JR 2019, 'The Applicability of Mouse Models to the Study of Human Disease', *Methods in Molecular Biology*, vol. 1940, pp. 3–22.

Sadovnick, AD, Eisen, K, Ebers, GC, & Paty, DW 1991, 'Cause of death in patients attending multiple sclerosis clinics.', *Neurology*, vol. 41, no. 8, pp. 1193–6.

Salehi, A, Zhang, JH, & Obenaus, A 2017, 'Response of the cerebral vasculature following traumatic brain injury.', *Journal of Cerebral Blood Flow and Metabolism*, vol. 37, no. 7, pp. 2320–2339.

Salou, M, Garcia, A, Michel, L, Gainche-Salmon, A, Loussouarn, D, Nicol, B, Guillot, F, Hulin, P, Nedellec, S, Baron, D, Ramstein, G, Soullillou, J, Brouard, S, Nicot, AB, Degauque, N, & Laplaud, DA 2015, 'Expanded CD8 T-cell sharing between periphery and CNS in multiple sclerosis', *Annals of clinical and translational neurology*, vol. 2, no. 6, pp. 609–622.

Salou, M, Nicol, B, Garcia, A, & Laplaud, DA 2015, 'Involvement of CD8+ T Cells in Multiple Sclerosis', *Frontiers in Immunology*, vol. 6, no. NOV.

Sandoval, KE & Witt, KA 2008, 'Blood-brain barrier tight junction permeability and ischemic stroke', *Neurobiology of Disease*, vol. 32, no. 2, pp. 200–219.

Sanoobar, M, Dehghan, P, Khalili, M, Azimi, A, & Seifar, F 2015, 'Coenzyme Q10 as a treatment for fatigue and depression in multiple sclerosis patients: A double blind randomized clinical trial', <http://dx.doi.org/10.1179/1476830515Y.0000000002>, vol. 19, no. 3, pp. 138–143.

Sanoobar, M, Egtesadi, S, Azimi, A, Khalili, M, Jazayeri, S, Mahmood, & Gohari, R, & Gohari, MR 2013, 'Coenzyme Q10 supplementation reduces oxidative stress and increases antioxidant enzyme activity in patients with relapsing-remitting multiple sclerosis', *International Journal of Neuroscience*, vol. 123, no. 11, pp. 776–782.

Sanoobar, M, Egtesadi, S, Azimi, A, Khalili, M, Khodadadi, B, Jazayeri, S, Gohari, R, Aryaeian, N, & Gohari, MR 2014, 'Coenzyme Q10 supplementation ameliorates inflammatory markers in patients with multiple sclerosis: a double blind, placebo, controlled randomized clinical trial Coenzyme Q10 supplementation ameliorates inflammatory markers in patients with multiple sclero', *Nutritional Neuroscience*, vol. 18, no. 4, pp. 169–176.

Saunders, NR, Ek, CJ, Habgood, MD, & Dziegielewska, KM 2008, 'Barriers in the brain: A renaissance?', *Trends in Neuroscience*, vol. 31, no. 6, pp. 279–286.

Savaskan, NE, Weinmann, O, Heimrich, B, & Eyupoglu, IY 2009, 'High resolution neurochemical gold staining method for myelin in peripheral and central nervous system at the light-

and electron-microscopic level', *Cell and Tissue Research* 2009 337:2, vol. 337, no. 2, pp. 213–221.

Savic, V, Yin, B, Maas, NL, Bredemeyer, AL, Carpenter, AC, Helmink, BA, Yang-Iott, KS, Sleckman, BP, & Bassing, CH 2009, 'Formation of Dynamic γ -H2AX Domains along Broken DNA Strands Is Distinctly Regulated by ATM and MDC1 and Dependent upon H2AX Densities in Chromatin', *Molecular Cell*, vol. 34, no. 3, pp. 298–310.

Savigni, DL, O'Hare Doig, RL, Szymanski, CR, Bartlett, CA, Lozić, I, Smith, NM, & Fitzgerald, M 2013, 'Three Ca²⁺ channel inhibitors in combination limit chronic secondary degeneration following neurotrauma', *Neuropharmacology*, vol. 75, pp. 380–390.

Scarpello, JH & Howlett, HC 2008, 'Metformin therapy and clinical uses', *Diabetes and Vascular Disease Research*, vol. 5, no. 3, pp. 157–167.

Schröder, M & Kaufman, RJ 2005, 'ER stress and the unfolded protein response', *Mutation Research/Fundamental and Molecular Mechanisms of Mutagenesis*, vol. 569, no. 1–2, pp. 29–63.

Schwab, N, Grenier, K, & Hazrati, LN 2019, 'DNA repair deficiency and senescence in concussed professional athletes involved in contact sports', *Acta Neuropathologica Communications*, vol. 7, no. 1, p. 182.

Schwartz, M 2004, 'Optic nerve crush: Protection and regeneration', *Brain Research Bulletin*, vol. 62, pp. 467–471.

Secchi, C, Carta, M, Crescio, C, Spano, A, Arras, M, Caocci, G, Galimi, F, La Nasa, G, Pippia, P, Turrini, F, & Pantaleo, A 2015, 'T cell tyrosine phosphorylation response to transient redox stress', *Cellular Signalling*, vol. 27, no. 4, pp. 777–788.

Selt, M, Bartlett, CA, Harvey, AR, Dunlop, SA, & Fitzgerald, M 2010, 'Limited restoration of visual function after partial optic nerve injury: A time course study using the calcium channel blocker lomerizine', *Brain Research Bulletin*, vol. 81, pp. 467–471.

Sen, MK, Almuslehi, MSM, Coorssen, JR, Mahns, DA, & Shortland, PJ 2020, 'Behavioural and histological changes in cuprizone-fed mice', *Brain, Behavior, and Immunity*, vol. 87, pp. 508–523.

Sen, MK, Mahns, DA, Coorssen, JR, & Shortland, PJ 2019, 'Behavioural phenotypes in the cuprizone model of central nervous system demyelination', *Neuroscience & Biobehavioral Reviews*, vol. 107, pp. 23–46.

Sengupta, P 2013, 'The Laboratory Rat: Relating Its Age With Human's', *International Journal of Preventive Medicine*, vol. 4, no. 6, p. 624.

Seo, JH, Maki, T, Maeda, M, Miyamoto, N, Liang, AC, Hayakawa, K, Pham, L-DD, Suwa, F, Taguchi, A, Matsuyama, T, Ihara, M, Kim, K-W, Lo, EH, & Arai, K 2014, 'Oligodendrocyte precursor cells support blood-brain barrier integrity via TGF- β signaling.', *PloS one*, vol. 9, no. 7, p. e103174.

Seo, JH, Miyamoto, N, Hayakawa, K, Pham, LDD, Maki, T, Ayata, C, Kim, KW, Lo, EH, & Arai, K 2013, 'Oligodendrocyte precursors induce early blood-brain barrier opening after white matter injury', *Journal of Clinical Investigation*, vol. 123, no. 2, pp. 782–786.

Sharma, V, Collins, LB, Chen, T-H, Herr, N, Takeda, S, Sun, W, Swenberg, JA, & Nakamura, J 2016, 'Oxidative stress at low levels can induce clustered DNA lesions leading to NHEJ mediated mutations.', *Oncotarget*, vol. 7, no. 18, pp. 25377–90.

Sharp, DJ & Jenkins, PO 2015, 'Concussion is confusing us all', *Practical Neurology*, vol. 15, pp. 172–186.

Shelestak, J, Singhal, N, Frankle, L, Tomor, R, Sternbach, S, McDonough, J, Freeman, E, & Clements, R 2020, 'Increased blood-brain barrier hyperpermeability coincides with mast cell activation early under cuprizone administration', *PLoS ONE*, vol. 15, no. 6, p. e0234001.

Shields, DC, Deiber, GE, & Banik, NL 1997, 'Calpain: A mediator of myelin breakdown in demyelinating diseases', *Annals of the New York Academy of Sciences*, vol. 825, no. 1, pp. 128–130.

Sibille, E, Wang, Y, Joeyen-Waldorf, J, Gaiteri, C, Surget, A, Oh, S, Belzung, C, Tseng, GC, & Lewis, DA 2009, 'A molecular signature of depression in the amygdala', *American Journal of Psychiatry*, vol. 166, no. 9, pp. 1011–1024.

Siegert, RJ 2005, 'Depression in multiple sclerosis: a review', *Journal of Neurology, Neurosurgery & Psychiatry*, vol. 76, pp. 469–475.

Sies, H 1997, 'Oxidative stress: oxidants and antioxidants', *Experimental Physiology*, vol. 82, no. 2, pp. 291–295.

Simpson, S, Blizzard, L, Otahal, P, Van der Mei, I, & Taylor, B 2011, 'Latitude is significantly associated with the prevalence of multiple sclerosis: a meta-analysis', *Journal of Neurology, Neurosurgery & Psychiatry*, vol. 82, no. 10, pp. 1132–1141.

Sims, DE 1986, 'The pericyte-A review', *Tissue and Cell*, vol. 18, no. 2, pp. 153–174.

Skogseid, IM, Nordby, HK, Urdal, P, Paus, E, & Lilleaas, F 1992, 'Increased serum creatine kinase BB and neuron specific enolase following head injury indicates brain damage', *Acta Neurochirurgica*, vol. 115, no. 3–4, pp. 106–111.

Skripuletz, T, Gudi, V, Hackstette, D, & Stangel, M 2011, 'De- and remyelination in the CNS white and grey matter induced by cuprizone: The old, the new, and the unexpected', *Histology and Histopathology*, vol. 26, no. 12, pp. 1585–1597.

Smith, NM, Gachulincova, I, Ho, D, Bailey, C, Bartlett, CA, Norret, M, Murphy, J, Buckley, A, Rigby, PJ, House, MJ, St. Pierre, T, Fitzgerald, M, Iyer, KS, & Dunlop, SA 2016, 'An unexpected transient breakdown of the blood brain barrier triggers passage of large intravenously administered nanoparticles', *Scientific Reports*, vol. 6, no. 1, p. 22595.

Smith, NM, Giacci, MK, Gough, A, Bailey, C, McGonigle, T, Black, AM, Clarke, TO,

Bartlett, CA, Swaminathan Iyer, K, Dunlop, SA, & Fitzgerald, M 2018, 'Inflammation and blood-brain barrier breach remote from the primary injury following neurotrauma', *Journal of Neuroinflammation*, vol. 15, no. 1, pp. 1–18.

Smyth, LCD, Rustenhoven, J, Scotter, EL, Schweder, P, Faull, RLM, Park, TIH, & Dragunow, M 2018, 'Markers for human brain pericytes and smooth muscle cells', *Journal of Chemical Neuroanatomy*, vol. 92, pp. 48–60.

Soon, D, Tozer, DJ, Altmann, DR, & Miller, DH 2007, 'Quantification of subtle blood-brain barrier disruption in non-enhancing lesions in multiple sclerosis: a study of disease and lesion subtypes', *ARTICLE Multiple Sclerosis*, vol. 13, pp. 884–894.

Sospedra, M & Martin, R 2005, 'Immunology of Multiple Sclerosis', *Annu. Rev. Immunol.*, vol. 23, pp. 683–747.

Sova, H, Puistola, U, Morin-Papunen, L, & Karihtala, P 2013, 'Metformin decreases serum 8-hydroxy-2'-deoxyguanosine levels in polycystic ovary syndrome', *Fertility and Sterility*, vol. 99, no. 2, pp. 593–598.

Spencer, J 2018, 'Vascular pathology in multiple sclerosis: reframing pathogenesis around the blood-brain barrier', *Journal of Neurology, Neurosurgery, and Psychiatry*, vol. 89, pp. 42–52.

Spitzer, SO, Sitnikov, S, Kamen, Y, & De Faria, O 2019, 'Oligodendrocyte Progenitor Cells Become Regionally Diverse and Heterogeneous with Age', *Neuron*, vol. 101, pp. 459-471.e5.

Srinivasan, R, Sailasuta, N, Hurd, R, Nelson, S, & Pelletier, D 2005, 'Evidence of elevated glutamate in multiple sclerosis using magnetic resonance spectroscopy at 3 T', *Brain*, vol. 128, pp. 1016–1025.

Sriram, S & Steiner, I 2005, 'Experimental Allergic Encephalomyelitis: A Misleading Model of Multiple Sclerosis', *Annals of Neurology*, vol. 58, pp. 939–945.

Staal, JA, Dickson, TC, Gasperini, R, Liu, Y, Foa, L, & Vickers, JC 2010, 'Initial calcium release from intracellular stores followed by calcium dysregulation is linked to secondary axotomy following transient axonal stretch injury', *Journal of Neurochemistry*, vol. 112, no. 5, pp. 1147–1155.

Stamatovic, S, Keep, R, & Andjelkovic, A 2008, 'Brain Endothelial Cell-Cell Junctions: How to "Open" the Blood Brain Barrier', *Current Neuropharmacology*, vol. 6, no. 3, pp. 179–192.

Steelman, AJ, Thompson, JP, & Li, J 2012, 'Demyelination and remyelination in anatomically distinct regions of the corpus callosum following cuprizone intoxication', *Neuroscience Research*, vol. 72, no. 1, pp. 32–42.

Steinman, L 2001, 'Multiple sclerosis: Two-stage disease', *Nature Immunology*, vol. 2, no. 9, pp. 762–764.

Stephenson, E, Nathoo, N, Mahjoub, Y, Dunn, JF, & Wee Yong, V 2014, 'Iron in multiple sclerosis: roles in neurodegeneration and repair', *Nature Publishing Group*, vol. 10, no. 10.

Stidworthy, MF, Genoud, S, Suter, U, Mantei, N, & Franklin, RJM 2003, 'Quantifying the early stages of remyelination following cuprizone-induced demyelination', *Brain Pathology*, vol. 13, no. 3, pp. 329–339.

Stinissen, P & Hellings, N 2008, 'Activation of myelin reactive T cells in multiple sclerosis: A possible role for T cell degeneracy?', *European Journal of Immunology*, vol. 38, pp. 1190–1193.

Stirling, DP, Cummins, K, Wayne Chen, SR, & Stys, P 2014, 'Axoplasmic reticulum Ca²⁺ release causes secondary degeneration of spinal axons', *Annals of Neurology*, vol. 75, no. 2, pp. 220–229.

Stirling, DP & Stys, PK 2010, 'Mechanisms of axonal injury: Internodal nanocomplexes and calcium deregulation', *Trends in Molecular Medicine*, vol. 16, no. 4, pp. 160–170.

Stys, PK, Zamponi, GW, van Minnen, J, & Geurts, JJG 2012, 'Will the real multiple sclerosis please stand up?', *Nature Reviews Neuroscience*, vol. 13, pp. 507–515.

Su, K, Bourdette, D, & Forte, M 2013, 'Mitochondrial dysfunction and neurodegeneration in multiple sclerosis.', *Frontiers in physiology*, vol. 4, p. 169.

Su, M, Yang, Y, & Yang, G 2006, 'Quantitative measurement of hydroxyl radical induced DNA double-strand breaks and the effect of N-acetyl-1-cysteine', *FEBS Letters*, vol. 580, no. 17, pp. 4136–4142.

Sun, SW, Liang, HF, Trinkaus, K, Cross, AH, Armstrong, RC, & Song, SK 2006, 'Noninvasive detection of cuprizone induced axonal damage and demyelination in the mouse corpus callosum', *Magnetic Resonance in Medicine*, vol. 55, no. 2, pp. 302–308.

Supko, JG & Malspeis, L 1995, 'Plasma pharmacokinetics of genistein in mice', *International Journal of Oncology*, vol. 7, no. 4, pp. 847–854.

Sutiwisesak, R, Burns, TC, Rodriguez, M, & Warrington, AE 2021, 'Remyelination therapies for multiple sclerosis: optimizing translation from animal models into clinical trials', *Expert Opinion on Investigational Drugs*, vol. 30, no. 8, pp. 857–876.

Sweeney, MD, Sagare, AP, & Zlokovic, B V. 2018, 'Blood-brain barrier breakdown in Alzheimer disease and other neurodegenerative disorders', *Nature Reviews Neurology*, vol. 14, no. 3, pp. 133–150.

Szabo, C & Ohshima, H 1997, 'DNA Damage Induced by Peroxynitrite: Subsequent Biological Effects', *Biology and Chemistry*, vol. 1, no. 5, pp. 373–385.

Szymanski, CR, Chiha, W, Morellini, N, Cummins, N, Bartlett, CA, O', RL, Doig, H, Savigni, DL, Payne, SC, Harvey, AR, Dunlop, SA, & Fitzgerald, M 2013, 'Paranode abnormalities and oxidative stress in optic nerve vulnerable to secondary degeneration: Modulation by 670 nm light treatment', *PLoS One*, vol. 8, no. 6.

Tagge, I, O'Connor, A, Chaudhary, P, Pollaro, J, Berlow, Y, Chalupsky, M, Bourdette, D,

Woltjer, R, Johnson, M, & Rooney, W 2016, 'Spatio-temporal patterns of demyelination and remyelination in the cuprizone mouse model', *PLoS ONE*, vol. 11, no. 4, pp. 1–24.

Takahashi, M, Kohara, A, Shishikura, J-I, Kawasaki-Yatsugi, S, Ni, JW, Yatsugi, S-I, Sakamoto, S, Okada, M, Shimizu-Sasamata, M, & Yamaguchi, T 2002, 'YM872: A selective, potent and highly water-soluble alpha-amino-3-hydroxy-5-methylisoxazole-4-propionic acid receptor antagonist', *CNS Drug Reviews*, vol. 8, no. 4, pp. 337–352.

Takahashi, M & Wei, JN 1998, 'Neuroprotective efficacy of YM872, an alpha-amino-3-hydroxy-5- methylisoxazole-4-propionic acid receptor antagonist, after permanent middle cerebral artery occlusion in rats', *Journal of Pharmacology and Experimental Therapeutics*, vol. 287, no. 2, pp. 559–566.

Tanner, DC, Cherry, JD, & Mayer-Pröschel, M 2011, 'Oligodendrocyte progenitors reversibly exit the cell cycle and give rise to astrocytes in response to interferon- γ .', *Journal of Neuroscience*, vol. 31, no. 16, pp. 6235–46.

Taraboletti, A, Walker, T, Avila, R, Huang, H, Caporoso, J, Manandhar, E, Leeper, TC, Modarelli, DA, Medicetty, S, & Shriver, LP 2017, 'Cuprizone Intoxication Induces Cell Intrinsic Alterations in Oligodendrocyte Metabolism Independent of Copper Chelation', *Biochemistry*, vol. 56, no. 10, pp. 1518–1528.

Taylor, LC, Gilmore, W, Ting, JPY, & Matsushima, GK 2010, 'Cuprizone induces similar demyelination in male and female C57BL/6 mice and results in disruption of the estrous cycle', *Journal of Neuroscience Research*, vol. 88, no. 2, pp. 391–402.

Thelin, EP, Nelson, DW, & Bellander, BM 2016, 'A review of the clinical utility of serum S100B protein levels in the assessment of traumatic brain injury', *Acta Neurochirurgica 2016 159:2*, vol. 159, no. 2, pp. 209–225.

Thelin, EP, Zeiler, FA, Ercole, A, Mondello, S, Büki, A, Bellander, BM, Helmy, A, Menon, DK, & Nelson, DW 2017, 'Serial sampling of serum protein biomarkers for monitoring human traumatic brain injury dynamics: A systematic review', *Frontiers in Neurology*, vol. 8, p. 300.

Thompson, AJ, Banwell, BL, Barkhof, F, Carroll, WM, Coetzee, T, Comi, G, Correale, J, Fazekas, F, Filippi, M, Freedman, MS, Fujihara, K, Galetta, SL, Hartung, HP, Kappos, L, Lublin, FD, Marrie, RA, Miller, AE, Miller, DH, Montalban, X, Mowry, EM, Sorensen, PS, Tintoré, M, Traboulsee, AL, Trojano, M, Uitdehaag, BMJ, Vukusic, S, Waubant, E, Weinshenker, BG, Reingold, SC, & Cohen, JA 2018, 'Diagnosis of multiple sclerosis: 2017 revisions of the McDonald criteria', *The Lancet Neurology*, vol. 17, no. 2, pp. 162–173.

Thorburne, SK & Juurlink, BH 1996, 'Low glutathione and high iron govern the susceptibility of oligodendroglial precursors to oxidative stress', *Journal of Neurochemistry*, vol. 67, no. 3, pp. 1014–1022.

Titus, HE, Chen, Y, Podojil, JR, Robinson, AP, Balabanov, R, Popko, B, & Miller, SD 2020, 'Pre-clinical and Clinical Implications of "Inside-Out" vs. "Outside-In" Paradigms in Multiple Sclerosis Etiopathogenesis', *Frontiers in Cellular Neuroscience*, vol. 14.

Toomey, LM, Bartlett, CA, Gavriel, N, McGonigle, T, Majimbi, M, Gopalasingam, G, Rodger, J, & Fitzgerald, M 2019, 'Comparing modes of delivery of a combination of ion channel inhibitors for limiting secondary degeneration following partial optic nerve transection', *Scientific Reports 2019 9:1*, vol. 9, no. 1, pp. 1–10.

Toomey, LM, Bartlett, CA, Rodger, J, & Fitzgerald, M 2018, 'Comparison of ion channel inhibitor combinations for limiting secondary degeneration following partial optic nerve transection', *Experimental Brain Research*, vol. 237, no. 1, pp. 161–171.

Toomey, LM, Papini, M, Lins, B, Wright, AJ, Warnock, A, McGonigle, T, Hellewell, SC, Bartlett, CA, Anyaegbu, C, & Fitzgerald, M 2021, 'Cuprizone feed formulation influences the extent of demyelinating disease pathology', *Scientific Reports*, vol. 11, no. 1, pp. 1–16.

Torkildsen, Brunborg, LA, Myhr, KM, & Bø, L 2008, 'The cuprizone model for demyelination', *Acta Neurologica Scandinavica*, vol. 117, pp. 72–76.

Torres-Gonzalez, M, Gawlowski, T, Kocalis, H, Scott, BT, & Dillmann, WH 2014, 'Mitochondrial 8-oxoguanine glycosylase decreases mitochondrial fragmentation and improves mitochondrial function in H9C2 cells under oxidative stress conditions.', *American Journal of Physiology*, vol. 306, no. 3, pp. 221–229.

Tran, H, Mittal, A, Sagi, V, Luk, K, Nguyen, A, Gupta, M, Nguyen, J, Lamarre, Y, Lei, J, Guedes, A, & Gupta, K 2019, 'Mast Cells Induce Blood Brain Barrier Damage in SCD by Causing Endoplasmic Reticulum Stress in the Endothelium', *Frontiers in Cellular Neuroscience*, vol. 13, pp. 1–12.

Trapp, BD & Nave, K-A 2008, 'Multiple Sclerosis: An immune or neurodegenerative disorder?', *The Annual Review of Neuroscience*, vol. 31, pp. 247–269.

Tremlett, H, Zhao, Y, & Devonshire, V 2008, 'Natural history of secondary-progressive multiple sclerosis', *Multiple Sclerosis*, vol. 14, pp. 314–324.

Trojano, M, Avolio, C, Manzari, C, Calò, A, De Robertis, F, Serio, G, & Livrea, P 1995, 'Multivariate analysis of predictive factors of multiple sclerosis course with a validated method to assess clinical events.', *Journal of Neurology, Neurosurgery & Psychiatry*, vol. 58, no. 3, pp. 300–6.

Tsai, JJ, Wu, T, Leung, H, Desudchit, T, Tiamkao, S, Lim, KS, & Dash, A 2018, 'Perampanel, an AMPA receptor antagonist: From clinical research to practice in clinical settings', *Acta Neurologica Scandinavica*, vol. 137, no. 4, pp. 378–391.

Tse, K-H, Cheng, A, Ma, F, & Herrup, K 2018, 'DNA damage-associated oligodendrocyte degeneration precedes amyloid pathology and contributes to Alzheimer's disease and dementia',

Alzheimer's & Dementia, vol. 14, no. 5, pp. 664–679.

Tsuchiya, M, Nijima-Yaoita, F, Yoneda, H, Chiba, K, Tsuchiya, S, Hagiwara, Y, Sasaki, K, Sugawara, S, Endo, Y, Tan-No, K, & Watanabe, M 2014, 'Long-term feeding on powdered food causes hyperglycemia and signs of systemic illness in mice', *Life Sciences*, vol. 103, no. 1, pp. 8–14.

Ttir, RK, Hamilton, NB, Bakiri, Y, Attwell, D, Káradóttir, R, Hamilton, NB, Bakiri, Y, & Attwell, D 2008, 'Spiking and nonspiking classes of oligodendrocyte precursor glia in CNS white matter', *Nature Neuroscience*, vol. 11, no. 4.

Turtzo, LC, Jikaria, N, Cota, MR, Williford, JP, Uche, V, Davis, T, MacLaren, J, Moses, AD, Parikh, G, Castro, MA, Pham, DL, Butman, JA, & Latour, LL 2020, 'Meningeal blood–brain barrier disruption in acute traumatic brain injury', *Brain Communications*, vol. 2, no. 2.

Uberti, D, Yavin, E, Gil, S, Ayasola, K, Goldfinger, N, & Rotter, V 1999, 'Hydrogen peroxide induces nuclear translocation of p53 and apoptosis in cells of oligodendroglia origin', *Molecular Brain Research*, vol. 65, pp. 167–175.

Ülger, H, Karabulut, AK, & Pratten, MK 2002, 'Labelling of rat endothelial cells with antibodies to vWF, RECA-1, PECAM-1, ICAM-1, OX-43 and ZO-1', *Anatomia, histologia, embryologia*, vol. 31, no. 1, pp. 31–35.

Underwood, EL, Redell, JB, Maynard, ME, Kobori, N, Hylin, MJ, Hood, KN, West, RK, Zhao, J, Moore, AN, & Dash, PK 2021, 'Metformin Reduces Repeat Mild Concussive Injury Pathophysiology', *eNeuro*.

Uranova, N, Orlovskaya, D, Vikhрева, O, Zimina, I, Kolomeets, N, Vostrikov, V, & Rachmanova, V 2001, 'Electron microscopy of oligodendroglia in severe mental illness.', *Brain Research Bulletin*, vol. 55, no. 5, pp. 597–610.

Uzunalli, G, Herr, S, Dieterly, AM, Shi, R, & Lyle, LT 2021, 'Structural disruption of the blood-brain barrier in repetitive primary blast injury', *Fluids and barriers of the CNS*, vol. 18, no. 1.

Valavanidis, A, Vlachogianni, T, & Fiotakis, C 2009, '8-hydroxy-2-deoxyguanosine (8-OHdG): A critical biomarker of oxidative stress and carcinogenesis', *Journal of Environmental Science and Health*, vol. 27, pp. 120–139.

Varatharaj, A & Galea, I 2017, 'The blood-brain barrier in systemic inflammation', *Brain, Behavior, and Immunity*, vol. 60, pp. 1–12.

Vasquez-Vivar, J, Kalyanaraman, B, & Kennedy, MC 2000, 'Mitochondrial aconitase is a source of hydroxyl radical. An electron spin resonance investigation.', *Journal of Biological Chemistry*, vol. 275, no. 19, pp. 14064–9.

Vega-Riquer, JM, Mendez-Victoriano, G, Morales-Luckie, RA, & Gonzalez-Perez, O 2019, 'Five Decades of Cuprizone, an Updated Model to Replicate Demyelinating Diseases', *Current Neuropharmacology*, vol. 17, no. 2, pp. 129–141.

Vercellino, M, Merola, A, Piacentino, C, Votta, B, Capello, E, Mancardi, GL, Mutani, R, Giordana, MT, & Cavalla, P 2007, 'Altered glutamate reuptake in relapsing-remitting and secondary progressive multiple sclerosis cortex: Correlation with microglia infiltration, demyelination, and neuronal and synaptic damage', *Journal of Neuropathology and Experimental Neurology*, vol. 66, no. 8, pp. 732–739.

Verkhratsky, A & Kettenmann, H 1996, 'Calcium signaling in glia', *Glia*, vol. 19, no. 8, pp. 346–352.

Verkhratsky, A & Nedergaard, M 2018, 'Physiology of Astroglia', *Physiology of Astroglia. Physiol Rev*, vol. 98, pp. 239–389.

Vignali, DAA 2000, 'Multiplexed particle-based flow cytometric assays', *Journal of Immunological Methods*, vol. 243, no. 1–2, pp. 243–255.

Vink, R 2018, 'Large animal models of traumatic brain injury', *Journal of Neuroscience Research*, vol. 96, no. 4, pp. 527–535.

Vos, CMP, Geurts, JJG, Montagne, L, van Haastert, ES, Bö, L, van der Valk, P, Barkhof, F, & de Vries, HE 2005, 'Blood–brain barrier alterations in both focal and diffuse abnormalities on postmortem MRI in multiple sclerosis', *Neurobiology of Disease*, vol. 20, no. 3, pp. 953–960.

Vukusic, S & Confavreux, C 2003, 'Prognostic factors for progression of disability in the secondary progressive phase of multiple sclerosis', *Journal of the Neurological Sciences*, vol. 206, no. 2, pp. 135–137.

Vuolo, F, Petronilho, F, Sonai, B, Ritter, C, Hallak, JEC, Zuardi, AW, Crippa, JA, & Dal-Pizzol, F 2015, 'Evaluation of Serum Cytokines Levels and the Role of Cannabidiol Treatment in Animal Model of Asthma', *Mediators of Inflammation*, pp. 1–5.

Walls, GL 1942, *The Vertebrate Eye and its Adaptive Radiation*. Hafner, New York.

Wang, HL & Lai, TW 2014, 'Optimization of Evans blue quantitation in limited rat tissue samples', *Scientific Reports 2014 4:1*, vol. 4, no. 1, pp. 1–7.

Wang, HN, Liu, GH, Zhang, RG, Xue, F, Wu, D, Chen, YC, Peng, Y, Peng, ZW, & Tan, QR 2016, 'Quetiapine Ameliorates Schizophrenia-Like Behaviors and Protects Myelin Integrity in Cuprizone Intoxicated Mice: The Involvement of Notch Signaling Pathway', *International Journal of Neuropsychopharmacology*, vol. 19, no. 2.

Wang, K, Song, F, Fernandez-Escobar, A, Luo, G, Wang, JH, & Sun, Y 2018, 'The Properties of Cytokines in Multiple Sclerosis: Pros and Cons', *The American Journal of the Medical Sciences*, vol. 356, no. 6, pp. 552–560.

Wang, KKW, Larner, SF, Robinson, G, & Hayes, RL 2006, 'Neuroprotection targets after traumatic brain injury', *Current Opinion in Neurology*, vol. 19, pp. 514–519.

Wang, P, Sui, HJ, Li, XJ, Bai, LN, Bi, J, & Lai, H 2021, 'Melatonin ameliorates microvessel

abnormalities in the cerebral cortex and hippocampus in a rat model of Alzheimer's disease', *Neural Regeneration Research*, vol. 16, no. 4, p. 757.

Wang, Qilong, Zhang, M, Torres, G, Wu, S, Ouyang, C, Xie, Z, & Zou, M-H 2017, 'Metformin Suppresses Diabetes-Accelerated Atherosclerosis via the Inhibition of Drp1-Mediated Mitochondrial Fission.', *Diabetes*, vol. 66, no. 1, pp. 193–205.

Wang, Y-C, Cui, Y, Cui, J-Z, Sun, L-Q, Cui, C-M, Zhang, H-A, Zhu, H-X, Li, R, Tian, Y-X, & Gao, J-L 2015, 'Neuroprotective effects of brilliant blue G on the brain following traumatic brain injury in rats', *Molecular Medicine Reports*, vol. 12, no. 2, pp. 2149–2154.

Wang, Yi-Wei, He, S-J, Feng, X, Cheng, J, Luo, Y-T, Tian, L, & Huang, Q 2017, 'Metformin: a review of its potential indications.', *Drug Design, Development and Therapy*, vol. 11, pp. 2421–2429.

Watts, ME, Pocock, R, & Claudianos, C 2018, 'Brain energy and oxygen metabolism: Emerging role in normal function and disease', *Frontiers in Molecular Neuroscience*, vol. 11, p. 216.

Weber, JT 2012, 'Altered Calcium Signaling Following Traumatic Brain Injury', *Frontiers in Pharmacology*, vol. 3, p. 60.

Weiland, NG, Orikasa, C, Hayashi, S, & McEwen, BS 1997, 'Distribution and hormone regulation of estrogen receptor immunoreactive cells in the hippocampus of male and female rats', *The Journal of Comparative Neurobiology*, vol. 388, no. 4, pp. 603–612.

Weiner, HL 2009, 'The challenge of multiple sclerosis: How do we cure a chronic heterogeneous disease?', *Annals of Neurology*, vol. 65, no. 3, pp. 239–248.

Weinshenker, BG, Bass, B, Rice, GP, Noseworthy, J, Carriere, W, Baskerville, J, & Ebers, GC 1989, 'The natural history of multiple sclerosis: a geographically based study. I. Clinical course and disability.', *Brain*, vol. 112, no. 1, pp. 133–46.

Weiskirchen, S, Weiper, K, Tolba, RH, & Weiskirchen, R 2020, 'All You Can Feed: Some Comments on Production of Mouse Diets Used in Biomedical Research with Special Emphasis on Non-Alcoholic Fatty Liver Disease Research', *Nutrients 2020, Vol. 12, Page 163*, vol. 12, no. 1, p. 163.

Wekerle, H & Kurschus, FC 2006, 'Animal models of multiple sclerosis', *Drug Discovery Today: Disease Models*, vol. 3, no. 4, pp. 359–367.

Wells, J, Kilburn, MR, Shaw, JA, Bartlett, CA, Harvey, AR, Dunlop, SA, & Fitzgerald, M 2012, 'Early in vivo changes in calcium ions, oxidative stress markers, and ion channel immunoreactivity following partial injury to the optic nerve', *Journal of Neuroscience Research*, vol. 90, no. 3, pp. 606–618.

Wens, I, Dalgas, U, Vandenabeele, F, Krekels, M, Grevendonk, L, & Eijnde, BO 2014, 'Multiple Sclerosis Affects Skeletal Muscle Characteristics', *PLOS ONE*, vol. 9, no. 9, p. e108158.

Werner, P, Pitt, D, & Raine, CS 2001, 'Multiple sclerosis: Altered glutamate homeostasis in lesions correlates with oligodendrocyte and axonal damage', *Annals of Neurology*, vol. 50, no. 2, pp. 169–180.

Witte, ME, Schumacher, AM, Mahler, CF, Bewersdorf, JP, Lehmitz, J, Scheiter, A, Sánchez, P, Williams, PR, Griesbeck, O, Naumann, R, Misgeld, T, & Kerschensteiner, M 2019, 'Calcium Influx through Plasma-Membrane Nanoruptures Drives Axon Degeneration in a Model of Multiple Sclerosis', *Neuron*, vol. 101, no. 4, pp. 615-624.e5.

Wolf, JA, Stys, PK, Lusardi, T, Meaney, D, & Smith, DH 2001, 'Traumatic axonal injury induces calcium influx modulated by tetrodotoxin-sensitive sodium channels', *Journal of Neuroscience*, vol. 21, no. 6, pp. 1923–1930.

Wong, HE, Qi, W, Choi, H-M, Fernandez, EJ, & Kwon, I 2011, 'A safe, blood-brain barrier permeable triphenylmethane dye inhibits amyloid- β neurotoxicity by generating nontoxic aggregates', *ACS Chemical Neuroscience*, vol. 2, pp. 645–657.

Woodbine, L, Brunton, H, Goodarzi, AA, Shibata, A, & Jeggo, PA 2011, 'Endogenously induced DNA double strand breaks arise in heterochromatic DNA regions and require ataxia telangiectasia mutated and Artemis for their repair.', *Nucleic acids research*, vol. 39, no. 16, pp. 6986–97.

van der Worp, HB, Howells, DW, Sena, ES, Porritt, MJ, Rewell, S, O'Collins, V, & Macleod, MR 2010, 'Can Animal Models of Disease Reliably Inform Human Studies?', *PLOS Medicine*, vol. 7, no. 3, p. e1000245.

Wu, QZ, Yang, Q, Cate, HS, Kemper, D, Binder, M, Wang, HX, Fang, K, Quick, MJ, Marriott, M, Kilpatrick, TJ, & Egan, GF 2008, 'MRI identification of the rostral-caudal pattern of pathology within the corpus callosum in the cuprizone mouse model', *Journal of Magnetic Resonance Imaging*, vol. 27, no. 3, pp. 446–453.

Xie, M, Tobin, JE, Budde, MD, Chen, CI, Trinkaus, K, Cross, AH, McDaniel, DP, Song, SK, & Armstrong, RC 2010, 'Rostrocaudal analysis of corpus callosum demyelination and axon damage across disease stages refines diffusion tensor imaging correlations with pathological features', *Journal of Neuropathology and Experimental Neurology*, vol. 69, no. 7, pp. 704–716.

Xing, YL, Röth, PT, Stratton, JAS, Chuang, BHA, Danne, J, Ellis, SL, Ng, SW, Kilpatrick, TJ, & Merson, TD 2014, 'Adult neural precursor cells from the subventricular zone contribute significantly to oligodendrocyte regeneration and remyelination', *Journal of Neuroscience*, vol. 34, no. 42, pp. 14128–14146.

Xu, C, Bailly-Maitre, B, & Reed, JC 2005, 'Endoplasmic reticulum stress: cell life and death decisions', *Journal of Clinical Investigation*, vol. 115, no. 10, pp. 2656–2664.

Xu, H, Yang, H-J, McConomy, B, Browning, R, & Li, X-M 2010, 'Behavioral and

neurobiological changes in C57BL/6 mouse exposed to cuprizone: effects of antipsychotics’, *Frontiers in Behavioral Neuroscience*, vol. 4, p. 8.

Xu, H, Yang, H-J, Zhang, Y, Clough, R, Browning, R, & Li, X-M 2009, ‘Behavioral and neurobiological changes in C57BL/6 mice exposed to cuprizone.’, *Behavioral Neuroscience*, vol. 123, no. 2, pp. 418–429.

Xu, L, Kong, L, Wang, J, & Ash, JD 2018, ‘Stimulation of AMPK prevents degeneration of photoreceptors and the retinal pigment epithelium’, *Proceedings of the National Academy of Sciences of the United States of America*, vol. 115, no. 41, pp. 10475–10480.

Xu, L, Nirwane, A, & Yao, Y 2019, ‘Basement membrane and blood-brain barrier’, *Stroke and Vascular Neurology*, vol. 4, no. 2, pp. 78–82.

Yakimov, V, Schweiger, F, Zhan, J, Behrangi, N, Horn, A, Schmitz, C, Hochstrasser, T, & Kipp, M 2019, ‘Continuous cuprizone intoxication allows active experimental autoimmune encephalomyelitis induction in C57BL/6 mice’, *Histochemistry and Cell Biology*, vol. 152, no. 2, pp. 119–131.

Yamada, C, Harada, K, Shimamoto, A, Sugimoto, H, Nishimura, N, & Sukamoto, H 1997, ‘Effects of lomerizine on cerebral blood flow and systemic arterial blood pressure in anesthetized dogs’, *Japanese Journal of Pharmacology*, vol. 25, pp. 797–802.

Yang, PK, Chou, CH, Chang, CH, Chen, SU, Ho, HN, & Chen, MJ 2020, ‘Changes in peripheral mitochondrial DNA copy number in metformin-treated women with polycystic ovary syndrome: A longitudinal study’, *Reproductive Biology and Endocrinology*, vol. 18, no. 1, pp. 1–10.

Yang, Q-K, Xiong, J-X, & Yao, Z-X 2013, ‘Neuron-NG2 cell synapses: novel functions for regulating NG2 cell proliferation and differentiation.’, *BioMed Research International*, vol. 2013, p. 402843.

Yates, Nathanael J., Lydiard, S, Fehily, B, Weir, G, Chin, A, Bartlett, CA, Alderson, J, & Fitzgerald, M 2017, ‘Repeated mild traumatic brain injury in female rats increases lipid peroxidation in neurons’, *Experimental Brain Research*, vol. 235, no. 7, pp. 2133–2149.

Yates, Richard L., Esiri, MM, Palace, J, Jacobs, B, Perera, R, & DeLuca, GC 2017, ‘Fibrin(ogen) and neurodegeneration in the progressive multiple sclerosis cortex’, *Annals of Neurology*, vol. 82, no. 2, pp. 259–270.

Yeung, MSY, Djelloul, M, Steiner, E, Bernard, S, Salehpour, M, Possnert, G, Brundin, L, & Frisén, J 2019, ‘Dynamics of oligodendrocyte generation in multiple sclerosis’, *Nature*, vol. 566, no. 7745, pp. 538–542.

Yu, Q, Hui, R, Park, J, Huang, Y, Kusnecov, AW, Dreyfus, CF, & Zhou, R 2017, ‘Strain differences in cuprizone induced demyelination.’, *Cell & Bioscience*, vol. 7, p. 59.

Zarini, D, Pasbakhsh, P, Nekoonam, S, Mojaverrostami, S, Ghasemi, S, Shabani, M, &

Kashani, IR 2021, 'Protective Features of Calorie Restriction on Cuprizone-induced Demyelination via Modulating Microglial Phenotype', *Journal of Chemical Neuroanatomy*, vol. 116, p. 102013.

Zatta, P, Raso, M, Zambenedetti, P, Wittkowski, W, Messori, L, Piccioli, F, Mauri, PL, & Beltramini, M 2005, 'Copper and zinc dismetabolism in the mouse brain upon chronic cuprizone treatment', *Cellular and Molecular Life Sciences*, vol. 62, pp. 1502–1513.

Zehendner, CM, Sebastiani, A, Hugonnet, A, Bischoff, F, Luhmann, HJ, & Thal, SC 2015, 'Traumatic brain injury results in rapid pericyte loss followed by reactive pericytosis in the cerebral cortex', *Scientific Reports*, vol. 5.

Zeis, T, Enz, L, & Schaeren-Wiemers, N 2016, 'The immunomodulatory oligodendrocyte', *Brain Research*, vol. 1641, pp. 139–148.

Zeis, T, Graumann, U, Reynolds, R, & Schaeren-Wiemers, N 2007, 'Normal-appearing white matter in multiple sclerosis is in a subtle balance between inflammation and neuroprotection', *Brain*, vol. 131, no. 1, pp. 288–303.

Zhan, J, Fegg, FN, Kaddatz, H, Rühling, S, Frenz, J, Denecke, B, Amor, S, Ponsaerts, P, Hochstrasser, T, & Kipp, M 2021, 'Focal white matter lesions induce long-lasting axonal degeneration, neuroinflammation and behavioral deficits', *Neurobiology of Disease*, vol. 155, p. 105371.

Zhan, J, Mann, T, Joost, S, Behrangi, N, Frank, M, & Kipp, M 2020, 'The Cuprizone Model: Dos and Do Nots', *Cells*, vol. 9, no. 4, p. 843.

Zhang, Q-G, Laird, MD, Han, D, Nguyen, K, Scott, E, Dong, Y, Dhandapani, KM, & Brann, DW 2012, 'Critical Role of NADPH Oxidase in Neuronal Oxidative Damage and Microglia Activation following Traumatic Brain Injury', *PLoS ONE*, vol. 7, no. 4, p. e34504.

Zhang, Y, Xu, H, Jiang, W, Xiao, L, Yan, B, He, J, Wang, Y, Bi, X, Li, X, Kong, J, & Li, X-M 2008, 'Quetiapine alleviates the cuprizone-induced white matter pathology in the brain of C57BL/6 mouse', *Schizophrenia Research*, vol. 106, no. 2–3, pp. 182–191.

Zhang, Z & David, G 2015, 'Stimulation-induced Ca²⁺ influx at nodes of Ranvier in mouse peripheral motor axons', *The Journal of Physiology*, vol. 594, no. 1, pp. 39–57.

Zhao, Z, Li, T, Dong, X, Wang, X, Zhang, Z, Zhao, C, Kang, X, Zheng, R, & Li, X 2021, 'Untargeted Metabolomic Profiling of Cuprizone-Induced Demyelination in Mouse Corpus Callosum by UPLC-Orbitrap/MS Reveals Potential Metabolic Biomarkers of CNS Demyelination Disorders', *Oxidative Medicine and Cellular Longevity*, vol. 2021.

Zheng, F, Lin, Y, & Boulas, P 2021, 'Development and validation of a novel HILIC method for the quantification of low-levels of cuprizone in cuprizone-containing chow', *Scientific reports*, vol. 11, no. 1, p. 17995.

Zhong, H & Yin, H 2015, 'Role of lipid peroxidation derived 4-hydroxynonenal (4-HNE) in

cancer: Focusing on mitochondria', *Redox Biology*, vol. 4, pp. 193–199.

Zhou, X, Qian, Y, Yuan, D, Feng, Q, & He, P 2019, 'H₂O₂-induced microvessel barrier dysfunction: the interplay between reactive oxygen species, nitric oxide, and peroxynitrite', *Physiological Reports*, vol. 7, no. 16, p. 14206.

Zhou, X, Yuan, D, Wang, M, & He, P 2013, 'H₂O₂-induced endothelial NO production contributes to vascular cell apoptosis and increased permeability in rat venules', *American Journal of Physiology - Heart and Circulatory Physiology*, vol. 304, no. 1, p. H82.

Zhu, X, Bergles, DE, & Nishiyama, A 2008, 'NG2 cells generate both oligodendrocytes and gray matter astrocytes.', *Development*, vol. 135, no. 1, pp. 145–57.

Ziabreva, I, Campbell, G, Rist, J, Zamboni, J, Rorbach, J, Wydro, MM, Lassmann, H, Franklin, RJM, & Mahad, D 2010, 'Injury and differentiation following inhibition of mitochondrial respiratory chain complex IV in rat oligodendrocytes', *Glia*, vol. 58, no. 15, pp. 1827–1837.

Zibara, K, Ballout, N, Mondello, S, Karnib, N, Ramadan, N, Omais, S, Nabbouh, A, Caliz, D, Clavijo, A, Hu, Z, Ghanem, N, Gajavelli, S, & Kobeissy, F 2019, 'Combination of drug and stem cells neurotherapy: Potential interventions in neurotrauma and traumatic brain injury', *Neuropharmacology*, vol. 145, pp. 177–198.

Ziebell, JM & Morganti-Kossmann, MC 2010, 'Involvement of Pro-and Anti-Inflammatory Cytokines and Chemokines in the Pathophysiology of Traumatic Brain Injury', *Neurotherapeutics*, vol. 7, pp. 22–30.

Zimmermann, T, Marrison, J, & Hogg, K 2014, 'Clearing Up the Signal: Spectral Imaging and Linear Unmixing in Fluorescence Microscopy', *Methods in Molecular Biology*, vol. 1075, pp. 129–148.

Zirngibl, M, Assinck, P, Sizov, A, Caprariello, A V., & Plemel, JR 2022, 'Oligodendrocyte death and myelin loss in the cuprizone model: an updated overview of the intrinsic and extrinsic causes of cuprizone demyelination', *Molecular Neurodegeneration* 2022 17:1, vol. 17, no. 1, pp. 1–28. Available from: <https://moleculareneurodegeneration.biomedcentral.com/articles/10.1186/s13024-022-00538-8>. [8 February 2023].

Zlokovic, B V. 2005, 'Neurovascular mechanisms of Alzheimer's neurodegeneration', *Trends in Neurosciences*, vol. 28, no. 4, pp. 202–208.

Every reasonable effort has been made to acknowledge the owners of copyright material. I would be pleased to hear from any copyright owner who has been omitted or incorrectly acknowledged.

Appendix A. Introducing “Comparing modes of delivery of a combination of ion channel inhibitors for limiting secondary degeneration following partial optic nerve transection”

As discussed in Chapter 2, during my candidature I was involved in work that successfully employed a combinatorial treatment of ion channel inhibitors for attenuating pathology in the partial optic nerve transection model of neurotrauma. For this study, the ion channel inhibitor combination employed comprised of lomerizine, YM872 and BBG to target VGCCs, AMPA receptors and P2X₇ receptors respectively for limiting excess intracellular Ca²⁺ influx. When rats were treated with this ion channel inhibitor combination for 3 days following a partial optic nerve transection, myelin structure was significantly preserved compared to vehicle treated injured rats. No effect of treatment was observed for preventing inflammation, either locally or in the periphery, nor for ameliorating the decreased density of oligodendroglia with injury. This study is presented below and has been published as:

Toomey L.M., Bartlett C.A., Gavriel N., McGonigle, T., Majimbi M., Gopalasingam G., Rodger J., Fitzgerald M. 2019. Comparing modes of delivery of a combination of ion channel inhibitors for limiting secondary degeneration following partial optic nerve transection. *Scientific Reports* 9: 1-10. doi.org/10.1038/s41598-019-51886-3

OPEN

Comparing modes of delivery of a combination of ion channel inhibitors for limiting secondary degeneration following partial optic nerve transection

Lillian M. Toomey^{1,2,3}, Carole A. Bartlett¹, Nikolas Gavriel¹, Terence McGonigle², Maimuna Majimbi², Gopana Gopalasingam¹, Jennifer Rodger^{1,3} & Melinda Fitzgerald^{1,2,3*}

Injury to the central nervous system is exacerbated by secondary degeneration. Previous research has shown that a combination of orally and locally administered ion channel inhibitors following partial optic nerve injury protects the myelin sheath and preserves function in the ventral optic nerve, vulnerable to secondary degeneration. However, local administration is often not clinically appropriate. This study aimed to compare the efficacy of systemic and local delivery of the ion channel inhibitor combination of lomerizine, brilliant blue G (BBG) and YM872, which inhibits voltage-gated calcium channels, P2X₂ receptors and Ca²⁺ permeable α -amino-3-hydroxy-5-methyl-4-isoxazolepropionic acid (AMPA) receptors respectively. Following a partial optic nerve transection, adult female PVG rats were treated with BBG and YM872 delivered *via* osmotic mini pump directly to the injury site, or *via* intraperitoneal injection, both alongside oral administration of lomerizine. Myelin structure was preserved with both delivery modes of the ion channel inhibitor combination. However, there was no effect of treatment on inflammation, either peripherally or at the injury site, or on the density of oligodendroglial cells. Taken together, the data indicate that even at lower concentrations, the combinatorial treatment may be preserving myelin structure, and that systemic and local delivery are comparable at improving outcomes following neurotrauma.

Damage to the CNS, known as neurotrauma¹, occurs in the context of traumatic brain and spinal cord injuries as well as optic neuropathy, leading to substantial loss of function for which there is currently no effective therapy. Cells adjacent to the injury site are vulnerable to secondary degeneration, a self-propagating cascade of reactive pathways characterised by glutamate- and ATP-induced excitotoxicity, intracellular Ca²⁺ overload, oxidative stress, microglial and macrophage activation and infiltration, dysmyelination and cellular apoptosis^{2–4}. Secondary degeneration has been shown to spread to initially undamaged tissue and is associated with chronic functional loss⁵. Therefore, therapeutic strategies to minimise damage following neurotrauma need to limit this secondary degeneration of tissue adjacent to the primary injury.

In order to develop effective treatments for limiting secondary degeneration, therapeutics need to be trialled in appropriate animal models of injury, and partial optic nerve transection has been utilised for this purpose. In this model, the right dorsal optic nerve of rats is partially transected leaving the ventral nerve vulnerable to secondary degeneration, and allowing for spatial segregation between the primary and secondary injury sites^{6,7}. This particular model has been utilised in pre-clinical studies whereby therapeutics for secondary degeneration are directly delivered to the injury site *via* an implanted osmotic mini-pump drug delivery system^{5,8–10}.

¹Experimental and Regenerative Neurosciences, School of Biological Sciences, The University of Western Australia, 35 Stirling Hwy, Perth, 6009, Western Australia, Australia. ²Curtin Health Innovation Research Institute, Curtin University, Sarich Neuroscience Research Institute Building, 8 Verdun St, Nedlands, 6009, Western Australia, Australia. ³Perron Institute for Neurological and Translational Science, Sarich Neuroscience Research Institute Building, 8 Verdun St, Nedlands, 6009, Western Australia, Australia. *email: lindy.fitzgerald@curtin.edu.au

Following milder injuries to the central nervous system there is contradictory literature as to what extent the blood-brain barrier (BBB) is breached^{11,12} or whether the BBB is compromised at all¹³. Nevertheless, efficacy of treatments for neurotrauma are frequently assessed in pre-clinical models that employ delivery systems to administer agents directly to an injury site, and the ability of an agent to access the brain from the periphery is not always considered. The partial optic nerve transection model results in disruption of the BBB at the optic nerve injury site for at least 3 days after injury¹⁴. As such, at 3 days after injury the model allows for direct pre-clinical assessment of therapeutics for neurotrauma and proof of principle investigations into treatments for secondary degeneration specifically, in which comparisons can be made between local and systemic delivery of agents where the blood brain barrier is known to be breached.

Using the partial optic nerve transection model, we have previously investigated a combinatorial treatment employing the ion channel inhibitors lomerizine, Brilliant Blue G (BBG) and YM872. This treatment is designed to limit intracellular Ca^{2+} influx through voltage-gated calcium channels (VGCC)¹⁵, P2X₇ receptors¹⁶ and Ca^{2+} permeable α -amino-3-hydroxy-5-methyl-4-isoxazolepropionic acid (AMPA) receptors¹⁷ respectively. When YM872 and BBG were locally delivered directly to the injury site *via* osmotic mini-pumps for 3 days following injury, alongside oral administration of lomerizine, we found that this treatment preserved function and partially protected the structure of the node of Ranvier¹⁰. All three ion channel inhibitors can cross the BBB^{18–21}, making it clinically suitable for systemic delivery. Therefore, this study aimed to compare the efficacy of local and systemic delivery of this combinatorial treatment for limiting secondary degeneration following a partial optic nerve transection, assessing inflammatory cell and oligodendroglial populations as well as structure of the node of Ranvier.

Results

Effects of ion channel inhibitor combinations on microglia and macrophages. To examine the effect of the ion channel inhibitor combination on local inflammation, changes in the cell densities of Iba1+ resident ramified microglia, ED1+ infiltrating phagocytic microglia/macrophages and Iba1+/ED1+ infiltrating activated microglial cells^{22–24} were quantified in the ventral optic nerve following a partial optic nerve transection relative to controls (Fig. 1D). Injury caused a significant increase in the number of Iba1+ resident ramified microglia in the presence of the osmotic mini-pump locally delivering vehicle (Fig. 1A; $F = 3.624$, $df = 5$, $p = 0.026$); this increase was not observed when vehicle treatment was delivered systemically *via* intraperitoneal injections ($p = 0.464$). The number of Iba1+ resident ramified microglia in the locally delivered ion channel inhibitor treatment group remained significantly increased compared to the uninjured, sham group ($p = 0.026$). Neither delivery mode of ion channel inhibitor treatment resulted in significant decreases in numbers of resident ramified microglia relative to their respective injured vehicle treated groups (systemic $p = 0.978$, local $p = 1.000$). There were no significant differences observed in the number of Iba1+ resident ramified microglia between the two uninjured control groups ($p = 0.992$) or between the two injured vehicle administration groups ($p = 0.970$).

Injury with systemic vehicle administration resulted in a significant increase in the number of ED1+ infiltrating phagocytic microglia/macrophage cells relative to uninjured controls (Fig. 1B; $F = 4.357$, $df = 5$, $p = 0.038$). However, injury combined with an osmotic mini-pump delivering vehicle did not show a significant increase in the level of ED1+ cells ($p = 0.115$), perhaps due to increased variability in inflammation caused by the delivery catheter at the injury site (Fig. 1B). Neither systemic nor local treatment with the ion channel inhibitors significantly reduced the numbers of ED1+ infiltrating phagocytic microglia/macrophage cells compared to the vehicle treatment groups (systemic $p = 0.111$, local $p = 0.997$). There were no significant differences observed in the number of ED1+ infiltrating phagocytic microglia/macrophage cells between the two uninjured control groups ($p = 0.968$) or between the two injured vehicle administration groups ($p = 0.789$).

Finally, injury caused a trend towards an increase in the numbers of Iba1+/ED1+ infiltrating activated microglial cells in the systemically delivered vehicle group ($F = 3.615$, $df = 5$, $p = 0.053$), but not in the injured group with osmotic mini-pumps delivering vehicle ($p = 0.144$). Neither delivery mode resulted in significant reductions in Iba1+/ED1+ infiltrating activated microglial cells with the ion channel inhibitors compared to their respective vehicle groups (systemic $p = 0.279$, local $p = 0.998$). There were no significant differences observed in the number of Iba1+/ED1+ infiltrating activated microglial cells between the two uninjured control groups ($p = 0.990$) or between the two injured vehicle administration groups ($p = 0.900$).

Effects of ion channel inhibitor combinations on plasma cytokine and chemokine concentrations. To determine whether the ion channel inhibitor combinations were having an effect on inflammation in the periphery, the effects of the ion channel inhibitor combination on the expression of 22 cytokines and chemokines were assessed in plasma samples. 15 of the analytes were below the detection limit of the assay and were excluded from analysis: i.e. IL-1 α (interleukin 1 alpha), G-CSF (granulocyte-colony stimulating factor), IL-10 (interleukin 10), IL-1 β (interleukin 1 beta), IL-6 (interleukin 6), TNF α (tumour necrosis factor alpha), IL-4 (interleukin 4), GM-CSF (granulocyte-macrophage colony-stimulating factor), IFN γ (interferon gamma), IL-2 (interleukin 2), IL-5 (interleukin 5), IL-13 (interleukin 13), IL-12p70 (interleukin 12p70), and MIP-2 (macrophage inflammatory protein 2); data not shown. Of those analysed, significant differences between groups were found for only one of the analytes, MCP-3 (monocyte-chemotactic protein 3; Fig. 2). While injury did not result in a significant effect on MCP-3 concentration ($F = 8.084$, $df = 5$) for either systemic ($p = 0.999$) or local vehicle delivery ($p = 0.467$), the systemically delivered ion channel inhibitor combination did result in a significantly decreased concentration of MCP-3 compared to when the ion channel inhibitor combination was locally delivered ($p = 0.005$). Neither delivery mode of the ion channel inhibitor combination affected the concentration of MCP-3 relative to their respective vehicle controls (systemic $p = 1.000$, local $p = 0.846$). There was a significant difference observed in the concentration of MCP-3 between the two uninjured control groups ($p = 0.005$), but there was no difference between groups for the two injured vehicle administration groups ($p = 0.151$). This result likely reflects the increased inflammation caused by the catheter attached to the osmotic mini-pump.

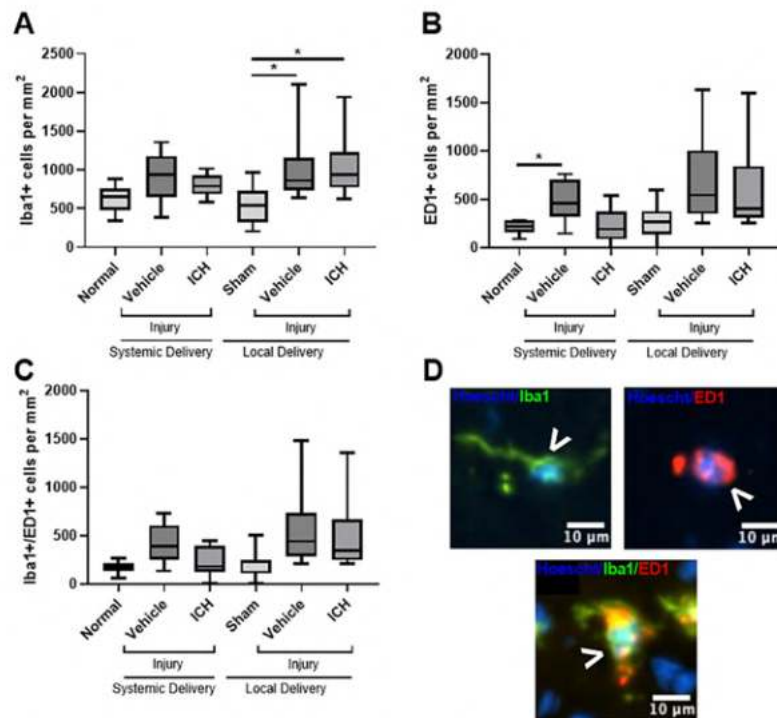


Figure 1. Effects of ion channel inhibitor combinations on densities of Iba1+ and ED1+ cells. Densities of Iba1+ (A), ED1+ (B) and Iba1+/ED1+ (C) cells in the ventral optic nerve from uninjured normal; sham injured, local vehicle treated animals; injured, systemic and local vehicle treated animals; and systemic and local ion channel inhibitor treated animals 3 days after partial optic nerve transection. N = 8–10 rats per group; graphs display min to max values, with the central line representing the median data point. Significant differences are indicated by * $p < 0.05$. (D) Representative images of Iba1+, ED1+ and Iba1+/ED1+ cells, indicated with arrow heads; scale bars = 10 μ m.

There were no significant differences detected in the plasma concentrations of Eotaxin ($F = 1.478$, $df = 5$), Gro- α (growth-regulated oncogene alpha; $F = 0.917$, $df = 5$), IP-10 (interferon gamma-induced protein 10; $F = 1.023$, $df = 5$), MCP-1 (monocyte chemoattractant protein-1; $F = 0.507$, $df = 5$), MIP-1 α (macrophage inflammatory protein 1 alpha; $F = 0.722$, $df = 5$), or RANTES (regulated on activation normal T cell expressed and secreted; $F = 1.089$, $df = 5$).

Effects of ion channel inhibitor combinations on oligodendroglia. Oligodendroglia are particularly vulnerable to damage following neurotrauma²⁵, and to examine the effect of the ion channel inhibitor combination on oligodendroglial cell numbers, the densities of Olig2+ cells were quantified (Fig. 3B). There were no effects of injury with either mode of vehicle administration, compared to the relevant uninjured control group, on the densities of Olig2+ oligodendroglial cells (Fig. 3A; $F = 3.308$, $df = 5$, systemic $p = 0.816$, local $p = 0.442$). Treatment with the ion channel inhibitor combination administered *via* either delivery mode also did not change the densities of oligodendroglial cells (systemic $p = 0.980$, local $p = 0.674$). There were no significant differences observed in the density of Olig2+ oligodendroglial cells between the two uninjured control groups ($p = 0.612$) or between the two injured vehicle administration groups ($p = 0.143$).

When analysing oligodendrocyte precursor cells (OPCs) specifically, by detection of Olig2 together with PDGF α R (Fig. 3D), there were also no effects of injury with either mode of vehicle administration when compared to their uninjured controls (Fig. 3C; $F = 4.344$, $df = 5$, systemic $p = 0.063$, local $p = 0.126$). Treatment with the ion channel inhibitor combination delivered by either mode also did not change the number of OPCs relative to relevant vehicle administered controls (systemic $p = 0.527$, local $p = 0.222$). There were no significant differences observed between the two delivery modes for the ion channel inhibitor treatments ($p = 0.958$). There were also no significant differences observed in the density of OPCs between the two uninjured control groups ($p = 0.597$) or between the two injured vehicle administration groups ($p = 0.751$).

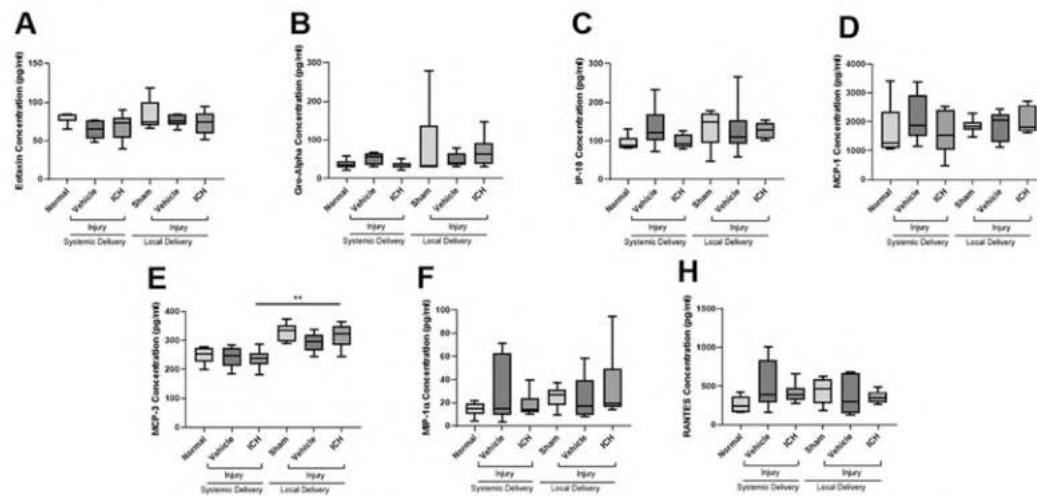


Figure 2. Effects of injury and ion channel inhibitor combinations on the plasma concentration of cytokine and chemokine analytes. Concentration of MIP-2 (A), IP-10 (B), RANTES (C), MIP-1 α (D), MCP-3 (E), MCP-1 (F), and Eotaxin (G) in the plasma of uninjured normal; sham injured, local vehicle treated animals; injured, systemic and local vehicle treated animals; and systemic and local ion channel inhibitor treated animals 3 days after partial optic nerve transection. Graphs display min to max values, with the central line representing the median data point; N = 5–6 rats per group. Significant differences indicated by * $p \leq 0.05$ and ** $p \leq 0.001$.

Effects of ion channel inhibitor combinations on node/paranode complexes. To determine the effects of the ion channel inhibitor combination on structure of the node of Ranvier following injury, the length of the paranode and the paranodal gap, indicative of the length of the Node of Ranvier, were measured, along with the proportion of atypical nodal complexes (Fig. 4). The paranode length increased with injury when vehicle was delivered either systemically (Fig. 4A; $F = 25.089$, $df = 5$, $p \leq 0.001$) or locally ($p \leq 0.001$). Both modes of delivery of the ion channel inhibitors resulted in significantly reduced paranode length compared to the relevant vehicle treatment groups (both $p \leq 0.001$), to paranode lengths not significantly different from their relevant uninjured controls (systemic $p = 0.197$, local $p = 0.088$). There were no significant differences observed in the length of the paranode between the two uninjured control groups ($p = 0.996$) or between the two injured vehicle administration groups ($p = 1.000$).

Injury also significantly increased the length of the paranodal gap following both systemic (Fig. 4B; $F = 22.898$, $df = 5$, $p \leq 0.001$) and local ($p \leq 0.001$) vehicle administration. Both modes of delivery of the ion channel inhibitors significantly reduced the paranodal gap length compared to the outcome following relevant vehicle administration ($p \leq 0.001$) to paranodal gap lengths not significantly different from their relevant uninjured controls (systemic $p = 1.000$, local $p = 0.683$). There were no significant differences observed in the length of the paranodal gap between the two uninjured control groups ($p = 0.966$) or between the two injured vehicle administration groups ($p = 0.589$).

Finally, there was a significant increase in the percentage of atypical node/paranode complexes with injury following both systemic and local vehicle administration compared to the relevant uninjured controls (Fig. 4C; $F = 445.292$, $df = 5$, both $p \leq 0.001$). Both modes of delivery of the ion channel inhibitors significantly reduced the percentage of atypical complexes compared to relevant vehicle treatment (both $p \leq 0.001$), however both remained significantly higher than the relevant uninjured control group (both $p \leq 0.001$). Interestingly, treatment with the systemically administered ion channel inhibitors significantly reduced the percentage of atypical node/paranode complexes compared to local administration ($p = 0.002$). There were no significant differences observed in the percentage of atypical complexes between the two uninjured control groups ($p = 1.000$) or between the two injured vehicle administration groups ($p = 0.583$).

Discussion

Following optic nerve injury, systemic delivery of a combination of ion channel inhibitors was just as effective at preserving the structure of the node of Ranvier in optic nerve vulnerable to secondary degeneration, as when two of the agents were administered directly to the injury site. Preservation of node of Ranvier structure has been demonstrated to be associated with preservation of function of the optic nerve, in the form of preservation of the number of visual responses in the optokinetic nystagmus test, including following local administration of this combination of ion channel inhibitors¹⁰. Although a local inflammatory response was observed with injury alone, in line with our previous work that has demonstrated increased microglia and macrophages at both the primary injury site along the optic nerve and remotely to the visual centres in the brain^{26,27}, there was no effect of

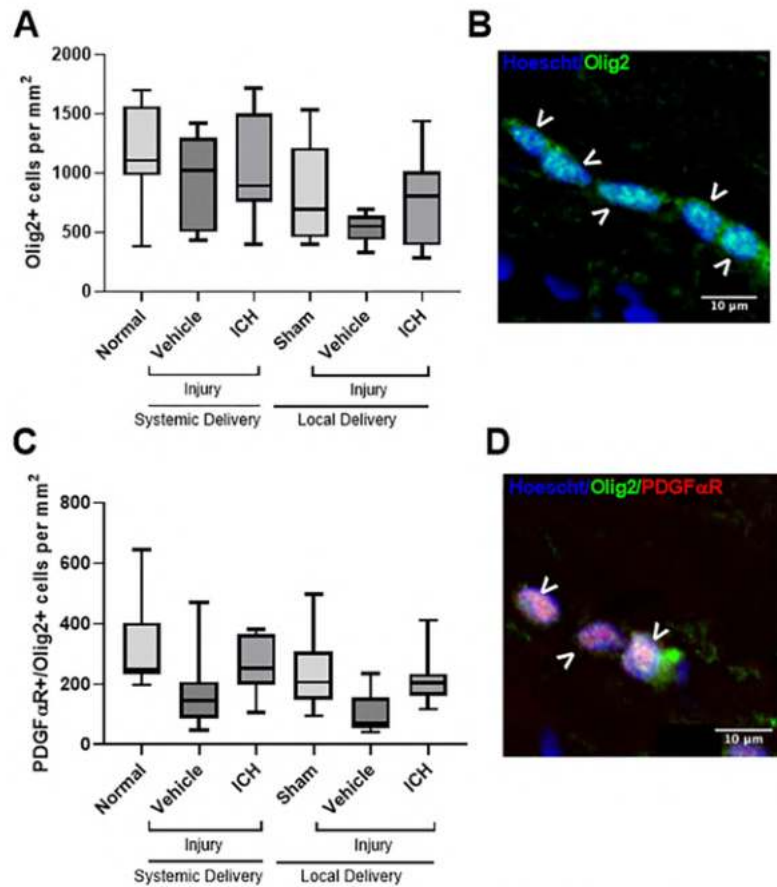


Figure 3. Effects of ion channel inhibitor combinations on oligodendroglial cells. Densities of Olig2+ oligodendroglial cells (A) and PDGF α R+/Olig2+ OPCs (C) in the ventral optic nerve from uninjured normal; sham injured, local vehicle treated animals; injured, systemic and local vehicle treated animals; and systemic and local ion channel inhibitor treated animals 3 days after partial optic nerve transection. N = 8–10 rats per group. Graphs display min to max values, with the central line representing the median data point. Representative image of Olig2+ cells (B) and OPCs (D), indicated with arrow heads; scale bars = 10 μ m.

the inhibitor combination on inflammation with either mode of delivery, either at the injury site or peripherally in the circulatory system. The lack of effect of the inhibitor combination is in line with studies assessing a similar combination of inhibitors in this model, showing that the ion channel inhibitor combination YM872, oxATP and lomerizine, when locally delivered for three days following injury as performed in the current study, has no significant effect on the number of Iba1+ and ED1+ cells at the primary injury site or in the ventral optic nerve vulnerable to secondary degeneration⁹ Furthermore, the current study extends outcomes to demonstrate no discernible changes in circulating chemokines either with injury or ion channel inhibitor treatment. There were also no changes observed in the numbers of oligodendroglial cells either with injury or with treatment. Overall, this indicates that the ion channel inhibitor combination is not working *via* ameliorating the immune response, but perhaps acting on the myelin sheath directly.

Myelin structural changes are a key feature of neurotrauma, with chronic dysmyelination observed following injury^{28,29}. Myelin degeneration has previously been associated with P2X₇ receptor activation³⁰, and P2X₇ receptor antagonists have been shown to protect white matter following injury^{31,32}. Ca²⁺ permeable AMPA receptors³³ are present on the myelin sheath, and myelin degeneration further exposes sub-myelin VGCCs³⁴. Oligodendroglia themselves have a higher concentration of AMPA and P2X₇ receptors than other neuroglia^{35,36}. Furthermore, oligodendroglia do not appear to possess the ability for receptor-mediated desensitisation of AMPA receptors during periods of overstimulation, thus increasing their risk of excitotoxic insult³⁷. Once the cell depolarises upon entry of Ca²⁺, this activates VGCCs which results in further Ca²⁺ influx³⁸. A similar ion channel inhibitor

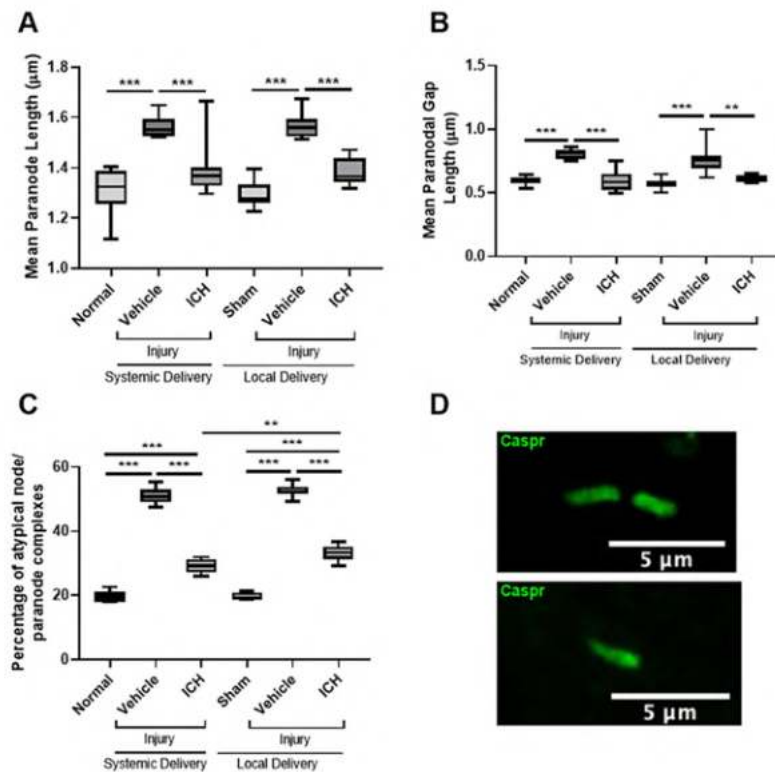


Figure 4. Effect of ion channel inhibitor combinations on node/paranode complexes. Paranode length (A), paranodal gap length (B), and percentage of atypical node/paranode complexes (C) from at least thirty nodal complexes per animal in the ventral optic nerve from uninjured normal; sham injured, local vehicle treated animals; injured, systemic and local vehicle treated animals; and systemic and local ion channel inhibitor treated animals 3 days after partial optic nerve transection. Graphs display min to max values, with the central line representing the median data point; $N = 8-10$ rats per group. Significant differences indicated by * $p \leq 0.05$, ** $p \leq 0.01$, and *** $p \leq 0.001$. (D) Representative image of two Caspr+ areas flanking a β -III tubulin+ area or a typical nodal complex; scale bar = $2 \mu\text{m}$. (E) Representative image of one Caspr+ area flanking a β -III tubulin+ area denoting an atypical nodal complex or a heminode; scale bars = $5 \mu\text{m}$.

combination, comprised of lomerizine, YM872 and the alternative $P2X_7$ receptor antagonist oxATP, has been assessed *in vitro* and was found to successfully limit excess Ca^{2+} entry³⁹. Taken together with the outcomes of this study, the data suggest that control of Ca^{2+} influx into cells is important for the preservation of the structure of the node of Ranvier. While the ion channel inhibitor combination of lomerizine, YM872 and oxATP has been shown to preserve axons both acutely⁹ and chronically⁵, densities of retinal ganglion cell somata were intermediate and not significantly different from densities in either normal or injured animals⁵. The data suggest that preservation of the myelin nodal complex does not necessarily guarantee retinal ganglion cell survival.

Excess intracellular Ca^{2+} contributes to mitochondrial dysfunction and subsequent oxidative damage, including lipid peroxidation⁴⁰. Oxidative damage does not always cause oligodendroglial death²⁹, but does cause oligodendroglial dysfunction and dysmyelination⁴¹. Being a highly lipid-rich structure⁴², myelin is extremely vulnerable to lipid peroxidation as a result of oxidative stress⁴³. By three days following a partial optic nerve transection, there is a significant increase in the levels of 4-hydroxynonenal, a marker of lipid peroxidation, colocalising with myelin basic protein⁴⁴, suggesting lipid peroxidation of the myelin sheath is a hallmark of white matter injury following neurotrauma. Lipid peroxidation of the myelin sheath also results in the aggregation and instability of myelin basic protein, resulting in further dysmyelination⁴⁵. Therefore, the observed preservation of node of Ranvier structure with treatment with the ion channel inhibitor combination may be due to reduced lipid peroxidation, which has also been observed when using a similar combination of inhibitors⁹.

The concentration of the ion channel inhibitor combination that would have reached the injury site when the combination was systemically delivered would likely be below that when the combination was delivered directly to the nerve⁴⁶. Based on the blood volume of a rat, and if 100% of the agent was absorbed into the bloodstream

from the intraperitoneal injection, the blood concentration would be 823.31 μM BBG and 943.41 μM YM872. However, while data on blood concentration of the agents employed following intraperitoneal injection are not available, a range of studies indicate that the average concentration of agents in blood is only 0.5% of that intraperitoneally injected^{47–49}. Therefore, the amount that would have reached the injury site is likely to have been considerably less than the 540 μM BBG and 240 μM YM872 delivered using injury site administration. Overall, this suggests that the ion channel inhibitor combination at the injury site may be at least as effective at lower concentrations.

Local drug delivery has limited clinical utility due to the difficulties associated with surgical implantation of delivery devices, risk of infection and the limited time for which devices can remain *in situ*⁵⁰. Systemic delivery of pharmacotherapeutics is generally preferred due to fewer delivery associated side effects⁴⁶. Nevertheless, systemic delivery is often hindered by the presence of the BBB, which limits entry of many pharmacotherapeutics into the CNS⁵¹.

This study demonstrated the efficacy of a clinically relevant systemically delivered ion channel inhibitor combination for limiting secondary degeneration following a partial optic nerve transection, when the BBB is known to be breached¹⁴. In most rodent models of mild traumatic brain injury, BBB dysfunction typically resolves within minutes to days^{52–55}, however some studies have found no BBB dysfunction following injury¹³. In human studies of mild traumatic brain injury, changes in BBB integrity have been found to be heterogeneous^{11,56}, with not all patients showing increased markers of BBB dysfunction following injury⁵⁷, whilst other patients displaying BBB dysfunction years following injury⁵⁸. Therefore, pharmacotherapies designed to treat neurotrauma need to possess the ability to cross a closed BBB to reach the site of damage. All three of the ion channel inhibitors in the combination assessed in the current study are able to cross the BBB^{18–21,59}. Therefore, this BBB permeable treatment may also be suitable for milder traumatic brain injuries, such as concussion, where the BBB is likely to only be transiently open^{55,56}.

Methods

Animals and study design. Adult, female PVG rats were acquired from the Animal Resource Centre in Murdoch, Western Australia. Animals were housed with *ad libitum* access to water and food under a 12-hour light/dark cycle. All procedures were approved by the University of Western Australia Animal Ethics Committee (Approval Number RA3/100/1485) and were in accordance with the National Health and Medical Research Council (NHMRC) of Australia Code of Practice for use of Animals for Scientific Purposes. Two cohorts of animals were utilised for this study. The first cohort had fifty-six rats that were divided into six experimental groups; a normal group ($n = 8$), an injured, systemically delivered vehicle group ($n = 10$), an injured, systemically delivered ion channel inhibitor combination treatment group ($n = 10$), an injured, locally delivered vehicle group ($n = 10$), an injured, ion channel inhibitor combination treated group ($n = 10$) and a sham injured, locally delivered vehicle group ($n = 8$). The normal group served as an uninjured control for systemic delivery and the sham group served as an uninjured control for local delivery; n 's are noted in the Figure legends. The second cohort had 48 rats ($n = 8/\text{group}$), with the same six experimental groups as cohort 1. The tissue from cohort 1 was processed for immunohistochemical analysis and bloods collected from cohort 2 were processed for a multiplex cytokine analysis.

Surgical procedures. Partial optic nerve transection (day 0) was performed as previously described^{8,60}, under intraperitoneal Ketamine (Ketamil, 50 mg/kg, Troy Laboratories) and Xylazine (Ilium Xylazil, 10 mg/kg, Troy Laboratories) anaesthesia. In summary, the skin overlying the skull behind the right eye was incised and retracted forwards to allow access to the orbit. About 1 mm behind the right eye, the optic nerve parenchyma was exposed by making a longitudinal cut in the sheath using fine iridectomy scissors. The dorsal aspect of the optic nerve was partially lesioned using a diamond radial keratotomy knife (Geuder) to a depth of approximately 200 μm . Sham injury included all procedures except the cut in the sheath and the partial optic nerve lesion. Implantation of Alzet osmotic mini-pumps was performed as described⁵. Subcutaneous injections of analgesia (2.8 mg/kg carprofen, Norbrook) and 1 mL sterile phosphate buffered saline (PBS) were administered to the animals directly following surgery.

Treatments. Lomerizine (30 mg/kg, LKT Labs®) was orally administered in butter vehicle twice daily 8 hours apart for the duration of the experiment as previously described⁸. For local delivery, BBG (540 μM) and YM872 (240 μM) in PBS vehicle were delivered *via* osmotic mini-pump at a rate of 0.5 $\mu\text{L}/\text{h}$. The concentrations employed for local delivery were consistent with our previous studies where efficacy was demonstrated^{5,10}. The sham injured and partial optic nerve transection injured, locally delivered vehicle treated experimental groups both received PBS *via* osmotic mini-pump and orally administered butter vehicle. For systemic delivery, BBG (45 mg/kg, Sigma-Aldrich) and YM872 (20 mg/kg, LKT Laboratories) in PBS were administered intraperitoneally 2 hours post-surgery on day 1, and in the afternoon of day 3. The dosages of systemically administered BBG and YM872 were based on previous studies^{17,61,62}. The partial optic nerve transection injured, systemically delivered vehicle treated experimental group received an equivalent volume intraperitoneal injection of PBS and butter orally, administered as described for the inhibitor treated group. The normal group did not receive any treatments.

Tissue processing. Three days after partial optic nerve transection, rats were euthanised with pentobarbitone sodium (160 mg/kg, Delvet). Rats in cohort 1 were transcardially perfused with 0.9% saline, followed by 4% paraformaldehyde (PFA; Sigma-Aldrich) in 0.1 M phosphate buffer. Optic nerves were dissected and fixed overnight in 4% PFA and subsequently transferred into 15% sucrose (Chem Supply), 0.1% sodium azide (Sigma-Aldrich) in PBS pH 7.2 for storage. Tissue was then cryosectioned longitudinally to a thickness of 14 μm and collected onto Superfrost Plus glass microscope slides. In cohort 2, blood samples were taken *via* cardiac

puncture from the rats following euthanasia. Blood samples were collected into heparinised tubes and spun at 3000 rpm, 4 °C for 10 minutes. Plasma was separated and stored at −80 °C until subsequent multiplex assay analysis.

Immunohistochemistry. Immunohistochemical analysis was conducted on tissue obtained from cohort 1 in accordance with established procedures²⁶. Primary antibodies were used that recognised: microglial activation markers Iba1 (1:500; Abcam, goat Ab5076) and ED1 (1:500; Merck Millipore, mouse MAB1435); oligodendroglial indicators oligodendrocyte transcription factor 2 (Olig2; 1:500; R&D Systems, goat AF2418) and platelet-derived growth factor alpha receptor (PDGFR α ; 1:500; Abcam Ab96806); and for paranode and node of Ranvier structures, Caspr (1:500; Abcam, rabbit Ab34151). Antibodies were diluted in PBS containing 0.2% Triton™ X-100 and 5% normal donkey serum. Secondary antibodies were Alexa Fluor 488 or 555 (1:400; Thermo Fisher Scientific™), with Hoechst 3342 (1:1000; Thermo Fisher Scientific™), diluted in PBS containing 0.2% Triton™ X-100. Finally, the sections were mounted and cover slipped using Fluoromount-G (Thermo Fisher Scientific).

Imaging and analysis. Imaging was performed as previously described¹⁰. The ventral optic nerve directly below the site of injury was visualised using either a Nikon Ni-E confocal fluorescence microscope (Nikon Corporation) or a Nikon Eclipse Ti inverted microscope, with one field of view from one section per animal imaged for each outcome measure. A series of 13 optical images were taken at 0.5 μ m increments along the z-axis, and deconvoluted using Nikon Elements AT software. Imaging for each outcome measure was performed in a single session with consistent capture settings. All image analysis was performed on Fiji image processing software (NIH) by a single investigator blinded to tissue identity.

Total numbers of Iba1+ resident ramified microglia, ED1+ activated phagocytic microglia/macrophages, Iba1+/ED1+ infiltrating activated microglia^{22–24}, Olig2+ oligodendroglia and Olig2+/PDGFR α + oligodendrocyte precursor cells (OPCs) were counted within a region of interest in a 20x image of the ventral nerve directly beneath the primary injury site and expressed as the mean number of cells/mm². For node/paranode analyses, a single 60x z-stack image per animal was divided into a 3 \times 3 grid and complexes with clearly defined Caspr immunostaining in a single randomly selected grid square were analysed. At least thirty complexes per animal were assessed for the length of the paranodal gap, defined as the distance between two Caspr+ areas; paranode length, as defined by the length of Caspr+ areas; the percentages of atypical nodal complexes were determined in the entire 60x image, all as previously described²⁸.

Multiplex assay. The concentration of 22 cytokine and chemokines (IL-1 α , G-CSF, IL-10, IL-17A, IL-1 β , IL-6, TNF α , IL-4, GM-CSF, IFN γ , IL-2, IL-5, IL-13, IL-12p70, Eotaxin, GRO α , IP-10, MCP-1, MCP-3, MIP-1 α , MIP-2, and RANTES) were assessed in the plasma samples collected from cohort 2, using a Cytokine and Chemokine 22-Plex Rat ProcartaPlex™ Panel (Invitrogen) according to manufacturer's instructions. 6 plasma samples per group were chosen using random sampling from the cohort of n = 8 and assessed in duplicate, alongside seven antigen standards in duplicate and two blank wells. The plate was then run on a BioPlex® 200 system and the amount of analyte plotted against the standard curve.

Statistics. Results were analysed using IBM SPSS software. Single one-way ANOVAs encompassing all six treatment groups were performed for each outcome measure and F and degrees of freedom (dF) outcomes described at first mention in the Results section. Normality was assumed, Levene's test was used to assess homogeneity of variances for each data set ($\alpha = 0.05$). If Levene's test showed equal variance, the Tukey post-hoc was used; for unequal variance, the Games-Howell post-hoc was applied; both used $p \leq 0.05$ to indicate statistical significance and these p values are provided in the results text. Statistical significances shown on graphs are hypothesis driven and may not display all significant differences obtained. Specifically, only significant differences within systemic and local delivery groups are presented on graphs, as well as differences between the local and systemic ion channel inhibitor treatment groups. No outliers were removed for any of the outcome measures; missing data points in the multiplex analyses were due to values outside of the detection limit of the assay.

Data availability

The datasets generated during and/or analysed during the current study are available from the corresponding author on reasonable request.

Received: 19 July 2019; Accepted: 7 October 2019;

Published online: 25 October 2019

References

- Kobeissy, F. H. *Brain Neurotrauma: Molecular, Neuropsychological, and Rehabilitation Aspects*. (CRC Press, 2015).
- Li, H.-Y., Ruan, Y.-W., Ren, C.-R., Cui, Q. & So, K.-F. Mechanisms of secondary degeneration after partial optic nerve transection. *Neural Regeneration Research* **9**, 565–574, <https://doi.org/10.4103/1673-5374.130093> (2014).
- Dong, X.-X., Wang, Y. & Qin, Z.-H. Molecular mechanisms of excitotoxicity and their relevance to pathogenesis of neurodegenerative diseases. *Acta Pharmacol Sin Acta Pharmacologica Sinica* **30**, 379–387, <https://doi.org/10.1038/aps.2009.24> (2009).
- Farooqui, A. A., Ong, W.-Y. & Horrocks, L. A. *Neurochemical Aspects of Excitotoxicity*. (Springer, 2008).
- Savigni, D. L. et al. Three Ca²⁺ channel inhibitors in combination limit chronic secondary degeneration following neurotrauma. *Neuropharmacology* **75**, 380–390, <https://doi.org/10.1016/j.neuropharm.2013.07.034> (2013).
- Blair, M. et al. Effect of glatiramer acetate on primary and secondary degeneration of retinal ganglion cells in the rat. *Investigative Ophthalmology & Visual Science* **46**, 884–890 (2005).
- Levkovitch-Verbin, H. et al. A model to study differences between primary and secondary degeneration of retinal ganglion cells in rats by partial optic nerve transection. *Investigative Ophthalmology & Visual Science* **44**, 3388–3388 (2003).

8. Fitzgerald, M. *et al.* Secondary degeneration of the optic nerve following partial transection: The benefits of lomerizine. *Experimental Neurology* **216**, 219–230, <https://doi.org/10.1016/j.expneurol.2008.11.026> (2009).
9. O'Hare Doig, R. *et al.* Specific ion channels contribute to key elements of pathology during secondary degeneration following neurotrauma. *BMC Neuroscience* **18** (2017).
10. Toomey, L. M. *et al.* Comparison of ion channel inhibitor combinations for limiting secondary degeneration following partial optic nerve transection. *Experimental Brain Research* **237**, 161–171 (2018).
11. Dash, P. K., Zhao, J., Hergenroeder, G. & Moore, A. N. Biomarkers for the diagnosis, prognosis, and evaluation of treatment efficacy for traumatic brain injury. *Neurotherapeutics* **7**, 100–114 (2010).
12. Morochović, R. *et al.* Serum S100B protein in early management of patients after mild traumatic brain injury. *European Journal of Neurology* **16**, 1112–1117, <https://doi.org/10.1111/j.1468-1331.2009.02653.x> (2009).
13. Deford, S. M. *et al.* Repeated mild brain injuries result in cognitive impairment in B6C3F1 mice. *Journal of Neurotrauma* **19**, 427–438 (2002).
14. Smith, N. *et al.* An unexpected transient breakdown of the blood brain barrier triggers passage of large intravenously administered nanoparticles. *Scientific Reports* **6**, 22595 (2016).
15. Hara, H. *et al.* Selective effects of lomerizine, a novel diphenylmethylpiperazine Ca²⁺ channel blocker, on cerebral blood flow in rats and dogs. *Clinical and Experimental Pharmacology and Physiology* **26**, 870–876, <https://doi.org/10.1046/j.1440-1681.1999.03154.x> (1999).
16. Murgia, M., Hanau, S., Pizzo, P., Rippla, M. & Virgilio, F. D. Oxidised ATP: An irreversible inhibitor of the macrophage P2Z receptor. *Journal of Biological Chemistry* **266**, 8199–8203 (1993).
17. Takahashi, M. *et al.* YM872: A selective, potent and highly water-soluble alpha-amino-3-hydroxy-5-methylisoxazole-4-propionic acid receptor antagonist. *CNS Drug Reviews* **8**, 337–352 (2002).
18. Atsumi, T. *et al.* The glutamate AMPA receptor antagonist, YM872, attenuates regional cerebral edema and IgG immunoreactivity following experimental brain injury in rats. *Brain Edema XII. Acta Neurochirurgica Supplements* **86**, 305–307, <https://doi.org/10.1089/089771503321532851> (2003).
19. Takahashi, M. & Wei, J. N. I. Neuroprotective efficacy of YM872, an alpha-amino-3-hydroxy-5-methylisoxazole-4-propionic acid receptor antagonist, after permanent middle cerebral artery occlusion in rats. *Journal of Pharmacology and Experimental Therapeutics* **287**, 559–566 (1998).
20. Wong, H. E., Qi, W., Choi, H.-M., Fernandez, E. J. & Kwon, I. A safe, blood-brain barrier permeable triphenylmethane dye inhibits amyloid- β neurotoxicity by generating nontoxic aggregates. *ACS Chemical Neuroscience* **2**, 645–657, <https://doi.org/10.1021/cn200056g> (2011).
21. Shahsuvaryan, M. L. Glaucomatous optic neuropathy management: The role of neuroprotective agents. *Medical Hypothesis, Discovery & Innovation Ophthalmology Journal* **2**, 41–46 (2013).
22. Wu, D. *et al.* Different expression of macrophages and microglia in rat spinal cord contusion injury model at morphological and regional levels. *Acta Medica Okayama* **59**, 121–127, <https://doi.org/10.18926/AMO/31950> (2005).
23. Sutherland, T. C., Mathews, K. J., Mao, Y., Nguyen, T. & Gorrie, C. A. Differences in the Cellular Response to Acute Spinal Cord Injury between Developing and Mature Rats Highlights the Potential Significance of the Inflammatory Response. *Frontiers in Cellular Neuroscience* **10**, 310 (2017).
24. Ito, D., Tanaka, K., Suzuki, S., Dembo, T. & Fukuchi, Y. Enhanced Expression of Iba1, Ionized Calcium-Binding Adapter Molecule 1, After Transient Focal Cerebral Ischemia In Rat Brain. *Stroke* **32**, 1208–1215 (2001).
25. Giacci, M. K. *et al.* Oligodendroglia are particularly vulnerable to oxidative damage after neurotrauma *in vivo*. *Journal of Neuroscience*, 1898–1917 (2018).
26. Fitzgerald, M., Bartlett, C. A., Harvey, A. R. & Dunlop, S. A. Early events of secondary degeneration after partial optic nerve transection: An immunohistochemical study. *Journal of Neurotrauma* **27**, 439–452 (2010).
27. Smith, N. *et al.* Inflammation and blood-brain barrier breach remote from the primary injury following neurotrauma. *Journal of Neuroinflammation* **15**, 201 (2018).
28. Szymanski, C. R. *et al.* Paranode abnormalities and oxidative stress in optic nerve vulnerable to secondary degeneration: Modulation by 670 nm light treatment. *PLoS One* **8**, <https://doi.org/10.1371/journal.pone.0066448> (2013).
29. Payne, S. C., Bartlett, C. A., Harvey, A. R., Dunlop, S. A. & Fitzgerald, M. Chronic swelling and abnormal myelination during secondary degeneration after partial injury to a central nervous system tract. *Journal of Neurotrauma* **28**, 1077–1088, <https://doi.org/10.1089/neu.2010.1665> (2011).
30. Matute, C. P2X7 receptors in oligodendrocytes: A novel target for neuroprotection. *Molecular Neurobiology* **38**, 123–128, <https://doi.org/10.1007/s12035-008-8028-x> (2008).
31. Matute, C. *et al.* P2X7 receptor blockade prevents ATP excitotoxicity in oligodendrocytes and ameliorates experimental autoimmune encephalomyelitis. *The Journal of neuroscience: the official journal of the Society for Neuroscience* **27**, 9525–9533, <https://doi.org/10.1523/JNEUROSCI.0579-07.2007> (2007).
32. Domercq, M. *et al.* P2X7 receptors mediate ischemic damage to oligodendrocytes. *Glia* **58**, <https://doi.org/10.1002/glia.20958> (2010).
33. Fowler, J., McCracken, E., Dewar, D. & McCulloch, J. Intracerebral injection of AMPA causes axonal damage *in vivo*. *Brain Research* **991**, 104–112, <https://doi.org/10.1016/j.BRAINRES.2003.08.004> (2003).
34. Zhang, Z. & David, G. Stimulation-induced Ca²⁺ influx at nodes of Ranvier in mouse peripheral motor axons. *The Journal of Physiology* **594**, 39–57, <https://doi.org/10.1113/JP271207> (2015).
35. Matute, C. *et al.* Neurobiology of disease P2X7 receptor blockade prevents ATP excitotoxicity in oligodendrocytes and ameliorates experimental autoimmune encephalomyelitis. *Journal of Neuroscience* **27**, 9525–9533, <https://doi.org/10.1523/JNEUROSCI.0579-07.2007> (2007).
36. Borges, K., Ohlemeyer, C., Trotter, J. & Kettenmann, H. AMPA/kainate receptor activation in murine oligodendrocyte precursor cells leads to activation of a cation conductance, calcium influx and blockade of delayed rectifying K⁺ channels. *Neuroscience* **63**, 135–149, [https://doi.org/10.1016/0306-4522\(94\)90012-4](https://doi.org/10.1016/0306-4522(94)90012-4) (1994).
37. Yamaya, Y. *et al.* Type-2 astrocyte-like cells are more resistant than oligodendrocyte-like cells against non-N-methyl-D-aspartate glutamate receptor-mediated excitotoxicity. *Journal of Neuroscience Research* **70**, 588–598, <https://doi.org/10.1002/jnr.10425> (2002).
38. Matute, C. *et al.* Excitotoxic damage to white matter. *Journal of Anatomy* **210**, 693–702, <https://doi.org/10.1111/j.1469-7580.2007.00733.x> (2007).
39. O'Hare Doig, R. L. *et al.* Specific combinations of Ca²⁺ channel inhibitors reduce excessive Ca²⁺ influx as a consequence of oxidative stress and increase neuronal and glial cell viability *in vitro*. *Neuroscience* **339**, 450–462, <https://doi.org/10.1016/j.neuroscience.2016.10.005> (2016).
40. Frantseva, M., Perez Velazquez, J. L., Tonkikh, A., Adamchik, Y. & Carlen, P. L. Neurotrauma/neurodegeneration and mitochondrial dysfunction. *Progress in Brain Research* **137**, 171–176 (2002).
41. Fitzgerald, M. Strategies to limit dysmyelination during secondary degeneration following neurotrauma. *Neural Regeneration Research* **9**, 1096–1099, <https://doi.org/10.4103/1673-5374.135307> (2014).
42. Norton, W. & Poduslo, S. Myelination in rat brain: changes in myelin composition during brain maturation. *Journal of Neurochemistry* **21**, 759–773 (1973).

43. Bongarzone, E. R., Pasquini, J. M. & Soto, E. F. Oxidative damage to proteins and lipids of CNS myelin produced by *in vitro* generated reactive oxygen species. *Journal of Neuroscience Research* **41**, 213–221, <https://doi.org/10.1002/jnr.490410209> (1995).
44. O'Hare Doig, R. L. *et al.* Reactive species and oxidative stress in optic nerve vulnerable to secondary degeneration. *Experimental Neurology* **261**, 136–146, <https://doi.org/10.1016/j.expneurol.2014.06.007> (2014).
45. Frid, K. *et al.* Aggregation of MBP in chronic demyelination. *Annals of Clinical and Translational Neurology* **2**, 711–721 (2015).
46. Serwer, L., Hashizume, R., Ozawa, T. & James, C. D. Systemic and local drug delivery for treating diseases of the central nervous system in rodent models. *Journal of Visualised Experiments* **42**, e1992 (2010).
47. Turner, P. V., Brabb, T., Pekow, C. & Vasbinder, M. A. Administration of substances to laboratory animals: routes of administration and factors to consider. *Journal of the American Association for Laboratory Animal Science* **50**, 600–613 (2011).
48. Chang, T., Olson, J., Proffitt, R. & Adler-Moore, J. Differences in tissue drug concentrations following intravenous versus intraperitoneal treatment with amphotericin B deoxycholate or liposomal amphotericin B. *Medical Mycology* **48**, 430–435 (2010).
49. Shimada, T. *et al.* Pharmacokinetic advantage of intraperitoneal injection of docetaxel in the treatment for peritoneal dissemination of cancer in mice. *Journal of Pharmacy and Pharmacology* **57**, 177–181 (2005).
50. Dash, A. & Cudworth, G. Therapeutic applications of implantable drug delivery systems. *Journal of Pharmacological and Toxicological Methods* **40**, 1–12, [https://doi.org/10.1016/S1056-8719\(98\)00027-6](https://doi.org/10.1016/S1056-8719(98)00027-6) (1998).
51. Kasinathan, N., Jagani, H. V., Alex, A. T., Volety, S. M. & Rao, J. V. Strategies for drug delivery to the central nervous system by systemic route. *Drug Delivery* **22**, 243–257 (2015).
52. Habgood, M. D. *et al.* Changes in blood–brain barrier permeability to large and small molecules following traumatic brain injury in mice. *European Journal of Neuroscience* **25**, 231–238 (2007).
53. Barzo, P., Marmarou, A., Fatouros, P., Corwin, F. & Dunbar, J. Magnetic resonance imaging-monitored acute blood–brain barrier changes in experimental traumatic brain injury. *Journal of Neurosurgery* **85**, 1113–1121 (1996).
54. Shapira, Y., Setton, D., Artru, A. & Shohami, E. Blood–brain barrier permeability, cerebral edema, and neurologic function after closed head injury in rats. *Anesthesia & Analgesia* **77**, 141–148 (1993).
55. Guérin, C. *et al.* The dynamics of blood–brain barrier breakdown in an experimental model of glial cell degeneration. *Neuroscience* **103**, 873–883 (2001).
56. Sahyouni, R., Gutierrez, P., Gold, E., Robertson, R. & Cummings, B. Effects of concussion on the blood–brain barrier in humans and rodents. *Journal of Concussion* (2017).
57. Skogseid, I. M., Nordby, H. K., Urdal, P., Paus, E. & Lilleaas, F. Increased serum creatine kinase BB and neuron specific enolase following head injury indicates brain damage. *Acta Neurochirurgica* **115**, 106–111 (1992).
58. Tomkins, O. *et al.* Blood–Brain Barrier Breakdown Following Traumatic Brain Injury: A Possible Role in Posttraumatic Epilepsy. *Cardiovascular Psychiatry and Neurology* (2011).
59. Yamada, C. *et al.* Effects of lomerizine on cerebral blood flow and systemic arterial blood pressure in anesthetized dogs. *Japanese Journal of Pharmacology* **25**, 797–802 (1997).
60. Bartlett, C. & Fitzgerald, M. Partial Transection of Adult Rat Optic Nerve as a Model of Secondary Degeneration in the Central Nervous System. *Bio-Protocol* **8** (2018).
61. Cervetto, C., Frattaroli, D., Maura, G. & Marcoli, M. Motor neuron dysfunction in a mouse model of ALS: Gender-dependent effect of P2X7 antagonism. *Toxicology* **311**, 69–77, <https://doi.org/10.1016/j.tox.2013.04.004> (2013).
62. Diaz-Hernandez, J. I. *et al.* *In vivo* P2X7 inhibition reduces amyloid plaques in Alzheimer's disease through GSK3 β and secretases. *Neurobiology of Aging* **33**, 1816–1828, <https://doi.org/10.1016/j.neurobiolaging.2011.09.040> (2012).

Acknowledgements

M.F. was supported by an NHMRC Career Development Fellowship (APP1087114). L.T. is supported by an MS Research Australia Postgraduate Scholarship. We thank Thomas Clarke for technical assistance.

Author contributions

M.F. conceived the experiments; L.T., C.B., N.G., M.M., G.G., T.M. and M.F. conducted the experiments; L.T., J.R. and M.F. analysed and interpreted data; L.T. and M.F. drafted the manuscript; all authors reviewed the manuscript.

Competing interests


The authors declare no competing interests.

Additional information

Correspondence and requests for materials should be addressed to M.F.

Reprints and permissions information is available at www.nature.com/reprints.

Publisher's note Springer Nature remains neutral with regard to jurisdictional claims in published maps and institutional affiliations.

 **Open Access** This article is licensed under a Creative Commons Attribution 4.0 International License, which permits use, sharing, adaptation, distribution and reproduction in any medium or format, as long as you give appropriate credit to the original author(s) and the source, provide a link to the Creative Commons license, and indicate if changes were made. The images or other third party material in this article are included in the article's Creative Commons license, unless indicated otherwise in a credit line to the material. If material is not included in the article's Creative Commons license and your intended use is not permitted by statutory regulation or exceeds the permitted use, you will need to obtain permission directly from the copyright holder. To view a copy of this license, visit <http://creativecommons.org/licenses/by/4.0/>.

© The Author(s) 2019

Appendix B. Introducing “The effects of a combination of ion channel inhibitors on pathology in a model of demyelinating disease”

As discussed in Chapter 2, I have also been involved in a study during this doctoral degree that successfully employed a combinatorial treatment of ion channel inhibitors for ameliorating pathology in the cuprizone model of demyelinating disease. For this work, the ion channel inhibitor combination employed comprised of lomerizine, YM872 and BBG to target VGCCs, AMPA receptors and P2X₇ receptors respectively for limiting excess intracellular Ca²⁺ influx. When mice were treated with this ion channel inhibitor combination for 3 weeks alongside concomitant cuprizone administration, we observed significantly lower levels of protein nitration, increases in the density of OPCs and reductions in the number of atypical Node of Ranvier complexes. This study is presented below and has been published as:

Gopalsingam G., Bartlett C.A., McGonigle T., Majimbi M., Warnock A., Ford A., Gough A., **Toomey L.M.**, Fitzgerald M. 2019. The effects of a combination of ion channel inhibitors on pathology in a model of demyelinating disease. *Multiple Sclerosis and Related Disorders* 34: 1-8. doi.org/10.1016/j.msard.2019.06.005



Contents lists available at ScienceDirect

Multiple Sclerosis and Related Disorders

journal homepage: www.elsevier.com/locate/msard

The effects of a combination of ion channel inhibitors on pathology in a model of demyelinating disease



Gopana Gopalasingam^{a,b}, Carole A. Bartlett^a, Terence McGonigle^c, Maimuna Majimbi^c, Andrew Warnock^c, Abbey Ford^a, Alexander Gough^a, Lillian M. Toomey^{c,d}, Melinda Fitzgerald^{a,b,c,d,*}

^a Experimental and Regenerative Neurosciences, School of Biological Sciences, The University of Western Australia, 35 Stirling Hwy, Nedlands, Western Australia 6009, Australia

^b School of Human Sciences, The University of Western Australia, 35 Stirling Hwy, Nedlands, Western Australia 6009, Australia

^c Curtin Health Innovation Research Institute, Curtin University, Belmont, Western Australia, Australia

^d Perron Institute for Neurological and Translational Science, Sarich Neuroscience Research Institute Building, 8 Verdun St, Nedlands, Western Australia 6009, Australia

ARTICLE INFO

Keywords:

Multiple sclerosis
Oxidative damage
Excess Ca²⁺
Ion channel inhibitors
Myelin structure

ABSTRACT

Background: Multiple sclerosis (MS) has been shown to feature oxidative damage, which can be modelled using the cuprizone model of demyelinating disease. Oxidative damage can occur as a result of excessive influx of calcium ions (Ca²⁺) and oligodendroglia are particularly vulnerable. However, the effects of limiting excess Ca²⁺ influx on oxidative damage, oligodendroglia and myelin structure are unknown.

Objective: This study investigated the effects of limiting excess Ca²⁺ flux on oxidative damage and associated changes in oligodendroglial densities and Node of Ranvier structure in the cuprizone model.

Methods: The effects of three weeks of cuprizone administration and of treatment with a combination of three ion channel inhibitors (Lomerizine, Brilliant Blue G (BBG) and YM872), were semi-quantified immunohistochemically. Outcomes assessed were protein nitration (3-nitrotyrosine (3NT)) oxidative damage to DNA (8-hydroxy deoxyguanosine (8OHdG)), advanced glycation end-products (carboxymethyl lysine (CML)), immunoreactivity of microglia (Iba1) and astrocytes (glial acidic fibrillary protein (GFAP)), densities of oligodendrocyte precursor cells (OPCs) (platelet derived growth factor alpha receptor (PDGFRα) with olig2) and oligodendrocytes (olig2 and CC1), and structural elements of the Node of Ranvier (contactin associated protein (Caspr)).

Results: The administration of cuprizone resulted in increased protein nitration, DNA damage, and astrocyte and microglial immunoreactivity, a decrease in the density of oligodendrocytes and OPCs, together with altered structure of the Node of Ranvier and reduced myelin basic protein immunoreactivity. Treatment with the ion channel inhibitor combination significantly lowered protein nitration, increased the density of OPCs and reduced the number of atypical Node of Ranvier complexes; other outcomes were unaffected.

Conclusion: Our findings suggest that excess Ca²⁺ influx contributes to protein nitration, and associated changes to OPC densities and Node of Ranvier structure in demyelinating disease.

1. Introduction

Multiple sclerosis (MS) is a chronic inflammatory, demyelinating and neurodegenerative disease, which is considered by many to have an autoimmune aetiology (Dalla Libera et al., 2011; Zozulya and Wiendl, 2008). It is increasingly understood that glutamate mediated activation of calcium (Ca²⁺) permeable ion channels is a major trigger in MS pathogenesis (Matute, 2007; McTigue and Tripathi, 2008; Franklin et al., 2012; Matute et al., 2007). As a consequence, excessive Ca²⁺

enters the axoplasm resulting in swelling of mitochondria, increased production of reactive oxygen species, oxidative stress and apoptotic cell death of neuronal and glial cells (Gandhi et al., 2009; Huang et al., 2009; Kowaltowski et al., 2009). In white matter injury, increased influx of Ca²⁺ through voltage-gated Ca²⁺ channels (VGCCs) (Gurkoff et al., 2013), ATP-binding purinergic P2X₇ receptors (Franke et al., 2004), and Ca²⁺ permeable α-amino-3-hydroxy-5-methyl-4-isoxazolepropionic acid (AMPA) receptors (Spaethling et al., 2008) increases cytosolic Ca²⁺ concentrations. Mitochondrial

* Corresponding author.

E-mail address: lindy.fitzgerald@curtin.edu.au (M. Fitzgerald).

<https://doi.org/10.1016/j.msard.2019.06.005>

Received 12 October 2018; Received in revised form 16 May 2019; Accepted 7 June 2019
2211-0348/ © 2019 Elsevier B.V. All rights reserved.

dysfunction impairs the Na^+/K^+ ATPase pump, leading to an increase in intracellular Na^+ (Biller et al., 2016). This ionic imbalance promotes an inverse mode of action of the $\text{Na}^+-\text{Ca}^{2+}$ exchanger resulting in further influx of Ca^{2+} (Stys et al., 1992; Friese et al., 2014), thereby propagating a feed forward loop of increasing oxidative damage (Camello-Almaraz et al., 2006).

Studies have found that enzymes involved in producing reactive oxygen and nitrogen species are upregulated in active MS lesions (Liu et al., 2001; Gray et al., 2008), with increased markers of oxidative stress in the blood (Fiorini et al., 2013) of people with MS. Oxidative damage has also been found to play a key role in various mouse models of demyelinating disease, including experimental autoimmune encephalomyelitis (Espejo et al., 2002), cuprizone-induced toxication (Liu et al., 2015), and Theiler's murine encephalomyelitis virus (Bhuyan et al., 2015). The damage occurs predominantly in oligodendrocyte nuclei which show signs of apoptosis (Haider et al., 2011). Oligodendroglia are highly susceptible to oxidative damage, due to their high iron content, low reduced-glutathione levels (Thorburne and Juurlink, 1996) and low antioxidant defences (French et al., 2009; Volpe, 2011). We have recently demonstrated that oligodendrocytes and OPCs are particularly vulnerable to oxidative damage following neurotrauma, using a partial optic nerve transection model where pathological changes similar to MS occur (Giacci et al., 2018; Witherick et al., 2010; Szymanski et al., 2013). Ion channel inhibitors can be used to probe the importance of excess Ca^{2+} flux in oxidative damage and loss of oligodendroglia. The combination of ion channel inhibitors lomerizine, oxidised ATP and YM872, limits the entry of excessive Ca^{2+} through VGCC, P2X_7 receptors and Ca^{2+} permeable AMPA receptors respectively (O'Hare Doig et al., 2016). When various combinations of the three inhibitors were delivered in the partial optic nerve transection model, only the three inhibitors in combination restored the length of the node of Ranvier and reduced the loss of OPCs (O'Hare Doig et al., 2017). Use of the inhibitor combination indicated that excess Ca^{2+} may contribute to oxidative damage and myelin deficits in neurotrauma (O'Hare Doig et al., 2017) and might be useful to probe the mechanisms of demyelination in MS facilitated by excess Ca^{2+} influx (Naziroglu et al., 2014).

The oxidative elements of MS can be appropriately modelled using cuprizone induced demyelination (Kipp et al., 2009; Skripuletz et al., 2011). Cuprizone is a copper chelating reagent (*bis*-cyclo-hexanone oxalaldihydrazone) which is added to normal chow (Hiremath et al., 1998), and inhibits copper-dependent mitochondrial enzymes including cytochrome c oxidase and monoamine oxidase, resulting in apoptosis of oligodendrocytes and subsequent demyelination (Acs and Komoly, 2012). Demyelination in the medial corpus callosum is apparent at 3 weeks, referred to as early demyelination (Hesse et al., 2010; Skripuletz et al., 2011) and proceeds to severe demyelination thereafter (Hiremath et al., 1998; Skripuletz et al., 2011). Here, we assess the effects of the combination of ion channel inhibitors lomerizine, Brilliant Blue G (BBG) and YM872, on parameters of oxidative damage, microglia, astrocyte and oligodendrocyte dynamics, as well as structure of the Node of Ranvier, in the cuprizone model of demyelinating disease. Each agent has been shown to cross the blood brain barrier (Peng et al., 2009; Yamada et al., 2006; Takahashi et al., 2002), and BBG is present at 200–220 nM in brain of mice treated with 45.5 mg/kg every 48 h for 4 months (Diaz-Hernandez et al., 2012).

2. Methods

2.1. Animals and study design

All procedures were approved by the Animal Ethics Committee (AEC) of The University of Western Australia (RA/3/100/1489) and were conducted in accordance with the principles of the National Health and Medical Research Council of Australia. Male C57 black (C57 Bl/6.J) young mice (25–30 g), were obtained from the Animal Resource

Centre (Murdoch, Western Australia) and housed in groups of four under standard conditions including 12-h light/dark cycles with access to water and food *ad libitum*. Two cohorts of animals were used with a total of 24 in each cohort, each cohort had two groups with 12 randomly assigned animals/group. Cohort 1 consisted of a control group on a standard chow diet and a cuprizone administered group. Cohort 2 consisted of a vehicle control group and a group receiving the ion channel inhibitor combination; both of these groups were administered cuprizone. 0.2% cuprizone (*bis*-cyclo-hexanone oxalaldihydrazone) (Teklad Custom Diet TD. 150183, Envigo) was administered in cuprizone-containing pellets. All animals were weighed every day, and cuprizone fed animals were given supplemental normal chow for that day if their weight was less than 90% of their weight at the start of the experimental period. Note that cohort 1 originally included an additional 24 animals with a control group on a standard chow diet and a cuprizone administered group to be euthanized at five weeks. However experimental and logistical difficulties led to outcomes from these animals not being included in the analyses.

2.2. Ion channel inhibitor administration

For cohort 2 animals treated with the ion channel inhibitors (group 2), lomerizine (30 mg/kg, LKT Labs[®]) dissolved in butter was delivered orally, while the animals were gently held. Treatment commenced on the first day of cuprizone feeding and continued twice daily 8 h apart for the 3 week experimental period (6 days/week). The BBG (Sigma-Aldrich[®]) and YM872 (LKT Labs[®]) were administered systemically via intraperitoneal injection of 1 mL of 45 mg/kg BBG and 20 mg/kg YM872 dissolved in phosphate buffered saline (PBS). Injections commenced on the first day of cuprizone feeding and continued every second day throughout the experimental period. Group 1 of cohort 2 received vehicle treatment i.e. orally delivered butter and intraperitoneal injections of 1 mL of PBS.

2.3. Tissue processing

After the three week experimental period, mice were euthanized with pentobarbitone sodium (160 mg/kg, Delvet[®]), transcardially perfused with 0.9% saline, followed by 4% paraformaldehyde (Sigma-Aldrich[®]) in 0.1 M PBS. The brains were dissected from the mice and fixed overnight in 4% paraformaldehyde and subsequently transferred into 15% sucrose in PBS, and the following day into 30% sucrose (Chem Supply[®]) for cryoprotection. Brains were stored at 4 °C, until they were embedded in optimal cutting temperature compound (OCT) and cryo-sectioned coronally. Sections of 25 µm were stored in twenty-four well plates immersed in PBS at 4 °C; sections of 18 µm were mounted directly onto glass slides and stored at –80 °C.

2.4. Immunohistochemistry

Immunohistochemical procedures were performed according to previously described procedures (Fitzgerald et al., 2010). The primary antibodies utilised for immunohistochemical assessments were: protein nitration indicator 3-NT (1:500; Abcam[®], mouse Ab61392); DNA oxidation indicator 8OHdG (1:500; Abcam[®], mouse Ab62623); carboxy methyl lysine, CML (1:500; Transgenic[®], mouse KAL-KH024); myelin basic protein, MBP (1:500; Abcam[®], rabbit Ab40390); microglial markers ionized calcium-binding adapter molecule 1, Iba1 (1:500; Abcam[®], goat Ab5076); astrocyte indicator glial fibrillary acidic protein, GFAP (1:1000; Abcam[®], goat Ab53554); OPC indicators oligodendrocyte transcription factor 2 (Olig2; 1:500; R&D Systems[®], goat AF2418) and receptor for platelet-derived growth factor alpha, PDGF α R (1:1000, Santa Cruz, rabbit SC-338); mature oligodendrocyte indicator CC1 (Anti-APC, 1:500; Calbiochem, mouse OP80-100); for paranode structures contactin associated protein-like 1, Caspr (1:500, Abcam[®], rabbit Ab34151). The sections were blocked prior to staining

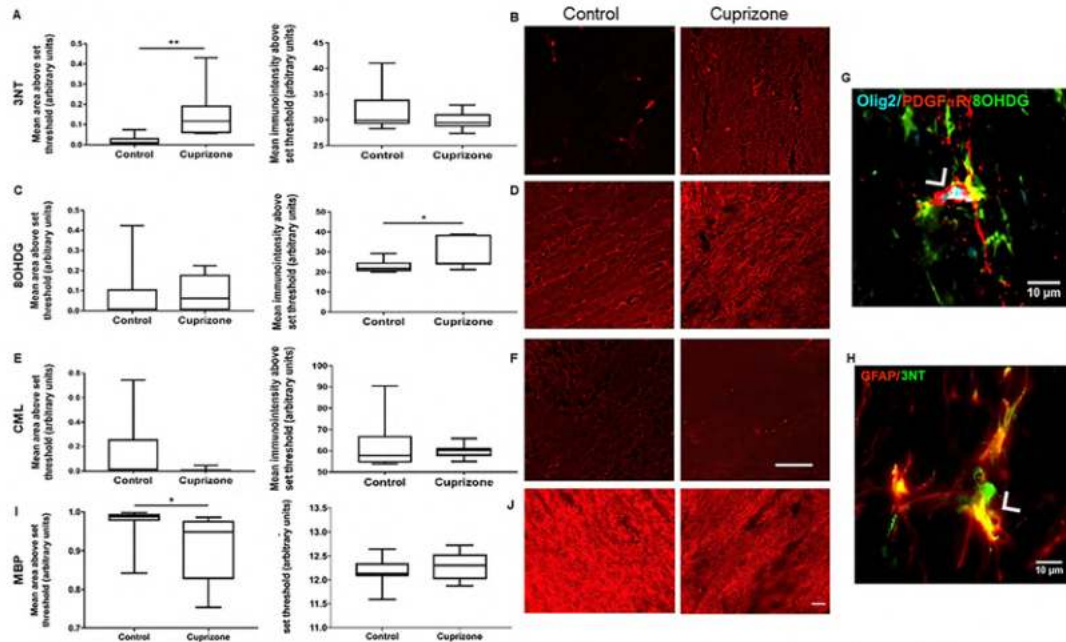


Fig. 1. Effects of cuprizone administration on immunointensity of oxidative stress indicators. Semi-quantification of 3NT (A), 8OHdG (C), CML (E) and MBP (I) immunointensity and area of immunointensity in the medial corpus callosum above an arbitrary set threshold following 3 weeks cuprizone feeding compared to control fed animals. Graphs display min to max values, with the central line representing the median data point, and statistical differences are indicated by * $p \leq 0.05$, ** $p \leq 0.01$. Representative images of immunointensity of the oxidative stress markers 3NT (B), 8OHdG (D), CML (F) and MBP (J) are shown; scale bar = 15 μ m. Representative images of 8OHdG immunoreactivity co-localised with PDGF α R + /Olig2 + OPCs (G) and 3NT immunoreactivity co-localised with GFAP + astrocytes (H) are shown (indicated by arrow heads); scale bars = 10 μ m.

with mouse antibodies (8OHdG, CML and 3NT) using unconjugated secondary goat anti-mouse IgG2a (1:1000; Thermo Fischer Scientific™) diluted in 0.2% Triton™ X-100 in PBS and 5% normal donkey serum for 1 h in room temperature followed by washing in PBS. The antibodies raised in mouse were incubated with sections immersed in wells. Staining using antibodies not raised in mouse was performed on slides. Secondary antibodies were species-specific Alexa Fluor 488, 555 or 647-conjugated antibodies (1:400; Thermo Fisher Scientific™, mouse, rabbit and/or goat) and Hoechst (1:1000; Thermo Fisher Scientific™) diluted in 0.2% Triton™ C-100 in PBS.

2.5. Imaging and statistical analyses

Sections encompassing the medial corpus callosum accompanied by the lateral corpus callosum on both sides were visualised using either a NikonEclipse Ti inverted microscope (Nikon Corporation®) with 20x objective, or a Nikon Ni-E confocal fluorescence microscope (Nikon Corporation®) with 60x oil objective. Images were acquired in a series of 13 steps at 0.5 μ m increments across the z-axis. Images acquired from the Nikon Ti inverted microscope were deconvoluted by Nikon Elements AT software (Nikon Corporation®). All images for the same outcome measure were captured using consistent microscope settings. The images were analysed using Fiji/ImageJ, by an investigator blinded to sample identity. Note that images were not able to be captured for some outcome measures in a few animals, due to the absence of the appropriate brain region in the available tissue sections, or occasional absence of immunohistochemical staining in a particular section.

The area and intensity of immunoreactivity of the oxidative stress markers (3-NT, 8OHdG and CML), and MBP, microglia (IBA1) and astrocytic marker (GFAP) were semi-quantified on 20x magnification

images. A defined, constant arbitrary threshold was set for each outcome measure, at which the immunopositive areas were detectable across all groups. For each image, the mean of four regions of background staining was subtracted from the intensity measure to adjust for subtle variations in section thickness and immunolabelling.

The total numbers of oligodendroglial cells (Olig2+, Olig2+ and PDGF α R+, and CC1+) were counted within a randomly selected and consistent region of interest in the medial corpus callosum containing 50–100 cells, using 20x magnification images, and expressed as densities (cells/mm²). PDGF α R+ cells were counted where immunoreactivity was co-localised with Olig2, thereby identifying OPCs (Harlow et al., 2014). Thirty Node of Ranvier complexes were characterised for each animal from a 60x magnification image of the corpus callosum. Images were divided into a grid, and starting from the left corner, all the complexes with defined Caspr+ immunostaining were measured to eliminate selection-bias toward a specific size of paranode. Two outcome measures were characterised; the length of the paranode, defined by the length of Caspr+ immunoreactivity, and the length of the paranodal gap measured by the distance between two Caspr+ nodes. Typical node/paranode complexes were characterised by two Caspr+ regions in the same plane of direction, separated by a paranodal gap. An atypical node complex was identified by a single Caspr+ paranode well within the z stack of images acquired.

Statistical analyses were performed using SPSS Statistics Software Version 24 (IBM), comparing the control and cuprizone group for cohort 1, and vehicle control and treatment for cohort 2, using independent sample T-tests, assuming equal variances. Data were presented in minimum to maximum box and whisker plots using GraphPad PRISM™ 7 software (GraphPad software).

3. Results

3.1. Indicators of oxidative damage in the cuprizone model

Oxidative damage as a consequence of cuprizone administration was semi-quantified as the mean immunointensity and area of immunointensity above arbitrary set thresholds, for 3NT, 8OHDG, and CML in the medial corpus callosum. Note that immunoreactivity of oxidative stress indicators is diffuse, of its nature, as the antibodies are recognising altered lipids and proteins that are present in multiple cell types and not necessarily confined to cellular boundaries. Independent sample t-tests demonstrated an increase in the area of 3NT immunoreactivity with 3 weeks cuprizone administration, compared to control animals ($dF = 20, p = 0.001$), whereas the intensity of that immunoreactivity was unchanged ($dF = 20, p \leq 0.13$; Fig. 1A, B). In contrast, the area of immunointensity of 8OHDG was unchanged by cuprizone administration ($dF = 16, p = 0.72$), but the intensity of that immunoreactivity was significantly increased ($dF = 16, p = 0.04$; Fig. 1C, D). However, the immunoreactivity of CML was unaffected by cuprizone administration compared to control (area $dF = 21, p = 0.06$; intensity $dF = 21, p = 0.44$; Fig. 1E, F). 8OHDG immunoreactivity was frequently co-localised with PDGF α R+/Olig2+ OPCs (arrow head, Fig. 1G), whereas 3NT immunoreactivity was frequently co-localised with GFAP+ astrocytes (arrow head, Fig. 1H). Oxidative damage was accompanied by decreased area of MBP immunoreactivity (area $dF = 21, p = 0.04$; intensity $dF = 21, p = 0.30$, Fig. 1I, J), indicating demyelination following three weeks of cuprizone administration.

3.2. Changes in indicators of oxidative stress with ion channel inhibitors

The combination of ion channel inhibitors was used to discern whether limiting excess Ca^{2+} flux affected oxidative damage as a result of cuprizone administration. The area of 3NT immunoreactivity was unaffected by the ion channel inhibitors ($dF = 22, p = 0.73$), but the intensity of that immunoreactivity was significantly decreased compared to vehicle treated control animals ($dF = 22, p = 0.048$; Fig. 2A, B). However, the immunoreactivity of 8OHDG was not affected by treatment with the three ion channel inhibitors (area $dF = 22, p = 0.38$; intensity $dF = 22, p = 0.98$; Fig. 2C, D), and neither was the immunoreactivity of CML (area $dF = 22, p = 0.64$; intensity $dF = 22, p = 0.20$; Fig. 2E, F).

3.3. Effects of the ion channel inhibitors on astrocytes and microglia / macrophages

As anticipated (Hibbitts et al., 2012), administration of cuprizone for 3 weeks led to a significantly increased area of immunoreactivity of GFAP relative to the control group, indicating increased number and / or size of astrocytes ($dF = 20, p \leq 0.001$; Fig. 3A). The combination of three ion channel inhibitors did not affect the area of GFAP immunoreactivity relative to vehicle control ($dF = 22, p = 0.896$; Fig. 3B, C). Similarly, the area of Iba1 immunoreactivity was also increased following cuprizone administration, indicative of increased numbers and / or size of microglial cells ($dF = 21, p \leq 0.0001$; Fig. 3D). The area of Iba1 immunoreactivity was not affected by treatment with the inhibitor combination ($dF = 22, p = 0.093$; Fig. 3E, F).

3.4. Effects of the ion channel inhibitors on oligodendroglial cells

Olig2 is present in both immature and maturing cells of the oligodendroglial lineage (Emery, 2010). Olig2+ positive oligodendroglial cell density was significantly decreased following 3 weeks of cuprizone administration ($dF = 21, p = 0.001$; Fig. 4A), as anticipated in this model of demyelinating disease (Acs et al., 2013). Treatment with the inhibitor combination to limit excess Ca^{2+} flux did not increase the density of Olig2+ cells ($dF = 22, p = 0.953$; Fig. 4B, C). The density of

OPCs was quantified by identifying cells immunoreactive for both Olig2 and PDGF α R (Rivers et al., 2008). A significant decrease was detected in the density of OPCs following three weeks of cuprizone administration ($dF = 21, p = 0.008$; Fig. 4D), and the density of OPCs was significantly increased in animals treated with the inhibitor combination compared to the vehicle control group ($dF = 21, p = 0.016$; Fig. 4E, F). In contrast, the number of CC1+ mature oligodendrocytes were decreased following cuprizone administration ($dF = 21, p \leq 0.0001$; Fig. 4G). However, limiting excess Ca^{2+} flux with the ion channel inhibitor combination did not increase the density of CC1+ oligodendrocytes ($dF = 22, p = 0.110$; Fig. 4H, I).

3.5. Effects of the ion channel inhibitors on structure of the Node of Ranvier

Node of Ranvier complexes were assessed immunohistochemically by quantifying the distributions of the paranodal protein, Caspr. The length of the paranode itself was not affected by 3 weeks of cuprizone administration ($dF = 18, p = 0.523$; Fig. 5A; representative images of quantified immunoreactivity are shown in Fig. 5G, H), nor by treatment with the ion channel inhibitor combination ($dF = 22, p = 0.564$; Fig. 5B). However, the length of the Node of Ranvier, indicated by the gap between two Caspr+ paranodes, was significantly increased with cuprizone administration ($dF = 18, p = 0.002$; Fig. 5C, G). Treatment with the inhibitor combination had no effect on the length of the paranodal gap ($dF = 22, p = 0.853$; Fig. 5D). In contrast, the percentage of atypical nodes was significantly increased in the cuprizone fed animals compared to controls ($dF = 14, p \leq 0.003$; Fig. 5E, G), and the percentage of these atypical nodes was significantly reduced in animals treated with ion channel inhibitors ($dF = 22, p \leq 0.001$; Fig. 5F). Note that Node of Ranvier complexes analysed lay well within the 13 image stack in the z plane (Fig. 5I), ensuring that atypical nodes were not classified as such due to projection beyond the z plane of the image.

4. Discussion

In this study a combination of ion channel inhibitors, which we have shown to reduce intracellular Ca^{2+} in a range of CNS cell types *in vitro* (O'Hare Doig et al., 2016) was used to provide insight into which elements of pathophysiology in the cuprizone model could be ameliorated by limiting excess influx of Ca^{2+} . It was found that the combination of inhibitors reduced protein nitration, increased numbers of OPCs and reduced the percentage of atypical Nodes of Ranvier, implying these elements of pathology are exacerbated by excess Ca^{2+} flux. In contrast, other measures of oxidative damage including DNA oxidation, increased microglia and astrocyte immunoreactivity and loss of oligodendrocytes were unaffected. The outcomes indicate that excess Ca^{2+} is not the only trigger that leads to oxidative damage and loss of oligodendrocytes, and that multiple mechanisms will need to be controlled to limit damage in demyelinating diseases.

Increased expression of markers of oxidative stress have been found in brain lesions in people with MS (Lin and Beal, 2006; Haider et al., 2011; Morel et al., 2017), and in the cuprizone mode of demyelinating disease (Liu et al., 2015). In the current study we demonstrate increased nitrosative damage and DNA oxidation in the early demyelination phases of cuprizone administration. The immunoreactivity of CML did not increase, in line with a previous clinical study demonstrating no significant differences in plasma CML between people with MS and healthy controls (Sternberg et al., 2010). Of these oxidative stress indicators, only protein nitration was reduced following administration of the combination of ion channel inhibitors. Previous studies have shown that following cuprizone administration, increased levels of nitrosative stress did not arise from microglial or macrophages (Schuh et al., 2014). Astrocytes have also been identified as key mediators of nitrosative stress in MS (Liu et al., 2001), potentially via AMPA receptor-mediated increases in nitric oxide synthase activity (Baltrons and Garcia, 1997). In the current study, we observed 3NT was colocalised within astrocytes

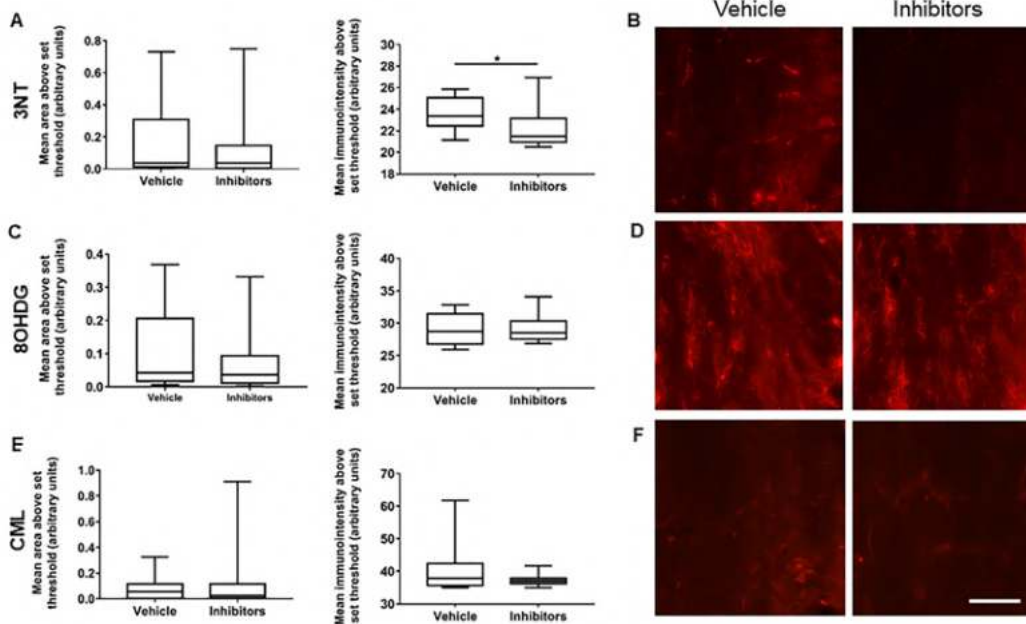


Fig. 2. Effects of treatment with the ion channel inhibitor combination on oxidative stress indicators. Semi-quantification of 3NT (A), 8OHdG (C) and CML (E) immunointensity and area of immunointensity in the medial corpus callosum above an arbitrary set threshold following treatment with the ion channel inhibitor combination or vehicle control for 3 weeks: all animals were administered cuprizone. Graphs display min to max values, with the central line representing the median data point, and statistical differences are indicated by * $p \leq 0.05$. Representative images of immunointensity of the oxidative stress markers 3NT (B), 8OHdG (D) and CML (F) are shown; scale bar = 15 μm .

following cuprizone administration, therefore the inhibitor combination may have been acting on astrocytes to produce the observed decrease in nitrosative stress with treatment. Though treatment of cuprizone fed animals with the inhibitor combination did not change

GFAP immunoreactivity, activated astrocytes have been found to play a dual role in MS lesions (Correale and Farez, 2015). In fact, genetic ablation of astrocytes delayed removal of myelin debris, limited remyelination, and reduced proliferation of OPCs in the cuprizone model

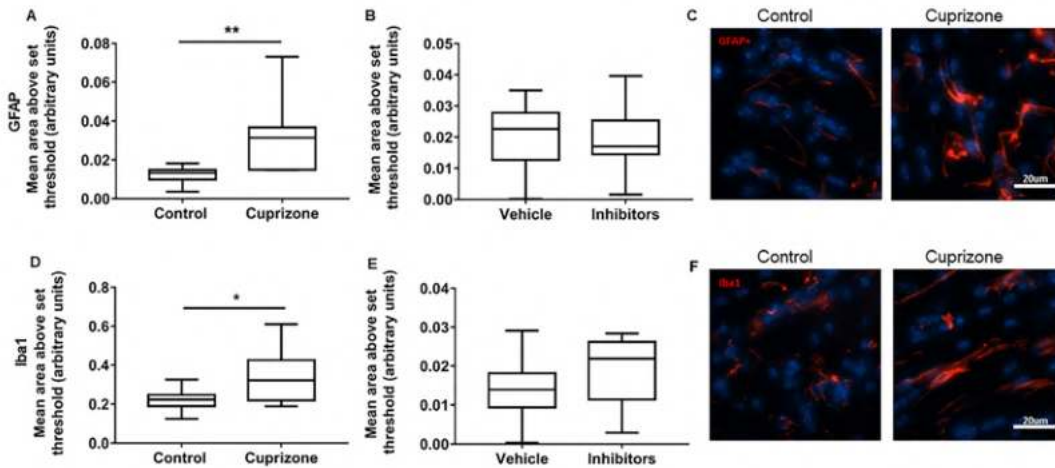


Fig. 3. Effects of cuprizone and the ion channel inhibitors on GFAP and Iba1 immunointensity. Semi-quantification of GFAP (A) and Iba1 (D) area of immunointensity above an arbitrary set threshold in the corpus callosum following 3 weeks cuprizone feeding compared to control fed animals; and (B, E) following treatment with the ion channel inhibitor combination or vehicle control for 3 weeks where all animals were administered cuprizone, (C, F) representative images. Graphs display min to max values, with the central line representing the median data point, and statistical significance indicated with * $p \leq 0.05$, ** $p \leq 0.01$; scale bars = 15 μm .

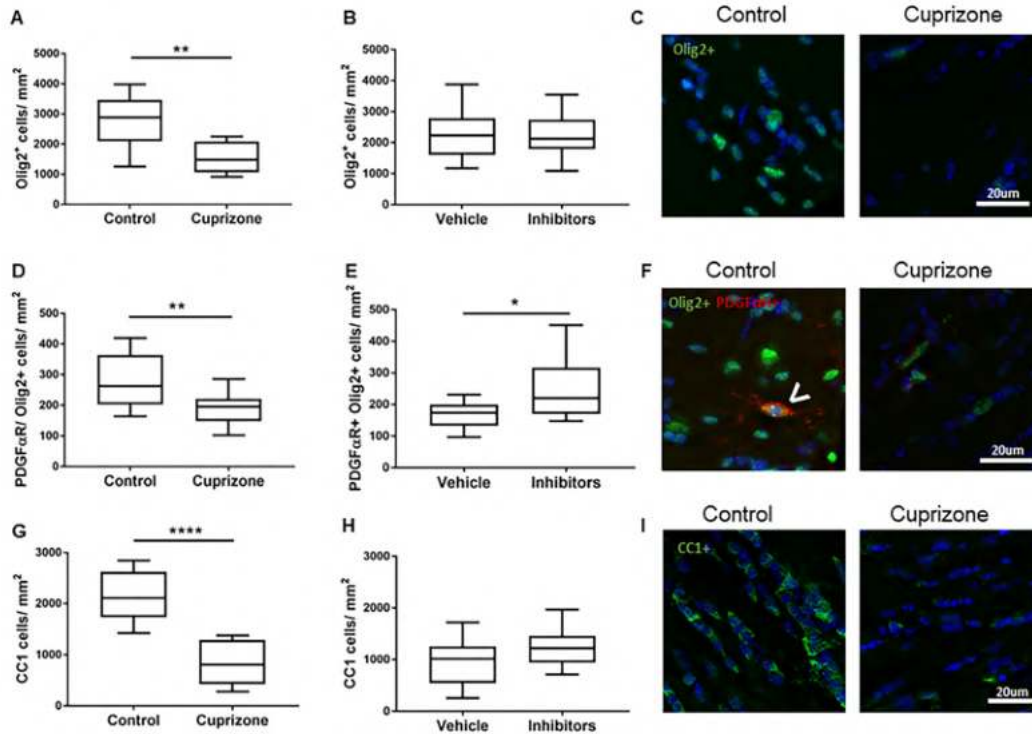


Fig. 4. Effects of cuprizone and the ion channel inhibitors on oligodendroglial cell densities. Densities of Olig2+ oligodendroglial cells (A), PDGFαR+/Olig2+ OPCs (D) and CC1+ oligodendrocytes (G) in the corpus callosum following 3 weeks cuprizone feeding compared to control fed animals; and (B, E, H) following treatment with the ion channel inhibitor combination or vehicle control for 3 weeks where all animals were administered cuprizone; (C, F, I) representative images with cells indicated with arrow heads; scale bar = 15 μm. Graphs display min to max values, with the central line representing the median data point, and statistical significance indicated with * $p \leq 0.05$, **** $p \leq 0.0001$.

(Bullard et al., 2007), which further supports that activated astrocytes can play a beneficial role in limiting cuprizone-induced damage, but further work is needed to investigate this possible mechanism further.

Treatment with the ion channel inhibitor combination did not alter the level of 8OHdG immunoreactivity in the current study. This may be due to the nature of cuprizone-induced toxicity, whereby cuprizone directly causes oxidative stress with increases in superoxide anions (Prael et al., 2014), inhibition of complex IV on the electron transport chain (Acs et al., 2013), decreased activity of copper-dependent cytochrome c (Matsushima and Morell, 2001) and copper-zinc superoxide dismutase (Zhang et al., 2008) within the mitochondria. Therefore, this early mitochondrial dysfunction and the subsequent intracellular oxidative damage to DNA may be upstream of ionic dyshomeostasis (Tameh et al., 2013) and not modulated by the current ion channel inhibitor treatment. However, altered Ca^{2+} flux also feeds forward to exacerbate oxidative stress via further increases in ROS (Kowaltowski et al., 2009). As such, Ca^{2+} influx and oxidative damage are inextricably linked and both substantially contribute to demyelinating disease. While it is difficult to conclude whether the observed outcomes were due to modulated Ca^{2+} influx or oxidative damage, we believe that no other model of demyelination would more effectively model these events. Cuprizone selectively targets oligodendroglial cells (Acs et al., 2013), and thus damage originating from other cellular subpopulations are largely secondary to the initial cuprizone insult, which may account for the selective improvements in 3NT, rather than both 3NT and 8OHdG.

Reactive nitrogen species are observed mediators of demyelination

in MS lesions (Smith et al., 1999), with 3NT being highly expressed on myelin membranes in acute MS lesions (Liu et al., 2001). The percentage of Node of Ranvier complexes with an atypical morphology was decreased by treatment with the combination of ion channel inhibitors in this study. Thus, the association between the decrease in this indicator of protein nitration and restoration of typically structured nodes may be causative. However, other structural elements of the Node of Ranvier were not preserved by treatment with the ion channel inhibitor combination, which suggests that damage to myelin is not solely mediated by nitrosative stress in the cuprizone model.

PDGFαR+/olig2+ cells are OPCs, whereas olig2+ cells are oligodendroglia in general i.e. precursor cells as well as more mature oligodendroglia. Interestingly, there was a significant increase in the number of OPCs when animals were given the ion channel inhibitor treatment, whereas oligodendrocytes were unaffected. This suggests a selective protective mechanism, perhaps in an attempt to produce additional myelinating oligodendrocytes for remyelination, however it is unknown whether this increase in OPCs is due to enhanced proliferation or recruitment. It has been proposed that failure to remyelinate is caused by the inability of OPCs to completely differentiate to a mature myelin producing oligodendrocyte, observed in both MS and the cuprizone model of demyelinating disease (Duncan et al., 2017; Kuhlmann et al., 2008; Fancy et al., 2010). In this study, we did observe colocalisation of 8OHdG in OPCs, and this DNA damage may have contributed to an inability of these cells to differentiate. Once an oligodendrocyte has myelinated an axon, it is relatively unable to remyelinate (Watkins et al., 2008), thus the production of new

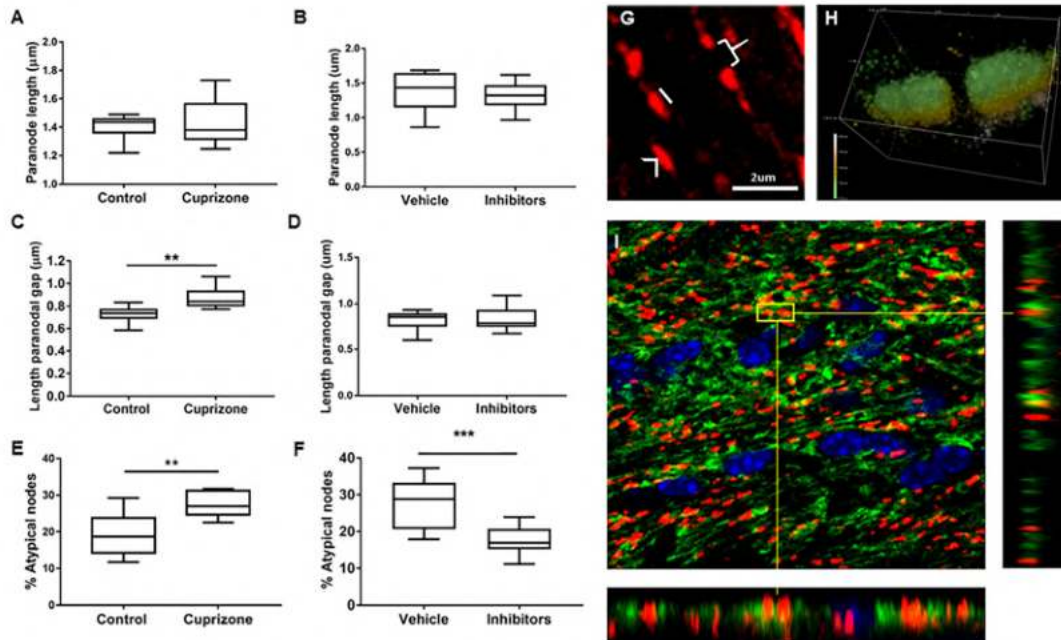


Fig. 5. Effects of cuprizone administration on Node of Ranvier complexes. Node/paranode complexes were analysed in the medial corpus callosum, quantifying (A) paranode length, (C) paranodal gap length and (E) percentage of atypical node/paranode complexes following 3 weeks cuprizone feeding compared to control fed animals; and (B, D, F) following treatment with the ion channel inhibitor combination or vehicle control for 3 weeks where all animals were administered cuprizone. Graphs display min to max values, with the central line representing the median data point, and significant differences are indicated by ** $p \leq 0.01$, *** $p \leq 0.001$. (G) Representative image illustrating measurements of paranode length (line), paranodal gap length (brace), and an atypical nodal complex (arrow head), scale bar = 2 µm. (H, I) Representative images showing the three dimensional nature of the Node of Ranvier complex and illustrating that complexes analysed lay within the z projection collected.

myelinating oligodendrocytes is essential for myelin repair (Franklin and Ffrench-Constant, 2008). Therefore, inhibition of OPC differentiation may account for the lack of effect of the ion channel inhibitor treatment on the number of oligodendrocytes. Furthermore, OPCs play an important role in neuroglial signalling, contacting the axon at the Node of Ranvier (Butt et al., 2004), and may be contributing to functional improvements and maintenance of Node of Ranvier structure. Future studies assessing the effects of limiting excess Ca^{2+} on functional outcomes will be necessary to elucidate the relative importance of the observed changes to pathophysiology.

5. Final conclusions

Usage of a combination of ion channel inhibitors has allowed a greater understanding of the contribution of excess Ca^{2+} influx to the various elements of pathology in demyelinating disease. The lack of consistent effect on all outcome measures illustrates the complexity of the disease process and the need to identify and modulate additional triggers of oxidative damage and myelin disruption.

Declaration of Competing Interest

None.

Acknowledgements

We thank Ms Storm Manning for technical assistance. We acknowledge financial support from MS Research Australia (16-002). MF has been supported by an NHMRC Career Development Fellowship

(APP1087114).

References

- Acs, P., Komoly, S., 2012. Selective ultrastructural vulnerability in the cuprizone-induced experimental demyelination. *Ideggyogy Sz.* 65, 266–270.
- Acs, P., Selak, M.A., Komoly, S., Kalman, B., 2013. Distribution of oligodendrocyte loss and mitochondrial toxicity in the cuprizone-induced experimental demyelination model. *J. Neuroimmunol.* 262, 128–131.
- Baltrons, M.A., Garcia, A., 1997. AMPA receptors are coupled to the nitric oxide/cyclic GMP pathway in cerebellar astroglial cells. *Eur. J. Neurosci.* 9, 2497–2501.
- Bhuyan, P., Patel, D., Wilcox, K., Patel, M., 2015. Oxidative stress in murine Theiler's virus-induced temporal lobe epilepsy. *Exp. Neurol.* 271, 329–334.
- Biller, A., Pflugmann, I., Badde, S., Diem, R., Wildemann, B., Nagel, A.M., Jordan, J., Benkhedah, N., Kleesiek, J., 2016. Sodium MRI in multiple sclerosis is compatible with intracellular sodium accumulation and inflammation-induced hyper-cellularity of acute brain lesions. *Sci. Rep.* 6, 31269.
- Bullard, D.C., Hu, X., Schoeb, T.R., Collins, R.G., Beaudet, A.L., Barnum, S.R., 2007. Intercellular adhesion molecule-1 expression is required on multiple cell types for the development of experimental autoimmune encephalomyelitis. *J. Immunol.* 178, 851–857.
- Butt, A.M., Pugh, M., Hubbard, P., James, G., 2004. Functions of optic nerve glia: axoglial signalling in physiology and pathology. *Eye (Lond.)* 18, 1110–1121.
- Camello-Almaraz, M.C., Pozo, M.J., Murphy, M.P., Camello, P.J., 2006. Mitochondrial production of oxidants is necessary for physiological calcium oscillations. *J. Cell Physiol.* 206, 487–494.
- Correale, J., Farez, M., 2015. The role of astrocytes in multiple sclerosis progression. *Front. Neurol.* 6.
- Dalla Libera, D., Di Mitri, D., Bergami, A., Centonze, D., Gasperini, C., Grasso, M.G., Galgani, S., Martinelli, V., Comi, G., Avolio, C., Martino, G., Borsellino, G., Sallusto, F., Battistini, L., Furlan, R., 2011. T regulatory cells are markers of disease activity in multiple sclerosis patients. *PLoS One* 6, e21386.
- Diaz-Hernandez, J.I., Gomez-Villafuertes, R., Leon-Otegui, M., Hontecillas-Prieto, L., Del Puerto, A., Trejo, J.L., Lucas, J.L., Garrido, J.J., Gualix, J., Miras-Portugal, M.T., Diaz-Hernandez, M., 2012. In vivo P2X7 inhibition reduces amyloid plaques in Alzheimer's disease through GSK3beta and secretases. *Neurobiol. Aging* 33, 1816–1828.

- Duncan, G.J., Pleml, J.R., Assinck, P., Manesh, S.B., Muir, F.G.W., Hirata, R., Berson, M., Liu, J., Wegner, M., Emery, B., Moore, G.R.W., Tetzlaff, W., 2017. Myelin regulatory factor drives remyelination in multiple sclerosis. *Acta Neuropathologica* 134, 403–422.
- Emery, B., 2010. Regulation of oligodendrocyte differentiation and myelination. *Science* 330, 779–782.
- Espejo, C., Penkowa, M., Saez-Torres, I., Hidalgo, J., Garcia, A., Montalbán, X., Martínez-Caceres, E., 2002. Interferon- γ regulates oxidative stress during experimental autoimmune encephalomyelitis. *Exp. Neurol.* 177, 21–31.
- Fancy, S.P.J., Kotter, M.R., Harrington, E.P., Huang, J.K., Zhao, C., Rowitch, D.H., Franklin, R.J.M., 2010. Overcoming remyelination failure in multiple sclerosis and other myelin disorders. *Experimental Neurology* 225, 18–23.
- Fiorini, A., Koudriavtseva, T., Bucaj, E., Coccia, R., Foppoli, C., Giorgi, A., Schininà, M.E., Di Domenico, F., De Marco, F., Perluigi, M., 2013. Involvement of oxidative stress in occurrence of relapses in multiple sclerosis: the spectrum of oxidatively modified serum proteins detected by proteomics and redox proteomics analysis. *PLoS One* 8, e65184.
- Fitzgerald, M., Bartlett, C.A., Harvey, A.R., Dunlop, S.A., 2010. Early events of secondary degeneration after partial optic nerve transection: an immunohistochemical study. *J. Neurotrauma* 27, 439–452.
- Franke, H., Gunther, A., Grosche, J., Schmidt, R., Rossner, S., Reinhardt, R., Faber-Zuschratter, H., Schneider, D., Illes, P., 2004. P2X7 receptor expression after ischemia in the cerebral cortex of rats. *J. Neurophysiol. Exp. Neurol.* 63, 686–699.
- Franklin, R., French-Constant, C., 2008. Remyelination in the CNS: from biology to therapy. *Nat. Rev. Neurosci.* 9, 839–855.
- Franklin, R.J., French-Constant, C., Edgar, J.M., Smith, K.J., 2012. Neuroprotection and repair in multiple sclerosis. *Nat. Rev. Neurol.* 8, 624–634.
- French, H.M., Reid, M., Mamontov, P., Simmons, R.A., Grinspan, J.B., 2009. Oxidative stress disrupts oligodendrocyte maturation. *J. Neurosci. Res.* 87, 3076–3087.
- Fries, M.A., Schattling, B., Fugger, L., 2014. Mechanisms of neurodegeneration and axonal dysfunction in multiple sclerosis. *Nat. Rev. Neurol.* 10, 225–238.
- Gandhi, S., Wood-Kaczmar, A., Yao, Z., Plun-Favreau, H., Deas, E., Klupsch, K., Downward, J., Latchman, D.S., Tabrizi, S.J., Wood, N.W., Duchon, M.R., Abramov, A.Y., 2009. PINK1-associated Parkinson's disease is caused by neuronal vulnerability to calcium-induced cell death. *Mol. Cell* 33, 627–638.
- Giacci, M.K., Bartlett, C.A., Smith, N.M., Iyer, K.S., Toomey, L.M., Jiang, H., Guagliardo, P., Kilburn, M.R., Fitzgerald, M., 2018. Oligodendroglia are particularly vulnerable to oxidative damage after neurotrauma in vivo. *J. Neurosci.* 38, 6491–6504.
- Gray, E., Thomas, T., Betmouni, S., Scolding, N., Love, S., 2008. Elevated myeloperoxidase activity in white matter in multiple sclerosis. *Neurosci. Lett.* 444, 195–198.
- Gurkoff, G., Shakhlaie, K., Lyeth, B., Berman, R., 2013. Voltage-gated calcium channel antagonists and traumatic brain injury. *Pharmaceuticals* 6, 788–812.
- Haider, L., Fischer, M.T., Frischer, J.M., Bauer, J., Hofberger, R., Botond, G., Esterbauer, H., Binder, C.J., Witzum, J.L., Lassmann, H., 2011. Oxidative damage in multiple sclerosis lesions. *Brain* 134, 1914–1924.
- Harlow, D.E., Saul, K.E., Culp, C.M., Vesely, E.M., Macklin, W.B., 2014. Expression of proteolipid protein gene in spinal cord stem cells and early oligodendrocyte progenitor cells is dispensable for normal cell migration and myelination. *J. Neurosci.* 34, 1333–1343.
- Hesse, A., Wagner, M., Held, J., Bruck, W., Salinas-Riester, G., Hao, Z., Waisman, A., Kuhlmann, T., 2010. In toxic demyelination oligodendroglial cell death occurs early and is FAS independent. *Neurobiol. Dis.* 37, 362–369.
- Hibbits, N., Yoshino, J., Le, T.Q., Armstrong, R.C., 2012. Astroglialosis during acute and chronic cuprizone demyelination and implications for remyelination. *ASN Neuro.* 4, 393–408.
- Hiremath, M.M., Saito, Y., Knapp, G.W., Ting, J.P., Suzuki, K., Matsushima, G.K., 1998. Microglial/macrophage accumulation during cuprizone-induced demyelination in C57BL/6 mice. *J. Neuroimmunol.* 92, 38–49.
- Huang, X., Li, Q., Li, H., Guo, L., 2009. Neuroprotective and antioxidative effect of cactus polysaccharides in vivo and in vitro. *Cell Mol. Neurobiol.* 29, 1211–1221.
- Kipp, M., Clamer, T., Dang, J., Copray, S., Beyer, C., 2009. The cuprizone animal model: new insights into an old story. *Acta Neuropathol.* 118, 723–736.
- Kowaltowski, A.J., De Souza-Pinto, N.C., Castilho, R.F., Vercesi, A.E., 2009. Mitochondria and reactive oxygen species. *Free Radic. Biol. Med.* 47, 333–343.
- Kuhlmann, T., Miron, V., Cui, Q., Wegner, C., Antel, J., Bruck, W., 2008. Differentiation block of oligodendroglial progenitor cells as a cause for remyelination failure in chronic multiple sclerosis. *Brain* 131, 1749–1758.
- Lin, M.T., Beal, M.F., 2006. Mitochondrial dysfunction and oxidative stress in neurodegenerative diseases. *Nature* 443, 787–795.
- Liu, J., Tian, D., Murugan, M., Eyo, U.B., Dreyfus, C.F., Wang, W., Wu, L.J., 2015. Microglial Hv1 proton channel promotes cuprizone-induced demyelination through oxidative damage. *J. Neurochem.* 135, 347–356.
- Liu, J.S., Zhao, M.L., Brosnan, C.F., Lee, S.C., 2001. Expression of inducible nitric oxide synthase and nitrotyrosine in multiple sclerosis lesions. *Am. J. Pathol.* 158, 2057–2066.
- Matsushima, G.K., Morell, P., 2001. The neurotoxicant, cuprizone, as a model to study demyelination and remyelination in the central nervous system. *Brain Pathol.* 11, 107–116.
- Matute, C., 2007. Interaction between glutamate signalling and immune attack in damaging oligodendrocytes. *Neuron Glia Biol.* 3, 281–285.
- Matute, C., Torre, I., Perez-Cerdá, F., Perez-Samartín, A., Alberdi, E., Etxebarria, E., Arranz, A.M., Ravid, R., Rodríguez-Antiguedad, A., Sánchez-Gómez, M., Domercq, M., 2007. P2X(7) receptor blockade prevents ATP excitotoxicity in oligodendrocytes and ameliorates experimental autoimmune encephalomyelitis. *J. Neurosci.* 27, 9525–9533.
- McTigue, D.M., Tripathi, R.B., 2008. The life, death, and replacement of oligodendrocytes in the adult CNS. *J. Neurochem.* 107, 1–19.
- Morel, A., Bijak, M., Niwald, M., Miller, E., Saluk, J., 2017. Markers of oxidative/nitritative damage of plasma proteins correlated with EDSS and BDI scores in patients with secondary progressive multiple sclerosis. *Redox Rep.* 22, 547–555.
- Naziroglu, M., Kutluhan, S., Ovey, I.S., Aykur, M., Yurekli, V.A., 2014. Modulation of oxidative stress, apoptosis, and calcium entry in leukocytes of patients with multiple sclerosis by Hypericum perforatum. *Nutr. Neurosci.* 17, 214–221.
- O'Hare Doig, R.L., Bartlett, C.A., Smith, N.M., Hodgetts, S.I., Dunlop, S.A., Hool, L., Fitzgerald, M., 2016. Specific combinations of ion channel inhibitors reduce excessive Ca(2+) influx as a consequence of oxidative stress and increase neuronal and glial cell viability in vitro. *Neuroscience* 339, 450–462.
- O'Hare Doig, R.L., Chiha, W., Giacci, M.K., Yates, N.J., Bartlett, C.A., Smith, N.M., Hodgetts, S.I., Harvey, A.R., Fitzgerald, M., 2017. Specific ion channels contribute to key elements of pathology during secondary degeneration following neurotrauma. *BMC Neurosci.* 18, 62.
- Peng, W., Cotrina, M.L., Han, X., Yu, H., Bekar, L., Blum, L., Takano, T., Tian, G.F., Goldman, S.A., Nedergaard, M., 2009. Systemic administration of an antagonist of the ATP-sensitive receptor P2 \times 7 improves recovery after spinal cord injury. *Proc. Natl. Acad. Sci. USA* 106, 12489–12493.
- Praet, J., Guglielmetti, C., Berneman, Z., Van der Linden, A., Ponsaerts, P., 2014. Cellular and molecular neuropathology of the cuprizone mouse model: clinical relevance for multiple sclerosis. *Neurosci. Biobehav. Rev.* 47, 485–505.
- Rivers, L.E., young, K.M., Rizzi, M., Jamen, F., Psachoulia, K., Wade, A., Kessaris, N., Richardson, W.D., 2008. PDGFRA/NG2 glia generate myelinating oligodendrocytes and piriform projection neurons in adult mice. *Nat. Neurosci.* 11, 1392–1401.
- Schuh, C., Wimmer, I., Hametner, S., Haider, L., Van Dam, A.-M., Liblau, R.S., Smith, K.J., Probert, L., Binder, C.J., Bauer, J., Bradl, M., Mahad, D., Lassmann, H., 2014. Oxidative tissue injury in multiple sclerosis is only partly reflected in experimental disease models. *Acta Neuropathol. (Berl.)* 128, 247–266.
- Skrupietz, T., Gudi, V., Hackstette, D., Stangel, M., 2011. De- and remyelination in the CNS white and grey matter induced by cuprizone: the old, the new, and the unexpected. *Histol. Histopathol.* 26, 1585–1597.
- Smith, K.J., Kapoor, R., Felts, P.A., 1999. Demyelination: the role of reactive oxygen and nitrogen species. *Brain Pathol.* 9, 69–92.
- Spaethling, J.M., Klein, D.M., Singh, P., Meaney, D.F., 2008. Calcium-permeable AMPA receptors appear in cortical neurons after traumatic mechanical injury and contribute to neuronal fate. *J. Neurotrauma* 25, 1207–1216.
- Sternberg, Z., Hennies, C., Sternberg, D., Wang, P., Kinkel, P., Hojnacki, D., Weinstock-Guttman, B., Munschauer, F., 2010. Diagnostic potential of plasma carboxymethyllysine and carboxyethyllysine in multiple sclerosis. *J. Neuroinflammation* 7, 72.
- Stys, P.K., Waxman, S.G., Ransom, B.R., 1992. Ionic mechanisms of anoxic injury in mammalian CNS white matter: role of Na⁺ channels and Na⁺/Ca²⁺ exchanger. *J. Neurosci.* 12, 430–439.
- Szymanski, C.R., Chiha, W., Morellini, N., Cummins, N., Bartlett, C.A., O'Hare Doig, R.L., Savigni, D.L., Payne, S.C., Harvey, A.R., Dunlop, S.A., Fitzgerald, M., 2013. Paranode abnormalities and oxidative stress in optic nerve vulnerable to secondary degeneration: modulation by 670nm light treatment. *PLoS One* 8, e66448.
- Takahashi, M., Kohara, A., Shishikura, J., Kawasaki-Yatsugi, S., Ni, J.W., Yatsugi, S., Sakamoto, S., Okada, M., Shimizu-Sasamata, M., Yamaguchi, T., 2002. YM872: a selective, potent and highly water-soluble alpha-amino-3-hydroxy-5-methylisoxazole-4-propionic acid receptor antagonist. *CNS Drug Rev.* 8, 337–352.
- Tameh, A.A., Clarner, T., Beyer, C., Atlasi, M.A., Hassanzadeh, G., Naderian, H., 2013. Regional regulation of glutamate signaling during cuprizone-induced demyelination in the brain. *Ann. Anat.* 195, 415–423.
- Thorburne, S.K., Juurlink, B.H., 1996. Low glutathione and high iron govern the susceptibility of oligodendroglial precursors to oxidative stress. *J. Neurochem.* 67, 1014–1022.
- Volpe, J.J., 2011. Systemic inflammation, oligodendroglial maturation, and the encephalopathy of prematurity. *Ann. Neurol.* 70, 525–529.
- Watkins, T., Emery, B., Mulinyawe, S., Barres, B.A., 2008. Distinct stages of myelination regulated by g-secretase and astrocytes in a rapidly myelinating CNS coculture system. *Neuron* 60, 555–569.
- Witherick, J., Wilkins, A., Scolding, N., Kemp, K., 2010. Mechanisms of oxidative damage in multiple sclerosis and a cell therapy approach to treatment. *Autoimmune Dis.* 2011, 164608.
- Yamada, H., Chen, Y.N., Aihara, M., Araie, M., 2006. Neuroprotective effect of calcium channel blocker against retinal ganglion cell damage under hypoxia. *Brain Res.* 1071, 75–80.
- Zhang, Y., Xu, H., Jiang, W., Xiao, L., Yan, B., He, J., Wang, Y., Bi, X., Li, X., Kong, J., Li, X.-M., 2008. Quetiapine alleviates the cuprizone-induced white matter pathology in the brain of C57BL/6 mouse. *Schizophr. Res.* 106, 182–191.
- Zozulya, A.L., Wiendl, H., 2008. The role of regulatory T cells in multiple sclerosis. *Nat. Clin. Pract. Neurol.* 4, 384–398.

Appendix C. Introducing “Secondary degeneration of oligodendrocyte precursor cells occurs as early as 24 hours after optic nerve injury in rats”

As discussed in Chapter 6, the study presented throughout that chapter has since been published as a journal article. This paper investigated the vulnerability of OPCs to early oxidative DNA damage in the partial optic nerve transection model of neurotrauma. At 1 day following injury, there was observable secondary degeneration within the ventral nerve, with a significant increase in oxidative damage, BBB dysfunction, and cell proliferation and apoptosis. OPCs were found to be the majority of the proliferating and DNA damaged cells, but they did not comprise a similar majority of apoptotic cells. This study is presented below and has been published as:

Toomey L.M., Papini, M.G., Clarke, T.O., Wright, A.J., Denham, E., Warnock, A., McGonigle, T., Fitzgerald M., Anyaegbu, C. 2023. Secondary degeneration of oligodendrocyte precursor cells occurs as early as 24 hours after optic nerve injury in rats. *International Journal of Molecular Sciences* 24(4): 3463. doi.org/10.3390/ijms24043463



Article

Secondary Degeneration of Oligodendrocyte Precursor Cells Occurs as Early as 24 h after Optic Nerve Injury in Rats

Lillian M. Toomey ^{1,2}, Melissa G. Papini ¹, Thomas O. Clarke ³, Alexander J. Wright ¹, Eleanor Denham ¹, Andrew Warnock ¹, Terry McGonigle ¹, Carole A. Bartlett ³, Melinda Fitzgerald ^{1,2} and Chidozie C. Anyaegbu ^{1,2,*}

¹ Curtin Health Innovation Research Institute, Curtin University, Bentley, WA 6102, Australia

² Perron Institute for Neurological and Translational Science, Sarich Neuroscience Research Institute Building, 8 Verdun St., Nedlands, WA 6009, Australia

³ Experimental and Regenerative Neurosciences, School of Biological Sciences, The University of Western Australia, Perth, WA 6009, Australia

* Correspondence: chidozie.anyaegbu@curtin.edu.au; Tel.: +61-8-6457-0505

Abstract: Optic nerve injury causes secondary degeneration, a sequela that spreads damage from the primary injury to adjacent tissue, through mechanisms such as oxidative stress, apoptosis, and blood-brain barrier (BBB) dysfunction. Oligodendrocyte precursor cells (OPCs), a key component of the BBB and oligodendrogenesis, are vulnerable to oxidative deoxyribonucleic acid (DNA) damage by 3 days post-injury. However, it is unclear whether oxidative damage in OPCs occurs earlier at 1 day post-injury, or whether a critical ‘window-of-opportunity’ exists for therapeutic intervention. Here, a partial optic nerve transection rat model of secondary degeneration was used with immunohistochemistry to assess BBB dysfunction, oxidative stress, and proliferation in OPCs vulnerable to secondary degeneration. At 1 day post-injury, BBB breach and oxidative DNA damage were observed, alongside increased density of DNA-damaged proliferating cells. DNA-damaged cells underwent apoptosis (cleaved caspase3+), and apoptosis was associated with BBB breach. OPCs experienced DNA damage and apoptosis and were the major proliferating cell type with DNA damage. However, the majority of caspase3+ cells were not OPCs. These results provide novel insights into acute secondary degeneration mechanisms in the optic nerve, highlighting the need to consider early oxidative damage to OPCs in therapeutic efforts to limit degeneration following optic nerve injury.

Keywords: oligodendrocyte precursor cells; secondary degeneration; oxidative stress; DNA damage; proliferation; blood-brain barrier; CNS injury; optic nerve injury



Citation: Toomey, L.M.; Papini, M.G.; Clarke, T.O.; Wright, A.J.; Denham, E.; Warnock, A.; McGonigle, T.; Bartlett, C.A.; Fitzgerald, M.; Anyaegbu, C.C. Secondary Degeneration of Oligodendrocyte Precursor Cells Occurs as Early as 24 h after Optic Nerve Injury in Rats. *Int. J. Mol. Sci.* **2023**, *24*, 3463. <https://doi.org/10.3390/ijms24043463>

Academic Editors: Neil R. Miller and Rongkung Tsai

Received: 22 December 2022

Revised: 6 February 2023

Accepted: 7 February 2023

Published: 9 February 2023



Copyright: © 2023 by the authors. Licensee MDPI, Basel, Switzerland. This article is an open access article distributed under the terms and conditions of the Creative Commons Attribution (CC BY) license (<https://creativecommons.org/licenses/by/4.0/>).

1. Introduction

Injury to the central nervous system (CNS) involves two components of damage: the initial mechanical insult and a subsequent cascade of spreading damage called secondary degeneration [1]. The initial primary injury typically manifests as axonal shearing, contusions, and hemorrhage or hematoma [1,2]. Secondary degeneration occurs as pathological factors released by injured neurons and glia spread to the surrounding tissue, causing additional self-propagating damage [3]. Glaucoma and other optic neuropathies follow similar sequelae, where axonal injury to retinal ganglion cells triggers a plethora of degenerative mechanisms that spread throughout the visual system to progressively impair visual function [4]. Hypoxia-induced vascular dysfunction can reduce blood flow to the optic nerve head, contributing to axonal injury and vision loss in optic neuropathies [5,6]. The BBB, comprising endothelial cells, neurons, astrocytes, pericytes, and OPCs, is a key component of vascular function [7].

The rodent partial optic nerve transection model is especially useful for characterizing mechanisms of secondary damage in the optic nerve, facilitating spatial segregation

between primary and secondary injury. Only the dorsal aspect of the right optic nerve is partially transected thus leaving the ventral aspect vulnerable solely to secondary degenerative processes [8]. Within the initially spared tissue, a multitude of secondary degeneration mechanisms occur, including oxidative stress, BBB dysfunction, reactive gliosis, axonal damage, dysmyelination, and oligodendrocyte death, associated with functional deficits post-injury [9,10]. Such secondary damage can spread as far into the brain as the superior colliculus via the visual pathways, to elicit a remote degenerative response following optic nerve injury [11].

A key feature of secondary degeneration that exacerbates acute pathology is oxidative stress. Oxidative stress occurs when the rate of reactive oxygen species production increases and overwhelms the detoxification capacity of the antioxidant system [12]. Excessive levels of reactive oxygen species can cause damage to a variety of cellular structures, including lipids, proteins, and DNA [13]. One form of oxidative DNA damage is nucleobase modifications, such as the guanine oxidation by-product 8-hydroxy-2-deoxyguanosine (8OHdG). Nucleobase modifications can cause particularly harmful effects by either modifying the genetic code or blocking DNA replication [14].

Within 5 min of a partial optic nerve transection, astrocytes are oxidatively stressed and become hypertrophic by 3 h [15]. No changes in Olig2+ oligodendroglia are observed by 24 h. However, at day 3, oligodendroglia, including OPCs, are significantly more likely to become oxidatively DNA damaged than other cell types within the ventral optic nerve [16]. The heightened vulnerability of OPCs is likely due in part to increased concentrations of Ca²⁺-permeable P2X₇ receptors and α -amino-3-hydroxy-5-methyl-4-isoxazolepropionic acid (AMPA) receptors [17,18], increased intracellular iron levels [19], and decreased concentrations of antioxidant defenses [19,20]. Similarly, a specific subpopulation of newly derived mature oligodendrocytes has been identified to have elevated oxidative DNA damage compared to their pre-existing counterparts at this same time point [16]. The newly derived oligodendrocyte subpopulation was also less likely to become apoptotic than pre-existing oligodendrocytes, but instead demonstrated a decreased long-term capacity for myelination [16]. The concurrent death of pre-existing oligodendrocytes alongside the reduced myelination capacity of newly derived, DNA-damaged oligodendrocytes likely contributes to chronic deficits in myelination observed at 1, 3, and 6 months after optic nerve injury [21–23]. However, the specific vulnerability of oligodendroglia to this oxidative DNA damage at the earlier 1 day timepoint, is yet to be investigated. It is possible that a therapeutic window exists prior to 3 days, where oligodendroglia show signs of oxidative damage but are not yet proliferative or apoptotic.

To address this knowledge gap, this study assessed the vulnerability of OPCs to oxidative DNA damage at an acute 1 day timepoint following a partial optic nerve transection. Within the ventral nerve susceptible to secondary degeneration, 8OHdG DNA damage increased and correlated to the extent of BBB dysfunction. DNA-damaged cells showed increased proliferation with injury and increased apoptosis. While OPCs accounted for the majority of proliferating, DNA-damaged cells, these were not the largest population of apoptotic cells.

2. Results

2.1. Secondary Degeneration in the Ventral Optic Nerve following Partial Injury

At 1 day following a partial optic nerve transection, the ventral nerve was immunohistochemically assessed for 8OHdG, immunoglobulin G (IgG) and 5'Ethynyl-2-deoxyuridine (EdU) to quantify oxidative DNA damage, BBB dysfunction and cellular proliferation respectively. There was a significant effect of injury on both the area ($t(4.448) = 17, p = 0.0004$, Figure 1A) and mean intensity ($t(4.197) = 17, p = 0.0006$, Figure 1B) of 8OHdG immunoreactivity relative to sham controls, indicating increased oxidative DNA damage post-injury (Figure 1C). Similarly, the mean area of IgG immunoreactivity significantly increased with injury compared to sham controls ($Mdn_{sham} = 2.018, Mdn_{injured} = 0.00825, U = 0, p < 0.0001$, Figure 1D,F). The observed increase in IgG extravasation indicates an injury-induced breach

of the BBB. A strong and significant positive monotonic relationship between the mean areas of IgG and 8OHdG immunoreactivities was also observed ($r_s = 0.752$, $p = 0.0003$, Figure 1E), suggesting that animals with increased DNA damage in the ventral optic nerve typically experience greater levels of BBB dysfunction.

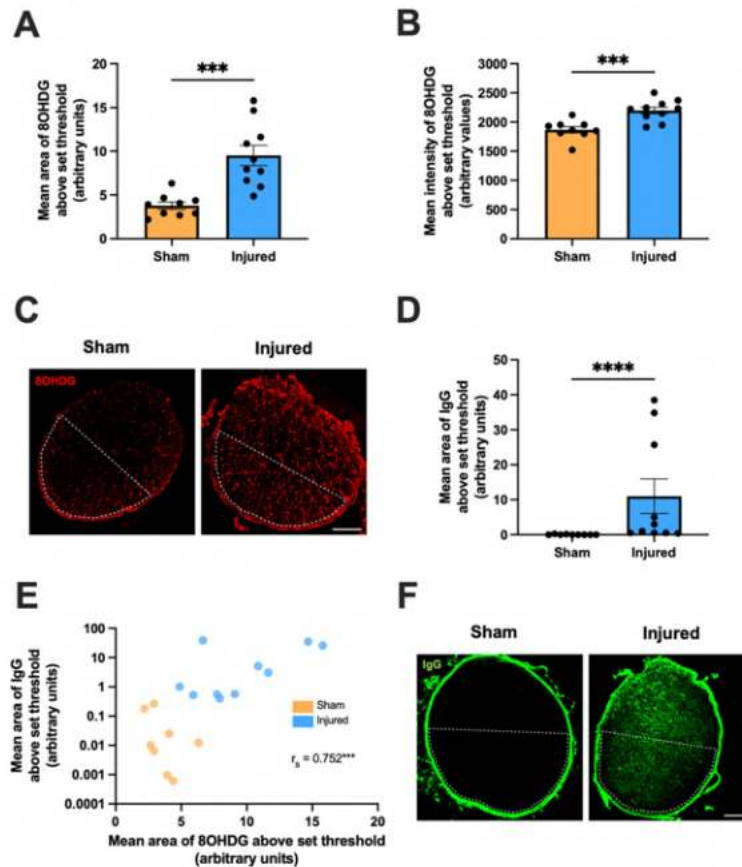


Figure 1. Effect of injury on oxidative DNA damage and BBB dysfunction within the ventral optic nerve, relative to sham injury. Area (A) and mean intensity (B) of 8OHdG immunoreactivity within the ventral optic nerve were assessed to determine the level of oxidative DNA damage. Graphs display individual data points overlaid on a bar displaying the mean \pm SEM. $n = 9$ – 10 rats per group. Statistical analysis by *t*-tests. (D) Area of IgG immunointensity within the ventral nerve was assessed to determine the extent of BBB breach. Graph displays individual data points overlaid on a bar displaying the mean \pm SEM. Statistical analysis by Mann-Whitney test. $n = 9$ – 10 rats per group. (E) The area of IgG immunointensity was correlated to the area of 8OHdG using Spearman's correlation, with the r_s value and corresponding *p*-value displayed on the graph. The mean area of IgG immunointensity was plotted on a log scale to best illustrate the overall relationship between IgG and 8OHdG on the scatterplot. Each data point on the graph represents an individual animal. $n = 8$ – 10 rats per group. (C,F) Representative images of both 8OHdG and IgG immunoreactivity in sham and injured rats are shown, scale bars = $100 \mu\text{m}$. Area of the ventral nerve is denoted by dotted lines. All areas above threshold measurements are presented in arbitrary units as the data have been normalized to the total area of the ventral nerve for each animal. No outliers were removed for any outcome measure. Significant differences are indicated by $*** p \leq 0.001$, $**** p \leq 0.0001$.

The effect of partial optic nerve transection on cellular proliferation as indicated by EdU+ staining in the ventral nerve was also assessed. There was a trend towards an increased density of EdU+ cells with injury compared to sham controls, although this difference did not reach statistical significance ($t(2,072) = 17, p = 0.0538$, Figure 2A). EdU+ cells were then categorized based on colocalization with 8OHdG above a set threshold and a two-way ANOVA was used to compare the densities of proliferating cells either with or without oxidative DNA damage ($F(1,34) = 2.947$, Figure 2B,D). A significant difference was observed by Tukey *post-hoc* comparisons in the density of EdU+ 8OHdG+ cells with injury compared to the sham group ($p = 0.0264$). There were no differences in the density of EdU+ 8OHdG− cells with injury compared to those without injury ($p > 0.05$). A weak but significant positive monotonic relationship between the mean area of IgG immunointensity and EdU+ densities was also observed ($r_s = 0.489, p = 0.0394$, Figure 2C).

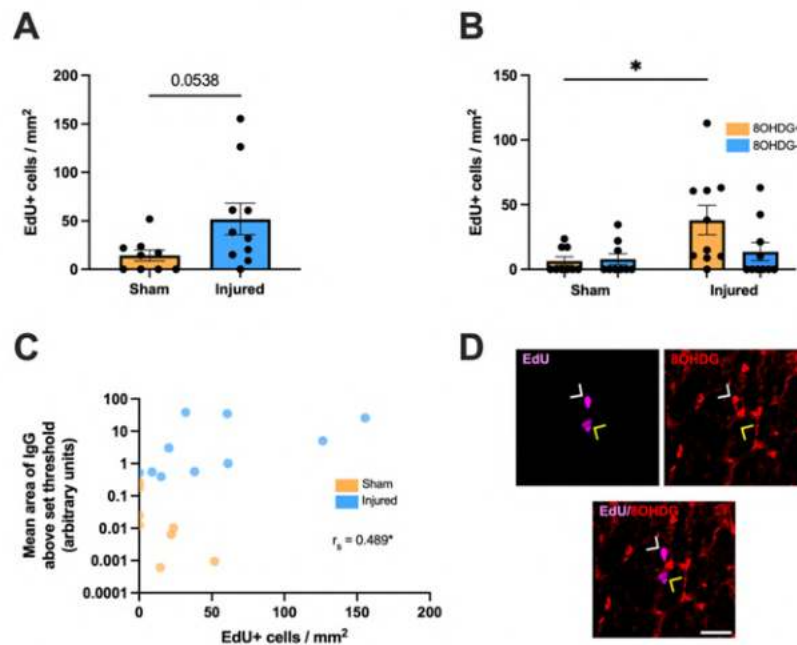


Figure 2. Effect of injury on cellular proliferation within the ventral optic nerve. (A) The density of EdU+ cells was quantified in the ventral optic nerve following partial optic nerve transection or sham injury. Graphs display individual data points overlaid on a bar displaying the mean \pm SEM. $n = 9$ – 10 rats per group. Statistical analysis by *t*-test. (B) The relative densities of EdU+ 8OHdG+ and EdU+ 8OHdG− cells were quantified. Statistical analysis by two-way ANOVA and Tukey *post-hoc* tests. Graphs display individual data points overlaid on a bar displaying the mean \pm SEM. $n = 9$ – 10 rats per group. (C) The area of IgG immunointensity was correlated to the density of EdU+ cells using Spearman's correlation, with the r_s value and corresponding *p*-value displayed on the graph. The mean area of IgG immunointensity was plotted on a log scale to best illustrate the overall relationship between IgG and EdU on the scatterplot. Each data point on the graph represents an individual animal. $n = 8$ – 10 rats per group. (D) Representative image of both an EdU+ 8OHdG+ cell (white arrow head) and an EdU+ 8OHdG− cell (yellow arrow head) is shown, scale bar = 25 μ m. No outliers were removed for any outcome measure. Significant differences are indicated by * $p \leq 0.05$.

Additionally, the effect of partial optic nerve transection on apoptosis was assessed by detecting Cleaved Caspase3, the proteolytically-cleaved and functionally-active form

of Caspase3 [24]. A significant increase was observed in the overall density of Cleaved Caspase3+ cells with injury compared to sham controls in the ventral nerve ($t(5.064) = 16$, $p = 0.0001$, Figure 3A). Cleaved Caspase3+ cells were then categorized based on colocalization with 8OHdG above a set threshold and a two-way ANOVA was used to compare the densities of apoptotic cells either with or without oxidative DNA damage ($F(1,32) = 25.64$, Figure 3B,D). A significant difference was observed by Tukey post hoc comparisons in the density of Cleaved Caspase3+ 8OHdG+ cells with injury compared to Cleaved Caspase3+ 8OHdG+ cells in the sham group ($p < 0.0001$). A significant increase was also found between Cleaved Caspase3+ cells with and without 8OHdG+ in both the injured ($p < 0.0001$) and sham groups ($p < 0.0001$). No differences were observed in the density of Cleaved Caspase3+ 8OHdG− cells with injury compared to Cleaved Caspase3+ 8OHdG− cells without injury ($p > 0.05$). A moderate and significant positive monotonic relationship between the mean area of IgG immunointensity and Cleaved Caspase3+ densities was also observed ($r_s = 0.694$, $p = 0.003$, Figure 3C).

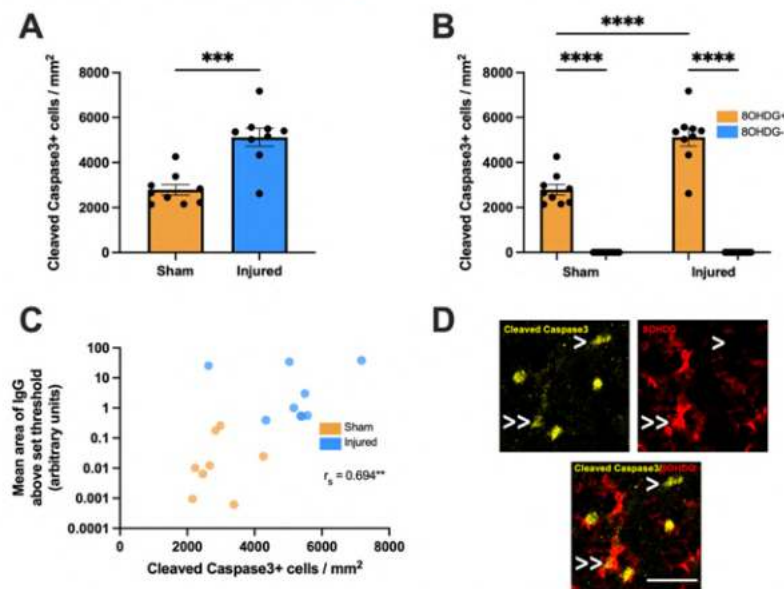


Figure 3. Effect of injury on apoptosis within the ventral optic nerve. (A) The density of Cleaved Caspase3+ cells was quantified in the ventral optic nerve following partial optic nerve transection or sham injury. Graphs display individual data points overlaid on a bar displaying the mean \pm SEM. $n = 9$ rats per group. Statistical analysis by t -test. (B) The relative densities of Cleaved Caspase3+ 8OHdG+ and Cleaved Caspase3+ 8OHdG− cells were quantified. Statistical analysis by two-way ANOVA and Tukey post hoc tests. Graphs display individual data points overlaid on a bar displaying the mean \pm SEM. $n = 9$ rats per group. (C) The area of IgG immunointensity was correlated to the density of Cleaved Caspase3+ cells using Spearman's correlation, with the r_s value and corresponding p -value displayed on the graph. The mean area of IgG immunointensity was plotted on a log scale to best illustrate the overall relationship between IgG and Cleaved Caspase3+ on the scatterplot. Each data point on the graph represents an individual animal. $n = 8$ – 9 rats per group. (D) Representative image of both a Cleaved Caspase3+ 8OHdG+ cell (indicated by >>) and a Cleaved Caspase3+ 8OHdG− cell (indicated by >) is shown, scale bar = 25 μ m. No outliers were removed for any outcome measure. Significant differences are indicated by ** $p \leq 0.01$, *** $p \leq 0.001$, **** $p \leq 0.0001$.

2.2. Heightened Vulnerability of OPCs to Oxidative DNA Damage

To identify oxidatively damaged OPCs, antibodies detecting neural/glial antigen 2 (NG2) [25] or platelet-derived growth factor receptor α (PDGFR α) [26] were utilized. Within NG2+ glia specifically, the mean intensity of 8OHdG immunoreactivity significantly increased compared to sham controls ($t(2.161) = 15, p = 0.0472$, Figure 4A,B). Correspondingly, there was a significant increase with injury in the mean intensity of 8OHdG within PDGFR α + glia ($t(3.992) = 17, p = 0.0007$, Figure 4C,D).

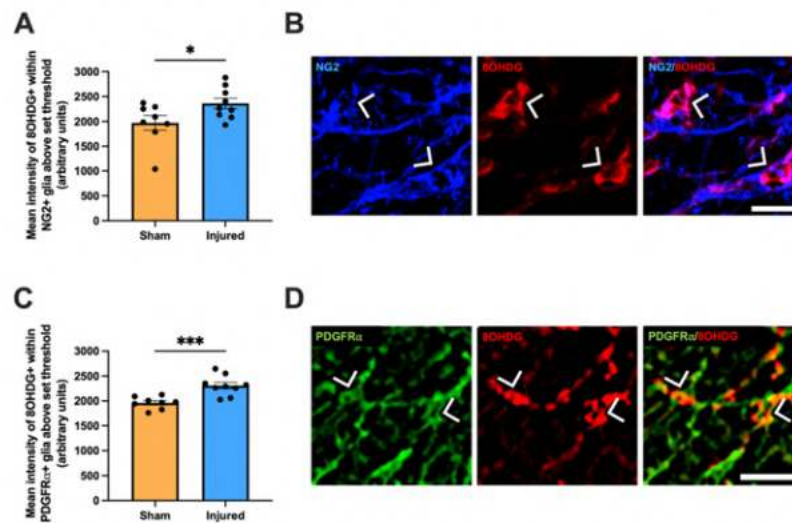


Figure 4. Effect of injury on oxidative DNA damage within NG2+ glia and PDGFR α + glia. The mean immunointensity of 8OHdG was specifically quantified in NG2+ glial cells (A) and PDGFR α + glia cells (C) in the ventral nerve. Graphs display individual data points overlaid on a bar displaying the mean \pm SEM. $n = 8$ –10 rats per group. Statistical analysis by t -tests. Representative images of NG2+ glia (B) and PDGFR α + glia (C) with 8OHdG+ DNA damage are shown, indicated with arrow heads, scale bars = 20 μ m. No outliers were removed for any outcome measure. Significant differences are indicated by * $p \leq 0.05$, *** $p \leq 0.001$.

2.3. Proliferative and Apoptotic Status of OPCs with Oxidative DNA Damage

The proliferative status of oxidatively DNA-damaged OPCs was then assessed within the ventral nerve. The EdU+ population was first identified as either PDGFR α + or PDGFR α – cells and analyzed using a two-way ANOVA ($F(1,36) = 1.457$, Figure 5A). Tukey post hoc comparisons revealed a significant increase in the density of EdU+ PDGFR α + OPCs with injury compared to sham ($p = 0.0466$). No significant difference was observed in the density of EdU+ PDGFR α – cells with injury ($p > 0.05$). The EdU+ PDGFR α + and EdU+ PDGFR α – populations were further classified by colocalization with 8OHdG DNA damage and analyzed via a three-way ANOVA with Tukey post hoc comparisons ($F(1, 64) = 1.958$, Figure 5B,C). There was a significant increase with injury in the density of EdU+ PDGFR α + 8OHdG+ cells compared to sham ($p = 0.0115$). Interestingly, the densities of EdU+ PDGFR α + 8OHdG+ cells were also significantly higher than EdU+ PDGFR α + 8OHdG– cells within injured animals ($p = 0.0033$). No significant differences were observed with injury for EdU+ PDGFR α + 8OHdG– OPCs ($p > 0.05$), or EdU+ PDGFR α – 8OHdG+ ($p > 0.05$) or EdU+ PDGFR α – 8OHdG– ($p > 0.05$) cells compared to sham. Altogether, this suggests that OPCs are the major proliferating, DNA-damaged cell type at 1 day following injury to the optic nerve.

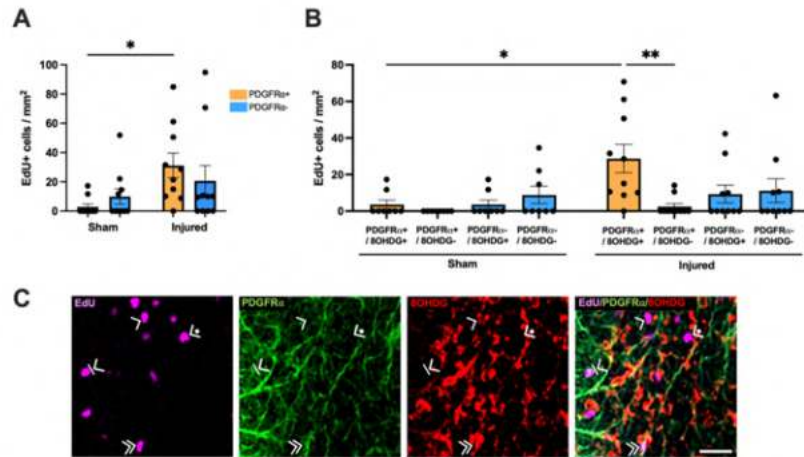


Figure 5. Effect of injury on proliferation and oxidative DNA damage within OPCs. (A) The relative densities of EdU+ PDGFR α + and EdU+ PDGFR α - OPCs were quantified. Statistical analysis by two-way ANOVA and Tukey post hoc tests. (B) The relative densities of EdU+ cells colocalized with PDGFR α and 8OHdG were quantified. Statistical analysis by three-way ANOVA with Tukey post hoc tests. Graphs display individual data points overlaid on a bar displaying the mean \pm SEM. $n = 8$ –10 rats per group. (C) Representative images illustrating EdU+ PDGFR α + 8OHdG+ OPCs (indicated by >>), EdU+ PDGFR α + 8OHdG- OPCs (indicated by >|), EdU+ PDGFR α - 8OHdG+ cells (indicated by >), EdU+ PDGFR α - 8OHdG- cells (indicated by >>) are shown, scale bar = 25 μ m. No outliers were removed for any outcome measure. Significant differences are indicated by * $p \leq 0.05$, ** $p \leq 0.01$.

The apoptotic status of oxidatively DNA-damaged OPCs was also assessed within the ventral nerve. The Cleaved Caspase3+ population was initially identified as either PDGFR α + or PDGFR α - cells and analyzed using a two-way ANOVA ($F(1,32) = 5.611$, Figure 6A). Tukey post hoc comparisons revealed no significant increase in the density of Cleaved Caspase3+ PDGFR α + OPCs with injury compared to sham ($p > 0.05$). A significant difference was observed in the density of Cleaved Caspase3+ PDGFR α - cells with injury ($p < 0.0001$). There was also a significant increase in the density of Cleaved Caspase3+ PDGFR α - cells compared to Cleaved Caspase3+ PDGFR α + cells within both injured ($p < 0.0001$) and sham groups ($p < 0.0001$). The Cleaved Caspase3+ PDGFR α + and Cleaved Caspase3+ PDGFR α - populations were further classified by colocalization with 8OHdG DNA damage and analyzed via a three-way ANOVA with Tukey *post-hoc* comparisons ($F(1, 64) = 33.37$, Figure 6B,C). There was a significant increase with injury in the density of both Cleaved Caspase3+ PDGFR α + 8OHdG+ OPCs ($p = 0.0304$) and Cleaved Caspase3+ PDGFR α - 8OHdG+ cells ($p < 0.0001$) compared to sham. Within the sham group, there were significantly more Cleaved Caspase3+ PDGFR α - 8OHdG+ cells than Cleaved Caspase3+ PDGFR α + 8OHdG+ OPCs ($p < 0.0001$), Cleaved Caspase3+ PDGFR α + 8OHdG- OPCs ($p < 0.0001$) and Cleaved Caspase3+ PDGFR α - 8OHdG- cells ($p < 0.0001$). Similarly, within the injured group, there were significantly more Cleaved Caspase3+ PDGFR α - 8OHdG+ cells than OPCs that were Cleaved Caspase3+ PDGFR α + 8OHdG+ ($p < 0.0001$) or Cleaved Caspase3+ PDGFR α + 8OHdG- ($p < 0.0001$) or Cleaved Caspase3+ PDGFR α - 8OHdG- cells ($p < 0.0001$). In addition, there was a significant increase in the density of Cleaved Caspase3+ PDGFR α + 8OHdG+ OPCs compared to both Cleaved Caspase3+ PDGFR α + 8OHdG- OPCs ($p = 0.0019$) and Cleaved Caspase3+ PDGFR α - 8OHdG- cells ($p = 0.0019$) within the injured group. These data indicate an

increase in apoptosis of DNA-damaged OPCs at 1 day following injury to the optic nerve, though these cells do not form the majority of the overall apoptotic cell population.

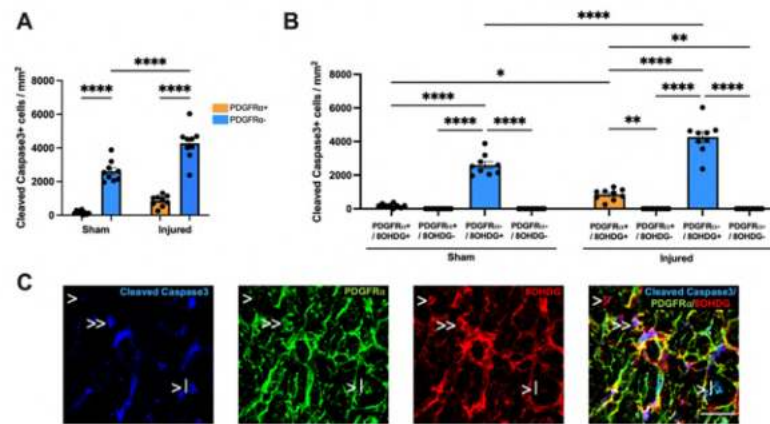


Figure 6. Effect of injury on apoptosis and oxidative DNA damage of OPCs. (A) The relative densities of Cleaved Caspase3+ PDGFR α + and Cleaved Caspase3+ PDGFR α - OPCs were quantified. Statistical analysis by two-way ANOVA and Tukey post hoc tests. (B) The relative densities of Cleaved Caspase3+ cells colocalized with PDGFR α and 8OHdG were quantified. Statistical analysis by three-way ANOVA with Tukey post hoc tests. Graphs display individual data points overlaid on a bar displaying the mean \pm SEM. $n = 9$ rats per group. (C) Representative image illustrating Cleaved Caspase3+ PDGFR α + 8OHdG+ cells (indicated by >>), Cleaved Caspase3+ PDGFR α + 8OHdG- cells (indicated by >|) and Cleaved Caspase3+ PDGFR α - 8OHdG+ cells (indicated by >) is shown. Cleaved Caspase3+ PDGFR α - 8OHdG- cells were not observed in the ventral nerve. Scale bar = 25 μ m. No outliers were removed for any outcome measure. Significant differences are indicated by * $p \leq 0.05$, ** $p \leq 0.01$, **** $p \leq 0.0001$.

3. Discussion

This study investigated the role of oxidative DNA damage to OPCs following optic nerve injury at an acute 1 day timepoint. Early pathological changes induced within the ventral nerve were indicative of secondary degeneration mechanisms, with observed increases in BBB dysfunction and 8OHdG DNA damage, as well as increased cellular proliferation specifically in DNA-damaged cells. Heightened DNA damage was also specifically identified within both NG2+ glia and PDGFR α + glia, indicating a vulnerability of OPCs to oxidative DNA damage. Apoptotic cells were DNA damaged, and associated with BBB breach. Finally, this study demonstrated that while the PDGFR α + OPC population was the major proliferating, DNA-damaged cell type following injury to the optic nerve, most of the apoptotic cells were not OPCs. While additional research is needed to further delineate the role of oxidative damage post-injury, these novel results provide valuable insights into early mechanisms that underpin secondary degeneration of the optic nerve at 1 day following injury.

In line with previous work that assessed outcomes at 1 day following a partial optic nerve transection, this study found significant increases in DNA damage and BBB dysfunction in the ventral optic nerve vulnerable to secondary degeneration [10,27]. A strong and significant relationship between the extent of oxidative DNA damage and BBB breach was also uncovered and observed across animals in both sham and injured groups. Though oxidative stress had already been closely associated with BBB dysfunction in a variety of CNS diseases and injuries [28], a direct relationship between the two has not been previously investigated within the partial optic nerve transection model. Taken together with the increased oxidative damage to OPCs, this direct relationship suggests that the

observed increase in parenchymal IgG relates to a breakdown of the OPC component of the BBB and not due to transcellular transport [29]. The density of DNA-damaged cells undergoing proliferation significantly increased with injury. Meanwhile, there was no change in the density of proliferating cells without DNA damage as indicated by 8OHdG immunoreactivity. This finding suggests a relationship between oxidative DNA damage and cellular proliferation that requires further elucidation. Additionally, it will be important to determine whether oxidative damage is driving, or is a consequence of, secondary pathological mechanisms.

Consistent with previous studies [25,30], this study used NG2 and PDGFR α separately to identify OPCs. In our hands, immunohistochemical detection reliably allowed quantification of one cell identifying marker together with the functional indicators 8OHdG and Cleaved Caspase3. We, therefore, identified OPCs using a combination of their expression of NG2 or PDGFR α and known morphology (i.e., round features with small processes; in line with several other studies [25,31]). The majority of the PDGFR α + cells in this study were most likely OPCs, as OPCs have the most abundant expression of PDGFR α in the CNS [26] and PDGFR α is the best singular marker for OPCs [25]. PDGFR α and NG2 likely identified a similar population of OPCs in this study, as the distribution and morphology of PDGFR α + cells coincide with NG2+ cells in the brain [30,32], and PDGFR α + and NG2+ cells showed a similar pattern of oxidative damage.

OPCs have previously been shown to be vulnerable to DNA damage at 3 days following a partial optic nerve transection [16]. The present study showed that this pathology occurs as early as 1 day after injury, with increases in oxidative DNA damage specifically observed within both NG2+ glia and PDGFR α + glia. The PDGFR α + OPC population was the major proliferating and DNA-damaged cell type. This finding builds on previous work in this model which showed that approximately 54% of proliferating cells were NG2+ Olig2+ OPCs at 1 day post-injury [33]. This early proliferative response of OPCs to injury occurs prior to the onset of cell death at 7 days, with OPC loss continuing out to 3 months post-injury [33]. Therefore, the observed early proliferation does not prevent a chronic depletion of OPCs later in the pathological sequelae. Combined with the observed increase in the proliferation of OPCs with oxidative DNA damage specifically within the injured nerve, these data suggest that proliferation could be an early indicator of OPC damage and dysfunction following optic nerve injury. However, whether increased OPC proliferation is actively induced by DNA damage or whether already proliferating OPCs are inherently more vulnerable to oxidative stress mechanisms post-injury is not yet known. Indeed, not all of the cells that are proliferating post-injury are OPCs, with a variety of cells known to proliferate following CNS injury, including astrocytes and microglia [34,35]. Nevertheless, the data suggest that oxidatively damaged OPCs drive the majority of cellular proliferation acutely post-injury.

As OPCs differentiate into mature oligodendrocytes post-injury, a peak ratio of proliferating to non-proliferating OPCs occurs at 3 days post-injury before these EdU+ OPCs differentiate through the stages of the oligodendroglial lineage towards mature myelinating oligodendrocytes [16]. By 3 days following a partial optic nerve transection, there is also a specific subpopulation of newly derived mature oligodendrocytes that have increased levels of DNA damage compared to their pre-existing counterparts [16]. Therefore, it is highly likely that a proportion of the identified proliferating and DNA-damaged OPC population at 1 day post-injury may differentiate into mature oligodendrocytes at later timepoints. This subpopulation of DNA-damaged, newly derived mature oligodendrocytes are less likely to become apoptotic than pre-existing oligodendrocytes but demonstrate a decreased long-term capacity for myelination [16]. The decreased apoptosis of newly derived and proliferating oligodendrocytes suggests that proliferation and differentiation may have been protective against the cell death associated with DNA damage post-injury. Nevertheless, the concurrent death of pre-existing oligodendrocytes alongside the reduced myelination capacity of newly derived, DNA-damaged oligodendrocytes likely contributes to chronic deficits in myelination following injury.

Heterogeneity within the overall OPC population [36] could convey varying degrees of susceptibility to oxidative damage. For example, some OPCs colocalize and interact with blood vessels, whilst others reside solely in the brain parenchyma [37]. OPCs with an intermediate phenotype have also been observed, whereby they are both simultaneously perivascular and parenchymal [38], suggesting a spectrum of OPC phenotypes based on association with the vasculature. Functional differences between OPC subpopulations identified here remain to be investigated. However, it may be that a portion of the observed DNA-damaged OPCs modulated detrimental effects at the BBB. OPCs located at the vasculature have already been found to play a key role in BBB integrity under pathological conditions, such as cerebral hypoperfusion [39] and MS [40,41]. Therefore, future studies should determine the relative vulnerability of OPC subpopulations to oxidative DNA damage to elucidate any potential contribution of perivascular OPC damage in pathological BBB dysfunction. It is also important to note that OPCs do not exist in isolation, and cross-talk between OPCs and other cells, both in the parenchyma and at the perivascular regions, is likely to contribute to outcomes.

Female rats were used in this study to enable initial comparison with our previously published work and to address the disproportionate overrepresentation of male animals within neuroscience literature. Future studies will include both male and female rats to identify possible sex-dependent changes. However, it is noteworthy that differences were observed between injured and uninjured female rats, indicating that any potential effect of female hormones does not preclude the detection of injury-induced changes in these animals.

This study identified OPCs as the major proliferating, DNA-damaged cells acutely following optic nerve injury. The observed early oxidative damage to this cell type likely plays a key role in exacerbating pathology post-injury, further highlighting oxidative stress as a therapeutic target worthy of future investigation. Pharmacological modulation of glial components of the BBB, such as the aquaporin-4 water channel on astrocytes, has been shown to reduce vasogenic edema and improve function in rats with CNS injury [42]. Given the importance of OPCs for BBB and CNS function, therapeutic interventions that attenuate oxidative DNA damage in OPCs are likely to mitigate the progression of secondary degeneration to axonal and functional loss after injury. Computer-aided, high-throughput drug screening platforms that investigate up to a hundred thousand compounds per day have the potential to accelerate the discovery or repurposing of drugs that effectively target oxidative stress-induced OPC dysfunction [43]. High-resolution imaging of OPCs and associated cells in humanized, self-organized 3D organoids or microvessel-on-a-chip platforms would facilitate the robust assessment of drug candidates likely to be effective in humans [44,45].

4. Materials and Methods

4.1. Animal Procedures and Study Design

Twenty adult, female PVG rats (180 g) were obtained from the Animal Resource Centre in Murdoch, Western Australia. All procedures were in accordance with the principles of the National Health and Medical Research Council (NHMRC) of Australia Code of Practice for use of Animals for Scientific Purposes and were approved by the Animal Ethics Committee of The University of Western Australia (RA/3/100/1485) and the Animal Ethics Committee of Curtin University (ARE2017-4). The rats were provided ad libitum access to both food and water and were housed under a 12 h light/dark cycle. Rats were also given a 1 week acclimatization period to the holding facility prior to commencing the experimental period. The cohort consisted of two experimental groups: a sham control group ($n = 10$) and an injured group ($n = 10$).

4.2. Surgical Procedures

Partial optic nerve transections were performed as previously described [8], under anesthesia with intraperitoneal Ketamine (Ketamil, 50 mg/kg, Troy Laboratories,

Glendenning, Australia) and Xylazine (Ilium Xylazil, 10 mg/kg, Troy Laboratories). In brief, the right optic nerve was surgically exposed about 1 mm behind the eye and the dorsal aspect of the nerve was partially lesioned to approximately 200 μm using a diamond radial keratotomy knife (Geuder, Heidelberg, Germany). Rats that underwent a sham injury received all surgical procedures except the cut in the surrounding nerve sheath and the partial transection into the optic nerve. Post-operative analgesia (Carprofen, 2.8 mg/kg, Norbook, Newry, UK) and sterile phosphate-buffered saline (PBS, 1 mL) were administered subcutaneously following surgery. To label cells actively undergoing the cell cycle, EdU (20 mg/kg, Invitrogen, Waltham, MA, USA) was delivered via intraperitoneal injection twice, once immediately following the surgical procedures during post-operative care and once the following morning at least 2 h prior to euthanasia. The total number of sham control animals was reduced to $n = 9$ due to $n = 1$ rat being resistant to the anesthesia necessary for surgery and thus omitted from the study. There were no deaths from the surgical procedure.

4.3. Tissue Processing

At 1 day post-injury, rats were euthanized with pentobarbitone sodium (160 mg/kg, Delvet) prior to being transcardially perfused with 0.9% saline followed by 4% paraformaldehyde (Sigma-Aldrich, St. Louis, MO, USA). The injured right optic nerves were dissected and immersed in a 4% paraformaldehyde solution overnight. The following day, the nerves were transferred to 5% sucrose (ChemSupply Australia, Bedford, South Australia, Australia), 0.1% sodium azide (Sigma-Aldrich) in PBS for cryoprotection. The optic nerves were then cryosectioned transversely at 14 μm , collected onto Superfrost Plus glass microscope slides, and stored at $-80\text{ }^{\circ}\text{C}$ prior to immunohistochemical analysis.

4.4. Multiplex Immunohistochemistry

Prior to commencing immunohistochemical analysis, the back surface of each slide was placed unsubsmerged in PBS within an electrophoresis tank for 1 h at 70 V to reinforce the electrostatic bond between the tissue and slide, mitigating the risk of tissue detachment during the multiple wash steps involved in the protocol. Slides were then dried in a $37\text{ }^{\circ}\text{C}$ oven for 10 min. Antigen retrieval involved heating the slides in 10 mM Tris-EDTA-0.5 M NaCl (pH 9.0) solution in the microwave for 2 min and 20 s, followed by a 20 min cooling period at room temperature. Slides were washed in a PBS bath prior to the application of a hydrophobic barrier around the tissue, using a PAP pen (Merck, Advanced PAP Pen, Darmstadt, Germany). Sections were washed with PBS three times before incubation with Peroxidized 1 solution (0.3% H_2O_2 , PX968M, 121219-2, Biocare Medical, Pacheco, CA, USA) for 10 min at room temperature. Slides were washed three times in PBS after the application period for each reagent was complete. Non-specific background was blocked using 3% bovine serum albumin solution (Merck, 12657) for 20 min at room temperature.

Primary antibodies used recognized: 8OHDG (1:250, 4 $\mu\text{g}/\text{mL}$, mouse, Abcam, ab62623, GR3284216-13), rat Immunoglobulin G (IgG, 1:150, 10 $\mu\text{g}/\text{mL}$, goat, BA-9400, ZG0108, Vector Laboratories, Burlingame, CA, USA), NG2 (1:50, 20 $\mu\text{g}/\text{mL}$, rabbit, AB5320B, 3218879, Merck), Cleaved Caspase3 (Asp175, 1:150; rabbit, D3E9, #9579, Lot 1, Cell Signaling Technology, Danvers, MA, USA) and PDGFR α (1:250, 4 $\mu\text{g}/\text{mL}$, rabbit, PA516571, VJ2870528A, ThermoFisher, Waltham, MA, USA). Primary antibodies were diluted in PBS and applied overnight at $4\text{ }^{\circ}\text{C}$. Target markers were detected sequentially in three separate combinations of antibodies/detection systems—Combination 1: PDGFR α , 8OHDG, EdU; Combination 2: PDGFR α , 8OHDG, Cleaved Caspase3; and Combination 3: NG2, 8OHDG. A separate section was used for each combination. IgG was detected alone on a separate section.

Fluorescence labeling of PDGFR α , 8OHDG, and Cleaved Caspase3 was performed using the following secondary antibodies, respectively: AF488-conjugated anti-rabbit IgG antibody (1:400; 5 $\mu\text{g}/\text{mL}$, donkey, A21206, 2289872, ThermoFisher), AF647-conjugated anti-mouse IgG antibody (1:100; 20 $\mu\text{g}/\text{mL}$, donkey, A31571, 2136787, ThermoFisher) and

AF555-conjugated anti-rabbit IgG antibody (1:400; 5 µg/mL, donkey, A31572, 1945911, ThermoFisher). Secondary antibodies were diluted in PBS and applied for 2 h at room temperature. To minimize cross-reactivity between the two anti-rabbit secondary antibodies for each combination, anti-rabbit IgG (H+L) antibody (1:100, 15 µg/mL, horse, BA-1100-1.5, ZH0421, Vector Laboratories) was applied for 1 h at room temperature after the full detection of the first rabbit antibody (i.e., after primary and secondary antibody application steps). The anti-rabbit IgG (H+L) antibody saturates the remaining binding sites for rabbit-specific secondary antibodies on the Fc region of the preceding rabbit primary antibody, restricting off-target binding when the next rabbit-specific secondary antibody is applied. The biotinylated NG2 and IgG antibodies were fluorescently labeled using the VECTASTAIN® Elite® ABC-HRP Kit (1:100, PK-6100, ZG0312, Vector Laboratories) in conjunction with a TSA FLUORESCENCE REAGENT PACK (NEL701A001KT, 191230019, Akoya Biosciences, Marlborough, MA, USA) according to manufacturers' instructions. To detect EdU+ cells, the Click-iT EdU AlexaFluor-647 Imaging Kit (C10340, 2284610, ThermoFisher) was utilized according to the manufacturer's instructions. Finally, sections were washed with PBS three times and coverslipped using Fluoromount-G (Thermo Fisher).

4.5. Imaging and Analysis

For each analysis, the entire optic nerve was visualized using a Nikon A1 confocal microscope (Nikon Corporation, Sydney, Australia) or a Dragonfly High Speed Confocal Microscope System (Andor Technology, Belfast, UK). A series of images were taken at 0.5 µm increments along the z-axis with consistent capture settings across all images for each outcome, at a magnification of 20× and numerical aperture of 0.75. Image analysis was performed using Fiji/ImageJ image processing software (National Institutes of Health, Bethesda, MD, USA).

The area of the ventral nerve region was segmented and quantified. Representative immunointensity thresholds for each outcome measure were determined to distinguish positive signals from the background prior to analyses within the ventral nerve. Using the most in-focus visual z-slice and the defined intensity thresholds, the mean area and intensity of immunoreactivity for IgG and 8OHdG were then semi-quantified. The areas above threshold measurements were normalized to the total area of the ventral nerve region. The number of EdU+ and Cleaved Caspase3+ cells was counted within the ventral nerve, normalized against the total ventral area, and expressed as the mean number of cells/mm². Both EdU+ 8OHdG+ and Cleaved Caspase3+ 8OHdG+ cells were detected by the colocalization of either EdU+ or Cleaved Caspase3+ cells with 8OHdG immunointensity above the set threshold similarly quantified.

Using the defined thresholds to identify NG2+ glia and PDGFRα+ glia, the intensity of 8OHdG was then also measured within the identified glia to assess the levels of DNA damage specifically within these cell types. EdU+ and Cleaved Caspase3+ cells were categorized into PDGFRα+ and PDGFRα- subpopulations based on immunoreactivity and cellular morphology. These subpopulations were further categorized via the colocalized detection of 8OHdG DNA damage.

4.6. Statistics

The obtained data were analyzed and plotted using GraphPad PRISM 9 software. All outcome measures, except for the area of IgG immunointensity, satisfied the assumption of normality according to a Kolmogorov-Smirnov test. Therefore, a t-test, two-way ANOVA with Tukey's post hoc or three-way ANOVA with Tukey's post hoc were used as appropriate. Given the area of IgG immunointensity did not satisfy the assumption of normality, the non-parametric Mann-Whitney test was used to assess the statistical difference between sham and injury for this outcome measure. A Spearman's correlation was used to assess the monotonic relationship between IgG and either 8OHdG, EdU or Cleaved Caspase3. Any reductions in final n's reflect a loss of tissue from slides during immunohistochemical analyses or the exclusion of sections that had become damaged during tissue processing and

analysis in a way that precluded reliable quantification of outcomes. Statistical significances shown on graphs are hypothesis-driven and may not display all significant differences obtained. Specifically, only significant differences in comparable cell types between the sham control and injured groups are shown, as well as any differences found between cells within each group. No data outliers were removed for any outcome measures.

Author Contributions: Conceptualization, L.M.T., M.G.P., T.O.C., M.F. and C.C.A.; methodology, L.M.T., M.G.P., T.O.C., E.D., M.F. and C.C.A.; software, L.M.T. and C.C.A.; validation, L.M.T., M.G.P., T.O.C., A.J.W., E.D. and C.C.A.; formal analysis, L.M.T. and C.C.A.; investigation, L.M.T., M.G.P., T.O.C., A.J.W., E.D., A.W., T.M., C.A.B. and C.C.A.; resources, M.F.; data curation, L.M.T. and C.C.A.; writing—original draft preparation, L.M.T. and C.C.A.; writing—review and editing, L.M.T., M.G.P., T.O.C., A.J.W., E.D., A.W., T.M., C.A.B., M.F. and C.C.A.; visualization, L.M.T. and C.C.A.; supervision, M.F. and C.C.A.; project administration, L.M.T., M.G.P., T.O.C., E.D., M.F. and C.C.A.; funding acquisition, M.F. and C.C.A. All authors have read and agreed to the published version of the manuscript.

Funding: This work was supported by the National Health and Medical Research Fund (APP1160691). L.M.T. was supported by an MS Research Australia Postgraduate Scholarship and a Byron Kakulas Prestige Scholarship from the Perron Institute for Neurological and Translational Science.

Institutional Review Board Statement: The animal study protocol was approved by the Animal Ethics Committee of The University of Western Australia (RA/3/100/1485, approved 30 September 2016) and the Animal Ethics Committee of Curtin University (ARE2017-4, approved 28 April 2017).

Data Availability Statement: The datasets generated during this study are available from the corresponding author upon request.

Conflicts of Interest: The authors declare no conflict of interest. The funders had no role in the design of the study; in the collection, analyses, or interpretation of data; in the writing of the manuscript; or in the decision to publish the results.

References

- Werner, C.; Engelhard, K. Pathophysiology of Traumatic Brain Injury. *Br. J. Anaesth.* **2007**, *99*, 4–9. [\[CrossRef\]](#) [\[PubMed\]](#)
- Kaur, P.; Sharma, S. Recent Advances in Pathophysiology of Traumatic Brain Injury. *Curr. Neuropharmacol.* **2018**, *16*, 1224–1238. [\[CrossRef\]](#) [\[PubMed\]](#)
- Li, H.-Y.; Ruan, Y.-W.; Ren, C.-R.; Cui, Q.; So, K.-F. Mechanisms of Secondary Degeneration after Partial Optic Nerve Transection. *Neural Regen. Res.* **2014**, *9*, 565–574. [\[CrossRef\]](#) [\[PubMed\]](#)
- Tezel, G. Multifactorial Pathogenic Processes of Retinal Ganglion Cell Degeneration in Glaucoma towards Multi-Target Strategies for Broader Treatment Effects. *Cells* **2021**, *10*, 1372. [\[CrossRef\]](#) [\[PubMed\]](#)
- Chidlow, G.; Wood, J.P.M.; Casson, R.J. Investigations into Hypoxia and Oxidative Stress at the Optic Nerve Head in a Rat Model of Glaucoma. *Front. Neurosci.* **2017**, *11*, 478. [\[CrossRef\]](#)
- Osborne, N.N.; Melena, J.; Chidlow, G.; Wood, J.P.M. A Hypothesis to Explain Ganglion Cell Death Caused by Vascular Insults at the Optic Nerve Head: Possible Implication for the Treatment of Glaucoma. *Br. J. Ophthalmol.* **2001**, *85*, 1252–1259. [\[CrossRef\]](#)
- Cash, A.; Theus, M.H. Mechanisms of Blood-Brain Barrier Dysfunction in Traumatic Brain Injury. *Int. J. Mol. Sci.* **2020**, *21*, 3344. [\[CrossRef\]](#)
- Bartlett, C.; Fitzgerald, M. Partial Transection of Adult Rat Optic Nerve as a Model of Secondary Degeneration in the Central Nervous System. *Bio-Protocol* **2018**, *8*, e3118. [\[CrossRef\]](#)
- Warnock, A.; Toomey, L.M.; Wright, A.J.; Fisher, K.; Won, Y.; Anyaegbu, C.; Fitzgerald, M. Damage Mechanisms to Oligodendrocytes and White Matter in Central Nervous System Injury: The Australian Context. *J. Neurotrauma* **2020**, *37*, 739–769. [\[CrossRef\]](#)
- Smith, N.M.; Gachulincova, I.; Ho, D.; Bailey, C.; Bartlett, C.A.; Norret, M.; Murphy, J.; Buckley, A.; Rigby, P.J.; House, M.J.; et al. An Unexpected Transient Breakdown of the Blood Brain Barrier Triggers Passage of Large Intravenously Administered Nanoparticles. *Sci. Rep.* **2016**, *6*, 22595. [\[CrossRef\]](#)
- Smith, N.M.; Giacci, M.K.; Gough, A.; Bailey, C.; McGonigle, T.; Black, A.M.; Clarke, T.O.; Bartlett, C.A.; Swaminathan Iyer, K.; Dunlop, S.A.; et al. Inflammation and Blood-Brain Barrier Breach Remote from the Primary Injury Following Neurotrauma. *J. Neuroinflammation* **2018**, *15*, 201. [\[CrossRef\]](#)
- Cornelius, C.; Crupi, R.; Calabrese, V.; Graziano, A.; Milone, P.; Pennisi, G.; Radak, Z.; Calabrese, E.J.; Cuzzocrea, S. Traumatic Brain Injury: Oxidative Stress and Neuroprotection. *Antioxid. Redox Signal.* **2013**, *19*, 836–853. [\[CrossRef\]](#)
- Ischiropoulos, H.; Beckman, J.S. Oxidative Stress and Nitration in Neurodegeneration: Cause, Effect, or Association? *J. Clin. Invest.* **2003**, *111*, 163–169. [\[CrossRef\]](#)

14. Laval, J.; Jurado, J.; Saporbaev, M.; Sidorkina, O. Antimutagenic Role of Base-Excision Repair Enzymes upon Free Radical-Induced DNA Damage. *Mutat. Res.* **1998**, *402*, 93–102. [[CrossRef](#)]
15. Fitzgerald, M.; Bartlett, C.A.; Harvey, A.R.; Dunlop, S.A. Early Events of Secondary Degeneration after Partial Optic Nerve Transection: An Immunohistochemical Study. *J. Neurotrauma* **2010**, *27*, 439–452. [[CrossRef](#)]
16. Giacci, M.K.; Bartlett, C.A.; Smith, N.M.; Iyer, K.S.; Toomey, L.M.; Jiang, H.; Guagliardo, P.; Kilburn, M.R.; Fitzgerald, M. Oligodendroglia Are Particularly Vulnerable to Oxidative Damage after Neurotrauma In Vivo. *J. Neurosci.* **2018**, *38*, 6491–6504. [[CrossRef](#)]
17. Matute, C.; Torre, I.; Pérez-Cerdá, F.; Pérez-Samartín, A.; Alberdi, E.; Etxebarria, E.; Arranz, A.M.; Ravid, R.; Rodríguez-Antigüedad, A.; Sánchez-Gómez, M.V.; et al. P2X7 Receptor Blockade Prevents ATP Excitotoxicity in Oligodendrocytes and Ameliorates Experimental Autoimmune Encephalomyelitis. *J. Neurosci.* **2007**, *27*, 9525–9533. [[CrossRef](#)]
18. Borges, K.; Ohlemeyer, C.; Trotter, J.; Kettenmann, H. AMPA/Kainate Receptor Activation in Murine Oligodendrocyte Precursor Cells Leads to Activation of a Cation Conductance, Calcium Influx and Blockade of Delayed Rectifying K⁺ Channels. *Neuroscience* **1994**, *63*, 135–149. [[CrossRef](#)]
19. Thorburne, S.K.; Juurlink, B.H. Low Glutathione and High Iron Govern the Susceptibility of Oligodendroglial Precursors to Oxidative Stress. *J. Neurochem.* **1996**, *67*, 1014–1022. [[CrossRef](#)]
20. Butts, B.D.; Houde, C.; Mehmet, H. Maturation-Dependent Sensitivity of Oligodendrocyte Lineage Cells to Apoptosis: Implications for Normal Development and Disease. *Cell Death Differ.* **2008**, *15*, 1178–1186. [[CrossRef](#)]
21. Fitzgerald, M.; Bartlett, C.A.; Evill, L.; Rodger, J.; Harvey, A.R.; Dunlop, S.A. Secondary Degeneration of the Optic Nerve Following Partial Transection: The Benefits of Lomerizine. *Exp. Neurol.* **2009**, *216*, 219–230. [[CrossRef](#)] [[PubMed](#)]
22. Payne, S.C.; Bartlett, C.A.; Harvey, A.R.; Dunlop, S.A.; Fitzgerald, M. Chronic Swelling and Abnormal Myelination during Secondary Degeneration after Partial Injury to a Central Nervous System Tract. *J. Neurotrauma* **2011**, *28*, 1077–1088. [[CrossRef](#)] [[PubMed](#)]
23. Payne, S.C.; Bartlett, C.A.; Harvey, A.R.; Dunlop, S.A.; Fitzgerald, M. Myelin Sheath Decompaction, Axon Swelling, and Functional Loss during Chronic Secondary Degeneration in Rat Optic Nerve. *Investig. Ophthalmol. Vis. Sci.* **2012**, *53*, 6093–6101. [[CrossRef](#)]
24. Nicholson, D.W.; Ali, A.; Thornberry, N.A.; Vaillancourt, J.P.; Ding, C.K.; Gallant, M.; Gareau, Y.; Griffin, P.R.; Labelle, M.; Lazebnik, Y.A.; et al. Identification and Inhibition of the ICE/CED-3 Protease Necessary for Mammalian Apoptosis. *Nature* **1995**, *376*, 37–43. [[CrossRef](#)]
25. Akay, L.A.; Effenberger, A.H.; Tsai, L.H. Cell of All Trades: Oligodendrocyte Precursor Cells in Synaptic, Vascular, and Immune Function. *Genes Dev.* **2021**, *35*, 180–198. [[CrossRef](#)] [[PubMed](#)]
26. Bergles, D.E.; Richardson, W.D. Oligodendrocyte Development and Plasticity. *Cold Spring Harb. Perspect. Biol.* **2016**, *8*, a020453. [[CrossRef](#)]
27. O'Hare Doig, R.L.; Bartlett, C.A.; Maghzal, G.J.; Lam, M.; Archer, M.; Stocker, R.; Fitzgerald, M. Reactive Species and Oxidative Stress in Optic Nerve Vulnerable to Secondary Degeneration. *Exp. Neurol.* **2014**, *261*, 136–146. [[CrossRef](#)]
28. Grammas, P.; Martinez, J.; Miller, B. Cerebral Microvascular Endothelium and the Pathogenesis of Neurodegenerative Diseases. *Expert Rev. Mol. Med.* **2011**, *13*, e19. [[CrossRef](#)]
29. Salman, M.M.; Kitchen, P.; Halsey, A.; Wang, M.X.; Törnroth-Horsefield, S.; Conner, A.C.; Badaut, J.; Iliff, J.J.; Bill, R.M. Emerging Roles for Dynamic Aquaporin-4 Subcellular Relocalization in CNS Water Homeostasis. *Brain* **2022**, *145*, 64–75. [[CrossRef](#)]
30. Nishiyama, A.; Lin, X.H.; Giese, N.; Heldin, C.H.; Stallcup, W.B. Co-Localization of NG2 Proteoglycan and PDGF α -Receptor on O2A Progenitor Cells in the Developing Rat Brain. *J. Neurosci. Res.* **1996**, *43*, 299–314. [[CrossRef](#)]
31. Jakovcevski, I.; Filipovic, R.; Mo, Z.; Rakic, S.; Zecevic, N. Oligodendrocyte Development and the Onset of Myelination in the Human Fetal Brain. *Front. Neuroanat.* **2009**, *3*, 5. [[CrossRef](#)]
32. Li, P.; Li, H.X.; Jiang, H.Y.; Zhu, L.; Wu, H.Y.; Li, J.T.; Lai, J.H. Expression of NG2 and Platelet-Derived Growth Factor Receptor Alpha in the Developing Neonatal Rat Brain. *Neural Regen. Res.* **2017**, *12*, 1843. [[CrossRef](#)]
33. Payne, S.C.; Bartlett, C.A.; Savigni, D.L.; Harvey, A.R.; Dunlop, S.A.; Fitzgerald, M. Early Proliferation Does Not Prevent the Loss of Oligodendrocyte Progenitor Cells during the Chronic Phase of Secondary Degeneration in a CNS White Matter Tract. *PLoS ONE* **2013**, *8*, 65710–65720. [[CrossRef](#)]
34. Karve, I.P.; Taylor, J.M.; Crack, P.J. The Contribution of Astrocytes and Microglia to Traumatic Brain Injury. *Br. J. Pharmacol.* **2016**, *173*, 692–702. [[CrossRef](#)]
35. Loane, D.J.; Byrnes, K.R. Role of Microglia in Neurotrauma. *Neurotherapeutics* **2010**, *7*, 366–377. [[CrossRef](#)]
36. Beiter, R.M.; Rivet-Noor, C.; Merchak, A.R.; Bai, R.; Johanson, D.M.; Slogar, E.; Sol-Church, K.; Overall, C.C.; Gaultier, A. Evidence for Oligodendrocyte Progenitor Cell Heterogeneity in the Adult Mouse Brain. *Sci. Rep.* **2022**, *12*, 12921. [[CrossRef](#)]
37. Maki, T. Novel Roles of Oligodendrocyte Precursor Cells in the Developing and Damaged Brain. *Clin. Exp. Neuroimmunol.* **2017**, *8*, 33–42. [[CrossRef](#)]
38. Maki, T.; Maeda, M.; Uemura, M.; Lo, E.K.; Terasaki, Y.; Liang, A.C.; Shindo, A.; Choi, Y.K.; Taguchi, A.; Matsuyama, T.; et al. Potential Interactions between Pericytes and Oligodendrocyte Precursor Cells in Perivascular Regions of Cerebral White Matter. *Neurosci. Lett.* **2015**, *597*, 164–169. [[CrossRef](#)]
39. Seo, J.H.; Miyamoto, N.; Hayakawa, K.; Pham, L.D.D.; Maki, T.; Ayata, C.; Kim, K.W.; Lo, E.H.; Arai, K. Oligodendrocyte Precursors Induce Early Blood-Brain Barrier Opening after White Matter Injury. *J. Clin. Investig.* **2013**, *123*, 782–786. [[CrossRef](#)]

40. Girolamo, F.; Errede, M.; Longo, G.; Annese, T.; Alias, C.; Ferrara, G.; Morando, S.; Trojano, M.; De Rosbo, N.K.; Uccelli, A.; et al. Defining the Role of NG2-Expressing Cells in Experimental Models of Multiple Sclerosis. A Biofunctional Analysis of the Neurovascular Unit in Wild Type and NG2 Null Mice. *PLoS ONE* **2019**, *14*, e0213508. [[CrossRef](#)]
41. Niu, J.; Tsai, H.H.; Hoi, K.K.; Huang, N.; Yu, G.; Kim, K.; Baranzini, S.E.; Xiao, L.; Chan, J.R.; Fancy, S.P.J. Aberrant Oligodendroglial–Vascular Interactions Disrupt the Blood–Brain Barrier, Triggering CNS Inflammation. *Nat. Neurosci.* **2019**, *22*, 709–718. [[CrossRef](#)] [[PubMed](#)]
42. Kitchen, P.; Salman, M.M.; Halsey, A.M.; Clarke-Bland, C.; MacDonald, J.A.; Ishida, H.; Vogel, H.J.; Almutiri, S.; Logan, A.; Kreida, S.; et al. Targeting Aquaporin-4 Subcellular Localization to Treat Central Nervous System Edema. *Cell* **2020**, *181*, 784–799.e19. [[CrossRef](#)] [[PubMed](#)]
43. Aldewachi, H.; Al-Zidan, R.N.; Conner, M.T.; Salman, M.M. High-Throughput Screening Platforms in the Discovery of Novel Drugs for Neurodegenerative Diseases. *Bioengineering* **2021**, *8*, 30. [[CrossRef](#)] [[PubMed](#)]
44. Papaspyropoulos, A.; Tsolaki, M.; Foroglou, N.; Pantazaki, A.A. Modeling and Targeting Alzheimer’s Disease With Organoids. *Front. Pharmacol.* **2020**, *11*, 396. [[CrossRef](#)]
45. Salman, M.M.; Marsh, G.; Kusters, L.; Delincé, M.; Di Caprio, G.; Upadhyayula, S.; de Nola, G.; Hunt, R.; Ohashi, K.G.; Gray, T.; et al. Design and Validation of a Human Brain Endothelial Microvessel-on-a-Chip Open Microfluidic Model Enabling Advanced Optical Imaging. *Front. Bioeng. Biotechnol.* **2020**, *8*, 1077. [[CrossRef](#)]

Disclaimer/Publisher’s Note: The statements, opinions and data contained in all publications are solely those of the individual author(s) and contributor(s) and not of MDPI and/or the editor(s). MDPI and/or the editor(s) disclaim responsibility for any injury to people or property resulting from any ideas, methods, instructions or products referred to in the content.

Appendix D. Detailed Copyright Statements

The review article, entitled *Damage mechanisms to oligodendrocytes and white matter in central nervous system injury: The Australian context*, was published in the *Journal of Neurotrauma* in volume 37, issue 5. This journal is published by Mary Ann Liebert, Inc., publishers, New Rochelle, NY. This article can be used for non-commercial, scholarly purposes in accordance with the Mary Ann Liebert, Inc., publishers' Terms and Conditions, and therefore I was not required to obtain specific permission to reproduce the article in this thesis.

The original research article, entitled *Cuprizone feed formulation influences the extent of demyelinating disease pathology*, was published in *Scientific Reports* in volume 11, issue 1. This journal is published by Springer Nature. The article is open access and distributed under the terms of a Creative Commons CC BY license, and therefore I was not required to obtain specific permission to reproduce the article in this thesis.

The original research article, entitled *Comparison of ion channel inhibitor combinations for limiting secondary degeneration following partial optic nerve transection*, was published in *Scientific Reports* in volume 9, issue 1. This journal is published by Springer Nature. The article is open access and distributed under the terms of a Creative Commons CC BY license, and therefore I was not required to obtain specific permission to reproduce the article in this thesis.

The original research article, entitled *The effects of a combination of ion channel inhibitors on pathology in a model of demyelinating disease*, was published in *Multiple Sclerosis and Related Disorders* in volume 34. This journal is published by Elsevier Inc. This article can be used for non-commercial, scholarly purposes in accordance with the Elsevier Inc. Terms and Conditions, and therefore I was not required to obtain specific permission to reproduce the article in this thesis.

The original research article, entitled *Secondary degeneration of oligodendrocyte precursor cells occurs as early as 24 hours after optic nerve injury in rats*, was published in the *International Journal of Molecular Sciences* in volume 24, issue 4. This journal is published by MDPI. The article is open access and distributed under the terms of a Creative Commons CC BY license, and therefore I was not required to obtain specific permission to reproduce the article in this thesis.